

**Characterisation of a plasmid segregational
stability determinant, *par*, of the
staphylococcal multiresistance plasmid, pSK1**

A thesis submitted in partial fulfilment of the requirements for
the degree of Doctor of Philosophy

by

Helena Yee-Wah Chan

B. Sc. (Molecular Biology and Genetics) (Hons)

Oct 2017

School of Life and Environmental Sciences

The University of Sydney

NSW 2006 Australia

TABLE OF CONTENTS

LIST OF TABLES	xi
LIST OF FIGURES	xii
SUMMARY	xviii
STATEMENT OF ORIGINALITY	xxi
ACKNOWLEDGMENTS	xxii
CHAPTER 1 Introduction	1
1.1. The staphylococci	1
1.2. Antimicrobial resistance in the staphylococci	2
1.2.1. Emergence of antimicrobial resistance in the staphylococci	2
1.2.2. Mechanisms of genetic exchange in the staphylococci	5
1.3. Mobile genetic elements associated with antibiotic resistance in the staphylococci	8
1.3.1. Transposons and insertion sequences	8
1.3.2. Staphylococcal plasmids	11
1.3.2.1. Small rolling-circle plasmids	11
1.3.2.2. pSK639-like plasmids	12
1.3.2.3. Multiresistance plasmids	13
1.3.2.4. Conjugative multiresistance plasmids	15
1.3.3. Staphylococcal cassette chromosome <i>mec</i>	16
1.3.4. <i>Staphylococcus aureus</i> pathogenicity islands	17
1.4. Plasmid maintenance mechanisms	18
1.4.1. Multimer resolution	18
1.4.2. Post-segregational killing	20
1.4.3. Active plasmid partitioning	21
1.5. Active plasmid partitioning systems	23

1.5.1. Type I active plasmid partitioning systems	23
1.5.2. Type II active plasmid partitioning systems	27
1.5.3. Type III active plasmid partitioning systems	30
1.5.4. Other plasmid partitioning systems	32
1.6. Staphylococcal multiresistance plasmid, pSK1	32
1.6.1. pSK1 plasmid segregational stability determinant, <i>par</i>	34
1.6.1.1. pSK1 Par N-terminal helix-turn-helix domain is involved in DNA-binding	35
1.6.1.2. pSK1 Par central coiled-coil domain is involved in multimerisation	36
1.6.1.3. pSK1 Par autoregulates its own expression	37
1.7. Scope of thesis	37
CHAPTER 2 Materials and methods	41
2.1. Microbial strains, plasmids and growth conditions	41
2.2. Reagents, solutions and oligonucleotides	42
2.3. Bacterial transformation procedures	42
2.3.1. Preparation of chemically-competent <i>E. coli</i> cells	42
2.3.2. Transformation of chemically-competent <i>E. coli</i> cells with plasmid DNA	43
2.3.3. Preparation of electrocompetent <i>S. aureus</i> cells	43
2.3.4. Electroporation of electrocompetent <i>S. aureus</i> cells with plasmid DNA	44
2.3.5. Preparation of electrocompetent <i>E. faecalis</i> cells	45
2.3.6. Electroporation of electrocompetent <i>E. faecalis</i> cells with plasmid DNA	45
2.4. DNA manipulations	46
2.4.1. Isolation of plasmid DNA	46

2.4.2. Isolation of genomic DNA	46
2.4.3. Agarose gel electrophoresis	47
2.4.4. Polymerase chain reaction	47
2.4.5. Site-directed mutagenesis	48
2.4.6. Reaction endonuclease digestion	49
2.4.7. DNA purification	49
2.4.8. Blunting of DNA ends	50
2.4.9. Phosphorylation of DNA ends	50
2.4.10. Dephosphorylation of DNA ends	50
2.4.11. DNA ligation	50
2.4.12. Ethanol precipitation of DNA	51
2.4.13. Quantification of DNA	51
2.4.14. DNA sequencing	51
2.5. Protein manipulations	52
2.5.1. Protein overproduction	52
2.5.2. Protein purification under non-denaturing conditions	53
2.5.3. Protein purification under denaturing conditions	53
2.5.4. Protein buffer exchange	54
2.5.5. Protein quantification	55
2.5.6. Sodium dodecyl-sulphate polyacrylamide gel electrophoresis (SDS-PAGE)	56
2.5.7. Non-reducing SDS-PAGE	57
2.5.8. Preparation of whole cell lysates for SDS-PAGE	57
2.5.9. Western blotting	58
2.5.9.1. Protein transfer	58
2.5.9.2. Immunological detection of proteins	59
2.6. Antibody preparation	61

2.6.1. Affinity purification of antiserum	61
2.6.2. Preadsorption of antibodies with <i>S. aureus</i> cell lysates	62
2.6.3. Production of anti-peptide antibodies	62
2.7. Plasmid segregational stability assays	62
2.8. Electrophoretic mobility shift assays	63
2.8.1. Preparation and radioactive end-labelling of DNA probes	63
2.8.2. Gel shift assays	64
2.9. Protein cross-linking	65
2.9.1. <i>in vitro</i> cross-linking of purified proteins using glutaraldehyde	65
2.9.2. <i>in vivo</i> cross-linking of proteins using dithiobis(succinimidyl propionate)	65
2.10. Yeast experiments	66
2.10.1. Preparation of competent <i>S. cerevisiae</i> cells	66
2.10.2. Transformation of yeast cells with plasmid DNA	67
2.10.3. Yeast two-hybrid assays	68
2.10.4. Yeast two-hybrid screening of <i>S. aureus</i> genomic DNA prey libraries	68
2.10.5. Quantitative α -galactosidase assays	70
2.11. Microscopy	71
2.11.1. Immunofluorescence microscopy	71
2.11.2. Epifluorescence microscopy	73
2.11.3. Fluorescence <i>in situ</i> hybridisation	74
2.11.3.1. Preparation of Cy3-labelled DNA probes	74
2.11.3.2. Fluorescence <i>in situ</i> hybridisation in <i>S. aureus</i>	74

CHAPTER 3 Functional significance of pSK1 Par domains	77
3.1. Introduction	77
3.2. Functional significance of the Par C-terminal domain	77
3.2.1. Construction of pSK1 minireplicons expressing Par CTD mutants	77
3.2.2. Effect of Par CTD mutations on plasmid segregational stability	80
3.3. Overproduction and purification of Par CTD mutants	81
3.3.1. Construction of expression plasmids for Par CTD mutants	81
3.3.2. Overproduction of Par CTD mutants	83
3.3.3. Small-scale purification of Par CTD mutants under non-denaturing conditions	84
3.3.4. Large-scale overproduction and purification of Par CTD mutants under denaturing conditions	85
3.4. DNA-binding activity of Par CTD mutants	87
3.4.1. Resolution of Par-DNA complexes formed in EMSAs	89
3.5. Multimerisation activity of Par CTD mutants	90
3.5.1. <i>in vitro</i> cross-linking of Par mutants using glutaraldehyde	90
3.5.2. <i>in vivo</i> cross-linking of Par mutants using dithiobis(succinimidyl propionate)	91
3.6. Self-interaction of Par proteins	94
3.6.1. Construction of Par bait and prey fusion proteins for yeast two-hybrid assays	95
3.6.2. Yeast two-hybrid assay of Par self-interaction	97
3.6.3. Contribution of Par domains to self-interaction	99
3.6.3.1. Construction of yeast two-hybrid bait and prey fusion proteins containing individual Par domains	99
3.6.3.2. Yeast two-hybrid assay of interactions between Par domains	100
3.6.4. Interactions involving Par N-terminal domain residues	103
3.6.4.1. Indications from preliminary Par structural data	103

3.6.4.2. Construction of pSK1 minireplicons expressing Par NTD mutants	103
3.6.4.3. Functionality of Par NTD mutants	104
3.7. Discussion	105
3.7.1. Functional studies of the Par CTD	106
3.7.2. Protein purification	109
3.7.3. DNA-binding studies	110
3.7.4. Multimerisation studies	112
3.7.5. Self-interaction studies	115
3.7.6. Functional studies of the Par NTD	121
CHAPTER 4 Interactions between pSK1 Par and <i>S. aureus</i> host factors	123
4.1. Introduction	123
4.2. Plasmid stabilisation by a distant pSK1 Par homologue	123
4.2.1. Construction of pSERP minireplicons to assess the functionality of a distant Par homologue	125
4.2.2. Effect of a distant Par homologue on plasmid segregational stability	126
4.3. Functionality of pSK1 <i>par</i> in a heterologous host	127
4.4. Interactions between Par and <i>S. aureus</i> proteins	129
4.4.1. Yeast two-hybrid screening of <i>S. aureus</i> genomic DNA prey libraries with full-length Par bait	129
4.4.1.1. Interaction between Par and FnBP	132
4.4.2. Contribution of <i>S. aureus</i> FnBP to Par function	133
4.4.3. Yeast two-hybrid assay to determine interaction between Par and DivIVA	135
4.4.3.1. Construction of DivIVA bait and prey plasmids for yeast two-hybrid assays	136

4.4.3.2. Yeast two-hybrid assay of Par and DivIVA interaction	137
4.4.4. Yeast two-hybrid screening of <i>S. aureus</i> genomic DNA prey libraries with the C-terminal domain of Par	138
4.5. Interactions between Par and non-specific DNA	139
4.5.1. Binding of Par to non-specific DNA	140
4.5.2. Potential Par binding sites on <i>S. aureus</i> chromosomal DNA	141
4.6. Discussion	142
4.6.1. Interaction of Par with <i>S. aureus</i> proteins	146
4.6.2. Interaction of Par with non-specific DNA	150
CHAPTER 5 Cell biology of pSK1 <i>par</i>-mediated plasmid segregation	154
5.1. Introduction	154
5.2. Generation of anti-Par peptide antibodies	155
5.2.1. Reactivity of anti-Par peptide antibodies in <i>S. aureus</i>	156
5.3. Immunofluorescence microscopy of Par in <i>S. aureus</i>	159
5.3.1. Immunofluorescence microscopy of Par using anti-Par peptide antibodies	159
5.3.2. Validation of <i>S. aureus</i> immunofluorescence microscopy protocol	160
5.3.3. Construction of a pSK1 minireplicon encoding RGS _{H6} -Par	161
5.3.4. Functionality of RGS _{H6} -Par in <i>S. aureus</i>	163
5.4. Live cell epifluorescence microscopy of fluorescently-tagged Par in <i>S. aureus</i>	164
5.4.1. Construction of pSK1 minireplicons encoding Par GFP fusions	164
5.4.2. Segregational stability of pSK1 minireplicons encoding Par GFP fusions	167
5.4.3. Epifluorescence microscopy of Par GFP fusions in <i>S. aureus</i>	169
5.4.4. Development of a pSK1 <i>par</i> system with inducible, <i>in trans</i> expression of Par	169

5.4.4.1. Construction of an IPTG-inducible <i>par</i> expression plasmid	170
5.4.4.2. Effect of Par on plasmid segregational stability <i>in trans</i>	171
5.4.4.3. Interaction between Par and Par-GFP	174
5.4.4.4. Epifluorescence microscopy of Par-GFP in <i>S. aureus</i> , supplied <i>in trans</i> with Par	176
5.4.4.4.1. Association between Par-GFP and nucleoid DNA in <i>S. aureus</i>	178
5.4.5. Development of a pSK1 <i>par</i> system with inducible, <i>in trans</i> expression of <i>par-gfp</i>	180
5.4.5.1. Construction of an IPTG-inducible <i>par-gfp</i> expression plasmid	180
5.4.5.2. Effect of Par-GFP on plasmid segregational stability <i>in trans</i>	181
5.4.5.3. Epifluorescence microscopy of Par-GFP in <i>S. aureus</i> , supplied <i>in trans</i> to Par	184
5.4.6. Epifluorescence microscopy of Par GFP fusions in <i>S. aureus</i> , in the absence of centromere DNA	185
5.4.7. Distribution of Par-GFP focus numbers in <i>S. aureus</i>	187
5.5. Immunofluorescence microscopy of Par in <i>E. coli</i>	188
5.6. Live cell epifluorescence microscopy of fluorescently-tagged Par in <i>E. coli</i>	190
5.6.1. Fluorescence localisation of GFP-Par mutants in <i>E. coli</i>	191
5.6.2. Construction of an IPTG-inducible <i>gfp-par</i> expression plasmid	192
5.6.3. Fluorescence localisation of GFP-Par in <i>E. coli</i> , in the absence of centromere DNA	194
5.7. Fluorescence <i>in situ</i> hybridisation of pSK1 minireplicons in <i>S.</i> <i>aureus</i>	195
5.8. Fluorescence localisation of pSK1 minireplicons in live <i>S. aureus</i> cells	196
5.8.1. Construction of pSK1 minireplicons carrying <i>tetO</i> arrays	197
5.8.2. Construction of an IPTG-inducible <i>tetR-gfp</i> expression plasmid	198

5.8.3. Effect of TetR-GFP on plasmid segregational stability	201
5.8.4. Fluorescence localisation of pSK1 minireplicons using a fluorescent repressor-operator system in live <i>S. aureus</i> cells	203
5.8.5. Distribution of TetR-GFP focus numbers in <i>S. aureus</i>	205
5.8.6. Association between TetR-GFP and nucleoid DNA in <i>S. aureus</i>	207
5.8.7. Time-lapse epifluorescence microscopy of plasmid localisation in <i>S. aureus</i>	208
5.9. Discussion	210
5.9.1. Fluorescence localisation of Par	210
5.9.2. Fluorescence localisation of plasmid DNA	224
CHAPTER 6 General Discussion	233
6.1. Functional significance of Par C-terminal domain in the partition complex	234
6.2. Potential mechanisms of pSK1 <i>par</i>-mediated plasmid segregational stability	239
6.2.1. Centromere-binding	240
6.2.2. Plasmid pairing	242
6.2.3. Plasmid segregation	243
6.2.3.1. Molecular switches	244
6.2.3.2. Pilot-fish or hitch-hiking	245
6.2.3.3. Host factors	246
6.2.3.3.1. Host factors: nucleoid DNA	247
6.2.3.3.2. Host factors: host-encoded proteins	249
6.2.4. Autoregulation	250
6.3. Concluding remarks	251
APPENDIX A Abbreviations	254
APPENDIX B Supplementary	260

Supplementary Methods S1. Bioinformatics techniques	260
BIBLIOGRAPHY	261

LIST OF TABLES

Table	Title	After page
Chapter 1		
Table 1.1	Staphylococcal transposons and insertion sequences	9
Chapter 2		
Table 2.1	Microbial strains	41
Table 2.2	Plasmids	41
Table 2.3	Microbial growth media	41
Table 2.4	Concentrations of antimicrobial compounds	41
Table 2.5	Reagents and solutions	42
Table 2.6	Oligonucleotides	42
Chapter 3		
Table 3.1	Summary of properties of Par and Par CTD mutants	106
Chapter 4		
Table 4.1	Summary of properties of Par derivatives (Chapter 4)	142
Chapter 5		
Table 5.1	Summary of properties of Par derivatives (Chapter 5)	210
Supplementary		
Table S1	pSK1 <i>par</i> centromere-like sites on <i>S. aureus</i> chromosomal DNA	260

LIST OF FIGURES

Figure	Title	After page
Chapter 1		
Figure 1.1	Genetic maps of pSK1 family plasmids	15
Figure 1.2	Genetic organisation of representative active plasmid partitioning systems	21
Figure 1.3	Structures of centromere-binding proteins bound to DNA	24
Figure 1.4	Mechanistic models of active plasmid partitioning systems	26
Figure 1.5	Genetic map of the staphylococcal multiresistance plasmid, pSK1	33
Figure 1.6	Organisation of the pSK1 <i>par</i> upstream promoter region	34
Figure 1.7	Predicted Par protein domains	34
Chapter 3		
Figure 3.1	Graphical representation of pSK1 <i>par</i> mutants generated in this study	77
Figure 3.2	Effect of Par CTD mutations on plasmid segregational stability	80
Figure 3.3	Overproduction of Par CTD mutant proteins in <i>E. coli</i>	83
Figure 3.4	Small-scale overproduction and purification of RGS _{H6} -tagged Par proteins under non-denaturing conditions	85

Figure	Title	After page
Figure 3.5	Large-scale overproduction and purification of RGS _{H6} -tagged Par proteins under denaturing conditions	86
Figure 3.6	DNA-binding activity of Par CTD mutant proteins	88
Figure 3.7	<i>in vitro</i> cross-linking of purified Par proteins using glutaraldehyde	90
Figure 3.8	<i>in vivo</i> cross-linking of Par proteins in <i>S. aureus</i> using DSP	92
Figure 3.9	<i>in vivo</i> cross-linking of Par proteins in <i>E. coli</i> using DSP	93
Figure 3.10	Self-interaction of Par proteins	98
Figure 3.11	Interactions between Par domains	100
Figure 3.12	Effect of Par NTD mutations on plasmid segregational stability	104
 Chapter 4		
Figure 4.1	Sequence analysis of pSK1 Par homologues	124
Figure 4.2	Effect of a distant Par homologue on plasmid segregational stability	126
Figure 4.3	Effect of pSK1 <i>par</i> on plasmid segregational stability in <i>Enterococcus faecalis</i>	128
Figure 4.4	Graphical overview of DNA inserts contained in yeast two-hybrid prey plasmids encoding fibronectin-binding protein	131
Figure 4.5	Amino acid sequence of FnBP identified by yeast two-hybrid screening of <i>S. aureus</i> genomic DNA library using a Par bait	131

Figure	Title	After page
Figure 4.6	Interaction between Par and FnBP	132
Figure 4.7	Plasmid segregational stability of pSK1 minireplicons in a <i>S. aureus</i> FnBP mutant	135
Figure 4.8	Putative RacA conserved domain of Par	135
Figure 4.9	Interaction between Par and DivIVA	137
Figure 4.10	DNA-binding of Par proteins to non-specific DNA	140
Figure 4.11	Map of potential pSK1 Par binding sites on <i>S. aureus</i> chromosome	142
 Chapter 5		
Figure 5.1	Prediction of Par antigenic peptides	155
Figure 5.2	Immunodetection of Par in <i>S. aureus</i> using anti-Par peptide antibodies	157
Figure 5.3	Immunofluorescence microscopy in <i>S. aureus</i>	159
Figure 5.4	Effect of RGSH ₆ -Par on plasmid segregational stability	163
Figure 5.5	Fusion of <i>gfp</i> to pSK1 <i>par</i> using overlap extension PCR	164
Figure 5.6	Effect of GFP fusions on plasmid segregational stability	167
Figure 5.7	Fluorescence localisation of Par GFP fusion proteins in <i>S. aureus</i> cells	169
Figure 5.8	Effect of Par on plasmid segregational stability, <i>in trans</i>	171
Figure 5.9	Immunodetection of Par, supplied <i>in trans</i> to pSK1 minireplicons	173

Figure	Title	After page
Figure 5.10	Interaction between Par and Par-GFP	175
Figure 5.11	Fluorescence localisation of the cell division marker, Spo0J-GFP, in <i>S. aureus</i> cells	177
Figure 5.12	Fluorescence localisation of Par-GFP in <i>S. aureus</i> cells, in the presence and absence of Par supplied <i>in trans</i>	177
Figure 5.13	Effect of nucleoid condensation on the fluorescence localisation of Par-GFP in <i>S. aureus</i> cells, in the presence and absence of Par supplied <i>in trans</i>	179
Figure 5.14	Effect of Par-GFP on plasmid segregational stability, <i>in trans</i>	182
Figure 5.15	Immunodetection of Par, supplied <i>in trans</i> to pSK1 minireplicons	183
Figure 5.16	Fluorescence localisation of Par-GFP in <i>S. aureus</i> cells, supplied <i>in trans</i> to pSK1 minireplicons	184
Figure 5.17	Fluorescence localisation of Par-GFP in <i>S. aureus</i> cells, in the absence of pSK1 <i>par</i> centromere-like site	186
Figure 5.18	Distribution of the number of fluorescent Par-GFP foci per cell	187
Figure 5.19	Immunofluorescence microscopy of Par in <i>E. coli</i> cells	189
Figure 5.20	Deconvolved immunofluorescence microscopy images of Par in <i>E. coli</i> cells	190
Figure 5.21	Fluorescence localisation of Par GFP fusion proteins in <i>E. coli</i> cells	190
Figure 5.22	Effect of nucleoid condensation on the fluorescence localisation of Par GFP fusion proteins in <i>E. coli</i> cells	190

Figure	Title	After page
Figure 5.23	Fluorescence localisation of GFP-ParK15A in <i>E. coli</i> cells	192
Figure 5.24	Fluorescence localisation of GFP-Par in <i>E. coli</i> cells, in the absence of pSK1 <i>par</i> centromere-like site	194
Figure 5.25	Construction of pSK1 minireplicons carrying <i>tetO</i> arrays	197
Figure 5.26	Construction of an inducible <i>tetR-gfp</i> expression plasmid	199
Figure 5.27	Effect of TetR-GFP on the segregational stability of pSK1 minireplicons containing <i>tetO</i> arrays	202
Figure 5.28	Fluorescence localisation of pSK1 minireplicons in <i>S. aureus</i> cells by tagging with TetR-GFP	203
Figure 5.29	Distribution of the number of plasmid foci per cell	205
Figure 5.30	Effect of nucleoid condensation on the fluorescence localisation of pSK1 minireplicons in <i>S. aureus</i> cells	207
Figure 5.31	Time-lapse microscopy of the fluorescence localisation of pSK1 minireplicons in <i>S. aureus</i> cells by tagging with TetR-GFP	208
 Chapter 6		
Figure 6.1	Proposed models for pSK1 <i>par</i> plasmid segregation	248
 Supplementary		
Figure S1	Identification of conserved residues in the Par CTD	260
Figure S2	Cross-linking of Par proteins	260
Figure S3	DNA-binding activity of Par mutants	260

Figure	Title	After page
Figure S4	Sequence alignment of pSK1 Par with an enterococcal Par homologue	260
Figure S5	Prediction of disordered Par protein regions	260

SUMMARY

Since the introduction of antibiotic use almost 80 years ago, bacterial resistance to antibiotics has posed significant problems in both hospital and community settings, and there is insufficient development of new antibiotics to keep ahead of the spread of antibiotic resistance. Plasmids act as vehicles to facilitate the rapid and widespread dissemination of antibiotic resistance determinants. To prevent plasmid mis-segregation and plasmid loss during cell division, low copy-number plasmids, such as the staphylococcal multiresistance plasmid, pSK1, encode plasmid segregational stability mechanisms to ensure that plasmids are stably inherited and maintained by progeny cells, even in the absence of selection.

pSK1 is the prototype of the pSK1 family of staphylococcal multiresistance plasmids. The *par* locus on pSK1 enhances plasmid segregational stability using a putative plasmid partitioning mechanism. Homologues of pSK1 *par* are widespread on staphylococcal multiresistance plasmids (~80%), and hence understanding the mechanism of *par* will contribute to our knowledge of plasmid maintenance and inheritance, particularly in coccoid-shaped staphylococcal cells. This, in turn, can provide insight into potential targets for the development of antimicrobial therapies aimed to disrupt plasmid inheritance and the dissemination of resistance genes.

Unique to pSK1 *par* is the production of a single protein, Par, from the partitioning locus. This is in contrast to the two proteins (a centromere-binding protein and a NTPase motor protein) that are encoded by other characterised plasmid partitioning systems. Previous studies on pSK1 Par revealed that the N-terminal helix-turn-helix (HTH) domain is essential for DNA-binding, while the central coiled-coil (CC)

domain is crucial for Par multimerisation. Mutations to either of these domains have severe effects on plasmid segregational stability.

The experimental data presented in this thesis reveal important mechanistic insights into pSK1 *par*-mediated plasmid segregational stability. Importantly, a distantly-related pSK1 Par homologue was identified on a *S. epidermidis* multiresistance plasmid, and was also shown to exhibit plasmid stabilisation activity, which highlights the relevance of pSK1 *par*-like systems to the maintenance of staphylococcal multiresistance plasmids and their antibiotic resistance determinants. Functional studies, performed both *in vivo* and *in vitro*, highlight the importance of the predicted disordered C-terminal domain (CTD) for Par self-interaction. These interactions appear to directly affect the formation of higher-order Par multimers, as well as the cooperativity of Par binding to the centromere-like site. These results are consistent with a role of the Par CTD in stabilisation of the partition complex.

With regard to mechanism, the functional characterisation of Par was complemented by experiments performed to explore the possibility of the involvement of host factors in Par function. Yeast two-hybrid screening of *S. aureus* genomic DNA libraries did not identify any functionally significant Par interaction partners, and no direct evidence of nucleoid interaction was obtained. However, the possibility remains open that a host-encoded protein or the host chromosome might contribute to Par function. This possibility should be explored further.

Finally, cytological studies of plasmid segregation by pSK1 *par* revealed that Par-GFP and plasmid DNA are localised around the cell periphery or near the division site in *S. aureus*. The fluorescence localisation experiments described in this thesis represent the first visualisation of plasmid segregation in *S. aureus*. Results from

these studies provide indications of plasmid pairing and demonstrate the functionality of pSK1 *par* in the accurate segregation and inheritance of plasmid DNA.

Taken together, the results presented in this thesis provide strong evidence to suggest that pSK1 *par* encodes a plasmid segregational stability determinant that functions using a mode of action that cannot be described by mechanisms proposed for active plasmid partitioning systems known to date. The results, therefore, imply a novel mechanism of plasmid partitioning mediated by pSK1 *par* and *par*-like loci.

STATEMENT OF ORIGINALITY

This is to certify that to the best of my knowledge, the content of this thesis is my own work. This thesis has not been submitted for any degree or other purposes. I certify that the intellectual content of this thesis is the product of my own work and that all the assistance received in preparing this thesis and sources have been acknowledged.



Helena Yee-Wah Chan

ACKNOWLEDGMENTS

I gratefully acknowledge the guidance and unwavering support given to me by my supervisor, A/Prof. Neville Firth, and my co-supervisors, A/Prof. Slade Jensen and Dr. Anthony Brzoska. Each has provided me with invaluable assistance, direction and discussions during my candidature. I am especially appreciative of Dr. Brzoska, for his continuous efforts to encourage, foster and challenge my scientific ideas and ambitions.

I am thankful to have studied alongside some fantastic lab members, especially Dr. Stephen Kwong, Dr. Michael Liu and Alvina Sarosh, who have provided many thoughtful exchanges and good company. In particular, I would like to acknowledge Dr. Kwong for sharing his laboratory expertise in staphylococcal biology and yeast two-hybrid methods, and for the generation of *S. aureus* genomic DNA prey libraries for yeast two-hybrid library screening.

I am appreciative to all those who have kindly shared resources for my project: Prof. Maria Schumacher (Duke University, USA) for sharing X-ray crystallography data of Par DNA-binding; Prof. Timothy Foster (Dublin University, UK) for providing *S. aureus* DU5883; Prof. Elizabeth Harry and Dr. Amy Bottomley (University of Technology, Sydney, Australia) for useful advice on immunofluorescence microscopy in *S. aureus* and for providing anti-FtsZ antibodies, and Dr. Ian Grainge (University of Newcastle, Australia) for providing pLAU44.

Finally, I would like to express my deepest gratitude to my friends and family, for their understanding, encouragement and unconditional support throughout my PhD candidature.

CHAPTER 1

INTRODUCTION

1.1. The staphylococci

The staphylococci are a group of Gram-positive opportunistic pathogenic bacteria that are coccoid shaped and 0.5–1 μm in diameter (Prescott *et al.* 2005). They are non-motile, salt-tolerant, facultative anaerobes that have a low G+C content of 30–38%, similar to other Gram-positive bacteria such as bacilli, streptococci and enterococci. Due to cell division in three orthogonal planes (Tzagoloff and Novick 1977, Pinho *et al.* 2013), staphylococci are differentiated from streptococci by their appearance as grape-like clusters, as opposed to chains, when observed by microscopy.

The staphylococci are part of the commensal bacteria of approximately 30% of the human population, with *S. aureus* colonising the nasal passage and axillae, and *S. epidermidis* commonly found on the skin (Kluytmans *et al.* 1997, Wertheim *et al.* 2005, Grice and Segre 2011). The most pathogenic species of the staphylococci, *S. aureus*, is characterised by its coagulase-producing properties, whereas most other species, including *S. epidermidis*, are coagulase-negative. *S. aureus*, also commonly known as “Golden Staph”, due to the production of a carotenoid pigment on solid growth media, is one of the most common causes of hospital-acquired, or nosocomial, infections world-wide (Klein *et al.* 2007, Laxminarayan *et al.* 2013). Infections caused by *S. aureus* include infections of the skin, such as boils, styes and impetigo, infections of the bone, such as osteomyelitis, and more serious conditions such as bacteraemia, pneumonia, meningitis, endocarditis and septicaemia (Baron

1996). Multiply-resistant *S. aureus* infections are a frequent cause of hospital outbreaks (Boucher and Corey 2008, Lindsay 2013), which can become epidemic and lead to increased morbidity and mortality, as well as increased health care costs (Klein *et al.* 2007). The success of *S. aureus* as a human pathogen that is commonly associated with antibiotic resistance can be attributed to its ability to rapidly evolve and adapt to changes in its environment (see Section 1.2.2). Although less pathogenic than *S. aureus*, other species of the staphylococci can also be pathogenic, such as *S. epidermidis*, which is commonly associated with infections from indwelling medical devices, and *S. saprophiticus*, which causes urinary tract infections.

1.2. Antimicrobial resistance in the staphylococci

1.2.1. Emergence of antimicrobial resistance in the staphylococci

With the discovery of penicillin by Alexander Fleming in 1928, and the prescribed use of penicillin for the treatment of infections in the 1940s, the prognosis for bacterial infections was greatly improved. However, less than two years after the introduction of penicillin use, reports emerged of *S. aureus* strains that had developed resistance to the drug (Rammelkamp and Maxon 1942). The emergence of antibiotic resistance in *S. aureus* was repeated following the introduction of other antibiotics in the mid-1940s, such as erythromycin, streptomycin and the tetracyclines (Mitsuhashi *et al.* 1965, Plorde and Sherris 1974, Brumfitt and Hamilton-Miller 1989). In 1959, a semi-synthetic penicillin, methicillin, was introduced to overcome penicillin resistance, however, strains of methicillin-resistant *S. aureus* (MRSA) were detected less than two years later (Jevons 1961). Over time, with increased widespread use of antibiotics, the efficacy of antibiotics for the

treatment of *S. aureus* infections has rapidly diminished. What was once used as a drug of last resort, vancomycin is now the drug of choice for serious MRSA infections. Alarming, strains of *S. aureus* with reduced susceptibility to vancomycin, vancomycin-intermediate *S. aureus* (VISA), were detected in Japan in 1997 (Hiramatsu *et al.* 1997) and are becoming more widespread (Howden *et al.* 2010). Although rare, a number of reports have identified strains of *S. aureus* that are highly resistant to vancomycin (CDC 2002, Weigel *et al.* 2003, Bataineh 2006, Tiwari and Sen 2006). Newer antibiotics introduced in the 1970s to 1980s, such as linezolid and daptomycin, remain largely effective against MRSA, although resistance to these drugs has also emerged (Tsiodras *et al.* 2001, Hayden *et al.* 2005, Mangili *et al.* 2005, Morales *et al.* 2010, Gu *et al.* 2013).

Whereas MRSA infections were traditionally hospital-acquired, cases of community-acquired MRSA (CA-MRSA) infections are increasing (Chambers 2001, Salgado *et al.* 2003, Sowash and Uhlemann 2014, Stryjewski and Corey 2014). CA-MRSA were found to be acquired and transmitted in populations that have no known risk factors for colonisation, such as exposure to healthcare environments or previous antimicrobial therapy (Herold *et al.* 1998, Gorak *et al.* 1999). CA-MRSA are often associated with mild skin or soft tissue infections (Stryjewski and Chambers 2008), although invasive and severe infections causing death have also been reported (CDC 1999, Gillet *et al.* 2002, Gonzalez *et al.* 2005). Unlike hospital-acquired MRSA, CA-MRSA isolates were initially susceptible to multiple drugs, and resistant only to β -lactams (Naimi *et al.* 2003). However, recent surveys have found resistance of CA-MRSA to non- β -lactams, such as cotrimoxazol, erythromycin and clindamycin (John *et al.* 2017). Indeed, isolates of one of the most predominant strains of CA-MRSA, clone USA300 (Diep *et al.* 2006, King *et al.* 2006, Carrel *et al.* 2015), were shown to

exhibit multiresistance to β -lactams, erythromycin, clindamycin, tetracycline, levofloxacin, ciprofloxacin, fluoroquinolones, gentamicin, mupirocin, vancomycin and/or daptomycin (Diep *et al.* , Tenover and Goering 2009, Stryjewski and Corey 2014), and contain genes encoding the Panton-Valentine leucocidin and resistance to arsenic, bacitracin, cadmium and fosfomycin (Tenover *et al.* 2006, Stryjewski and Corey 2014).

Today, resistance to methicillin by *S. aureus* is indicative of resistance to multiple antibiotics. MRSA is a major cause of hospital- and community-acquired infections world-wide (Stefani *et al.* 2012), accounting for 72,444 cases of severe infections, and causing 9,194 deaths in 2014, in the US alone (CDC 2014). MRSA infections are associated with prolonged hospital stays, heightened risk of morbidity and increased healthcare costs compared to non-resistant forms of the infection (Filice *et al.* 2010, Gould *et al.* 2010). As such, the Centers for Disease Control and Prevention (CDC) identified MRSA as a serious threat level pathogen, and acknowledged that antibiotic resistance in MRSA needs to be addressed urgently (CDC 2013). The World Health Organisation (WHO) has recognised that the world is now facing an antibiotic crisis, wherein there is a substantial threat that effective antimicrobials will no longer be available for simple invasive surgical procedures or for the treatment of common infections. In May 2015, the WHO developed a global action plan on antimicrobial resistance to support the surveillance and management of drug resistance (WHO 2015). Without proper management of antibiotic resistance, the prognosis for once-treatable *S. aureus* infections, and infections caused by other antibiotic resistant pathogenic bacteria, could potentially revert to those of pre-antimicrobial days.

1.2.2. Mechanisms of genetic exchange in the staphylococci

Rather than arising from spontaneous mutations in the chromosome, it is believed that antibiotic resistance in the staphylococci most likely results from the acquisition of pre-existing resistance determinants (Lyon and Skurray 1987, Jensen and Lyon 2009, Lindsay 2010, Malachowa and DeLeo 2010, Ramsay *et al.* 2016). The exchange of genetic material between staphylococcal cells occurs via four main mechanisms: transformation, transduction, conjugation and mixed-culture transfer. Although observed in the laboratory, the occurrence of these mechanisms of horizontal gene transfer in the natural environment is unclear, however, it is thought that genetic exchange is facilitated predominantly by transduction and conjugation (Firth and Skurray 2000, Lindsay 2014, Ramsay *et al.* 2016).

Transformation is the process of the cellular uptake of naked exogenous DNA. Transformation of staphylococcal cells with DNA occurs in the presence of calcium ions and relies on cells having attained competency, for example, by lysogeny with phage (Rudin *et al.* 1974) or heat inactivation of nucleases (Sjöström *et al.* 1979). Additionally, sigma H factor has been shown to induce bacterial competency, albeit with very low transformation frequencies (Morikawa *et al.* 2012). However, due to intrinsic deoxyribonucleases and restriction modification systems present in the staphylococci (Waldron and Lindsay 2006, Corvaglia *et al.* 2010, Lindsay 2014), genetic exchange by transformation is not expected to occur frequently in the natural environment.

In the staphylococci, transduction involves the packing of genetic material into the heads of transducing phage particles from a donor strain, which then attach to glycosylated wall teichoic acid of a recipient strain to mediate transfer of genetic

material in the presence of calcium ions (Rountree 1951, Xia *et al.* 2011, Winstel *et al.* 2013). Transduction is predicted to be a major contributor to the horizontal transfer of genetic material between staphylococcal cells (Iandolo *et al.* 2002, Lindsay 2010, Lindsay 2014), since phage are widespread amongst *S. aureus* isolates, which often harbour one to four different phage types (Kwan *et al.* 2005, Lindsay *et al.* 2006, Lindsay 2010).

In a laboratory setting, transduction frequencies of between 10^{-6} and 10^{-8} transductants per PFU have been observed for chromosomal DNA fragments, and between 10^{-4} and 10^{-6} for plasmid DNA (Novick 1990). The phage head is capable of packaging up to 45 kb of DNA from the donor strain (Bächi 1980, Löfdahl *et al.* 1981, Stewart *et al.* 1985), with higher transduction frequencies observed for plasmids smaller than 40 kb (Rush *et al.* 1969, Chopra 1976, McDonnell *et al.* 1983). Phage-mediated transfer of genetic material is often associated with the transfer of antibiotic resistance genes, such as chloramphenicol (Dyer *et al.* 1985) and tetracycline (Novick *et al.* 1986), virulence factors, such as enterotoxin A (Betley and Mekalanos 1985), exfoliative toxin A (Yamaguchi *et al.* 2000) and Panton-Valentine leucocidin (Kaneko *et al.* 1998, Narita *et al.* 2001), as well as *S. aureus* pathogenicity islands (SAPIs) (Section 1.3.4) (Ruzin *et al.* 2001, Kwan *et al.* 2005). Once injected into the recipient cell, the packaged DNA then either integrates into the chromosome or is resolved as plasmid DNA (Canchaya *et al.* 2003).

Plasmid-mediated conjugation involves the transfer of plasmid DNA from donor to recipient cells via direct cell-to-cell contact. Conjugative plasmids are vehicles for genetic exchange, although the prevalence of conjugative plasmids in staphylococci is predicted to be relatively low, with only 5–20% of strains carrying plasmids that

contain conjugative transfer regions (Shearer *et al.* 2011, McCarthy and Lindsay 2012). Despite this, mobilisation of non-conjugative staphylococcal plasmids has been observed in the presence of a co-resident conjugative plasmid. For example, early observations showed that the mobilisation of a staphylococcal chloramphenicol resistance plasmid, pC221 (Archer and Johnston 1983, McDonnell *et al.* 1983, Projan and Archer 1989), occurred at even higher frequencies than the transfer of the co-resident conjugative plasmid itself, pGO1 (Projan and Archer 1989), which suggests that conjugation and mobilisation of plasmids play major roles in the spread of antibiotic resistance determinants in the staphylococci.

Interestingly, a recently described relaxase-*in trans* mechanism of plasmid transfer was identified for relaxases encoded by staphylococcal plasmids from the pWBG749 and pSK41 family of conjugative multiresistance plasmids (Section 1.3.2.4) (O'Brien *et al.* 2015, Pollet *et al.* 2016, Ramsay *et al.* 2016). This mechanism describes the mobilisation of non-conjugative staphylococcal plasmids that contain origin of transfer (*oriT*) sequences that mimic the *oriT* sequences recognised by the relaxase from a co-resident conjugative multiresistance plasmid (SmpP or Nes for pWBG749 and pSK41, respectively). Approximately 89% of large staphylococcal plasmids (>14.5 kb), which includes multiresistance plasmids (Section 1.3.2.3), carry at least one *oriT* mimic sequence, which highlights the significant potential of these non-conjugative plasmids to be mobilised *in trans*. Therefore, plasmid-mediated conjugation, which includes relaxase-*in trans* mobilisation of non-conjugative staphylococcal plasmids, is a potentially significant contributor to the dissemination of antimicrobial resistance determinants in *S. aureus* (McDonnell *et al.* 1983, Ramsay *et al.* 2016).

Phage-mediated conjugation, or mixed-culture transfer, requires phage in either the donor or recipient cell, as well as a high cell density and calcium ions (Lacey 1980). While little is known about the mechanism of genetic exchange, high transfer frequencies have been reported, with transfer frequencies of plasmid-located resistance determinants reaching 10^{-1} transipients per donor cell (Lacey 1980). Lacey (1980) proposed that phage, or components of phage, may alter cell surface proteins to increase adhesiveness. Indeed, evidence suggests that conditions such as sub-inhibitory concentrations of β -lactam antibiotics, increase the frequency of phage-mediated conjugation, possibly by promoting aggregation and cell-to-cell contact, thus allowing plasmid DNA to be transferred from donor to recipient (Barr *et al.* 1986).

1.3. Mobile genetic elements associated with antibiotic resistance in the staphylococci

1.3.1. Transposons and insertion sequences

Transposons and insertion sequences are mobile genetic elements that are able to independently translocate between genetic locations, using a mechanism called transposition. The simplest of the transposable elements, insertion sequences are typically comprised of a transposase gene, which encodes the transposase that mediates transposition, flanked by a pair of inverted repeats (IRs). Transposons, in addition to encoding the transposase, also often contain genes that confer antibiotic resistance. Composite transposons are transposons that are bound by insertion sequences.

Transposable genetic elements are widespread on the staphylococcal chromosome and on multiresistance plasmids. Table 1.1 provides a list of transposons and insertion sequences that have been identified in the staphylococci, along with the resistance genes associated with the mobile elements. The mobility of transposons and insertion sequences results in genetic rearrangements in the staphylococcal genome, such as insertions, deletions, inversions and replicon fusions. Due to the replicative nature of transposition, insertion elements are often present in multiple copies in the genome. As such, further recombination and insertion events are promoted, and can lead to clustering of resistance determinants and mobile elements (Firth and Skurray 1998). The transposition of transposons and insertion sequences within and between staphylococcal genomes and plasmids is, therefore, a significant contributor to the evolution of multiresistance plasmids in the staphylococci.

Amongst the staphylococci, IS257 is a widespread transposable element that is often responsible for the acquisition and clustering of resistance determinants on staphylococcal chromosomes and multiresistance plasmids. IS257 is associated with a range of antibiotic resistance genes (Table 1.1), and is frequently identified bordering composite transposons, such as Tn4003 and Tn4004, and bordering the sequences of small resistance plasmids that have cointegrated with the host genome (Firth and Skurray 1998). For example, on pSK41-like plasmids, IS257 is found flanking pUB110, pSK108-like, pSK89-like and pSK639-like plasmid sequences (Byrne *et al.* 1990, Berg *et al.* 1998, Liu *et al.* 2013), while on pSK1, IS257 elements are found flanking the insertion of a pSK639-like plasmid (Jensen *et al.* 2010).

Tn4001 is a composite transposon that is prevalent on the chromosomes and multiresistance plasmids of clinical *S. aureus* and coagulase-negative staphylococcal

Table 1.1 Staphylococcal transposons and insertion sequences

Element	Associated resistance(s)	Associated resistance gene(s)	Reference
IS256	Gentamicin, kanamycin, tobramycin	<i>aacA-aphA</i>	Rouch <i>et al.</i> (1987), Byrne <i>et al.</i> (1989)
IS257 (IS431)	Antiseptics, disinfectants	<i>smr</i>	Littlejohn <i>et al.</i> (1991), Leelaporn <i>et al.</i> (1996)
	Bacitracin	<i>bcrAB</i>	Chalker <i>et al.</i> (2000)
	Bleomycin	<i>ble</i>	Byrne <i>et al.</i> (1991)
	Cadmium	<i>cadD</i>	Crupper <i>et al.</i> (1999)
	Fusidic acid	<i>fusB</i>	O'Brien <i>et al.</i> (2002)
	Gentamicin, kanamycin, tobramycin	<i>aacA-aphA</i>	Byrne <i>et al.</i> (1990)
	Kanamycin, neomycin, paromomycin, tobramycin	<i>aadD</i>	Byrne <i>et al.</i> (1991), Dubin <i>et al.</i> (1991)
	Lysostaphin immunity factor	<i>lif</i>	Thumm and Götzt (1997)
	Macrolides, lincosamides, streptogramin B (MLS)	<i>ermC</i>	(Holden <i>et al.</i> 2013)
	Mercury	<i>merA, merB</i>	Gillespie <i>et al.</i> (1987a), Stewart <i>et al.</i> (1994)
	Methicillin	<i>mecA</i>	Stewart <i>et al.</i> (1994)
	Mupirocin	<i>mupA</i>	Needham <i>et al.</i> (1994), Morton <i>et al.</i> (1995)

Table 1.1 Staphylococcal transposons and insertion sequences (continued)

Element	Associated resistance(s)	Associated resistance gene(s)	Reference
IS257 (IS431)	Preprolysostaphin	<i>lss</i>	Thumm and Götz (1997)
	Streptogramin A	<i>vatA</i> , <i>vgaA</i>	Haroche <i>et al.</i> (2003)
	Streptothricin	<i>sat4</i>	(Derbise <i>et al.</i> 1997)
	Tetracycline	<i>tetA(K)</i>	Leelaporn <i>et al.</i> (1996), Stewart <i>et al.</i> (1994), Needham <i>et al.</i> (1994), Werckenthin <i>et al.</i> (1996)
	Trimethoprim	<i>dfrA</i>	Leelaporn <i>et al.</i> (1996), Rouch <i>et al.</i> (1989)
	Virginiamycin	<i>vgb</i>	Allignet <i>et al.</i> (1988)
IS1181	Kanamycin, neomycin	<i>aphA-3</i>	Derbise <i>et al.</i> (1994)
	Streptomycin	<i>aadE</i>	
IS1182	Kanamycin, neomycin	<i>aphA-3</i>	Derbise <i>et al.</i> (1994)
	Streptomycin	<i>aadE</i>	
IS1272	Methicillin	<i>mecA</i>	Archer and Niemeyer (1994), Archer <i>et al.</i> (1996)
ISSau9 (IS21-558)	Chloramphenicol, florfenicol	<i>fexA</i>	Kehrenberg and Schwarz (2006)
	Chloramphenicol, florfenicol, clindamycin	<i>cfr</i>	

Table 1.1 Staphylococcal transposons and insertion sequences (continued)

Element	Associated resistance(s)	Associated resistance gene(s)	Reference
ISSau10	Macrolides, lincosamides, streptogramin B	<i>erm(T)</i>	Kadlec and Schwarz (2010a)
	Tetracycline	<i>tet(L)</i>	
	Trimethoprim	<i>dfrK</i>	
Tn551	Macrolides, lincosamides, streptogramin B	<i>ermB</i>	Khan and Novick (1980)
Tn552	Penicillins	<i>blaZ</i>	Rowland and Dyke (1989), Rowland and Dyke (1990)
Tn554	Macrolides, lincosamides, streptogramin B	<i>ermA</i>	Murphy <i>et al.</i> (1985)
	Spectinomycin	<i>spc</i>	
Tn558	Chloramphenicol, florfenicol	<i>fexA</i>	Kehrenberg and Schwarz (2005)
Tn559	Trimethoprim	<i>dfrK</i>	Kadlec and Schwarz (2010b)
Tn1546	Vancomycin, teicoplanin	<i>vanHAX</i>	Weigel <i>et al.</i> (2003)
Tn3854	Kanamycin, neomycin	Unknown	Udo and Grubb (1991)
Tn4001	Gentamicin, kanamycin, tobramycin	<i>aacA-aphD</i>	Rouch <i>et al.</i> (1987), Byrne <i>et al.</i> (1989), Gillespie <i>et al.</i> (1987b)
Tn4003	Trimethoprim	<i>dfrA</i>	Rouch <i>et al.</i> (1989)

Table 1.1 Staphylococcal transposons and insertion sequences (continued)

Element	Associated resistance(s)	Associated resistance gene(s)	Reference
Tn4004	Mercury	<i>merA, merB</i>	Lyon and Skurray (1987)
Tn4291	Methicillin	<i>mecA</i>	Trees and Iandolo (1988)
Tn5404	Kanamycin, neomycin	<i>aphA-3</i>	Derbise <i>et al.</i> (1995)
	Streptomycin	<i>aadE</i>	
Tn5405	Kanamycin, neomycin	<i>aphA-3</i>	Derbise <i>et al.</i> (1996)
	Streptomycin	<i>aadE</i>	
Tn5406	Streptogramin A	<i>vgaAv</i>	Haroche <i>et al.</i> (2002)
Tn5801	Tetracycline, minocycline	<i>tet(M)</i>	Kuroda <i>et al.</i> (2001)
Tn6072	Gentamicin, kanamycin, tobramycin	<i>aacA-aphD</i>	Chen <i>et al.</i> (2010)
	Spectinomycin	<i>spc</i>	
Tn6133	Macrolides, lincosamides, streptogramin B	<i>ermA</i>	Schwendener and Perreten (2011)
	Streptogramin A, lincosamides, pleuromutilin	<i>vga(E)</i>	

strains (Gillespie *et al.* 1987). Along with the related transposable elements, Tn3851 and Tn4031, Tn4001 is largely responsible for the spread of aminoglycoside resistance (gentamicin, tobramycin and kanamycin resistance) amongst the staphylococci, via the dissemination of the *aacA-aphD* gene that it carries (Table 1.1) (Lyon *et al.* 1984b, Lyon and Skurray 1987). Tn4001 is flanked by inverted copies of IS256, the upstream element of which contains the promoter that drives expression of *aacA-aphD* (Rouch *et al.* 1987, Byrne *et al.* 1989).

First identified on pSK1, Tn4003 (Table 1.1) is a composite transposon that carries three copies of IS257 (Rouch *et al.* 1989). This transposon is associated with high-level trimethoprim resistance in the staphylococci, which is driven by expression of the *dfrA* gene by a hybrid promoter located in the upstream copy of IS257 (Leelaporn *et al.* 1994). Deletions within the flanking region lead to reduced trimethoprim resistance (Leelaporn *et al.* 1994). An IS257-associated hybrid promoter also drives expression of high-level tetracycline resistance from the *tetA(K)* gene located in the chromosomal *mec* region of some MRSA strains (Simpson *et al.* 2000).

Transposons in the Tn3 family, which include Tn552 and the related transposons, Tn3852 and Tn4002 (Table 1.1), do not rely on insertion sequences for transposition (Rowland and Dyke 1989, Dyke and Gregory 1997). Instead, these elements encode other transposition determinants in addition to the transposase. Tn552, which is thought to be the source of β -lactamase determinants in the staphylococci (Dyke and Gregory 1997), carries the β -lactamase resistance gene, *blaZ*, as well as *blaRI* and *blaI*, which encode the coinducer and repressor, respectively (Rowland and Dyke 1989). The transposon is flanked by inverted repeats, and transposition is mediated

by its transposase, Orf480, and a putative accessory transposition protein, Orf271 (Rowland and Dyke 1989, Rowland and Dyke 1990). Tn552 has been found to integrate into both the chromosome and plasmids of the staphylococci, however, in many plasmids, only remnants of Tn552 can be identified, due to recombination events that have disrupted the transposon (Gillespie *et al.* 1988, Paulsen *et al.* 1994, Berg *et al.* 1998).

1.3.2. Staphylococcal plasmids

Plasmids are extrachromosomal DNA elements that replicate independently of the chromosome (Lederberg 1952). They are typically double-stranded, circular molecules that encode accessory genes that often benefit the host. Importantly, plasmids frequently encode antibiotic resistance determinants, and are, therefore, vehicles for the transfer of resistance genes amongst cell populations.

In the staphylococci, plasmids are believed to play an integral role in the acquisition, maintenance and dissemination of antibiotic resistance determinants (Firth and Skurray 1998, Ramsay *et al.* 2016). Approximately 90% of naturally-occurring staphylococcal strains carry plasmids, and it is not uncommon for strains (approximately 80%) to carry one or more plasmids larger than 20 kb, which typically include multiresistance plasmids (Shearer *et al.* 2011). Four different groups of staphylococcal antibiotic resistance plasmids are described in Sections 1.3.2.1–1.3.2.4, below.

1.3.2.1. Small rolling-circle plasmids

Small rolling-circle (RC) plasmids are the most widely characterised plasmids amongst staphylococcal species. This class of plasmids is further divided into at least

four families, primarily based on the sequence relatedness of their replication regions (Novick 1989, Khan 1997). RC plasmids are relatively small in size (1–10 kb), which enables them to replicate via a rolling-circle mechanism to reach high copy-numbers (15–50 copies) within the cell (Koepsel *et al.* 1985, Khan 2005). Most RC plasmids, such as pT181 (Khan and Novick 1983), are either phenotypically cryptic or carry only one antibiotic resistance gene, although a *Bacillus*-related plasmid, pUB110, was found to carry two resistance genes (Semon *et al.* 1987). Many RC plasmids share regions of sequence similarity, defined as cassettes, which can encode replication signals and resistance genes (Novick 1989). The RS_A/pre mobilisation system on some RC plasmids is thought to mediate horizontal exchange of cassettes between RC plasmids of different families (Gennaro *et al.* 1987, Selinger *et al.* 1990).

1.3.2.2. pSK639-like plasmids

Similar to the RC class of plasmids, the prototype of the pSK639 family plasmids, pSK639, is a small, 8 kb plasmid that carries a single trimethoprim resistance gene, *dfrA* (Apsiridej *et al.* 1997). Other members of the pSK639 family of plasmids carry genes that confer resistance to antimicrobials, such as tetracycline, and antiseptics and disinfectants (Leelaporn *et al.* 1996). However, unlike RC plasmids, which replicate via rolling-circle replication (Khan 2005), pSK639 family plasmids utilise a theta-mode of replication (Apsiridej *et al.* 1997), similar to that of multiresistance plasmids (Sections 1.3.2.3–1.3.2.4). Indeed, pSK639 family plasmids are reminiscent of intermediates between RC and multiresistance plasmids, as demonstrated by the pSK639 family plasmids, pSK697 and pSK818, which seem to

have arisen from IS257-mediated cointegration of staphylococcal RC plasmids (Leelaporn *et al.* 1996).

1.3.2.3. Multiresistance plasmids

Staphylococcal multiresistance plasmids are relatively large (15–45 kb) and exist in low copy-numbers (approximately 5 copies per cell) (Novick 1989, Simpson *et al.* 2003, Jensen *et al.* 2010). Plasmids in this group utilise a theta-mode replication system (Firth *et al.* 2000), with the vast majority (90%) of plasmids >10 kb encoding a highly conserved replication initiation protein, RepA, from the RepA_N family (Weaver *et al.* 2009a, Shearer *et al.* 2011). The RepA_N family of plasmid replication initiation proteins is also encoded by many staphylococcal conjugative multiresistance plasmids (Section 1.3.2.4) (Firth *et al.* 2000, Shearer *et al.* 2011, Liu *et al.* 2013), as well as plasmids from other Gram-positive bacteria, such as pAD1 from *Enterococcus faecalis* (Francia *et al.* 2004, Weaver *et al.* 2009a). Expression of staphylococcal *repA* is regulated by an antisense RNA and its promoter, P_{RNAI} (Kwong *et al.* 2004, Kwong *et al.* 2006, Kwong *et al.* 2008, Kwong and Firth 2015), which was initially thought to be the promoter of a closely-associated plasmid maintenance gene, *par*, on the staphylococcal multiresistance plasmid, pSK1 (Section 1.6) (Simpson *et al.* 2003). RepA binds to iterative sequences in the origin of replication, *oriV*, located within the *repA* gene (Kwong *et al.* 2004, Kwong *et al.* 2008). Studies on the evolutionarily related, but phylogenetically distinct (Firth *et al.* 2000), RepA_N family replication initiation protein from the staphylococcal conjugative multiresistance plasmid, pSK41 (Section 1.3.2.4), revealed that binding of RepA to *oriV*, via its N-terminal winged helix-turn-helix (HTH) domain, appears to facilitate hand-cuffing of replicated plasmid pairs at the origin (Schumacher *et al.*

2014). RepA-DNA complexes subsequently interact with the host primase, DnaG, via the RepA C-terminal domain (Schumacher *et al.* 2014), which is believed to result in recruitment of the replicative helicase, DnaC, to stimulate primosome formation and plasmid replication (Corn and Berger 2006, Koepsell *et al.* 2006).

Staphylococcal multiresistance plasmids carry genes that provide resistances to multiple antibiotics, often acquired from the integration of mobile genetic elements, such as transposons and insertion sequences (Firth and Skurray 1998, Jensen *et al.* 2010). There are two major groups of staphylococcal multiresistance plasmids: the β -lactamase/heavy metal resistance plasmids, and the pSK1 family plasmids.

β -lactamase/heavy metal resistance plasmids were initially identified in clinical *S. aureus* isolates in the 1960s and 1970s (Shalita *et al.* 1980). These plasmids frequently contain a Tn552-like transposon that encodes β -lactamase, resulting in resistance to antibiotics such as cephalosporins and penicillin (Rowland and Dyke 1990). Furthermore, β -lactamase/heavy metal resistance plasmids have been found to carry Tn4001 and Tn551, which confer resistance to aminoglycosides, and the macrolide-lincosamide-streptogramin B antibiotics, respectively (Table 1.1) (Lyon *et al.* 1983). Other plasmids of this family encode resistances to dyes, inorganic ions, quaternary ammonium compounds and organomercurial reagents (Lyon and Skurray 1987).

pSK1 family plasmids, of which pSK1 is the prototype (Jensen *et al.* 2010), were first isolated from *S. aureus* strains in the 1980s, and characteristically carry the *qacA* gene, which confers multidrug resistance to antiseptics and disinfectants (Lyon *et al.* 1983, Lyon *et al.* 1984a, Townsend *et al.* 1987, Tennent *et al.* 1989). Other resistance determinants identified on pSK1 family plasmids include Tn4001, which

confers aminoglycoside resistance (Lyon *et al.* 1984b), Tn4002, which confers β -lactamase resistance (Gillespie *et al.* 1988), and Tn4003, which confers trimethoprim resistance (Rouch *et al.* 1989). The genetic organisation of representative pSK1 family plasmids is shown in Figure 1.1.

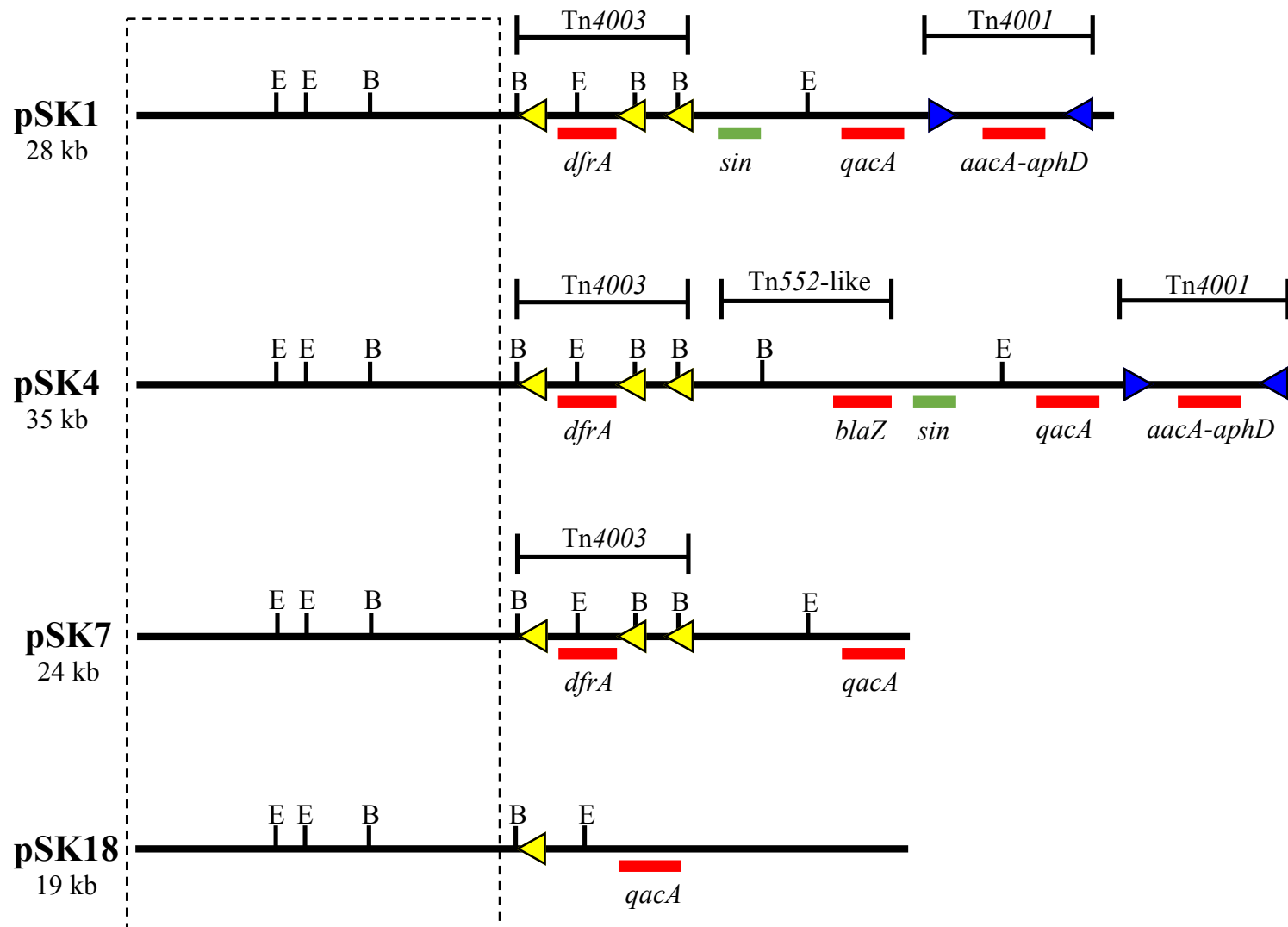
1.3.2.4. Conjugative multiresistance plasmids

Conjugative multiresistance plasmids, conventionally represented by pSK41, are the largest of the staphylococcal plasmids, at 30–60 kb in size (Novick 1989, Berg *et al.* 1998, Liu *et al.* 2013). These plasmids are capable of mediating their own conjugative transfer using a system consisting of a transfer (*tra*) region and *oriT* sequences (Firth *et al.* 1993, Berg *et al.* 1998, Edwards *et al.* 2013, Liu *et al.* 2013). Similar to staphylococcal non-conjugative multiresistance plasmids, the majority of staphylococcal conjugative multiresistance plasmids utilise a theta-mode of replication that is facilitated by RepA_N family replicons (Section 1.3.2.3) (Weaver *et al.* 2009a, Shearer *et al.* 2011, Liu *et al.* 2013, Schumacher *et al.* 2014). A number of antibiotic resistance determinants are encoded by pSK41 family conjugative multiresistance plasmids, including aminoglycoside (Byrne *et al.* 1990), trimethoprim (Leelaporn *et al.* 1994), mupirocin (Morton *et al.* 1995), penicillin (Gillespie *et al.* 1988), vancomycin (Weigel *et al.* 2003) and mupirocin resistance (Diep *et al.* 2006, Pérez-Roth *et al.* 2006, Pérez-Roth *et al.* 2010), as well as resistance to antiseptics and disinfectants (Littlejohn *et al.* 1991, Liu *et al.* 2013).

In addition to the pSK41 family, two other families of staphylococcal conjugative plasmids have been identified, pWBG749 and pWBG4 family plasmids, each carrying conjugation gene clusters that are distinct from pSK41 family plasmids (Ramsay *et al.* 2016). pWBG749 family plasmids are not usually associated with

Figure 1.1 Genetic maps of pSK1 family plasmids

Linear maps of selected pSK1 family multiresistance plasmids (pSK1, pSK4, pSK7 and pSK18) are shown with their approximate sizes on the left. The positions of transposons are indicated above the linear maps. Insertion sequences, IS256 and IS257, are represented by blue and yellow arrowheads, respectively. Genes encoding resistance to trimethoprim (*dfrA*), β -lactams (*blaZ*), antiseptics and disinfectants (*qacA*) and aminoglycosides (*aacA-aphD*), are indicated by red lines below the maps. The locations of *sin*, which encodes a putative multimer resolution system, are indicated by green lines below the maps. The positions of *EcoRI* (E) and *BglII* (B) restriction sites are indicated on the maps. Regions shown inside the dashed box indicate conserved regions amongst pSK1 family multiresistance plasmids. Figure adapted from Firth and Skurray (1998).



antimicrobial resistance genes, however, genes encoding resistance to penicillin, aminoglycosides and vancomycin, have been identified on some plasmids (Rossi *et al.* 2014, O'Brien *et al.* 2015). Conjugative plasmids from the pWBG4 family have been found to encode resistance to trimethoprim, spectinomycin, aminoglycosides, macrolides, lincosamides and linezolid (Townsend *et al.* 1985, Udo *et al.* 1992, Mendes *et al.* 2013, Shore *et al.* 2016). Furthermore, pSK41 and pWBG749 plasmids have demonstrated mobilisation of co-resident non-conjugative plasmids using a relaxase-*in trans* mechanism, described in Section 1.2.2 (O'Brien *et al.* 2015, Ramsay *et al.* 2016).

1.3.3. Staphylococcal cassette chromosome *mec*

All MRSA strains contain staphylococcal cassette chromosome *mec* (SCC*mec*), which is a large DNA fragment that inserts into the *orfX* site on the chromosome (Katayama *et al.* 2000, Ito *et al.* 2001, Ito *et al.* 2003, Turlej *et al.* 2011). SCC*mec* carries the methicillin resistance gene, *mecA*, which encodes penicillin-binding protein (PBP) 2a and confers resistance to β -lactam antibiotics (Hartman and Tomasz 1984, Ito *et al.* 1999). In addition to the *mecA* gene, SCC*mec* also carries two regulatory genes, *mecI* and *mecRI*, as well as genes encoding site-specific recombinases, *ccrAB* or *ccrC* (Ito *et al.* 1999, Katayama *et al.* 2000, Ito *et al.* 2004). The Ccr recombinases facilitate excision and integration of SSC*mec* complexes at a specific attachment site at the *orfX* locus (Katayama *et al.* 2000, Ito *et al.* 2004). The type of *ccr* and *mec* genes contained in SCC*mec* complexes usually defines the SCC*mec* type (type I–XII) (IWG-SCC 2009, Turlej *et al.* 2011, Wu *et al.* 2015). SCC*mec* joining, or junk-yard (J), regions often contain mobile genetic elements, such as plasmids, transposons or insertion sequences, that have integrated into the

region and confer additional antibiotic resistance phenotypes, such as spectinomycin (*spc*), erythromycin (*ermA*), bleomycin (*ble*), tobramycin and kanamycin (*aadD*) resistance (Dubin *et al.* 1991, Ito *et al.* 1999, Hiramatsu *et al.* 2001, Ito *et al.* 2001, Ito *et al.* 2003, Malachowa and DeLeo 2010). The genetic content contained in SCC*mec* J regions is used to further divide SCC*mec* types into subtypes (IWG-SCC 2009). Perhaps due to the large size of SCC*mec* complexes, horizontal transfer of complexes is predicted to be rare (Hanssen and Ericson Sollid 2006, Nübel *et al.* 2008). However, smaller SCC*mec* types, such as type IV SCC*mec*, are more prominent amongst staphylococcal isolates, and hence appear to be mobilised more readily (Daum *et al.* 2002).

Other SCCs, which do not encode methicillin resistance, are known as non-*mec* SCCs, and often encode virulence determinants, such as mercury (Chongtrakool *et al.* 2006) or phagocytosis resistance (Luong *et al.* 2002). Similar to SCC*mec*, these complexes contain *ccr* recombinase genes and integrate at the *orfX* site of the staphylococcal chromosome (Katayama *et al.* 2003, Mongkolrattanothai *et al.* 2004). However, some non-*mec* SCCs, such as SCC*cap1* (Luong *et al.* 2002), lack functional *ccr* recombinase genes, and hence are non-mobilisable.

1.3.4. *Staphylococcus aureus* pathogenicity islands

Although often not associated with antibiotic resistance determinants, *S. aureus* pathogenicity islands (SaPIs) are 15–17 kb DNA regions that usually contain genes for superantigen toxins, such as enterotoxins and toxic shock syndrome toxin-1 (TSST-1) (Novick *et al.* 2001, Novick *et al.* 2010). The prototypical SaPI, SaPI1, contains genes encoding TSST-1, an enterotoxin, and an integrase (Lindsay *et al.* 1998). SaPIs exhibit high transfer efficiencies and are commonly found at one or

more locations on the chromosomes of most *S. aureus* strains (Lindsay *et al.* 1998, Novick and Subedi 2007, Subedi *et al.* 2007, Úbeda *et al.* 2008). Mobilisation of SaPIs is facilitated by excision, replication and transduction by helper phages, followed by site-specific integration into the host chromosome using the SaPI-encoded integrase (Lindsay *et al.* 1998, Ruzin *et al.* 2001, Maiques *et al.* 2007, Úbeda *et al.* 2008).

1.4. Plasmid maintenance mechanisms

Plasmids that exist in high copy-numbers in the bacterial cell, such as RC plasmids (Section 1.3.2.1), do not require specialised plasmid maintenance systems, since passive diffusion is sufficient to ensure that daughter cells receive at least one plasmid copy (Nordström and Austin 1989). Furthermore, being smaller in size, the high replication rate of RC plasmids is usually sufficient to restore plasmid copy-number to characteristic levels, even if plasmids are not equally segregated. However, larger plasmids, such as the staphylococcal multiresistance and conjugative multiresistance plasmids (Sections 1.3.2.3–1.3.2.4), typically exist in lower copy-numbers, and hence passive diffusion would not be adequate for mediating equal plasmid segregation between daughter cells. As a result, low copy-number plasmids commonly encode plasmid maintenance systems, such as multimer resolution systems (Section 1.4.1), post-segregational killing systems (Section 1.4.2), and active plasmid partitioning systems (Section 1.4.3), to ensure that plasmids are accurately inherited.

1.4.1. Multimer resolution

Multimer resolution systems facilitate the separation of plasmid multimers that may have formed due to recombination events between identical plasmid copies, for

example, during plasmid replication. Assuming plasmids are randomly distributed to daughter cells during cell division, the chances of plasmid inheritance would be directly correlated with plasmid copy-number – the higher the copy-number, the less chance of plasmid-free cells (Nordström and Austin 1989). For unresolved plasmid multimers, the unit of segregation is the multimer, rather than the plasmid number, and therefore, the copy-number of discrete replicons is effectively reduced. This results in worse-than-random segregation (Summers and Sherratt 1984), since the chance of plasmid inheritance would no longer be equal between daughter cells (Nordström and Austin 1989).

Multimer resolution is particularly important for low copy-number plasmids, whereby plasmid multimerisation can reduce the copy-number to one. Multimer resolution systems have been shown to enhance the segregational stability of low copy-number plasmids, such as R1 of *E. coli* (Weitao *et al.* 2000), and the engineered plasmid, pBR322 (Summers *et al.* 1993). In *S. aureus*, the multimer resolution system, *res*, on the staphylococcal conjugative multiresistance plasmid, pSK41 (Berg *et al.* 1998), encodes a resolvase, Res, that binds to resolution sites upstream of the resolvase coding sequence (LeBard *et al.* 2008). The presence of pSK41 *res* on an unrelated plasmid resulted in the resolution of plasmid multimers into monomers, as judged by electrophoresis of plasmid DNA (LeBard *et al.* 2008). Importantly, pSK41 *res* enhanced the segregational stability of both its cognate replicon and an unstable heterologous replicon, whereas plasmids carrying a pSK41 *res* knock-out mutation were significantly less stable (LeBard *et al.* 2008). This study, therefore, demonstrates a correlation between multimer resolution and increased plasmid segregational stability, which may be attributed to the generation of single plasmid units that can be independently segregated to daughter cells.

1.4.2. Post-segregational killing

In post-segregational killing (*psk*) systems encoded by plasmid DNA, plasmid-free cells are selectively killed using a toxin-antitoxin (TA) mechanism. In this system of programmed cell death, plasmids encode a stable toxin and an unstable antitoxin. There are two main classes of *psk* systems, defined by the type of antitoxin encoded – type I systems, which encode an antisense RNA antitoxin (Gerdes and Wagner 2007, Fozo *et al.* 2008), and type II systems, which encode a protein antitoxin (Van Melderen and Saavedra De Bast 2009, Rocker and Meinhart 2016). Essentially, in both types of mechanisms, plasmids carrying the TA system encode the antitoxin, which binds with high affinity to the toxin or toxin mRNA. In this toxin-antitoxin complex, the toxin is inactive and unable to exert its effect on cell survival. However, in plasmid-free cells, antitoxin production is absent, and hence any labile antitoxin molecules that may have been inherited during cell division are degraded more rapidly than the toxin (Unterholzner *et al.* 2013). This results in reduced antitoxin levels relative to the toxin, and thus the stable toxin remains unbound and active, selectively killing plasmid-free cells.

Toxins usually target essential cellular proteins, such as DNA gyrase for the *ccd* system of F plasmid (Bernard and Couturier 1992), and DnaB for the *parD* system of R1 (Ruiz-Echevarría *et al.* 1995). The type I Fst TA system on the *E. faecalis* plasmid, pAD1, is the prototypical TA system for Gram-positive bacteria (Weaver *et al.* 1996). Type I Fst-like TA systems have been identified on numerous plasmids from Gram-positive bacteria, such as *Enterococcus*, *Staphylococcus*, *Lactococcus*, *Macrococcus* and *Carnobacterium* (Weaver *et al.* 2009b, Kwong *et al.* 2010). In Fst-like TA systems, translation of a 27–35 residue Fst-like toxin is inhibited by the

binding of an antisense RNA antitoxin to complementary sequences in the toxin mRNA (Greenfield *et al.* 2000, Greenfield and Weaver 2000, Greenfield *et al.* 2001) which results in the formation of a stem loop structure that obstructs translation of the toxin transcript (Shokeen *et al.* 2008, Shokeen *et al.* 2009). Notably, putative Fst-like TA systems have been detected on staphylococcal multiresistance (Section 1.3.2.3) (Jensen *et al.* 2010, Kwong *et al.* 2010) and conjugative multiresistance plasmids (Section 1.3.2.4) (Kwong *et al.* 2010, Liu *et al.* 2013), which may provide an additional means of plasmid maintenance and acquisition and dissemination of antimicrobial resistance determinants.

Interestingly, Fst-like TA systems are also commonly present on the chromosomes of Gram-positive bacteria (Weaver *et al.* 2009b, Kwong *et al.* 2010), although the role of chromosomally-encoded TA systems is unclear. It has been proposed that chromosomal TA systems may be involved in the stress response; under conditions of external cell stress, the antitoxin might be less stable, which could enable the toxin to remain active and target essential cellular processes to induce a stress response, such as attenuation of cell growth, or formation of biofilms and persister cells (Gerdes *et al.* 2005, Wang and Wood 2011, Wen *et al.* 2014, Page and Peti 2016).

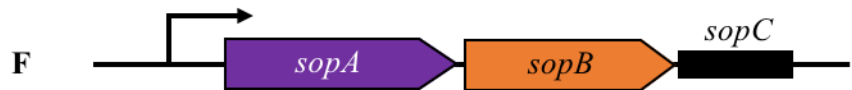
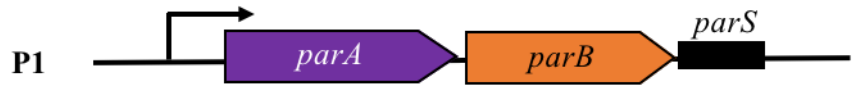
1.4.3. Active plasmid partitioning

Active plasmid partitioning (*par*) systems are tripartite systems that consist of a centromere-like site, a centromere-binding protein (CBP) and a force-generating NTPase. These systems are generally divided into three types (types I–III), primarily based on the type of NTPase involved. Examples of the genetic organisation of prototypical partitioning systems from each type are shown in Figure 1.2.

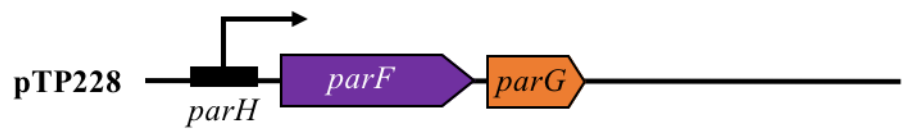
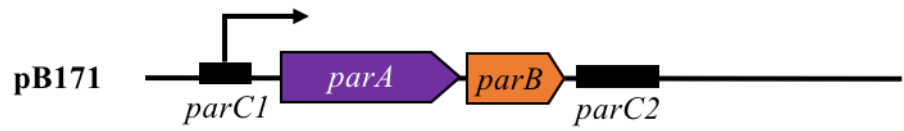
Figure 1.2 Genetic organisation of representative active plasmid partitioning systems

Prototypical active plasmid partitioning systems from type Ia (plasmids P1 and F), type Ib (plasmids pB171 and pTP228), type II (plasmid R1) and type III (plasmid pBtoxis) systems are shown. Promoters are represented by bent arrows. Solid boxes represent centromere-like sites. Genes encoding NTPase proteins and centromere-binding proteins are represented by purple and orange block arrows, respectively.

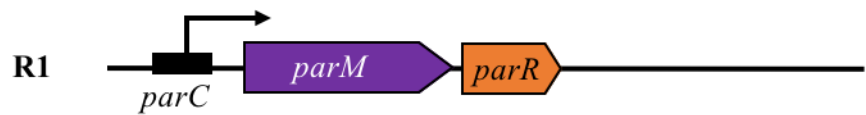
Type Ia



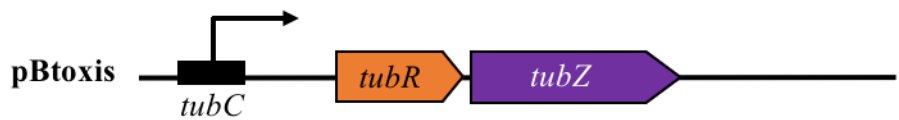
Type Ib



Type II



Type III



Studies of the three types of plasmid partitioning systems indicate the requirement of all three components of the partitioning locus for function. Although the mechanism of plasmid segregation differs between the three systems (Sections 1.5.1–1.5.3) (reviewed in Hayes and Barilla (2006), Schumacher (2008) and Baxter and Funnell (2014)), in all characterised active plasmid partitioning systems, the CBPs bind specifically to their cognate centromere-like site, which consists of repetitive DNA sequences. This DNA-binding triggers the recruitment of additional CBPs, which bind cooperatively as multimers to the DNA at the centromere-like site. Cooperative binding of CBPs results in the formation of a nucleoprotein complex known as the segrosome, or partition complex. Plasmid pairing has been described for most partitioning systems, whereby the CBPs pair two separate plasmid molecules, via their partition complexes, in a fashion analogous to the pairing of sister chromatids during eukaryotic mitosis (Skibbens 2008).

To date, three types of NTPase motor proteins have been identified in active plasmid partitioning systems: Walker-type ATPases, actin-like ATPases and tubulin/FtsZ-like GTPases (Gerdes *et al.* 2010, Schumacher 2012, Baxter and Funnell 2014). The motor proteins of all three types of partitioning systems are, therefore, nucleotide-binding proteins. As anticipated, different mechanisms of plasmid segregation have been proposed, based on the type of motor protein utilised by each of the three systems, as described below (Sections 1.5.1–1.5.3). In all cases, motor proteins interact with the partition complex to stimulate separation of plasmid copies. Additionally, the binding of either the CBP (in types Ib, II and III systems), or the motor protein (in type Ia systems), to the centromere-like site results in autoregulation of the *par* operon. Further details on the mechanisms of types I–III active plasmid partitioning systems are provided in Section 1.5, below.

1.5. Active plasmid partitioning systems

1.5.1. Type I active plasmid partitioning systems

Type I systems are the most widespread of the active plasmid partitioning systems (Ebersbach and Gerdes 2005, Schumacher 2008), and are characterised by motor proteins containing the Walker-type ATPase motif (Walker *et al.* 1982, Motallebi-Veshareh *et al.* 1990). In type I systems, the gene encoding the motor protein is located upstream of the gene encoding the CBP (Figure 1.2). Type I systems are divided into type Ia and type Ib systems, based on their genetic organisation and the size of the motor protein. The centromere-like site of the type Ia partitioning system is located distal to the *par* promoter, P_{par} , downstream of the protein-encoding genes, whereas in type Ib systems, the centromere-like site overlaps P_{par} , upstream of the *par* operon (Figure 1.2).

The *parABS* system, of the *E. coli* P1 plasmid, is the archetype of the type I partitioning system. Like all type Ia partitioning systems, the centromere-like site, *parS*, is located downstream of the genes encoding the centromere-binding protein, *parB*, and the Walker-type ATPase motor protein, *parA* (Figure 1.2) (Austin and Abeles 1983, Abeles *et al.* 1985). However, the P1 *parS* site is unusual because it is multipartite; *parS* consists of two ParB binding sites, each containing at least one heptameric A-box and a hexameric B-box, flanking a binding site for integration host factor (IHF) (Funnell and Gagnier 1993).

ParB binds *parS* via a C-terminal domain that consists of a HTH DNA-binding motif that is connected to a β -sheet dimerisation domain by a short flexible linker (4

A) (Surtees and Funnell 2001, Schumacher and Funnell 2005). X-ray crystallography of P1 ParB DNA-binding revealed that the structure of the HTH domain is similar to the HTH structures solved for other type Ia CBPs, such as the RP4 KorB (Khare *et al.* 2004) and F plasmid SopB proteins (Schumacher *et al.* 2010). Furthermore, structural data showed that P1 ParB binds *parS* as dimers, with the recognition helix of the HTH domain binding the A-boxes, and the dimerisation domain binding the B-boxes (Figure 1.3A) (Schumacher and Funnell 2005, Schumacher *et al.* 2007b). Binding of ParB to *parS* is stimulated by the binding of IHF to a DNA region located between the two ParB binding sites (Funnell 1988b, Funnell 1991, Funnell and Gagnier 1993). Binding of IHF induces a bend in the DNA, which is thought to align the A- and B- boxes for optimal ParB binding (Funnell 1991, Schumacher and Funnell 2005). The *parABS* system of P1 is the only known system to utilise such a host-encoded factor for plasmid segregation.

Additionally, non-specific DNA-binding by ParB, and its homolog SopB from F plasmid, is known to cause spreading of ParB for several kilobases around *parS* (Łobocka and Yarmolinsky 1996, Rodionov *et al.* 1999, Rodionov and Yarmolinsky 2004). Although the mechanism and purpose of spreading is not clear, ParB spreading has been shown to cause silencing of adjacent genes (Rodionov *et al.* 1999, Hao and Yarmolinsky 2002). However, spreading does not appear to be a requirement for plasmid segregational stability, since mutants of ParB spreading were still able to partition plasmids (Rodionov and Yarmolinsky 2004). Recently, it was proposed that for chromosomal ParB proteins, spreading may have a role in bridging DNA regions to facilitate re-structuring and condensation of nucleoid DNA (Broedersz *et al.* 2014, Funnell 2014, Graham *et al.* 2014, Sanchez *et al.* 2015, Taylor *et al.* 2015).

Figure 1.3 Structures of centromere-binding proteins bound to DNA

A. Structure of one P1 ParB (aa 142–333) dimer binding to two pseudo-continuous 16-mer DNA duplexes, each containing one A-box and one B-box of the *parS* site (PDB ID 2NTZ) (Schumacher *et al.* 2007b).

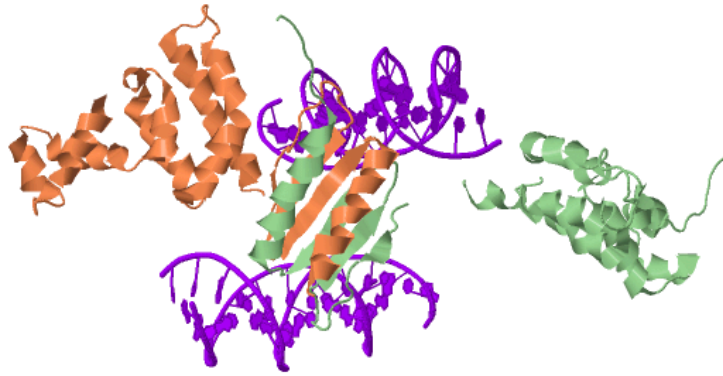
B. Structure of one pSK41 ParR (aa 1–53) dimer-of-dimer binding to a 20-mer duplex containing the minimal centromeric repeat (PDB ID 2Q2K) (Schumacher *et al.* 2007a).

C. Structure of pBtoxis TubR binding to 24-mer duplexes of *tubC* (PDB ID 4ASS) (Aylett and Löwe 2012).

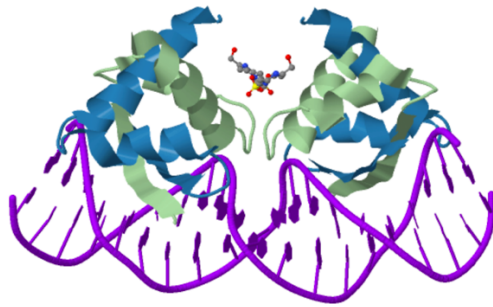
Centromere-binding proteins are represented as ribbons, with subunits coloured differently. Images were visualised using Jmol software (<http://www.jmol.org/>).

Detailed structures can be found in the referenced articles.

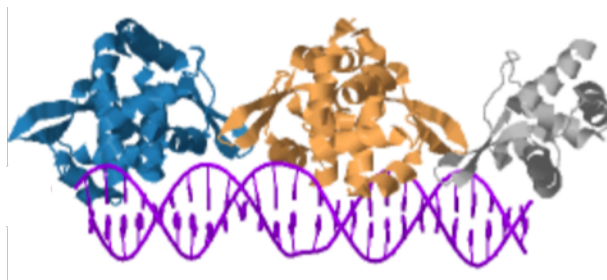
A.



B.



C.



Following the specific binding of ParB dimers to *parS*, additional ParB dimers are cooperatively loaded to the centromere to form a higher-order nucleoprotein partition complex (Bouet and Funnell 1999, Bouet *et al.* 2000). Edgar *et al.* (2001) showed that ParB is capable of mediating plasmid pairing via the *parS* centromere-like sites. Structural data has since shown that the ParB HTH DNA-binding domain bridges adjacent A-boxes, and that the ParB dimer domain bridges adjacent B-boxes, forming a ParB-DNA bridged complex that signifies the potential of ParB to mediate plasmid pairing (Schumacher *et al.* 2007b). Pairing of plasmid copies is thought to be critical to successful plasmid partitioning; paired plasmids act as substrates for ParA interaction, and hence, for plasmid localisation and partitioning (Erdmann *et al.* 1999, Sengupta *et al.* 2010).

Once paired, ParA Walker-type ATPases interact with the partition complex in an ATP-dependent manner (Bouet and Funnell 1999, Fung *et al.* 2001, Havey *et al.* 2012, Vecchiarelli *et al.* 2013a). In its ATP-bound form, ParA interacts with the ParB/*parS* partition complex (Vecchiarelli *et al.* 2010, Havey *et al.* 2012, Vecchiarelli *et al.* 2013b). The ATPase activity of ParA is stimulated by interaction with an arginine residue at the N-terminus of ParB (Barillà *et al.* 2007, Ah-Seng *et al.* 2009), and results in dissociation of ParA from the partition complex (Vecchiarelli *et al.* 2010, Havey *et al.* 2012).

The exact mechanism of how ParA segregates plasmids has only recently become clearer. Fluorescence microscopy studies showed that P1 plasmids are localised to the quarter-cell positions, which become the mid-cell positions in daughter cells following cell division (Gordon *et al.* 1997, Erdmann *et al.* 1999, Gordon *et al.* 2004). Earlier studies suggested that ParA family proteins form filaments, or helices,

that oscillate over the nucleoid (Ebersbach and Gerdes 2004, Lim *et al.* 2005, Adachi *et al.* 2006, Hatano *et al.* 2007, Ringgaard *et al.* 2009). Based on these observations, it was proposed that stimulation of ParA ATPase activity by ParB/*parS* results in depolymerisation of ParA filaments, which consequently pulls plasmids towards the quarter-cell positions, as plasmids rebind ParA-ATP at the ends of retracting ParA filaments (Ringgaard *et al.* 2009).

However, in recent years, data has come to light, which show that ParA-ATP binds non-specifically to DNA via residues in its C-terminal domain (Hester and Lutkenhaus 2007, Vecchiarelli *et al.* 2010). Thus, interaction of ATP-bound ParA with non-specific DNA, i.e. nucleoid DNA, and with ParB/*parS* partition complexes, suggests that the bacterial nucleoid plays a key role in type I plasmid partitioning systems (Vecchiarelli *et al.* 2010, Vecchiarelli *et al.* 2013b). At present, research seems to favour a diffusion-ratchet model for type I plasmid partitioning, which involves exploitation of the nucleoid as a scaffold for the movement of ParB-bound plasmid DNA along a gradient of nucleoid-bound ParA-ATP molecules, driven by ATP-binding and hydrolysis (Figure 1.4) (Vecchiarelli *et al.* 2010, Vecchiarelli *et al.* 2013b).

In addition to its role in plasmid partitioning, type Ia ParA proteins also act as transcriptional repressors of the *parAB* operon (Friedman and Austin 1988, Davis *et al.* 1992). Similar to its interactions with ParB, the specificity of ParA for the *par* operator and for the ParB/*parS* complex is dictated by its nucleotide-bound state; when bound to ATP, ParA interacts with the partition complex, whereas ParA-ADP carries out *parAB* autoregulation activities (Davey and Funnell 1997, Bouet and Funnell 1999). ATP binding and hydrolysis, therefore, act as a molecular switch,

Figure 1.4 Mechanistic models of active plasmid partitioning systems

A. Diffusion-ratchet model of Type I active plasmid partitioning. ParA-ATP binds non-specifically to nucleoid DNA. ParB-bound plasmids interact with ParA-ATP and stimulate ATP hydrolysis, resulting in dissociation of ParB/*parS* complexes from ParA, and dissociation of ParA-ADP from the nucleoid, where it becomes diffuse in the cytoplasm. ParB/*parS* complexes on plasmid DNA re-bind nucleoid-bound ParA-ATP, such that plasmids move along a gradient of Par-ATP, towards the cell poles, where higher concentrations of ParA-ATP are present (Section 1.5.1).

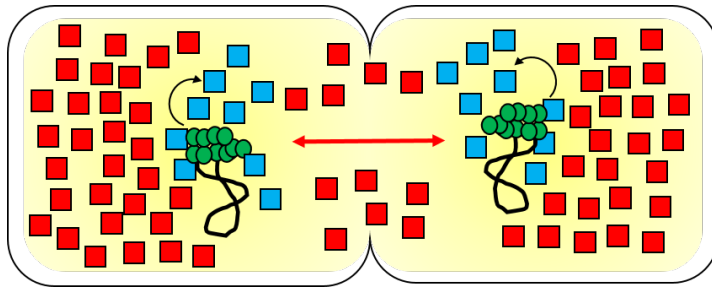
B. Insertional polymerisation model of Type II active plasmid partitioning. Dynamically unstable ParM filaments form in the presence of ATP, and are stabilised by ParR/*parC* partition complexes on plasmid DNA by interaction with the barbed end of ParM filaments. Antiparallel ParM filaments form a bipolar ParM spindle, which is stabilised at both ends when capped by ParR/*parC* partition complexes. ParM-ATP inserts at the interface with ParR/*parC* complexes to extend the ParM spindle bidirectionally, pushing plasmids to the cell poles (Section 1.5.2).

C. Trimming model of Type III active plasmid partitioning. TubZ filaments exhibit treadmilling behaviour, with polymerisation occurring in the presence of TubZ-GTP at the plus (+) end, and depolymerisation occurring at the minus (–) end. TubR/*tubC* complexes attach plasmid DNA to the flexible C-terminal tails presented on the surface of TubZ filaments. Plasmids are pulled along the filament in a cable-car, or tramming, motion until the filament reaches the cell poles, where the plasmids are unloaded (Section 1.5.3).

Bacterial cells are represented by black ovals, and nucleoid DNA is shown in yellow. Red arrows indicate the direction of plasmid movement. For clarity, only one pair of

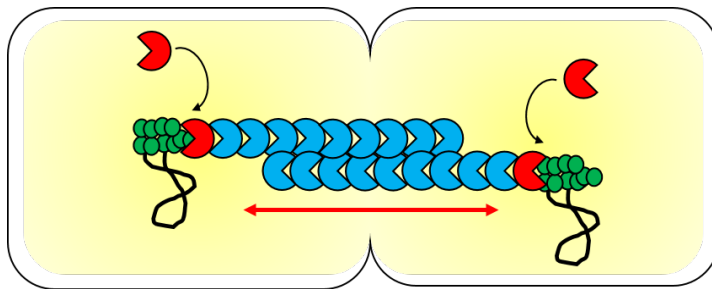
plasmids is shown for each dividing cell in (A) and (B), and a single plasmid is shown in (C). Figures adapted from Baxter and Funnell (2014).

A.



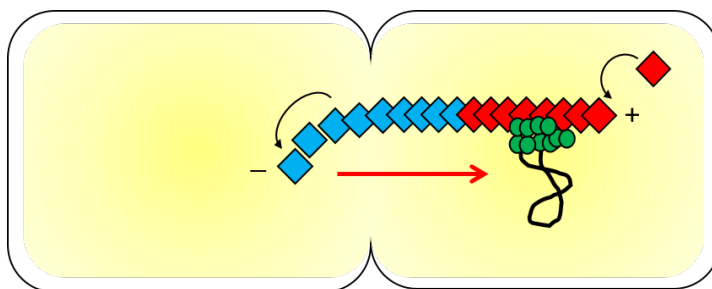
- ParB
- ⌘ ParB-bound plasmid DNA
- ParA-ATP
- ParA-ADP

B.



- ParR
- ⌘ ParR-bound plasmid DNA
- ◐ ParM-ATP
- ◐ ParM-ADP

C.



- TubR
- ⌘ TubR-bound plasmid DNA
- ◆ TubZ-GDP
- ◆ TubZ-GTP

defining the function of ParA in plasmid partitioning or transcriptional repression (Bouet and Funnell 1999).

Type Ib active plasmid partitioning systems include *parABC* from plasmid pB171 (Ebersbach and Gerdes 2001) and *parFGH* from plasmid TP228 (Hayes 2000). Importantly, the DNA-binding proteins of the type Ib system differ from those of the type Ia system; type Ib DNA-binding proteins bind centromere-DNA as a dimer (Barillà and Hayes 2003), utilising a ribbon-helix-helix (RHH) instead of a HTH motif (Golovanov *et al.* 2003). Also, because the centromere-like site of type Ib systems overlaps the operator site (Figure 1.2), transcriptional repression of the partitioning locus is mediated by the CBP rather than by the motor protein, as in type Ia systems (Carmelo *et al.* 2005).

1.5.2. Type II active plasmid partitioning systems

The genetic organisation of type II active plasmid partitioning systems is reminiscent of the type Ib systems, whereby the centromere-like site and P_{par} are located upstream of the *par* operon (Figure 1.2). Type II partitioning systems are distinguished by their motor proteins, which function as actin-like ATPases (Bork *et al.* 1992, Møller-Jensen *et al.* 2002, van den Ent *et al.* 2002), and by their CBPs, which contain a RHH motif (Schreiter and Drennan 2007, Schumacher *et al.* 2007a).

The type II *parMRC* system of the R1 plasmid from *E. coli* is one of the most well-characterised active plasmid partitioning systems. It consists of a centromere-like site, *parC*, located upstream of *parM* and *parR*, which encode the actin-like ATPase and the CBP, respectively (Figure 1.2) (Dam & Gerdes, 1994). *parC* comprises two sets of five 11-bp direct repeats that flank the *par* promoter (Breüner *et al.*, 1996).

The *parMR* promoter is located within *parC*, such that binding of ParR to *parC* results in transcriptional repression of the *par* operon (Jensen *et al.* 1994).

The structure of apo-pB171 ParR was solved using X-ray crystallography, and revealed an N-terminal RHH DNA-binding domain and packing of ParR crystals as tight dimers (Møller-Jensen *et al.* 2007). However, the first structure of the ParR/*parC* partition complex was obtained for the functionally homologous ParR protein from the staphylococcal conjugative multiresistance plasmid, pSK41 (Berg *et al.* 1998, Schumacher *et al.* 2007a). The pSK41 ParR/*parC* structure revealed that ParR binds as a dimer-of-dimers to a set of two centromeric repeats (Figure 1.3B), and that by doing so, forms a novel superhelical nucleoprotein complex, the segrosome, with *parC* DNA wrapped around 6 pairs of ParR dimers per helical turn (Schumacher *et al.* 2007a). Binding of ParR to *parC* is cooperative (Møller-Jensen *et al.* 2003), and stabilisation of the segrosome is thought to involve interactions between the disordered C-terminal domains of ParR dimers (Schumacher *et al.* 2007a). Importantly, the structure showed that the pore of the helical segrosome, which is believed to be filled with disordered ParR C-terminal tails, could facilitate the capture of ParM filaments (Schumacher *et al.* 2007a, Popp *et al.* 2010). Indeed, studies have confirmed that ParR interacts with ParM via its flexible C-terminal end (Jensen and Gerdes 1997, Schumacher *et al.* 2007a, Salje and Löwe 2008, Gayathri *et al.* 2012).

Meanwhile, the actin-like ATPase, ParM, polymerises in the presence of ATP, to form helical filaments that are made up of one or more protofilaments (Møller-Jensen *et al.* 2002, van den Ent *et al.* 2002, Orlova *et al.* 2007, Salje *et al.* 2009, Popp *et al.* 2010, Gayathri *et al.* 2013, Bharat *et al.* 2015). However, these filaments

are dynamically unstable, and rapidly disassemble unless capped by ATP or ParR/*parC* complexes (Møller-Jensen *et al.* 2002, Garner *et al.* 2004). Consistent with this, the localisation of ParR/*parC* at the ends of ParM filaments has been visualised using numerous fluorescence methods, including *in vivo* (Jensen and Gerdes 1999, Møller-Jensen *et al.* 2003, Campbell and Mullins 2007) and *in vitro* assays (Garner *et al.* 2007, Salje and Löwe 2008, Gayathri *et al.* 2012). In all cases, ParR/*parC* complexes stabilised otherwise dynamically unstable ParM filaments, suggesting that ParM filamentation requires interaction of ParM-ATP with the partition complex. This led to the proposal of a ‘search and capture’ model, which emphasises the dynamic instability of ParM filaments as an essential component of plasmid segregation, allowing unstable ParM filaments to search the intracellular space until it is stabilised by interactions with ParR/*parC* partition complexes on plasmid DNA (Garner *et al.* 2004, Campbell and Mullins 2007, Garner *et al.* 2007). It has been suggested that stabilisation of ParM filaments by the segrosome may be facilitated, in part, by the ParR ring structure, which might act as a molecular clamp to secure ParM filaments to the helical segrosome (Salje and Löwe 2008).

Recent crystal structures and cryo-electron microscopy reconstructions of ParM filaments revealed that filaments consist of a barbed end and a pointed end (Gayathri *et al.* 2012, Bharat *et al.* 2015). Furthermore, structures of a C-terminal ParR peptide bound to ParM indicate that ParR, and hence the partition complex on plasmids, bind exclusively to the barbed end of ParM filaments (Gayathri *et al.* 2012). In addition to stabilising the ParM filament, binding of the partition complex stimulates ParM polymerisation at the interaction interface, from which the insertional polymerisation model of ParM-mediated plasmid partitioning was derived (Figure 1.4) (Møller-

Jensen *et al.* 2002, Møller-Jensen *et al.* 2003, Campbell and Mullins 2007, Garner *et al.* 2007, Gayathri *et al.* 2012).

Since ParR stabilises ParM filamentation, and since ParR only interacts with the barbed end of ParM filaments (Gayathri *et al.* 2012), ParM, therefore, only polymerises at one end of the filament. Consequently, in order for ParM filaments to facilitate bidirectional separation of plasmid copies, ParM filaments interact in an antiparallel fashion to form bipolar spindles (Gayathri *et al.* 2012). Plasmids are, therefore, paired for plasmid segregation when both ends of the ParM spindle are captured by ParR/*parC* complexes. In this way, capping at the barbed end of each antiparallel ParM filament results in insertional polymerisation and bidirectional growth of the ParM spindle, which ultimately pushes plasmids to opposite cell poles, as observed by fluorescence microscopy (Møller-Jensen *et al.* 2003, Campbell and Mullins 2007). Once ParM spindles reach the cell poles, they depolymerise due to ATP hydrolysis, which is stimulated by ParR/*parC* complexes (Jensen and Gerdes 1997, Møller-Jensen *et al.* 2002, Campbell and Mullins 2007). The trigger for this hydrolysis remains unclear, and may involve dissociation of the partition complex from the filament, or unwinding of antiparallel ParM filaments in the spindle (Gayathri *et al.* 2012).

1.5.3. Type III active plasmid partitioning systems

More recently, the partitioning loci of two *Bacillus* plasmids, pXO1 from *B. anthracis* (Tinsley and Khan 2006) and pBtoxis from *B. thuringiensis* (Tang *et al.* 2006), were classified as type III active plasmid partitioning systems. Notably, the type III partitioning system differs from the type I and type II systems by encoding a tubulin/FtsZ-like GTPase motor protein rather than an ATPase motor protein

(Vaughan *et al.* 2004). Also, the gene encoding the motor protein, *tubZ*, is located downstream, rather than upstream, of the gene encoding the CBP, *tubR* (Figure 1.2).

In pBtoxis, TubR dimers bind cooperatively to the centromere-like site, *tubC*, which consists of four 12-bp repeats (Tang *et al.* 2007, Aylett and Löwe 2012, Fink and Löwe 2015). Binding of TubR to *tubC* also mediates autoregulation of the *par* operon (Larsen *et al.* 2007, Tang *et al.* 2007). The first structure of pBtoxis TubR revealed a novel mode of DNA-binding that involves a winged-HTH motif that also facilitates dimerisation of TubR (Ni *et al.* 2010). Binding of *tubC* by a structurally homologous protein, TubR from *B. megaterium*, resulted in TubR-DNA filaments that formed a helical structure, with DNA wrapped external to the helix (Figure 1.3C) (Aylett and Löwe 2012), analogous to the superhelical segrosome structure described for ParR-*parC* binding (Schumacher *et al.* 2007a).

The GTPase partitioning protein, TubZ, forms double-helical filaments that are dependent on GTP-binding (Larsen *et al.* 2007, Chen and Erickson 2008, Akhtar *et al.* 2009, Aylett *et al.* 2010, Ni *et al.* 2010, Hoshino and Hayashi 2012, Fink and Löwe 2015). TubZ filaments are dynamic and move using a treadmilling mechanism, whereby TubZ filaments polymerise at one end and depolymerise at the other (Larsen *et al.* 2007, Chen and Erickson 2008, Aylett *et al.* 2010, Fink and Löwe 2015), which is characteristic of microtubules (Erickson and O'Brien 1992). TubZ filamentation is stimulated, and stabilised, by interaction with TubR/*tubC* complexes (Ni *et al.* 2010, Aylett and Löwe 2012, Oliva *et al.* 2012, Fink and Löwe 2015). Interaction with the partition complex has been delimited to the flexible C-terminal regions of TubZ, which are believed to be localised to the shrinking end of TubZ filaments, and rotated outwards along the sides of the filament (Aylett *et al.*

2010, Ni *et al.* 2010, Kraemer *et al.* 2012, Aylett *et al.* 2013, Montabana and Agard 2014). In this way, plasmids attach to the sides and shrinking ends of TubZ filaments via their TubR/*tubC* complexes, and are pulled by treadmilling TubZ filaments using a predicted cable-car, or tramming, mechanism (Figure 1.4) (Ni *et al.* 2010, Fink and Löwe 2015). Plasmids are then thought to be released when filaments reach the cell poles (Ni *et al.* 2010).

1.5.4. Other plasmid partitioning systems

A non-conventional plasmid maintenance system, *stbABC*, has been described for the *E. coli* plasmid, R388 (Guynet *et al.* 2011). The *stbABC* operon has both plasmid conjugation and plasmid maintenance functions, and much remains to be revealed about the mechanism of segregational stability (Guynet *et al.* 2011). Remarkably, it has been shown that plasmid maintenance is dependent only on the DNA-binding protein, StbA, and not StbB, which plays a role in plasmid conjugation (Guynet *et al.* 2011). Hence, R388 plasmid partitioning does not appear to require a motor protein (Guynet and de la Cruz 2011). Fluorescently-labelled R388 plasmids were localised to the bacterial nucleoid (Guynet *et al.* 2011), prompting Guynet and de la Cruz (2011) to propose a pilot-fish mechanism of plasmid segregation, in which plasmids attach to, and segregate with, the bacterial nucleoid.

1.6. Staphylococcal multiresistance plasmid, pSK1

The staphylococcal multiresistance plasmid, pSK1, is the prototype of the pSK1 family of multiresistance plasmids that were first isolated from clinical *S. aureus* strains in Australia and the United Kingdom in the 1980s (Lyon *et al.* 1983, Lyon *et al.* 1984a, Townsend *et al.* 1987, Cookson and Phillips 1988). As illustrated in Figures 1.1 and 1.4, pSK1 family plasmids typically carry antimicrobial resistance

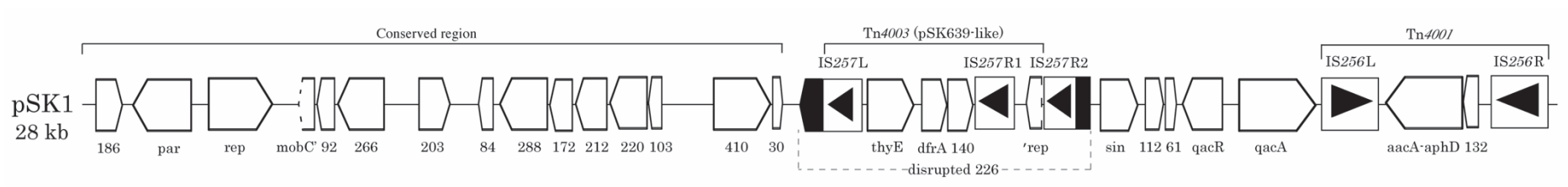
determinants, such as *qacA*, *dfrA* and *Tn4001*, which confer resistance to antiseptics and disinfectants, trimethoprim and aminoglycosides, respectively (Firth and Skurray 1998).

The 28 kb nucleotide sequence of pSK1 has been analysed, and was found to contain a 14 kb DNA segment that is conserved amongst pSK1 family plasmids (Jensen *et al.* 2010). Within this conserved plasmid backbone (Figure 1.5), are the previously characterised genes for plasmid replication (*rep*) (Firth *et al.* 2000, Kwong *et al.* 2008) and plasmid maintenance (*par*) (Firth *et al.* 2000, Simpson *et al.* 2003), as well as a newly-identified gene product encoded by *orf30*, that is similar to the Fst toxin of the type I TA system on the *E. faecalis* plasmid, pAD1 (Section 1.4.2) (Weaver *et al.* 1996, Jensen *et al.* 2010, Kwong *et al.* 2010). Other deduced gene products encoded by the pSK1 conserved backbone region include membrane transport and cell envelope proteins (Jensen *et al.* 2010).

The remaining 14 kb of the pSK1 sequence is less conserved amongst pSK1 family plasmids, most likely due to genetic rearrangements caused by mobile genetic elements, including the integration of a pSK639-like plasmid, which disrupts *orf226* (Figure 1.5) (Jensen *et al.* 2010). Along with antibiotic resistance determinants, the putative multimer resolution system, *sin* (Paulsen *et al.* 1994), is also encoded by this region (Jensen *et al.* 2010). Notably, carriage of pSK1 was found to have minimal effect on host gene expression, which might contribute to the success and prevalence of pSK1-like plasmids as vehicles for the carriage and dissemination of multiple antibiotic resistance genes amongst the staphylococci (Jensen *et al.* 2010).

Figure 1.5 Genetic map of the staphylococcal multiresistance plasmid, pSK1

A linear map of the staphylococcal multiresistance plasmid, pSK1, is shown. The positions of insertions by a pSK639-like element, and the transposon, Tn4001, are indicated above the map. Black arrowheads within boxes denote the transposase (and direction of its transcription) of IS256 and IS257 elements. Filled boxes represent the *orf226* gene that was disrupted by insertion of Tn4003, pSK639-like DNA. Genes encoding aminoglycoside resistance (*aacA-aphD*), trimethoprim resistance (*dfrA*) and resistance to antiseptics and disinfectants (*qacA*), are indicated on the map. The 14 kb conserved DNA region is indicated with a bracket above the map. Figure adapted from Jensen *et al.* (2010).



1.6.1. pSK1 plasmid segregational stability determinant, *par*

In addition to putative multimer resolution and TA systems, pSK1 also encodes a gene, *par* (originally named *orf245*), which is located upstream of, and transcribed divergently from, the replication initiation gene, *rep* (Figure 1.5) (Firth *et al.* 2000, Simpson *et al.* 2003, Jensen *et al.* 2010). Consistent with staphylococcal multiresistance plasmids, pSK1 Rep belongs to the RepA_N family of replication initiation proteins, described in Section 1.3.2.3 (Kwong *et al.* 2008, Weaver *et al.* 2009a). Plasmid segregational stability assays demonstrated that *par* was able to enhance the segregational stability of a pSK1 minireplicon (Firth *et al.* 2000), as well as heterologous replicons (Simpson *et al.* 2003). By elimination of post-segregational killing and multimer resolution as potential mechanisms of stability, pSK1 *par* is predicted to play a role in plasmid maintenance by encoding a plasmid partitioning system (Simpson *et al.* 2003).

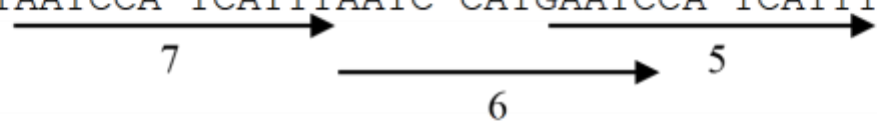
Genes homologous to pSK1 *par* are carried on approximately 80% of staphylococcal plasmids >10 kb (Shearer *et al.* 2011), and homologues have also been identified in other Gram-positive bacteria, such as *Streptococcus*, *Lactococcus*, *Lactobacillus*, *Clostridium* and *Tetragenococcus* (Simpson *et al.* 2003). Consistent with its predicted role in plasmid partitioning, the sequence immediately upstream of pSK1 *par* contains seven 12-bp direct repeats (Figure 1.6), and was shown to mediate incompatibility, thus implicating this region as a potential centromere-like site for plasmid partitioning (Simpson *et al.* 2003). Analysis of the 245-residue Par protein sequence predicted a highly-conserved N-terminal HTH DNA-binding domain and a highly-conserved, centrally-located coiled-coil (CC) domain, which is thought to be involved in protein-protein interactions (Figure 1.7) (Firth *et al.* 2000, Simpson *et al.*

Figure 1.6 Organisation of the pSK1 *par* upstream promoter region

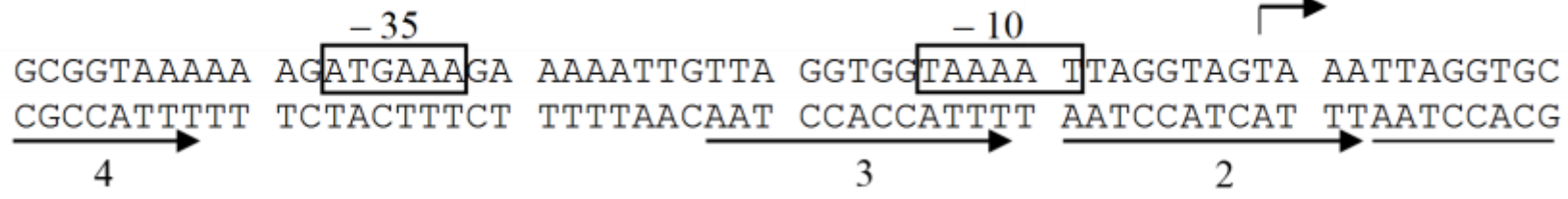
Sequence of the *par* upstream promoter region, including the translated sequence of the 5' end of *par*, shown above the nucleotide sequence. Numbers at the ends of each line indicate the pSK1 sequence position (GenBank entry GU565967). The -10 and -35 sequences of the *par* promoter, P_{*par*}, are shown in boxes. The positions of direct repeats are indicated by arrows. The transcriptional start point (TSP) is denoted by a bent arrow, and the ribosome binding site (RBS) is double-underlined.

1920 ATAAAGCGTT TTAAGTACAG ATCAGAATCA TGTTATGACC TTAAAACAAC AAAATTTATT 1861
 1920 TATTTGCGCA AATTCATGTC TAGTCTTAGT ACAATACTGG AATTTTGTTG TTTTAAATAA 1861

1860 ATTTTAGTGG CTAATTAGGT AGTAAATTAG GTRACTTAGGT AGTAAAAATG ATATATTTAG 1801
 1860 TAAAATCACC GATTAATCCA TCATTTAATC CATGAATCCA TCATTTTTTAC TATATAAATC 1801



1800 GCGGTAAAAA AGATGAAAGA AAAATTGTTA GGTGGTAAAA TTAGGTAGTA AATTAGGTGC 1741
 1800 CGCCATTTTT TCTACTTTCT TTTAACAAT CCACCATTTT AATCCATCAT TTAATCCACG 1741



RBS *par* M K T I K M V A D E L N V T K
 1740 CTAAGGGTGG ATGATATGAA AACTATAAAA ATGGTTGCTG ATGAATTGAA TGTA ACTAAA 1681
 1740 GATTCCCACC TACTATACTT TTGATATTTT TACCAACGAC TACTTAACTT ACATTGATTT 1681

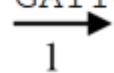
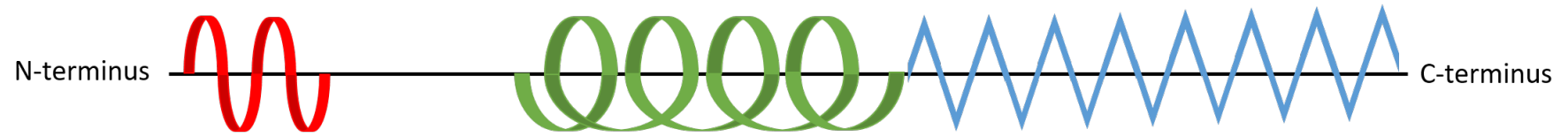


Figure 1.7 Predicted Par protein domains

Diagrammatic representation of predicted Par protein domains. Par is predicted to contain an N-terminal helix-turn-helix domain (red), central coiled-coil domain (green) and disordered C-terminal domain (blue). The predicted locations of Par domains are shown, with reference to the Par amino acid sequence (GenBank Accession Number AAF63251). The function of each predicted Par domains is given, as determined by previous studies (Lai (2008), Jensen, S. O. and Firth, N., unpublished data).



Predicted structure:

Helix-turn-helix
(aa 3–24)

Coiled-coil
(aa 83–155)

Disordered
(aa 156–245)

Function:

DNA-binding

Multimerisation

Unknown

2003). Taken together, Par, therefore, has the potential to perform both the DNA-binding and protein-protein interaction activities that are central to active plasmid partitioning mechanisms (Sections 1.5.1–1.5.3). The significance of this is highlighted by the fact that only a single protein, Par, is encoded by the pSK1 partitioning locus, compared to separate CBP and NTPase proteins encoded by most other characterised plasmid partitioning systems (Sections 1.5.1–1.5.3). This, therefore, implies that pSK1 *par* encodes a novel mechanism of plasmid segregational stability.

1.6.1.1. pSK1 Par N-terminal helix-turn-helix domain is involved in DNA-binding

DNaseI footprinting and electrophoretic mobility shift assays (EMSAs) have confirmed that Par exhibits DNA-binding activity (LeBard 2005, Lai 2008). Par binds specifically to the repeat sequences located immediately upstream of pSK1 *par*, in the *par-rep* intergenic region, which encompasses the promoter, P_{par} , and the putative centromere-like site (LeBard 2005).

A predicted N-terminal HTH domain is encoded by residues 3–24 of Par (Figure 1.7) (Firth *et al.* 2000). HTH domains are commonly associated with DNA-protein interactions, and the specificity of DNA-binding is often dependent on the interaction between the second recognition helix and the major groove of the DNA (Brennan and Matthews 1989). Consistent with its predicted structure and function, EMSAs on a Par N-terminal HTH mutant, ParK15A, revealed that this mutant was incapable of binding to a DNA probe that contained the *par-rep* intergenic region to which Par was shown to bind (Lai 2008). Therefore, as expected, the DNA-binding activity of Par is localised to the N-terminal HTH domain. Accordingly, a pSK1

minireplicon encoding ParK15A was less stable compared to a minireplicon encoding wild-type Par, when grown in the absence of selection (Lai 2008). It is presumed that the K15A mutation interferes with possible electrostatic interactions between the positively-charged lysine residue and the negatively-charged DNA backbone. Par proteins with mutations in the CC domain (described below in Section 1.6.1.2) also have impaired DNA-binding activity, although not to the same extent as ParK15A (Figgett 2007, Lai 2008).

1.6.1.2. pSK1 Par central coiled-coil domain is involved in multimerisation

Cross-linking studies of pSK1 Par revealed the formation of dimers, trimers and even higher-order multimers (Lai (2008), Jensen, S. O. and Firth, N., unpublished data), which could potentially assemble into filaments in the absence of any nucleotide co-factor, as shown by electron microscopy of purified Par proteins (Barton, D. A., Jensen, S. O. and Firth, N., unpublished data). The multimerisation activity of Par is believed to be mediated by the predicted central CC domain (Figure 1.7) (Simpson *et al.* 2003). CC domains consist of heptad repeats that coil around each other such that the nonpolar first and fourth residues of each heptad form a hydrophobic core, which mediates protein-protein interactions, especially oligomerisation (Burkhard *et al.* 2001). In previous studies, the Par L132 residue, located at the first residue of the most highly-conserved heptad repeat amongst Par homologues, was replaced with an alanine residue to generate a ParL132A mutant (Figgett 2007). An additional mutant, Par Δ CC, in which the entire putative CC domain is absent, was also generated to ensure functional disruption (Figgett 2007, Lai 2008).

pSK1 minireplicons encoding the CC domain mutants, ParL132A and Par Δ CC, exhibited reduced segregational stability compared to a minireplicon harbouring the wild-type *par* system (Figgett 2007). The reduced functionality of the CC mutants corresponded with an impairment in the ability of ParL132A to form multimers, and a complete inability of Par Δ CC to multimerise (Lai (2008), Jensen, S. O. and Firth, N., unpublished data) or form filaments (Barton, D. A., Jensen, S. O. and Firth, N., unpublished data). These results indicate a role of the putative central CC domain of Par in self-interaction and multimerisation.

1.6.1.3. pSK1 Par autoregulates its own expression

The pSK1 *par* promoter, P_{*par*}, is located within the centromere-like site of the partitioning locus (Figure 1.6), suggesting possible autoregulation of *par* expression upon Par DNA-binding, consistent with other partitioning systems (Sections 1.5.1–1.5.3). Indeed, transcriptional reporter gene assays performed using P_{*par*} fused upstream of a promoterless chloramphenicol acetyltransferase (*cat*) reporter gene, revealed that CAT activity was reduced in the presence of Par (LeBard 2005). This suggests that Par autoregulates its own expression, presumably by binding across the pSK1 *par* centromere-like site and promoter region (Section 1.6.1.1).

1.7. Scope of thesis

Traditional approaches to combating antibiotic resistance primarily focus on treating the infection, or infected individual, by eliminating the pathogen using drugs that target essential cellular processes (Bonhoeffer *et al.* 1997, Fischbach and Walsh 2009, Dandekar and Dandekar 2010). However, the naturally-occurring reservoir of antibiotic resistance determinants in the environment (Alonso *et al.* 2001, Martínez 2008, Forsberg *et al.* 2012), combined with the adaptability of bacteria to acquire

such resistance determinants through mobile genetic elements (Section 1.3), suggests that complete elimination of antibiotic resistant bacterial populations is impossible. Several views have been presented, which advocate the control of antibiotic resistance using an ecological and evolutionary (eco-evo) approach that takes into consideration the ecological and evolutionary history, behaviour and environment of antibiotic resistant bacterial populations (Amábile-Cuevas and Heinemann 2004, Pallen and Wren 2007, Garneau *et al.* 2010, Baquero *et al.* 2011, Ojala *et al.* 2013, Henriques-Normark and Normark 2014, Baquero *et al.* 2015). Eco-evo drugs and therapies, therefore, aim to reduce, and eventually eliminate, the acquisition, maintenance or spread of antibiotic resistance determinants (Baquero *et al.* 2011).

Since 90% of staphylococcal isolates carry one or more plasmids (Shearer *et al.* 2011), and since almost 80% of these plasmids are multiresistance plasmids that carry pSK1 *par*-like plasmid maintenance genes (Shearer *et al.* 2011), pSK1 *par* represents an ideal target for “promiscuity inhibitors” and “plasmid decontamination” eco-evo strategies (Amábile-Cuevas and Heinemann 2004, Baquero *et al.* 2011) aimed at disrupting the maintenance and dissemination of antibiotic resistance determinants carried by staphylococcal multiresistance plasmids. A greater understanding of the functional and mechanistic details of plasmid segregation by pSK1 *par*, and *par*-like systems, is paramount to the identification of targets for antiplasmid drugs that could be used to interfere with the acquisition, maintenance and dissemination of antibiotic resistance determinants in staphylococcal populations. Ultimately, it is envisaged that such eco-evo strategies could promote plasmid loss, or decontamination, within antibiotic resistant populations such that a reversion to antibiotic susceptible staphylococci might be achieved.

In the context of identifying and understanding potential targets for eco-evo therapies aimed at interfering with the maintenance of staphylococcal multiresistance plasmids and their resistance determinants, this study aims to elucidate the mechanism of pSK1 *par* by:

- a) determining the functional significance of the predicted disordered C-terminal domain (CTD),
- b) investigating whether pSK1 Par interacts with *S. aureus* host factors to enhance plasmid maintenance, and
- c) examining the intracellular localisation of Par and plasmid DNA in *S. aureus* cells.

Chapter 3 of this thesis describes experiments that were undertaken to determine the role of the predicted disordered Par CTD. A number of Par CTD mutants were generated and their effect on Par function, i.e. plasmid segregational stability, was assessed. The contribution of the CTD to Par activity, specifically, to DNA-binding, multimerisation and self-interaction, was determined using a range of *in vitro* studies, including electrophoretic mobility shift assays, cross-linking assays, and yeast two-hybrid assays.

The potential for the involvement of *S. aureus* host factors in Par mechanism is explored in Chapter 4 of this thesis. The ability of a distant pSK1 Par homologue to stabilise a pSK1 minireplicon was investigated in *S. aureus*, and the functionality of pSK1 *par* was examined in a heterologous host, *E. faecalis*. Potential Par interaction partners in *S. aureus* were identified by yeast two-hybrid screening of *S. aureus* genomic DNA libraries with a Par bait fusion protein, and potential interactions were tested by performing pairwise yeast two-hybrid assays. Furthermore, the role of the

bacterial nucleoid in pSK1 *par*-mediated plasmid partitioning was investigated using epifluorescence microscopy, electrophoretic mobility shift assays using non-specific DNA, and searching the *S. aureus* chromosome sequence for potential Par binding sites.

Lastly, epifluorescence microscopy was used to perform cytological studies on the localisation of Par and plasmid DNA in *S. aureus* cells. Presented in Chapter 5 of this thesis, the results describe the construction of Par GFP fusions and the genetic manipulations performed to achieve a balance between Par GFP functionality and fluorescence localisation. The localisation pattern of Par was also analysed by expressing fluorescent Par fusions in a heterologous host, *E. coli*. Additionally, for the first time, plasmid DNA was localised in *S. aureus* cells using a fluorescent repressor-operator system, which enabled plasmid segregation to be tracked during cell division.

A discussion of the results obtained from this study, and how they contribute to the understanding of Par function and mechanism, is presented in Chapter 6.

CHAPTER 2

Materials and methods

2.1. Microbial strains, plasmids and growth conditions

The microbial strains used throughout this study are described in Table 2.1. A description of the plasmids used and constructed in this study is provided in Table 2.2. Growth media for bacterial and yeast cells are described in Table 2.3. Media and solutions to be added to growth media were sterilised by autoclaving at 121°C for 20 min. Solutions containing heat labile compounds were sterilised at 105°C for 25 min or by filtration through a 0.45 µm pore size Millex® syringe-driven filter unit (Millipore). Where necessary, antibiotics were added to growth media at the final concentrations indicated in Table 2.4. Stock antibiotic solutions were prepared according to Sambrook and Russell (2001) and filter sterilised.

Unless otherwise specified, bacterial cells were grown on solid media at either 37°C or 30°C for approximately 16 h. For stationary phase bacterial cultures, 3–10 ml of liquid medium were inoculated with a single bacterial colony and incubated at 37°C or 30°C with aeration at 220 rpm on a G10 gyratory shaker (New Brunswick Scientific), or in an Innova 42 incubator shaker (New Brunswick Scientific). Yeast cells were cultured on solid growth media by incubation at 30°C for 2–7 days. For stationary phase yeast cultures, 5–150 ml of liquid media were inoculated with 1–5 yeast colonies and incubated at 30°C with aeration at 250 rpm for approximately 20 h in an Innova 42 incubator shaker (New Brunswick Scientific). When required, the

Table 2.1 Microbial strains

Strain	Genotype/Description	Reference
<i>E. coli</i>		
BL21	F ⁻ <i>ompT hsdS_B (r_B⁻m_B⁻) dcm gal</i>	Studier <i>et al.</i> (1990)
DC10B	Δ <i>dcm</i> in the DH10B background; Dam methylation only	Monk <i>et al.</i> (2012)
DH10B (K-12 strain)	<i>dam⁺ dcm⁺ ΔhsdRMS endA1 recA1</i>	Invitrogen
DH5α	<i>supE44 ΔlacU169 (Φ80lacZΔM15) hsdR17 recA1 endA1 gyrA96 thi-1 relA1</i>	Bethesda Research Laboratories
<i>E. faecalis</i>		
JH2-2	Clinical isolate harbouring defective ϕFL1C prophage. <i>rif, fus</i>	Jacob and Hobbs (1974)
<i>S. aureus</i>		
DU5883	Mutant of NCTC 8325-4 defective in expression of FnBPA and FnBPB <i>fnbA::Tc^R fnbB::Em^R</i>	Greene <i>et al.</i> (1995)
RN4220	Restrictionless derivative of NCTC 8325-4	Kreiswirth <i>et al.</i> (1983)
SK8250	RN4220 with the L1.LtrB-ΔORF intron inserted into the <i>spa</i> gene	Liu (2012)

Table 2.1 Microbial strains (continued)

Strain	Genotype/Description	Reference
<i>S. cerevisiae</i>		
AH109	<i>MATa, trp1-901, leu2-3, 112, ura3-52, his3-200, gal4Δ, gal80Δ, LYS2::GAL1_{UAS}-GAL1_{TATA}-HIS3, MEL1 GAL2_{UAS}-GAL2_{TATA}-ADE2, URA3::MEL1_{UAS}-MEL1_{TATA}-lacZ</i>	James <i>et al.</i> (1996)

Table 2.2 Plasmids

Plasmid	Description ^a	Resistance ^b	Reference
Staphylococcal plasmids			
pSERP	Multiresistance plasmid from <i>S. epidermidis</i> ; 27.3 kb	Pn ^R , Km ^R , Gm ^R , multidrug resistance	Gill <i>et al.</i> (2005)
pSK1	Multiresistance plasmid from <i>S. aureus</i> ; 28.2 kb	Km ^R , Tp ^R , Gm ^R , multidrug resistance	Lyon <i>et al.</i> (1983), Jensen <i>et al.</i> (2010)
pSK41	Conjugative multiresistance plasmid from <i>S. aureus</i> ; 46.4 kb	Gm ^R , Tm ^R , Km ^R , multidrug resistance	Wood <i>et al.</i> (1977), Berg <i>et al.</i> (1998)
<i>E. coli</i> plasmids			
pLAU44	pUC18 carrying an ~9 kb fragment containing an array of 120 copies of the 19-bp Tn10 <i>tetO</i> binding site separated by 10-bp random spacer sequence, flanking either side of a gentamicin resistance gene	Ap ^R , Gm ^R	Lau <i>et al.</i> (2003)
pQE30	<i>E. coli</i> expression vector containing IPTG-inducible T5 promoter and <i>lac</i> operator; 3.4 kb	Ap ^R	Qiagen
pREP4	<i>E. coli</i> repressor plasmid carrying <i>lacI</i> repressor gene; 3.7 kb	Km ^R	Qiagen

Table 2.2 Plasmids (continued)

Plasmid	Description ^a	Resistance ^b	Reference
pTTQ18-RGSH ₆	<i>E. coli</i> expression plasmid containing IPTG-inducible <i>tac</i> promoter, <i>lac</i> operator, and <i>lacI</i> ^Q repressor; 4.6 kb	Ap ^R	Stark (1987)
Recombinant plasmids			
<i>E. coli</i> – <i>S. aureus</i> shuttle plasmids			
pJEG015	pLOW-GFP with <i>ermC</i> replaced by <i>tetA(K)</i> ; 8.0 kb	Ap ^R <i>E. coli</i> ; Tc ^R <i>S. aureus</i>	Jensen, S. O. (Western Sydney University, Australia)
pLOW-GFP	<i>E. coli</i> – <i>S. aureus</i> shuttle plasmid containing IPTG-inducible P _{spac} promoter and <i>lacI</i> for controlled expression of <i>gfp</i> fusions in <i>S. aureus</i> ; 7.9 kb	Ap ^R <i>E. coli</i> ; Em ^R <i>S. aureus</i>	Liew <i>et al.</i> (2011)
pSK4829	pWE180 carrying a 2.3 kb <i>Bam</i> HI/ <i>Hind</i> III fragment containing the pSK1 <i>par-rep</i> region; 7.0 kb	Ap ^R <i>E. coli</i> ; Em ^R <i>S. aureus</i>	Firth <i>et al.</i> (2000)
pSK4833	pWE180 carrying a 1.4 kb <i>Bam</i> HI/ <i>Hind</i> III fragment containing pSK1 <i>rep</i> and the <i>par-rep</i> intergenic region; 6.1 kb	Ap ^R <i>E. coli</i> ; Em ^R <i>S. aureus</i>	Firth <i>et al.</i> (2000)

Table 2.2 Plasmids (continued)

Plasmid	Description ^a	Resistance ^b	Reference
pSK5623	<i>E. coli</i> - <i>S. aureus</i> shuttle vector containing <i>rrnBT1</i> transcription terminator	Ap ^R <i>E. coli</i> ; Cm ^R <i>S. aureus</i>	Grkovic <i>et al.</i> (2003)
pSK5630	pSK5623 carrying a 2.3 kb <i>Bgl</i> II fragment containing the pSK1 <i>par</i> - <i>rep</i> region; 5.9 kb	Ap ^R <i>E. coli</i> ; Cm ^R <i>S. aureus</i>	Grkovic <i>et al.</i> (2003)
pSK6195	pSK5623 carrying a 1.4 kb <i>Bam</i> HI/ <i>Hind</i> III fragment containing pSK1 <i>rep</i> and the <i>par</i> - <i>rep</i> intergenic region; 5.0 kb	Ap ^R <i>E. coli</i> ; Cm ^R <i>S. aureus</i>	Firth, N. (The University of Sydney, Australia)
pSK7721	pSK4829 site-directed mutant; <i>par</i> loop-out deletion of nucleotides 247–465 (aa 83–155; ΔCC); 7.0 kb	Ap ^R <i>E. coli</i> ; Em ^R <i>S. aureus</i>	Figgett (2007)
pSK7726	pSK4829 site-directed mutant; <i>par</i> double point mutation TT395GC (L132A); 7.0 kb	Ap ^R <i>E. coli</i> ; Em ^R <i>S. aureus</i>	Figgett (2007)
pSK7764	pSK4829 site-directed mutant; <i>par</i> double point mutation AA44GC (K15A); 7.0 kb	Ap ^R <i>E. coli</i> ; Em ^R <i>S. aureus</i>	Lai (2008)

Table 2.2 Plasmids (continued)

Plasmid	Description ^a	Resistance ^b	Reference
pSK9059	pSK4829 site-directed mutant; <i>par</i> double point mutation CG722GC (R241A). Also, <i>par</i> triple point mutation ACT724GGA to introduce silent <i>AvaII</i> restriction site; 7.0 kb	Ap ^R <i>E. coli</i> ; Em ^R <i>S. aureus</i>	This study
pSK9065	<i>E. coli</i> – <i>S. aureus</i> shuttle plasmid containing tetracycline-inducible P _{<i>xyl/tetO</i>} promoter and <i>tetR</i> for controlled expression of <i>mRFPmars</i> fusions in <i>S. aureus</i> ; 6.9 kb	Ap ^R <i>E. coli</i> ; Nm ^R <i>S. aureus</i>	Brzoska and Firth (2013)
pSK9067	pLOW-GFP containing an additional <i>lacO</i> _{id} operator upstream of P _{<i>spac</i>} ; 7.9 kb	Ap ^R <i>E. coli</i> ; Em ^R <i>S. aureus</i>	Brzoska and Firth (2013)
pSK9069	pWE180 carrying a 1.9 kb <i>BamHI/HindIII</i> fragment containing pSK1 <i>rep</i> and the C-terminally truncated pSK1 <i>par</i> coding region (<i>par</i> ΔCTD, aa 1–170); 6.6 kb	Ap ^R <i>E. coli</i> ; Em ^R <i>S. aureus</i>	This study
pSK9070	pSK4829 site-directed mutant; <i>par</i> double point mutation TG716GC (W239A). Includes silent <i>NruI</i> restriction site; 7.0 kb	Ap ^R <i>E. coli</i> ; Em ^R <i>S. aureus</i>	This study

Table 2.2 Plasmids (continued)

Plasmid	Description^a	Resistance^b	Reference
pSK9075	pSK9065 carrying a 1.2 kb <i>SalI/SacI</i> fragment containing <i>S. aureus</i> RN4220 <i>ftsZ</i> to create a C-terminal FtsZ-mRFPmars fusion protein; 8.1 kb	Ap ^R <i>E. coli</i> ; Nm ^R <i>S. aureus</i>	Brzoska and Firth (2013)
pSK9086	pSK9067 carrying a 0.9 kb <i>SalI/BamHI</i> fragment containing <i>S. aureus</i> <i>spo0J</i> and the superoxide dismutase (SOD) RBS to create a C-terminal Spo0J-GFP fusion protein; 8.8 kb	Ap ^R <i>E. coli</i> ; Em ^R <i>S. aureus</i>	This study
pSK9087	pWE180 carrying a 2.9 kb <i>BamHI/HindIII</i> fragment containing pSK1 <i>rep</i> and pSK1 <i>gfpmut-1-par</i> . N-terminal GFP-Par fusion protein expressed from native pSK1 <i>par</i> promoter, P _{par} ; 7.6 kb	Ap ^R <i>E. coli</i> ; Em ^R <i>S. aureus</i>	This study
pSK9088	pWE180 carrying a 2.9 kb <i>BamHI/HindIII</i> fragment containing pSK1 <i>rep</i> and pSK1 <i>par-gfpmut-1</i> . C-terminal Par-GFP fusion protein expressed from native pSK1 <i>par</i> promoter, P _{par} ; 7.6 kb	Ap ^R <i>E. coli</i> ; Em ^R <i>S. aureus</i>	This study
pSK9097	pJEG015 carrying a 0.8 kb <i>SalI/BamHI</i> fragment containing pSK1 <i>par</i> and the native <i>par</i> RBS to create a C-terminal Par-GFP fusion protein; 8.7 kb	Ap ^R <i>E. coli</i> ; Tc ^R <i>S. aureus</i>	This study

Table 2.2 Plasmids (continued)

Plasmid	Description^a	Resistance^b	Reference
pSK9102	pJEG015 carrying a 0.8 kb <i>SalI/BamHI</i> fragment containing pSK1 <i>parK15A</i> and the native <i>par</i> RBS to create a C-terminal Par-GFP fusion protein; 8.7 kb	Ap ^R <i>E. coli</i> ; Tc ^R <i>S. aureus</i>	This study
pSK9103	pJEG015 carrying a 0.5 kb <i>SalI/BamHI</i> fragment containing pSK1 <i>parΔCC</i> and the native <i>par</i> RBS to create a C-terminal Par-GFP fusion protein; 8.5 kb	Ap ^R <i>E. coli</i> ; Tc ^R <i>S. aureus</i>	This study
pSK9104	pJEG015 carrying a 0.8 kb <i>SalI/HindIII</i> fragment containing pSK1 <i>par</i> and the native <i>par</i> RBS cloned into the <i>SalI</i> and <i>SmaI</i> sites. Stop codon is located between <i>par</i> and <i>gfp</i> ; 8.7 kb	Ap ^R <i>E. coli</i> ; Tc ^R <i>S. aureus</i>	This study
pSK9135	pWE180 carrying a 2.2 kb <i>BamHI/HindIII</i> fragment containing pSK1 <i>rep</i> and pSK1 <i>RGSH₆-par</i> . N-terminal RGSH ₆ -Par fusion protein expressed from native pSK1 <i>par</i> promoter, P _{par} ; 6.9 kb	Ap ^R <i>E. coli</i> ; Em ^R <i>S. aureus</i>	This study
pSK9136	pWE180 carrying a 2.3 kb <i>BamHI/HindIII</i> fragment containing <i>S. epidermidis</i> RP62A pSERP <i>rep</i> and the gene for replication-associated protein; 7.0 kb	Ap ^R <i>E. coli</i> ; Em ^R <i>S. aureus</i>	This study

Table 2.2 Plasmids (continued)

Plasmid	Description ^a	Resistance ^b	Reference
pSK9137	pWE180 carrying a 1.4 kb <i>Bam</i> HI/ <i>Hind</i> III fragment containing <i>S. epidermidis</i> RP62A pSERP <i>rep</i> and intergenic region to gene for replication associated protein; 6.1 kb	Ap ^R <i>E. coli</i> ; Em ^R <i>S. aureus</i>	This study
pSK9140	pSK9067 with 1.2 kb <i>Kpn</i> I/ <i>Cla</i> I fragment containing <i>ermC</i> gene (Em ^R) removed and replaced with blunted 1.0 kb <i>Nco</i> I/ <i>Sph</i> I fragment containing <i>aadD</i> gene (Nm ^R) from pSK9065; 7.7 kb	Ap ^R <i>E. coli</i> ; Nm ^R <i>S. aureus</i>	This study
pSK9142	pSK9140 carrying a 0.7 kb <i>Sal</i> I/ <i>Bam</i> HI fragment containing Tn10 <i>tetR</i> (amplified from pSK9065), SOD RBS and SCGAS linker; 8.3 kb	Ap ^R <i>E. coli</i> ; Nm ^R <i>S. aureus</i>	This study
pSK9144	pSK4829 carrying a 2.2 kb <i>Kas</i> I fragment containing Tn10 <i>tetO</i> array (amplified from pLAU44); 9.2 kb	Ap ^R <i>E. coli</i> ; Em ^R <i>S. aureus</i>	This study
pSK9145	pSK4833 carrying a 2.2 kb <i>Kas</i> I fragment containing Tn10 <i>tetO</i> array (amplified from pLAU44); 8.4 kb	Ap ^R <i>E. coli</i> ; Em ^R <i>S. aureus</i>	This study

Table 2.2 Plasmids (continued)

Plasmid	Description ^a	Resistance ^b	Reference
pSK9166	pWE180 carrying a 2.9 kb <i>Bam</i> HI/ <i>Hind</i> III fragment containing pSK1 <i>rep</i> and pSK1 <i>gfpmut-1-parK15A</i> . GFP-ParK15A fusion protein expressed from native pSK1 <i>par</i> promoter; 7.6 kb	Ap ^R <i>E. coli</i> ; Em ^R <i>S. aureus</i>	This study
pSK9169	pSK4829 site-directed mutant; <i>par</i> double point mutation AA4GC (K2A); 7.0 kb	Ap ^R <i>E. coli</i> ; Em ^R <i>S. aureus</i>	This study
pSK9170	pSK4829 site-directed mutant; <i>par</i> point mutation A29C (E10A). Includes silent <i>Nsi</i> I site; 7.0 kb	Ap ^R <i>E. coli</i> ; Em ^R <i>S. aureus</i>	This study
pSK9171	pSK4829 site-directed mutant; <i>par</i> triple point mutation TAT127GCA (Y43A). Includes silent <i>Nsi</i> I site; 7.0 kb	Ap ^R <i>E. coli</i> ; Em ^R <i>S. aureus</i>	This study
pWE180	pUC18 carrying a <i>Pst</i> I/ <i>Cla</i> I fragment containing the pE194 erythromycin resistance gene (<i>ermC</i>) cloned into a blunted <i>Nde</i> I site; 4.7 kb	Ap ^R <i>E. coli</i> ; Em ^R <i>S. aureus</i>	Firth <i>et al.</i> (2000)

Table 2.2 Plasmids (continued)

Plasmid	Description ^a	Resistance ^b	Reference
<i>E. coli</i>–<i>E. faecalis</i> shuttle plasmids			
pAM401	<i>E. coli</i> – <i>E. faecalis</i> shuttle vector with pACYC184 and pIP501 replicons; 10.4 kb	Cm ^R , Tc ^R <i>E. coli</i> ; Cm ^R <i>S. aureus</i>	Wirth <i>et al.</i> (1986)
pSK5378	pAM401 carrying a 1.3 kb <i>Bam</i> HI fragment containing pSK1 <i>par</i> and the <i>par</i> - <i>rep</i> intergenic region; 11.7 kb	Cm ^R , Tc ^R <i>E. coli</i> ; Cm ^R <i>S. aureus</i>	Simpson <i>et al.</i> (2003)
pSK6110	pAM401 carrying a 0.2 kb DNA fragment containing the pSK1 <i>par</i> - <i>rep</i> intergenic region; 10.6 kb	Cm ^R , Tc ^R <i>E. coli</i> ; Cm ^R <i>S. aureus</i>	Simpson <i>et al.</i> (2003)
<i>E. coli</i>–<i>S. cerevisiae</i> shuttle plasmids			
pGADT7	<i>E. coli</i> – <i>S. cerevisiae</i> shuttle vector encoding the GAL4 activation domain (AD) (aa 768–881). Generates N-terminal GAL4 AD prey protein fusions; 8.0 kb	Ap ^R <i>E. coli</i> ; LEU ⁺ <i>S. cerevisiae</i>	Clontech
pGADT7-T	pGADT7 encoding SV40 large T-antigen (aa 84–708) as a C-terminal fusion to GAL4 AD	Ap ^R <i>E. coli</i> ; LEU ⁺ <i>S. cerevisiae</i>	Clontech

Table 2.2 Plasmids (continued)

Plasmid	Description ^a	Resistance ^b	Reference
pGBKT7	<i>E. coli</i> - <i>S. cerevisiae</i> shuttle vector encoding the GAL4 DNA-binding domain (BD) (aa 1–147). Generates N-terminal GAL4 DNA-BD bait protein fusions; 7.3 kb	Km ^R <i>E. coli</i> ; TRP ⁺ <i>S. cerevisiae</i>	Clontech
pGBKT7-53	pGBKT7 encoding murine p53 (aa 72–390) as a C-terminal fusion to GAL4 BD	Km ^R <i>E. coli</i> ; TRP ⁺ <i>S. cerevisiae</i>	Clontech
pGBKT7-Lam	pGBKT7 encoding human lamin C (aa 66–230) as a C-terminal fusion to GAL4 BD	Km ^R <i>E. coli</i> ; TRP ⁺ <i>S. cerevisiae</i>	Clontech
pSK9107	pGBKT7 carrying a 0.7 kb <i>EcoRI/BamHI</i> fragment containing pSK1 <i>par</i> ; 8.0 kb	Km ^R <i>E. coli</i> ; TRP ⁺ <i>S. cerevisiae</i>	This study
pSK9108	pGBKT7 carrying a 1.5 kb <i>EcoRI/BamHI</i> fragment containing pSK1 <i>par-gfp</i> (SCGAS linker); 8.8 kb	Km ^R <i>E. coli</i> ; TRP ⁺ <i>S. cerevisiae</i>	This study
pSK9109	pGBKT7 carrying a 0.6 kb <i>EcoRI/BamHI</i> fragment containing <i>S. aureus</i> <i>divIVA</i> ; 7.9 kb	Km ^R <i>E. coli</i> ; TRP ⁺ <i>S. cerevisiae</i>	This study
pSK9110	pGADT7 carrying a 0.7 kb <i>EcoRI/BamHI</i> fragment containing pSK1 <i>par</i> ; 8.7 kb	Ap ^R <i>E. coli</i> ; LEU ⁺ <i>S. cerevisiae</i>	This study

Table 2.2 Plasmids (continued)

Plasmid	Description^a	Resistance^b	Reference
pSK9111	pGADT7 carrying a 1.5 kb <i>EcoRI/BamHI</i> fragment containing pSK1 <i>par-gfp</i> (SCGAS linker); 9.5 kb	Ap ^R <i>E. coli</i> ; LEU ⁺ <i>S. cerevisiae</i>	This study
pSK9112	pGADT7 carrying a 0.6 kb <i>EcoRI/BamHI</i> fragment containing <i>S. aureus divIVA</i> ; 8.6 kb	Ap ^R <i>E. coli</i> ; LEU ⁺ <i>S. cerevisiae</i>	This study
pSK9121	pGBKT7 carrying a 0.7 kb <i>EcoRI/BamHI</i> fragment containing pSK1 <i>parK15A</i> ; 8.0 kb	Km ^R <i>E. coli</i> ; TRP ⁺ <i>S. cerevisiae</i>	This study
pSK9122	pGBKT7 carrying a 0.5 kb <i>EcoRI/BamHI</i> fragment containing pSK1 <i>parΔCC</i> ; 7.8 kb	Km ^R <i>E. coli</i> ; TRP ⁺ <i>S. cerevisiae</i>	This study
pSK9123	pGBKT7 carrying a 0.7 kb <i>EcoRI/BamHI</i> fragment containing pSK1 <i>parL132A</i> ; 8.0 kb	Km ^R <i>E. coli</i> ; TRP ⁺ <i>S. cerevisiae</i>	This study
pSK9124	pGBKT7 carrying a 0.5 kb <i>EcoRI/SmaI</i> fragment containing pSK1 <i>parΔCTD</i> ; 7.8 kb	Km ^R <i>E. coli</i> ; TRP ⁺ <i>S. cerevisiae</i>	This study
pSK9125	pGADT7 carrying a 0.7 kb <i>EcoRI/BamHI</i> fragment containing pSK1 <i>parK15A</i> ; 8.7 kb	Ap ^R <i>E. coli</i> ; LEU ⁺ <i>S. cerevisiae</i>	This study

Table 2.2 Plasmids (continued)

Plasmid	Description^a	Resistance^b	Reference
pSK9126	pGADT7 carrying a 0.5 kb <i>EcoRI/BamHI</i> fragment containing pSK1 <i>parΔCC</i> ; 8.5 kb	Ap ^R <i>E. coli</i> ; LEU ⁺ <i>S. cerevisiae</i>	This study
pSK9127	pGADT7 carrying a 0.7 kb <i>EcoRI/BamHI</i> fragment containing pSK1 <i>parL132A</i> ; 8.7 kb	Ap ^R <i>E. coli</i> ; LEU ⁺ <i>S. cerevisiae</i>	This study
pSK9128	pGADT7 carrying a 0.5 kb <i>EcoRI/SmaI</i> fragment containing pSK1 <i>parΔCTD</i> ; 8.5 kb	Ap ^R <i>E. coli</i> ; LEU ⁺ <i>S. cerevisiae</i>	This study
pSK9130	pGBKT7 carrying a 0.7 kb <i>EcoRI/BamHI</i> fragment containing pSK1 <i>parR241A</i> ; 8.0 kb	Km ^R <i>E. coli</i> ; TRP ⁺ <i>S. cerevisiae</i>	This study
pSK9131	pGBKT7 carrying a 0.7 kb <i>EcoRI/BamHI</i> fragment containing pSK1 <i>parW239A</i> ; 8.0 kb	Km ^R <i>E. coli</i> ; TRP ⁺ <i>S. cerevisiae</i>	This study
pSK9132	pGADT7 carrying a 0.7 kb <i>EcoRI/BamHI</i> fragment containing pSK1 <i>parR241A</i> ; 8.7 kb	Ap ^R <i>E. coli</i> ; LEU ⁺ <i>S. cerevisiae</i>	This study
pSK9133	pGADT7 carrying a 0.7 kb <i>EcoRI/BamHI</i> fragment containing pSK1 <i>parW239A</i> ; 8.7 kb	Ap ^R <i>E. coli</i> ; LEU ⁺ <i>S. cerevisiae</i>	This study

Table 2.2 Plasmids (continued)

Plasmid	Description^a	Resistance^b	Reference
pSK9172	pGBKT7 carrying a 0.2 kb <i>EcoRI/BamHI</i> fragment encoding pSK1 Par N-terminal domain (aa 1–82); 7.5 kb	Km ^R <i>E. coli</i> ; TRP ⁺ <i>S. cerevisiae</i>	This study
pSK9173	pGBKT7 carrying a 0.2 kb <i>EcoRI/BamHI</i> fragment encoding pSK1 Par CC domain (aa 83–155); 7.5 kb	Km ^R <i>E. coli</i> ; TRP ⁺ <i>S. cerevisiae</i>	This study
pSK9174	pGBKT7 carrying a 0.3 kb <i>EcoRI/BamHI</i> fragment encoding pSK1 Par C-terminal domain (aa 156–245); 7.5 kb	Km ^R <i>E. coli</i> ; TRP ⁺ <i>S. cerevisiae</i>	This study
pSK9175	pGADT7 carrying a 0.2 kb <i>EcoRI/BamHI</i> fragment encoding pSK1 Par N-terminal domain (aa 1–82); 8.2 kb	Ap ^R <i>E. coli</i> ; LEU ⁺ <i>S. cerevisiae</i>	This study
pSK9176	pGADT7 carrying a 0.2 kb <i>EcoRI/BamHI</i> fragment encoding pSK1 Par CC domain (aa 83–155); 8.2 kb	Ap ^R <i>E. coli</i> ; LEU ⁺ <i>S. cerevisiae</i>	This study
pSK9177	pGADT7 carrying a 0.3 kb <i>EcoRI/BamHI</i> fragment encoding pSK1 Par C-terminal domain (aa 156–245); 8.2 kb	Ap ^R <i>E. coli</i> ; LEU ⁺ <i>S. cerevisiae</i>	This study

Table 2.2 Plasmids (continued)

Plasmid	Description ^a	Resistance ^b	Reference
<i>E. coli</i> overexpression plasmids			
pSK5344	pQE30 carrying a 0.7 kb <i>Bam</i> HI/ <i>Hind</i> III fragment containing the pSK1 <i>par</i> coding region; 4.2 kb	Ap ^R	Simpson (2002)
pSK9071	pQE30 carrying a 0.5 kb <i>Bam</i> HI/ <i>Hind</i> III fragment containing pSK1 <i>par</i> Δ <i>CTD</i> (aa 1–170); 3.9 kb	Ap ^R	This study
pSK9073	pSK5344 site-directed mutant; <i>par</i> double point mutation CG722GC (R241A). Also, <i>par</i> triple point mutation ACT724GGA to introduce silent <i>Ava</i> II restriction site; 4.2 kb	Ap ^R	This study
pSK9074	pSK5344 site-directed mutant; <i>par</i> double point mutation TG716GC (W239A). Includes silent <i>Nru</i> I restriction site; 4.2 kb	Ap ^R	This study
pSK9178	pTTQ18-RGSH ₆ carrying a 1.5 kb <i>Sma</i> I/ <i>Hind</i> III fragment containing <i>gfp-par</i> ; 6.1 kb	Ap ^R	This study

^a Nucleotide positions refer to the pSK1 nucleotide sequence (GenBank Accession Number GU565967). Amino acid positions refer to the pSK1 Par sequence (GenBank Accession Number AAF63251)

^b Ap^R, ampicillin resistance; Cm^R, chloramphenicol resistance; Gm^R, gentamicin resistance; Em^R, erythromycin resistance; Km^R, kanamycin resistance; Pn^R, penicillin resistance; Tc^R, tetracycline resistance; Tm^R, tobramycin resistance; Tp^R, trimethoprim resistance; LEU⁺, leucine autotrophy; TRP⁺, tryptophan autotrophy

Medium	Composition	Source/Reference
B2	1% (w/v) casein hydrolysate 2.5% (w/v) yeast extract 0.1% (w/v) K ₂ HPO ₄ 0.5% (w/v) glucose 2.5% (w/v) NaCl pH 7.5	Schenk and Laddaga (1992)
Brain heart infusion (BHI)	3.7% (w/v) BHI 1.5% (w/v) agar (for solid media)	Oxoid
Luria-Bertani (LB)	1% (w/v) tryptone 0.5% (w/v) yeast extract 1% (w/v) NaCl 1.5% (w/v) agar (for solid media)	Willets and Finnegan (1970)
NYE	1% (w/v) casein hydrolysate 0.5% (w/v) yeast extract 0.5% (w/v) NaCl 1.5% (w/v) agar (for solid media)	Schenk and Laddaga (1992)
SD/-Leu	0.67% (w/v) yeast nitrogen base 1× Dropout solution (Table 2.5) 0.002% (w/v) L-tryptophan 0.002% (w/v) L-histidine HCl monohydrate 0.002% (w/v) L-adenine hemisulphate 2% (w/v) glucose 1.5% (w/v) agar (for solid media)	Yeast Protocols Handbook (Clontech)

Table 2.3 Microbial growth media (continued)

Medium	Composition	Source/Reference
SD/-Leu/-Trp	0.67% (w/v) yeast nitrogen base 1× Dropout solution (Table 2.5) 0.002% (w/v) L-histidine HCl monohydrate 0.002% (w/v) L-adenine hemisulphate 2% (w/v) glucose 1.5% (w/v) agar (for solid media)	Yeast Protocols Handbook (Clontech)
SD/-Leu/-Trp/-His	0.67% (w/v) yeast nitrogen base 1× Dropout solution (Table 2.5) 0.002% (w/v) L-adenine hemisulphate 2% (w/v) glucose 1.5% (w/v) agar (for solid media)	Yeast Protocols Handbook (Clontech)
SD/-Leu/-Trp/-His/-Ade/X- α -Gal	0.67% (w/v) yeast nitrogen base 1× Dropout solution (Table 2.5) 2% (w/v) glucose 33 μ g/ml 5-bromo-4-chloro-3-indolyl α -D-galactopyranoside (X- α -Gal) 1.5% (w/v) agar (for solid media)	Yeast Protocols Handbook (Clontech)
SD/-Trp	0.67% (w/v) yeast nitrogen base 1× Dropout solution (Table 2.5) 0.01% (w/v) L-leucine 0.002% (w/v) L-histidine HCl monohydrate 0.002% (w/v) L-adenine hemisulphate 2% (w/v) glucose 1.5% (w/v) agar (for solid media)	Yeast Protocols Handbook (Clontech)

Table 2.3 Microbial growth media (continued)

Medium	Composition	Source/Reference
Synthetic dropout (SD)	0.67% (w/v) yeast nitrogen base 1× Dropout solution (Table 2.5) 2% (w/v) glucose 1.5% (w/v) agar (for solid media)	Yeast Protocols Handbook (Clontech)
YPD	2% (w/v) bacteriological peptone 1% (w/v) yeast extract 2% (w/v) glucose 1.5% (w/v) agar (for solid media)	Yeast Protocols Handbook (Clontech)

Table 2.4 Concentrations of antimicrobial compounds

Antimicrobial compound	Final concentration used (µg/ml)
Ampicillin	100
Chloramphenicol	25 (<i>E. coli</i>); 10 (<i>S. aureus</i>)
Erythromycin	10
Kanamycin	25
Neomycin	15
Tetracycline	3

optical density of cell cultures was measured at 600 nm (OD_{600nm}) using a SPECTROstar *Nano* microplate reader (BMG LABTECH).

For long-term storage of microbial strains, stationary phase cultures were supplemented with 33% (v/v) glycerol and stored at -70°C.

2.2. Reagents, solutions and oligonucleotides

The compositions of reagents and solutions used in this study are presented in Table 2.5. When required, reagents and solutions were sterilised as described in Section 2.1.

Oligonucleotide primers used in this study were synthesised by GeneWorks Pty Ltd (Adelaide, SA) and are listed in Table 2.6. Oligonucleotides were provided in lyophilised form and resuspended in sterile Milli-Q water to a stock concentration of 100 µM, from which working stocks of 10 µM were prepared. Stock solutions of oligonucleotides were stored at -20°C.

2.3. Bacterial transformation procedures

2.3.1. Preparation of chemically-competent *E. coli* cells

Chemically-competent *E. coli* cells were prepared based on the protocol by Kahn *et al.* (1979). Stationary phase *E. coli* cells were inoculated 1:50 in fresh LB-broth (Table 2.3) containing antibiotic selection where appropriate (Table 2.4). Cells were incubated at 37°C with agitation at 220 rpm until mid-exponential phase (OD_{600nm} approximately 0.6), and then harvested by centrifugation (2,150 ×g / 5 min / 4°C; Heraeus Biofuge Primo). Cell pellets were washed with 0.2 volumes of ice-cold 0.1

Table 2.5 Reagents and solutions

Reagent/Solution	Composition
α -galactosidase Assay Buffer	333 mM NaOAc (pH 4.5) 33 mM <i>p</i> -nitrophenyl α -D-Galactopyranoside
α -galactosidase Stop Solution (10 \times)	1 M Na ₂ CO ₃
Adenine dropout solution (10 \times)	0.02% (w/v) L-adenine hemisulphate
Blocking buffer	3% (w/v) BSA or 5% (w/v) skim milk powder 10 mM Tris-HCl (pH 7.5) 150 mM NaCl
Bromophenol Blue loading dye	50 mM EDTA (pH 7.0) 50% (w/v) sucrose 0.05% (w/v) bromophenol blue
Coomassie Brilliant Blue stain	30% (v/v) methanol 10% (v/v) glacial acetic acid 0.25% (w/v) Coomassie Brilliant Blue R-250
Denaturing Protein Elution Buffer	100 mM NaH ₂ PO ₄ 10 mM Tris-Cl (pH 4.5) 8 M urea
Denaturing Protein Lysis Buffer	100 mM NaH ₂ PO ₄ 10 mM Tris-Cl (pH 8.0) 8 M urea

Table 2.5 Reagents and solutions (continued)

Reagent/Solution	Composition
Denaturing Protein Wash Buffer I	100 mM NaH ₂ PO ₄ 10 mM Tris-Cl (pH 6.3) 8 M urea
Denaturing Protein Wash Buffer II	100 mM NaH ₂ PO ₄ 10 mM Tris-Cl (pH 5.5) 8 M urea
Destain solution	30% (v/v) methanol 10% (v/v) glacial acetic acid
dNTP mix (20 mM)	20 mM dATP 20 mM dCTP 20 mM dGTP 20 mM dTTP
Dropout solution (10×)	0.02% (w/v) L-arginine HCl 0.03% (w/v) L-isoleucine 0.03% (w/v) L-lysine HCl 0.02% (w/v) L-methionine 0.05% (w/v) L-phenylalanine 0.2% (w/v) L-threonine 0.03% (w/v) L-tyrosine 0.02% (w/v) L-uracil 0.15% (w/v) L-valine
Electroporation solution	500 mM sucrose 10% (v/v) glycerol

Table 2.5 Reagents and solutions (continued)

Reagent/Solution	Composition
EMSA binding buffer	15 mM Tris-HCl (pH 7.5) 1 mM EDTA 100 mM KCl 7.5% (v/v) glycerol
FISH blocking solution	2× SSC buffer 70% (v/v) formamide 1 mg/ml sheared salmon sperm DNA
FISH hybridisation solution	3× SSC buffer 50% (v/v) formamide
GTE buffer	50 mM glucose 20 mM Tris-Cl (pH7.5) 10 mM EDTA
High ionic strength polyacrylamide gel mixture	5% (w/v) acrylamide (19:1) 0.5× TBE buffer 0.2% (w/v) APS 0.4% (w/v) TEMED
Histidine dropout solution (100×)	0.2% (w/v) L-histidine HCl monohydrate
HRP staining solution	7 mM Tris-HCl (pH 7.5) 107 mM NaCl 0.04% (v/v) H ₂ O ₂ 0.04% (w/v) 4-chloro-naphthol 28.5% (v/v) methanol
Leucine dropout solution (100×)	1% (w/v) L-leucine

Table 2.5 Reagents and solutions (continued)

Reagent/Solution	Composition
Native Elution Buffer	50 mM NaH ₂ PO ₄ (pH 8.0) 300 mM NaCl 250 mM imidazole
Native Protein Lysis Buffer	50 mM NaH ₂ PO ₄ (pH 8.0) 300 mM NaCl 10 mM imidazole
Native Wash Buffer A	50 mM NaH ₂ PO ₄ (pH 8.0) 300 mM NaCl 20 mM imidazole
Non-reducing SDS-PAGE sample buffer	50 mM Tris-HCl (pH 6.8) 2% (w/v) SDS 0.1% (w/v) bromophenol blue 10% (v/v) glycerol
PBS	137 mM NaCl 2.7 mM KCl 10 mM Na ₂ HPO ₄ 2 mM KH ₂ PO ₄
PEG/LiAc solution	40% (w/v) PEG 4000 10 mM Tris-HCl (pH 7.5) 1 mM EDTA 100 mM LiAc

Table 2.5 Reagents and solutions (continued)

Reagent/Solution	Composition
Polyacrylamide/agarose hybrid gel	3% (w/v) acrylamide (19:1) 0.5% (w/v) agarose 0.5× TBE buffer 0.2% (w/v) APS 0.04% (v/v) TEMED
SDS-PAGE resolving gel mixture	10% (w/v) acrylamide (29:1) 125 mM Tris-HCl (pH 8.8) 0.1% (w/v) SDS 0.2% (w/v) APS 0.04% (v/v) TEMED
SDS-PAGE running buffer	25 mM Tris-HCl 250 mM glycine 0.1% (w/v) SDS
SDS-PAGE sample buffer	50 mM Tris-HCl (pH 6.8) 2% (w/v) SDS 0.1% (w/v) bromophenol blue 10% (v/v) glycerol 100 mM DTT
SDS-PAGE stacking gel mixture	5% (w/v) acrylamide (29:1) 375 mM Tris-HCl (pH 6.8) 0.1% (w/v) SDS 0.3% (w/v) APD 0.03% (v/v) TEMED
SSC buffer (20×)	3 M NaCl 300 mM sodium citrate pH 7.0

Table 2.5 Reagents and solutions (continued)

Reagent/Solution	Composition
SSCT buffer (20×)	3 M NaCl 300 mM sodium citrate 1% (v/v) Tween 20 pH 7.0
TAE buffer	40 mM Tris-HCl (pH 8.5) 5 mM glacial acetic acid 1 mM EDTA
TBE buffer	90 mM Tris-HCl (pH 8.3) 90 mM boric acid 2.5 mM EDTA
TBS buffer	10 mM Tris-HCl (pH 7.5) 150 mM NaCl
TBS-Tween buffer	10 mM Tris-HCl (pH 7.5) 150 mM NaCl 0.05% (v/v) Tween 20
TE buffer	10 mM Tris-HCl (pH 7.5) 1 mM EDTA
TE/LiAc solution	10 mM Tris-HCl (pH 7.5) 1 mM EDTA 100 mM LiAc
Tryptophan dropout solution (100×)	0.2% (w/v) L-tryptophan

Table 2.5 Reagents and solutions (continued)

Reagent/Solution	Composition
Western transfer buffer	25 mM Tris-HCl (pH 8.3) 190 mM glycine 20% (v/v) methanol
WL buffer	25 mM Tris-HCl (pH 8.0) 10 mM EDTA

Table 2.6 Oligonucleotides

Oligonucleotide	Sequence
3'AD sequencing ¹	5' – agatggtgcacgatgcacag – 3'
3' DNA-BD sequencing ¹	5' – atcataaatcataagaaattcgcc – 3'
879BamHI	5' – cgcgatccaaaactataaaaatggttgctgatg – 3'
HC2	5' – gaaatcttgaaactagagc – 3'
HC3	5' – tgaaacggtgaaactatgc – 3'
HC6	5' – gccaccaaacaaagcggaccagaagccttt – 3'
HC7	5' – aaaggcttctggtccgctttgttggtggc – 3'
HC8	5' – gcgaagcttcatcgatcattagtagattatc – 3'
HC9	5' – ccaaacaaacgactcgcgaagccttttttag – 3'
HC10	5' – ctaaaaaaggcttcgcgagtcgtttgtttgg – 3'
HC11	5' – gcgaagcttttagccatctgaattattatc – 3'
HC16	5' – catggaggcgccgcaggagccaccaaacgactcc – 3'
HC17	5' – ggctcctgcggcgctccatgagtaaaggagaagaac – 3'
HC18	5' – gcgaagctttattgtatagttcatcc – 3'
HC19	5' – gttcttctcttactcatatcatccacccttaggc – 3'
HC20	5' – aaatcctgcggcgctccatgaaaactataaaaatgg – 3'
HC21	5' – gcgaagcttttagccaccaaacg – 3'
HC22	5' – gcctaagggtggatgatagtaaggagaagaac – 3'
HC23	5' – catggaggcgccgcaggattgtatagttcatcc – 3'

Table 2.6 Oligonucleotides (continued)

Oligonucleotide	Sequence
HC24	5' – cgcggaattcatgaaaactataaaaatgg – 3'
HC25	5' – gccggatccttagccaccaaaacaacg – 3'
HC26	5' – cgcgatccttattgtatagttcatcc – 3'
HC27	5' – cgcggaattcatgcctttacaccaaag – 3'
HC28	5' – cgcgatccttacttcttagttg – 3'
HC33	5' – gtgatggtgatggtgatgcgatcctctcatatcatccacccttaggc – 3'
HC34	5' – cgcatcaccatcaccatcacggcggtggcatgaaaactataaaaatgg – 3'
HC35	5' – gccggatccgttgcttagcaaccactg – 3'
HC36	5' – gcgaagcttgcaacagaacctagttatg – 3'
HC37	5' – gcgaagcttctaactccaattcttcac – 3'
HC38	5' – cgctcgacttaggaggatgattattatgtctagattagataaaaagt – 3'
HC39	5' – cgcgatcccggaggcgccgcaggaagaccacttccacatt – 3'
HC43	5' – atcgggcgccgctagcggccagtccaagcttag – 3'
HC45	5' – atcgggcgccgctagcgtgatgcactttgatatcg – 3'
HC56	5' – gccggatccttagccatctgaattattatc – 3'
HC57	5' – cgcggaattcttgagacattaaaaacaaaag – 3'
HC58	5' – gccggatccttattctctaatgatg – 3'
HC59	5' – cgcggaattcgagagacaattaagtattc – 3'
HC60	5' – ggggtggatgatatggcaactataaaaatggtg – 3'
HC61	5' – gcaaccattttatagttgccatatcatccacc – 3'

Table 2.6 Oligonucleotides (continued)

Oligonucleotide	Sequence
HC62	5' – ctataaaaatggttgctgatgcattgaatgtaactaac – 3'
HC63	5' – gtttagttacattcaatgcatcagcaaccatTTTTatag – 3'
HC64	5' – gaattatattgatgataatgatgcattgaaaatagtagaaaaaac – 3'
HC65	5' – gatttttctactattttcaatgcatcattatcatcaatataattc – 3'
NFRepDwn4829 ²	5' – gcgggatcctttctgttgacttaattcc – 3'
SJ37	5' – atcagaatcatgttatgacc – 3'
SJ38	5' – cattcaattcatcagcaacc – 3'
SJ69	5' – gattgtcgactgcctaagggtggatgatatg – 3'
SJ70	5' – ttaaggatccagccaccaaacgactcc – 3'
T7 sequencing ¹	5' – taatacgactcactatagggc – 3'

¹ Oligonucleotide sequence from Matchmaker GAL4 Two-hybrid System 3 & Libraries User Manual (Clontech)

² Oligonucleotide sequence from Firth *et al.* (2000)

M CaCl₂ (2,150 ×g / 5 min / 4°C; Heraeus Biofuge Primo), and then resuspended in 0.2 volumes of ice-cold 0.1 M CaCl₂. Cell suspensions were incubated on ice for at least 30 min, before being harvested as above. Harvested cells were resuspended in 0.04 volumes of 0.085 M ice-cold CaCl₂ containing 15% (v/v) glycerol. Chemically-competent *E. coli* cells were stored in 100 µl aliquots at -80°C.

2.3.2. Transformation of chemically-competent *E. coli* cells with plasmid DNA

A 50 µl aliquot of chemically-competent *E. coli* cells (Section 2.3.1) was thawed and incubated on ice for 30 min with approximately 100–200 ng of each plasmid DNA to be transformed. The mixtures were heated at 42°C for 2 min and then returned to ice for a further 2 min. Heat-shocked cells were allowed to recover in 350 µl of LB-broth (Table 2.3) at 37°C with agitation at 220 rpm for 45–60 min. Cells were spread in 100 µl aliquots on LB-agar plates (Table 2.3) containing the appropriate antibiotic selection (Table 2.4), and plates were incubated overnight at 37°C or 30°C.

2.3.3. Preparation of electrocompetent *S. aureus* cells

Electrocompetent *S. aureus* cells were prepared according to the method of Schenk & Laddaga (1992). *S. aureus* cells were grown overnight to stationary phase in B2-broth (Table 2.3) at 37°C with agitation at 220 rpm. Overnight cultures were diluted 1:25 in fresh B2-broth (Table 2.3) and grown at 37°C with agitation until the cells reached mid-exponential phase (OD_{600nm} approximately 0.4). Cells were harvested (2,150 ×g / 8 min / RT; Heraeus Biofuge Primo), and washed three times with 0.4 volumes of Milli-Q water (2,150 ×g / 8 min / RT; Heraeus Biofuge Primo), followed by a single wash with 0.2 volumes of 10% (v/v) glycerol (2,150 ×g / 8 min / RT;

Heraeus Biofuge Primo). Cells were then resuspended in 0.1 volumes of 10% (v/v) glycerol and incubated at RT for 15 min before cells were pelleted by centrifugation ($2,150 \times g$ / 8 min / RT; Heraeus Biofuge Primo). Harvested cells were resuspended in 0.03 volumes of 10% (v/v) glycerol and stored in 70 μ l aliquots at -80°C .

2.3.4. Electroporation of electrocompetent *S. aureus* cells with plasmid DNA

Electroporation of electrocompetent *S. aureus* RN4220 or SK8250 cells was performed according to the method of Schenk and Laddaga (1992). A 70 μ l aliquot of electrocompetent *S. aureus* cells (Section 2.3.3) was thawed and mixed with 1 μ g of plasmid DNA. The mixture was electroporated using a Gene Pulser electroporator (Bio-Rad) or Gene Pulser XCell electroporation system (Bio-Rad) at 23 kV/cm with 100 Ω resistance and 25 μ F capacitance. Electroporated cells were allowed to recover in 390 μ l of B2-broth (Table 2.3) at 37°C with agitation at 220 rpm for 1 h. Cells were then spread in 100 μ l aliquots on NYE-agar plates (Table 2.3) containing the appropriate antibiotic selection (Table 2.4), and plates were incubated overnight at 37°C or 30°C .

Electroporation of electrocompetent *S. aureus* DU5883 cells (Table 2.1), which contain restriction modification systems, was performed according to the method described by Löfblom *et al.* (2007). Thawed aliquots of electrocompetent *S. aureus* DU5883 cells (Section 2.3.3) were harvested ($16,060 \times g$ / 1 min / RT; Heraeus Biofuge Pico) and resuspended in electroporation solution (Table 2.5). Cells were incubated at RT for 30 min, after which 2 μ g of plasmid DNA were added. Electroporation mixtures were incubated at RT for 10 min prior to electroporation as described above.

2.3.5. Preparation of electrocompetent *E. faecalis* cells

Preparation of electrocompetent *E. faecalis* JH2-2 cells (Table 2.1) was performed based on the protocol of Dunny *et al.* (1991). *E. faecalis* JH2-2 cells were cultured at 37°C with agitation at 220 rpm overnight in BHI-broth (Table 2.3) supplemented with 2% (w/v) glycine. Stationary phase cultures were inoculated 1:20 in fresh BHI-broth (Table 2.3) containing 2% (w/v) glycine and subcultured at 37°C with aeration until mid-exponential phase (OD_{600nm} approximately 0.5). Cells were chilled on ice for 5 min, and then harvested by centrifugation (2,150 ×g / 5 min / 4°C; Heraeus Biofuge Primo). Cells were washed with 1 volume of sterile Milli-Q water (2,150 ×g / 5 min / 4°C; Heraeus Biofuge Primo), followed by 0.4 volumes and then 0.2 volumes of electroporation solution (Table 2.5) (2,150 ×g / 5 min / 4°C; Heraeus Biofuge Primo). Cells were resuspended in 0.1 volumes of electroporation solution and incubated at RT for 15 min. After incubation, cells were harvested (16,060 ×g / 1 min / RT; Heraeus Biofuge Pico), resuspended in 0.02 volumes of electroporation solution and then stored in 70 µl aliquots at -70°C.

2.3.6. Electroporation of electrocompetent *E. faecalis* cells with plasmid DNA

Electrocompetent *E. faecalis* JH2-2 cells (Section 2.3.5) were electroporated with plasmid DNA as described by Dunny *et al.* (1991). A 70 µl aliquot of electrocompetent *E. faecalis* cells was thawed on ice and mixed with 1 µg of plasmid DNA. The mixture was electroporated at 23 kV/cm with 200 Ω resistance and 25 µF capacitance, as described in Section 2.3.4. Electroporated cells were allowed to recover in 390 µl of BHI-broth (Table 2.3) at 37°C with agitation at 220 rpm for 2 h. Cells were then spread in 100 µl aliquots on BHI-agar plates (Table 2.3) containing

the appropriate antibiotic selection (Table 2.4), and plates were incubated at 37°C overnight.

2.4. DNA manipulations

2.4.1. Isolation of plasmid DNA

Plasmid DNA was isolated from stationary phase *E. coli* cultures (Section 2.1) using the ISOLATE Plasmid Mini Kit (BioLine), according to the manufacturer's instructions. For the isolation of plasmid DNA from *S. aureus*, cell suspensions were lysed with 0.4 mg/ml lysostaphin (Sigma) in resuspension buffer at 37°C for 30–60 min before proceeding with plasmid isolation as described above. For the isolation of plasmid DNA from *S. cerevisiae* yeast cells, the resuspension buffer was supplemented with 0.1 U/μl lyticase (Sigma) and cells were lysed by incubation at 37°C with agitation at 220 rpm for 1–1.5 h before proceeding with plasmid isolation as described above. Isolated plasmid DNA was quantified (Section 2.4.13) and stored at -20°C in sterile Milli-Q water.

2.4.2. Isolation of genomic DNA

Genomic DNA was isolated from 2 ml of stationary phase *S. aureus* cultures (Section 2.1). Cells were harvested by centrifugation (16,060 ×g / 1 min / RT; Heraeus Biofuge Pico) and resuspended in 50 μl of WL buffer (Table 2.5). Cells were lysed with 0.4 mg/ml lysostaphin (Sigma) at 37°C for 30–60 min, before genomic DNA isolation using the ISOLATE Genomic DNA Mini Kit (Bioline), according to the manufacturer's instructions. Isolated genomic DNA was quantified (Section 2.4.13) and stored at -20°C in sterile Milli-Q water.

2.4.3. Agarose gel electrophoresis

Prestained 0.8–3 % (w/v) agarose gels containing 1× SYBR Safe DNA gel stain (Invitrogen) were prepared in TAE buffer (Table 2.5). DNA samples were mixed with Bromophenol Blue loading dye (Table 2.5) prior to loading. Samples were electrophoresed alongside 1 kb DNA ladder or 100 bp DNA ladder (New England BioLabs) size markers at 100 V in TAE buffer (Table 2.5) until the bromophenol blue tracking dye had migrated approximately three quarters of the gel length. DNA was visualised by UV transillumination at 302 nm using the GelDoc-It TS Imaging System (UVP).

2.4.4. Polymerase chain reaction

Amplification of DNA fragments was achieved by polymerase chain reaction (PCR) using the appropriate oligonucleotide primer pair and template DNA. PCRs were performed in a total volume of 20 µl or 50 µl using either iProof High-Fidelity DNA polymerase (Bio-Rad) or KAPA Taq DNA polymerase (Kapa Biosystems) in a T100 thermal cycler (Bio-Rad) or an iCycler thermocycler (Bio-Rad). For PCRs using iProof High-Fidelity DNA polymerase, reactions contained 1–20 ng of template DNA, 0.5 µM of each forward and reverse primer, 0.2 mM deoxynucleotide triphosphate (dNTP) mix (Table 2.5) and 0.02 U/µl of iProof High-Fidelity DNA polymerase, in 1× iProof High-Fidelity DNA polymerase buffer (Bio-Rad). Amplification was carried out with an initial denaturation step of 98°C for 30 s, followed by 25 cycles of the following conditions: denaturation at 98°C for 10 s, annealing at 40–60°C for 30 s, and extension at 72°C for 15–30 s/kb. A final extension was carried out at 72°C for 7 min. For DNA amplification using KAPA

Taq DNA polymerase, reactions included 10–20 ng of template DNA, 0.4 μ M of each forward and reverse primer, 0.2 mM dNTP mix (Table 2.5) and 0.02 U/ μ l of KAPA Taq DNA polymerase in 1 \times Buffer B (Kapa Biosystems). Amplification was carried out with an initial denaturation step of 95°C for 2 min, followed by 25 cycles of the following conditions: denaturation at 95°C for 30 s, annealing at 40–60°C for 30 s, and extension at 72°C for 1 min/kb. A final extension was carried out at 72°C for 2 min. PCRs were held in the thermal cycler at 4°C and processed immediately, or stored at -20°C until required.

2.4.5. Site-directed mutagenesis

Site-directed mutagenesis (SDM) of plasmid DNA was performed according to the QuikChange protocol (Stratagene). Site-directed mutations were introduced using complementary mutagenic primers, listed in Table 2.6. Where possible, silent restriction sites were introduced into the primers to facilitate screening of plasmid DNA for incorporation of the mutagenic primer. Each SDM reaction consisted of approximately 10–20 ng of template plasmid DNA, 0.2 μ M of each forward and reverse mutagenic primer, 0.2 mM dNTP mix and 0.02 U/ μ l of iProof High-Fidelity DNA polymerase (Bio-Rad) in 1 \times iProof High-Fidelity DNA polymerase buffer (Bio-Rad), made up to a total reaction volume of 50 μ l with Milli-Q water. Mutagenesis reactions were performed using a T100 thermal cycler (Bio-Rad) or an iCycler thermocycler (Bio-Rad) with an initial denaturation step of 98°C for 30 s, followed by 15 cycles of the following conditions: denaturation at 98°C for 10 s, annealing at 40–60°C for 30 s, and extension at 72°C for 1 min/kb. A final extension was carried out at 72°C for 7 min.

Following SDM, the reaction mixtures were incubated with 0.4 U/ μ l of *DpnI* restriction endonuclease (New England BioLabs) at 37°C for 2–16 h to specifically digest the methylated, wild-type parental DNA template, leaving the unmethylated, newly-synthesised mutant DNA undigested. After restriction digestion, *DpnI* was heat-inactivated by incubation at 80°C for 20 min, and the *DpnI*-digested SDM reactions were used to transform chemically-competent *E. coli* DH5 α cells (Section 2.3.2).

2.4.6. Restriction endonuclease digestion

Restriction endonuclease digestion of DNA was performed at 37°C in the restriction buffer recommended by the manufacturer (New England BioLabs). Each reaction contained 300 ng–2 μ g of DNA and 0.2–0.4 U/ μ l of restriction endonuclease (New England BioLabs) in 1 \times restriction buffer (New England BioLabs), made up to a total volume of 20 μ l or 50 μ l. Restriction endonuclease digestions were incubated at 37°C for a minimum of 1 h. Digestions were terminated by purification of the DNA (Section 2.4.7), or by heat-inactivation of the restriction endonucleases at 65°C or 80°C for 20 min.

2.4.7. DNA purification

DNA fragments were purified, either from agarose gels or directly from reactions, using the ISOLATE PCR and Gel Kit (Bioline), according to the manufacturer's instructions. For the extraction of DNA from agarose gels, fragments were visualised by UV transillumination at 302 nm using a Mighty Bright UV transilluminator (Hoefer) or the GelDoc-It TS Imaging System (UVP). The desired DNA fragment was excised from the gel with a scalpel before proceeding with DNA purification.

2.4.8. Blunting of DNA ends

Blunting of overhangs from DNA ends was performed using DNA polymerase I, large (Klenow) fragment (New England BioLabs). DNA was treated with Klenow (1 U/ μ g DNA) in the presence of 33 μ M dNTP mix (Table 2.5) in 1 \times T4 DNA Ligase Buffer (New England BioLabs) at 25°C for 15 min. Reactions were terminated by the addition of 10 mM EDTA, followed by heat-inactivation of the enzyme at 75°C for 20 min.

2.4.9. Phosphorylation of DNA ends

Blunt DNA ends were phosphorylated using T4 polynucleotide kinase (PNK) (New England BioLabs). T4 PNK (0.33 U/ μ l) was added to DNA fragments and reactions were incubated at 37°C for 30 min in 1 \times T4 DNA Ligase Buffer. Reactions were terminated by heat-inactivation of T4 PNK at 65°C for 20 min.

2.4.10. Dephosphorylation of DNA ends

Dephosphorylation of DNA ends was performed using Antarctic phosphatase (AnP) (New England BioLabs). DNA ends were treated with 0.67 U/ μ l of AnP in 1 \times Antarctic Phosphatase Reaction Buffer (New England BioLabs) at 37°C for 15 min for 5' overhangs and blunt ends, or for 60 min for 3' overhangs. Following dephosphorylation, AnP was heat-inactivated at 70°C for 5 min.

2.4.11. DNA ligation

DNA ligation reactions were conducted in a total volume of 10 μ l using an insert:vector molar ratio of 3:1. Each reaction contained 50–100 ng of digested

(Section 2.4.6), purified (Section 2.4.7) and dephosphorylated (2.4.10) vector DNA and the appropriate amount of digested (Section 2.4.6) and purified (Section 2.4.7) insert DNA. For blunt-end ligations, approximately 200 ng of vector DNA was used. Ligation reactions proceeded at 16°C overnight using 2 U/μl T4 DNA ligase (New England BioLabs) in 1× T4 DNA Ligase Buffer (New England BioLabs).

2.4.12. Ethanol precipitation of DNA

DNA was precipitated with the addition of 0.1 volumes of 3 M NaOAc pH 5.2 (4°C) followed by 3 volumes of 100% (v/v) ethanol (-20°C). DNA was allowed to precipitate at -70°C for at least 1 h before recovery of the DNA by centrifugation (16,060 ×g / 30 min / 4°C; Heraeus Biofuge Pico). The DNA pellet was washed twice with 1 ml of 70% (w/v) ethanol (-20°C), and the ethanol was removed by centrifugation (16,060 ×g / 5 min / 4°C; Heraeus Biofuge Pico). The DNA pellet was dried and then resuspended in sterile Milli-Q water or in the appropriate buffer.

2.4.13. Quantification of DNA

The concentration of DNA samples was measured spectrophotometrically using a NanoDrop ND-1000 UV/Vis Spectrophotometer with NanoDrop software (NanoDrop Technologies).

2.4.14. DNA sequencing

Automated sequencing of DNA was performed by the Australian Genome Research Facility (Sydney). Reactions comprised approximately 1 μg of purified plasmid DNA (Section 2.4.1) with 10 pmol of oligonucleotide primer, made up to a total

volume of 12 μ l with sterile Milli-Q water. Nucleotide sequences were analysed using Sequencher 4.5 software (Gene Codes Corporation).

2.5. Protein manipulations

2.5.1. Protein overproduction

pQE30-based *E. coli* expression constructs (Table 2.2) were used to transform chemically-competent *E. coli* BL21 cells (Table 2.1) (Section 2.3.2) containing the repressor plasmid, pREP4 (Table 2.2). Single colonies of transformants were used to inoculate 10 ml of LB-broth (Table 2.3) containing ampicillin and kanamycin selection (Table 2.4), and cultures were grown at 37°C with agitation at 220 rpm overnight (Section 2.1). Overnight cultures were diluted 1:50 in 500 ml of selective LB-broth (Table 2.3) for large-scale protein overproduction, or in 25 ml for small-scale overproduction. Cultures were grown at 37°C with aeration at 220 rpm until mid-exponential phase (OD_{600nm} approximately 0.6), whereupon production of Par proteins was induced by the addition of isopropyl- β -D-thiogalactopyranoside (IPTG) to a final concentration of 0.1 mM. Induced cultures were incubated at a reduced temperature of 30°C with aeration at 220 rpm for 3.5 h. Following protein overproduction, cells were harvested ($9,820 \times g$ / 10 min / 4°C; Beckman JA-14 rotor for large-scale protein overproduction cultures, and $2,150 \times g$ / 5 min / 4°C; Heraeus Biofuge Primo for small-scale cultures) and cell pellets were stored at -80°C until required.

2.5.2. Protein purification under non-denaturing conditions

Small-scale protein purifications were performed under non-denaturing conditions using cells that were harvested from small-scale protein overproduction experiments (Section 2.5.1). Cell pellets from 2 ml of induced protein overproduction cultures were thawed and resuspended in 100 μ l of Native Protein Lysis Buffer (Table 2.5) and incubated with 1 mg/ml lysozyme (Sigma) on ice for 30 min. Lysed cells were sonicated on ice for 5 s on Setting 4 using a Sonifier B-12 Cell Disrupter (Branson). Cell lysates were cleared by centrifugation (16,060 $\times g$ / 10 min / 4°C; Heraeus Biofuge Pico) and mixed with 20 μ l of a 50% slurry of ProBond Ni²⁺-NTA metal chelate affinity agarose (Thermo Fisher Scientific) that had been pre-equilibrated with Native Protein Lysis Buffer (Table 2.5). Mixtures were incubated at 4°C for 30 min with gentle rotation on a RSM-6 rotary mixer (Ratek Instruments). Following incubation, the resin was recovered by centrifugation (1000 $\times g$ / 30 s / RT; Heraeus Biofuge Pico) and washed twice with 100 μ l of Native Wash Buffer A (Table 2.5) at RT with gentle rotation for 5–10 min. The resin was recovered by centrifugation (1000 $\times g$ / 30 s / RT; Heraeus Biofuge Pico) between each wash step. Proteins were then eluted from the resin three times with 20 μ l of Native Elution Buffer (Table 2.5) at RT with gentle rotation for 5–10 min. Elution fractions were kept on ice until required.

2.5.3. Protein purification under denaturing conditions

Overproduced proteins from large-scale protein overproduction cultures were purified under denaturing conditions by batch affinity chromatography. Cell pellets from 500 ml protein overproduction cultures (Section 2.5.1) were thawed and

resuspended in 15 ml of Denaturing Protein Lysis Buffer (Table 2.5). Resuspended cells were lysed using a pre-chilled French pressure cell (Sim-Aminco Spectronic Instruments) at 20,000 psi up to six times, and cell lysates were then cleared by centrifugation (17,400 $\times g$ / 10 min / 4°C; Beckman JA-20 rotor). The supernatant was mixed with 2 ml of a 50% slurry of Ni²⁺-NTA resin (Thermo Fisher Scientific) that had been pre-equilibrated by washing three times with Denaturing Protein Wash Buffer I (Table 2.5). The resin was recovered by centrifugation (35 $\times g$ / 2 min / 4°C; Heraeus Biofuge Pico) between each wash step. Soluble proteins were incubated with the resin at 4°C for 3 h or overnight with gentle rotation on a RSM-6 rotary mixer (Ratek Instruments). The resin was recovered by centrifugation (35 $\times g$ / 2 min / 4°C; Heraeus Biofuge Pico) and washed two times with 9 ml of Denaturing Protein Wash Buffer I (Table 2.5) at 4°C with gentle rotation for 1 h each wash. The resin was recovered (35 $\times g$ / 2 min / 4°C; Heraeus Biofuge Pico) after each wash, and then washed a further two times with 9 ml of Denaturing Protein Wash Buffer II (Table 2.5) at RT with gentle rotation for 15 min each wash. After centrifugation to pellet the resin after each wash (35 $\times g$ / 2 min / RT; Heraeus Biofuge Pico), proteins were eluted with 2.5 ml of Denaturing Protein Elution Buffer (Table 2.5) at RT with gentle rotation for 1 h. Elutions were kept on ice until buffer exchange (Section 2.5.4) was performed.

2.5.4. Protein buffer exchange

Protein buffer exchange was performed in order to renature proteins that had been purified under denaturing conditions (Section 2.5.3) and to replace the Denaturing Protein Elution Buffer with buffers compatible with downstream experiments.

Proteins were exchanged into EMSA binding buffer or PBS (Table 2.5), as described in Simpson (2002), LeBard (2005) and Lai (2008), using PD-10 Desalting Columns (GE Healthcare), according to the manufacturer's instructions. Columns were pre-equilibrated with 25 ml of the new buffer, subsequent to which 2.5 ml of denatured protein samples from Section 2.5.3 were passed through the column by gravity force. Proteins were re-buffered with the addition of 3.5 ml of the new buffer, and eluates were collected in three fractions. The concentrations of re-buffered protein fractions were measured using Bradford assays (Section 2.5.5), and fractions containing satisfactory amounts of protein were stored in 100 μ l aliquots at -80°C until required.

2.5.5. Protein quantification

Estimates of total protein concentration were performed using the colorimetric method of Bradford (1976). Assays were performed in a 96-well microplate using bovine serum albumin (BSA) (New England BioLabs) as the protein standard. BSA was diluted in EMSA binding buffer or PBS (Table 2.5) to give final concentrations of 0–1000 μ g/ml. To 5 μ l of each protein sample and standard, 200 μ l of Quick Start Bradford 1 \times Dye Reagent (Bio-Rad) was added to start the reaction. The absorbance of each reaction was measured spectrophotometrically at 595 nm using a SPECTROstar *Nano* microplate reader (BMG LABTECH). Standard curves and protein concentrations were calculated using the data analysis software, MARS 1.20 (BMG LABTECH). When necessary, protein samples were appropriately diluted in EMSA binding buffer or PBS to obtain absorbance readings within the linear range of the BSA standard curve.

2.5.6. Sodium dodecyl-sulphate polyacrylamide gel electrophoresis (SDS-PAGE)

Separation of proteins by sodium dodecyl-sulphate polyacrylamide gel electrophoresis (SDS-PAGE) was performed as described by Laemmli (1970), using the Mini-PROTEAN 3 cell (Bio-Rad), assembled according to the manufacturer's instructions. Glass gel plates were secured in a casting frame and sealed on a casting stand, before a 10% (w/v) SDS-PAGE resolving gel mixture (Table 2.5) was poured between the plates to approximately 1 cm below the bottom of the wells. The resolving gel was then overlaid with Milli-Q water to facilitate polymerisation (approximately 1 h). Following polymerisation of the resolving gel, the Milli-Q water was removed and a 5% (w/v) SDS-PAGE stacking gel mixture (Table 2.5) was poured on top of the resolving gel, and the appropriate well comb put in place. The stacking gel was allowed to polymerise (approximately 30 min), after which the well comb was removed and the wells flushed with SDS-PAGE running buffer (Table 2.5) in preparation for sample loading.

Prior to loading, protein samples were heated in SDS-PAGE sample buffer (Table 2.5) at 95°C for 5 minutes and then centrifuged ($16,060 \times g$ / 3 min / RT; Heraeus Biofuge Pico) to pellet the insoluble material. Section 2.5.8 below describes the preparation of whole cell lysates for SDS-PAGE. A 10 μ l sample of the supernatant was loaded into the wells of the stacking gel, and the samples were co-electrophoresed with Prestained Protein Ladder, Broad Range (10–230 kDa) (New England BioLabs) or Precision Plus Protein All Blue Standards (Bio-Rad) at 150 V in SDS-PAGE running buffer (Table 2.5) until the blue dye front reached the bottom

of the glass plates. Visualisation of fractionated proteins was achieved by staining the gels overnight with Coomassie Brilliant Blue stain (Table 2.5), followed by destaining with two washes of Destain solution (Table 2.5) until protein bands could be clearly visualised. Gels were scanned using a GS710 densitometer (Bio-Rad) and Quantity One software (Bio-Rad).

2.5.7. Non-reducing SDS-PAGE

Non-reducing SDS-PAGE was performed essentially as described in Section 2.5.6, except the reducing agent, dithiothreitol (DTT) was omitted from the sample buffer. Protein samples were instead mixed with non-reducing SDS-PAGE sample buffer (Table 2.5) and loaded directly onto SDS polyacrylamide gels, without heat treatment.

2.5.8. Preparation of whole cell lysates for SDS-PAGE

For the preparation of *E. coli* whole cell lysates, 1 ml samples were obtained from mid-exponential phase cultures, pelleted by centrifugation (16,060 $\times g$ / 1 min / RT; Heraeus Biofuge Pico) and resuspended in PBS (Table 2.5) to 12 OD_{600nm} units. SDS-PAGE sample buffer (Table 2.5) was added to the cell suspension to a final concentration of 1 \times , before cells were lysed by heating at 95°C for 5 min as described in Section 2.5.6.

For the preparation of *S. aureus* cell lysates, 25 ml of mid-exponential phase cultures were pelleted (16,060 $\times g$ / 1 min / RT; Heraeus Biofuge Pico) and resuspended in WL buffer (Table 2.5) to 30 OD_{600nm} units. Cell lysis was induced with 0.4 mg/ml lysostaphin (Sigma) at 37°C for 30–60 min, followed by sonication with three 5 s

bursts (Setting 4; Sonifier B-12 Cell Disrupter (Branson)) on ice. Lysates were cleared by centrifugation (16,060 $\times g$ / 30 min / 4°C; Heraeus Biofuge Pico) and then 10 μ l of the supernatant was mixed with SDS-PAGE sample buffer (Table 2.5) and prepared for SDS-PAGE as described in Section 2.5.6.

Preparation of *S. cerevisiae* whole cell lysates was performed according to the method described by Kushnirov (2000). The equivalent of 2.5 OD_{600nm} units of mid-exponential phase yeast cultures were pelleted (16,060 $\times g$ / 1 min / RT; Heraeus Biofuge Pico) and resuspended in 100 μ l of sterile Milli-Q water. An equal volume of 0.2 M NaOH (final concentration of 0.1 M) was added to the cell suspension, and cells were incubated at RT with gentle rotation on a RSM-6 rotary mixer (Ratek Instruments) for 10 min. Cells were pelleted by centrifugation (16,060 $\times g$ / 1 min / RT; Heraeus Biofuge Pico) and then prepared for SDS-PAGE (Section 2.5.6) by resuspension of the cells in 50 μ l of SDS-PAGE sample buffer (Table 2.5).

2.5.9. Western blotting

2.5.9.1. Protein transfer

Proteins separated by SDS-PAGE (Section 2.5.6 and Section 2.5.7) were transferred by the wet transfer method (Towbin *et al.* 1979) onto Amersham Hybond-P polyvinylidene difluoride (PVDF) membranes (GE Healthcare) using a Mini Trans-Blot cell (Bio-Rad), according to the manufacturer's instructions. The SDS polyacrylamide gel and a methanol-activated PVDF membrane were sandwiched between two fibre pads and two pieces of filter paper, and secured by a gel holder cassette (Bio-Rad). The trans-blot cell was assembled and Western transfer was

conducted at 4°C in Western transfer buffer (Table 2.5) at 30 V overnight or at 100 V for 1 h.

2.5.9.2. Immunological detection of proteins

Unless otherwise stated, all incubations and washes were performed at RT on an orbital mixer (Ratek Instruments). PVDF membranes containing the transferred proteins (Section 2.5.9.1) were activated with 100% (v/v) methanol and then washed twice in TBS buffer (Table 2.5). In order to prevent non-specific binding of antibodies, membranes were blocked for 1 h with blocking buffer (Table 2.5), and then washed twice with TBS-Tween buffer (Table 2.5) and once with TBS. For the detection of Par proteins in *S. aureus* SK8250 cells using anti-Par peptide antibodies, 5% (v/v) normal goat serum (Sigma) was added to the blocking buffer.

Membranes were incubated with the appropriate primary antibodies diluted in blocking buffer as follows: for the detection of purified proteins or proteins from *E. coli* whole cell lysates (Section 2.5.8), a 1:1,000 dilution of mouse penta-His antibodies (Qiagen) or a 1:2,000 dilution of rabbit anti-Par antiserum was incubated with the membrane for 1 h with gentle agitation. Membranes containing *S. aureus* or *S. cerevisiae* whole cell lysates (Section 2.5.8) were incubated with either a 1:100 dilution of affinity-purified (Section 2.6.1) and preadsorbed (Section 2.6.2) rabbit anti-Par antiserum, a 1:100 dilution of anti-Par peptide antibodies (Section 2.6.3) or a 1:100 dilution of anti-HA antibodies (Abcam) at 4°C overnight with gentle rotation on a RSM-6 rotary mixer (Ratek Instruments).

Following incubation with primary antibodies, membranes were washed twice with TBS-Tween and once with TBS. Membranes were then incubated with a 1:2,000

dilution of goat-anti-mouse or goat-anti-rabbit IgG HRP-conjugated secondary antibodies (Bio-Rad) in blocking buffer, with gentle agitation for 1 h. Membranes were subsequently washed four times with TBS-Tween and detection of secondary antibodies was performed using either chromogenic or enhanced chemiluminescence (ECL) detection methods.

Chromogenic detection methods were used for the detection of purified proteins or proteins from *E. coli* whole cell lysates. HRP staining solution (Table 2.5) containing the HRP substrate, 4-chloro-1-naphthol and H₂O₂, was prepared immediately before immunodetection. Membranes were incubated in the dark with the staining solution until protein bands became visible, whereupon the reaction was stopped by rinsing the membrane with Milli-Q water. Membranes were air-dried and scanned using a GS710 Imaging Densitometer (Bio-Rad) and analysed using Quantity One software (Bio-Rad).

ECL detection methods were used for the detection of proteins from *S. aureus* or *S. cerevisiae* whole cell lysates. ECL detection was performed using the Clarity ECL Western Blotting Substrate (Bio-Rad). Detection was facilitated by mixing equal volumes of Clarity Western Peroxide Reagent (Bio-Rad) and Clarity Western Luminol/Enhancer reagent (Bio-Rad) immediately prior to immunodetection. Membranes were incubated for 5 min in the dark with the prepared solution, and then imaged using chemiluminescence imaging on a G:BOX Chemi gel documentation system (Syngene) with GeneSnap image acquisition software (Syngene).

2.6 Antibody preparation

2.6.1 Affinity purification of antiserum

When required, rabbit anti-Par antisera were affinity-purified using batch chromatography with a Par-coupled Affigel-15 activated immunoaffinity support (Bio-Rad). Affinity columns were prepared using the aqueous coupling method, as described by the manufacturer. To prepare the affinity column, 500 μ l of a 50% slurry of Affigel-15 resin were pre-equilibrated by washing three times with ice-cold Milli-Q water (1000 \times g / 2 min / 4°C; Heraeus Biofuge Primo). Purified RGS_{H6}-Par protein (approximately 1 mg in PBS) was incubated with the Affigel-15 matrix at 4°C overnight with gentle rotation on a RSM-6 rotary mixer (Ratek Instruments). Following the coupling reaction, the resin was recovered by centrifugation (1000 \times g / 2 min / 4°C; Heraeus Biofuge Primo) and the supernatant was subjected to Bradford assays (Section 2.5.5) to verify protein coupling efficiency. The Par-coupled Affigel-15 support was washed two times with ice-cold Milli-Q water (1000 \times g / 2 min / 4°C; Heraeus Biofuge Primo) to remove unbound reactants, and then resuspended in 2.5 ml of ice-cold Milli-Q water. The slurry was transferred to a column that was assembled using a 3-ml syringe packed with glass wool at the base, and the resin was washed two times with five column volumes of Milli-Q water by gravity force.

For affinity-purification of rabbit anti-Par antisera, 1 ml of antiserum was heated at 56°C for 20 min to inactivate complement factors, and then passed five times through the Par-coupled Affigel-15 column. The column was washed with five column volumes of 10 mM Tris-HCl (pH 7.5), followed by five column volumes of 10 mM Tris-HCl, 0.5 M NaCl (pH 7.5). Bound antibodies were eluted three times

with 0.5 column volumes of 4.5 M MgCl₂, 10 mM Tris-HCl (pH 7.5) into an equal volume of 2× PBS, 80% (v/v) glycerol, 1% (w/v) BSA and 0.04% (w/v) sodium azide. Affinity-purified anti-Par antibodies were stored in 50 µl aliquots at -80°C.

2.6.2 Preadsorption of antibodies with *S. aureus* cell lysates

Where applicable, affinity-purified anti-Par antibodies were further purified by preadsorption with whole cell lysates prepared from *S. aureus* SK8250 cells (Table 2.1) carrying pSK4833 (no Par) (Table 2.2). Cell lysates were prepared essentially as described in Section 2.5.8, but without the addition of SDS-PAGE sample buffer. Preadsorption of affinity-purified antibodies was conducted by incubating 500 µl of cleared *S. aureus* lysates with 10 µl of affinity-purified antibodies at 4°C overnight with gentle rotation on a RSM-6 rotary mixer (Ratek Instruments). Following preadsorption, aggregates were precipitated by centrifugation (16,060 ×g / 30 min / 4°C; Heraeus Biofuge Pico), and the supernatant containing preadsorbed affinity-purified antibodies was used immediately.

2.6.3 Production of anti-peptide antibodies

Polyclonal antibodies against two predicted antigenic peptides from RGS_{H6}-Par were raised in two individual New Zealand White rabbits by Mimotopes Pty Ltd (Victoria, Australia). Details on the selection of predicted antigenic Par peptides are provided in Section 5.2.

2.7 Plasmid segregational stability assays

Strains harbouring the plasmid to be assayed were grown overnight in liquid broth containing the appropriate antibiotic selection (Table 2.4). The following day,

stationary phase cultures were diluted 10^{-4} in fresh selective media and subcultured for 4 h. This constituted Day 0 of the assay. The culture was serially diluted in 0.1% (w/v) NaCl, and viable counts were performed on non-selective solid media. The culture was used to inoculate 10 ml of fresh broth without antibiotic selection (10^{-4} dilution) and the cells were grown overnight. Cell cultures were serially diluted and viable counts were performed. The number of generations per day was calculated using the formula $\log(\Delta\text{cfu/ml}) / \log(2)$, where $\Delta\text{cfu/ml}$ is the difference in cfu/ml between the end and start of subculture. This process was repeated until 70–260 generations of growth had been reached. After each day of subculture, 50–100 individual colonies from the non-selective viable count plates were patched in duplicate onto selective and non-selective agar plates and incubated overnight to determine the proportion of the population that retained the plasmid. Plasmid DNA was isolated from selected colonies (Section 2.4.1) and visualised by agarose gel electrophoresis (Section 2.4.3) to confirm the presence or absence of the assayed plasmid.

2.8. Electrophoretic mobility shift assays

2.8.1. Preparation and radioactive end-labelling of DNA probes

A 212 bp DNA fragment encompassing the *par-rep* intergenic region, including the seven 12-bp direct repeats of the *par* centromere-like site (nt 1689–1900, GenBank entry GU565967, Figure 1.6), was PCR-amplified (Section 2.4.4) from pSK4829 template DNA (Table 2.2) using primers SJ37 and SJ38 (Table 2.6). The PCR product was electrophoresed on an agarose gel (Section 2.4.3) and the 212 bp DNA fragment was excised and purified as described in Section 2.4.7.

For the generation of radiolabelled DNA probes, end-labelling reactions were performed using 500 ng of the purified DNA probe with 3 μ l of [γ - 32 P]-ATP (Perkin-Elmer) and 0.5 U/ μ l of T4 PNK (New England BioLabs) in 1 \times T4 PNK buffer in a total volume of 20 μ l. Labelling reactions proceeded at 37°C for 30 min, after which labelled DNA probes were purified as described in Section 2.4.7. The radioactivity of labelled probes was estimated in counts per minute (cpm) using a mini Geiger-Muller tube. Labelled DNA probes were stored in lead pots at -20°C.

2.8.2. Gel shift assays

Electrophoretic mobility shift assays (EMSAs) were performed by incubating end-labelled DNA probes (approximately 500 cpm) with 100 μ g/ml of poly(dI-dC) (Sigma) and various amounts of purified protein in EMSA binding buffer for 30 min at RT. Binding reactions were electrophoresed on a non-denaturing and non-reducing 5% (w/v) high ionic strength polyacrylamide gel (Table 2.5) in 0.5 \times TBE buffer (Table 2.5) at 100 V for 30 min. Following electrophoresis, the gel was transferred to Whatman filter paper and dried at 80°C for 1 h in a vacuum gel drying apparatus (Haeffer Scientific Instruments). The gel was then exposed to a phosphor screen (Kodak), which was scanned using a Molecular Imager FX (Bio-Rad) after overnight exposure.

DNA-binding reactions that were electrophoresed on polyacrylamide/agarose hybrid gels (Table 2.5) were performed as described above, using approximately 135 ng of unlabelled DNA probe in place of the radiolabelled probe. Binding reactions were electrophoresed on hybrid gels under the conditions described above, and gels was stained in the dark with 1 \times SYBR Safe DNA gel stain (Invitrogen) in 0.5 \times TBE

buffer with gentle agitation for 30 min at RT. Gels were imaged using UV transillumination at 302 nm on the GelDoc-It TS Imaging System (UVP).

2.9. Protein cross-linking

2.9.1. *in vitro* cross-linking of purified proteins using glutaraldehyde

in vitro cross-linking of purified RGS_{H6}-Par and mutant derivatives was performed based on the method described by Abajy *et al.* (2007) using a glutaraldehyde cross-linker. Cross-linking reactions (20 μ l) consisted of 5–6 μ g of purified RGS_{H6}-Par proteins in EMSA binding buffer (Table 2.5) along with the specified concentration of glutaraldehyde, which was prepared from a stock solution of 25% (v/v) glutaraldehyde (Electron Microscopy Services). Reactions were incubated for 10 min at RT and then quenched with 0.1 M Tris-HCl (pH 8.0). Samples were fractionated by SDS-PAGE and analysed by Coomassie Brilliant Blue staining (Section 2.5.6).

2.9.2. *in vivo* cross-linking of proteins using dithiobis(succinimidyl propionate)

in vivo cross-linking of Par proteins in *S. aureus* was performed using dithiobis(succinimidyl propionate) (DSP) (Thermo Scientific) and adapted from Ogura *et al.* (2003). 10 ml of mid-exponential phase *S. aureus* SK8250 cells (containing pSK4829 or mutant derivatives thereof) (Table 2.2) were washed and resuspended in an equal volume of PBS (Table 2.5), and then incubated with various concentrations of DSP (0, 0.1, 0.25, 0.5 and 1 mM) in dimethyl sulfoxide (DMSO) for 30 min at RT. Cells were pelleted by centrifugation (16,060 $\times g$ / 1 min / RT; Heraeus Biofuge Pico) and the cross-linking solution was removed. Cells were

resuspended in 10 ml of PBS and cross-linking reactions were quenched with 20 mM Tris-HCl (pH 7.5) for 15 min at RT. Cells were pelleted (16,060 $\times g$ / 1 min / RT; Heraeus Biofuge Pico) and then resuspended in 200 μ l of WL buffer (Table 2.5) and lysed as described in Section 2.5.8. Cell lysates were fractionated by non-reducing SDS-PAGE (Section 2.5.7) and analysed by Western blotting (Section 2.5.9) using affinity-purified (Section 2.6.1) and preadsorbed (Section 2.6.2) anti-Par antibodies. For cleavage of cross-linked complexes, samples were boiled in SDS-PAGE sample buffer (Table 2.5) containing 100 mM DTT for 10 min prior to SDS-PAGE.

in vivo cross-linking of proteins in *E. coli* was performed as described above for *S. aureus*, except 3 ml of mid-exponential phase cultures were treated with the DSP cross-linking solution, and cells were resuspended in 100 μ l of PBS (Table 2.5) following the quenching of cross-linking reactions. Cells were lysed by vortexing in non-reducing SDS-PAGE sample buffer (Table 2.5) without heating, and cross-linked proteins were analysed by non-reducing SDS-PAGE (Section 2.5.7) and Western blotting (Section 2.5.9) using rabbit anti-Par antiserum.

2.10. Yeast experiments

2.10.1. Preparation of competent *S. cerevisiae* cells

Competent *S. cerevisiae* AH109 cells were prepared according to the small-scale lithium acetate (LiAc) yeast transformation procedure in the Yeast Protocols Handbook (Clontech). Liquid YPD medium (Table 2.3) or synthetic dropout (SD) medium, SD/-Trp (Table 2.3) (50 ml), was inoculated with 3–5 single colonies of *S. cerevisiae* AH109 and cells were grown to stationary phase at 30°C with aeration at

250 rpm for approximately 20 h, as described in Section 2.1. The entire 50 ml stationary phase culture was added to 250 ml of fresh medium and cells were subcultured at 30°C with aeration at 230 rpm until mid-exponential phase (OD_{600nm} approximately 0.4–0.5). Cells were harvested by centrifugation ($2,150 \times g$ / 5 min / RT; Heraeus Biofuge Primo), washed with 30 ml of sterile Milli-Q water ($2,150 \times g$ / 5 min / RT; Heraeus Biofuge Primo), and then resuspended in 1.5 ml of freshly-prepared, sterile TE/LiAc solution (Table 2.5). Competent *S. cerevisiae* AH109 cells were transformed immediately with plasmid DNA (Section 2.10.2).

2.10.2. Transformation of yeast cells with plasmid DNA

Transformation of competent *S. cerevisiae* AH109 cells (Section 2.10.1) was performed using the small-scale LiAc yeast transformation procedure described in the Yeast Protocols Handbook (Clontech). In cases where yeast cells were to be transformed with two plasmids, both plasmids were introduced simultaneously. Each transformation reaction contained 100 μ l of competent *S. cerevisiae* AH109 cells, approximately 500 ng of each plasmid to be introduced, 0.1 mg of sheared salmon sperm DNA (Invitrogen) and 600 μ l of freshly-prepared, sterile PEG/LiAc solution (Table 2.5). Mixtures were incubated at 30°C for 30 min with shaking at 200 rpm, after which 70 μ l of DMSO was added to each mixture and mixed by gentle inversion. Cells were heat-shocked for 15 min in a 42°C water bath, and chilled on ice for 2 min. Cells were then centrifuged ($16,060 \times g$ / 30 s / RT; Heraeus Biofuge Pico) and cell pellets were resuspended in 500 μ l of sterile TE buffer (Table 2.5) for transformations with a single plasmid, and in 200 μ l for simultaneous transformations with two plasmids. A 100 μ l sample of the cell suspension was

spread onto solid SD media containing the appropriate nutritional selection, and plates were incubated at 30°C for 3–5 days until colonies appeared.

2.10.3. Yeast two-hybrid assays

Yeast two-hybrid (Y2H) assays were carried out as described by the Yeast Protocols Handbook (Clontech). Competent *S. cerevisiae* AH109 cells (Section 2.10.1) were simultaneously transformed with pGBKT7 bait and pGADT7 prey plasmid derivatives (Table 2.2) as described in Section 2.10.2. Co-transformants were selected on low-stringency selection medium (SD/-Leu/-Trp) (Table 2.3) to select for the presence of both bait and prey plasmids. Single colonies were triplicate-patched onto low-, medium- (SD/-Leu/-Trp/-His) and high- (SD/-Leu/-Trp/-His/-Ade/X- α -Gal) stringency selection media (Table 2.3) and incubated at 30°C for 3–5 days to identify co-transformants that showed activation of the reporter genes from interaction between the GAL4 BD bait and GAL AD prey fusion proteins. The presence of blue pigment on high-stringency selection medium provided an indication of α -galactosidase activity.

2.10.4. Yeast two-hybrid screening of *S. aureus* genomic DNA prey libraries

A small-scale transformation procedure (Section 2.10.2) was used to initially transform competent *S. cerevisiae* AH109 cells (Section 2.10.1) with pSK9107 (Table 2.2), which encodes the GAL4 BD-Par bait protein. *S. cerevisiae* AH109 transformants carrying pSK9107 were subsequently made competent and transformed with *S. aureus* genomic DNA libraries according to the library-scale yeast transformation procedure outlined in the Matchmaker GAL4 Two-hybrid System 3 & Libraries User Manual (Clontech). Approximately five large colonies of

S. cerevisiae cells harbouring pSK9107 were used to inoculate 150 ml of SD/-Trp broth (Table 2.3) and cells were grown to stationary phase at 30°C with aeration at 250 rpm for approximately 20 h (Section 2.1). The overnight culture was added to 1 L of fresh YPD liquid medium (Table 2.3) and cells were subcultured to mid-exponential phase (OD_{600nm} approximately 0.5) at 30°C with shaking at 250 rpm. Mid-exponential phase cultures were harvested by centrifugation (1,000 ×g / 5 min / RT; Beckman JA-14 rotor), washed with 400 ml of sterile Milli-Q water (1,000 ×g / 5 min / RT; Beckman JA-14 rotor), and then resuspended in 8 ml of freshly-prepared, sterile TE/LiAc solution (Table 2.5).

Twelve *S. aureus* genomic DNA Y2H prey libraries were generated by Schumacher *et al.* (2014) by restriction digestion of *S. aureus* genomic DNA with four restriction enzymes, and fusion with GAL4 AD in all three reading frames. Competent *S. cerevisiae* cells containing pSK9107 were mixed with 6 µg of an equal mix of the twelve genomic prey libraries in the presence of 60 ml of freshly-prepared, sterile PEG/LiAc solution (Table 2.5) and 20 mg of high molecular weight salmon sperm DNA (Sigma). The mixture was incubated at 30°C for 30 min with shaking at 200 rpm, after which 7 ml of DMSO was added and mixed with gentle inversion. Cells were subsequently heat-shocked for 15 min in a 42°C water bath, and then chilled on ice for 2 min. Cells were harvested (1,000 ×g / 5 min / RT; Beckman JA-14 rotor) and the pellet was resuspended in 7.5 ml of TE buffer (Table 2.5). A small aliquot of the resuspended cells was used to prepare dilutions (undiluted, 10⁻¹, 10⁻², 10⁻³) that were spread on SD/-Leu, SD/-Trp, and SD/-Leu/-Trp agar plates (Table 2.3) to evaluate cell viability and transformation efficiency. The remaining cell suspension was spread on medium-stringency selection agar plates (SD/-Leu/-Trp/-His) (Table

2.3) and incubated at 30°C for 5–7 days, or until colonies appeared. Colonies from medium-stringency selection plates were triplicate-patched onto low-, medium- and high- stringency selection agar and incubated at 30°C for 3–5 days to verify co-transformants that showed activation of the reporter genes from interaction between the GAL4 BD-Par bait and GAL AD-library prey fusion proteins. The presence of blue pigment on high-stringency selection medium provided an indication of α -galactosidase activity.

The number of colony-forming units (cfu) on appropriate SD/-Leu/-Trp dilution plates (containing 30–300 colonies) was counted and transformation efficiency was calculated using the formula:

$$\frac{\text{cfu} \times \text{total suspension volume } (\mu\text{l})}{\text{volume plated } (\mu\text{l}) \times \text{dilution factor} \times \mu\text{g of limiting DNA used}}$$

The total number of library clones screened was calculated using the formula:

$$\text{cfu}/\mu\text{g DNA} \times \mu\text{g of library plasmid used}$$

2.10.5. Quantitative α -galactosidase assays

Quantitative α -galactosidase assays were performed according to the α -Gal quantitative assay protocol described in the Yeast Protocols Handbook (Clontech). *S. cerevisiae* AH109 strains showing interaction between bait and prey fusion proteins were grown at 30°C with aeration at 250 rpm for approximately 20 h (Section 2.1) in 5 ml of SD/-Leu/-Trp/-His liquid medium (Table 2.3), or in SD/-Leu/-Trp (Table 2.3) for the negative control strain (which harbours pGBKT7-Lam and pGADT7-T) (Table 2.2). The optical density of overnight cultures was recorded at 600 nm as

described in Section 2.1, and 1 ml of the culture was pelleted by centrifugation (16,060 $\times g$ / 1 min / RT; Heraeus Biofuge Pico) and the supernatant transferred to fresh tubes.

α -galactosidase assays were performed by adding 16 μ l of the supernatant to 48 μ l of α -galactosidase Assay Buffer (Table 2.5) in the wells of a 96-well microplate. Reactions were incubated at 30°C for 3 h and then terminated by the addition of 136 μ l of 10 \times α -galactosidase Stop Solution (Table 2.5). The absorbance of each reaction was measured at 410 nm using a SPECTROstar *Nano* microplate reader (BMG LABTECH) and α -galactosidase activity [milliunits/(cell \times ml)] was calculated using the formula: $OD_{410nm} \times V_f \times 1000 / [(\epsilon \times b) \times t \times V_i \times OD_{600nm}]$, where t = time elapsed (in min) of incubation; V_f = final volume of assay (μ l); V_i = volume of culture medium supernatant added (μ l); OD_{600nm} = optical density of overnight culture; $(\epsilon \times b)$ = *p*-nitrophenol molar absorbtivity at 410 nm \times the light path (cm), which was calculated at 10.5 ml/ μ mol for 200 μ l-format assays (Clontech).

2.11. Microscopy

2.11.1. Immunofluorescence microscopy

Immunofluorescence microscopy (IFM) of Par proteins in *S. aureus* SK8250 and *E. coli* DH5 α cells was performed based on protocols described by Pinho and Errington (2003) and Addinall *et al.* (1996). A 500 μ l aliquot of mid-exponential phase cultures was fixed with an equal volume of 2.7% (v/v) paraformaldehyde (Electron Microscopy Services) and 0.005% (v/v) glutaraldehyde (Electron Microscopy Services) in PBS (Table 2.5) for 15 min at RT. Cells were pelleted by centrifugation

(16,060 $\times g$ / 1 min / RT; Heraeus Biofuge Pico), washed three times with an equal volume of PBS (16,060 $\times g$ / 1 min / RT; Heraeus Biofuge Pico), and then resuspended in 90–500 μ l of GTE buffer (Table 2.5). *S. aureus* cells were lysed with 60 μ g/ml of lysostaphin (Sigma), and *E. coli* cells were lysed with 20 μ g/ml of lysozyme (Sigma) for 1 min at 37°C on a poly-L-lysine (Sigma) treated multitest slide. The liquid was aspirated from the wells, and the wells were washed twice with PBS and then air-dried. Wells were rehydrated with PBS for 4 min at RT, and then blocked with 2% (w/v) BSA and 5% (v/v) normal goat serum in PBS for 15 min at RT. The blocking solution was removed, and wells were incubated at 4°C overnight with 10 μ l of the primary antibody diluted in blocking buffer. Rabbit anti-FtsZ antibodies (Prof. Elizabeth Harry, University of Technology, Sydney, Australia) were used at a 1:20,000 dilution, and anti-Par anti-peptide antibodies (Section 2.6.3) were diluted 1:100 or 1:10,000 for *S. aureus* and *E. coli* IFM, respectively. Following incubation with primary antibodies, each well was washed eight times with PBS and 10 μ l of a 1:2,000 (for *S. aureus*) or 1:5,000 (for *E. coli*) dilution of goat anti-rabbit IgG Alexa Fluor 488-conjugated antibodies (Invitrogen) were added to the wells and incubated in the dark for 1 h at RT. Wells were washed eight times with PBS and, where appropriate, DNA staining was performed by incubating the wells in the dark with 1 μ g/ml of DAPI (Sigma) for 5 min at RT. Slides were mounted in 50% (v/v) glycerol in PBS and microscopy was performed at 100 \times magnification using a Zeiss AxioImager Z.1 microscope equipped with an AxioCam MRm cooled charge-coupled device (CCD) camera controlled using Zen software (Blue edition, 2012, Carl Zeiss). Cells were visualised using brightfield microscopy, and Alexa Fluor 488 and DAPI fluorescence were visualised using filter sets 44 and

49 (Carl Zeiss), respectively. Image analysis and processing, including deconvolution of image stacks, were performed using Zen software (Blue edition, 2012, Carl Zeiss) and Adobe Photoshop CS3 Extended (version 10.0).

2.11.2. Epifluorescence microscopy

S. aureus or *E. coli* cells harbouring the relevant plasmids were grown overnight in 10 ml of selective LB-broth (Table 2.3) at 30°C and 37°C, respectively, with aeration at 220 rpm (Section 2.1). Overnight cultures were used to inoculate (1:50 dilution) 25 ml of fresh selective LB-broth, and cells were grown under the conditions described above until mid-exponential phase (OD_{600nm} approximately 0.6). Where applicable, nucleoid condensation was achieved by the addition of 25 µg/ml or 300 µg/ml of chloramphenicol to mid-exponential phase *S. aureus* and *E. coli* cultures, respectively. Incubation of the cultures in the presence of chloramphenicol was continued for 1 h or 1.5 h for *S. aureus* and *E. coli*, respectively, after which 750 µl of cells were harvested by centrifugation (16,060 ×g / 1 min / RT; Heraeus Biofuge Pico) and resuspended in 500 µl of PBS (Table 2.5). Where applicable, nucleoids were stained in the dark with 1 µg/ml of DAPI for 5 min at RT. Cells were harvested (16,060 ×g / 1 min / RT; Heraeus Biofuge Pico) and then resuspended in 250 µl of PBS, and 3 µl of the cell suspension were mounted on 2% (w/v) agarose pads prepared either directly on the slide, or within a Gene Frame (Thermo Fisher Scientific) assembled on the slide.

Epifluorescence microscopy was performed at 100× magnification using a Zeiss AxioImager Z.1 microscope equipped with an AxioCam MRm cooled charge-coupled device (CCD) camera controlled using Zen software (Blue edition, 2012,

Carl Zeiss). Cells were visualised using brightfield microscopy, and GFP, mRFPmars and DAPI fluorescence were visualised using filter sets 44, 20 and 49 (Carl Zeiss), respectively. Image analysis and processing were performed using Zen software (Blue edition, 2012, Carl Zeiss) and Adobe Photoshop CS3 Extended (version 10.0). Cell counts were performed using the Cell Tracker plugin on ImageJ software (version 1.49, National Institutes of Health, USA).

2.11.3. Fluorescence *in situ* hybridisation

2.11.3.1. Preparation of Cy3-labelled DNA probes

Cy3-labelled DNA probes for fluorescence *in situ* hybridisation (FISH) were prepared as described by Pogliano *et al.* (2001). DNA fragments were end-labelled at the 3'-terminus with 5-Propargylamino-dCTP-Cy3 (Cy3-dCTP) (Jena Bioscience) using terminal deoxynucleotidyl transferase (Thermo Fisher Scientific). End-labelling reactions consisted of 1 pmol of DNA ends, 60 pmol of Cy3-dCTP and 30 U of terminal transferase in 1× reaction buffer in a total volume of 20 µl. Reactions were conducted at 37°C for 15 min, before the enzyme was heat-inactivated at 70°C for 10 min. Cy3-labelled DNA probes were purified (Section 2.4.7) and stored in the dark at -20°C.

2.11.3.2. Fluorescence *in situ* hybridisation in *S. aureus*

The detection of pSK1 minireplicons in *S. aureus* was performed based on protocols described by Jensen and Shapiro (1999) and Lawson *et al.* (2011b). Stationary phase cultures of *S. aureus* SK8250 strains (Table 2.1) carrying the appropriate plasmid were diluted 1:50 in fresh LB-broth (Table 2.3) with antibiotic selection. Cells were

subcultured at 37°C with agitation at 220 rpm until mid-exponential phase (OD_{600nm} approximately 0.6), whereupon 500 μ l of cells were fixed with 2.6% (v/v) paraformaldehyde in 32 mM sodium phosphate buffer (pH 7.5) for 15 min at RT. Fixed cells were washed three times with PBS (Table 2.5) (16,060 $\times g$ / 1 min / RT; Heraeus Biofuge Pico), and resuspended in 90 μ l of GTE buffer (Table 2.5). 10 μ l of the cell suspension were applied to the wells of a multitest slide, air-dried, and then fixed with 100% (v/v) ethanol (-20 °C) for 1 min. Cells were lysed with 15 mg/ml of lysozyme (Sigma) at 37°C for 6 min and then rinsed with PBS and air-dried. A second cell lysis was performed with 100 μ g/ml of lysostaphin (Sigma) at 47°C for 6 min. The lysostaphin was removed and slides were rinsed with 100% (v/v) ethanol (-20°C) for 1 min and then dried at 60°C for 1 min. Wells were blocked with FISH blocking solution (Table 2.5) at 75°C for 2 min and then washed two times with 2 \times SSCT buffer (Table 2.5) at RT for 5 min each wash. Slides were then incubated with 2 \times SSCT buffer containing 50% (v/v) formamide at 37°C for 30–60 min, during which the Cy3-labelled DNA probe (Section 2.11.3.1) was denatured at 75°C for 5 min and then kept on ice. 10 μ l of FISH hybridisation solution (Table 2.5), containing approximately 100 ng of Cy3-labelled DNA probe, was added to the wells and covered with a coverslip. Slides were heated at 94°C for 2 min to denature the DNA, and hybridisation reactions proceeded at 42°C overnight in a humidity chamber. After overnight hybridisation, wells were washed two times with 2 \times SSCT buffer containing 50% (v/v) formamide at 37°C for 30 min each wash. This was followed by a wash with 2 \times SSCT buffer containing 25% (v/v) formamide and three washes with 2 \times SSCT buffer, performed at RT for 5 min each wash. Slides were briefly rinsed twice with PBS, and DNA was stained in the dark with 1 μ g/ml of 4',6-

diamidino-2-phenylindole (DAPI) for 5 min at RT. Slides were mounted in 10% (v/v) glycerol in PBS and microscopy was performed at 100× magnification using a Zeiss AxioImager Z.1 microscope equipped with an AxioCam MRm cooled charge-coupled device (CCD) camera controlled using Zen software (Blue edition, 2012, Carl Zeiss). Cells were visualised using brightfield microscopy, and Cy3 fluorescence was visualised using filter set 20 (Carl Zeiss). Image analysis and processing were performed using Zen software (Blue edition, 2012, Carl Zeiss) and Adobe Photoshop CS3 Extended (version 10.0).

CHAPTER 3

Functional significance of pSK1 Par domains

3.1. Introduction

pSK1 Par was shown to enhance plasmid segregational stability (Simpson *et al.* 2003) via a single protein using a mechanism that distinguishes itself from the three characterised plasmid partitioning systems. Structural predictions indicate three putative domains: an N-terminal helix-turn-helix (HTH) domain (aa 3–24), a central coiled-coil (CC) domain (aa 132–155), and an acidic, disordered C-terminal domain (CTD) (aa 156–245) (Simpson *et al.* 2003). Previous functional studies have revealed that the HTH domain is involved in DNA-binding to the centromere-like site of pSK1 *par* (LeBard 2005, Lai 2008), while the CC domain is required for Par multimerisation (Lai 2008). This chapter details experiments that were performed to elucidate the contribution of the disordered CTD to Par DNA-binding and multimerisation activities, and explores potential inter- and intra-molecular interactions between Par domains.

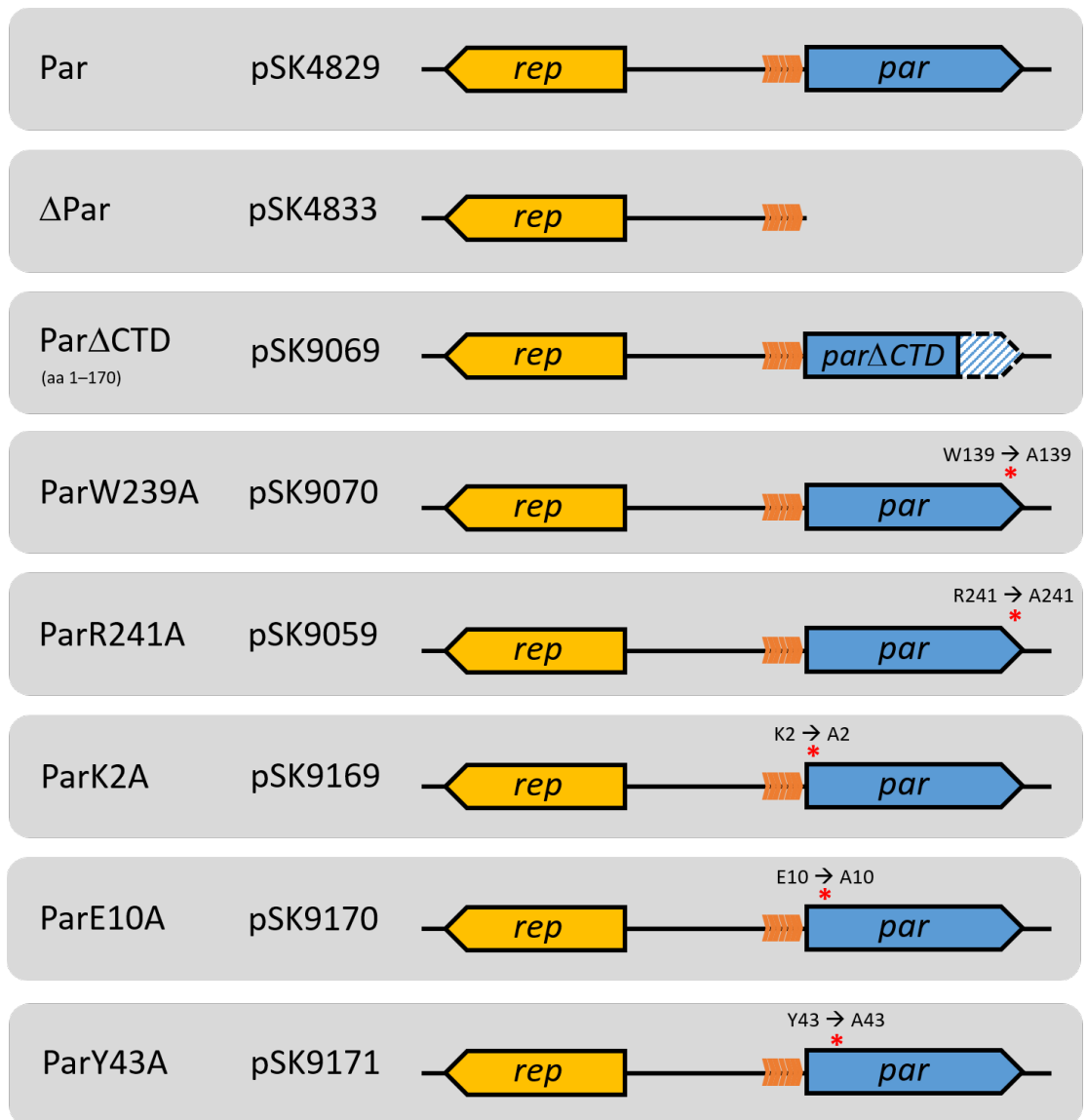
3.2. Functional significance of the Par C-terminal domain

3.2.1. Construction of pSK1 minireplicons expressing Par CTD mutants

Par functionality has been demonstrated by plasmid segregational stability assays, which show that a pSK1 minireplicon containing pSK1 *par* (pSK4829) is substantially more stable in *S. aureus* populations compared to a *par*-deficient pSK1 minireplicon (pSK4833) (Table 2.2, Figure 3.1) (Simpson *et al.* 2003). Therefore, in

Figure 3.1 Graphical representation of pSK1 *par* mutants generated in this study

Par protein mutants generated in this study are listed, along with the names of pSK1 minireplicons encoding the respective mutant protein. The genetic organisation of the wild-type *par-rep* region of pSK1 is shown with block arrows representing the *rep* (yellow) and *par* (blue) genes. Orange arrowheads represent the seven 12-bp repeats of the *par* centromere-like site to which Par binds. For Par Δ CTD, deletion of the last 228 nucleotides of the *par* sequence (nt 1498–1725 of pSK1, GenBank Accession Number GU565967) is denoted by a hatched block arrow with dashed lines. Red stars denote the relative positions of alanine codon substitutions introduced for the generation of Par point mutations.



order to determine whether the CTD of Par is functionally important, CTD mutants were generated such that their functionality could be assessed using plasmid segregational stability assays. Studies conducted as part of an honours project had generated two Par CTD mutants, including a CTD deletion of residues 161–245, as well as a CTD point mutant, ParR241A, which was generated by site-directed mutagenesis of the conserved R241 residue identified by a multiple sequence alignment of the Par CTD with similar proteins (Supplementary Figure S1) (Chan 2011). However, the C-terminally truncated mutant was not able to be overproduced in *E. coli* BL21 cells (possibly due to protein degradation) and hence the extent of the CTD deletion was altered to include a further nine amino acids of the CTD, resulting in a truncated protein encompassing residues 1–170 (Par Δ CTD).

In order to generate a pSK1 minireplicon that encodes Par Δ CTD for plasmid segregational stability assays, a nucleotide fragment encompassing pSK1 *rep* and encoding the first 170 residues of Par was amplified by PCR (Section 2.4.4) from pSK4829 template DNA (Table 2.2) using primers NFRepDwn4829 and HC8 (Table 2.6). The resulting amplicon was gel-purified (Section 2.4.7) and then restricted with *Bam*HI and *Hind*III (Section 2.4.6). The restricted amplicons were purified (Section 2.4.7) and then ligated (Section 2.4.11) to the similarly digested pWE180 plasmid (Table 2.2) that had been dephosphorylated with Antarctic phosphatase (Section 2.4.10). The ligations were used to transform *E. coli* DH5 α cells to ampicillin resistance (Section 2.3.2). Plasmid DNA was isolated from selected transformants (Section 2.4.1), and clones carrying recombinant plasmid DNA were identified by restriction digestion of the plasmids with *Bam*HI and *Hind*III (Section 2.4.6) and subsequent agarose gel electrophoresis (Section 2.4.3) of the digestion reactions.

Recombinant plasmids were sequenced (Section 2.4.14) using primers NFRepDwn4829, HC2, HC3 and HC11 (Table 2.6), and the resultant pSK1 minireplicon containing the correct sequence encoding Par Δ CTD was named pSK9069 (Table 2.2).

Since ParR241A was shown to retain some functionality (Chan 2011), a second CTD mutant, ParW239A, was generated to determine whether mutation of the conserved W239 residue of the CTD would impart a greater loss of functionality. Similar to R241, W239 was identified as a conserved residue by a multiple sequence alignment of the Par CTD with Par homologues (Chan 2011) (Supplementary Figure S1). Alanine substitution of W239 was generated by site-directed mutagenesis (Section 2.4.5) of pSK4829 template DNA (Table 2.2) using primers HC9 and HC10 (Table 2.6). A silent *NruI* restriction site was incorporated into each of the primers to facilitate screening of mutagenised plasmid DNA. Mutagenesis reactions were used to transform *E. coli* DH5 α cells to ampicillin resistance (Section 2.3.2) and plasmid DNA was isolated from selected transformants (Section 2.4.1). Isolated plasmids were subjected to restriction endonuclease digestion by *NruI* (Section 2.4.6) followed by agarose gel electrophoresis (Section 2.4.3) in order to identify potential plasmid mutants. The W239A mutation was verified by DNA sequencing (Section 2.4.14) using primers NFRepDwn4829, HC2, HC3 and HC11 (Table 2.6), and the pSK1 minireplicon encoding ParW239A was designated pSK9070 (Table 2.2). An overview of the Par CTD mutants used in this study is provided in Figure 3.1.

3.2.2. Effect of Par CTD mutations on plasmid segregational stability

To determine the functionality of the Par CTD mutants, pSK9069 (*par* Δ CTD), pSK9059 (*parR241A*) and pSK9070 (*parW239A*) (Table 2.2), were each individually introduced into *S. aureus* RN4220 cells by electroporation (Section 2.3.4), and plasmid segregational stability assays were performed (Section 2.7). Figure 3.2A shows that after five days (approximately 75 generations) of serial subculture in the absence of antibiotic selection, approximately 52 \pm 5% of the bacterial population retained pSK4829 (*par*), whereas pSK4833 (Δ *par*) was completely lost from the population by Day 4. The assays also revealed that the CTD mutations negatively affected Par function; Par Δ CTD and ParW239A were both entirely non-functional, with plasmid loss comparable to the loss of pSK4833 (Δ *par*) from the population (Figure 3.2A). In comparison, pSK9059, which encodes ParR241A, was less stable than pSK4829 (*par*), but more stable than pSK4833 (Δ *par*), with approximately 35 \pm 5% of the population retaining the plasmid after five days (Figure 3.2A), which suggests that ParR241A retains some functionality.

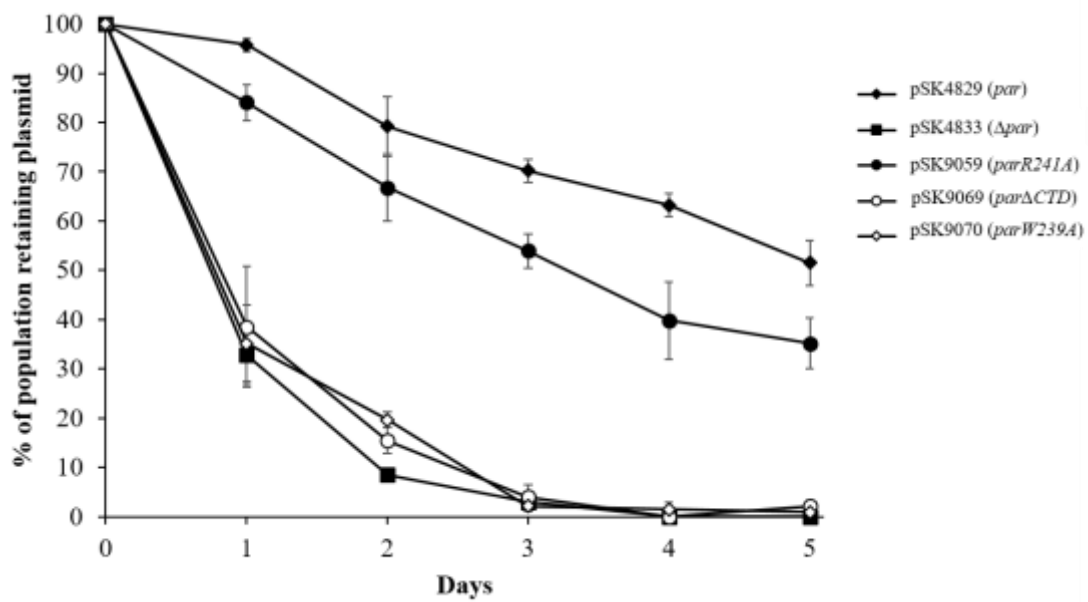
To ensure that plasmid instability was due to loss of Par function rather than absence of Par protein, the production of Par CTD mutants in *S. aureus* was confirmed by Western blotting using anti-Par antibodies (Section 2.5.9). Chromogenic detection methods provided insufficient sensitivity for the immunodetection of Par (data not shown), and hence all subsequent Western blotting of Par in *S. aureus* was performed using enhanced chemiluminescent (ECL) detection methods. However, when rabbit anti-Par antiserum was used for the immunodetection of Par in *S. aureus*, the increased sensitivity of ECL detection resulted in significant background

Figure 3.2 Effect of Par CTD mutations on plasmid segregational stability

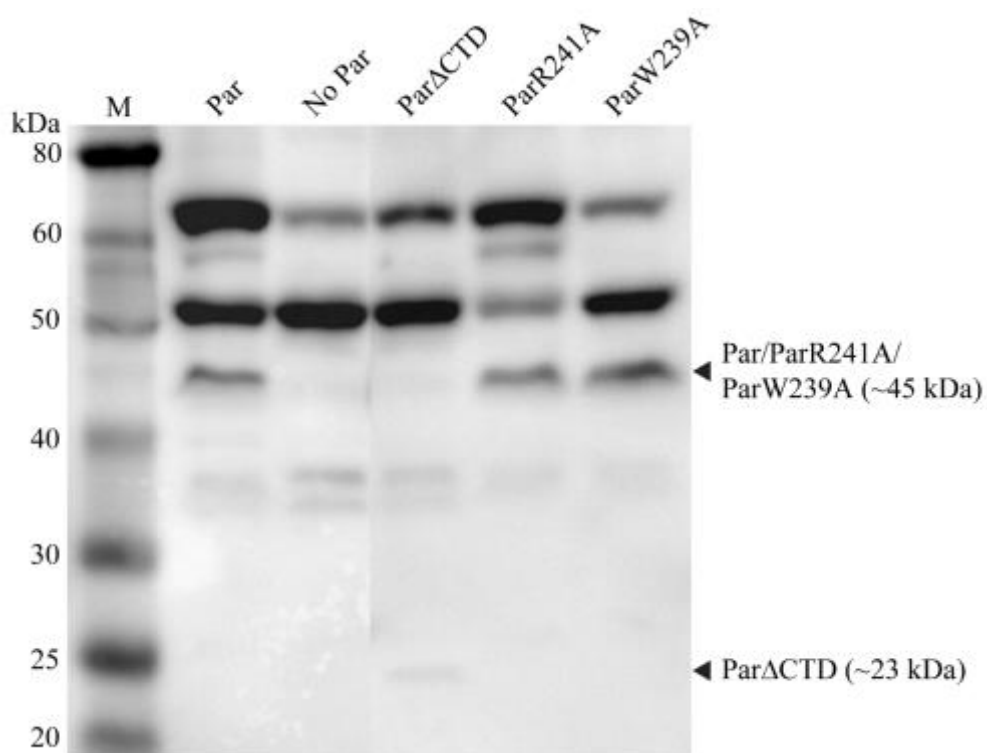
A. Plasmid segregational stability assay of pSK1 minireplicons encoding Par CTD mutants. The retention of pSK1 minireplicons pSK4829 (*par*) (◆), pSK4833 (Δ *par*) (■), pSK9059 (*parR241A*) (●), pSK9069 (*par* Δ CTD) (○) and pSK9070 (*parW239A*) (◇) in *S. aureus* RN4220 cells was determined as described in Section 2.7. Five days of serial subculture represents approximately 75 generations. Data are normalised to 100% plasmid retention on Day 0. The averages of at least three independent assays are shown. Error bars represent standard error of the mean.

B. Immunodetection of Par CTD mutants in *S. aureus* by Western blotting. Cleared lysates from *S. aureus* SK8250 cells carrying pSK4829 (Par), pSK4833 (No Par), pSK9069 (Par Δ CTD), pSK9059 (ParR241A) or pSK9070 (ParW239A) were fractionated on a 10% (w/v) SDS polyacrylamide gel (Section 2.5.6) and subjected to Western blotting (Section 2.5.9) using affinity-purified anti-Par antibodies (Section 2.6.1) that had been preadsorbed against *S. aureus* SK8250 cell lysates (Section 2.6.2). Lane M contains prestained protein markers, with marker sizes indicated in kDa on the left of the blot. Positions of relevant proteins and their approximate measured sizes are indicated by black arrowheads.

A.



B.



signals, which obscured the Par protein band and rendered interpretation of the blots difficult (data not shown). Therefore, the anti-Par antiserum was affinity-purified and preadsorbed against *S. aureus* SK8250 lysates (Table 2.1), as described in Sections 2.6.1 and 2.6.2. This process reduced background signals and, as shown in Figure 3.2B, Western blotting using affinity-purified and preadsorbed anti-Par antiserum confirmed the production of Par and all Par CTD mutants in the *S. aureus* strains assayed. Par, ParR241A and ParW239A appeared as 45 kDa bands of similar intensity, and Par Δ CTD appeared as a faint band of approximately 23 kDa (Figure 3.2B). Notably, the 45 kDa protein size determined for full-length Par proteins is larger than their expected size of 29 kDa, which is consistent with observations from previous studies (Simpson *et al.* 2003, LeBard 2005, Figgett 2007, Lai 2008). On the other hand, Par Δ CTD migration was more consistent with its predicted size of 20 kDa.

3.3. Overproduction and purification of Par CTD mutants

3.3.1. Construction of expression plasmids for Par CTD mutants

In order to further investigate the contribution of the CTD to Par function, Par CTD mutants were overproduced and purified for *in vitro* analysis of DNA-binding and multimerisation activities. Protein overproduction was performed using the pQE30 expression vector (Table 2.2), which contains sequences encoding a N-terminal RGS₆ tag upstream of the multiple cloning site (MCS) to facilitate immunodetection using anti-polyhistidine antibodies and protein purification using nickel-nitrilotriacetic acid (Ni²⁺-NTA) metal affinity chromatography. Regulated gene expression is provided by an IPTG-inducible T5 promoter/*lac* operator element

and a *trans*-acting Lac repressor, encoded by *lacI*, on a compatible co-resident repressor plasmid, pREP4 (Table 2.2).

To generate an overexpression plasmid encoding RGSH₆-Par Δ CTD, the coding region for amino acids 1–170 of Par was amplified by PCR (Section 2.4.4) from pSK9069 (Table 2.2) using primers 879BamHI and HC8 (Table 2.6), and then restricted with *Bam*HI and *Hind*III (Section 2.4.6). The doubly-digested amplicon was purified (Section 2.4.7) and ligated to restricted and dephosphorylated (Section 2.4.10) *Bam*HI and *Hind*III sites of pQE30, to be in-frame with the vector-encoded N-terminal RGSH₆ tag. *E. coli* DH5 α cells (Table 2.1) carrying the pREP4 repressor plasmid were transformed with the ligation reaction and selected for ampicillin and kanamycin resistance (Section 2.3.2). Plasmid DNA was isolated from selected transformants (Section 2.4.1), restricted with *Bam*HI and *Hind*III (Section 2.4.6), and then analysed by agarose gel electrophoresis (Section 2.4.3) to identify recombinant plasmids. Restricted plasmids displaying the anticipated restriction profile were verified by DNA sequencing (Section 2.4.14) using primers 879BamHI and HC11 (Table 2.6). The overexpression plasmid encoding RGSH₆-Par Δ CTD was named pSK9071 (Table 2.2).

Overexpression plasmids encoding RGSH₆-ParR241A and RGSH₆-ParW239A were constructed by site-directed mutagenesis (Section 2.4.5) of pSK5344, which contains *RGSH₆-par* in pQE30 (Table 2.2). Site-directed mutagenesis was performed essentially as described in Section 3.2.1 for the construction of pSK9070 (Table 2.2), except that primer pairs HC6/HC7 and HC9/HC10 (Table 2.6) were used to generate nucleotide substitutions for the R241A and W239A mutations, respectively.

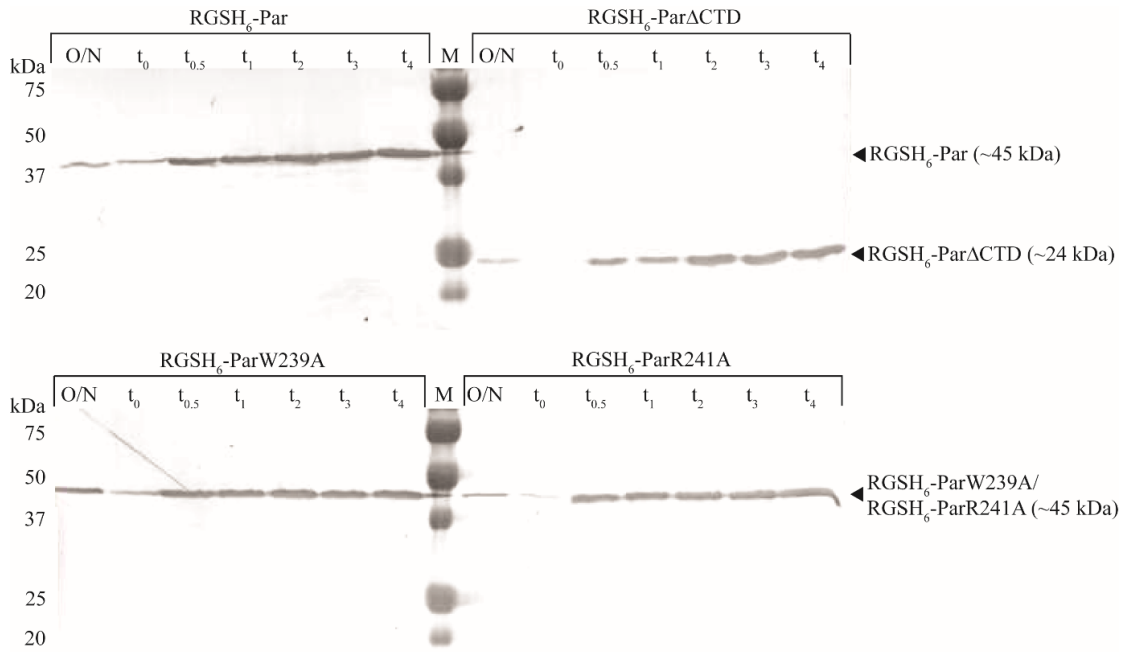
Mutagenesis reactions were then used to transform *E. coli* DH5 α cells carrying the repressor plasmid, pREP4, to ampicillin and kanamycin resistance (Section 2.3.2). *Nru*I restriction digestion (Section 2.4.6) was used to identify plasmids that had incorporated the W239A mutation. Overexpression plasmids encoding RGS_{H6}-ParR241A and RGS_{H6}-W239A were verified by DNA sequencing (Section 2.4.14) using primers 879BamHI and HC11 (Table 2.6), and were named pSK9073 and pSK9074, respectively (Table 2.2).

3.3.2. Overproduction of Par CTD mutants

In order to obtain sufficient quantities of purified protein for subsequent *in vitro* studies on Par DNA-binding and multimerisation activities, the pREP4 repressor plasmid and one of each of the overexpression plasmids generated in Section 3.3.1, pSK9071, pSK9073 or pSK9074 (Table 2.2), were used to sequentially transform the protease-deficient *E. coli* strain BL21 (Table 2.1) by heat shock (Section 2.3.2). Small-scale protein overproduction studies were initially performed as described in Section 2.5.1, using induction conditions of 100 μ M IPTG at 30°C, which were the conditions established for the overproduction of RGS_{H6}-Par from pSK5344 (Table 2.2) (LeBard 2005). Aliquots of the culture were taken pre-induction (t_0) and post-induction at hourly intervals for 4 h (t_{1-4}). Whole cell extracts were prepared from the samples (Section 2.5.8) and analysed by SDS-PAGE (Section 2.5.6) and Western blotting (Section 2.5.9) to confirm protein production. As shown in Figure 3.3, induction of Par protein production was evident, with small amounts of Par protein detected in uninduced cells, and production of higher quantities of recombinant proteins apparent within 0.5 h of induction. Full-length RGS_{H6}-Par proteins were

Figure 3.3 Overproduction of Par CTD mutant proteins in *E. coli*

Immunodetection of overproduced Par and Par CTD mutant proteins in *E. coli* BL21 cells by Western blotting. Protein overproduction for RGS_{H6}-Par, RGS_{H6}-Par Δ CTD, RGS_{H6}-ParR241A, and RGS_{H6}-ParW239A, was induced with 100 μ M IPTG for 4 h as described in Section 3.3.2. Aliquots of the cultures were sampled at various time points and whole cell lysates (Section 2.5.8) were fractionated on 10% (w/v) SDS polyacrylamide gels (Section 2.5.6) and analysed by Western blotting using rabbit anti-Par antiserum (Section 2.5.9). O/N: uninduced cells from overnight cultures; t₀: cells sampled pre-induction; t_{0.5}, t₁, t₂, t₃, t₄: cells sampled 0.5, 1, 2, 3 and 4 h post-induction, respectively. Lane M contains prestained protein markers, with marker sizes indicated in kDa on the left of each blot. Positions of overproduced proteins and their approximate measured sizes are indicated by black arrowheads.



detected as protein bands of approximately 45 kDa, whereas RGS_{H6}-Par Δ CTD appeared as a 24 kDa band (Figure 3.3). The blots did not show any visible protein degradation for up to 4 h post-induction (Figure 3.3).

3.3.3. Small-scale purification of Par CTD mutants under non-denaturing conditions

Previous studies have employed denaturing conditions for the purification of overproduced RGS_{H6}-Par proteins, as purification under native, or non-denaturing, conditions did not yield sufficient quantities of purified protein (LeBard 2005, Figgett 2007, Lai 2008). To determine whether the Par CTD mutant proteins could be purified under non-denaturing conditions, RGS_{H6}-Par, RGS_{H6}-Par Δ CTD, RGS_{H6}-ParR241A and RGS_{H6}-ParW239A were overproduced in small-scale overexpression cultures of *E. coli* BL21 with 100 μ M IPTG, as described in Section 3.3.2. Small-scale protein purifications were subsequently performed under non-denaturing conditions using Ni²⁺-NTA metal affinity chromatography (Section 2.5.2). In order to evaluate the protein purification process, samples were taken throughout the procedure, and included the cleared lysate prior to incubation with the Ni²⁺-NTA resin (to check cell lysis and confirm the presence of overproduced protein in the soluble fraction of the cells), the unbound proteins after incubation with the Ni²⁺-NTA resin (to confirm that Par had bound to the resin and that other proteins did not bind non-specifically), and the proteins released after each wash and elution step. Protein fractions were analysed by SDS-PAGE and Coomassie Brilliant Blue staining (Section 2.5.6).

Figure 3.4 shows overproduced protein bands (migrating as approximately 45 kDa for full-length RGSH₆-Par proteins, and approximately 23 kDa for RGSH₆-Par Δ CTD) in the whole cell lysates of cells sampled 3.5 h post-induction. Following two brief washes, RGSH₆-Par Δ CTD, RGSH₆-ParR241A and RGSH₆-ParW239A proteins were detected in the elution fractions (Figures 3.4B–D), which indicates that they could be purified under non-denaturing conditions, albeit with low efficiency. Consistent with previous findings (LeBard 2005), RGSH₆-Par could not be purified under non-denaturing conditions, possibly due to poor binding to the Ni²⁺-NTA resin, since the 45 kDa protein band was present in the unbound fraction but absent in the washes and elutions (Figure 3.4A). Therefore, for the purposes of consistency, denaturing conditions were used for the purification of all Par protein derivatives (see Section 3.3.4 below).

3.3.4. Large-scale overproduction and purification of Par CTD mutants under denaturing conditions

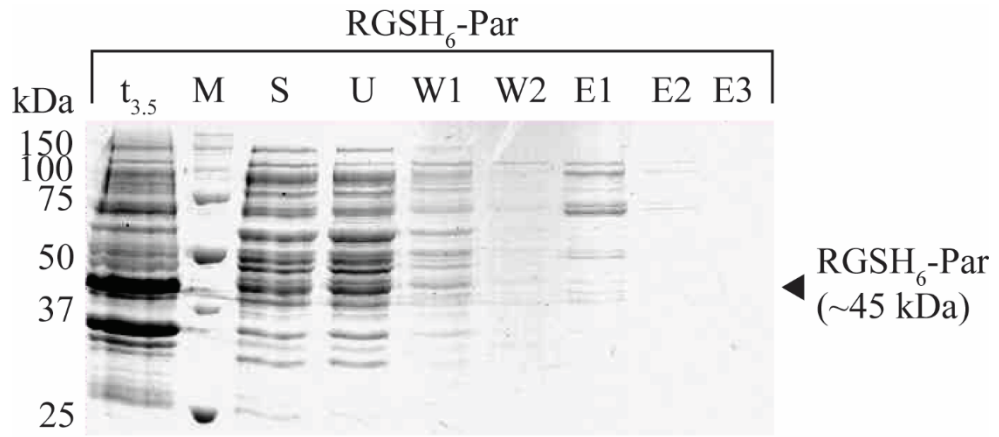
For the purification of large quantities of protein required for downstream experiments, RGSH₆-Par, RGSH₆-Par Δ CTD, RGSH₆-ParR241A and RGSH₆-ParW239A were overproduced in large-scale overexpression cultures as described in Section 2.5.1, using 100 μ M IPTG induction at 30°C for 3.5 h. In order to confirm protein overproduction, samples of the culture were taken pre-induction (t_0) and at the conclusion of the induction period ($t_{3.5}$). The samples and remaining cultures were harvested and cell pellets were stored at -80 °C until required.

Overproduced proteins were purified by Ni²⁺-NTA metal affinity chromatography under denaturing conditions (Section 2.5.3). As performed in Section 3.3.3, samples

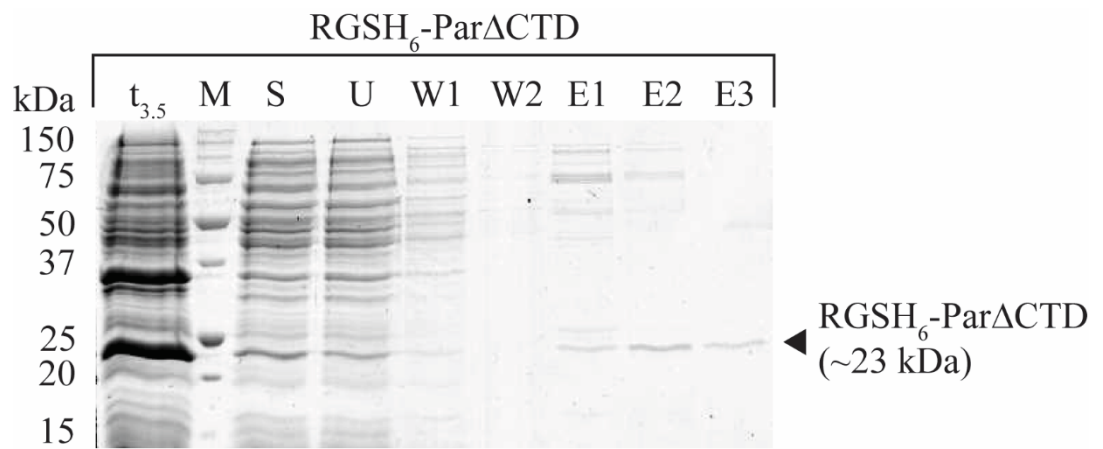
Figure 3.4 Small-scale overproduction and purification of RGS_{H6}-tagged Par proteins under non-denaturing conditions

Coomassie-stained 10% (w/v) SDS polyacrylamide gels showing the overproduction and purification process for RGS_{H6}-Par **(A)**, RGS_{H6}-Par Δ CTD **(B)**, RGS_{H6}-ParW239A **(C)**, and RGS_{H6}-ParR241A **(D)**. RGS_{H6}-tagged proteins were overproduced in *E. coli* BL21 cells with 100 μ M IPTG induction for 3.5 h (Section 2.5.1) and purified using Ni²⁺-NTA resin under non-denaturing conditions (Section 2.5.2). Protein fractions were collected at each stage of the protein purification process and analysed by SDS-PAGE and Coomassie Brilliant Blue staining (Section 3.3.3). t_{3.5}: whole cell lysates from cells 3.5 h post-induction; S: supernatant from lysed *E. coli* cells; U: unbound fraction following incubation of cleared lysate with Ni²⁺-NTA resin; W1: fraction obtained after first wash with Native Protein Wash Buffer A; W2: fraction obtained after second wash with Native Protein Wash Buffer A; E1: first elution; E2: second elution; E3: third elution. Lane M contains prestained protein markers, with marker sizes indicated in kDa on the left of each gel; for clarity, some marker sizes are omitted (Marker sizes from top to bottom: 250, 150, 100, 75, 50, 37, 25, 20, 15, 10 kDa). Positions of RGS_{H6}-tagged Par proteins and their approximate measured sizes are indicated by black arrowheads.

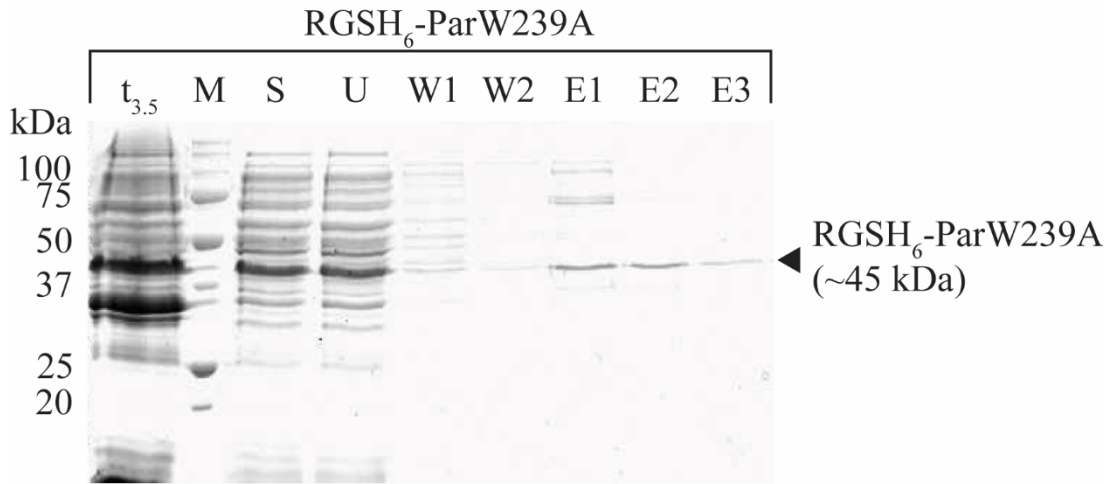
A.



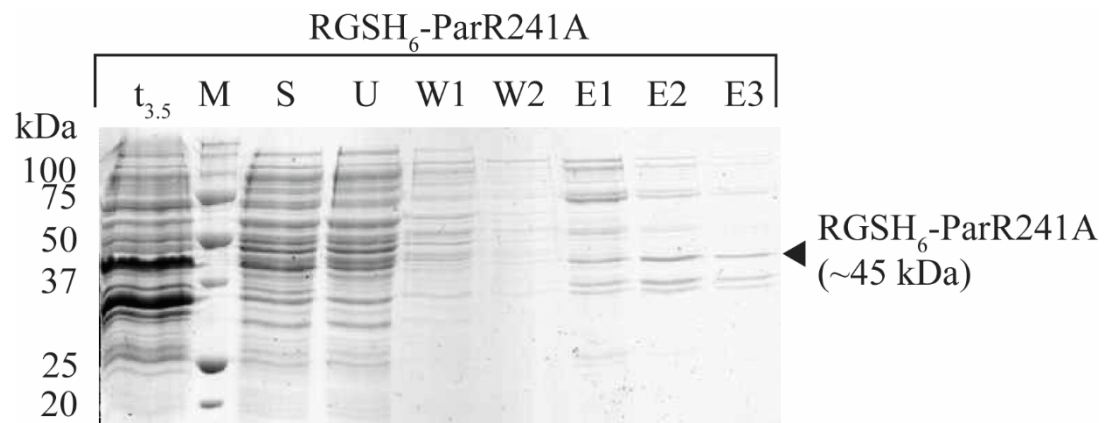
B.



C.



D.



were taken from each stage of the purification procedure, and protein fractions were analysed by SDS-PAGE and Coomassie Brilliant Blue staining (Section 2.5.6). As illustrated in Figures 3.5A, C and D, an overproduced protein band of approximately 45 kDa was observed in whole cell extracts from cells that had induced expression of *RGSH₆-par*, *RGSH₆-parR241A* and *RGSH₆-parW239A* for 3.5 h ($t_{3.5}$). An overproduced protein band for *RGSH₆-Par Δ CTD* was not visible by Coomassie Brilliant Blue staining of cell lysates from induced cells (Figure 3.5B). During the protein purification process, most proteins were removed in the first wash step (Figures 3.5A–D, lane W1), with some of the *RGSH₆*-tagged proteins removed in subsequent washes (Figures 3.5A–D, lanes W2–W4). The elution samples showed relatively pure protein of the expected sizes (approximately 45 kDa for full-length *RGSH₆-Par* proteins and approximately 25 kDa for *RGSH₆-Par Δ CTD*), with the exception of an approximately 30 kDa protein that was co-purified with the *RGSH₆*-tagged proteins (Figures 3.5A–D, lane E, asterisk).

To encourage refolding of the eluted proteins from their denatured states and to ensure buffer compatibility for downstream experiments, buffer exchange was performed using PD-10 desalting columns (Section 2.5.4) to replace the elution buffer (Table 2.5) with EMSA binding buffer or PBS (Table 2.5). To ensure that the purified and desalted proteins were indeed Par proteins, the desalted proteins were electrophoresed on polyacrylamide gels (Section 2.5.6) and immunologically detected by Western blotting (Section 2.5.9) using rabbit anti-Par antiserum. The Western blot shown in Figure 3.5E confirms the presence of *RGSH₆*-tagged proteins of the expected sizes in the final protein preparations. *RGSH₆-Par*, *RGSH₆-ParW239A* and *RGSH₆-ParR241A* appeared as protein bands of approximately 45

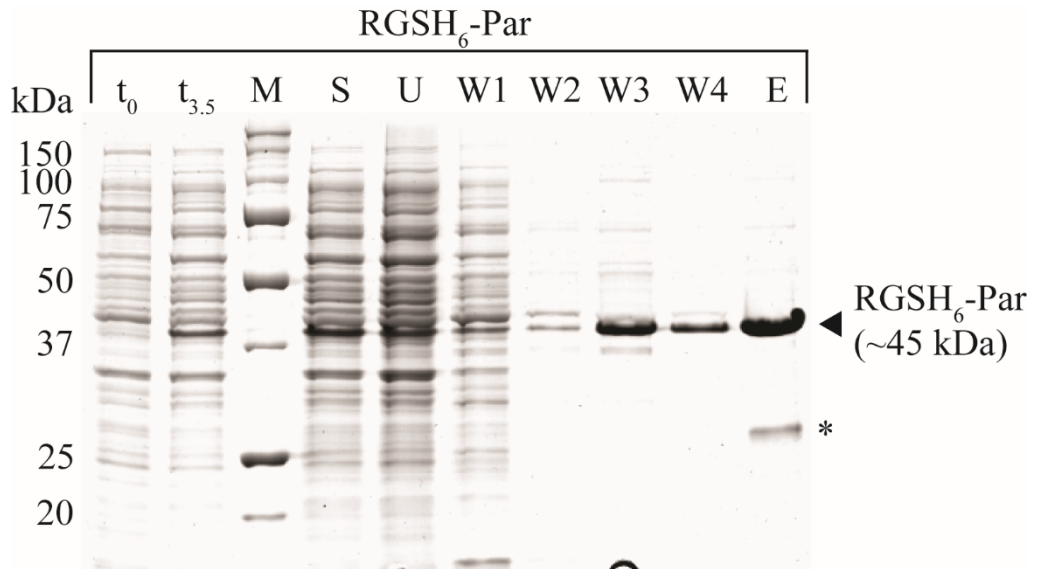
Figure 3.5 Large-scale overproduction and purification of RGSH₆-tagged Par proteins under denaturing conditions

Coomassie-stained 10% (w/v) SDS polyacrylamide gels showing the overproduction and purification process for RGSH₆-Par **(A)**, RGSH₆-Par Δ CTD **(B)**, RGSH₆-ParW239A **(C)**, and RGSH₆-ParR241A **(D)**. RGSH₆-tagged proteins were overproduced in *E. coli* BL21 cells with 100 μ M IPTG induction for 3.5 h (Section 2.5.1) and purified using Ni²⁺-NTA resin under denaturing conditions (Section 2.5.3). Protein fractions were collected at each stage of the protein purification process and analysed by SDS-PAGE and Coomassie Brilliant Blue staining (Section 3.3.4). t₀: whole cell lysates from cells pre-induction; t_{3.5}: whole cell lysates from cells 3.5 h post-induction; S: supernatant from lysed *E. coli* cells; U: unbound fraction following incubation of cleared lysate with Ni²⁺-NTA resin; W1: fraction obtained after first wash with Denaturing Protein Wash Buffer I; W2: fraction obtained after second wash with Denaturing Protein Wash Buffer I; W3: fraction obtained after first wash with Denaturing Protein Wash Buffer II; W4: fraction obtained after second wash with Denaturing Wash Buffer II; E: elution. Lane M contains prestained protein markers, with marker sizes indicated in kDa on the left of each gel; for clarity, some marker sizes are omitted (Marker sizes from top to bottom: 250, 150, 100, 75, 50, 37, 25, 20, 15, 10 kDa). Positions of RGSH₆-tagged Par proteins and their approximate measured sizes are indicated by black arrowheads. The position of a co-purified contaminant protein is indicated by an asterisk.

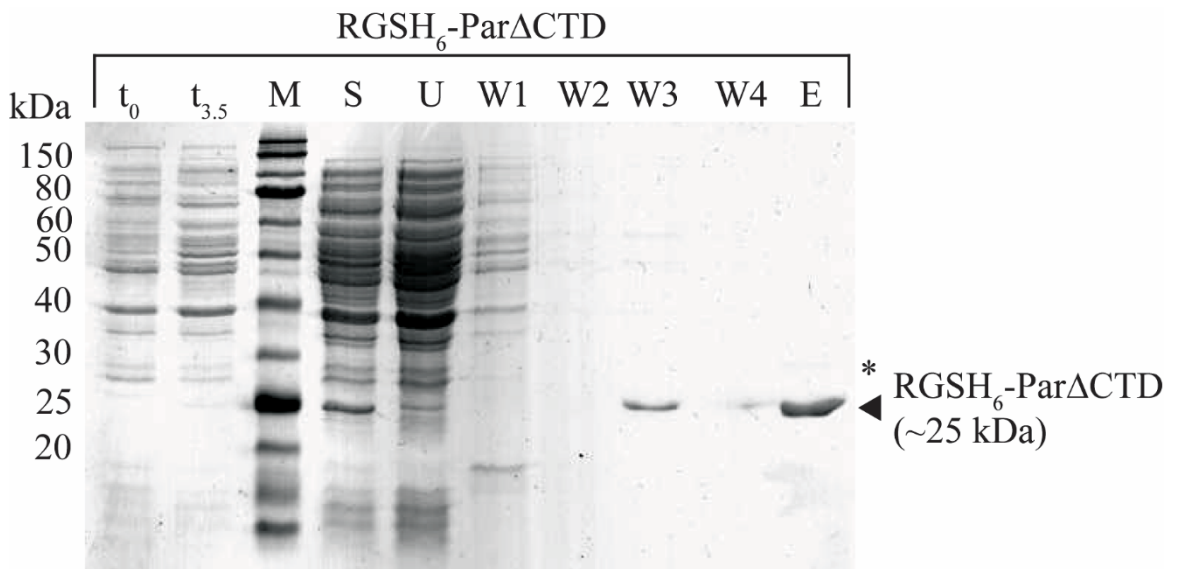
E. Western blot of purified RGSH₆-tagged Par proteins following buffer exchange. RGSH₆-tagged Par proteins were purified under denaturing conditions and then desalted and re-buffered in EMSA binding buffer as described in Section 3.3.4. Desalted proteins were fractionated on a 10% (w/v) SDS polyacrylamide gel (Section

2.5.6) and transferred to a PVDF membrane for Western blotting (Section 2.5.9) using rabbit anti-Par antiserum. Lane M contains prestained protein markers, with marker sizes indicated in kDa on the left of the blot. Positions of desalted proteins and their approximate measured sizes are indicated by black arrowheads.

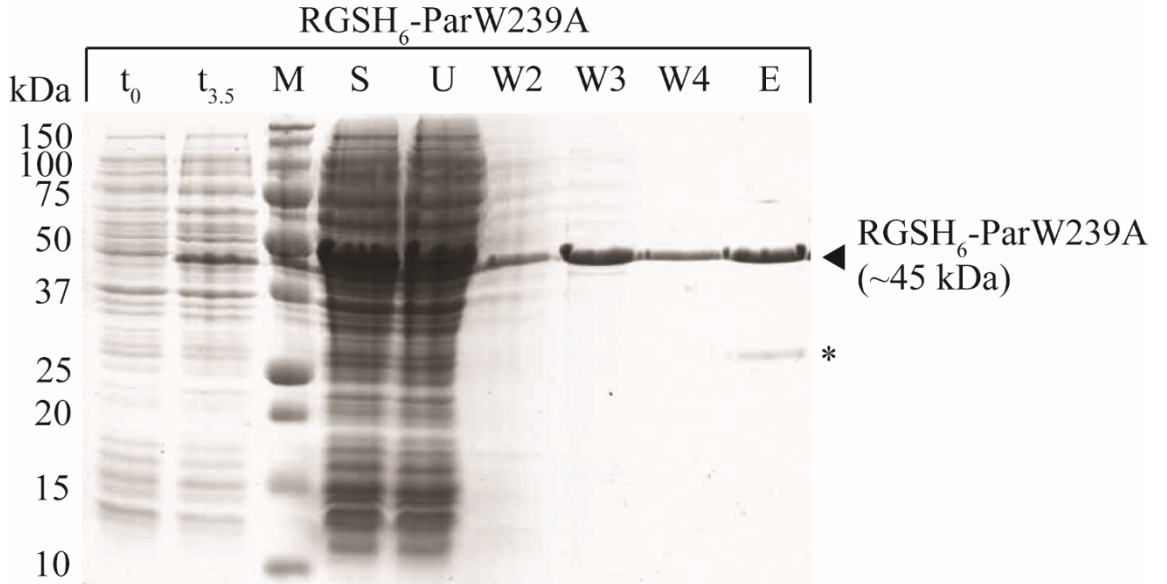
A.



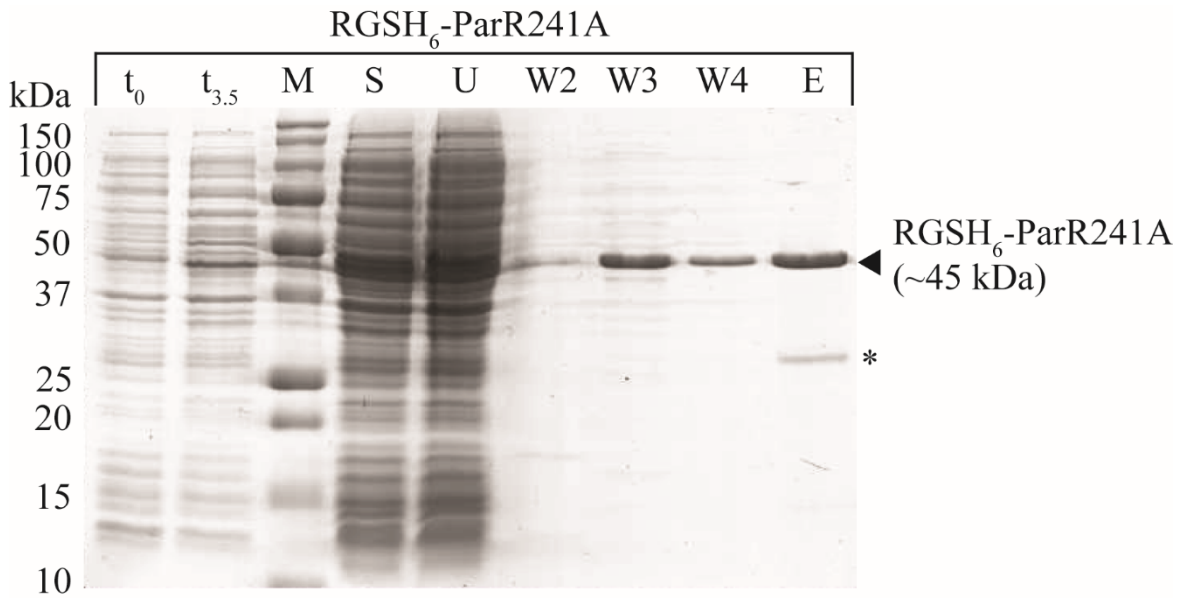
B.



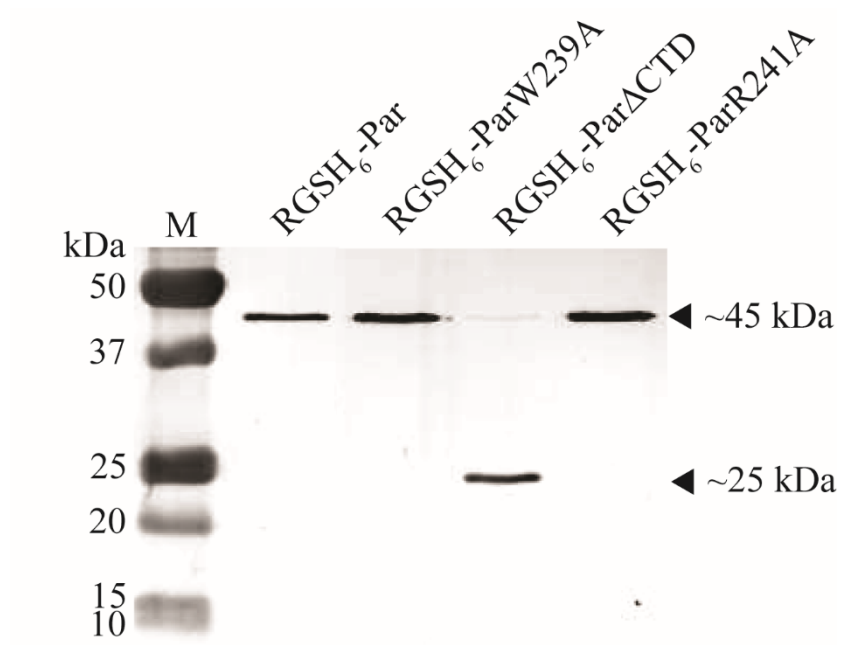
C.



D.



E.



kDa, while RGSH₆-Par Δ CTD appeared as a 25 kDa band (Figure 3.5E). No protein degradation products were detected, since only a single protein band was observed for each purified protein sample (Figure 3.5E). The low-intensity band of around 45 kDa in the RGSH₆-Par Δ CTD lane most likely represents cross-contamination with other full-length RGSH₆-Par proteins during the gel loading process. The Western blot also suggests that the 30 kDa protein band that was co-purified with RGSH₆-tagged proteins (Figures 3.5A–D) was most likely a contaminating protein. The desalted proteins were quantified using Bradford assays (Section 2.5.5), which indicated final protein concentrations of 300–500 μ g/ml (corresponding to protein yields of 0.9–1.5 mg/L of expression culture), which was deemed sufficient for use in downstream *in vitro* experiments.

3.4. DNA-binding activity of Par CTD mutants

In order to establish whether the CTD contributes to DNA-binding, electrophoretic mobility shift assays (EMSAs) (Section 2.8) were performed on Par CTD mutants. EMSAs rely on the detection of changes in the migration of a labelled DNA probe through a polyacrylamide gel. Free, unbound DNA probes migrate further on a gel compared to protein-bound DNA probes, and hence EMSAs can be used to determine whether a particular protein binds to a specific labelled DNA sequence.

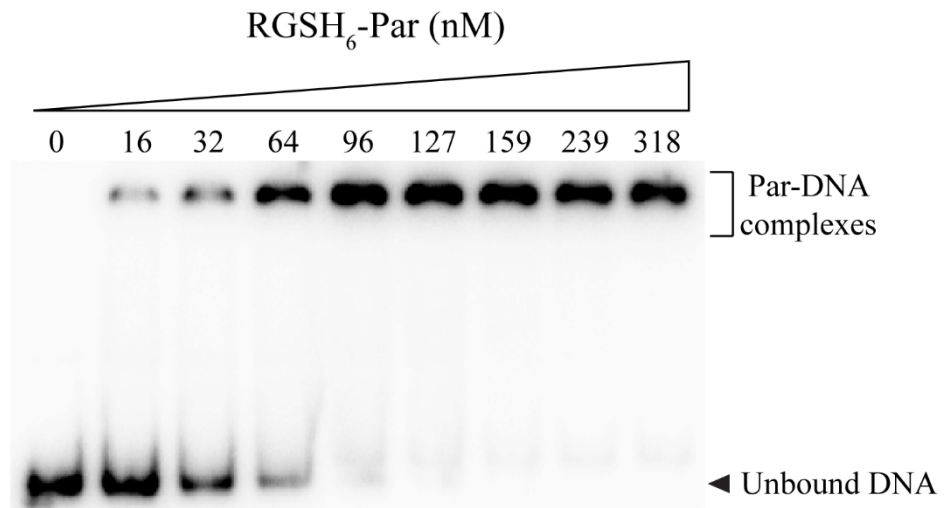
Previous EMSAs established that RGSH₆-Par binds specifically to a 212 bp DNA fragment that encompasses the seven 12-bp direct repeats of the *par* centromere-like site (nt 1689–1900 of pSK1, GenBank Accession Number GU565967, Figure 1.6) (LeBard 2005, Figgett 2007, Lai 2008). To compare the DNA-binding activity of the CTD mutants with RGSH₆-Par, the same 212 bp DNA fragment was PCR-amplified

(Section 2.4.4) from pSK4829 (Table 2.2) using primers SJ37 and SJ38 (Table 2.6). The resulting fragment was purified (Section 2.4.7) and then end-labelled with ^{32}P from $[\gamma\text{-}^{32}\text{P}]\text{-ATP}$ using T4 PNK (Section 2.8.1). EMSAs were performed as described in Section 2.8.2, using approximately 500 cpm of purified, labelled DNA probe in each EMSA reaction, and increasing amounts of purified RGSH₆-tagged protein (Section 3.3.4). Figure 3.6A reveals that RGSH₆-Par bound the radiolabelled DNA probe efficiently, as DNA-binding was evident with 16 nM of RGSH₆-Par, and a complete retardation of DNA probe migration was observed with protein concentrations greater than 96 nM. The competition EMSA shown in Figure 3.6B reveals that RGSH₆-Par-DNA complexes could be titrated with unlabelled centromere competitor DNA (specific DNA), but not with non-specific DNA (181 bp region downstream of pSK1 *rep*, nt 2950–3130 of pSK1, GenBank Accession Number GU565967), which confirms previous findings that Par binds specifically to the centromere-like site (LeBard 2005, Figgett 2007, Lai 2008). RGSH₆-ParW239A and RGSH₆-ParR241A bound the probe as efficiently as RGSH₆-Par, with no visible distinction between the DNA-binding profiles of the full-length proteins (Figures 3.6D–E). Similar concentrations of RGSH₆-Par Δ CTD and RGSH₆-Par were required to completely shift the mobility of the labelled probe (approximately 96 nM), however, the binding of RGSH₆-Par Δ CTD to the DNA probe produced additional bands between the unbound probe and the completely shifted probe (Figure 3.6C). This was not observed from the DNA-binding of RGSH₆-Par, RGSH₆-ParW239A or RGSH₆-ParR241A (compare Figure 3.6C with A, D and E). It should be noted that protein-DNA complexes involving full-length Par and Par mutants appeared unable to migrate into the gel and remained in the wells (Figure 3.6A, D and E), which

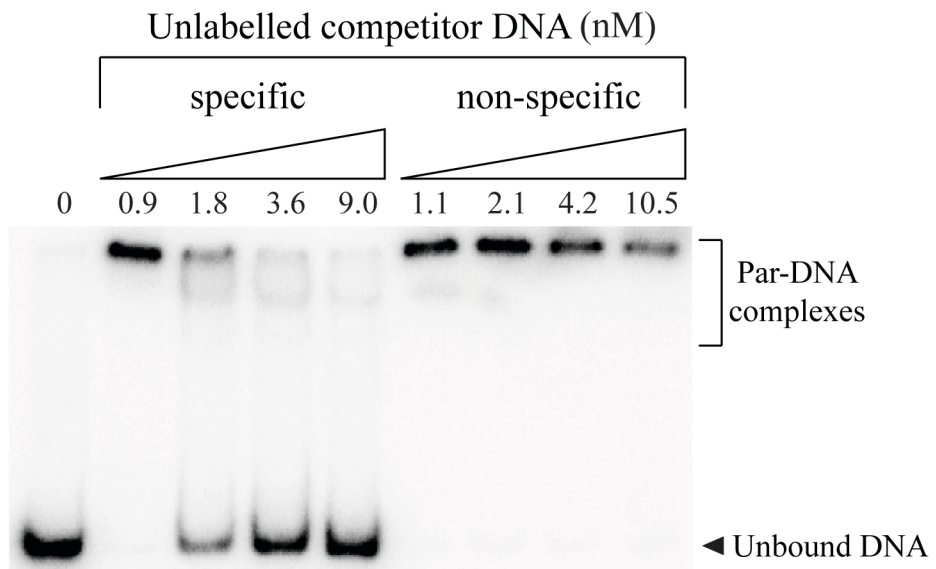
Figure 3.6 DNA-binding activity of Par CTD mutant proteins

Electrophoretic mobility shift assays (EMSAs) of Par proteins binding to the pSK1 *par-rep* intergenic region. A 212 bp *par-rep* intergenic DNA probe (nt 1689–1900 of pSK1, GenBank Accession Number GU565967, Figure 1.5) was incubated with increasing concentrations of purified RGS_{H6}-tagged Par proteins as described in Section 3.4. **A–E.** EMSAs performed using 500 cpm of radiolabelled DNA probe and electrophoresed on 5% (w/v) polyacrylamide gels. Radiolabelled DNA probes were detected by phosphor imaging. **B.** Competition EMSA performed as described in Section 3.4 using a fixed concentration of RGS_{H6}-Par (556 nM) and increasing amounts of unlabelled competitor DNA, either specific (same as labelled probe) or non-specific (181 bp DNA fragment downstream of pSK1 *rep*, nt 2950–3130 of pSK1, GenBank Accession Number GU565967). **F–I.** EMSAs performed using 135 ng of unlabelled DNA probe and electrophoresed on polyacrylamide/agarose hybrid gels. DNA probes were detected using SYBR Safe DNA gel stain and UV transillumination. The bottom of the wells is indicated by a dashed line. The concentration of protein (nM) or amount of unlabelled competitor DNA (ng) is shown above each lane. The positions of unbound DNA are indicated by black arrowheads. Par-DNA complexes are bracketed on the right.

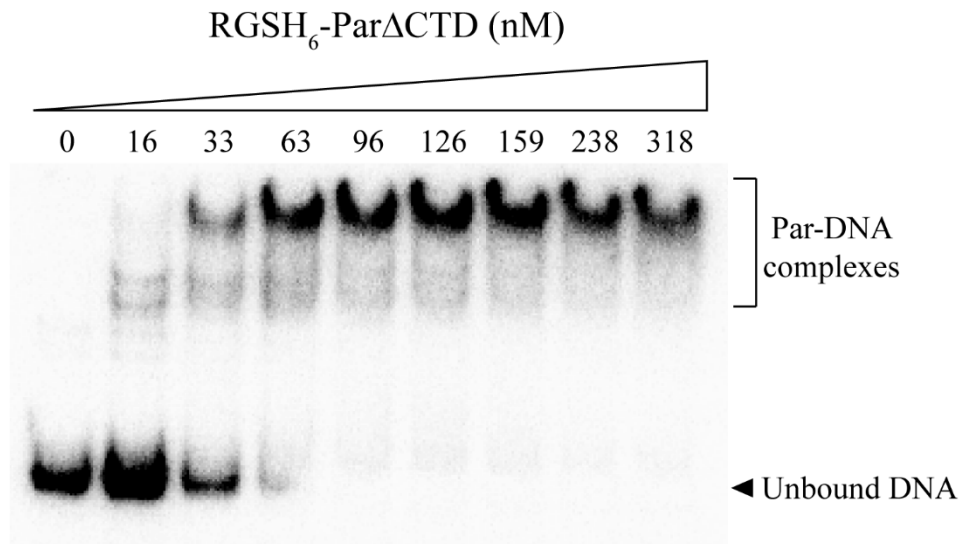
A.



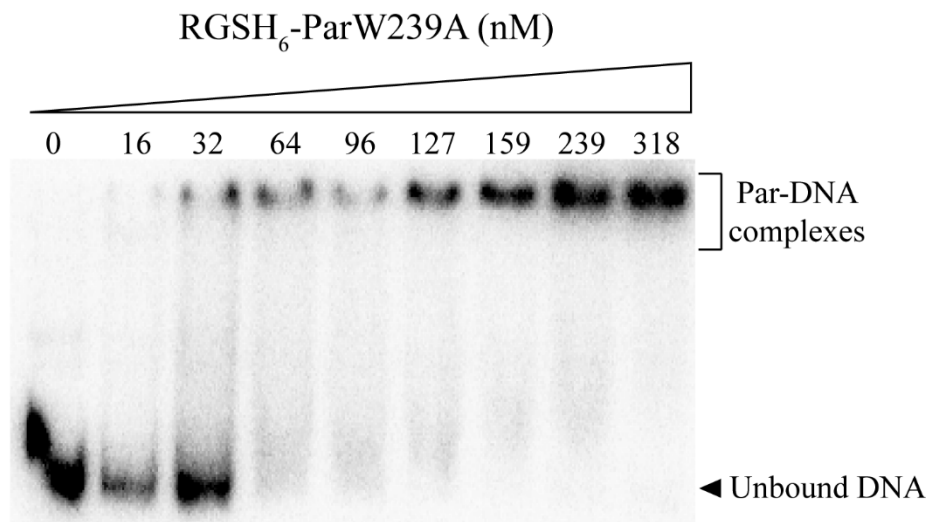
B.



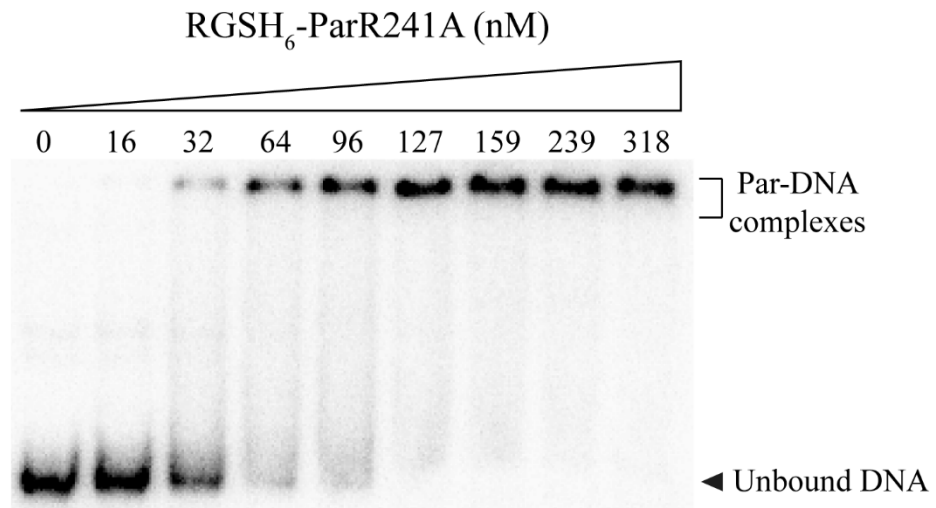
C.



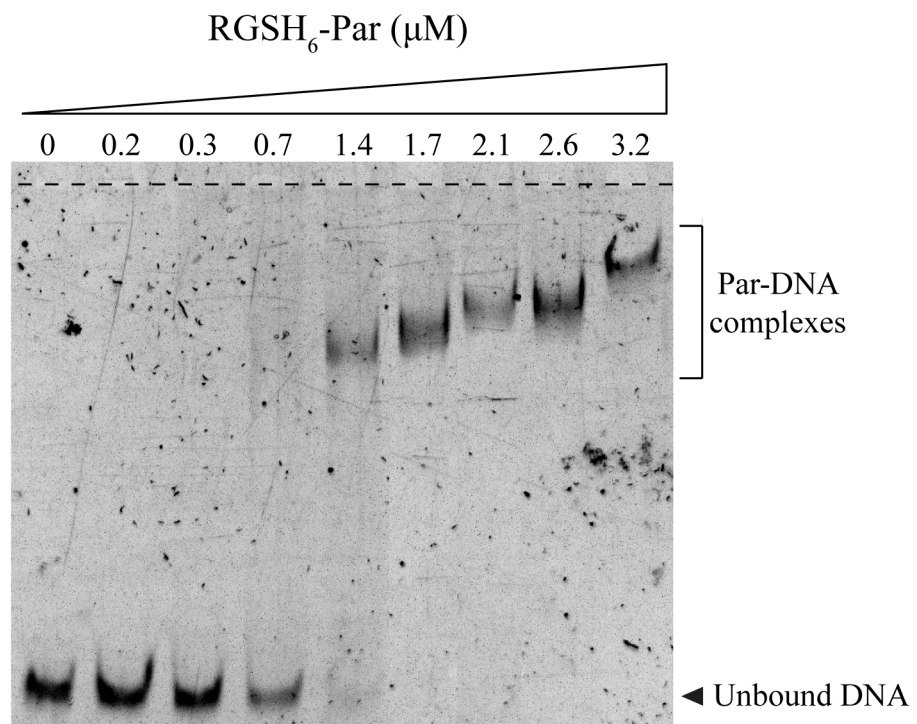
D.



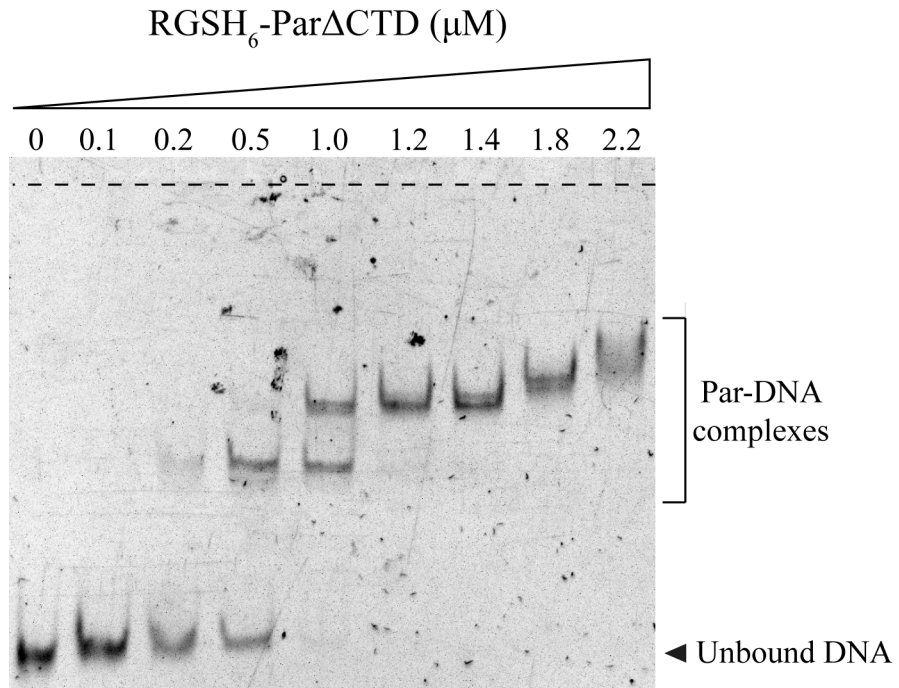
E.



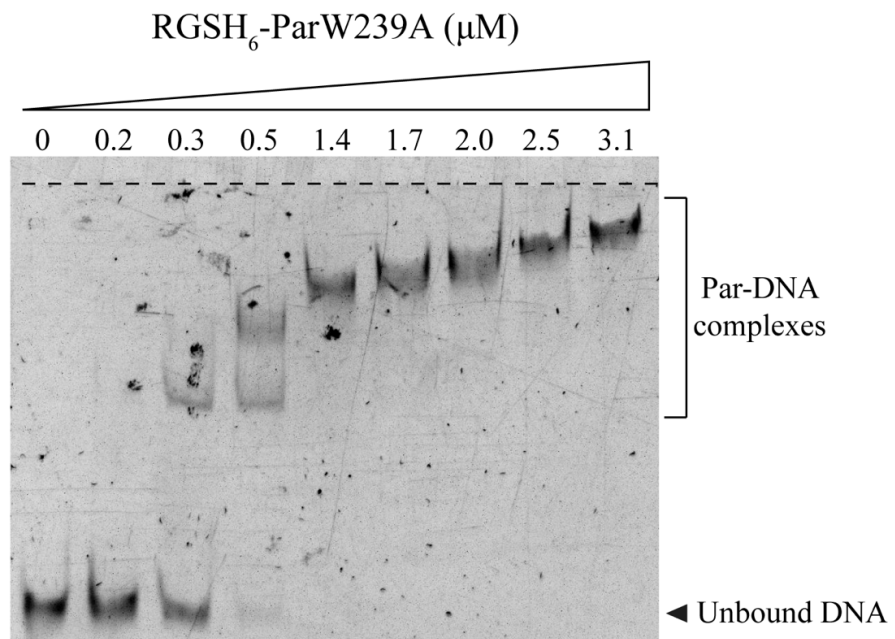
F.



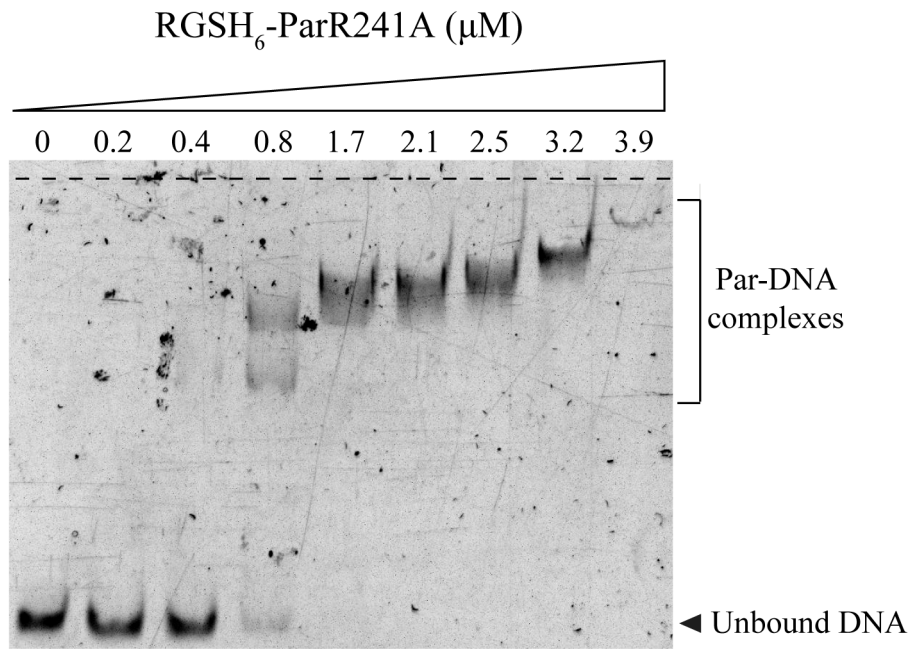
G.



H.



I.



made it difficult to determine whether intermediate protein-DNA species were formed.

3.4.1. Resolution of Par-DNA complexes formed in EMSAs

Electrophoresis of the above EMSAs on 5% (w/v) polyacrylamide gels appeared to restrict the migration of full-length Par-DNA complexes into the gel, which prevented the identification of potential protein-DNA complexes of different sizes (Section 3.4). Therefore, in order to facilitate the migration of large Par-DNA complexes into the gel, EMSAs were electrophoresed on polyacrylamide/agarose hybrid gels (Table 2.5), which have a larger pore matrix. As depicted in Figure 3.6F, RGSH₆-Par-DNA complexes migrated completely into the hybrid gels, with 1.7 μ M RGSH₆-Par required to bind the total amount of DNA probe. This was comparable to the concentrations of RGSH₆-Par Δ CTD, RGSH₆-ParW239A and RGSH₆-ParR241A protein required to observe a loss of unbound probe (approximately 1.2–1.7 μ M of protein) (Figures 3.6G–I). The hybrid gels also revealed that DNA-binding by RGSH₆-Par Δ CTD, RGSH₆-ParW239A and RGSH₆-ParR241A caused a step-wise retardation of the DNA probe, with intermediate protein-DNA species observed (Figures 3.6G–I). This was in contrast to RGSH₆-Par DNA-binding, which produced a rapid shift of the DNA probe between 0.7 μ M and 1.4 μ M of protein, with no intermediate protein-DNA species observed (Figure 3.6F).

3.5. Multimerisation activity of Par CTD mutants

3.5.1. *in vitro* cross-linking of Par mutants using glutaraldehyde

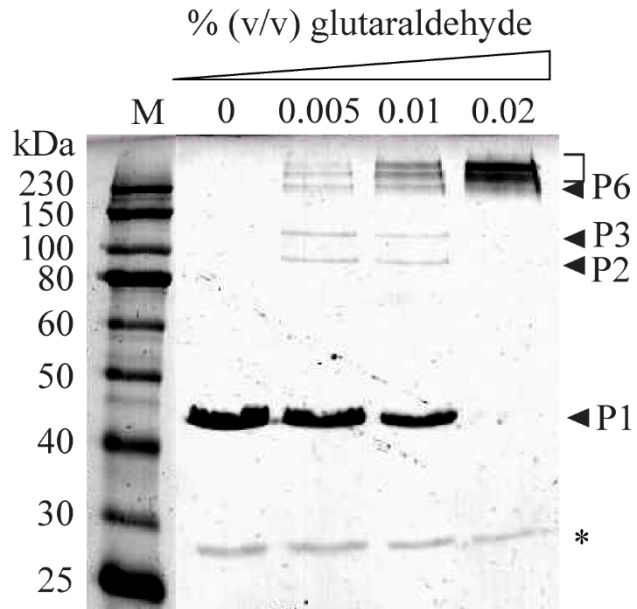
Previous studies on Par established that Par multimerisation was primarily driven by the central CC domain (Lai 2008). To determine whether the CTD also has a role in multimerisation, *in vitro* multimerisation studies were carried out on purified Par proteins using glutaraldehyde as a chemical cross-linker. Glutaraldehyde is a non-cleavable, homobifunctional amine-reactive cross-linker that forms covalent bonds between closely associated proteins, such as interacting proteins or protein multimers. Electrophoresis under reducing conditions separates the cross-linked proteins according to size, allowing for multimeric forms of Par to be identified.

To determine the optimum amount of cross-linker for use in the *in vitro* cross-linking reactions, purified Par proteins were incubated in PBS with increasing concentrations of glutaraldehyde (Section 2.9.1) and then resolved by SDS-PAGE (Section 2.5.6). As shown in Figure 3.7A, increasing glutaraldehyde concentrations increased the proportion of high-molecular weight cross-linked complexes. RGS_{H6}-Par formed dimers, trimers, hexamers and higher-order complexes when cross-linked with 0.01% (v/v) glutaraldehyde, with dimers and trimers in apparently similar proportions (Figure 3.7A). To minimise artefactual cross-linking, subsequent cross-linking studies were performed using 0.01% (v/v) glutaraldehyde. All proteins remained as monomers when untreated with glutaraldehyde (Figure 3.7B), which indicates that the observed protein bands in the treated samples were a result of cross-linking. There was no observable difference in multimerisation profiles between RGS_{H6}-Par and the full-length CTD point mutants when cross-linked with

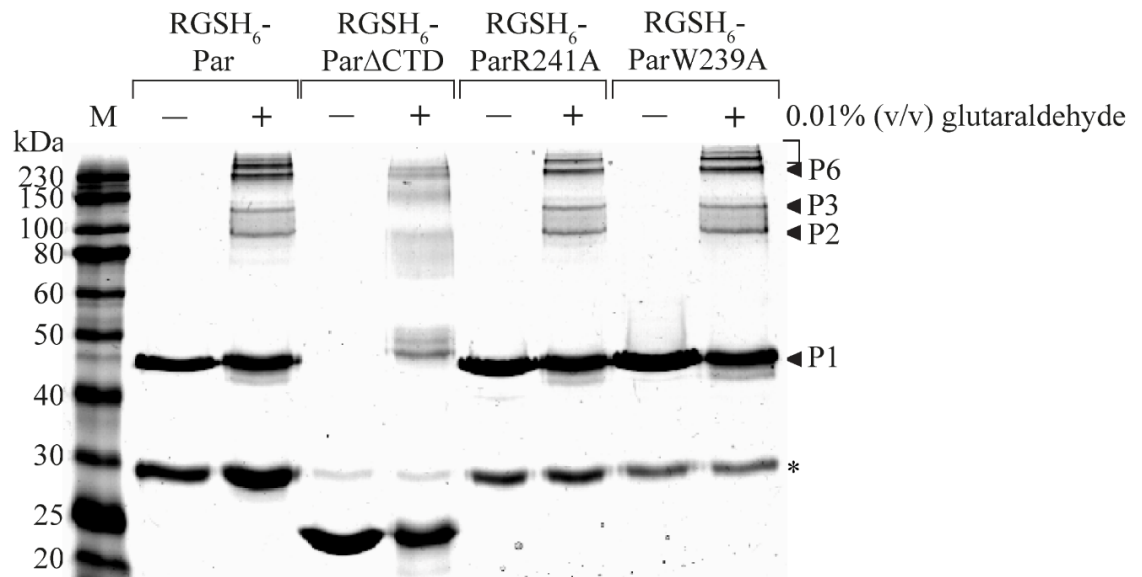
Figure 3.7 *in vitro* cross-linking of purified Par proteins using glutaraldehyde

10% (w/v) SDS polyacrylamide gels of cross-linked RGSH₆-Par proteins. Purified RGSH₆-Par proteins were cross-linked with the indicated concentrations of glutaraldehyde, as described in Section 2.9.1. Cross-linking reactions were analysed by SDS-PAGE and Coomassie Brilliant Blue staining (Section 2.5.6). **A.** Titration of RGSH₆-Par with glutaraldehyde cross-linker. **B.** RGSH₆-Par proteins incubated with (+) or without (-) 0.01% (v/v) glutaraldehyde. **C.** Titration of RGSH₆-Par Δ CTD with glutaraldehyde cross-linker. Lane M contains prestained protein markers, with marker sizes indicated in kDa on the left of each gel. Where appropriate, the positions of monomers (P1) and potential dimers (P2), trimers (P3), tetramers (P4) and hexamers (P6) are indicated by solid arrowheads for full-length RGSH₆-Par proteins, and by open arrowheads for RGSH₆-Par Δ CTD proteins. The positions of higher-order multimers are bracketed. The position of a contaminant protein from the purification process is indicated with an asterisk.

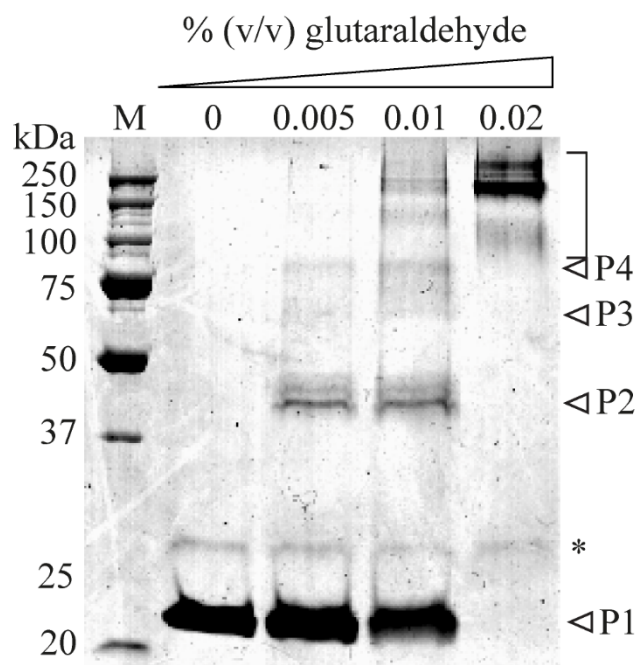
A.



B.



C.



0.01% (v/v) glutaraldehyde (Figure 3.7B). Cross-linking of RGSH₆-Par Δ CTD resulted in a higher observed proportion of dimers compared to trimers and higher-order multimers (Figure 3.7B). This was also observed at a lower glutaraldehyde concentration of 0.005% (v/v) (Figure 3.7C). Additionally, possible tetramers were present upon cross-linking of RGSH₆-Par Δ CTD, which were not observed for RGSH₆-Par (compare Figures 3.7B–C). The contaminant protein from the purification process (Section 3.3.4) did not appear to interfere with the cross-linking assay, since it remained in the form of a monomer even in the presence of 0.02% (v/v) glutaraldehyde (Figures 3.7A–C).

3.5.2. *in vivo* cross-linking of Par mutants using dithiobis(succinimidyl propionate)

To determine whether the multimeric forms of Par observed in the above *in vitro* cross-linking experiments (Section 3.5.1) are also formed *in vivo*, cross-linking experiments were also performed *in vivo* using the homobifunctional, thiol-cleavable, amine-reactive cross-linker dithiobis(succinimidyl propionate) (DSP). Unlike glutaraldehyde, DSP is membrane-permeable, allowing it to enter cells and covalently cross-link proteins intracellularly. *S. aureus* SK8250 cells (Table 2.1) carrying pSK4829 (Table 2.2), and expressing Par in the presence of the pSK1 *par* centromere-like site, were treated with increasing concentrations of DSP as described in Section 2.9.2. Cells were then lysed, and the cleared lysates (Section 2.5.8) were fractionated by SDS-PAGE under non-reducing conditions (Section 2.5.7) to ensure that the cross-links remained intact. Subsequent Western blotting (Section 2.5.9) using affinity-purified (Section 2.6.1) and preadsorbed (Section

2.6.2) anti-Par antibodies facilitated the detection of Par multimers that had been cross-linked *in vivo*.

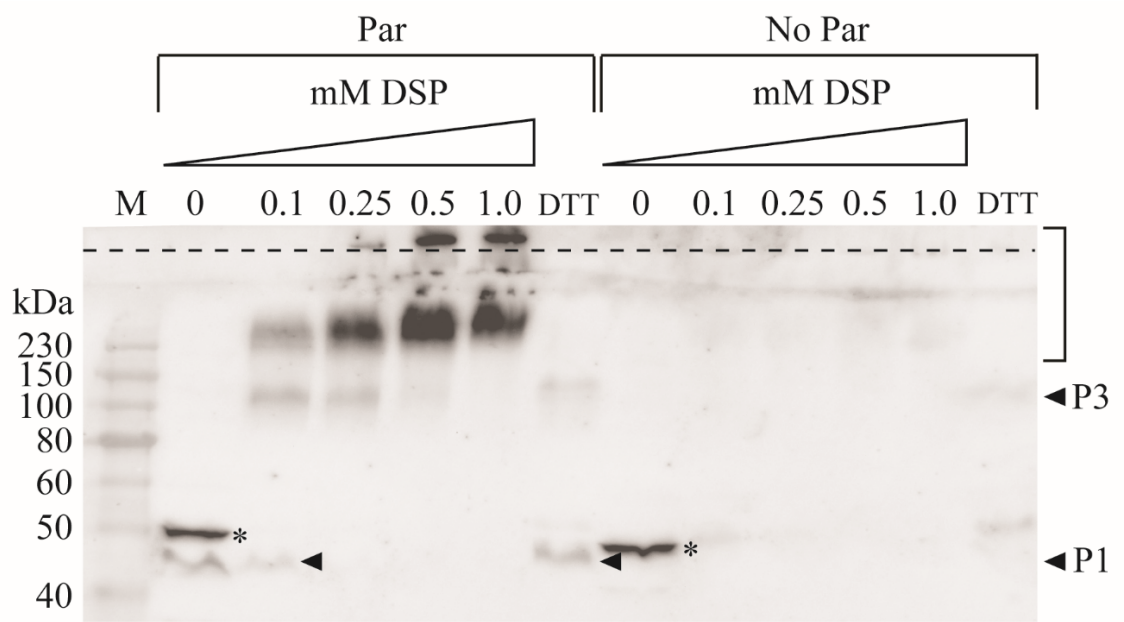
As shown in Figure 3.8A, DSP treatment of *S. aureus* SK8250 cells carrying pSK4829 (Table 2.2) resulted in the cross-linking of Par complexes corresponding to the estimated sizes of Par trimers, and, at elevated DSP levels, higher-order multimers, which could be cleaved upon treatment with the reducing agent, dithiothreitol (DTT) prior to electrophoresis (Section 2.9.2). A proportion of Par multimers was unable to migrate into the gel under non-reducing conditions and remained in the wells (Figure 3.8A). No Par proteins were detected in *S. aureus* SK8250 cells carrying pSK4833 (Table 2.2), which lacks the Par coding sequence (Figure 3.8A), suggesting that the detected bands corresponded specifically to Par and Par complexes. Note that the absence of the non-specific band in the cross-linked samples may indicate cross-linking of this protein with itself or with Par protein. However, the relatively low amounts of the non-specific protein are unlikely to affect interpretation of the most intense Par protein bands.

To minimise artefactual cross-linking of proteins, a concentration of 0.1 mM DSP was chosen for subsequent cross-linking experiments on *S. aureus* cells expressing mutant derivatives of Par in the presence of pSK1 *par* centromere DNA. Cross-linking experiments were repeated at least three times, however, due to considerable amounts of background signals, it was difficult to detect Par proteins and their complexes amongst the non-specific staphylococcal protein bands. In Figure 3.8B, which shows the most presentable of the blots, it was possible to discern protein bands corresponding to the sizes of Par trimers and higher-order complexes from the

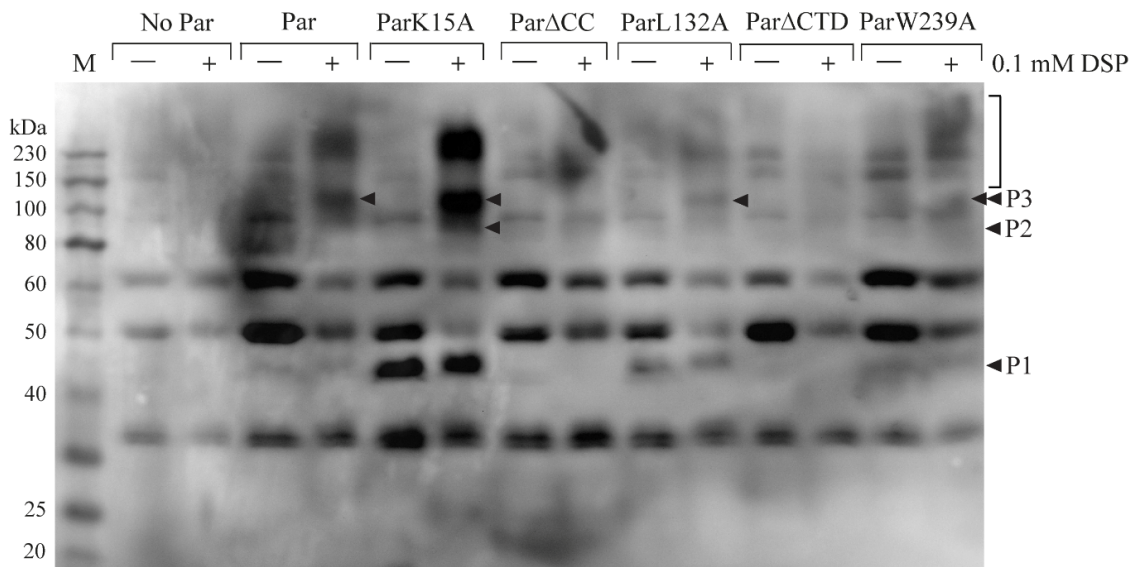
Figure 3.8 *in vivo* cross-linking of Par proteins in *S. aureus* using DSP

Western blots of cross-linked Par proteins in *S. aureus*. *S. aureus* SK8250 cells were treated with the indicated concentrations of DSP and lysates were electrophoresed on 10% (w/v) SDS polyacrylamide gels under non-reducing conditions (Section 3.5.2). Par proteins were transferred to a PVDF membrane and detected by Western blotting (Section 2.5.9) using affinity-purified rabbit anti-Par antiserum (Section 2.6.1) preadsorbed with *S. aureus* SK8250 whole-cell lysates (Section 2.6.2). **A.** DSP titration of *S. aureus* SK8250 cells carrying pSK4829 (Par) or pSK4833 (No Par). Lanes marked DTT contain samples treated with 1 mM DSP and subsequently reduced with 100 mM DTT prior to electrophoresis (Section 2.9.2). **B.** *S. aureus* SK8250 cells carrying pSK4833 (No Par), pSK4829 (Par), pSK7764 (ParK15A), pSK7721 (Par Δ CC), pSK7726 (ParL132A), pSK9069 (Par Δ CTD) or pSK9070 (ParW239A) incubated with (+) or without (-) 0.1 mM DSP. Lane M contains prestained protein markers, with marker sizes indicated in kDa on the left of each blot. Where appropriate, arrowheads indicate the positions of Par monomers (P1) and potential dimers (P2) and trimers (P3). For clarity, arrowheads are also positioned adjacent to protein bands corresponding to Par monomers in (A) and to potential Par multimers in (B). The positions of higher-order multimers are bracketed. In (A), the position of a non-specific protein band detected by Western blotting is indicated by an asterisk, and the bottom of the wells is indicated by a dashed line.

A.



B.



in vivo cross-linking of Par (pSK4829), ParK15A (pSK7764), ParL132A (pSK7726) and ParW239A (pSK9070) (Table 2.2). Potential dimers were also detected from DSP treatment of *S. aureus* cells producing ParK15A (Figure 3.8B). Signals from Par Δ CC (pSK7721) and Par Δ CTD (pSK9069) (Table 2.2) in *S. aureus* were too weak for detection by Western blotting (Figure 3.8B).

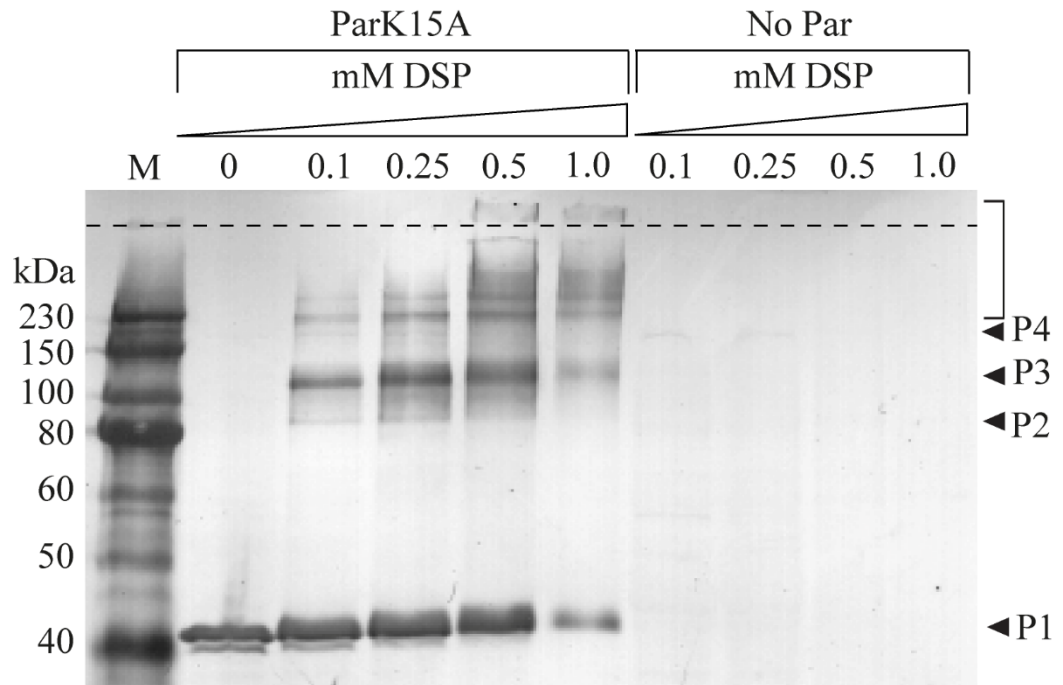
In an attempt to improve the sensitivity of detection of Par multimers *in vivo*, DSP cross-linking was also performed in *E. coli*, since anti-Par antibodies were shown to have less cross-reactivity with *E. coli* whole cell lysates (for example, see Figure 3.3). Since ParK15A is overproduced *in vivo*, and hence more easily detected by Western blotting (Figure 3.8B), pSK7764 (Table 2.2), which contains *parK15A* expressed from P_{par} in the presence of centromere DNA, was used in preliminary DSP cross-linking experiments in *E. coli*. *E. coli* DH5 α cells carrying pSK7764 were titrated with DSP cross-linker as described in Section 2.9.2, subsequent to which whole cell extracts (Section 2.5.8) were fractionated by SDS-PAGE under non-reducing conditions (Section 2.5.7). Figure 3.9A shows that in the absence of cross-linker, only ParK15A monomers were present, however, treatment with DSP resulted in the detection of protein bands corresponding to the approximate sizes of ParK15A dimers, trimers and tetramers, as well as higher-order complexes at elevated DSP concentrations. No Par protein bands were detected from *E. coli* cells carrying pSK4833 (Δ *par*) (Figure 3.9A).

A DSP concentration of 0.5 mM was used for further cross-linking experiments to determine the effect of CTD mutations on Par multimerisation in *E. coli*. Cross-linking had been performed previously for *E. coli* cells independently producing

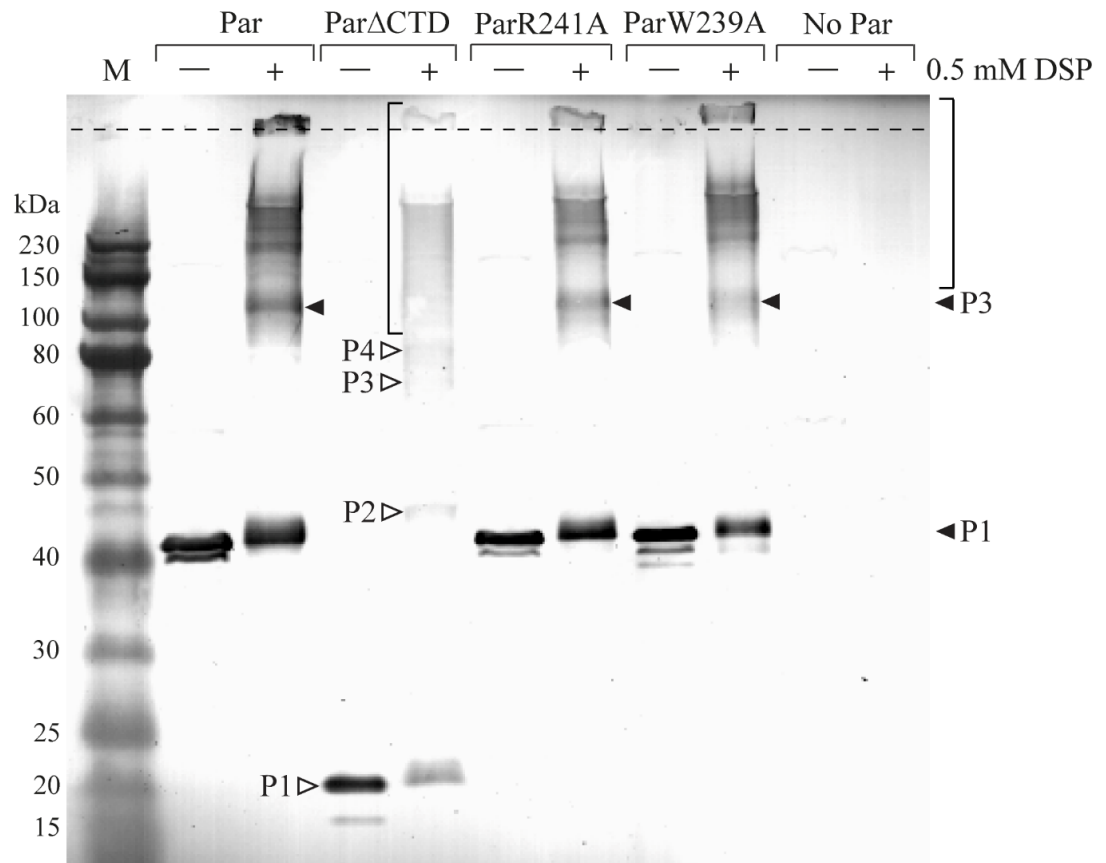
Figure 3.9 *in vivo* cross-linking of Par proteins in *E. coli* using DSP

Western blots of cross-linked Par proteins in *E. coli*. *E. coli* DH5 α cells were treated with the indicated concentrations of DSP and lysates were electrophoresed on 10% (w/v) SDS polyacrylamide gels under non-reducing conditions (Section 3.5.2). Par proteins were transferred to a PVDF membrane and detected by Western blotting (Section 2.5.9) using rabbit anti-Par antiserum. **A.** DSP titration of *E. coli* DH5 α cells carrying pSK7764 (ParK15A) or pSK4833 (No Par). **B.** *E. coli* DH5 α cells carrying pSK4829 (Par), pSK9069 (Par Δ CTD), pSK9059 (ParR241A), pSK9070 (ParW239A) or pSK4833 (No Par) incubated with (+) or without (–) 0.5 mM DSP. **C.** DSP titration of *E. coli* DH5 α cells carrying pSK9069 (Par Δ CTD). Lane M contains prestained protein markers, with marker sizes indicated in kDa on the left of each blot. Where appropriate, the positions of monomers (P1) and potential dimers (P2), trimers (P3) and tetramers (P4) are indicated by solid arrowheads for full-length Par proteins, and by open arrowheads for Par Δ CTD proteins. For clarity, arrowheads are also positioned adjacent to protein bands corresponding to the sizes of Par multimers in (B). The positions of higher-order multimers are bracketed. The bottom of the wells is indicated by a dashed line.

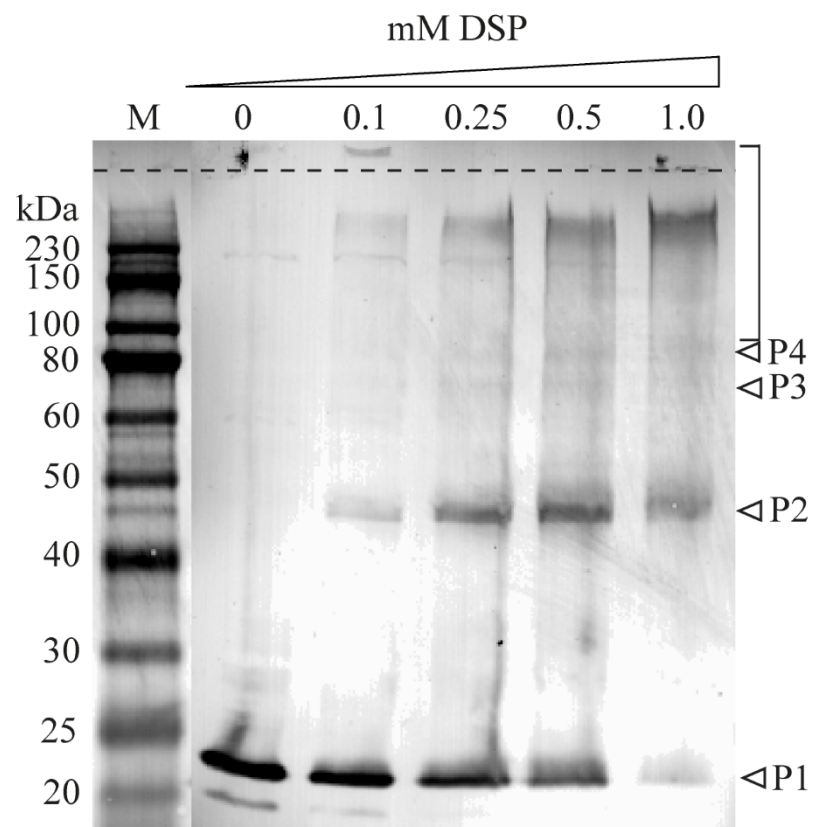
A.



B.



C.



ParK15A and Par Δ CC (Supplementary Figure S2B) (Jensen, S. O. and Firth, N., unpublished data), and hence the cross-linking experiments described here were performed only for the CTD mutants. The Western blot in Figure 3.9B shows little variation between the banding profiles of DSP-treated *E. coli* cells producing Par (pSK4829), ParR241A (pSK9059) or ParW239A (pSK9070). When cross-linked with 0.5 mM DSP, a clear band of the expected size of a trimer was visible, as well as bands of higher molecular weight (Figure 3.9B). It is unclear from the Western blot whether dimers were present for these full-length Par proteins, however, *in vivo* cross-linking of Par Δ CTD (pSK9069) revealed a 46 kDa band corresponding to the approximate size of Par Δ CTD dimers, which appeared at a higher proportion than bands predicted to be Par Δ CTD trimers or tetramers (Figure 3.9B). Probable Par Δ CTD dimers were also readily detected at lower cross-linker concentrations when *E. coli* cells carrying pSK9069 (*par* Δ CTD) were titrated with DSP (Figure 3.9C). No bands were detected by Western blotting using anti-Par antibodies on an *E. coli* strain lacking Par (Figure 3.9B), which indicates that the bands detected from the *in vivo* cross-linking experiments corresponded specifically to Par and Par multimers, either homo-multimers or hetero-multimers of Par in complex with other *E. coli* proteins.

3.6. Self-interaction of Par proteins

Whilst the cross-linking studies described in Section 3.5 provided insights into Par multimerisation, further insight into the interactions between two individual Par proteins could be gained by performing yeast two-hybrid (Y2H) assays (Fields and Song 1989). In Y2H assays, yeast cells carry two plasmids: 1) a bait plasmid (for

example pGBKT7; Table 2.2) that encodes GAL4 DNA-binding domain (BD) fused to a protein of interest, and 2) a prey plasmid (for example pGADT7; Table 2.2) that encodes GAL4 activation domain (AD) fused to a potential protein interaction partner. GAL4 is a yeast transcription factor that binds to the regulatory and promoter regions upstream of GAL4-responsive genes. In *Saccharomyces cerevisiae* AH109 (Table 2.1), the yeast strain used in this study, the GAL4-responsive reporter genes are *HIS3*, *ADE2*, *lacZ* and *MEL1*, which encode enzymes involved in histidine biosynthesis, adenine biosynthesis, β -galactosidase and α -galactosidase, respectively. Since *S. cerevisiae* AH109 lacks the GAL4 transcription factor, activation of GAL4-responsive reporter genes occurs when the GAL4 BD and AD regions are brought into close proximity by interaction between the plasmid-encoded bait and prey fusion proteins. Activation of these reporter genes is indicated by growth on minimal media (lacking histidine and/or adenine), or by detection of β -galactosidase and/or α -galactosidase activity, either qualitatively or quantitatively. In the following studies, Y2H assays were performed to determine the contribution of the predicted Par domains to interactions between Par proteins, i.e. Par self-interaction.

3.6.1. Construction of Par bait and prey fusion proteins for yeast two-hybrid assays

To facilitate Y2H assays for examining Par self-interaction, Par bait and prey fusion proteins were constructed in pGBKT7 and pGADT7 vectors, respectively (Table 2.2). pGBKT7 is an *E. coli-S. cerevisiae* shuttle vector that encodes GAL4 BD upstream of a multiple cloning site, such that a N-terminal GAL4 BD-bait fusion protein is generated when a protein-coding sequence is cloned in-frame. The vector

also incorporates a c-Myc epitope tag between GAL4 BD and the bait protein to facilitate immunodetection and purification. Similarly, pGADT7 encodes GAL4 AD, such that a N-terminal GAL4 AD-prey fusion protein is generated when a protein-coding sequence is cloned in-frame. A SV40 nuclear localisation signal is fused to the N-terminus of GAL4 AD in order to target the prey fusion protein to the yeast nucleus. A haemagglutinin (HA) epitope tag is also incorporated between the GAL4 AD and the prey protein. Constitutive expression of both BD- and AD- fusion proteins in yeast is driven by the P_{ADHI} promoter.

The *Par* coding region was amplified from pSK4829 template DNA (Table 2.2) by PCR (Section 2.4.4) using primers HC24 and HC25 (Table 2.6). PCR reactions were electrophoresed on an agarose gel (Section 2.4.3), after which the 0.7 kb band of interest was excised and purified (Section 2.4.7). A double digestion with *EcoRI* and *BamHI* (Section 2.4.6) was performed on the purified amplicon, as well as on the bait (pGBKT7) and prey (pGADT7) vectors (Table 2.2). Following purification of the restricted insert and vectors, the *par* insert was ligated to the dephosphorylated (Section 2.4.10) ends of each of the restricted bait and prey vectors. The *par* pGBKT7 and pGADT7 ligation reactions were then used to transform *E. coli* DH5 α cells to kanamycin and ampicillin resistance (Section 2.3.2), respectively. Recombinant clones were identified by agarose gel electrophoresis (Section 2.4.3) of isolated plasmid DNA (Section 2.4.1) that had been restricted with *EcoRI* and *BamHI* (Section 2.4.6). Recombinant plasmids displaying the anticipated restriction profiles were sequenced (Section 2.4.14) using primers HC24 and HC25 (Table 2.6). Plasmids containing the correct coding sequence for full-length *Par* (ParFL) in

pGBKT7 and pGADT7 were named pSK9107 and pSK9110 (Table 2.2), encoding GAL4 BD-ParFL bait and GAL4 AD-ParFL prey protein fusions, respectively.

Bait and prey fusion proteins for ParK15A, Par Δ CC, ParL132A, Par Δ CTD, ParR241A and ParW239A were generated as described above for the generation of pSK9107 and pSK9110 (Table 2.2), using pSK7764, pSK7721, pSK7726, pSK9069, pSK9059 and pSK9070 template DNA (Table 2.2), respectively. The resultant plasmids encoding mutant Par bait and prey fusion proteins are listed in Table 2.2.

3.6.2. Yeast two-hybrid assay of Par self-interaction

As a means to verify the results obtained from cross-linking studies of Par and Par mutants (Section 3.5), Y2H assays were performed, as described in Section 2.10.3, to determine the self-interaction abilities of Par proteins. *S. cerevisiae* AH109 cells (Table 2.1) were simultaneously transformed (Section 2.10.2) with pairs of bait and prey plasmids constructed in Section 3.6.1, such that yeast cells contained bait and prey fusion proteins encoding either ParFL, ParK15A, Par Δ CC, ParL132A, Par Δ CTD, ParR241A or ParW239A. Par bait and prey fusion proteins were also tested for self-activation of the reporter genes and interaction with GAL4 BD or GAL4 AD by performing Y2H assays with empty pGBKT7 bait and pGADT7 prey plasmids (Table 2.2). Co-transformants from low-stringency selection medium (SD/-Leu/-Trp) (Table 2.3) were patched in triplicate onto low-, medium- (SD/-Leu/-Trp/-His) and high- (SD/-Leu/-Trp/-His/-Ade/X- α -Gal) stringency selection media (Table 2.3) in order to identify clones that activated the GAL4-responsive reporter genes, *HIS3*, *ADE2* and *MEL1*. A positive indication of interaction between the GAL4 BD-bait and GAL4 AD-prey fusion proteins was provided by growth on medium- and

high- stringency selection media, as well as detection of α -galactosidase activity, as indicated by the production of a blue pigment on media containing 5-bromo-4-chloro-3-indolyl α -D-galactopyranoside (X- α -Gal).

The results of the Y2H assays of Par self-interaction are shown in Figure 3.10A. The Y2H assays indicated that ParFL interacts with itself, as determined by growth on high-stringency selection medium (Figure 3.10A). Additionally, all Par mutants tested (ParK15A, Par Δ CC, ParL132A, Par Δ CTD, ParR241A and ParW239A) showed evidence of self-interaction, since growth was detected on high-stringency selection medium for all strains (Figure 3.10A). No growth was detected on high-stringency selection medium when bait and prey fusion proteins were tested for interaction with empty Y2H vectors (Figure 3.10A). This demonstrated that activation of the reporter genes was not due to non-specific interaction with GAL4 BD or GAL4 AD, nor due to self-activation of the reporter genes by the protein fusions.

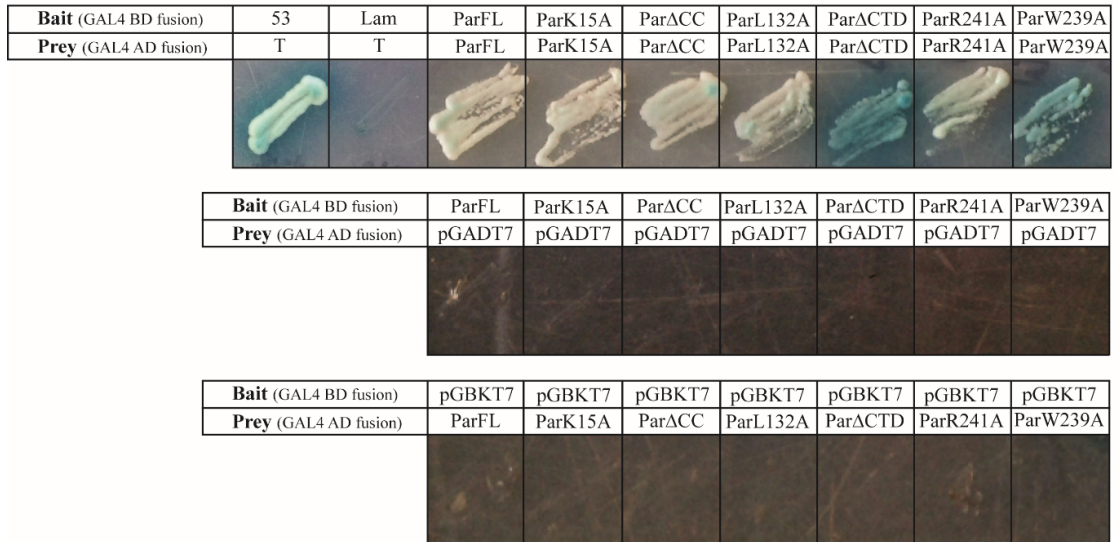
Notably, self-interaction of Par Δ CTD and ParW239A appeared to result in higher α -galactosidase activities, as suggested by the darker blue pigment produced on media containing X- α -Gal (Figure 3.10A). The relative strengths of the self-interactions were quantified using α -galactosidase assays as described in Section 2.10.5, and expressed as fold-change relative to the negative control strain, which encodes GAL4 BD-Lam and GAL4 AD-T (Table 2.2). Overall, the findings supported the results from the Y2H assays, and showed that Par Δ CTD and ParW239A self-interactions generated a 969 ± 285 -fold and 200 ± 79 -fold increase in α -galactosidase activities, respectively, compared to the negative control strain (Figure 3.10B). These

Figure 3.10 Self-interaction of Par proteins

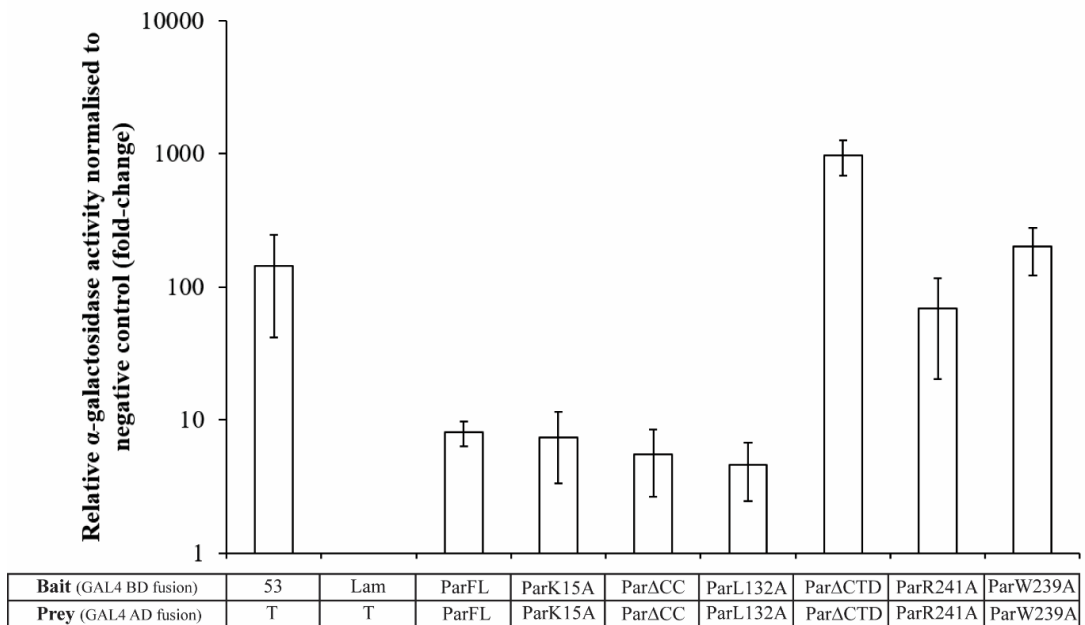
A. Yeast two-hybrid (Y2H) assays of Par self-interaction. Y2H assays were performed between pairs of Par bait and prey fusion proteins according to the methods described in Section 3.6.2. Growth of *S. cerevisiae* AH109 cells containing bait and prey plasmids is shown on high-stringency selection medium (SD/-Leu/-Trp/-His/-Ade/X- α -Gal) (Table 2.3). Growth indicates activation of the *HIS3* and *ADE2* reporter genes. Blue pigmentation indicates α -galactosidase activity from yeast cells. *S. cerevisiae* AH109 cells expressing the prey protein fusion, simian virus T antigen (GAL4 AD-T), and the bait protein fusions, murine p53 (GAL4 BD-53) or human lamin protein (GAL4 BD-Lam), were included as positive and negative controls, respectively.

B. α -galactosidase assays of Par self-interaction. α -galactosidase assays were performed between pairs of Par bait and prey fusion proteins according to the methods described in Section 3.6.2. For comparison of relative interaction strengths, α -galactosidase activity was calculated (Section 2.10.5) and expressed as fold-change relative to the negative control strain containing GAL4 BD-Lam and GAL4 AD-T. Each data point represents the mean of at least three independent assays, each performed in triplicate. Error bars represent standard error of the mean.

A.



B.



interactions caused greater induction of α -galactosidase activity compared to ParFL self-interaction, which produced an 8 ± 2 -fold increase in α -galactosidase activity compared to the negative control strain (Figure 3.10B). ParR241A self-interaction resulted in a calculated α -galactosidase activity that was 69 ± 48 -fold higher than the negative control, while the self-interaction of all other Par mutants (ParK15A, Par Δ CC and ParL132A) produced similar levels of α -galactosidase activity to ParFL self-interaction (Figure 3.10B).

3.6.3. Contribution of Par domains to self-interaction

The Y2H assays performed in Section 3.6.2 demonstrated that self-interaction occurs between Par proteins and that self-interactions are maintained between Par mutants. To further delineate Par self-interaction, the three putative Par domains were individually expressed and assessed for their ability to interact with each other. In this way, Y2H assays might provide insight into the contribution of the Par domains to intermolecular Par self-interaction, and/or interactions that take place intramolecularly, between Par domains of the same protein.

3.6.3.1. Construction of yeast two-hybrid bait and prey fusion proteins containing individual Par domains

The full-length Par coding sequence was divided into three parts, corresponding to each of the three putative Par domains: the N-terminal domain (NTD; aa 1–82), CC domain (aa 83–155) and CTD (aa 156–245). pSK4829 template DNA (Table 2.2) was PCR-amplified (Section 2.4.4) using the primer pairs HC24/HC56, HC57/HC58, and HC59/HC25 (Table 2.6) to generate protein-coding sequences corresponding to the Par NTD, CC domain, and CTD, respectively. The three protein-coding regions

were each individually cloned into the pGBKT7 bait and pGADT7 prey plasmids (Table 2.2), essentially as described in Section 3.6.1 for the construction of pSK9107 and pSK9110 (Table 2.2). The resultant plasmids encoding Par NTD, CC domain and CTD bait and prey fusion proteins are listed in Table 2.2.

3.6.3.2. Yeast two-hybrid assay of interactions between Par domains

In order to localise inter- and/or intra-molecular Par self-interactions to specific Par domains, pairwise Y2H assays (Section 2.10.3) were performed between full-length Par fusion proteins and each of the Par domain fusions. As shown in Figure 3.11A, full-length Par (ParFL) bait protein interacted with ParFL prey protein (Figure 3.11A, panel A), but did not show an interaction with the Par NTD, CC domain or CTD prey fusions (Figure 3.11A, panels B–D). ParFL, only when fused to GAL4-AD as the prey protein, appeared to interact with ParCC and ParCTD bait proteins (Figure 3.11A, panels K and P). When the interactions were examined further, it was revealed that the ParCC bait protein interacted with the ParCC prey fusion (Figure 3.11A, panel M), and that the ParCTD bait protein interacted with the ParCTD prey fusion (Figure 3.11A, panel S). Note that although the yeast strain containing both the ParCC bait and prey plasmids did not grow on high-stringency selection medium, there was evidence of α -galactosidase activity on the medium (Figure 3.11A, panel M), and this was interpreted as a positive interaction that resulted in activation of the *MEL1* reporter gene. There were no indications of interactions involving ParNTD with any other fragment tested, nor were interactions observed between ParCC and ParCTD, in either pairing (Figure 3.11A). This was despite the growth of all yeast strains on low-stringency selection medium (Figure 3.11B), which confirmed the

Figure 3.11 Interactions between Par domains

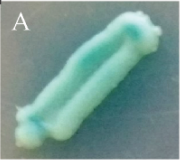
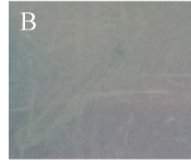
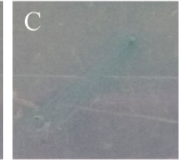







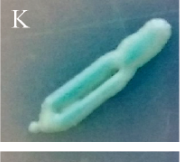



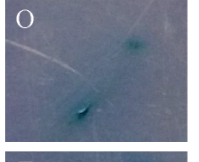
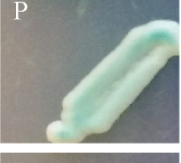



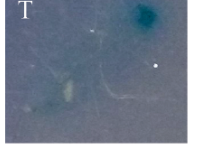
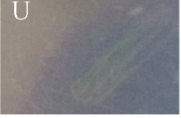
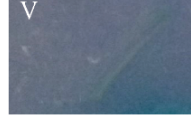
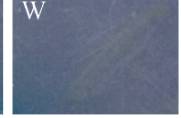
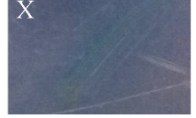


A–B. Yeast two-hybrid (Y2H) assays of interactions between Par domains. Pairwise Y2H assays were performed between GAL4 BD (bait) and GAL4 AD (prey) protein fusions to full-length Par (ParFL, residues 1–245), ParNTD (residues 1–82), ParCC (residues 83–155) and ParCTD (residues 156–245), according to the methods described in Section 3.6.3.2. **A.** Growth of *S. cerevisiae* AH109 cells containing bait and prey plasmids on high-stringency selection medium (SD/-Leu/-Trp/-His/-Ade/X- α -Gal) (Table 2.3). Growth indicates activation of the *HIS3* and *ADE2* reporter genes. Blue pigmentation indicates α -galactosidase activity from yeast cells. **B.** Growth of *S. cerevisiae* AH109 cells containing bait and prey plasmids on low-stringency selection medium (SD/-Leu/-Trp) (Table 2.3). Growth indicates the presence of both bait (pGBKT7) and prey (pGADT7) plasmids or plasmid derivatives. *S. cerevisiae* AH109 cells expressing the prey protein fusion, simian virus T antigen (GAL4 AD-T), and the bait protein fusions, murine p53 (GAL4 BD-53) or human lamin protein (GAL4 BD-Lam), were included as positive and negative controls, respectively.

C–D. Immunodetection of Par bait and prey fusion proteins in *S. cerevisiae*. *S. cerevisiae* AH109 whole cell lysates (Section 2.5.8) were fractionated on 10% (w/v) SDS polyacrylamide gels (Section 2.5.6) and proteins were detected by Western blotting (Section 2.5.9). **C.** Western blot of GAL4-BD fusions to Par protein domains using affinity-purified anti-Par antibodies (Section 2.6.1). *S. cerevisiae* cells contained pSK9107 (GAL4 BD-ParFL), pSK9172 (GAL4 BD-ParNTD), pSK9173 (GAL4 BD-ParCC) or pSK9174 (GAL4 BD-ParCTD). **D.** Western blot of GAL4-AD fusions to Par protein domains using anti-HA antibodies. *S. cerevisiae* cells contained pSK9110 (GAL4 AD-ParFL), pSK9175 (GAL4 AD-ParNTD), pSK9176 (GAL4 AD-ParCC) or pSK9177 (GAL4 AD-ParCTD). Lane M contains prestained protein markers, with

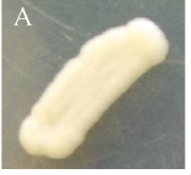
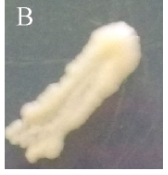
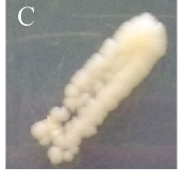
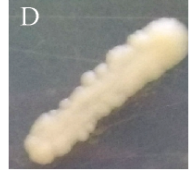


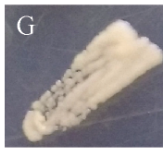
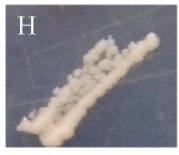




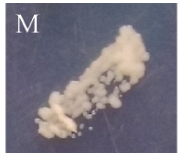

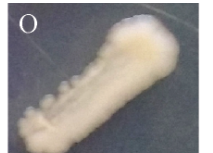






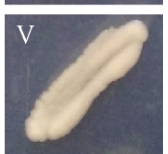



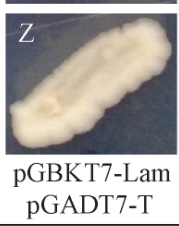
marker sizes indicated in kDa on the left of each blot. Positions of fusion proteins and their approximate measured sizes are indicated by black arrowheads.

E. Relative interaction strengths between Par domain fusions. α -galactosidase assays were performed for *S. cerevisiae* AH109 cells containing interacting Par domains according to the protocol described in Section 2.10.5. *S. cerevisiae* AH109 cells expressing the prey protein fusion, simian virus T antigen (GAL4 AD-T), and the bait protein fusions, murine p53 (GAL4 BD-53) or human lamin protein (GAL4 BD-Lam), were included as positive and negative controls, respectively. For comparison of relative interaction strengths, α -galactosidase activity was calculated (Section 2.10.5) and expressed as fold-change relative to the negative control strain containing GAL4 BD-Lam and GAL4 AD-T. Each data point represents the mean of at least three independent assays, each performed in triplicate. Error bars represent standard error of the mean.

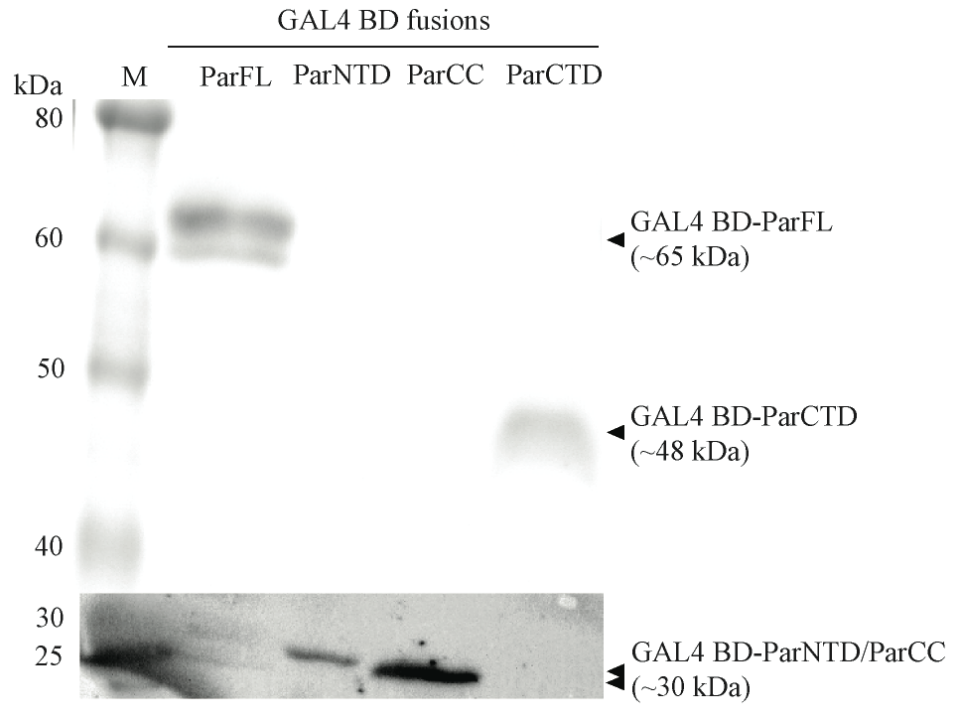
A.

Prey <small>(GAL4 AD fusion)</small> Bait <small>(GAL4 BD fusion)</small>	pSK9110 (ParFL)	pSK9175 (ParNTD)	pSK9176 (ParCC)	pSK9177 (ParCTD)	pGADT7 empty
pSK9107 (ParFL)					
pSK9172 (ParNTD)					
pSK9173 (ParCC)					
pSK9174 (ParCTD)					
pGBKT7 empty					
					
		pGBKT7-53 pGADT7-T	pGBKT7-Lam pGADT7-T		

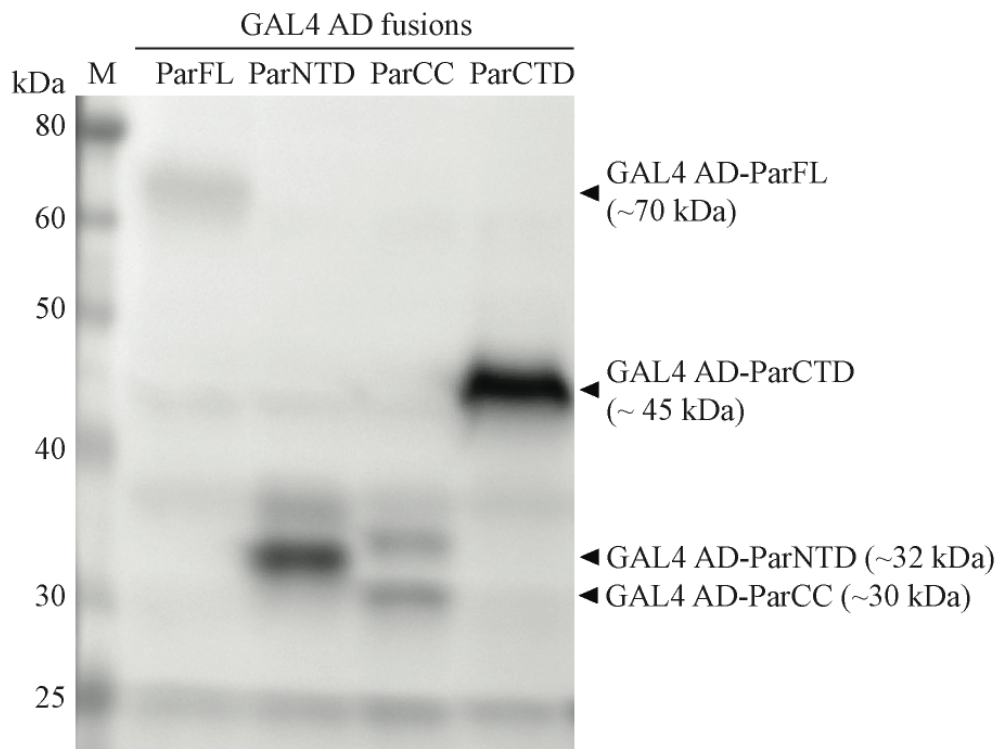
B.

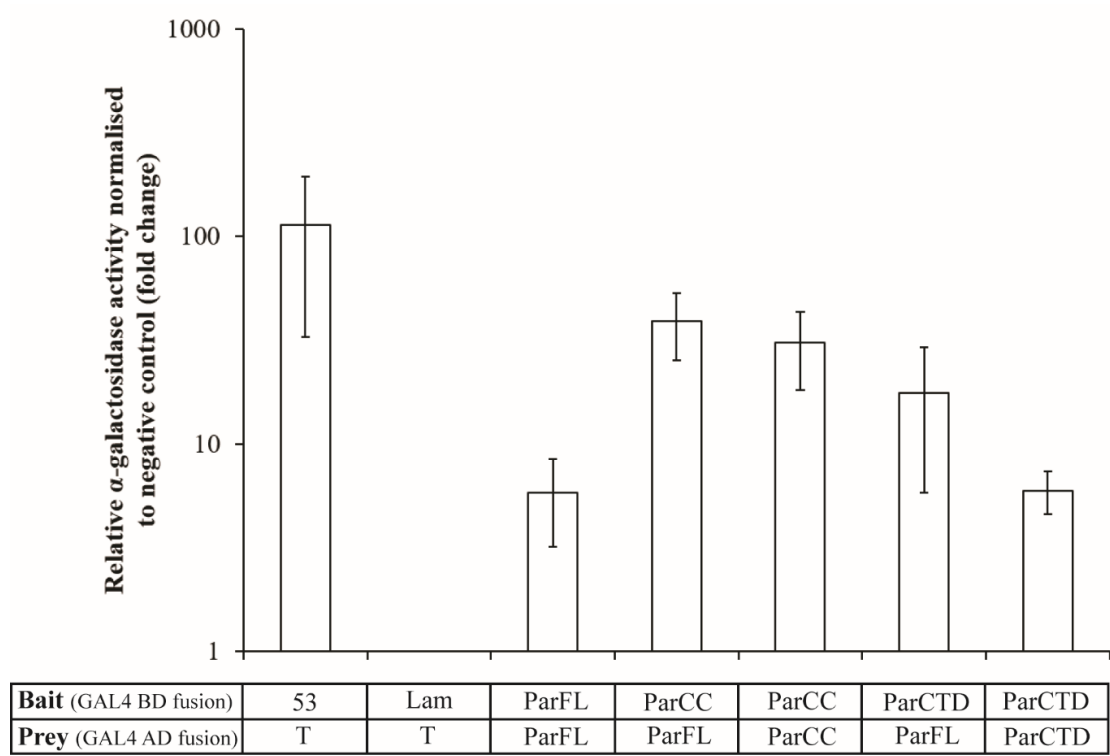
Prey <small>(GAL4 AD fusion)</small> Bait <small>(GAL4 BD fusion)</small>	pSK9110 (Par FL)	pSK9175 (Par NTD)	pSK9176 (Par CC)	pSK9177 (Par CTD)	pGADT7 empty
pSK9107 (Par FL)	A 	B 	C 	D 	E 
pSK9172 (Par NTD)	F 	G 	H 	I 	J 
pSK9173 (Par CC)	K 	L 	M 	N 	O 
pSK9174 (Par CTD)	P 	Q 	R 	S 	T 
pGBKT7 empty	U 	V 	W 	X 	
		Y  pGBKT7-53 pGADT7-T	Z  pGBKT7-Lam pGADT7-T		

C.



D.



E.

presence of both bait and prey plasmids in each strain. No bait or prey fusion proteins showed self-activation of the reporter genes, or interactions with the empty Y2H plasmids (Figure 3.11A), which indicates that any interaction detected was the result of specific interactions between the bait and prey fusion proteins.

To eliminate the possibility that a lack of growth on high-stringency selection medium was due to problems with protein production, a Western blot analysis (Section 2.5.9) was performed to detect the presence of Par bait and prey fusion proteins in yeast whole cell extracts, prepared as described in Section 2.5.9. Figure 3.11C shows the immunodetection of all GAL4 BD fusions to Par, NTD, CC and CTD bait proteins using affinity-purified rabbit anti-Par antiserum (Section 2.6.1). GAL4 BD-ParNTD and GAL4 BD-ParCC proteins were not readily detected, and visualisation of these proteins required darkening of the imaged blot (Figure 3.11C). GAL4 BD-ParNTD and GAL4 BD-ParCC were subsequently detected at their expected sizes of 30.4 kDa and 29.5 kDa, respectively (Figure 3.11C). The apparent sizes of GAL4 BD-ParFL and GAL4 BD-ParCTD were approximately 65 kDa and 48 kDa, which differed from their calculated sizes of 49.9 kDa and 31.3 kDa, respectively. This aberrant electrophoretic mobility is consistent with the aberrant mobility of Par proteins observed previously (for example, see Figures 3.2B and 3.3–3.5), and is addressed further in Section 3.7.5.

GAL4 AD fusions to Par and Par domains could not be detected using anti-Par antiserum (data not shown), however, all protein fusions could be detected using anti-HA antibodies against the HA tag (Figure 3.11D). The apparent sizes of GAL4 AD-ParNTD and GAL4 AD-ParCC were approximately 30–32 kDa (Figure 3.11D),

which were similar to their expected sizes of 28.1 kDa and 27.3 kDa, respectively. In contrast, GAL4 AD-ParFL and GAL4 AD-ParCTD had apparent sizes of 70 kDa and 45 kDa (Figure 3.11D), which were larger than their expected sizes of 47.4 kDa and 29.1 kDa, respectively. The immunodetection of all Par, NTD, CC and CTD bait and prey fusion proteins confirmed their production in yeast, and hence any lack of growth on high-stringency selection media was not due to a complete absence of protein.

To provide further insight into the contribution of Par domains to Par self-interaction, α -galactosidase assays (Section 2.10.5) were conducted on yeast cells containing bait and prey fusions to Par domains that showed positive interactions, as indicated by growth and α -galactosidase activity on high-stringency selection medium (Figure 3.11A). The results from the assays, shown in Figure 3.11E, revealed that ParFL self-interaction had a relative α -galactosidase activity 5 ± 3 -fold greater than that of the negative control strain (containing GAL4 BD-Lam and GAL4 AD-T). This was comparable to results obtained in Section 3.6.2, which showed an 8 ± 2 -fold increase in α -galactosidase activity from ParFL self-interaction (Figure 3.10B). A similar level of α -galactosidase activity was observed from the interaction between GAL4 BD-ParCTD and GAL4 AD-ParCTD (Figure 3.11E). The highest levels of α -galactosidase activities were observed from interactions involving the CC domain fusions, with a 39 ± 14 -fold increase in α -galactosidase activity from the interaction between GAL4 BD-ParCC and GAL4 AD-ParFL compared to the negative control, and a 31 ± 13 -fold increase in α -galactosidase activity from the interaction between GAL4 BD-ParCC and GAL4 AD-ParCC (Figure 3.11E). The interaction between GAL4 BD-ParCTD and GAL4 AD-ParFL also produced a

similar level of α -galactosidase activity (18 ± 12 -fold increase relative to negative control; Figure 3.11E).

3.6.4. Interactions involving Par N-terminal domain residues

3.6.4.1. Indications from preliminary Par structural data

Preliminary structural data shared by a collaborator, Prof. Maria Schumacher (Duke University, USA), suggested that Par binds centromere DNA as a dimer, and that residues in the NTD of Par might be involved in interactions between pairs of DNA-bound dimers (Schumacher, M. A. and Firth, N., unpublished data). Potential interactions were predicted to involve the K2, E10 and/or Y43 residues of the NTDs of neighbouring Par dimers. This structural data provided reason to further examine the functionality of the NTD. To this end, the functional significance of each of the three NTD residues identified from the structural data above was investigated by determining the effect of NTD mutations on Par function.

3.6.4.2. Construction of pSK1 minireplicons expressing Par NTD mutants

In order to determine their functional significance, site-directed mutagenesis (Section 2.4.5) was performed on pSK4829 plasmid DNA (Table 2.2) using primer pairs HC60/HC61, HC62/HC63 and HC64/HC65 (Table 2.6) to generate individual alanine substitutions at residues K2, E10 and Y43 of the Par NTD, respectively. DNA from mutagenesis reactions were used to transform *E. coli* DH5 α cells, and transformants were selected for ampicillin resistance (Section 2.3.2). Plasmid DNA was isolated (Section 2.4.1) from selected transformants to identify mutated plasmids. For the generation of E10A and Y43A mutations, the mutagenic primers

contained a silent *NsiI* restriction site that was used to facilitate the identification of successfully mutated plasmids by *NsiI* restriction digestion (Section 2.4.6) and agarose gel electrophoresis (Section 2.4.3). No silent restriction sites were suitable for incorporation into the primers for generating the K2A mutation, and hence screening for mutant plasmids by restriction digestion could not be performed. Plasmid DNA was sequenced (Section 2.4.14) using primers SJ37 and HC11 (Table 2.6) to ensure that the correct mutations were introduced. Successfully mutated plasmids were designated pSK9169 (*parK2A*), pSK9170 (*parE10A*) and pSK9171 (*parY43A*) (Table 2.2). An overview of the Par NTD mutants generated in this study is shown in Figure 3.1.

3.6.4.3. Functionality of Par NTD mutants

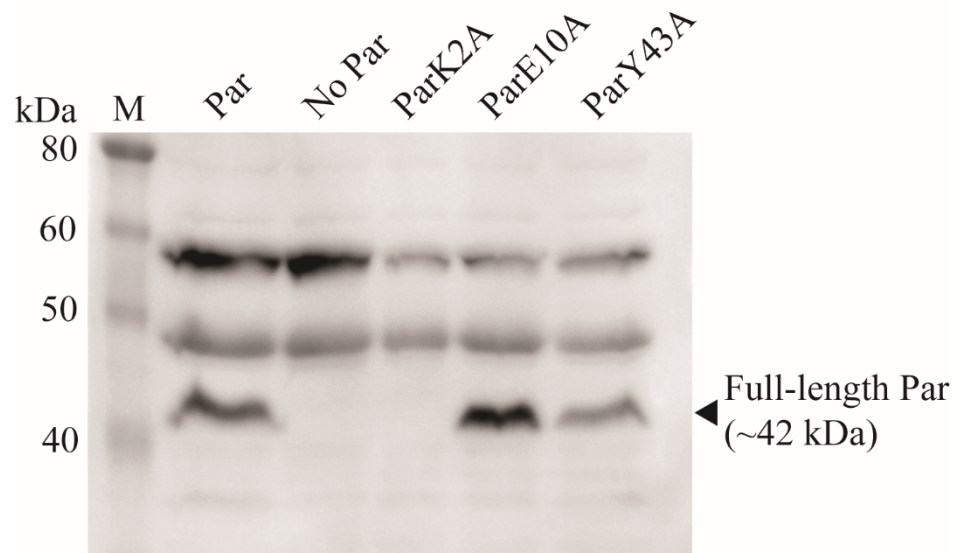
To determine the functionality of the Par NTD mutants generated in Section 3.6.4.2 above, *S. aureus* SK8250 cells were electroporated (Section 2.3.4) with pSK9169, pSK9170 or pSK9171 plasmid DNA (Table 2.2), which encode ParK2A, ParE10A and ParY43A, respectively. To ensure that the Par NTD mutants were produced *in vivo*, whole cell lysates from exponentially growing *S. aureus* SK8250 cells (Section 2.5.8) were subjected to SDS-PAGE (Section 2.5.6) and Western blot analysis (Section 2.5.9) using anti-Par anti-peptide antibodies (Section 2.6.3). The immunoblot shown in Figure 3.12A revealed the detection of protein bands of approximately 42 kDa for Par, ParE10A and ParY43A. However, a similar band was not detected for ParK2A (Figure 3.12A), which suggests that this protein was not produced at detectable levels in *S. aureus*. To verify these findings, a Western blot analysis (Section 2.5.9) was also performed on the cell lysates of *E. coli* DH5 α cells

Figure 3.12 Effect of Par NTD mutations on plasmid segregational stability

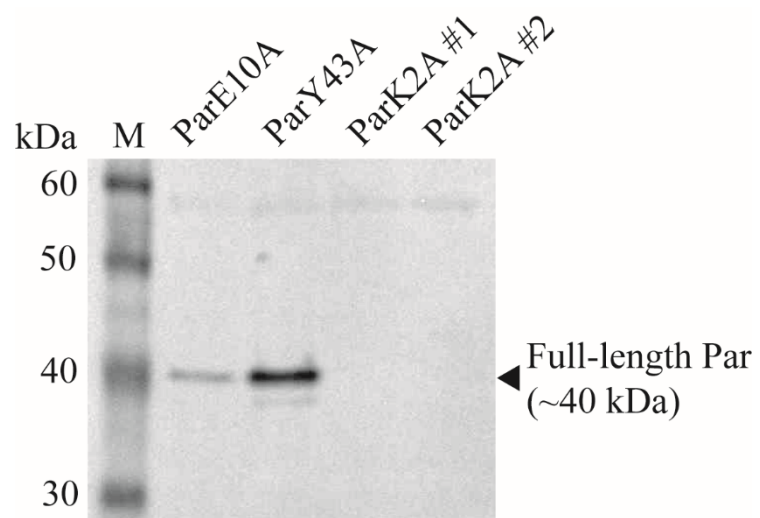
A–B. Immunodetection of Par NTD mutants by Western blotting. **A.** Western blot of Par NTD mutants in *S. aureus*. Immunodetection was performed on *S. aureus* SK8250 cell lysates (Section 2.5.8) containing pSK4829 (Par), pSK4833 (No Par), pSK9169 (ParK2A), pSK9170 (ParE10A) or pSK9171 (ParY43A). Proteins were detected using anti-Par peptide antibodies (Section 2.6.3) as described in Section 2.5.9. **B.** Western blot of Par NTD mutants in *E. coli*. Immunodetection was performed on *E. coli* DH5 α cell lysates (Section 2.5.8) containing pSK9170 (ParE10A), pSK9171 (ParY43A) or pSK9169 obtained from two independent clones (ParK2A #1 and ParK2A #2). Proteins were detected using rabbit anti-Par antiserum as described in Section 2.5.9. Lane M contains prestained protein markers, with marker sizes indicated in kDa on the left of each blot. Positions of relevant proteins and their approximate measured sizes are indicated by black arrowheads.

C. Plasmid segregational stability assay of pSK1 minireplicons encoding Par NTD mutants. The retention of pSK1 minireplicons pSK9169 (*parK2A*) (●), pSK9170 (*parE10A*) (△), pSK9171 (ParY43A) (▲), pSK4829 (*par*) (◆) and pSK4833 (Δ *par*) (■) in *S. aureus* SK8250 cells was determined as described in Section 2.7. Five days of serial subculture represents approximately 75 generations. Data are normalised to 100 % plasmid retention on Day 0. The averages of at least three independent assays are shown. Error bars represent standard error of the mean.

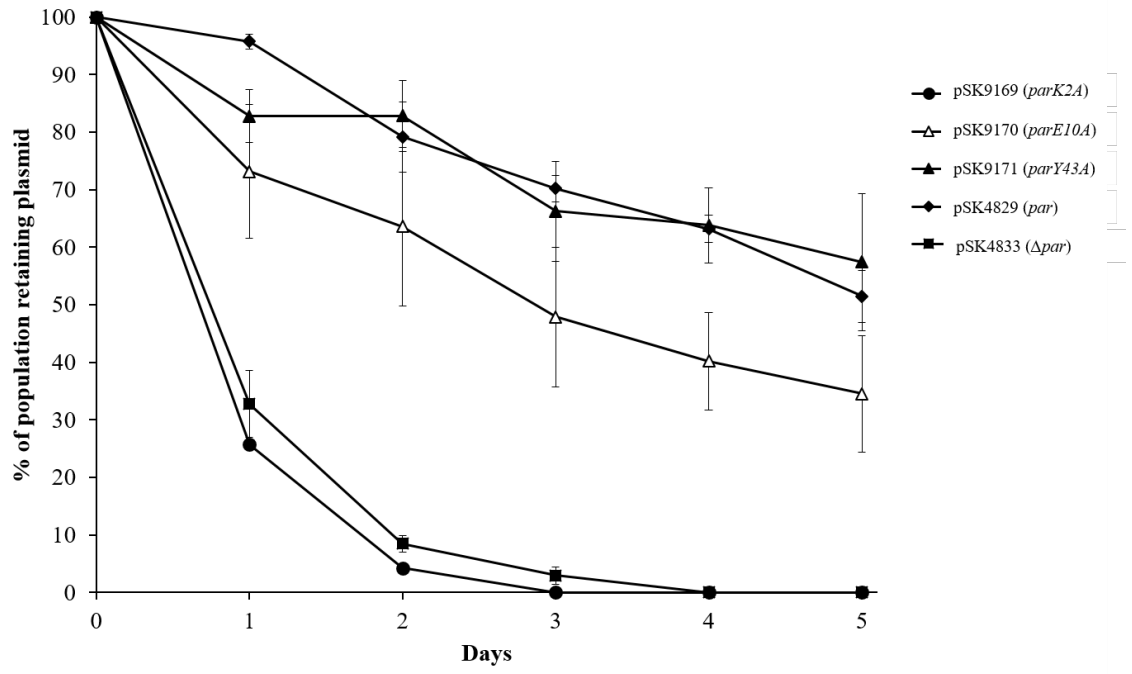
A.



B.



C.



carrying either pSK9169 (*parK2A*), pSK9170 (*parE10A*) or pSK9171 (*parY43A*) (Table 2.2) (Section 2.5.8). Two *E. coli* clones that carried the *parK2A* mutation (pSK9169 #1 and pSK9169 #2), isolated from two independent cloning experiments, were included in the Western blot analysis to minimise the possibility that the absence of detection of ParK2A was specific to the plasmid generated from a single clone. The Western blot analysis on *E. coli* cell lysates, shown in Figure 3.12B, corroborated the findings from the Western blot analysis of *S. aureus* lysates, namely, that ParE10A and ParY43A were readily detected in *E. coli*, but ParK2A could not be detected from either of the two independent clones.

To determine the functionality of the Par NTD mutants, *S. aureus* SK8250 cells carrying pSK9169 (*parK2A*), pSK9170 (*parE10A*) or pSK9171 (*parY43A*) (Table 2.2) were subjected to plasmid segregational stability assays as described in Section 2.7. The assays showed that after five days of subculture in the absence of antibiotic selection, the segregational stability of pSK9169 (*parK2A*) was similar to the stability of the *par*-deficient plasmid, pSK4833 (Figure 3.12C), which was expected, given the undetectable levels of ParK2A in *S. aureus* (Figure 3.12A). There was also little difference in plasmid stability between plasmids encoding Par, ParE10A or ParY43A (Figure 3.12C), which suggests that there was minimal, if any, effect of the E10A or Y43A mutations on plasmid stability, and hence on Par function.

3.7. Discussion

The objective of this chapter is to establish the functional significance and role of the three predicted domains of the pSK1 Par protein. Since the N-terminal HTH domain and central CC domains had previously been implicated in Par DNA-binding and

multimerisation activities, respectively (LeBard 2005, Figgett 2007, Lai 2008), many of the experiments described in this chapter were dedicated to establishing the significance of the predicted C-terminal disordered domain, for which a role had not previously been demonstrated. Table 3.1 summarises the properties of Par and Par CTD mutants as determined by experiments described in this chapter.

3.7.1. Functional studies of the Par CTD

Three separate mutations were generated in the CTD of Par, including a deletion of residues 171–245 (Par Δ CTD), and two individual alanine substitutions at conserved residues of the CTD, R241A and W239A (Section 3.2.1). Plasmid segregational stability assays revealed that the CTD is required for Par function, since Par Δ CTD was unable to maintain the segregational stability of a pSK1 minireplicon (Figure 3.2A). Although this might have been expected from a gross deletion of part of the protein, the stability assays also highlighted the importance of residues R241 and W239 (Figure 3.2A). The partial loss of function imparted by the R241A mutation suggests that R241 contributes to plasmid stability, while the complete loss of function caused by the W239A mutation suggests that W239 is critical for Par function.

It is unclear what role W239 might play in Par function. Tryptophan residues are generally associated with anchoring membrane proteins to the lipid bilayer (Yau *et al.* 1998, Hong *et al.* 2007), however, as yet, there is no data to suggest that Par is a membrane-bound protein. It is possible that, being an aromatic amino acid, W239 might be involved in maintaining proper protein folding or interactions involving the CTD (Ridder *et al.* 2005, Moreira *et al.* 2013). Protein structural studies, such as X-

Table 3.1 Summary of properties of Par and Par CTD mutants

Protein	Plasmid stabilisation^a	DNA-binding^b	Multimerisation^d	Self-interaction^e
Par	Yes	Yes, cooperative	Yes	Yes
Par Δ CTD (aa 1–170)	No	Yes, lower cooperativity ^c	Yes, high proportion of potential dimers	Yes
ParW239A	No	Yes, lower cooperativity ^c	Yes, multimeric profile same as Par	Yes
ParR241A	Partial	Yes, lower cooperativity ^c	Yes, multimeric profile same as Par	Yes

^aPlasmid stabilisation ability assessed by plasmid segregational stability assays (Section 3.2.2).

^bDNA-binding activity assessed by electrophoretic mobility shift assays (EMSAs) (Section 3.4).

^cLower cooperativity based on observation of intermediate protein-DNA species in EMSAs (Section 3.4).

^dMultimerisation activity assessed by cross-linking assays using glutaraldehyde and DSP (Section 3.5).

^eSelf-interaction ability assessed by yeast two-hybrid (Y2H) assays (Section 3.6.2).

ray crystallography (Ilari and Savino 2008), circular dichroism (Pelton and McLean 2000), and nuclear magnetic resonance (Montelione *et al.* 2000), could be used to compare the structures or folding of Par and ParW239A, which might reveal a role of W239 in Par function.

Western blotting confirmed the production of all Par CTD mutants in *S. aureus*, however, only a faint signal was detected for Par Δ CTD (Figure 3.2B). It is unclear whether this was the result of a reduction in the number of epitopes following the removal of 75 amino acids from the C-terminal end of Par, or the result of low Par Δ CTD levels. Therefore, the possibility cannot be excluded that low protein levels may have led to the observed inability of Par Δ CTD to stabilise a pSK1 minireplicon in *S. aureus*. However, the similar band intensities between Par, ParR241A and ParW239A (Figure 3.2B) suggests that the Par CTD point mutants were present at similar levels to Par in *S. aureus*. The reduced functionality of ParR241A and ParW239A can, therefore, be directly attributed to the introduced mutations, which in turn implicates these residues in Par functionality.

It is also worth noting that from the Western blot in Figure 3.2B, the electrophoretic migrations of Par, ParR241A and ParW239A reflected apparent protein sizes that were larger than expected. Full-length Par proteins migrated with an apparent size of 45 kDa, which is approximately 50% larger than their calculated size of 29 kDa. This phenomenon has been observed previously with other Par mutants, including a CC deletion mutant (Par Δ CC) (Supplementary Figures S2A– B) (Lai 2008, Jensen, S. O. and Firth, N., unpublished data). Since only Par Δ CTD migrated close to its expected size of 20 kDa (Figure 3.2B), the aberrant migration was most likely a consequence

of the highly acidic nature of the CTD. Aberrant migration of proteins in SDS-PAGE gels is not unprecedented. Shirai *et al.* (2008) analysed the proteome of the yeast *Schizosaccharomyces pombe* and found that 40% of proteins did not migrate according to their calculated molecular weights when electrophoresed on SDS-PAGE gels. Furthermore, they observed that acidic proteins, with isoelectric points less than 6, tended to have reduced mobility through gels, possibly due to repulsion with negatively charged SDS (Shirai *et al.* 2008). In general, the difference between apparent and calculated molecular weights increased as isoelectric points decreased (Shirai *et al.* 2008). The calculated isoelectric points of Par, Par Δ CC and Par Δ CTD are 4.97, 4.90 and 5.70, respectively. Based on these figures, the difference between apparent and calculated molecular weights would be greater for Par and Par Δ CC than for Par Δ CTD, which is consistent with observations in this study (for example, see Figures 3.2B and 3.3–3.5).

Western blotting was performed on cell lysates from *S. aureus* SK8250 cells (Table 2.1), a *spa*⁻ strain that was used for the purpose of eliminating non-specific binding of immunoglobulins by the staphylococcal immunoglobulin-binding protein, Protein A (Forsgren and Sjöquist 1966). As expected, Protein A (42 kDa) was not detected, however, despite using affinity-purified and preadsorbed anti-Par antibodies for the immunodetection of Par proteins (Section 3.2.2), the Western blot showed non-specific binding and cross-reactivity of the antibodies with staphylococcal proteins, including an approximately 50 kDa protein that appeared as an intense band on the blot (Figure 3.2B). This band most likely corresponds to a second staphylococcal immunoglobulin-binding protein, Sbi, which has also demonstrated non-specific binding to antibodies (Zhang *et al.* 1998).

3.7.2. Protein purification

For *in vitro* analysis of Par DNA-binding and multimerisation activities, purification of overproduced Par proteins was performed under denaturing conditions (Section 3.3.4). Although it would have been preferable to purify proteins under native, or non-denaturing, conditions to minimise protein denaturation, it was demonstrated that RGS_{H6}-Par could not be purified under these conditions (Section 3.3.3 and LeBard 2005), possibly due to inaccessibility of the RGS_{H6} tag to the Ni²⁺-NTA purification resin. It is interesting to note that the ability of the Par CTD mutants to be purified under non-denaturing conditions (Section 3.3.3) suggests that the conformation of these mutants possibly differs from that of RGS_{H6}-Par, in such a way that allows the RGS_{H6} tag to be exposed and accessible to the purification resin. Because RGS_{H6}-Par could not be purified under non-denaturing conditions, and to maintain consistency between all protein preparations, denaturing conditions were employed for the purification of all Par protein variants. In this regard, it was assumed that buffer exchange facilitated the refolding of purified proteins from their denatured states (Section 3.3.4), since DNA-binding and multimerisation activities were detected for Par (Sections 3.4 and 3.5). Further detailed analysis of protein conformation and structure, using techniques such as circular dichroism (Pelton and McLean 2000), X-ray crystallography (Ilari and Savino 2008) or nuclear magnetic resonance (Montelione *et al.* 2000), would be needed to confirm these propositions.

It should also be noted that the purified protein preparations contained a contaminant protein of approximately 30 kDa (Figures 3.5A–D), which was unlikely to have been the product of Par degradation, since it was not detected by Western blotting with

anti-Par antibodies (Figure 3.5E). Rather, the contaminant protein is possibly SlyD, a 30 kDa histidine-rich protein that has been reported to co-purify with His-tagged proteins (Andersen *et al.* 2013). This contaminant did not appear to pose any problems for downstream experiments, as the protein preparations remained consistent, and proper experimental controls were in place.

3.7.3. DNA-binding studies

Due to the propensity of disordered domains to interact with proteins (Dunker *et al.* 2002), it was reasoned that the CTD might be involved in interactions intra- or inter-molecularly with the HTH or CC domains of Par, and in turn affect DNA-binding or multimerisation activities. It has been shown previously that Par binds specifically to seven 12-bp direct repeats of the centromere-like site encompassed by the 212 bp DNA probe used in the EMSAs described in Section 3.4 (LeBard 2005, Figgett 2007, Lai 2008). The EMSAs on Par CTD mutants showed that RGSH₆-Par Δ CTD, RGSH₆-ParW239A and RGSH₆-ParR241A bound the DNA probe containing the centromere-like site as efficiently as RGSH₆-Par (Section 3.4), suggesting that the CTD is not essential for DNA-binding. This is unsurprising, since Par DNA-binding activity is most likely restricted to the N-terminal HTH domain, as a K15A mutation completely abolished DNA-binding (Supplementary Figure S3A) (Lai 2008).

However, it appears that the CTD contributes in some capacity to Par DNA-binding, since the binding of RGSH₆-Par Δ CTD resulted in the production of intermediate Par-DNA complexes that had not completely shifted the electrophoretic mobility of the DNA probe (Figure 3.6C). This might have been due in part to the smaller size of Par Δ CTD-DNA complexes, which might have enabled their complete migration into

the gel. This was in contrast to the full-length Par-DNA complexes that remained in the wells of the polyacrylamide gel (Figures 3.6A–B and D–E). However, when the EMSAs were electrophoresed on polyacrylamide/agarose hybrid gels, which have larger pores in the gel matrix, the complete migration of protein-DNA complexes into the hybrid gels allowed for better separation of the complexes (Figures 3.6F–I). This led to the revelation of intermediate protein-DNA species that were observed upon binding of the DNA probe by RGS_{H6}-Par Δ CTD, RGS_{H6}-ParW239A and RGS_{H6}-ParR241A, but not by RGS_{H6}-Par (Figures 3.6F–I). In order to better resolve the intermediate protein-DNA complexes, and to possibly allow for quantification of binding parameters, EMSAs could be performed using a finer concentration range within that observed for intermediate shifting.

Note that poly(dI-dC) was not included in the EMSAs performed using the polyacrylamide/agarose hybrid gels, since SYBR-Safe staining of DNA would have likely stained both poly(dI-dC) and the DNA probe, obscuring interpretation of results. Therefore, it would not be accurate to derive quantitative data from these results, since non-specific DNA-binding cannot be excluded. The EMSAs on hybrid gels are only useful for qualitative analysis of the protein-DNA complexes formed in stepwise DNA-binding.

Taken together, these results suggest that the CTD plays a non-essential role in DNA-binding; it would appear that the CTD is not directly involved in DNA-binding, but rather, that the CTD might have a role in enhancing the cooperativity of DNA-binding, or enhancing the binding of Par to the second highest affinity site. Quantitative biophysical techniques such as surface plasmon resonance (Szabo *et al.*

1995, Nguyen *et al.* 2007), isothermal titration calorimetry (Liang 2008) or fluorescence polarisation assays (Lundblad *et al.* 1996) would be required to determine the effects of mutations to the CTD on DNA-binding kinetics and cooperativity. It might also be useful to determine the affinity of Par, and Par mutants, for individual binding sites in isolation, in order determine the effect of mutations to cooperativity, and to derive a possible DNA-binding order. Implications of the perceived reduction in the cooperativity of DNA-binding by Par CTD mutants are discussed further in Chapter 6.

3.7.4. Multimerisation studies

When studying the multimerisation activity of Par using cross-linking methods, it was important to use a cross-linker concentration that would minimise artefactual cross-linking. A glutaraldehyde concentration of 0.01% (v/v) was used for *in vitro* cross-linking of purified proteins (Section 3.5.1), and a DSP concentration of 0.1 mM and 0.5 mM was used for *in vivo* cross-linking in *S. aureus* and *E. coli*, respectively (Section 3.5.2). These concentrations produced cross-linked multimers of a range of sizes, whereas higher cross-linker concentrations resulted in high molecular weight complexes, presumably corresponding to protein aggregates formed as a result of excessive cross-linking.

From both *in vitro* and *in vivo* cross-linking experiments, conducted in Sections 3.5.1 and 3.5.2, respectively, ParR241A and ParW239A produced similar multimeric profiles to that of cross-linked Par, whereby the proportion of dimers and trimers appeared equal in *in vitro* assays (Figure 3.7B), and trimers were prominent in *in vivo* assays (Figure 3.9B). However, cross-linking of Par Δ CTD produced a higher

proportion of dimers compared to trimers or higher-order multimers in both *in vitro* and *in vivo* cross-linking assays (Figures 3.7B and 3.9B). These dimers were present even at lower cross-linker concentrations (Figures 3.7C and 3.9C), which suggests that they were unlikely to be the product of artefactual cross-linking. Although it would have been preferable to gain insights into Par Δ CTD multimerisation in its native *S. aureus* host, Western blots using affinity-purified (Section 2.6.1) and preadsorbed (Section 2.6.2) anti-Par antiserum could not readily detect Par Δ CTD in *S. aureus* cell lysates (Figure 3.8B), which, combined with non-specific background signals from anti-Par antibodies, was problematic for meaningful interpretation of results. Nevertheless, considering the above multimerisation results alone, it would appear that the R241A and W239A mutations did not have a visible effect on Par multimerisation, whereas a gross deletion of the CTD favoured dimer formation and reduced the formation of trimers and higher-order complexes. The dimers formed by Par Δ CTD were likely mediated by the CC domain, since previous cross-linking studies showed that a Par Δ CC mutant, which lacks the CC domain from residues 83–155, was unable to multimerise to any significant extent and remained largely as monomers in the presence of cross-linker (Supplementary Figures S2A–B) (Lai 2008, Jensen, S. O. and Firth, N., unpublished data). This, therefore, implicated the CC domain, and not the CTD, in Par multimerisation. However, the multimerisation behaviour of Par Δ CTD demonstrated in cross-linking studies (Section 3.5) suggests that, although the CTD might not contribute directly to Par dimerisation, it might contribute to the formation or stabilisation of trimers and higher-order complexes, perhaps by mediating interactions between existing Par multimers. This supports the EMSA results, which suggest that CTD mutations affect the ability of Par to bind

cooperatively to DNA (Section 3.4). The impaired ability of Par Δ CTD to form higher-order complexes might, therefore, explain the presence of intermediate protein-DNA species that were observed in the EMSAs (Figures 3.6C and G). The potential role of the Par CTD in DNA-binding and multimerisation is explored further in Chapter 6.

Interestingly, in contrast to the *in vitro* cross-linking results, cross-linked dimers were not readily detected for Par, ParR41A or ParW239A in *S. aureus* nor in *E. coli*, but rather, distinct bands of approximately 130 kDa, the predicted size of trimers, were observed (Figures 3.8B and 3.9B). It is unclear why a discrepancy in the presence of dimers was observed between *in vitro* and *in vivo* cross-linking results. The electrophoresis of lysates from DSP-treated cells under non-reducing conditions may have caused some proteins to retain their quaternary structures, especially those involving disulphide bonds, and this may have resulted in aberrant migration and miscalculation of protein size. However, it seems unlikely that the 130 kDa band represents Par dimers that have migrated aberrantly under non-reducing conditions, because Par does not contain any cysteine residues that might participate in disulphide bonding. Furthermore, cross-linking studies performed on the Par DNA-binding mutant, ParK15A, in *E. coli* and *S. aureus*, revealed protein bands of approximately 90 kDa and 130 kDa, corresponding to the sizes of dimers and trimers, respectively (Figures 3.8B and 3.9A). Note that the high levels of ParK15A detected in *S. aureus* is presumably due to its inability to bind centromere DNA and thus mediate autoregulation (LeBard 2005, Lai 2008). The absence of the 90 kDa band from cells producing Par, ParR241A or ParW239A suggests that these protein variants do not form dimers (or the 90 kDa protein complex) *in vivo*, and that the 130

kDa band most likely corresponds to Par trimers, or to protein complexes involving Par and other *S. aureus* or *E. coli* proteins. However, the complete absence of Par dimers *in vivo* seems unlikely, and the Western blotting results shown in Figures 3.8B and 3.9B possibly reflects the cross-linking of closely-interacting Par proteins that might have been bound as multimers to the centromere-like site present on the plasmid DNA. The dimers detected for ParK15A might, therefore, have been the result of Par dimerisation combined with an inability to bind DNA. This has implications for the mechanism of Par-DNA binding, which is addressed in Chapter 6. A more accurate gauge on Par multimerisation states might be gained through size exclusion chromatography (Wen *et al.* 1996), which would provide better resolution of high molecular weight multimers, whilst also reducing the ambiguities associated with calculating multimeric states based on electrophoretic migration.

3.7.5. Self-interaction studies

The multimerisation activity of Par revealed in the cross-linking assays (Section 3.5) is supported by Y2H assays, which provided evidence of self-interaction between Par bait and prey fusion proteins (Figures 3.10A–B). Self-interaction was also detected for all Par mutants, including Par Δ CC (Figures 3.10A–B), which contradicts previous cross-linking results that showed little or no multimerisation of Par CC mutants (Supplementary Figures S2A–B) (Lai 2008, Jensen, S. O. and Firth, N., unpublished data). It should be noted that the interpretation of a positive interaction from Y2H assays only requires interaction between two proteins (the bait and prey fusion proteins), and does not directly provide evidence of multimerisation.

Although both *in vitro* and *in vivo* cross-linking studies indicate that the CTD has a role in Par multimerisation, particularly in the formation of higher-order multimers, the studies revealed similar multimerisation patterns between Par, ParW239A and ParR241A (Figures 3.7B and 3.9B), which suggests that these mutations did not significantly affect Par multimerisation. However, the cross-linking assays are qualitative rather than quantitative assays, and so the possibility cannot be excluded that the point mutations in the CTD might result in changes to multimerisation activity at the molecular level. Indeed, the α -galactosidase assays performed in Section 3.6.2 revealed that the highest levels of α -galactosidase activity were generated by the self-interaction of Par CTD mutants – Par Δ CTD, ParR241A and ParW239A (Figure 3.10B). The increased α -galactosidase activities suggest that the absence of, or alterations to, the CTD promotes stronger self-interaction, presumably due to an increase in the accessibility of multimerisation domains. Taking into account previous findings that identified the CC domain as the domain responsible for Par multimerisation (Figgett 2007, Lai 2008), this would lead one to speculate that the CTD might have a role in modulating interactions between Par proteins, possibly by obstructing interactions between CC domains. In this regard, the CTD might be important for preventing strong, inappropriate Par self-interactions that could otherwise be detrimental to Par function. It should also be noted, however, that differences in α -galactosidase activities might also be due to differences in the expression levels of bait and prey proteins, or the effect of fusion proteins on GAL4-dependent activation of the *MEL1* reporter gene. Therefore, α -galactosidase assays in yeast might not provide an absolute indication of protein-protein interaction strength. Techniques such as surface plasmon resonance (Szabo *et al.* 1995), isothermal

titration calorimetry (Liang 2008) or fluorescence polarisation (Lundblad *et al.* 1996), which can be used to quantitatively measure protein interaction kinetics, might be able to substantiate the results from α -galactosidase assays.

A potential role for the CTD in modulating Par self-interactions gave reason for further investigations into the interactions between individual Par domains, which might provide insights into the intermolecular interactions between Par domains in Par multimers, or into the intramolecular contacts made between Par domains within a single Par protein. Despite interaction between GAL4 BD-ParFL and GAL4 AD-ParFL, no apparent interactions were detected between GAL4 BD-ParFL and the Par domain prey fusions (Figure 3.11A). These conflicting results highlight the caution that must be taken with the interpretation of negative Y2H results, as negative results are not necessarily indicative of the absence of protein interaction. The activation of reporter genes in the Y2H assay relies on interaction between bait and prey proteins that are fused to GAL4 BD and GAL4 AD proteins, respectively, the fusion of which may interfere with, or hinder, interactions that might otherwise take place. Furthermore, identification of positive interactions is dependent on activation of the *HIS3*, *ADE2*, *lacZ* and/or *MEL1* reporter genes in *S. cerevisiae* AH109. Activation of transcription is driven by a functional GAL4 transcription factor, and thus the transcription factor assembled by the interacting bait and prey fusion proteins must be able to recognise and bind to the promoter region of reporter genes in order to activate their transcription. Another consideration in the interpretation of negative Y2H results is the use of a heterologous, eukaryotic host to produce bacterial *S. aureus* proteins. Yeast cells might introduce protein modifications or changes to protein folding which differ from the natural host, and hence a bacterial two-hybrid

system (Karimova *et al.* 1998) might be more suitable for performing interaction studies with Par proteins.

With the above considerations in mind, the Y2H assays did, however, show that GAL4 AD-ParFL interacted with both GAL4 BD-ParCC and GAL4 BD-ParCTD (Figure 3.11A, panels K and P), thus implicating the CC domain and CTD in Par interactions. Further assays to delimit the interacting domains suggested that the CC domain interacts only with itself, and that the CTD interacts only with itself (Figure 3.11A, panels M and S). Notably, strains expressing ParCTD and ParCC fusions consistently showed weaker growth on low-stringency selection medium (results from four biological replicates) (Figure 3.11B, panels M, R and S), possibly as a result of impaired cell growth due to the production of these two specific fusion proteins. Furthermore, yeast cells containing Par CC bait and prey fusion proteins did not show growth on high-stringency selection media, but did show α -galactosidase activity on the media and in α -galactosidase assays (Figures 3.11A and 3.11E). The lack of growth was possibly due to a failure of the interacting protein pair to activate the *HIS3* or *ADE2* reporter genes, with *MEL1* activation and α -galactosidase activity driven by cells that were initially patched but failed to multiply. Four biological replicates were patched, and this phenomenon was observed in all replicates. The conformation of the interacting fusion proteins and the assembled GAL4 transcription factor, combined with differences in the upstream activation sequence and promoters of the reporter genes, may have led to differences in the outcomes of reporter gene activation. Nevertheless, the positive interaction between CC domains corroborates previous cross-linking results, which implicated the CC domain as the multimerisation domain (Lai 2008). Note that α -galactosidase

activities resulting from interactions between CC domains alone were higher than those from interactions between full-length Par (31 ± 13 -fold and 6 ± 3 -fold increase in α -galactosidase activity, respectively, compared to GAL4 BD-Lam and GAL4 AD-T interaction; Figure 3.11E), which again suggests that the CTD might interfere with interactions between CC domains.

The α -galactosidase activity generated from interactions between Par CTDs alone was not substantially higher than the activity from the interaction between full-length Par proteins, presumably due to the absence of the CC domains, which have been demonstrated to promote high levels of α -galactosidase activity (Figure 3.11E). The positive interaction between Par CTD bait and prey fusion proteins is consistent with data obtained from DNA-binding and cross-linking experiments (Sections 3.4 and 3.5), which suggest that the CTDs of Par might interact with each other to stabilise Par complexes (for example, multimers) to facilitate DNA-binding and the formation of higher-order multimers.

It was anticipated that, given the possible role of the CTD in modulating Par self-interaction (Section 3.6.2 and 3.6.3.2), the CTD might interact with either the NTD or CC domain to fulfil this function. However, Y2H assays did not show a direct interaction between the CTD and either the NTD or CC domains (Figure 3.11A). This may have been due to weak or transient interactions between the CTD and other Par domains that were not detected by the Y2H assays, or problems with protein conformation or reporter gene activation as described above. It is also possible that the Par CTD modulates Par self-interaction by steric means, rather than by direct

interactions with Par domains. Mechanistic insights gained from Y2H experiments between Par domains will be revisited in Chapter 6.

For positive Y2H interactions between Par domains, it was assumed that the yeast cells produced both bait and prey fusion proteins, since all fusion proteins did not exhibit self-activation of the reporter genes or non-specific interaction with the GAL4 BD or GAL4 AD proteins (Figure 3.11A). However, for negative Y2H results, it was important to verify the production of both bait and prey fusion proteins in yeast to ensure that both proteins were available for potential interactions. All bait fusions to Par domains could be detected by Western blotting using anti-Par antibodies, however, GAL4 BD-ParNTD and GAL4 BD-ParCC were not as readily detected as GAL4 BD-ParFL and GAL4 BD-ParCTD (Figure 3.11C). This may have been due to lower protein levels or fewer epitopes, which would result in less efficient immunodetection. For reasons unknown, GAL4 AD fusions to the Par domains could not be detected using anti-Par antibodies, but were detected using anti-HA antibodies against the HA epitope (Figure 3.11D). The apparent sizes of ParFL and ParCTD bait and prey fusion proteins, as determined by Western blotting (Figures 3.11C–D), were different to their expected sizes (Section 3.6.3.2). This aberrant migration was consistent with previous gel electrophoresis observations (Sections 3.2.2, 3.3.2 – 3.3.4 and 3.5), and is most likely a result of the acidic nature of the CTD, since migration of ParNTD and ParCC fusion proteins, both of which lack the CTD, was consistent with their expected sizes (Section 3.6.3.2). The immunodetection of all GAL4 BD and GAL4 AD fusions to Par and the three Par domains, therefore, confirmed their production in yeast and suggests that any lack of

growth on high-stringency selection media was not due to the absence of either the bait or prey protein.

3.7.6. Functional studies of the Par NTD

Preliminary structural data obtained by a collaborator, Prof. Maria Schumacher (Duke University, USA), identified three residues in the Par NTD (K2, E10 and Y43) that might be involved in interactions between pairs of Par dimers when bound to pSK1 *par* centromere DNA (Section 3.6.4.1). Although the Y2H assays performed in Section 3.6.3.2 did not indicate any interaction between Par NTDs (Figure 3.11A), the assays did not contain the pSK1 *par* centromere-like site to which Par binds. For this reason, potential interactions between Par NTDs, that might be dependent on Par DNA-binding, would have been overlooked. Therefore, to explore the involvement of K2, E10 and Y43 in interactions of the NTD, Par mutants were generated using alanine substitution (Section 3.6.4.2). However, Western blotting failed to detect the presence of ParK2A in *S. aureus* and from two independent clones in *E. coli* (Figures 3.12A–B). Since the protein-coding sequence and promoter region of *parK2A* from both clones were correct, it is possible that the substitution of a lysine codon (AAA) at the second codon for an alanine codon (GCA) may have altered the translational efficiency of the *parK2A* transcript. Indeed, several studies have reported on the importance of the second codon in translation initiation efficiency and gene expression levels (Looman *et al.* 1987, Stenström *et al.* 2001, Tang *et al.* 2010). It is also possible that substituting K2 with an alanine residue resulted in targeting of the protein for degradation, based on the N-end rule (Dougan *et al.* 2012). Therefore, substitution of the K2 residue of Par

may have resulted in degradation or poor protein expression, which was reflected in undetectable protein levels in Western blots (Figures 3.12A–B). Perhaps substituting the K2 residue with another residue, for example, glutamic acid, might produce a more stable protein.

Of the two NTD mutants that were expressed, ParE10A and ParY43A, neither showed any drastic effect on plasmid segregational stability (Figure 3.12C). It is possible, therefore, that these residues are not functionally significant, and that the contacts inferred from the structural data were crystal contacts and not true interaction between residues. However, it is also possible that the effect of a single ParE10A or ParY43A mutation, in isolation, might have only had a subtle effect on plasmid stability. Hence, it might be useful to generate a ParE10A/Y43A double mutant to determine whether a more severe effect might be observed.

CHAPTER 4

Interactions between pSK1 Par and *S. aureus* host factors

4.1. Introduction

Par was shown to exhibit both DNA-binding and multimerisation activities *in vitro* (Sections 3.4 and 3.5), however, details of the mechanism of plasmid segregation remain elusive. Investigating the mechanism of plasmid maintenance by pSK1 *par* is of particular significance, since the pSK1 *par* system is unique, largely because it encodes a single protein, as opposed to a separate DNA-binding protein and NTPase that are encoded by most characterised plasmid partitioning systems (Gerdes *et al.* 2010, Schumacher 2012, Baxter and Funnell 2014). It is, therefore, conceivable that Par might act in concert with one or more host factors to facilitate efficient plasmid segregation. In this regard, it is envisaged that Par might serve as a bridging protein between plasmid DNA and a host element, such as a host-encoded protein or nucleoid DNA. This chapter, therefore, describes experiments that were performed to determine whether host-encoded proteins or nucleoid DNA might interact with pSK1 Par to contribute to Par function.

4.2. Plasmid stabilisation by a distant pSK1 Par homologue

Because the pSK1 *par* locus encodes only a single protein, this partitioning system represents a potentially novel mechanism of plasmid stability. However, many of the

studies performed to date on the effect of this system on plasmid maintenance have focussed on the *par* system from pSK1. Therefore, to determine whether plasmid segregational stability is a function of Par homologues, or whether this function is unique to pSK1 Par, the contribution of a distant Par homologue to plasmid stability was assessed.

A BLASTP search (Altschul *et al.* 1990) using the Par amino acid sequence (GenBank Accession Number AAF63251) identified a distant Par homologue that is encoded by the *S. epidermidis* multiresistance plasmid, pSERP (GenBank Accession Number NC_006663). This protein, annotated as replication-associated protein (GenBank Accession Number WP_011251343), and hereafter referred to as Par-pSERP, showed 40% sequence identity to Par, as shown by the Clustal Omega alignment (Sievers *et al.* 2011) of pSK1 Par with Par-pSERP (Figure 4.1A). For comparison, the sequence of a Par homologue identified by Firth *et al.* (2000), RepB287 (GenBank Accession Number CAA53279), encoded on the *Tetragenococcus halophilus* plasmid pUCL287, is included in the sequence alignment. Similar to pSK1 Par, RepB287 has also been implicated in plasmid maintenance (Benachour *et al.* 1997), however, the sequence alignment in Figure 4.1A shows that pSK1 Par is more closely related to Par-pSERP than to RepB287.

The genes encoding pSK1 Par and Par-pSERP also share the same genetic organisation relative to the replication initiation gene, *rep*, of their cognate plasmids (Figure 4.1B). Namely, the *par*-like gene is located upstream of, and transcribed divergently from, the associated *rep* gene (Figure 4.1B). In contrast, *repB287* is located downstream of, overlapping with, and transcribed in the same direction as,

Figure 4.1 Sequence analysis of pSK1 Par homologues

A. Multiple sequence alignment of selected pSK1 Par homologues. Amino acid sequences of pSK1 Par (GenBank Accession Number AAF63251) and homologues encoded by pSERP (GenBank Accession Number WP_011251343) and pUCL287 (GenBank Accession Number CAA53279) were aligned using Clustal Omega as described in Section 4.2. Names of the plasmids on which Par-like proteins are encoded are shown on the left. Amino acid positions for individual sequences are shown on the right; positions for the alignment are shown above the alignment. Amino acid residues common to all three aligned sequences are shaded in orange and denoted in uppercase below the alignment. Amino acid residues common to two of the three aligned sequences are shaded in yellow and denoted in lower case below the alignment. Insertions and deletions are indicated by dashes.

B. Illustrative representation of the genetic organisation of pSK1 *par*-like genes (blue arrows) relative to the respective replication initiation genes (yellow arrows) on pSK1 (GenBank Accession Number GU565967), pSERP (GenBank Accession Number NC_006663) and pUCL287 (GenBank Accession Number X75607). Names of the plasmids are shown on the left. The directionality of the arrows indicates the direction of transcription.

C. Intergenic sequence between the genes encoding Par-pSERP and Rep on pSERP. Nucleotides in the pSERP plasmid sequence are numbered on the left. The sequences of eight potential repeats are underlined and numbered below the sequence. Coding sequences for the start of Par-pSERP and Rep are shown in blue and yellow, respectively. Amino acids at the start of replication-associated protein and Rep are shown above the nucleotide sequence.

A.

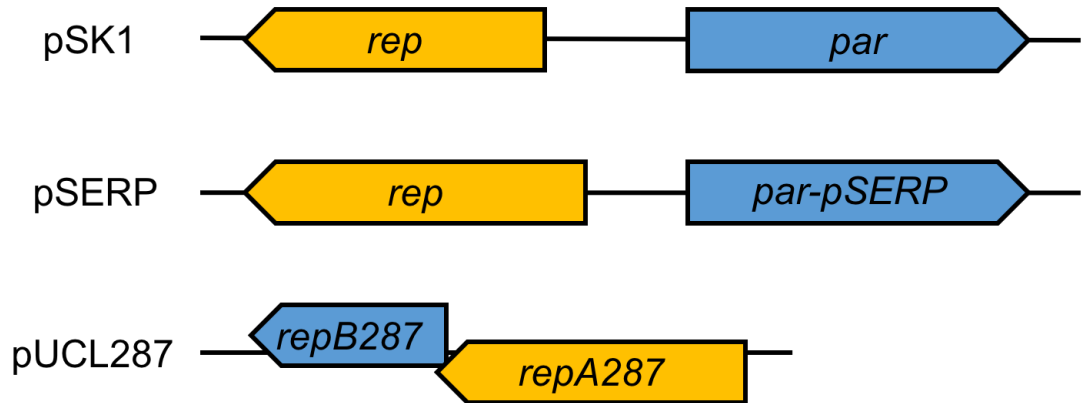
```

                *           20           *           40           *           60           *           80           *
pSK1      : ~MKTIKMVADELNVTKQTVVNNAKNLNISFE-KENGVNYIDDND-YLKIIVEKITKKERTTQNKENKKSEITYENTEKNRYNNS-----D : 81
pSERP     : ~MKSVKKEISEELEVSKQTVFNNIKRLNIETV-KQDNTSFKNDVDVEKIIQRVIRNKKKYGF---ESTNISSEKVKTDNKKNESKYDV--Q : 84
pUCL287   : MPKTIRELADDELGVSKQRIQQIIAKLSPSKTPNKEGNRYVLSAQDVK-----NIKALMGFENNKSSSTSEST----NR---LVDYDVYLD : 77
           mKtike adEL VsKQtv nnik Lnis  k g yi  dv ki  k  gf nkss i se  nr  n  ydv  d

                100           *           120           *           140           *           160           *           180
pSK1      : GFETLKTQVNELEKQVEIFETRAKNDKQYIENLTKQLDQQNSNVNTLNKLLLENQQILALESNKKIQKLEHQLEEERQLSYSFDKSTNDREN : 172
pSERP     : IIEELLEKQIDTLNKQLEKQEKR---HETT-----IEFYRKELQERSKLLLENQQVLALESNKKIQKLESQLEEERQLNYSFDATNNRQN : 165
pUCL287   : VIDSIKEDQIKSLLEV-----QKQTQNLLDQQRLAIQDKKLLLEEKTEIKELKSLNIPKQGSSE----- : 138
           ie lk k  l kqlE  e r  e  kLLenQQ LALesnKkiqkle qleEerqLnysfd stn r n

                *           200           *           220           *           240           *           260
pSK1      : FDVQEASYSVSDSVNTDQYQKEEKKPEVQPKDISESQQDEKSQQ---QDDSFN---QNDKDIAIEETQTKKGFWSRFFGG~~ : 245
pSERP     : IDPQEATFTEESQNINQQQTKCQPTQEVNYKDIAEEKENDSTNEGELIKEDKQVEETKSLPDDNKEVEPPKKGFWSRFFGN~~ : 245
pUCL287   : -----KDD SIP---KENSAENRVKEPQNKKWH--FGRRM : 168
           d qea  t  s n  q q  ev  kdi e  kdDsf  k d d n e ep kKgfWsr FG
```

B.



C.

K I N K R S M **rep**
27061 CATAACTTTT TGACTTGCAA ACTGTAGATA TTGTTGTATA TAATACATAT ATCAAATTA
27111 ATAGCTAACG TATTGTAACG TTTTATTACC CAGTCCCAAC TATTACCAGT AGTTGGGACT
27211 AAAACGTATT ATGAACATTA TATCATTAAA AAAGAACATA TAAAAGATAT TATAATCCCA
27261 TTA AAAACCT TTTATAACA GTTGACAAGA TCATCGTCAA CTGTTTATAA AAGGTTTTTT
8 7 6
1 AAGACTGCTC AAGCTCCCTT TATAAAAGTA TTTATGATAA AATTTATTTA TAAAGGGTTG
5 4 3
replication-associated protein M K S V
51 ATAAAGTGTT TATAAAGGGT TGAAGATATG AAGAGCGTT
2 1

the *repA287* replication gene on pUCL287 (Figure 4.1B) (Benachour *et al.* 1997). Furthermore, the region between pSERP *rep* and *par-pSERP* contains a number of almost identical 8-bp sequences with the consensus sequence ‘TTTATAAA’ (Figure 4.1C), which might represent a potential centromere-like site. With these factors in consideration, Par-pSERP could potentially be functionally homologous to pSK1 Par and be involved in plasmid maintenance.

4.2.1. Construction of pSERP minireplicons to assess the functionality of a distant Par homologue

To determine whether Par-pSERP is involved in plasmid segregational stability, the ability of Par-pSERP to enhance the segregational stability of a pSERP minireplicon was assessed. For the construction of a pSERP minireplicon, a 1.4 kb DNA fragment encompassing the *rep* coding region and upstream intergenic region was PCR-amplified (Section 2.4.4) from pSERP plasmid DNA (Table 2.2) using primers HC35 and HC37 (Table 2.6). The resulting amplicon was purified (Section 2.4.7) and then restriction digested with *Bam*HI and *Hind*III (Section 2.4.6). The pUC18 plasmid derivative, pWE180 (Table 2.2), which carries the *ermC* erythromycin resistance gene for antibiotic selection in staphylococci, was concurrently restricted with *Bam*HI and *Hind*III, after which the digestion reaction was electrophoresed on an agarose gel (Section 2.4.3). The 4.7 kb restricted vector DNA band was gel-purified (Section 2.4.7) and then dephosphorylated using Antarctic phosphatase (Section 2.4.10). The restricted and dephosphorylated vector DNA was ligated (Section 2.4.11) to the restricted insert DNA containing pSERP *rep*. The ligation reaction was used to transform competent *E. coli* DH5 α cells (Section 2.3.2), and

plasmid DNA was isolated from selected ampicillin-resistant transformants (Section 2.4.1) to screen for recombinant plasmids. Isolated plasmid DNA was restricted with *Bam*HI and *Hind*III (Section 2.4.6), and restriction digestion reactions were electrophoresed on an agarose gel (Section 2.4.3). Restricted plasmids displaying the restriction profile of recombinant plasmid DNA were sequenced (Section 2.4.14) using primers HC35 and HC37 (Table 2.6). The *E. coli*–*Staphylococcus* shuttle plasmid containing the correct sequence of pSERP *rep* was named pSK9137 (Table 2.2).

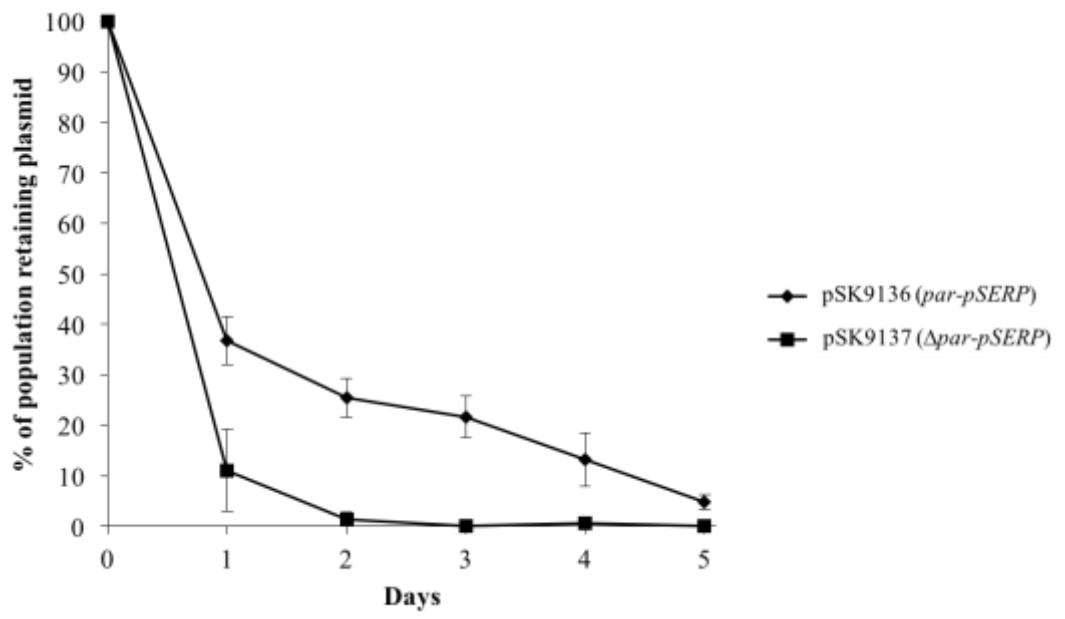
A pSERP minireplicon encoding Par-pSERP was constructed essentially as described above, using primers HC35 and HC36 (Table 2.6) to PCR-amplify (Section 2.4.4) a 2.3 kb DNA fragment encompassing pSERP *rep* and *par-pSERP*. Recombinant plasmids were sequenced (Section 2.4.14) using primers HC35, HC36 and HC37, and the pSERP minireplicon encoding Par-pSERP was named pSK9136 (Table 2.2).

4.2.2. Effect of a distant Par homologue on plasmid segregational stability

In order to determine whether a distant pSK1 Par homologue identified on the *S. epidermidis* multiresistance plasmid, pSERP, is involved in plasmid maintenance, plasmid segregational stability assays were performed on pSERP minireplicons in the presence and absence of Par-pSERP. *S. aureus* RN4220 cells were electroporated (Section 2.3.4) with either pSK9137 (Δ *par-pSERP*) or pSK9136 (*par-pSERP*) (Table 2.2) and subjected to plasmid segregational stability assays as described in Section 2.7. The graph in Figure 4.2 shows that in the absence of Par-pSERP, pSK9137 was rapidly lost from the population, with only a small proportion of the population

Figure 4.2 Effect of a distant Par homologue on plasmid segregational stability

Plasmid segregational stability assay of pSERP minireplicons in the presence and absence of *par-pSERP*. The retention of the pSERP minireplicons pSK9137 (Δ *par-pSERP*) (■) and pSK9136 (*par-pSERP*) (◆) in *S. aureus* RN4220 cells was determined as described in Section 2.7. Five days of serial subculture represents approximately 75 generations. Data are normalised to 100% plasmid retention on Day 0. The averages of three independent assays are shown. Error bars represent standard error of the mean.



(<1%) retaining the plasmid after two days of subculture. In comparison, when Par-pSERP was present, approximately 25±4% of the population retained the pSERP minireplicon on Day 2 of the assay, and 5±1% of the population retained the plasmid at the end of the assay (Figure 4.2). The stability assays, therefore, showed that Par-pSERP enhanced the segregational stability of pSERP minireplicons in *S. aureus*, which suggests that Par-like proteins may have plasmid maintenance functions.

4.3. Functionality of pSK1 *par* in a heterologous host

The involvement of Par-pSERP in the segregational stability of a pSERP minireplicon in *S. aureus* (Section 4.2.2) gives rise to the possibility that Par and other Par-like proteins that have been identified in different bacterial species (Firth *et al.* 2000), might function in plasmid maintenance. However, given that a single plasmid-encoded Par-like protein appears to be sufficient for enhanced plasmid segregational stability (Section 4.2.2, Benachour *et al.* 1997, Simpson *et al.* 2003), and that most characterised plasmid partitioning systems encode a DNA-binding protein and a NTPase (Gerdes *et al.* 2010, Schumacher 2012, Baxter and Funnell 2014), the involvement of host-specific factors in pSK1 *par* functionality cannot be excluded. Therefore, to investigate whether pSK1 *par* relies on *S. aureus* host factors for the mediation of plasmid segregational stability, the effect of *par* on plasmid maintenance was assessed in a heterologous host, *Enterococcus faecalis*.

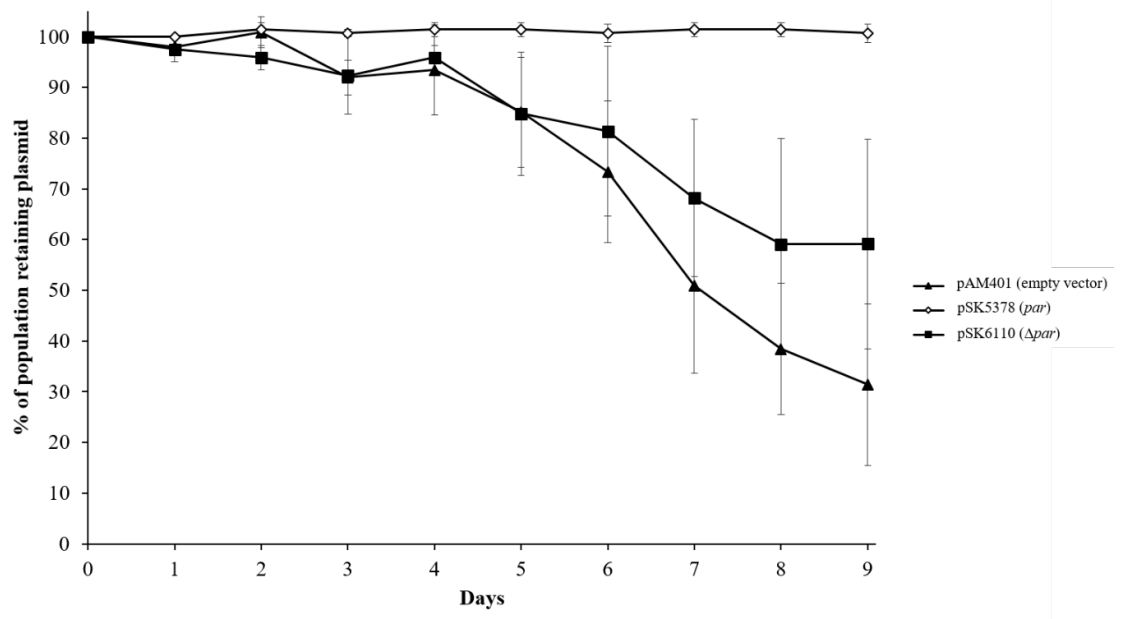
Plasmid segregational stability assays were performed in *E. faecalis* using the *E. coli*-*E. faecalis* shuttle plasmid pAM401 (Table 2.2), which carries the Gram-positive broad host-range replicon of pIP501 (Thompson and Collins 2003). pIP501 minireplicons carrying either the pSK1 *par* gene (pSK5378) or only the pSK1 *par*

centromere-like site (pSK6110) (Table 2.2) were constructed from pAM401 by Simpson *et al.* (2003). The study showed that pSK1 *par* was able to stabilise the pIP501 minireplicon, pSK5378, in *S. aureus* (Simpson *et al.* 2003). For this reason, pSK5378 was used for plasmid segregational stability assays in *E. faecalis* to determine whether pSK1 *par* enhances plasmid segregational stability in the absence of *S. aureus*-specific factors.

E. faecalis JH2-2 (Table 2.1) cells were separately electroporated with pAM401 (empty vector), pSK5378 (*par*) or pSK6110 (Δ *par*) (Table 2.2) (Section 2.3.6), and plasmid segregational stability assays were performed as described in Section 2.7. The stability assays revealed that continuous subculture in the absence of antibiotic selection resulted in a decline in the proportion of the population retaining the *par*-deficient plasmids pAM401 and pSK6110, with $<59\pm 21\%$ of the population retaining pSK6110 at the completion of the assay (Figure 4.3). However, in the presence of pSK1 *par*, pSK5378 was stably retained over nine days by close to 100% of the population, even in the absence of antibiotic selection (Figure 4.3). These results, therefore, demonstrate functionality of pSK1 *par* in the heterologous *E. faecalis* host, which suggests that either pSK1 *par* may be functional as a discrete unit, independent of *S. aureus* host factors, or that Par is able to utilise *E. faecalis* host factors to enhance plasmid segregation (see Section 4.6).

Figure 4.3 Effect of pSK1 *par* on plasmid segregational stability in *Enterococcus faecalis*

Plasmid segregational stability assay of pIP501 minireplicons in the presence and absence of pSK1 *par*. The retention of the pIP501 minireplicons pAM401 (empty vector) (▲), pSK5378 (*par*) (◇) and pSK6110 (Δ *par*) (■) in *E. faecalis* JH2-2 cells was determined as described in Section 2.7. Nine days of serial subculture represents approximately 255 generations. Data are normalised to 100% plasmid retention at Generation 0. The averages of three independent assays are shown. Error bars represent standard error of the mean.



4.4. Interactions between Par and *S. aureus* proteins

4.4.1. Yeast two-hybrid screening of *S. aureus* genomic DNA prey libraries with full-length Par bait

The ability of pSK1 *par* to enhance the segregational stability of a pIP501 minireplicon in *E. faecalis* (Section 4.3) suggests that the mechanism of *par*-mediated plasmid stability might not involve *S. aureus* host factors. However, this does not exclude the possibility that factors in common to *S. aureus* and *E. faecalis* might contribute to Par function. Therefore, to further investigate whether host-encoded factors, in particular *S. aureus* proteins, contribute to the mechanism of pSK1 *par*, yeast two-hybrid (Y2H) studies were undertaken using a Par bait fusion protein. Screening of *S. aureus* genomic DNA prey libraries was performed as described in Section 2.10.4. Briefly, *S. cerevisiae* AH109 cells were first transformed with pSK9107 plasmid DNA (Table 2.2), which encodes the full-length Par (ParFL) bait fusion, GAL4 BD-ParFL, constructed in Section 3.6.1. Yeast cells containing pSK9107 were then made competent and transformed with 6 µg of an equal mixture of twelve existing *S. aureus* genomic DNA prey libraries (Schumacher *et al.* 2014). The prey libraries were constructed from *S. aureus* genomic DNA that had been separately partially-digested with four frequent-cutting enzymes (*Hin*PI, *Taq*^oI, *Aci*I and *Ac*I), and then ligated to pGADT7 vector derivatives in all three reading frames, such that twelve separate libraries were generated (Schumacher *et al.* 2014). These prey libraries have previously been used to identify an interaction between the replication initiator protein, RepA, of the staphylococcal conjugative multiresistance plasmid pSK41, and the staphylococcal protein, DnaG (Schumacher *et al.* 2014).

Yeast transformation reactions were spread on medium-stringency selection medium (SD/-Leu/-Trp/-His) (Table 2.3) to identify clones that potentially contained interacting pairs of GAL4 BD-ParFL bait and *S. aureus* prey protein fusions to GAL4 AD. Serial dilutions of the transformation mixture were also spread on low-stringency selection medium (SD/-Leu/-Trp) (Table 2.3) to calculate the transformation efficiency. A total of approximately 5.7×10^5 library clones were screened. From the medium-stringency selection medium, 280 individual transformants were patched onto low-, medium- and high-stringency (SD/-Leu/-Trp/-His/-Ade/X- α -Gal) selection media (Table 2.3). Following incubation at 30°C for 3–5 days, 17 patches showed growth on high-stringency selection medium. These potential interactions were re-tested and the prey proteins were investigated for self-activation of the reporter genes. Prey plasmids encoding candidate Par interaction partners were isolated from prey clones (Section 2.4.1), and *S. cerevisiae* AH109 cells were co-transformed (Section 2.10.2) with the isolated prey plasmids and either pSK9107 (GAL4 BD-ParFL) or empty pGBKT7 bait plasmid (Table 2.2). Subsequent Y2H assays (Section 2.10.3) revealed that, of the 17 prey plasmids tested, five prey clones activated the reporter genes only in the presence of GAL4 BD-ParFL and not the empty pGBKT7 bait plasmid. The remaining interactions were false-positives, most likely due to interaction between the *S. aureus* prey protein and GAL4 BD, or self-activation of the reporter genes by the prey protein. The *S. aureus* genomic DNA inserts in the five prey plasmids were sequenced (Section 2.4.14) using the T7 sequencing primer (Table 2.6), and open reading frames (ORFs) in each sequence were identified using ORF Finder (Wheeler *et al.* 2003).

The ORF in-frame with GAL4 AD in each of the sequenced prey inserts was used in a BLASTP search (Altschul *et al.* 1990) to identify the Par interaction partner encoded by the prey plasmid. BLASTP searches revealed that four of the five plasmids encoded regions of a staphylococcal cell-surface anchored protein, fibronectin-binding protein (FnBP) (for example, GenBank Accession Number WP_000841432). *S. aureus* expresses two FnBPs, FnBPA and FnBPB, which are involved in adhesion to host matrix proteins, such as fibrinogen and fibronectin, during *S. aureus* infection (Signäs *et al.* 1989). Although the sequences of the *S. aureus* genomic DNA contained in the four prey plasmids were of various lengths, a 761 bp sequence was mostly common to all of the four prey inserts (Figure 4.4). This sequence contains the coding region for the last 177 amino acids of the C-terminal end of FnBP (Figure 4.5), which is common to both FnBPA and FnBPB, and encompasses a LPXTG motif that is a feature of Gram-positive cell wall anchored proteins (Schneewind *et al.* 1992). Importantly, cleavage of the LPXTG motif between the threonine and glycine residues leaves the hydrophobic domain attached to the cell membrane, and the C-terminal end exposed on the cytosolic side of the membrane (Ton-That *et al.* 1997). Therefore, it might be envisaged that interaction of Par with the membrane-bound cleavage product of FnBPs could facilitate anchoring of plasmid DNA to the cell periphery to prevent mis-segregation of plasmids. As a result, the interaction between Par and FnBP was investigated further, as described in Sections 4.4.1.1 and 4.4.2.

The prey plasmid harboured by the fifth prey clone was found to contain a sequence encoding part of *S. aureus* ribonuclease Y (GenBank Accession Number WP_064288115). Staphylococcal ribonuclease Y is involved in RNA degradation

Figure 4.4 Graphical overview of DNA inserts contained in yeast two-hybrid prey plasmids encoding fibronectin-binding protein

Fibronectin-binding protein (FnBP) was identified as a potential Par interaction partner by yeast two-hybrid (Y2H) screening of *S. aureus* genomic DNA libraries using a Par bait protein (Section 4.4.1). The *fnbA/B* gene is shown as a black box. Chromosomal DNA downstream of the *fnbA/B* gene is shown as a black line. Graphical representations of the *fnbA/B* sequence contained in each of the four prey plasmids (FnBP prey 1–4) are shown as coloured boxes. The region of DNA common to all four prey inserts is shaded in yellow.

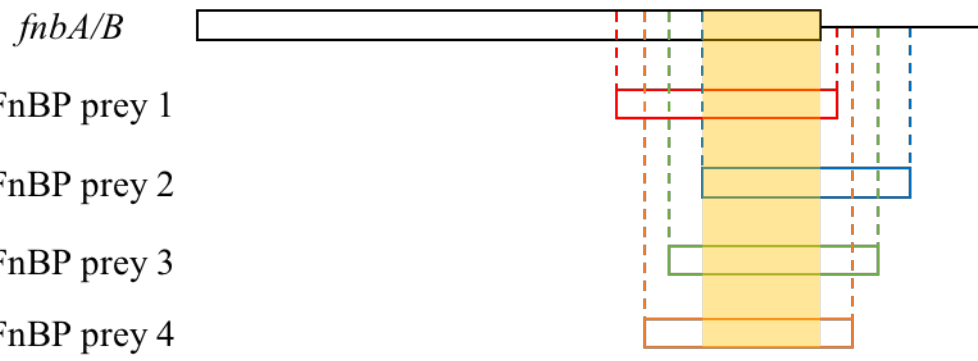


Figure 4.5 Amino acid sequence of FnBP identified by yeast two-hybrid screening of *S. aureus* genomic DNA library using a Par bait

S. aureus genomic DNA prey libraries were screened by yeast two-hybrid (Y2H) analysis using GAL4 BD-ParFL bait as described in Section 4.4.1. Subsequent BLASTP searches using open reading frames from the insert DNA of prey plasmids encoding potential Par interaction partners revealed matches to *S. aureus* fibronectin-binding protein A (FnBPA) and fibronectin-binding protein B (FnBPB). The amino acid sequence of *S. aureus* FnBPA (GenBank Accession Number WP_000841432) is shown. Amino acid residues are numbered on the left. Sequences common to all prey clones that contained sequences encoding fragments of FnBP are shown in red. The sequence of an LPXTG motif is boxed and shown in bold. The site of cleavage between the threonine and glycine residues by sortase is indicated by a purple arrow and dashed lines. Residues comprising the hydrophobic domain are boxed and shaded blue. Positively-charged residues at the C-terminal end of the FnBPA sequence are denoted by green “+” symbols below the sequence.

```

1  MKSNLRYGIR  KHKLGAASVF  LGTMIVVGMG  QEKEAAASEQ  NNTTVEESGS  SATESKASET
61  QTTTNNVNTI  DETQSYSATS  TEQPSQSTQV  TTEEAPTTVQ  APKVETSRVD  LASEKVADKK
121  TTGTQVDTAQ  PSNVSEIKPR  MKRSTDVAEV  AEKEVVEEAK  ATGTDVTSKV  TVENGSEIVG
181  HKQDTNVVNP  HNAERVTLKY  KWKFGEGIKA  GDYFDFTLSD  NVETHGISTL  RKVPEIKSST
241  EDKVMANGQV  IGERKIRYTF  TDYIDNKKDL  TAELTLNLFI  DPTTVTKQGM  EKVEVSLGQN
301  KVSKEFDIKY  LDGVKDRMGV  TVNGRIDTLN  KADGKFHFA  YVKPNNQSLS  SVTVTGQVTS
361  GYKQNVKNPT  VKVYKHIGSD  ELAESIYAKL  DDVSKFEDVT  GELTLQYTSN  GGYSLNFNNL
421  DQSKNYVIKY  EGDYDSNAST  LEFQTHLFGY  YNYYYNTSN  LTWKNVAFY  SNNAQGDGKD
481  KPNDPIIEKS  EPIDLDIKSE  PPVEKHELTG  TIEESNDSKP  IDFEYHTAVE  GAEGHAEGII
541  ETEEDSIHVD  FEESTHENSK  HHADVVEYEE  DTNPGGGQVT  TESNLVEFDE  DSTKGIVTGA
601  VSDHTTVEDT  KEYTTESNLI  ELVDELPEEH  GQAQGPIEEI  TENYQHISHS  GLGTENGHGN
661  YGVIEEIEEN  SHVDIKSELG  YEGGQNSGNQ  SFEEDTEEDK  PKYEQGGNIV  DIDFDSVPQI
721  QGQNGDQSF  EEDTEEDKPK  YEQGGNIIDI  DFDSVPHIHG  FNKHTEIIIEE  DTNKDKPNYQ
781  FGGHSSVDFE  EDTLPQVSGH  NEGQQTIEED  TTPPIVPPTP  PTPEVPSEPE  VPTPPTSEIP
841  SEPGKPVPPA  KEEPKKPSKP  VEQGKVTPV  IEINEKVAV  APTKKAQSKK  SELPETGEE
901  STNKGMLFGG  LFSILGLALL  RRNKKNHKA

```

Hydrophobic domain

++ ++ ++
Positively-
charged C-
terminal tail

Cleavage site

and regulation of virulence genes (Marincola *et al.* 2012, Bonnin and Bouloc 2015). Because of these roles, it was considered that the interaction between Par and ribonuclease Y was unlikely to be biologically relevant, and hence this interaction was not examined further.








4.4.1.1. Interaction between Par and FnBP

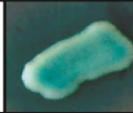

In order to delimit the region of the Par bait protein that might be involved in the interaction with FnBP, Y2H assays were performed between the C-terminal fragment of FnBP and mutant Par proteins (Section 2.10.3). Prey plasmid DNA that was isolated from one of the FnBP preys, FnBP prey 3 (Section 4.4.1), was used to simultaneously transform *S. cerevisiae* AH109 cells (Section 2.10.2) with a bait plasmid encoding either ParFL (pSK9107), ParK15A (pSK9121), Par Δ CC (pSK9122), ParL132A (pSK9123), Par Δ CTD (pSK9124), ParR241A (pSK9130) or ParW239A (pSK9131) (Table 2.2). Co-transformants from low-stringency selection medium were patched onto low-, medium- and high- stringency selection media (Table 2.3) in order to identify clones that activated the GAL4-responsive reporter genes, *HIS3*, *ADE2* and *MEL1*. A positive indication of interaction between the GAL4 BD-bait and GAL4 AD-prey fusion proteins was provided by growth on medium- and high-stringency selection media, and the detection of α -galactosidase activity, as indicated by the production of a blue pigment on media containing X- α -Gal.

The Y2H assays, shown in Figure 4.6, revealed growth on high-stringency selection medium for *S. cerevisiae* strains carrying the prey plasmid encoding the C-terminal end of FnBP and the bait plasmid encoding either ParFL, ParK15A, Par Δ CC,

Figure 4.6 Interaction between Par and FnBP

Yeast two-hybrid (Y2H) assays of interactions between FnBP prey and mutant Par bait fusion proteins. A prey fusion protein of GAL4 AD to a fragment of FnBP that was identified from Y2H screening of a *S. aureus* genomic DNA library using Par bait (Section 4.4.1), was used in pairwise Y2H assays to detect interactions with GAL4 BD bait protein fusions to full-length Par (ParFL), ParK15A, Par Δ CC, ParL132A, Par Δ CTD, ParR241A and ParW239A. Y2H assays were performed as described in Section 4.4.1.1. Growth of *S. cerevisiae* AH109 cells containing bait and prey plasmids is shown on high-stringency selection medium (SD/-Leu/-Trp/-His/-Ade/X- α -Gal) (Table 2.3). Growth indicates activation of the *HIS3* and *ADE2* reporter genes. Blue pigmentation indicates α -galactosidase activity from yeast cells. *S. cerevisiae* AH109 cells expressing the prey protein fusion, simian virus T antigen (GAL4 AD-T), and the bait protein fusions, murine p53 (GAL4 BD-53) or human lamin protein (GAL4 BD-Lam), were included as positive and negative controls, respectively.

		Bait (GAL4 BD fusion)						
		ParFL	ParK15A	Par Δ CC	ParL132A	Par Δ CTD	ParR241A	ParW239A
Prey (GAL4 AD fusion) FnBP fragment								

		pGBKT7-53	pGBKT7-Lam
pGADT7-T			

ParL132A or ParR241A. Conversely, no growth was observed for yeast strains carrying the FnBP prey plasmid and the bait plasmids encoding Par Δ CTD or ParW239A (Figure 4.6). Therefore, interaction between the C-terminal end of FnBP and Par was abolished when the CTD of Par was removed or altered with a W239A mutation, which suggests that interaction with FnBP occurred via the CTD of Par.

4.4.2. Contribution of *S. aureus* FnBP to Par function

Y2H screening of *S. aureus* genomic DNA prey libraries using Par bait protein identified an interaction between Par and *S. aureus* FnBP that was subsequently confirmed using Y2H assays (Section 4.4.1.1). In order to determine the biological significance of this interaction, and the relevance of FnBP to *par*-mediated plasmid segregation, *par* functionality was assessed in a *S. aureus* FnBP mutant, DU5883 (Table 2.1). *S. aureus* DU5883, obtained from Prof. Timothy Foster (Trinity College, Dublin), is a derivative of *S. aureus* 8325-4 that is deficient in both FnBPA and FnBPB. This strain was generated by Greene *et al.* (1995) by insertion mutations of the *fnbA* and *fnbB* genes with tetracycline and erythromycin resistance genes, respectively, which abolished production of FnBPA and FnBPB proteins in *S. aureus*, as determined by Western blotting. The functionality of pSK1 *par* in *S. aureus* 8325-4 and the FnBP mutant, *S. aureus* DU5883, was assessed by performing plasmid segregational stability assays on pSK5630 and pSK6195, which are pSK1 minireplicons with and without *par*, respectively (Table 2.2). Unlike previous assays that were used to assess *par* functionality in *S. aureus*, these assays were not performed using the erythromycin resistance-encoding plasmids, pSK4829 and pSK4833 (Table 2.2), due to the chromosomally-encoded erythromycin resistance of

S. aureus DU5883. Hence, stability assays in *S. aureus* 8325-4 and DU5883 (*fnbA*⁻, *fnbB*⁻) were performed using pSK5630 (*par*) and pSK6195 (Δ *par*), since the chloramphenicol resistance conferred by these plasmids could be used for strain generation and monitoring of plasmid retention.

Unlike *S. aureus* RN4220 and its *spa*⁻ derivative used in most other studies described in this thesis, strains 8325-4 and DU5883 possess normal restriction modification systems. As a result, electroporation of these cells with pSK5630 or pSK6195 did not yield any transformants. This was likely due to the presence of *S. aureus* restriction modification systems, which recognise the methylation state of foreign DNA and inhibit its uptake, thereby preventing the ability of *S. aureus* cells to be transformed (Waldron and Lindsay 2006, Corvaglia *et al.* 2010, Monk *et al.* 2012). To circumvent this problem, plasmids were first passaged through a *dcm*⁻ *E. coli* strain, DC10B (Table 2.1), to prevent cytosine methylation of plasmid DNA (Monk *et al.* 2012), so as to bypass the *S. aureus* restriction barrier. Chemically-competent *E. coli* DC10B cells (Section 2.3.1) were transformed with pSK5630 (*par*) or pSK6195 (Δ *par*) (Table 2.2) then selected for ampicillin resistance (Section 2.3.2), and un-methylated plasmid DNA was subsequently isolated from transformants (Section 2.4.1). Isolated plasmids were then introduced into electrocompetent *S. aureus* 8325-4 and DU5883 cells (Table 2.1) using a sucrose-enriched electroporation buffer, as described in Section 2.3.4.

Plasmid segregational stability assays on pSK5630 and pSK6195 were performed in *S. aureus* 8325-4 and in the FnBP mutant derivative, DU5883, according to the method described in Section 2.7. In both *S. aureus* 8325-4 and DU5883, pSK6195

(Δpar) was lost rapidly from the population, with $<8\pm 1\%$ of the population retaining the plasmid on Day 5 of the assay (Figure 4.7). In the presence of *par*, pSK5360 was retained by a much larger proportion of the population at all stages of the assay, with $>71\pm 11\%$ of the population retaining the plasmid at the conclusion of the assay (Figure 4.7). The stability assays revealed no difference in the retention of pSK5630 (*par*) or pSK6195 (Δpar) between the *S. aureus* FnBP wild-type and mutant strains. Since the absence of FnBP did not result in a noticeable reduction in plasmid stability, it is likely that FnBP is not required for plasmid segregation, and that an interaction between FnBP and Par, detected in Section 4.4.1, is not essential for Par function.

4.4.3. Yeast two-hybrid assay to determine interaction between Par and DivIVA

Plasmid segregational stability assays in a *S. aureus* FnBP mutant indicated that the interaction between Par and FnBP, which was identified by Y2H screening of *S. aureus* genomic DNA prey libraries (Section 4.4.1), was not likely to be biologically significant (Section 4.4.2). However, BLASTP searches using the pSK1 Par amino acid sequence (GenBank Accession Number AAF63251) resulted in the detection of a putative conserved domain, from residues 2–171, that matched to the RacA superfamily in the NCBI conserved domains database (CDD) (Figure 4.8). The region of Par containing the putative conserved RacA domain encompasses the predicted HTH and CC domains of Par (Figure 4.8), which are also predicted structural features of the *Bacillus* polar chromosome division protein, RacA (Ben-Yehuda *et al.* 2003). In *B. subtilis*, RacA interacts with chromosomal DNA and the

Figure 4.7 Plasmid segregational stability of pSK1 minireplicons in a *S. aureus* FnBP mutant

Plasmid segregational stability assay of pSK1 minireplicons in *S. aureus* 8325-4 and a FnBP mutant derivative, DU5883. The retention of the pSK1 minireplicons pSK5630 (*par*) (squares) and pSK6195 (Δ *par*) (circles) in *S. aureus* 8325-4 (solid lines) and DU5883 cells (dashed lines) was determined as described in Section 2.7. Five days of serial subculture represents approximately 75 generations. Data are normalised to 100% plasmid retention on Day 0. The averages of three independent assays are shown. Error bars represent standard error of the mean.

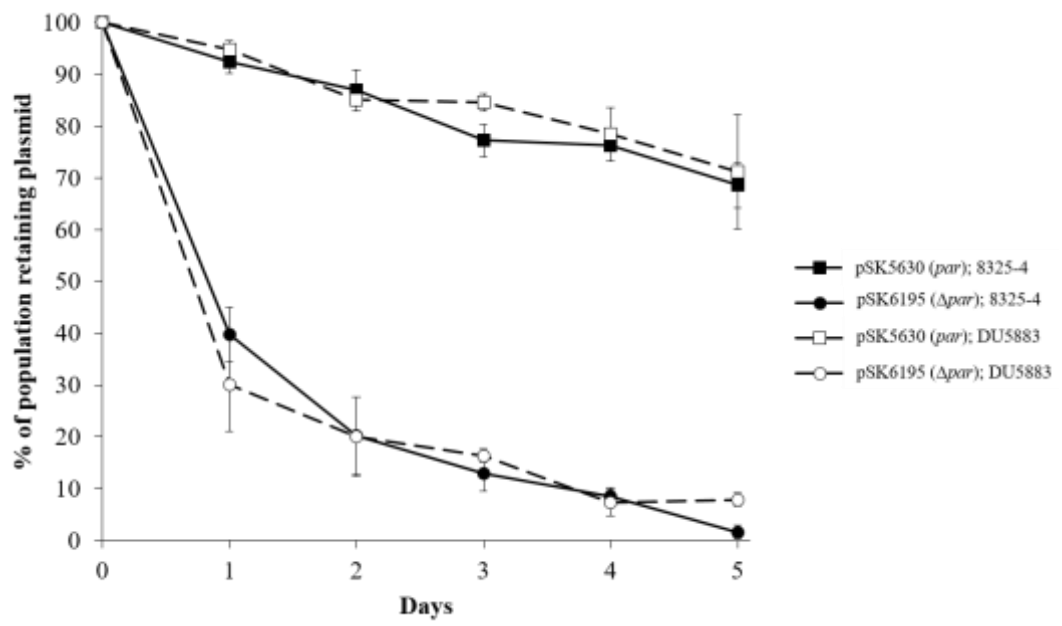


Figure 4.8 Putative RacA conserved domain of Par

Amino acid sequence of pSK1 Par (GenBank Accession Number AAF63251) showing the residues of Par that represent a putative conserved domain of the RacA superfamily in the NCBI Conserved Domains Database (highlighted in blue). Amino acid residues are numbered on the left. For reference, the Par sequence is divided by red dashed lines into amino acids that form the predicted helix-turn-helix (HTH) (aa 1–53), coiled-coil (CC) (aa 54–155) and disordered C-terminal domains (CTD) (aa 156–245).

HTH (aa 1–53)

1 MKTIKMLVADE LNVTKQTVVN NAKNLNISFE KENGVNYIDD NDYKIVEKI TKKERTTQNK

CC (aa 54–155)

61 ENKKSEITYE NTEKNRYNNS DGFETLTKTV NELEKQVEIF ETRAKNDEKY IENLTKQLDQ

121 QNSNVNTLNK LLENQQILAL ESNKKIQKLE HQLEEEERQLS YSFDKSTNDR ENFDVQEASY

CTD (aa 156–245)

181 TSDSVNTDQY QKEEKKPEVQ PKDISESQOD EKSQQQDDSF NQNDKDIAIE ETQTKKGFWS

241 RLFGG

membrane-bound protein, DivIVA, to anchor chromosomes to the cell poles during sporulation (Ben-Yehuda *et al.* 2003, Wu and Errington 2003). In *S. aureus*, DivIVA is localised at the division septum, and does not appear to be involved in chromosome segregation (Pinho and Errington 2004). Notably, a TBLASTN search (Altschul *et al.* 1997) of the translated *S. aureus* nucleotide database using the *B. subtilis* RacA nucleotide sequence (GenBank Accession Number NP_391584) did not identify any RacA homologues in *S. aureus* (data not shown). Thus, due to the putative conserved domain between Par and *B. subtilis* RacA, and the interaction between RacA and DivIVA in *B. subtilis*, it was hypothesised that Par might interact with *S. aureus* DivIVA in a manner similar to the RacA-DivIVA interaction in *B. subtilis*. In this way, Par might act as a bridging protein to tether plasmid DNA to DivIVA during plasmid segregation. Therefore, because no other potentially relevant Par interaction partners were identified from the Y2H library screen, except for a ribonuclease that was not investigated further (Section 4.4.1), pairwise Y2H assays were performed between Par and a candidate interaction partner of interest, DivIVA.

4.4.3.1. Construction of DivIVA bait and prey plasmids for yeast two-hybrid assays

S. aureus genomic DNA was isolated (Section 2.4.2) from stationary phase cultures of *S. aureus* RN4220 cells, and a 0.6 kb DNA fragment containing the DivIVA coding region was PCR-amplified (Section 2.4.4) using primers HC27 and HC28 (Table 2.6). The amplified DNA was inserted into the pGBKT7 bait and pGADT7 prey vectors (Table 2.2), essentially as described in Section 3.6.1 for the construction of the Par bait and prey Y2H plasmids, pSK9107 and pSK9110, respectively (Table


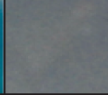


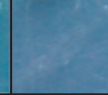
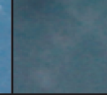

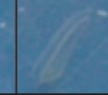
2.2). Following the identification of recombinant bait and prey plasmids by screening with *EcoRI* and *BamHI* restriction digestion (Section 2.4.6) and agarose gel electrophoresis (Section 2.4.3), plasmids were sequenced (Section 2.4.14) using T7 sequencing and 3' DNA-BD sequencing primers (Table 2.6) for recombinant pGBKT7 bait plasmids, and T7 sequencing and 3'AD sequencing primers (Table 2.6) for recombinant pGADT7 prey plasmids. The plasmid containing the correct *divIVA* sequence in pGBKT7 was named pSK9109, and pSK9112 for *divIVA* in pGADT7 (Table 2.2).

4.4.3.2. Yeast two-hybrid assay of Par and DivIVA interaction

To investigate whether Par and DivIVA interact, pairwise Y2H assays were performed between Par and DivIVA bait and prey fusion proteins, according to the methods described in Section 2.10.3. As expected, yeast cells containing ParFL bait (pSK9107) and prey (pSK9110) plasmids (Table 2.2) grew on high-stringency selection medium, as did cells carrying DivIVA bait (pSK9109) and prey (pSK9112) plasmids (Table 2.2) (Figure 4.9). However, no growth was observed for cells containing ParFL bait (pSK9107) and DivIVA prey (pSK9112) plasmids, or DivIVA bait (pSK9109) and ParFL prey (pSK9110) plasmids (Figure 4.9). There were also no indications of interactions between empty Y2H vectors and DivIVA (Figure 4.9) or Par (Figure 3.11). The Y2H assays, therefore, did not provide any evidence of an interaction between Par and DivIVA.

Figure 4.9 Interaction between Par and DivIVA

Yeast two-hybrid (Y2H) assays of interactions between Par and DivIVA bait and prey fusion proteins. Pairwise Y2H assays were performed between GAL4 BD (bait) and GAL4 AD (prey) protein fusions to full-length Par (ParFL) and DivIVA, according to the methods described in Section 4.4.3.2. *S. cerevisiae* AH109 cells containing bait and prey plasmids were patched on high-stringency selection medium (SD/-Leu/-Trp/-His/-Ade/X- α -Gal) (Table 2.3). Growth indicates activation of the *HIS3* and *ADE2* reporter genes. Blue pigmentation indicates α -galactosidase activity from yeast cells. Y2H assays of the prey fusion protein encoding simian virus T antigen (GAL4 AD-T) and the bait fusion proteins encoding murine p53 (GAL4 BD-53) and human lamin protein (GAL4 BD-Lam) were included as positive and negative controls, respectively.

Bait (GAL4 BD fusion)	53	Lam	ParFL	DivIVA	ParFL	DivIVA	DivIVA	pGBKT7
Prey (GAL4 AD fusion)	T	T	ParFL	DivIVA	DivIVA	ParFL	pGADT7	DivIVA
								

4.4.4. Yeast two-hybrid screening of *S. aureus* genomic DNA prey libraries with the C-terminal domain of Par

The above Y2H assays did not detect any interaction between Par and a candidate interaction partner, DivIVA (Section 4.4.3.2). Furthermore, the interaction between Par and FnBP, that was detected from Y2H screening of *S. aureus* genomic DNA prey libraries, was shown not to be biologically significant (Section 4.4.2). It is possible that by performing Y2H assays, the fusion of Par to GAL4 BD or GAL4 AD to generate bait and prey fusion proteins, respectively, may have interfered with Par protein structure and possibly impeded potential protein-protein interactions. Therefore, since it was anticipated that potential protein-protein interactions would most likely involve the predicted disordered CTD of Par (Dunker *et al.* 2002), Y2H screening of *S. aureus* genomic DNA prey libraries was repeated using the Par CTD (aa 156–245) as the bait protein. In this way, potential steric hindrances that might have prevented protein interactions with the Par CTD might be overcome by removing the NTD and CC domains to potentially increase the accessibility of the CTD to protein interactions.

S. aureus genomic DNA prey libraries were screened for interactions with the GAL4 BD-ParCTD bait fusion protein encoded by pSK9174 (Table 2.2) essentially as described above for the Y2H library screen using full-length Par bait (Section 4.4.1). From the Y2H screening of *S. aureus* genomic DNA prey libraries using ParCTD bait, approximately 3×10^7 library clones were screened, and 220 individual transformants that indicated an interaction between ParCTD and a library prey protein were patched onto high-stringency selection medium (Table 2.3). Prey

plasmids were isolated (Section 2.4.1) from 27 yeast colonies that grew on high-stringency selection medium, and the interactions with ParCTD bait were re-tested and examined for self-activation of the reporter genes. Y2H assays performed using the prey plasmids and pGBKT7 bait plasmids with and without the ParCTD coding region (Section 2.10.3), identified 10 prey clones that showed activation of the reporter genes only in the presence of ParCTD bait. The *S. aureus* genomic DNA fragments contained in these prey plasmids were sequenced (Section 2.4.14) using the T7 sequencing primer (Table 2.6), and subsequent BLASTP searches revealed that all 10 prey plasmids contained sequences that matched the coding region of the C-terminal end of FnBP. Since FnBP was found to be non-essential to Par function (Section 4.4.2), the interaction between ParCTD and FnBP was not investigated further.

4.5. Interactions between Par and non-specific DNA

Y2H screening of *S. aureus* genomic DNA prey libraries using Par or ParCTD bait protein did not reveal any biologically relevant interactions involving Par and *S. aureus* proteins (Sections 4.4.1 and 4.4.4). Although this may appear to suggest that pSK1 *par* functions independently of host-encoded proteins, there remains the possibility that the bacterial nucleoid might play a role in plasmid segregation, in a manner similar to the role of the nucleoid as a scaffold for plasmid segregation in the proposed diffusion-ratchet mechanism of Type Ia plasmid partitioning systems (Vecchiarelli *et al.* 2010) and in the pilot-fish mechanism of R388 plasmid partitioning (Gynet and de la Cruz 2011). Therefore, to investigate whether Par

might interact with the bacterial nucleoid, *in vitro* DNA-binding studies were performed using non-specific DNA, as described in Section 4.5.1 below.

4.5.1. Binding of Par to non-specific DNA

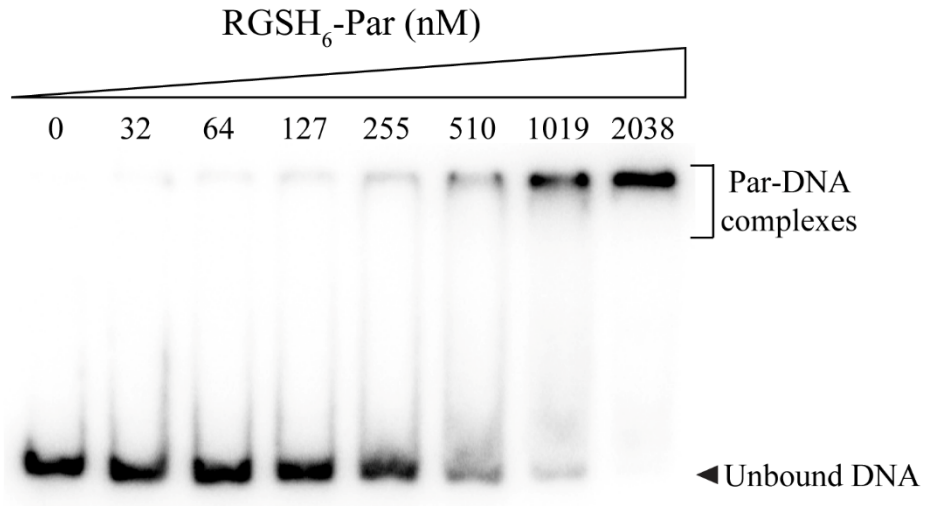
To determine whether Par binds to non-specific DNA, electrophoretic mobility shift assays (EMSAs) were performed using a non-specific DNA probe. A 181 bp DNA region located downstream of pSK1 *rep* (nt 2950–3130 of pSK1, GenBank Accession Number GU565967) was PCR-amplified (Section 2.4.4) from pSK4829 template DNA (Table 2.2) using primers NFRepDwn4829 and HC3 (Table 2.6). The resulting amplicon was electrophoresed on an agarose gel (Section 2.4.3) and then gel-purified as described in Section 2.4.7. The purified DNA fragment was subsequently end-labelled with ³²P from [γ -³²P]-ATP using T4 PNK (Section 2.8.1). EMSAs were performed as described in Section 2.8.2, with each EMSA reaction consisting of approximately 500 cpm of purified, radiolabelled non-specific DNA probe and increasing amounts of purified RGSH₆-tagged Par proteins (Section 3.3.4). EMSAs were electrophoresed on polyacrylamide gels, rather than polyacrylamide/agarose hybrid gels, since the main purpose was to determine whether Par could bind non-specific DNA, and hence, the need to resolve Par-DNA complexes was not relevant.

As shown in Figure 4.10A, the electrophoretic migration of a small amount of labelled non-specific DNA probe was shifted with 64–127 nM of RGSH₆-Par, and a complete shift of the DNA probe was observed at protein concentrations >1 μ M. Competition EMSAs performed using labelled non-specific DNA with 1.8 μ M of RGSH₆-Par protein showed that unlabelled specific competitor DNA (212 bp DNA

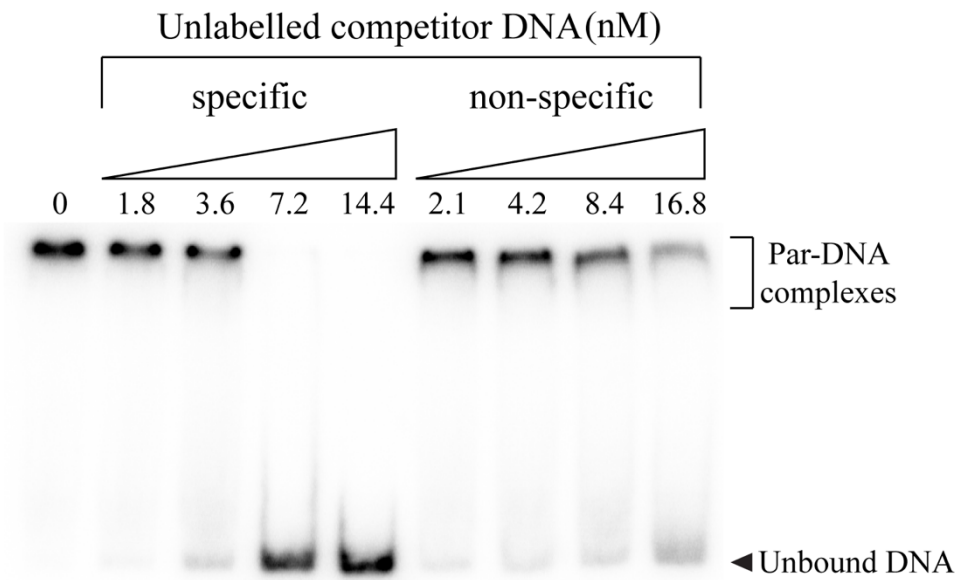
Figure 4.10 DNA-binding of Par proteins to non-specific DNA

Electrophoretic mobility shift assays (EMSAs) of Par binding to non-specific DNA. A 181 bp DNA probe corresponding to a region downstream of pSK1 *rep* (nt 2950–3130 of pSK1, GenBank Accession Number GU565967) was incubated with increasing concentrations of purified RGSH₆-Par (A) or RGSH₆-ParK15A (C) as described in Section 4.5.1. B. Competition EMSA performed as described in Section 4.5.1 using a fixed concentration of RGSH₆-Par (1.8 μM) and increasing amounts of unlabelled competitor DNA, either specific (212 bp fragment from pSK1 *par-rep* intergenic DNA, nt 1689–1900 of pSK1, GenBank Accession Number GU565967) or non-specific (same as labelled probe). EMSAs were performed using 500 cpm of radiolabelled non-specific DNA probe and electrophoresed on 5% (w/v) polyacrylamide gels. Radiolabelled DNA probes were detected by phosphor imaging. The concentration of protein (nM) or amount of unlabelled competitor DNA (ng) is shown above each lane. The positions of unbound DNA are indicated by black arrowheads. Par-DNA complexes are bracketed on the right.

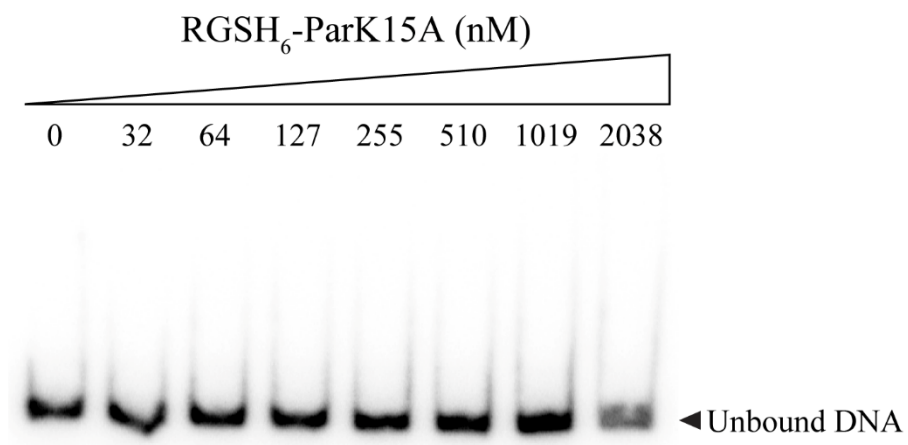
A.



B.



C.



probe containing pSK1 *par-rep* intergenic region, nt 1689–1900 of pSK1, GenBank Accession Number GU565967) could compete with labelled non-specific DNA for Par DNA-binding sites, since titration with unlabelled specific competitor DNA resulted in a loss of RGS_{H6}-Par binding to labelled non-specific DNA (Figure 4.10B). Titration with unlabelled non-specific competitor DNA had a less pronounced effect on the binding of RGS_{H6}-Par to labelled non-specific DNA (Figure 4.10B), which suggests that Par showed greater DNA-binding affinity for specific, rather than non-specific, DNA. Interestingly, the Par DNA-binding mutant, RGS_{H6}-ParK15A, did not bind to the non-specific DNA probe at the protein concentrations tested (Figure 4.10C), which suggests that Par DNA-binding, to both specific (Supplementary Figure S3) and non-specific DNA, is dependent on the K15 residue. Therefore, the above EMSA results show that RGS_{H6}-Par could bind to non-specific DNA, and hence potentially to nucleoid DNA, although whether the DNA-binding was a product of excess protein relative to DNA is unclear and is discussed further in Section 4.6.

4.5.2. Potential Par binding sites on *S. aureus* chromosomal DNA

In addition to the possible non-specific binding of Par to nucleoid DNA, it is also possible that Par binds specifically to sequences on the *S. aureus* chromosome. To investigate this possibility, the *S. aureus* NCTC 8325 genome sequence (GenBank Accession Number CP000253) was searched using the Sequence Searcher program (Marass and Upton 2009) in both the sense and antisense directions to identify potential Par DNA-binding sites. DNaseI footprinting showed that Par binds to seven 12-bp repeats in the pSK1 *par-rep* intergenic region, with a consensus sequence of

TTAGGTAGTAAA (Figure 1.6) (LeBard 2005). Three of the seven Par binding sites have the same sequence as the consensus (Figure 1.6). Assuming that Par might bind to similar sequences on the chromosome, the search was performed against the consensus sequence of the Par centromere-binding site.

A search using the Sequence Searcher program, allowing for a maximum of two mismatches from the consensus sequence, revealed that the consensus sequence of the Par centromere-binding site is present at two locations on the *S. aureus* NCTC 8325 chromosome (Supplementary Table S1). It was also found that the consensus sequence differed from 49 sites on the chromosome by one nucleotide, and differed from 592 sites by two nucleotides (Supplementary Table S1). Furthermore, the resulting matches appeared to be dispersed throughout the sequence of the *S. aureus* genome, and did not appear to cluster around particular positions (Figure 4.11 and Supplementary Table S1). The closest pairs of sites were located 11 bp apart – one pair at position 589,634 and another at position 1,013,864 on the chromosome (Supplementary Table S1). Other pairs of sites were located 37, 58 and 74 bp apart, however these were not clustered either, located at positions 2,111,228, 1,110,195 and 579,065, respectively (Supplementary Table S1). Distances between all other pairs of potential binding sites were greater than 100 bp. No matches were found in the *S. aureus* genome sequence for the four remaining Par centromere-binding sites.

4.6. Discussion

A summary of the properties of Par derivatives described in this chapter is presented in Table 4.1. Par-pSERP, encoded on the *S. epidermidis* multiresistance plasmid, pSERP, was identified as a distant homologue of pSK1 Par, sharing 40% amino acid

Figure 4.11 Map of potential pSK1 Par binding sites on *S. aureus* chromosome

The genomic DNA sequence of *S. aureus* NCTC 8325 (GenBank Accession Number NC_007795) was searched for potential pSK1 Par binding sites using Sequence Searcher software (Section 4.5.2). A circular map of *S. aureus* NCTC 8325 chromosomal DNA is shown, with marks inside the map representing the location of potential Par binding sites. Blue, red and black marks denote potential Par binding sites that differ by no, one and two nucleotides from the consensus Par binding sequence of the pSK1 *par* centromere-like site, respectively.

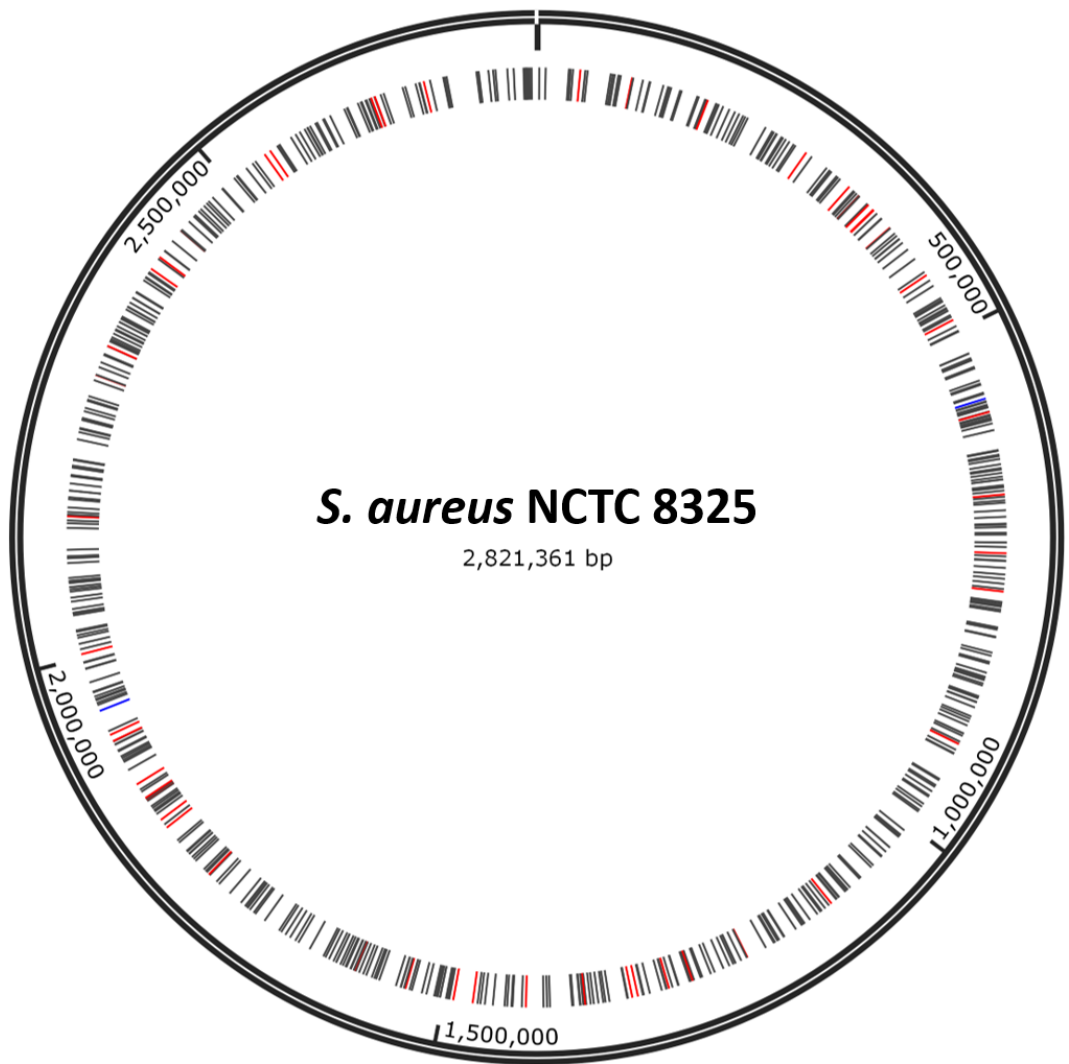


Table 4.1 Summary of properties of Par derivatives (Chapter 4)

Protein	Plasmid stabilisation	Protein interactions^a	No interaction^b	Interaction with non-specific DNA^c
Par-pSERP	Yes ^d	N. D.	N. D.	N. D.
pSK1 Par (in <i>E. faecalis</i>)	Yes ^e	N. D.	N. D.	N. D.
pSK1 Par (in <i>S. aureus</i> DU5883 <i>fnbA</i> ⁻ , <i>fnbB</i> ⁻)	Yes ^f	N. D.	N. D.	N. D.
GAL4 BD-ParFL	N. D.	GAL4 AD -ParFL, -FnBP	GAL4 AD-DivIVA	N. D.
GAL4 BD-FnBP fragment	N. D.	GAL4 AD -ParFL, -ParK15A, - Δ CC, -L132A, -ParR241A	GAL4 AD -Par Δ CTD, -ParW239A	N. D.
GAL4 BD-DivIVA	N. D.	GAL4 AD-DivIVA	GAL4 AD-ParFL	N. D.
GAL4 BD-ParCTD	N. D.	GAL4 AD-FnBP	N. D.	N. D.
RGSH ₆ -Par	N. D.	N. D.	N. D.	Yes
RGSH ₆ -ParK15A	N. D.	N. D.	N. D.	No

^{a,b}Protein interactions assessed by yeast two-hybrid (Y2H) assays (Section 4.4.1, 4.4.3.2, 4.4.4).

^cInteraction with non-specific DNA assessed by electrophoretic mobility shift assays (EMSAs) (Section 4.5.1).

^dPlasmid stabilisation ability assessed by plasmid segregational stability assays (Section 4.2.2).

^ePlasmid stabilisation ability assessed by plasmid segregational stability assays (Section 4.3).

^fPlasmid stabilisation ability assessed by plasmid segregational stability assays (Section 4.4.2).

N. D. Not determined in experiments described in Chapter 4.

sequence identity (Figure 4.1A). Prior to this study, the function of this protein had yet to be demonstrated. Despite being a distant pSK1 Par homologue, the location of the gene encoding Par-pSERP, relative to pSERP *rep*, is similar to the genetic organisation of *par* and *rep* on pSK1, i.e. *par* is located upstream of, and transcribed divergently from, *rep* (Figure 4.1B). Furthermore, the sequence between the genes encoding Rep and Par-pSERP appears to contain several 8-bp repeats (Figure 4.1C), possibly indicative of a centromere-like site. These factors gave reason to suspect a potential role of Par-pSERP in plasmid maintenance.

Indeed, plasmid segregational stability assays described in Section 4.2.2 showed that the segregational stability of pSERP minireplicons was enhanced in the presence of Par-pSERP, thus implicating Par-pSERP in plasmid maintenance. It should be noted that the relatively low segregational stability of the pSERP minireplicons, even in the presence of *par-pSERP* (Figure 4.2), might be due to the absence of other putative plasmid stabilisation factors, such as a resolvase and several hypothetical proteins annotated on the pSERP sequence (GenBank Accession Number NC_006663), that might also contribute to the overall plasmid stability of pSERP.

Whereas plasmid stabilisation function might have been expected for Par-pSERP, based on the similarities with pSK1 *par* outlined above, the more distantly-related Par homologue, RepB287, encoded by the *T. halophilus* plasmid pUCL287, was also shown to demonstrate plasmid maintenance functionality (Benachour *et al.* 1997). However, unlike the Par homologue encoded by pSERP, *repB287* is located downstream of, overlapping with, and transcribed in the same direction of, the plasmid replication gene, *repA287*, on pUCL287 (Figure 4.1B) (Benachour *et al.*

1997). Therefore, the ability of at least two distantly-related Par homologues to enhance plasmid segregational stability strongly suggests that plasmid maintenance is a function shared by Par-like proteins, and is not exclusive to pSK1 Par.

It is worth noting that the sequence alignment shown in Figure 4.1A demonstrates the conserved nature of the acidic Par CTD between the distant homologues, which implies a role of the CTD in Par function, as investigated in Chapter 3. Furthermore, the Par K2 and E10 residues appear highly conserved, whereas Y43 does not. This stresses the potential importance of K2 and E10 to Par function, possibly in Par NTD interactions (Section 3.6.4). Although little effect of K2A and E10A mutations were found in isolation (Figure 3.12C), the highly conserved nature of these residues warrants further investigation into their significance, as discussed in Section 3.7.6.

The single protein encoded by pSK1 *par* is intriguing, as it differs from most characterised plasmid partitioning systems that encode two separate proteins (Gerdes *et al.* 2010, Schumacher 2012, Baxter and Funnell 2014). Furthermore, Par homologues have been identified in several other bacterial species, such as *Tetragenococcus*, *Streptococcus*, *Lactococcus*, *Lactobacillus*, *Clostridium* and *Enterococcus* (Supplementary Figure S1, Firth *et al.* 2000), which raises the question of whether *par* functions as a discrete unit, or whether host factors might be involved in Par function. Plasmid segregational stability assays performed to assess the functionality of pSK1 *par* in the heterologous *E. faecalis* host, appeared to support the former proposition, that pSK1 *par* is a discrete functional unit, since a pIP501 minireplicon containing pSK1 *par* was remarkably more stable than its *par*-deficient counterpart (Figure 4.3). The enhanced plasmid segregational stability observed in

both *S. aureus* (Simpson *et al.* 2003) and *E. faecalis* (Figure 4.3), therefore, suggests that *par* might function independently of *S. aureus*-specific factors. A similar situation is observed in the Types II and III plasmid partitioning systems, whereby the partitioning systems appear to be self-contained units consisting of a centromere-like site, DNA-binding protein and NTPase, that are sufficient for plasmid segregational stability (Schumacher 2012, Baxter and Funnell 2014). However, unlike characterised partitioning systems, the functionality of pSK1 *par* in *E. faecalis* has great significance due to the potential for plasmid segregation by a single partitioning protein, instead of two separate DNA-binding and NTPase proteins. This suggests a novel mechanism of plasmid maintenance using a single protein without interaction with host-specific factors.

It should be noted that since enterococci and staphylococci are both low G+C, Gram-positive cocci belonging to the Firmicutes phylum, the possibility cannot be excluded that factors in common, or similar, between *E. faecalis* and *S. aureus* may have played a role in the functionality of pSK1 *par* in both species. Indeed, a Par homologue with 72% sequence identity has been identified in *E. faecalis* (Supplementary Figure S4), and therefore, it is not inconceivable that pSK1 Par may have utilised enterococcal host factors to impart plasmid segregational stability in this heterologous host. Interestingly, the sequence alignment shows that most of the sequence differences are located in the NTD, which is likely due to differences in the recognition of their cognate centromere-like sites. The CC and CTD sequences share a higher degree of identity, and hence these domains of pSK1 Par may have been involved in interactions with *E. faecalis* host factors, if such interactions exist. A more comprehensive investigation of the functionality of pSK1 *par* in a range of

bacterial hosts, such as *Bacillus* or the Gram-negative *E. coli*, could be performed to provide further insight into the dependence on host-encoded factors in the mechanism of *par*-mediated plasmid segregation.

4.6.1. Interaction of Par with *S. aureus* proteins

S. aureus genomic DNA prey libraries were screened by Y2H using ParFL bait to identify potential host-encoded proteins that might interact with Par to mediate plasmid segregational stability (Section 4.4.1). Interestingly, of the five library clones that contained potential Par interaction partners, four prey inserts contained sequences of varying lengths that encoded fragments of the C-terminal end of *S. aureus* FnBPA and FnBPB (Figure 4.4). These proteins are *S. aureus* cell-surface proteins that are involved in adhesion to host matrix proteins during infection (Signäs *et al.* 1989). This result was surprising, because the relevance of FnBP to plasmid segregation was not immediately obvious. Rather, it was expected that potential Par interaction partners would be involved in processes that might be associated with plasmid activities, such as chromosome segregation or cell division.

The interaction between FnBP and the ParFL bait protein involved the 177 most C-terminal residues of FnBP (Figure 4.5). This region includes the LPXTG cell-wall anchoring motif that is cleaved by the sortase enzyme to anchor FnBP to the peptidoglycan cell wall, leaving the hydrophobic region lodged in the cell membrane, and the positively-charged C-terminal amino acids exposed to the cytoplasmic side of the cell membrane (Ton-That *et al.* 1997). Therefore, it was conceivable that Par might interact with the cytoplasmic end of the membrane-bound

cleavage product to anchor plasmids to the cell wall to ensure plasmid segregation into daughter cells.

Further characterisation of the Par-FnBP interaction using Par mutants revealed that the interaction specifically involved the CTD of Par (Figure 4.6), which was confirmed by the detection of an interaction between FnBP and ParCTD from Y2H library screening of *S. aureus* genomic DNA prey libraries using ParCTD bait protein (Section 4.4.4). This was not unexpected, since the Par CTD is predicted to be disordered (Simpson *et al.* 2003), which would result in a high propensity for involvement in protein-protein interactions (Dunker *et al.* 2002). Nonetheless, despite showing a specific interaction between Par and FnBP via Y2H assays (Figure 4.6), plasmid segregational stability assays in a *S. aureus* FnBP mutant, DU5883, revealed that disruption of the FnBP genes had no effect on *par* functionality (Figure 4.7).

It should be noted that the intracellular localisation of GAL4 AD-FnBP fragment and the absence of sortase in *S. cerevisiae* means that the FnBP prey protein was unlikely to have been cleaved at the LPXTG motif and anchored to the cell surface. It is, therefore, possible that the interaction between Par and the FnBP fragment in Y2H assays may have involved the surface-exposed regions of FnBP, which would not otherwise be accessible to intracellular Par proteins in its natural host, *S. aureus*. In light of the plasmid stability results, the Par-FnBP interaction is unlikely to be biologically relevant, and is, therefore, most likely a technical artefact of the Y2H assay.

The other potential Par interaction partner, ribonuclease Y, that was identified from Y2H screening of *S. aureus* genomic DNA libraries (Section 4.4.1), was not investigated further because its role in RNA processing and virulence (Marincola *et al.* 2012, Bonnin and Bouloc 2015) implied that ribonuclease Y is unlikely to interact with Par in plasmid segregation. With time permitting, this potential interaction could be pursued by examining the functionality of pSK1 *par* in a *S. aureus* ribonuclease Y mutant to determine the biological significance of this interaction.

It was anticipated that Y2H screening of *S. aureus* genomic DNA prey libraries using the ParCTD bait, instead of the full-length Par bait, could result in the identification of a greater number and wider variety of library clones that contain potential interaction partners. This was based on the assumption that removal of the Par NTD and CC domains might increase accessibility of the CTD to protein-protein interactions, even if interactions are technical artefacts and not biologically relevant. However, this was not the case, and FnBP-encoding prey clones were again identified from the *S. aureus* library screen (Section 4.4.4).

Although the Y2H library screens using Par or ParCTD bait did not detect any meaningful interactions between Par and *S. aureus* proteins, it is possible that the fusion of Par and potential interaction partners to the GAL4 BD and AD proteins, respectively, may have disrupted protein structure and hindered potential protein-protein interactions. It is also possible that potential interactions between Par and host proteins might be dependent on Par binding to centromere DNA, which was absent in the Y2H system. In this case, a change in the structure of Par upon binding

to DNA might be required to facilitate subsequent protein-protein interactions, which would not have been detected using Y2H assays. To overcome the absence of the pSK1 *par* centromere in Y2H assays, the yeast strains could be modified so as to replace the upstream activation sequence of the yeast reporter genes with the *par* centromere-like site. In this way, GAL4 BD-Par fusions bind to the centromere-like site, such that interactions with GAL4 AD fusions result in activation of the GAL4-responsive reporter genes. This could potentially capture Par protein interactions that are dependent on DNA-binding.

These factors could also explain why the Y2H assays did not reveal any interaction between Par and a candidate interaction partner, DivIVA (Figure 4.9). To eliminate this possibility, and to examine whether Par interacts with DivIVA, plasmid segregational stability assays could be performed to assess *par* functionality in a *S. aureus* DivIVA mutant. Pinho and Errington (2004) showed that a *S. aureus* DivIVA null mutant is viable, and hence assessing plasmid segregational stability in a DivIVA mutant would be a strong indicator of the requirement of DivIVA for Par function.

It should also be noted that although a BLASTP search of the non-redundant protein database using the pSK1 Par amino acid sequence identified a match to the RacA superfamily in the conserved domain database (Section 4.4.3), the search did not detect RacA as a protein that showed significant sequence identity to the Par sequence. The identification of a RacA conserved domain was, therefore, most likely based on the structures of the predicted Par HTH and CC domains, which are also present in RacA (Schumacher *et al.* 2016). Implications of the structural similarity

between Par and RacA for the mechanism of plasmid segregational stability is discussed in Chapter 6.

To overcome some of the limitations of the Y2H method for identifying Par interaction partners, such as false positive interactions, potential structural hindrances resulting from fusions to GAL4 BD and AD proteins, and the absence of pSK1 *par* centromere DNA, alternative techniques such as co-immunoprecipitation and mass spectrometry (Free *et al.* 2001) could be used. Bacterial two-hybrid studies could also be performed to more closely resemble the natural bacterial host of Par and its potential interaction partners. In such screens, pSK1 plasmid genes could be included to account for interactions that might involve plasmid-encoded proteins. The functional significance of interactions between Par and proteins identified by these studies can then be confirmed by performing plasmid segregational stability assays in *S. aureus* mutants. Note that the possibility remains that the mechanism of Par in plasmid segregational stability might not involve interactions with other proteins. Additional protein interaction studies, such as those mentioned above, should be performed to confirm this.

4.6.2. Interaction of Par with non-specific DNA

EMSAs using a radiolabelled non-specific DNA probe, which corresponded to a 181 bp sequence downstream of pSK1 *rep*, showed that RGSH₆-Par was capable of binding to non-specific DNA (Figure 4.10A). However, binding to non-specific DNA occurred at much higher protein concentrations (approximately 10-fold higher) than those observed for a complete mobility shift of radiolabelled specific DNA probe (compare Figures 4.10A and 3.6A). This suggests that RGSH₆-Par has greater

DNA-binding affinity to specific, compared to non-specific, DNA. This is supported by the competition EMSAs in Figure 4.10B, which show the release of RGS_{H6}-Par from radiolabelled non-specific DNA probe using 200 ng of specific competitor DNA, compared to 400 ng of non-specific competitor DNA that could not entirely compete with the labelled probe for Par binding sites. Similar observations have been made for other DNA-binding proteins, such as the ParB proteins that are involved in spreading and binding to non-specific DNA during chromosome and plasmid segregation. For example, EMSAs have shown that the ParB-like proteins, Spo0J and SopB, both bind specifically to their cognate DNA sequences, but also bind non-specifically to DNA, albeit with lower affinities (Sanchez *et al.* 2013, Taylor *et al.* 2015). Interestingly, whereas approximately 10 times more Par protein was required to bind non-specific compared to specific DNA, the binding of non-specific DNA by SopB required more than 20-fold more protein than the concentration required to shift the mobility of specific DNA, while greater than 60 times was required to observe a complete mobility shift (Sanchez *et al.* 2013). This suggests that Par exhibits non-specific DNA-binding activity, however, further biophysical experiments such as surface plasmon resonance (Szabo *et al.* 1995, Nguyen *et al.* 2007), isothermal titration calorimetry (Liang 2008) or fluorescence polarisation assays (Lundblad *et al.* 1996) would be required to more accurately quantitate the DNA-binding parameters of Par to specific and non-specific DNA.

Unlike the R219 residue of SopB, which is essential for binding to its cognate centromere-like site, *sopC*, but not for binding to non-specific DNA (Sanchez *et al.* 2013), the inability of the RGS_{H6}-ParK15A DNA-binding mutant to bind to the non-specific probe (Figure 4.10C), suggests that K15 is essential for both specific

(Supplementary Figure S3) (Lai 2008), and potentially non-specific, DNA-binding. However, although RGS_{H6}-Par demonstrated non-specific DNA-binding *in vitro*, it is unclear whether these observations are artefacts of an excess of protein compared to DNA, or whether they are representative of true non-specific DNA-binding activity of Par. Being a DNA-binding protein, it was predicted that Par might exhibit some degree of non-specific DNA-binding, as would be expected given an excess of any DNA-binding protein in the presence of DNA. However, since the ParK15A DNA-binding mutant did not bind non-specific DNA, this suggests that, under the conditions tested *in vitro*, Par exhibited genuine binding to non-specific DNA. Further studies (see below) should, therefore, be performed to determine whether binding to non-specific DNA is biologically relevant.

The binding of purified RGS_{H6}-Par to non-specific DNA (Figure 4.10A), gives rise to a potential mechanism of plasmid segregation that involves interactions between Par and chromosomal DNA. A search of the *S. aureus* genome sequence identified two sites on the chromosome that matched the consensus sequence of the Par centromere binding site, and another 49 sites that differed from the consensus sequence by one nucleotide (Supplementary Table S1). These sites might represent potential chromosome binding sites of Par, assuming that Par binds to sequences on the chromosome that are similar to the sequences bound by Par at the pSK1 *par* centromere-like site. However, the matching sites were located throughout the chromosome, with no obvious co-location of potential binding sites (Figure 4.11 and Supplementary Table S1). This is unlike the chromosomal binding sites of chromosome segregation proteins such, as RacA or Spo0J, which are located near the chromosomal origins (Lin and Grossman 1998, Ben-Yehuda *et al.* 2003, Ben-

Yehuda *et al.* 2005). Of course, it is possible that Par binds specifically to sequences on the chromosome that are different to the DNA-binding sites on pSK1 *par*, or that Par binds non-specifically to the nucleoid, as is the case with Type I ParA proteins (Castaing *et al.* 2008, Vecchiarelli *et al.* 2013b). Regardless, more insight could be gained into the potential interactions of Par with nucleoid DNA, in particular with specific sites on the chromosome, by performing protein-DNA binding experiments, such as chromatin immunoprecipitation (ChIP), followed by sequencing of the ChIP products (ChIP-Seq) (Collas 2010) to identify possible Par binding sites on the *S. aureus* chromosome. The potential for interactions between Par and nucleoid DNA is explored further using epifluorescence microscopy, and is addressed in Chapter 5 (Sections 5.4.4.4.1 and 5.8.6).

CHAPTER 5

Cell biology of pSK1 *par*-mediated plasmid segregation

5.1. Introduction

The results from Chapter 3, combined with previous findings (LeBard 2005, Figgett 2007, Lai 2008), have contributed to the understanding of Par DNA-binding and multimerisation activities. However, it remains unclear how these activities contribute to the mechanism of pSK1 *par*-mediated plasmid segregation. Epifluorescence microscopy studies have provided invaluable understanding of the dynamics and potential mechanisms utilised by characterised plasmid partitioning systems (Gordon *et al.* 1997, Jensen and Gerdes 1999, Li and Austin 2002, Møller-Jensen *et al.* 2003, Ebersbach and Gerdes 2004, Gordon *et al.* 2004, Lim *et al.* 2005, Adachi *et al.* 2006, Hatano *et al.* 2007, Derman *et al.* 2008, Ringgaard *et al.* 2009, Guynet *et al.* 2011). For example, fluorescence microscopy studies to simultaneously visualise ParM and plasmid DNA have led to the insertional polymerisation model of the Type II plasmid partitioning system (Møller-Jensen *et al.* 2003), while studies by Guynet *et al.* (2011) have led to the proposal of a pilot-fish mechanism for the partitioning of R388. Therefore, in order to gain insight into the possible mechanism of plasmid segregational stability by pSK1 *par*, fluorescence microscopy was performed to localise Par and pSK1 minireplicons in *S. aureus*. Fluorescence

microscopy was also performed in *E. coli* cells to observe the structural characteristics of Par.

5.2. Generation of anti-Par peptide antibodies

Immunofluorescence microscopy (IFM) was employed to determine the localisation of Par in *S. aureus* cells. This method relies on the detection of proteins in fixed and permeabilised cells using a primary antibody specific to the protein of interest, followed by a fluorophore-conjugated secondary antibody to facilitate protein localisation by fluorescence microscopy. However, because of problems encountered with the sensitivity and cross-reactivity of rabbit anti-Par antiserum with *S. aureus* proteins, even after affinity purification and preadsorption of the antiserum with *S. aureus* cell lysates (Sections 3.2.2), these antibodies were not suitable for IFM of Par in *S. aureus*. Hence, in an attempt to improve the sensitivity and reduce the cross-reactivity of anti-Par antibodies in IFM, antibodies were generated against predicted antigenic Par peptides, as described below.

Rabbit polyclonal antibodies raised against predicted antigenic Par peptides were generated by Mimotopes Pty Ltd (Victoria, Australia). Prediction of antigenic Par peptides was performed by Mimotopes using the Par amino acid sequence (GenBank Accession Number AAF63251) and the epitope prediction programs PREDITOP (Pellequer and Westhof 1993) and ElliPro (Ponomarenko *et al.* 2008). Figure 5.1 shows the results of the epitope predictions, with potentially antigenic peptides highlighted. Following discussions with Mimotopes consultants, two Par peptides, with the sequences SYSFDKSTNDRENFD (residues 160–174) and SQQQDDSFNQNDKDI (residues 213–227), were predicted as potentially antigenic

Figure 5.1 Prediction of Par antigenic peptides

Antigenic peptides were predicted using PREDITOP (Pellequer and Westhof 1993) and ElliPro (Ponomarenko *et al.* 2008) software for the Par protein sequence (GenBank Accession Number AAF63251). The Par protein sequence is shown with amino acid positions indicated on the left. Predicted antigenic peptides are highlighted. The position, antigenicity score and peptide length, in amino acids (aa), of predicted antigenic peptides are provided in separate tables for results generated by PREDITOP and ElliPro. In each table, peptides are listed in order of decreasing antigenicity. For PREDITOP, higher scores indicate higher antigenicity, and for ElliPro, higher scores indicate lower antigenicity. The sequences of the two peptides used for the generation of anti-Par peptide antibodies are outlined by boxes.

PREDITOP

1 MKTIKMLVADE LNVTKQTVVN NAKNLNISFE KENGVNYIDD NDYLKIVEKI TKKERTTQNK
61 ENKKSEITYE NTEKNRYNNS DGFETLTKTV NELEKQVEIF ETRAKNDEKY IENLTKQLDQ
121 QNSNVNTLNK LLENQQILAL ESNKKIQKLE HQLEEERQLS YSFDKSTNDR ENFDVQEASY
181 TSDSVNTDQY QKEEKKPEVQ PKDISESQOD EK SQQQDSSF NQNDKDTAIE ETQTKKGFWS
241 RLFGG

Amino acid position	Score	Peptide length (aa)
213 – 227	3.0000	15
160 – 174	2.6433	15
116 – 130	2.2126	15

ElliPro

1 MKTIKMLVADE LNVTKQTVVN NAKNLNISFE KENGVNYIDD NDYLKIVEKI TKKERTTQNK
61 ENKKSEITYE NTEKNRYNNS DGFETLTKTV NELEKQVEIF ETRAKNDEKY IENLTKQLDQ
121 QNSNVNTLNK LLENQQILAL ESNKKIQKLE HQLEEERQLS YSFDKSTNDR ENFDVQEASY
181 TSDSVNTDQY QKEEKKPEVQ PKDISESQOD EK SQQQDSSF NQNDKDTAIE ETQTKKGFWS
241 RLFGG

Amino acid position	Score	Peptide length (aa)
155 – 173	0.626	19
194 – 217	0.670	24
179 – 188	0.733	10
236 – 245	0.782	10

by both programs (shown in boxes in Figure 5.1) and were selected for the production of anti-peptide antibodies. The two peptides were individually conjugated to the keyhole limpet hemocyanin carrier protein, and each conjugated peptide was used to inject two rabbits for the production of anti-peptide antisera. Polyclonal antisera isolated from the rabbits were affinity-purified against the peptides before being dispatched from Mimotopes.

5.2.1 Reactivity of anti-Par peptide antibodies in *S. aureus*

Upon receipt of the anti-Par peptide antibodies from Mimotopes (Section 5.2), the antibodies were tested for their ability to recognise the full-length Par protein. Cell lysates from mid-exponential phase cultures of *S. aureus* SK8250 cells (Table 2.1) harbouring pSK4829 (*par*) or pSK4833 (Δ *par*) (Table 2.2) were prepared as described in Section 2.5.8 and fractionated by SDS-PAGE (Section 2.5.6). Approximately 300 ng of purified RGS_{H6}-Par, prepared as described in Section 3.3.4, was loaded in one lane to serve as a positive control for Par immunodetection. Since Par signals from *S. aureus* lysates were generally weak (see Figures 3.8 and 3.12), Western blotting (Section 2.5.9) was performed using an equal mixture of the affinity-purified antisera obtained from the four rabbits (two rabbits for each of the two peptides) (Section 5.2), in order to increase the number of antibodies that can potentially bind each Par protein. In this way, it was anticipated that the strength of specific signals might be increased. The blot was divided into strips, which were incubated with 1:100 or 1:50 dilutions of either affinity-purified and preadsorbed rabbit anti-Par antiserum (Section 2.6.1 and 2.6.2), or anti-Par peptide antibodies (Section 5.2), diluted in 5% (w/v) skim milk powder in TBS (Table 2.5). Detection

was facilitated by a 1:2,000 dilution of goat anti-rabbit IgG HRP-conjugated secondary antibodies, followed by enhanced chemiluminescence detection, as described in Section 2.5.9.2.

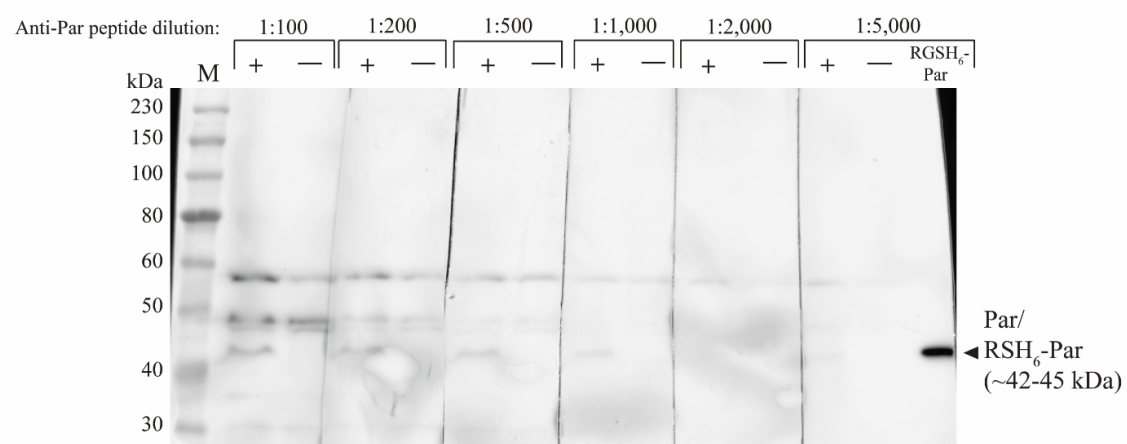
As shown in Figure 5.2A, the anti-peptide antibodies performed similarly to the affinity-purified and preadsorbed anti-Par antiserum raised against full-length Par protein, with the detection of an approximately 42 kDa band in cell lysates containing pSK4829 (*par*) but not pSK4833 (Δ *par*). This protein band was consistent with the size of purified RGS_{H6}-Par, which was detected with a 1:100 dilution of the affinity-purified and preadsorbed anti-Par antibodies (Figure 5.2A). Therefore, the reactivity of the anti-Par peptide antibodies against full-length Par protein was confirmed. However, significant non-specific binding and cross-reactivity with *S. aureus* proteins remained, which contributed to background signals that would be problematic for downstream IFM experiments.

Although higher dilutions of the anti-Par peptide antibodies reduced background bands in Western blotting experiments, the relatively low specificity of the anti-peptide antibodies compromised the detection of Par (data not shown). Hence, in order to increase specificity while decreasing cross-reactivity, normal goat serum was added to the blocking buffer, with the anticipation that immunoglobulin-binding *S. aureus* proteins might bind initially to the antibodies in the goat serum, and thus be blocked from binding non-specifically to anti-Par peptide antibodies. Importantly, goat serum should not interfere with immunodetection using anti-rabbit IgG secondary antibodies. Western blotting was subsequently performed on *S. aureus*

Figure 5.2 Immunodetection of Par in *S. aureus* using anti-Par peptide antibodies

Cleared lysates from *S. aureus* SK8250 cells carrying pSK4829 (*par*) (+) or pSK4833 (Δ *par*) (-), were fractionated by SDS-PAGE (Section 2.5.6) and subjected to Western blotting (Section 2.5.9) using either 1:100 or 1:50 dilutions of affinity-purified and preadsorbed anti-Par antibodies (Sections 2.6.1 and 2.6.2), or anti-Par peptide antibodies (Section 2.6.3). As a positive control, approximately 300 ng of purified RGS_{H6}-Par was loaded into one lane of each gel. **A.** Western blot of Par in *S. aureus* using either 1:100 or 1:50 dilutions of affinity-purified and preadsorbed anti-Par antibodies (Sections 2.6.1 and 2.6.2), or anti-Par peptide antibodies (Section 2.6.3) in the absence of normal goat serum. **B.** Western blot of Par in *S. aureus* using 1:100 dilution of anti-Par peptide antibodies, in the presence of 5% (v/v), 10% (v/v) or 20% (v/v) normal goat serum in the blocking buffer. **C.** Western blot of Par in *S. aureus* using anti-Par peptide antibodies diluted 1:100–1:5,000 in blocking buffer containing 5% (v/v) normal goat serum. Lane M contains prestained protein markers, with marker sizes indicated in kDa on the left of each blot. The position and approximate measured size of Par is indicated by a black arrowhead.

C.



cell lysates as described above, with the addition of 5% (v/v), 10% (v/v) or 20% (v/v) normal goat serum to the blocking buffer.

Figure 5.2B reveals a significant reduction in non-specific background bands when blots were detected using a 1:100 dilution of anti-Par peptide antibodies in the presence of normal goat serum. Par (and RGS_{H6}-Par) was detected as a clear band of approximately 42 kDa, with only two non-specific bands detected at approximately 48 kDa and 58 kDa (Figure 5.2B). There appeared to be no visible difference in the signal:noise ratios between blots treated with 5% (v/v), 10% (v/v) or 20% (v/v) normal goat serum, and hence a concentration of 5% (v/v) normal goat serum was added to subsequent blocking buffers.

In order to determine the minimum concentration that could be used for the immunodetection of Par with anti-Par peptide antibodies whilst minimising non-specific background bands, blots containing lysates and purified RGS_{H6}-Par, prepared as described above, were titrated with anti-Par peptide antibodies (1:100–1:5,000 dilutions) in the presence of 5% (v/v) normal goat serum in the blocking buffer. The results, shown in Figure 5.2C, revealed that the Par protein band of approximately 42 kDa could be detected using anti-Par peptide antibodies diluted up to 1:1,000 in blocking buffer (albeit very weakly). However, the blots also demonstrated the relatively low specificity of the anti-Par peptide antibodies for Par, as both the Par protein band and the non-specific protein bands showed a reduction in signal intensity as the dilution of primary antibodies increased. Since Par could be readily detected using a 1:100 dilution of anti-Par peptide antibodies, and since the signal:noise ratio was independent of the primary antibody concentration, subsequent

Western blotting experiments using anti-Par peptide antibodies for the immunodetection of Par in *S. aureus* were performed using the optimised conditions of anti-Par peptide antibodies diluted 1:100 in blocking buffer containing 5% (v/v) normal goat serum, as described in Section 2.5.9.2.

5.3. Immunofluorescence microscopy of Par in *S. aureus*

5.3.1 Immunofluorescence microscopy of Par using anti-Par peptide antibodies

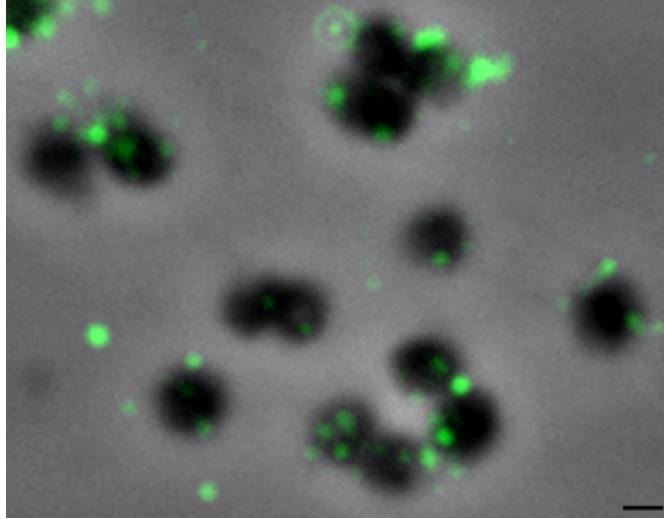
Using the optimised conditions established by Western blotting for the detection of Par in *S. aureus* (Section 5.2.1), immunofluorescence microscopy (IFM) was performed on fixed *S. aureus* cells to determine the cellular localisation of Par. Mid-exponential phase *S. aureus* SK8250 cells harbouring either pSK4829 (*par*) or pSK4833 (Δ *par*) (Table 2.2) were fixed and prepared for IFM on multitest slides as described in Section 2.11.1. A number of parameters were varied, such as lysostaphin concentration (0.1–300 μ g/ml), lysis time (1 min–30 min), lysis temperature (25°C–42°C), dilution of anti-Par peptide antibodies (1:100–1:10,000), incubation time with primary antibodies (1 h–overnight) and incubation temperature with primary antibodies (4°C–25°C). For each of the conditions tested, fluorescent foci were observed regardless of whether the cells produced Par or not (for representative images, see Figures 5.3A–B). No fluorescence was detected when anti-Par peptide antibodies were omitted from the procedure (Figure 5.3C), which indicates that the fluorescent foci were not caused by the secondary antibody alone. Since there were no distinguishable differences in the outcomes of IFM performed on *S. aureus* cells harbouring pSK4829 or pSK4833, it appeared that the low

Figure 5.3 Immunofluorescence microscopy in *S. aureus*

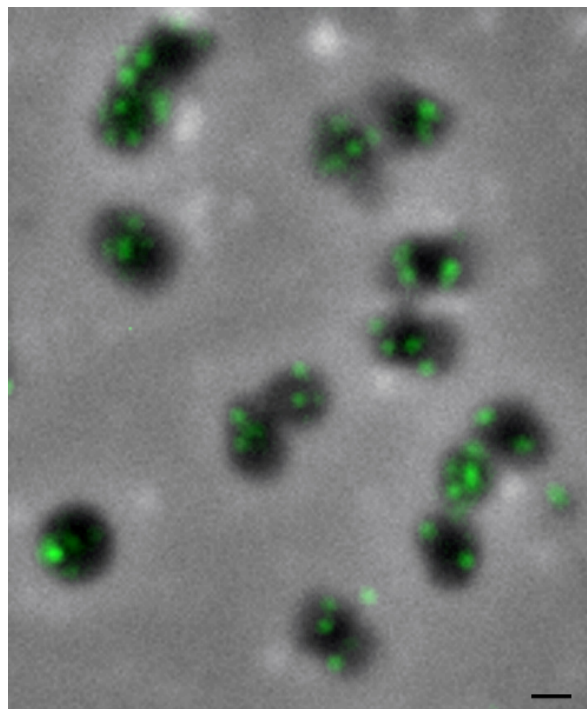
A–C. Immunofluorescence microscopy (IFM) of Par in *S. aureus*. Mid-exponential phase *S. aureus* SK8250 cells harbouring pSK4829 (*par*) (**A**) or pSK4833 (Δ *par*) (**B**) were prepared for IFM using anti-Par peptide antibodies and goat anti-rabbit IgG Alexa Fluor 488-conjugated antibodies, as described in Section 5.3.1. **C.** Immunofluorescence detection of Par in *S. aureus* cells carrying pSK4829, as described in (A), with the omission of anti-Par peptide antibodies. Images shown are overlays of bright-field and fluorescence micrographs. Scale bar = 1 μ m.

D. IFM of FtsZ and FtsZ-mRFPmars in *S. aureus*. *S. aureus* SK8250 cells harbouring pSK9075 ($P_{xyl/tet}::ftsZ\text{-}mRFPmars$) were grown to early-exponential phase and *ftsZ\text{-}mRFPmars* was induced with 2.5 ng/ μ l anhydrous tetracycline for 1 h. Cells were prepared for IFM using anti-FtsZ antibodies and goat anti-rabbit IgG Alexa Fluor 488-conjugated antibodies, as described in Section 2.11.1. From top left to bottom right: FtsZ and FtsZ-mRFPmars detected by IFM; FtsZ-mRFPmars detected by fluorescence microscopy; bright-field (BF); overlay of fluorescence images; overlay of bright-field (BF) and fluorescence images. Scale bar = 1 μ m.

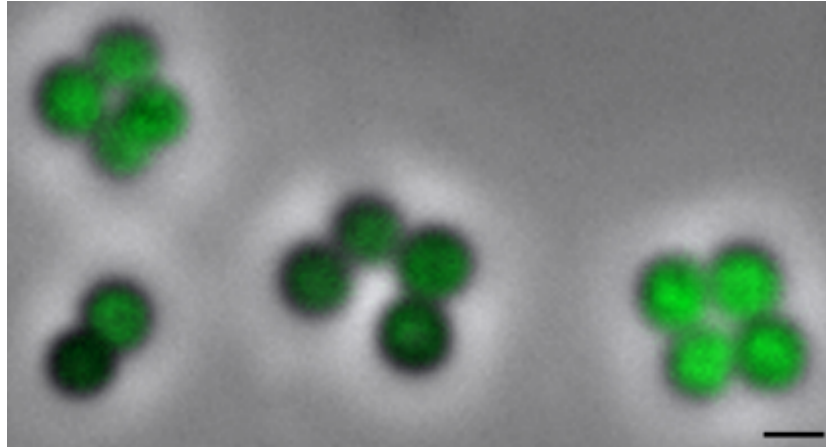
A. *S. aureus* (*par*)



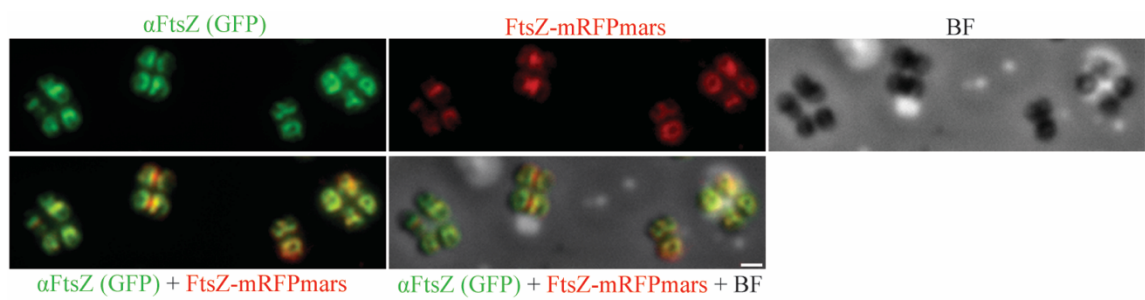
B. *S. aureus* (Δ *par*)



C. *S. aureus* (*par*), no anti-Par peptide antibodies



D. *S. aureus* (*ftsZ-mRFPmars*) + anti-FtsZ



sensitivity and cross-reactivity of anti-Par peptide antibodies remained problematic for the generation of meaningful IFM results, despite showing significant improvement with the addition of normal goat serum (as demonstrated by Western blots in Section 5.2.1).

5.3.2 Validation of *S. aureus* immunofluorescence microscopy protocol

To verify that the difficulties experienced with the detection of Par in *S. aureus* by IFM were not due to technical problems with the IFM protocol, IFM was performed on the staphylococcal cell division protein, FtsZ. The localisation of FtsZ in *S. aureus* is well-documented (Pinho and Errington 2005, Liew *et al.* 2011, Veiga *et al.* 2011, Strauss *et al.* 2012, Brzoska and Firth 2013, Bottomley *et al.* 2014) and anti-FtsZ antibodies from Prof. Elizabeth Harry (University of Technology, Sydney, Australia) have successfully localised FtsZ in *S. aureus* using IFM (Liew *et al.* 2011). As a further validation of the IFM protocol, *S. aureus* SK8250 cells were electroporated (Section 2.3.4) with pSK9075 (Table 2.2), which expresses *ftsZ-mRFPmars* from the inducible $P_{xyl/tet}$ promoter. The fluorescence localisation of FtsZ-mRFPmars in *S. aureus* has been published by Brzoska and Firth (2013). IFM using anti-FtsZ primary antibodies and Alexa Fluor 488-conjugated secondary antibodies (GFP) should, therefore, detect endogenous FtsZ as well as FtsZ-mRFPmars, while FtsZ-mRFPmars fluorescence would be detected using epifluorescence microscopy (RFP) (Section 2.11.2). In this way, colocalisation of GFP and RFP fluorescence should verify the IFM protocol used.

S. aureus SK8250 cells carrying pSK9075 ($P_{xyl/tet}::ftsZ-mRFPmars$) (Table 2.2) were grown at 37°C in LB-broth (Table 2.3) containing antibiotic selection (Table 2.4)

until early-exponential phase (approximately 2 h) (Section 2.1), before expression of *ftsZ-mRFPmars* was induced from pSK9075 for 1 h with 2.5 ng/ml anhydrotetracycline. Cells were prepared for IFM as described in Section 2.11.1, and FtsZ was immunodetected using 60 µg/ml lysostaphin and a 1:20,000 dilution of anti-FtsZ antibodies, followed by a 1:2,000 dilution of goat anti-rabbit IgG Alexa Fluor 488-conjugated secondary antibodies. Figure 5.3D shows the fluorescence localisation of FtsZ-mRFPmars and FtsZ as detected by epifluorescence microscopy and IFM using anti-FtsZ antibodies. Consistent with published images, FtsZ appeared as arcs, rings or lines (Pinho and Errington 2005, Liew *et al.* 2011, Veiga *et al.* 2011, Strauss *et al.* 2012, Brzoska and Firth 2013, Bottomley *et al.* 2014). Furthermore, the localisation pattern of FtsZ corresponded well with the localisation of FtsZ-mRFPmars, which confirms that the fluorescence pattern resulting from IFM with anti-FtsZ antibodies was specific and reflective of FtsZ localisation. The specific detection of FtsZ in *S. aureus* by IFM, therefore, verified the IFM protocol, and suggests that the inability to specifically detect Par in *S. aureus* was not the result of methodological limitations, but rather, the result of factors related to Par IFM (discussed further in Section 5.9.1).

5.3.3 Construction of a pSK1 minireplicon encoding RGS_{H6}-Par

Because Par localisation could not be detected specifically by IFM using anti-Par peptide antibodies (Section 5.3.1), an alternative strategy for protein localisation was considered, whereby monoclonal antibodies would be used to perform IFM on an epitope-tagged derivative of Par. It was anticipated that monoclonal antibodies might have higher specificity and greater affinity for the epitope and hence reduce

background signals, which have proven to be problematic with the anti-Par peptide antibodies (Section 5.3.1). To this end, an N-terminal RGSH₆ tag was fused in-frame of the Par coding sequence on the pSK1 minireplicon, pSK4829 (Table 2.2), using overlap extension PCR. Fusion of the epitope to the N-terminus of Par was favoured because a C-terminally-tagged Par-RGSH₆ protein could not be purified using Ni²⁺-NTA affinity chromatography (Simpson *et al.* 2003). This suggests that the tag might have been inaccessible to the purification resin, and as such, a C-terminal RGSH₆ tag might also be inaccessible to anti-His antibodies in IFM.

For overlap extension PCR, primers NFRepDwn4829 and HC33 (Table 2.6) were used to PCR-amplify (Section 2.4.4) a 1.4 kb DNA fragment containing pSK1 *rep* and the region upstream of *par* from pSK4829 template DNA (Table 2.2). A separate reaction was used to amplify the Par coding sequence using primers HC34 and HC21 (Table 2.6) from pSK4829 template DNA. Primers HC33 and HC34 contain complementary sequences that encode RGSH₆ followed by three glycine residues, such that subsequent fusion of NFRepDwn4829/HC33 and HC34/HC21 PCR products by overlap extension PCR, using primers NFRepDwn4829 and HC21, incorporates the RGSH₆ tag and three glycine residues upstream and in-frame of the Par coding sequence. In this way, P_{par} drives expression of an N-terminal RGSH₆-tagged Par fusion protein. The amplicon from the overlap extension PCR was digested with *Bam*HI and *Hind*III (Section 2.4.6) and ligated (Section 2.4.11) to the dephosphorylated (Section 2.4.10) sites of the similarly-digested pWE180 plasmid (Table 2.2). Ligation reactions were used to transform *E. coli* DH5a cells to ampicillin resistance (Section 2.3.2), after which plasmid DNA was isolated from selected transformants (Section 2.4.1) and screened for recombination by restriction

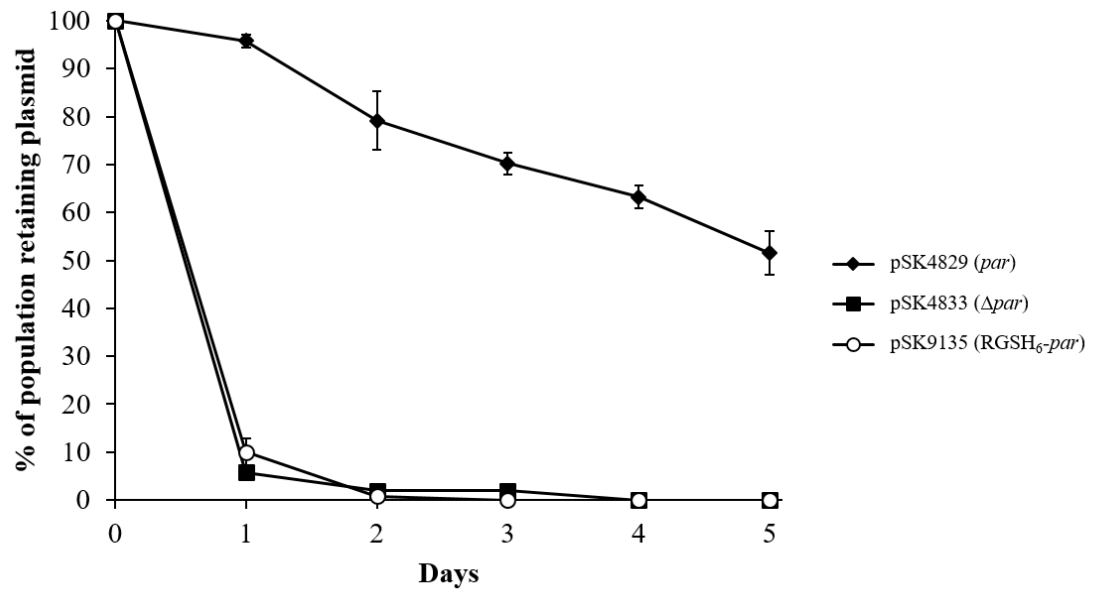
digestion using *Bam*HI and *Hind*III (Section 2.4.6). Following agarose gel electrophoresis (Section 2.4.3) of the digestion reactions, plasmids displaying the anticipated restriction profile were sequenced (Section 2.4.14) using primers HC2, HC3, HC21, NFRepDwn4829, SJ37 and SJ38 (Table 2.6). The pSK1 minireplicon encoding an in-frame N-terminal fusion of RGS_{H6} and three glycine residues to the Par coding sequence was named pSK9135 (Table 2.2).

5.3.4 Functionality of RGS_{H6}-Par in *S. aureus*

In order for the localisation of RGS_{H6}-Par to be representative of Par localisation in *S. aureus*, it was necessary to demonstrate the functionality of the tagged Par derivative. *S. aureus* SK8250 cells were separately electroporated (Section 2.3.4) with pSK4829 (*par*), pSK4833 (Δ *par*) and pSK9135 ($P_{par}::RGS_{H6}$ -*par*) (Table 2.2) and selected for erythromycin resistance (Table 2.4). Plasmid segregational stability assays were performed on individual transformants, as described in Section 2.7. The results shown in Figure 5.4 reveal that during five days of serial subculture in the absence of antibiotic selection, the segregational stability of pSK9135 ($P_{par}::RGS_{H6}$ -*par*) was similar to that of pSK4833 (Δ *par*), with the plasmid completely lost from the population after three days. This was compared to approximately 51±5% of the population that retained pSK4829 (*par*) at the completion of the assay (Figure 5.4). The stability assays, therefore, suggested that RGS_{H6}-Par was non-functional, and hence would not be suitable as a substitute for Par in IFM studies. Because IFM using anti-Par peptide antibodies could not specifically detect Par in *S. aureus* (Section 5.3.1), and because a functional epitope-tagged Par derivative could not be obtained, further attempts to localise Par in *S. aureus* by IFM were suspended.

Figure 5.4 Effect of RGS_{H6}-Par on plasmid segregational stability

Plasmid segregational stability assay of pSK1 minireplicons encoding an RGS_{H6}-tagged derivative of Par. The retention of the pSK1 minireplicon pSK9135 ($P_{par}::RGS_{H6}-par$) (○) in *S. aureus* SK8250 cells was determined as described in Section 2.7. For reference, segregational stability data for pSK4829 (*par*) (◆) and pSK4833 (Δpar) (■) from Figure 3.2A is also shown. Five days of serial subculture represents approximately 75 generations. Data are normalised to 100% plasmid retention on Day 0. The averages of three independent assays are shown. Error bars represent standard error of the mean.



5.4. Live cell epifluorescence microscopy of fluorescently-tagged Par in *S. aureus*

Since IFM localisation of Par in fixed *S. aureus* cells proved challenging (Section 5.3.1), epifluorescence microscopy of green fluorescent protein (GFP)-tagged Par fusion proteins was performed on live *S. aureus* cells. The functionality of GFP-tagged Par derivatives was evaluated using plasmid segregational stability assays to ensure that fluorescence localisation would be representative of Par localisation. As detailed in Sections 5.4.1–5.4.5 below, a number of *par-gfp* systems were developed in an attempt to obtain a system that demonstrated functionality of Par GFP fusions in the stabilisation of pSK1 minireplicons.

5.4.1 Construction of pSK1 minireplicons encoding Par GFP fusions

In order to maintain wild-type protein levels, N- and C- terminal fusions of Par to a GFP variant, GFPmut1 (Cormack *et al.* 1996), were generated by overlap extension PCR such that expression of the Par GFP fusions was under the control of the P_{par} promoter. The construction of DNA fragments encoding Par GFP fusions using overlap extension PCR is shown diagrammatically in Figure 5.5 and is described in detail below.

For the construction of a DNA fragment encoding an N-terminal GFP-Par fusion, pSK4829 (Table 2.2) was used as the template DNA in two separate PCRs (Section 2.4.4), using primer set NFRRepDwn4829/HC19 (Table 2.6) to amplify a 1.4 kb fragment encompassing pSK1 *rep* and the region upstream of *par* including the *par* RBS, and primer set HC20/HC21 (Table 2.6) to amplify a 0.7 kb fragment

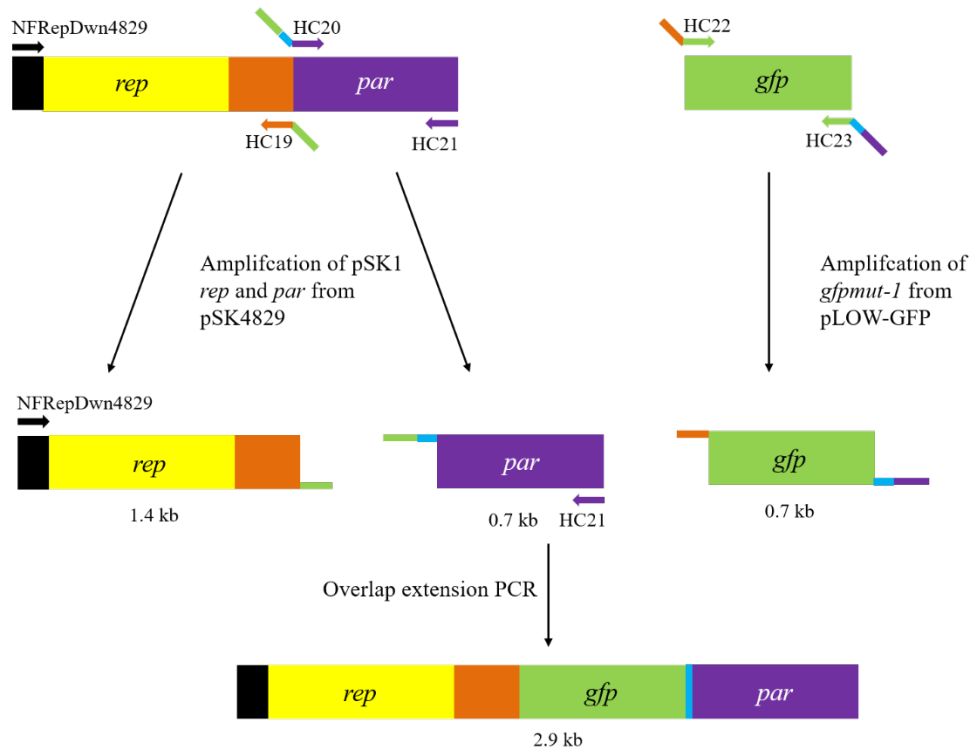
Figure 5.5 Fusion of *gfp* to pSK1 *par* using overlap extension PCR

Diagrammatic overview of the construction of *gfp-par* (A) and *par-gfp* (B) fusion products using overlap extension PCR. A detailed description is provided in Section 5.4.1.

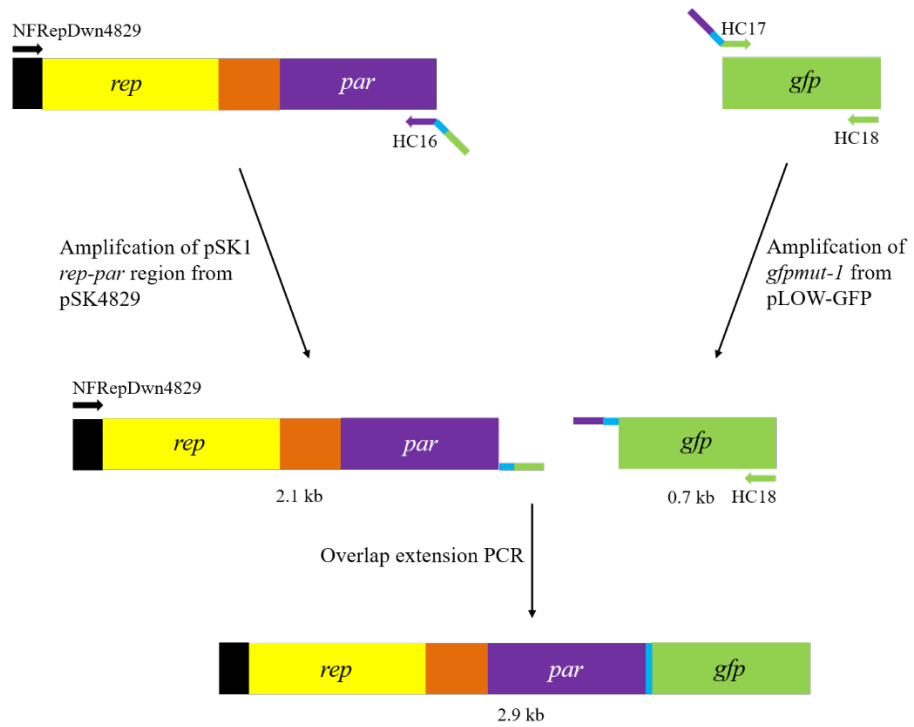
A. For the construction of *gfp-par*, primers NFRRepDwn4829 and HC19 were used to PCR-amplify a DNA fragment containing pSK1 *rep* (yellow) and the *par-rep* intergenic region (orange), and primers HC20 and HC21 were used to amplify the *par* coding sequence (purple) from pSK4829 template DNA. pLOW-GFP was used as the template for PCR-amplification of *gfpmut-1* (green) using primers HC22 and HC23. To enable fusion of PCR products, complementary sequences were appended to the 5' ends of primers. Blue boxes represent the sequence of the SCGAS linker between *gfp* and *par*. Black boxes represent sequences downstream of *rep* on pSK4829. The 2.9 kb *gfp-par* fusion product was generated by overlap extension PCR of the three amplicons using oligonucleotides NFRRepDwn4829 and HC21.

B. For the construction of *par-gfp*, primers NFRRepDwn4829 and HC16 were used to PCR-amplify a DNA fragment containing pSK1 *rep*, the *par-rep* intergenic region and the *par* coding sequence from pSK4829 template DNA. pLOW-GFP was used as the template for PCR-amplification of *gfpmut-1* using primers HC17 and HC18. To enable fusion of PCR products, complementary sequences were appended to the 5' ends of primers. Blue boxes represent the sequence of the SCGAS linker between *par* and *gfp*. Black boxes represent sequences downstream of *rep* on pSK4829. The 2.9 kb *gfp-par* fusion product was generated by overlap extension PCR of the two amplicons using oligonucleotides NFRRepDwn4829 and HC18.

A.



B.



containing the *par* gene. A third PCR was performed using primer set HC22/HC23 (Table 2.6) to amplify a 0.7 kb fragment encoding *gfpmut-1* from pLOW-GFP template DNA (Table 2.2). Complementary sequences encoding a five-residue linker, SCGAS (Veiga *et al.* 2011), to be located between GFP and Par, were incorporated into primers HC20 and HC23 to minimise potential interference of Par structure and function by GFP (Chen *et al.* 2013). The SCGAS linker has previously been used for successful localisation of *S. aureus* fluorescent protein fusions, such as FtsZ, EzrA, Spo0J, Noc and ParM, as described in Veiga *et al.* (2011) and Brzoska and Firth (2013). HC19 and HC22 contain complementary sequences encompassing the start of the GFP coding sequence as well as the sequence upstream of *par*, such that subsequent overlap extension PCR using primers NFRepDwn4829 and HC21 fused the *gfp*-containing amplicon to the *rep*-containing amplicon. The resulting 2.9 kb fusion product, therefore, contained pSK1 *rep* and the coding sequence for GFP-Par, arranged in the same genetic organisation as *rep* and *par* on pSK1 (Figure 5.5A).

The generation of a DNA fragment encoding a C-terminal Par-GFP fusion was also performed by overlap extension PCR. Primer set NFRepDwn4829/HC16 (Table 2.6) was used to PCR-amplify (Section 2.4.4) a 2.1 kb fragment encompassing pSK1 *rep* and *par* from pSK4829 template DNA (Table 2.2). A separate reaction was used to amplify (Section 2.4.4) *gfpmut-1* from pLOW-GFP template DNA (Table 2.2) using primer set HC17/HC18 (Table 2.6). Primers HC16 and HC17 contain complementary sequences encoding an SCGAS linker (Veiga *et al.* 2011) to be introduced between Par and GFP such that overlap extension PCR using primers NFRepDwn4829 and HC18 fused the GFP coding region downstream of the *rep-par*

fragment, producing a 2.9 kb fusion product containing pSK1 *rep* and *par-gfp* in the same genetic organisation as *rep* and *par* on pSK1 (Figure 5.5B).

The 2.9 kb overlap extension PCR products, encoding GFP-Par and Par-GFP, were individually ligated to the restricted (Section 2.4.6) and dephosphorylated (Section 2.4.10) *Bam*HI and *Hind*III sites of pWE180 (Table 2.2), essentially as described above for the construction of pSK9135 ($P_{par}::RGS_{H6}-par$) (Section 5.3.3). Ligation reactions were used to transform *E. coli* DH5 α cells to ampicillin resistance (Section 2.3.2), and plasmid DNA was isolated from selected transformants (Section 2.4.1) to screen for recombinants by restriction digestion with *Bam*HI and *Hind*III (Section 2.4.6). Restricted plasmids were fractionated by agarose gel electrophoresis (Section 2.4.3), and plasmids showing the expected banding pattern were sequenced (Section 2.4.14) using primers NFRepDwn4829, HC2, HC11, HC20 and SJ37 (Table 2.6) for the *gfp-par* fusion, and using primers NFRepDwn4829, HC2, HC11, HC16 and SJ37 (Table 2.6) for the *par-gfp* fusion. Plasmids containing pSK1 *rep* and encoding GFP-Par or Par-GFP fusions of the correct sequence were designated pSK9087 and pSK9088, respectively (Table 2.2).

A Western blot analysis (Section 2.5.9) was performed to confirm the production of GFP-Par and Par-GFP in *S. aureus*. The pSK9087 ($P_{par}::gfp-par$) and pSK9088 ($P_{par}::par-gfp$) plasmids generated above, as well as the pSK1 minireplicons pSK4829 (*par*) and pSK4833 (Δpar) (Table 2.2), were each separately introduced into *S. aureus* SK8250 cells by electroporation (Section 2.3.4). Single transformants were cultured to mid-exponential phase (Section 2.1) and whole cell lysates were prepared as described in Section 2.5.8. Lysates were fractionated by SDS-PAGE

(Section 2.5.6), and immunodetection of Par and Par GFP fusion proteins was carried out by Western blotting (Section 2.5.9) using anti-Par peptide antibodies (Section 2.6.3).

The Western blot shown in Figure 5.6A reveals the presence of an approximately 42 kDa band that is consistent with the apparent size of Par (for example, see Figure 3.2B). Note that the apparent size of Par differs from its expected size of 29 kDa, as discussed in Section 3.7.1. The fusion of GFP to Par adds another 27 kDa, resulting in a theoretical size of 56 kDa for Par GFP fusion proteins. Consistent with this, GFP-Par was detected as a band of approximately 63 kDa, while Par-GFP appeared as a band of approximately 60 kDa (Figure 5.6A). The detection of both GFP-Par and Par-GFP by Western blotting, therefore, confirmed their production in *S. aureus*.

5.4.2 Segregational stability of pSK1 minireplicons encoding Par GFP fusions

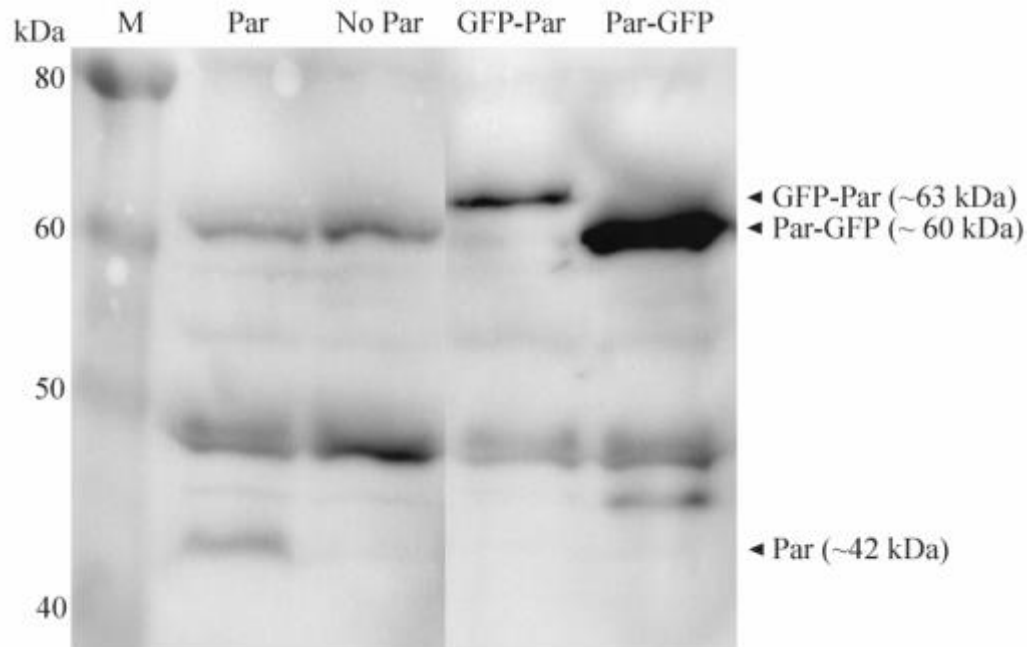
To evaluate the impact of the fused GFP domains on Par activity, the functionality of the GFP-Par and Par-GFP fusion proteins, generated above (Section 5.4.1), was assessed using plasmid segregational stability assays. pSK1 minireplicons pSK4829 (*par*), pSK4833 (Δ *par*), pSK9087 ($P_{par}::gfp-par$) and pSK9088 ($P_{par}::par-gfp$) (Table 2.2) were used to separately electroporate *S. aureus* SK8250 cells to erythromycin resistance, as described in Section 2.3.4. Transformants were subjected to plasmid segregational stability assays (Section 2.7) to determine the segregational stability of each of the pSK1 minireplicons during five days (approximately 75 generations) of serial subculture in the absence of antibiotic selection. As shown in Figure 5.6B, pSK4829 (*par*) was retained by approximately 50±9% of the cell

Figure 5.6 Effect of GFP fusions on plasmid segregational stability

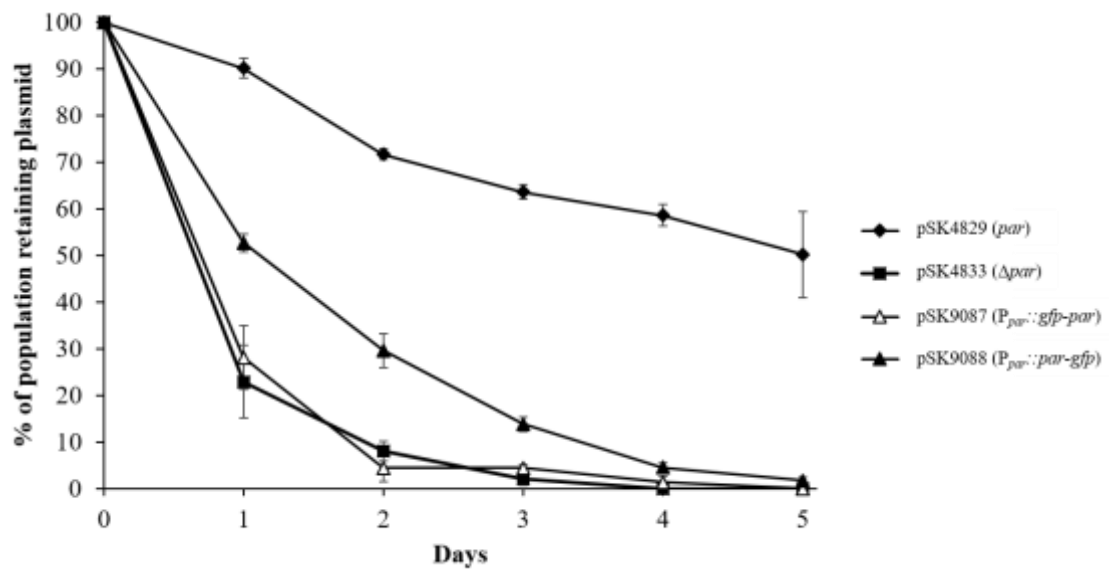
A. Immunodetection of Par GFP protein fusions in *S. aureus* by Western blotting. Cleared lysates from *S. aureus* SK8250 cells carrying pSK4829 (Par), pSK4833 (No Par), pSK9087 (GFP-Par) or pSK9088 (Par-GFP) were fractionated by SDS-PAGE (Section 2.5.6) and subjected to Western blotting (Section 2.5.9) using anti-Par peptide antibodies (Section 2.6.3). Lane M contains prestained protein markers, with marker sizes indicated in kDa on the left of the blot. Positions of relevant proteins and their approximate measured sizes are indicated by black arrowheads.

B. Plasmid segregational stability assay of pSK1 minireplicons encoding Par GFP protein fusions. The retention of pSK1 minireplicons pSK4829 (*par*) (◆), pSK4833 (Δ *par*) (■), pSK9087 ($P_{par}::gfp-par$) (△) and pSK9088 ($P_{par}::par-gfp$) (▲) in *S. aureus* SK8250 cells was determined as described in Section 2.7. Five days of serial subculture represents approximately 75 generations. Data are normalised to 100% plasmid retention on Day 0. The averages of three independent assays are shown. Error bars represent standard error of the mean.

A.



B.



population after five days, whereas pSK4833 (Δpar) was lost from the population by Day 4, which is consistent with previous findings (Sections 3.2.2 and 5.3.4). GFP-Par was unable to stabilise the pSK1 minireplicon, with the segregational stability of pSK9087 similar to that of pSK4833 (Figure 5.6B). However, there was a slight improvement in the segregational stability of pSK9088 ($P_{par}::par-gfp$) compared to pSK4833, with a slower observed rate of plasmid loss, which eventuated in $5\pm 1\%$ of the population retaining the pSK9088 plasmid on Day 4 and $2\pm 1\%$ retaining the plasmid on Day 5 of the assay (Figure 5.6B). Differences in plasmid stability between pSK4833 and pSK9088 were more pronounced at earlier stages of the assay, with $30\pm 4\%$ retention of pSK9088 compared to $8\pm 2\%$ retention of pSK4833 on Day 2, and $14\pm 2\%$ compared to $2\pm 1\%$ retention of pSK9088 and pSK4833, respectively, on Day 3 of the assay (Figure 5.6B). Taken together, the results from the stability assays suggest that GFP-Par was non-functional, and that Par-GFP might have partial functionality.

The severe reduction in the functionality of Par GFP fusion proteins when expressed *in cis* to the pSK1 *par* centromere-like site from P_{par} , compromised the utility of these fusion proteins for fluorescence localisation studies of Par in *S. aureus*, since the localisation of Par GFP fusions might not accurately reflect Par localisation. However, since Par-GFP is at least partially functional and the nature of the partial loss of function is unknown, it is possible that the localisation of Par-GFP in *S. aureus* might be unaffected by the loss of functionality. Therefore, epifluorescence microscopy was performed in *S. aureus* to determine whether Par-GFP might localise differently to non-functional GFP-Par.

5.4.3 Epifluorescence microscopy of Par GFP fusions in *S. aureus*

S. aureus SK8250 cells carrying either pSK9087 ($P_{par}::gfp-par$) or pSK9088 ($P_{par}::par-gfp$) (Table 2.2) were grown to mid-exponential phase and prepared for epifluorescence microscopy as described in Section 2.11.2. As shown in Figures 5.7A–B, there did not appear to be a dramatic difference between the localisation of GFP-Par and Par-GFP in *S. aureus*. Both fusion proteins appeared to produce one to four fluorescent foci that were located around the cell periphery (Figures 5.7A–B). Since no obvious differences in localisation were observed, and considering that Par-GFP is only partially functional, alternative Par GFP expression systems were developed in an attempt to obtain a more reliable representation of Par localisation.

5.4.4 Development of a pSK1 *par* system with inducible, *in trans* expression of Par

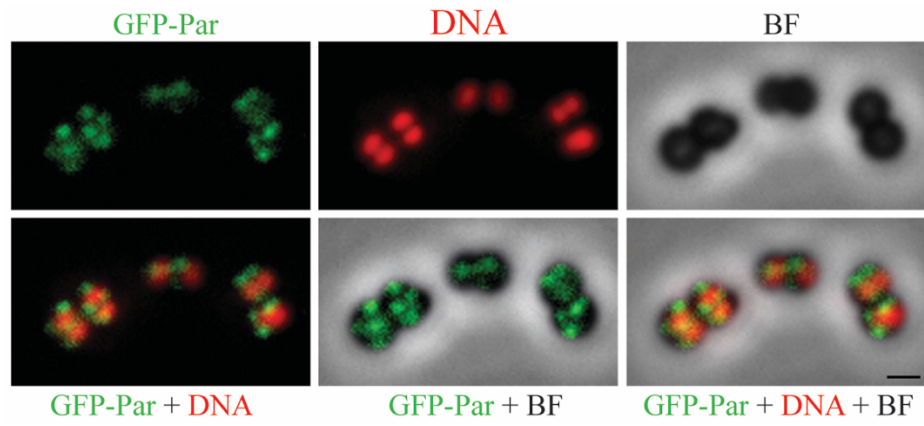
In order to determine whether the segregational stability of pSK9088 ($P_{par}::par-gfp$) (Table 2.2) could be improved such that Par-GFP might be more representative of Par localisation, the *par-gfp* partitioning system on pSK9088 was titrated *in trans* with wild-type Par from a compatible, co-resident plasmid. In this way, functional, wild-type Par might be able to complement the partial functionality of *par-gfp* and increase the stability of pSK9088, for example by interacting with the centromere-like site or with Par-GFP to improve its partitioning function. Co-expression of untagged and fluorescently-tagged proteins has been widely used as a strategy to overcome the partial functionality of tagged proteins. Specifically, in *S. aureus*, fluorescent protein fusions to the cell division proteins FtsZ, Spo0J, EzrA, PBP4 and Noc, have all been expressed and localised in the presence of their untagged

Figure 5.7 Fluorescence localisation of Par GFP fusion proteins in *S. aureus* cells

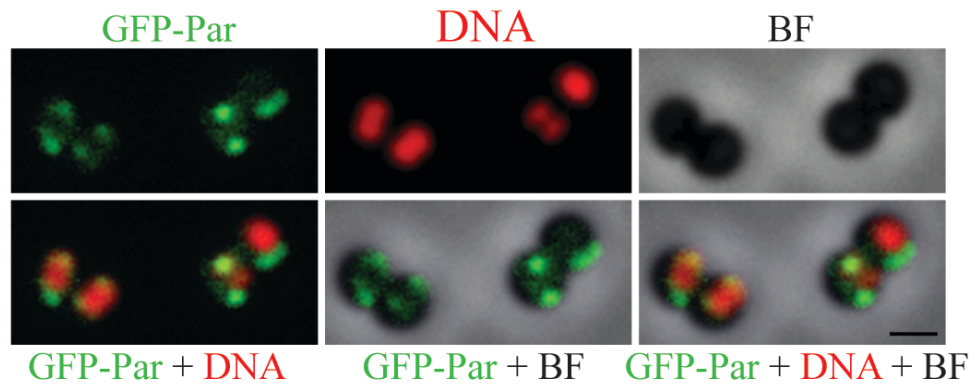
The localisation of Par GFP fusion proteins was visualised by epifluorescence microscopy on *S. aureus* SK8250 cells harbouring pSK9087 ($P_{par}::gfp-par$) (**Ai-iii**) or pSK9088 ($P_{par}::par-gfp$) (**Bi-ii**). Cells were grown to mid-exponential phase and prepared for epifluorescence microscopy as described in Section 2.11.2. Nucleoid DNA was stained with DAPI. Cells in each of (A) and (B) are biological replicates. From top left to bottom right: Par GFP fusion protein; DNA; bright-field (BF); overlay of GFP and DNA; overlay of bright-field (BF) and GFP; overlay of bright-field (BF), GFP and DNA. Scale bar = 1 μm .

A. *S. aureus* (*gfp-par*)

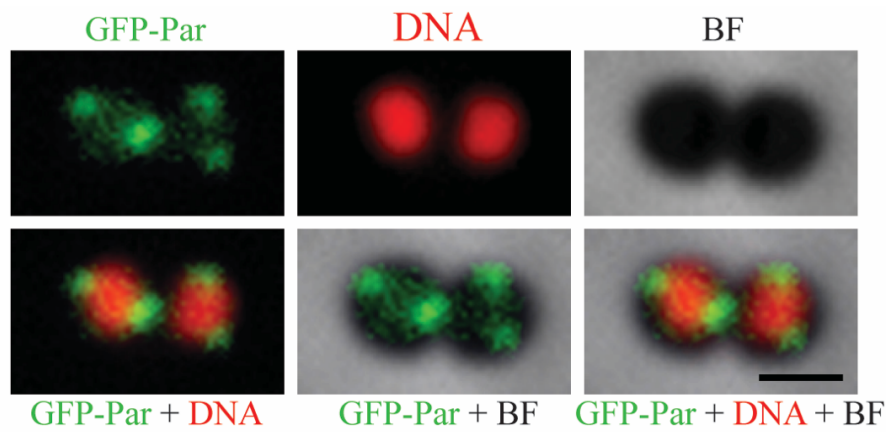
i.



ii.

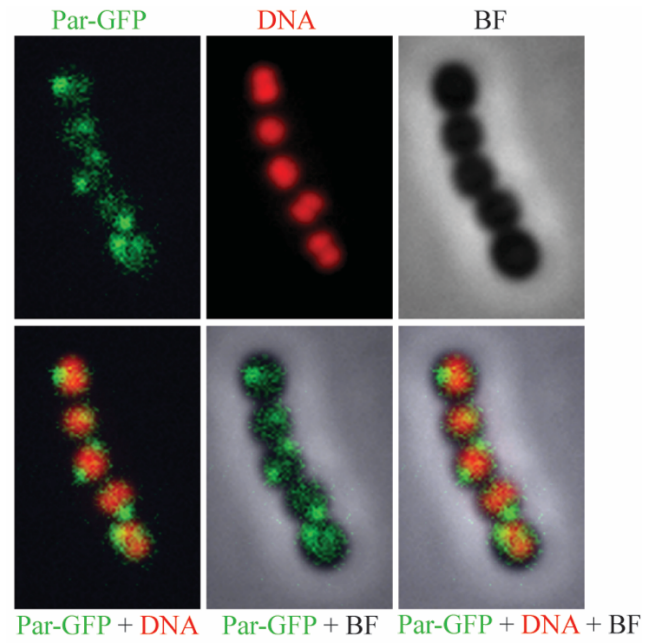


iii.

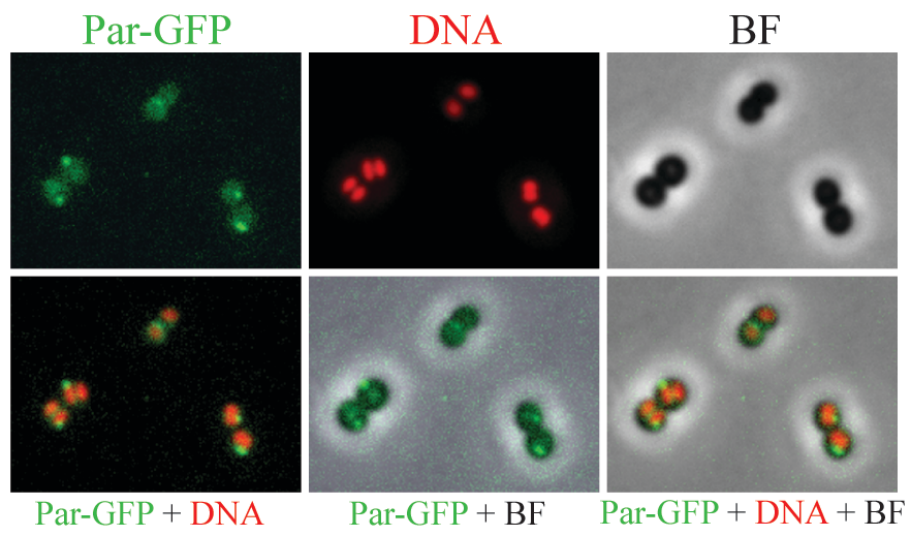


B. *S. aureus* (*par-gfp*)

i.



ii.



counterparts (Pereira *et al.* 2010, Veiga *et al.* 2011, Strauss *et al.* 2012). The interplay between Par and Par-GFP in the stabilisation of pSK9088 would result in a more accurate reflection of Par localisation by Par-GFP.

5.4.4.1 Construction of an IPTG-inducible *par* expression plasmid

An inducible *par* expression plasmid for the supply of Par *in trans* to pSK9088 ($P_{par}::par-gfp$) (Table 2.2) was constructed from pJEG015 (Table 2.2). pJEG015 is a derivative of pLOW-GFP (Table 2.2) (Liew *et al.* 2011) and contains the *tetA*(K) tetracycline resistance gene in place of the *ermC* erythromycin resistance gene on pLOW-GFP. As such, the selection for pJEG015 is compatible with the erythromycin selection used for pSK9088 in *S. aureus*. Furthermore, pJEG015 contains the pSK41 staphylococcal replicon, which is compatible with the pSK1 replicon on pSK9088. Importantly, pJEG015 features an IPTG-inducible P_{spac} promoter that is controlled by the Lac repressor, encoded by *lacI* on the same plasmid. Titratable protein production has been demonstrated by Liew *et al.* (2011), and hence Par induction levels can be optimised for the stabilisation of pSK1 minireplicons *in trans*.

A 0.8 kb DNA fragment containing the *par* ribosome binding site (RBS) and Par coding region, including the stop codon, was amplified by PCR (Section 2.4.4) from pSK4829 template DNA (Table 2.2) using primers SJ69 and HC21 (Table 2.6). The PCR was electrophoresed on a 2% (w/v) agarose gel (Section 2.4.3), gel-purified (Section 2.4.7) and digested with *SalI* and *HindIII* (Section 2.4.6). The digests were then purified (Section 2.4.7) and ligated (Section 2.4.11) to the dephosphorylated ends (Section 2.4.10) of the *SalI* and *HindIII* digested (Section 2.4.6) pJEG015

plasmid (Table 2.2), such that the stop codon was located between the *par* and *gfp* sequences. The ligation reaction was used to transform *E. coli* DH5 α cells to ampicillin resistance (Section 2.3.2), and selected transformants were screened by restriction digestion (Section 2.4.6) of isolated plasmid DNA (Section 2.4.1) with *SalI* and *HindIII*. Plasmids containing the correct restriction profile were identified by agarose gel electrophoresis (Section 2.4.3) of the digests, and were sequenced (Section 2.4.14) using primers SJ69 and HC21 (Table 2.6). The IPTG-inducible expression construct containing the *par* RBS and *par* coding region of the correct sequence was named pSK9104 (Table 2.2).

5.4.4.2 Effect of Par on plasmid segregational stability *in trans*

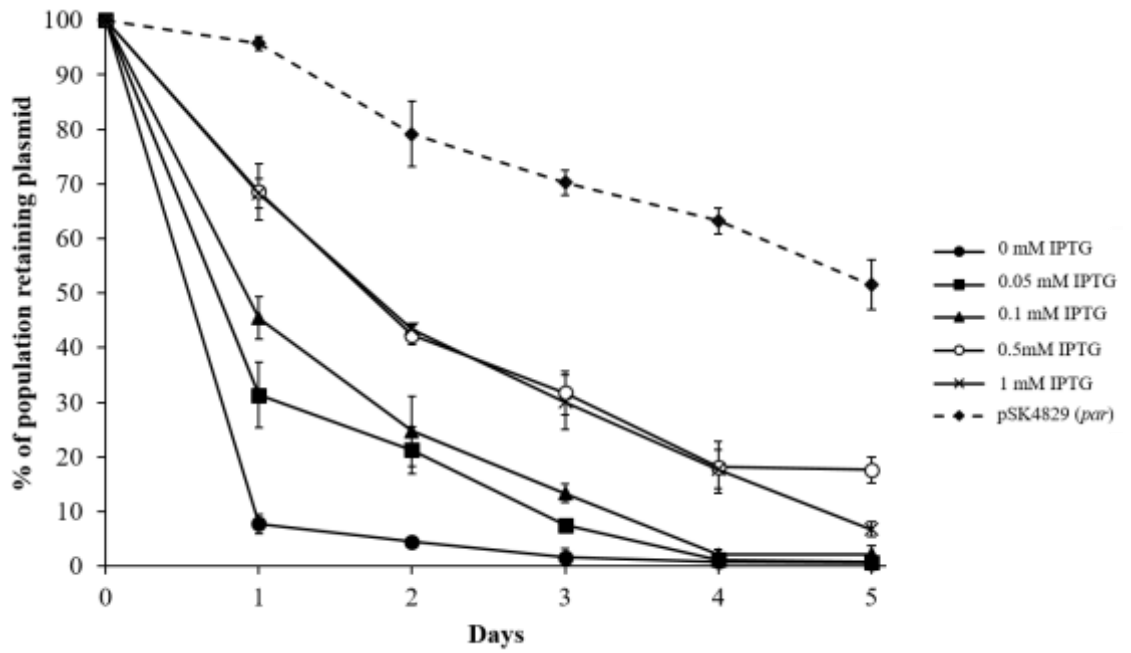
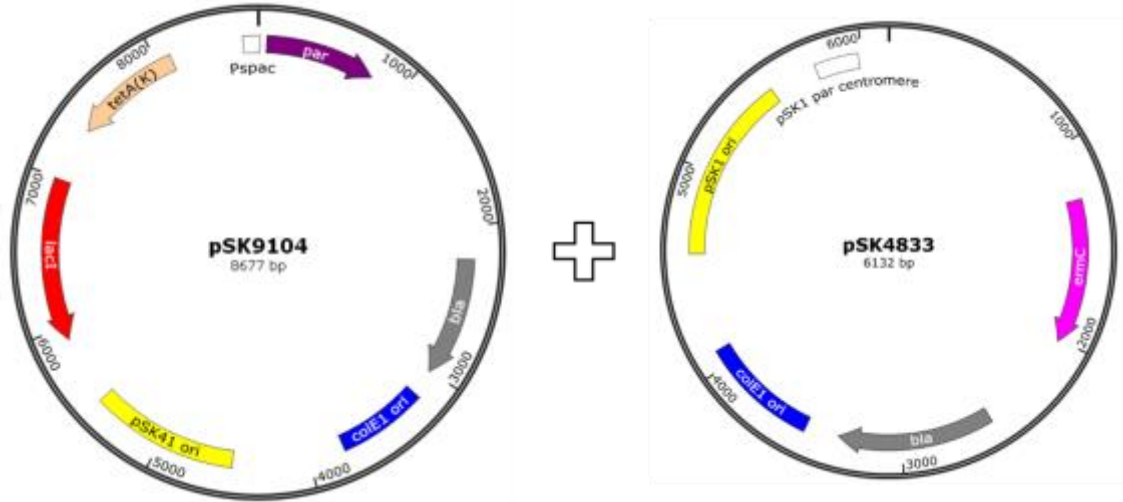
The ability of Par to stabilise an unstable pSK1 minireplicon *in trans* was assessed using plasmid segregational stability assays. *S. aureus* SK8250 cells were electroporated (Section 2.3.4) simultaneously with pSK9104 ($P_{spac}::par$) (Table 2.2) and one of the following pSK1 minireplicons containing the pSK1 *par* centromere-like site: pSK4833 (Δpar), pSK9087 ($P_{par}::gfp-par$) or pSK9088 ($P_{par}::par-gfp$) (Table 2.2). The segregational stability of the pSK1 minireplicon carried in each strain was determined by performing plasmid segregational stability assays (Section 2.7) in the presence of various levels of *par* induction (0, 0.05, 0.1, 0.5 and 1 mM IPTG; Liew *et al.* 2011), and with constant tetracycline selection for pSK9104.

The stability assay results in Figure 5.8A show that titration with Par *in trans* was capable of increasing the segregational stability a pSK1 minireplicon containing only the *par* centromere-like site (pSK4833). However, at the induction levels tested, Par was unable to fully complement the *par* deletion *in trans*, since the segregational

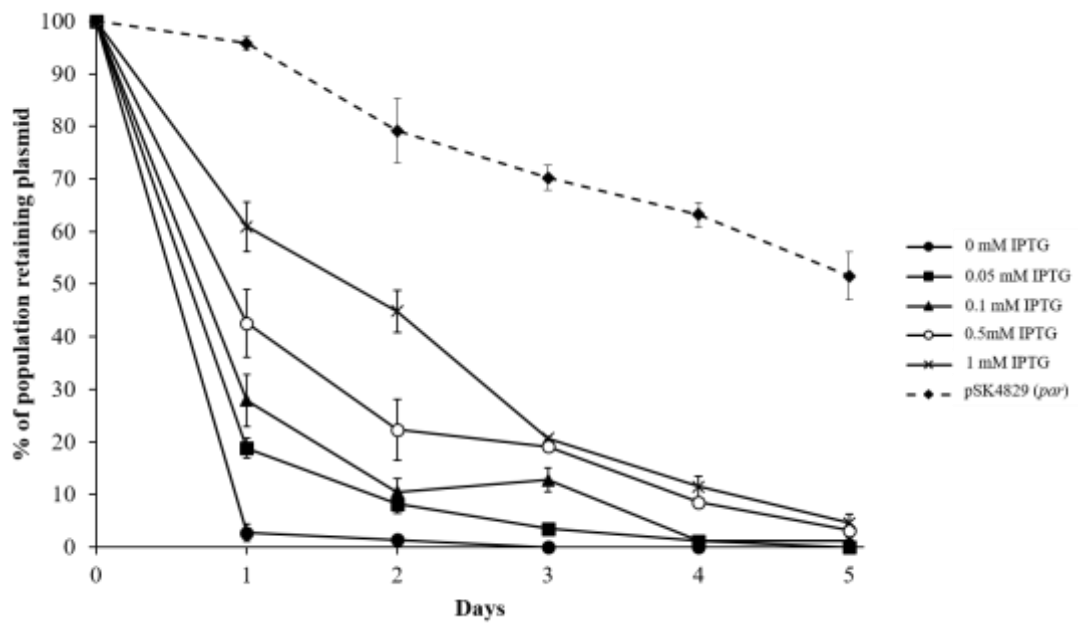
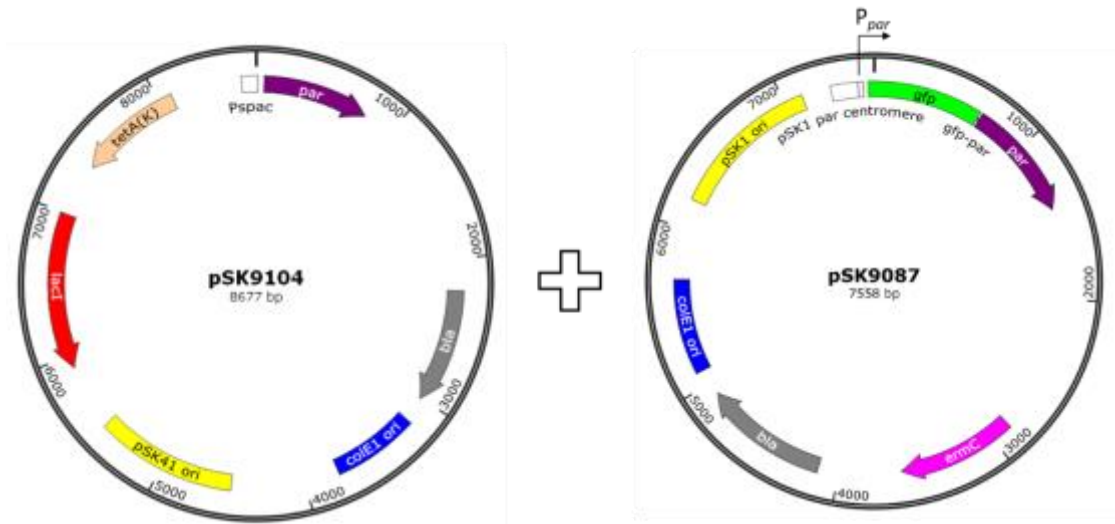
Figure 5.8 Effect of Par on plasmid segregational stability, *in trans*

Plasmid segregational stability assays of pSK1 minireplicons in the presence of Par, supplied *in trans*. The retention of pSK4833 (Δpar) (A), pSK9087 ($P_{par}::gfp-par$) (B) and pSK9088 ($P_{par}::par-gfp$) (C) in *S. aureus* SK8250 cells was determined as described in Section 2.7. Par was supplied *in trans* from a co-resident plasmid, pSK9104 ($P_{spac}::par$), by induction with 0 (●), 0.05 (■), 0.1 (▲), 0.5 (○) or 1 mM (×) IPTG. Assays were performed with continuous tetracycline selection for pSK9104. For reference, segregational stability data for pSK4829 (*par*) (◆) from Figure 3.2A is shown with a dashed line. Five days of serial subculture represents approximately 75 generations. Data are normalised to 100% plasmid retention on Day 0. The averages of three independent assays are shown. Error bars represent standard error of the mean. Illustrative maps of the plasmids contained in the assayed *S. aureus* strains are shown above the graphs.

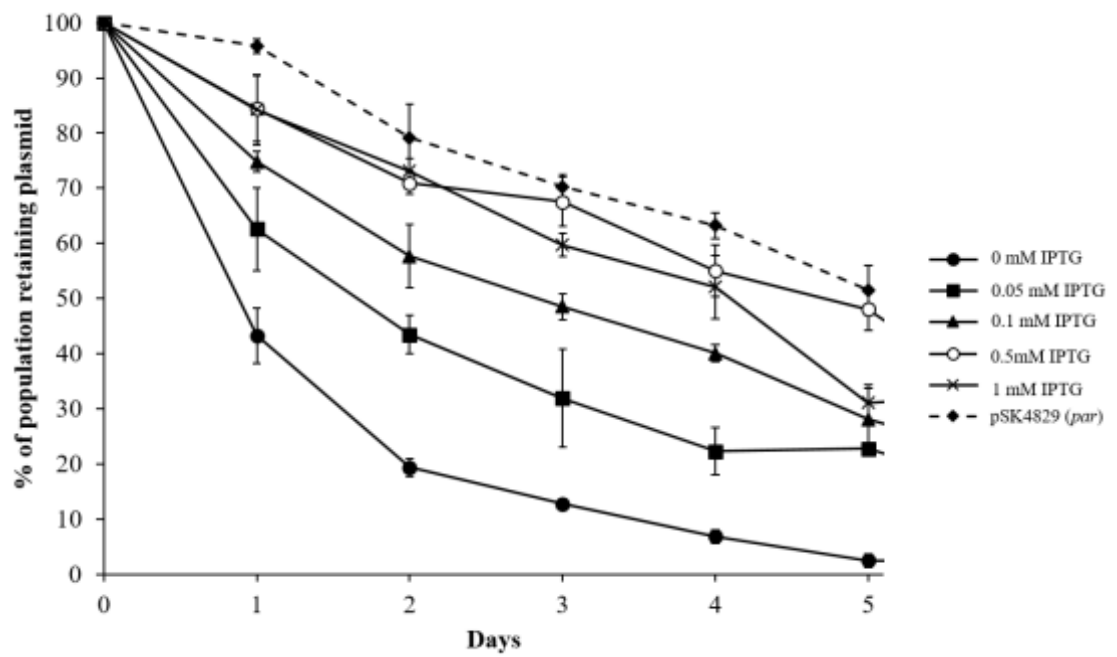
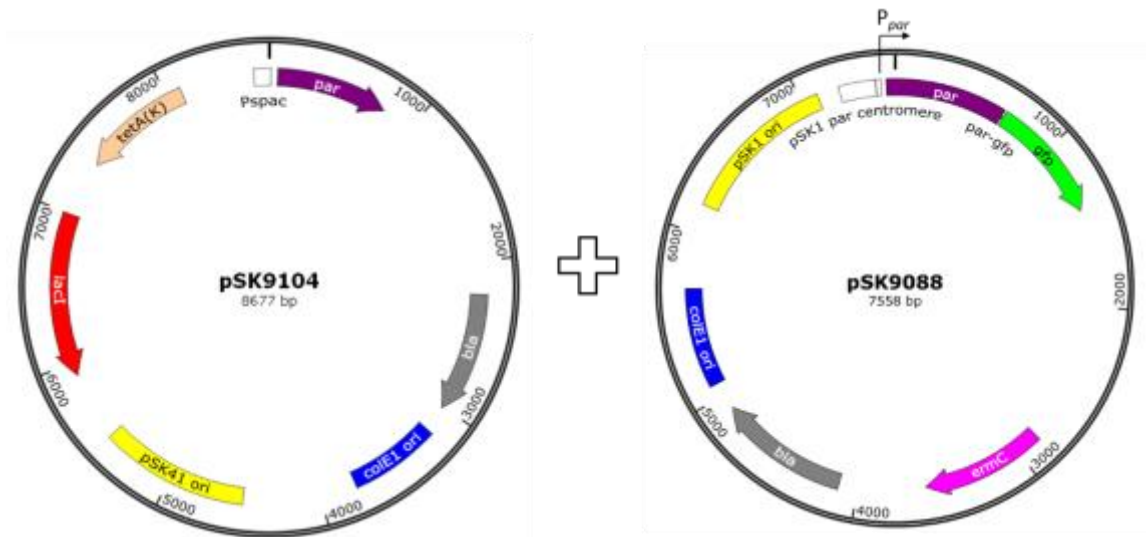
A.



B.



C.



stability of pSK4833 did not reach the level of stability observed for pSK4829, which contains the wild-type pSK1 *par* system (Figure 5.8A). A similar outcome was observed for the titration of pSK9087 ($P_{par}::gfp-par$) with Par, as increased *par* induction levels resulted in a noticeable increase in plasmid stability, especially during the first three days of the assay (Figure 5.8B). However, as was the case for pSK4833 (Δpar), the segregational stability of pSK9087 did not approach that of pSK4829 (*par*), even with maximum induction of *par* expression (Figure 5.8B). Conversely, when pSK9088 ($P_{par}::par-gfp$) was titrated with Par *in trans* from pSK9104 ($P_{spac}::par$), segregational stability increased from being partially stable in the absence of *par* induction, to displaying a similar level of stability to pSK4829 when *par* expression was induced with 0.5 mM or 1 mM IPTG (Figure 5.8C). This suggests that maximum induction of *par in trans* to pSK9088 was sufficient to fully complement the partial functionality of the *par-gfp* system.

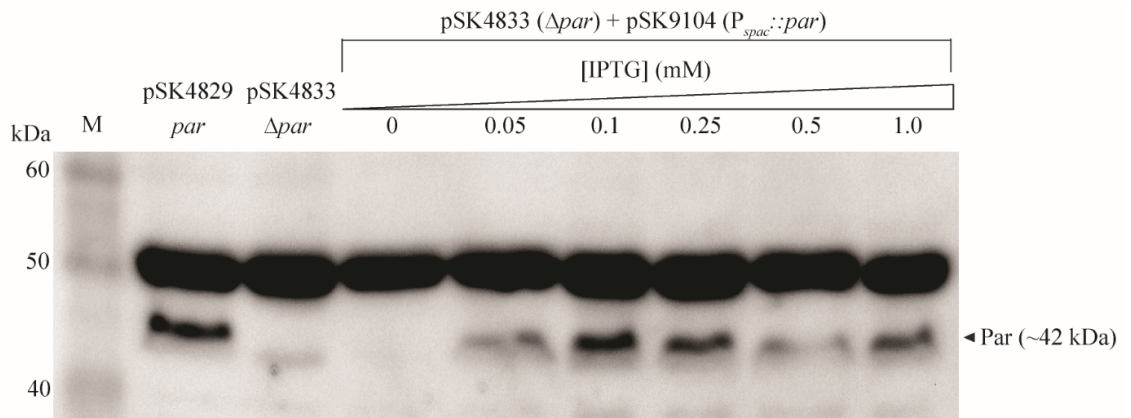
Taken together, the stability assay data presented in Figures 5.8A–C reveal a stabilisation effect on pSK4833, pSK9087 and pSK9088 when Par was provided *in trans*. Since plasmid stability generally increased with increasing IPTG levels, it appeared that the stability of the pSK1 minireplicons could be titrated with Par, which suggests some degree of Par functionality *in trans*. Furthermore, because maximum induction of *par* was unable to increase the stability of pSK4833 (Δpar) to pSK4829 (*par*) levels *in trans* (Figure 5.8A), the restored stability of pSK9088 ($P_{par}::par-gfp$) was, therefore, most likely a combination of the partial functionality of Par-GFP *in cis*, and the partial complementation provided by Par *in trans*.

To correlate the observed increases in plasmid segregational stability with increased Par protein levels, rather than increased concentrations of IPTG, Western blot analyses were performed for each of the assayed *S. aureus* strains at each of the IPTG levels tested. *S. aureus* SK8250 cells carrying pSK9104 ($P_{spac}::par$) and either pSK4833 (Δpar), pSK9087 ($P_{par}::gfp-par$) or pSK9088 ($P_{par}::par-gfp$) (Table 2.2) were grown to mid-exponential phase (Section 2.1) with selection for both co-resident plasmids (Table 2.4), and in the presence either 0, 0.05, 0.1, 0.5 or 1 mM IPTG. *S. aureus* SK8250 cells carrying either pSK4829 (*par*) or pSK4833 (Table 2.2) were included as positive and negative controls for Par immunodetection, respectively. *S. aureus* whole cell lysates, prepared as described in Section 2.5.8, were fractionated by SDS-PAGE (Section 2.5.6) and proteins were transferred to PVDF membranes for Western blotting (Section 2.5.9) using anti-Par peptide antibodies (Section 2.6.3). The Western blots in Figures 5.9A–C show the detection of Par as an approximately 42 kDa band from *S. aureus* cells carrying pSK4829 (*par*), but not from cells carrying pSK4833 (Δpar). In cells carrying pSK4833 and pSK9104 ($P_{spac}::par$), Par was not detected in the absence of IPTG induction, however, a 42 kDa band appeared in the lysates of all cells where *par* expression was induced (Figure 5.9A). This confirms that IPTG induction resulted in the specific production of Par from pSK9104. Notably, a band corresponding to the size of Par-GFP (approximately 60 kDa) did not appear from IPTG induction of the P_{spac} promoter on pSK9104, which suggests that the stop codon incorporated between *par* and *gfp* on pSK9104 was adequate in preventing translational read-through of the *gfp* coding sequence.

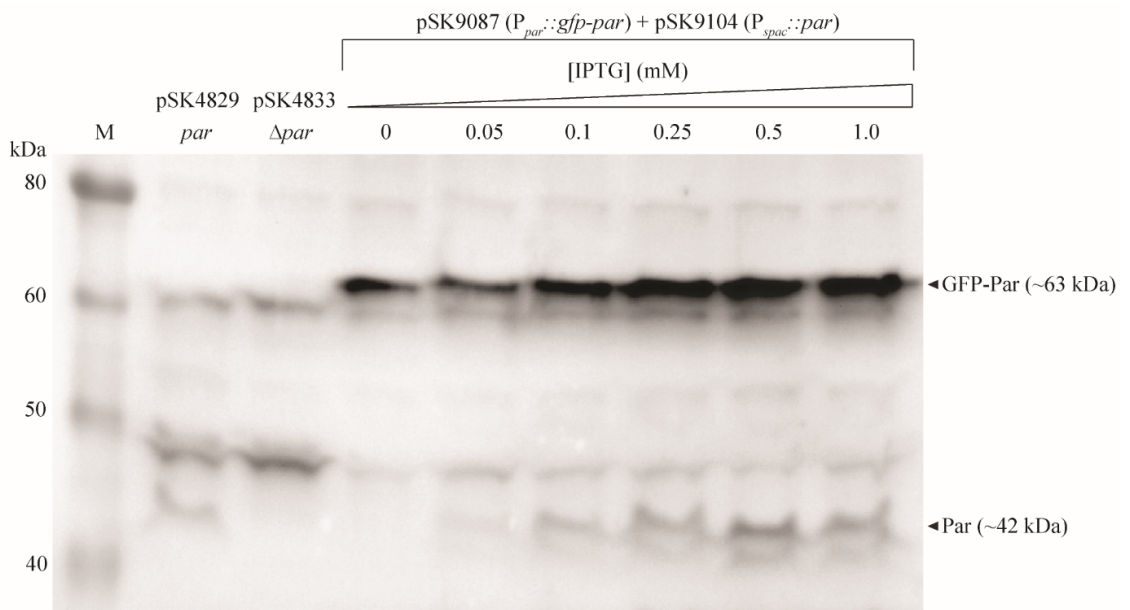
Figure 5.9 Immunodetection of Par, supplied *in trans* to pSK1 minireplicons

S. aureus SK8250 cells carrying pSK9104 ($P_{spac}::par$) and either pSK4833 (Δpar) (A), pSK9087 ($P_{par}::gfp-par$) (B) or pSK9088 ($P_{par}::par-gfp$) (C) were grown to mid-exponential phase in the presence of 0, 0.05, 0.1, 0.25, 0.5 or 1 mM IPTG induction of *par* expression from pSK9104 (Section 5.4.4.2). Cleared cell lysates were fractionated by SDS-PAGE (Section 2.5.6) and subjected to Western blotting (Section 2.5.9) using affinity-purified and preadsorbed anti-Par antibodies (Sections 2.6.1 and 2.6.2) (A and C) or anti-Par peptide antibodies (Section 2.6.3) (B). Samples were co-electrophoresed with cleared lysates from mid-exponential phase *S. aureus* SK8250 cells carrying pSK4829 (*par*) or pSK4833 (Δpar), for positive and negative controls, respectively. Lane M contains prestained protein markers, with marker sizes indicated in kDa on the left of each blot. Positions of relevant proteins and their approximate measured sizes are indicated by black arrowheads.

A.



B.



C.

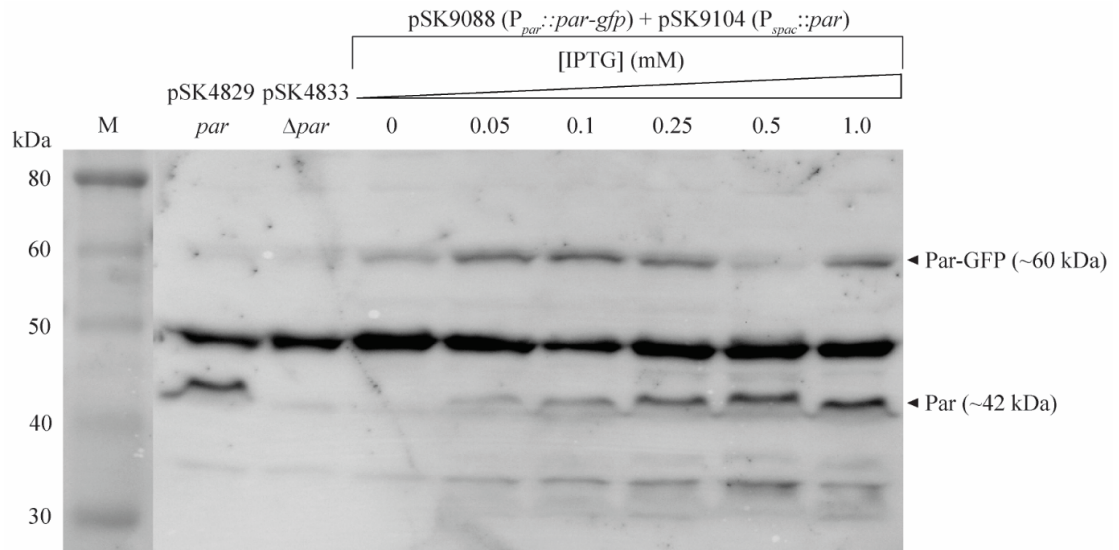


Figure 5.9B shows the Western blot of *S. aureus* lysates containing pSK9087 ($P_{par}::gfp-par$) and pSK9104 ($P_{spac}::par$). GFP-Par, produced from pSK9087, appeared as a band of approximately 63 kDa, with the production of Par evident from the appearance of a 42 kDa protein band in cells treated with IPTG (Figure 5.9B). Similarly, cells carrying pSK9088 ($P_{par}::par-gfp$) and pSK9104 ($P_{spac}::par$) showed an approximately 60 kDa band corresponding to Par-GFP produced from pSK9088, and a 42 kDa Par protein band that was present in cells induced with IPTG (Figure 5.9C). These results, therefore, confirm that titration of pSK1 minireplicons with IPTG led to detectable levels of Par produced from pSK9104, which correlated with an increase in the segregational stability of pSK1 minireplicons in *S. aureus* (Figures 5.8A–C).

5.4.4.3 Interaction between Par and Par-GFP

The stability assays described in Section 5.4.4.2 demonstrated that the segregational stability of pSK9088 ($P_{par}::par-gfp$) (Table 2.2) could be improved by providing Par *in trans* from pSK9104 ($P_{spac}::par$) (Table 2.2). In order for this result to be meaningful for fluorescence localisation studies, which are based on the premise that Par-GFP localisation is indicative of Par localisation, it was necessary to show interaction between Par and Par-GFP. To achieve this, Y2H assays were performed between Par and Par-GFP bait and prey fusion proteins. Par-GFP fusions to GAL4 BD and GAL4 AD were generated using pGBKT7 and pGADT7 plasmids, respectively (Table 2.2), using primers HC24 and HC26 (Table 2.6) for the PCR-amplification (Section 2.4.4) of the Par-GFP coding region from pSK9088 template DNA (Table 2.2). All other steps in the construction of bait and prey plasmids

encoding Par-GFP were performed essentially as described in Section 3.6.1 for the construction of Y2H plasmids encoding Par bait and prey fusion proteins. Plasmids of the correct sequence were named pSK9108, encoding GAL4 BD-Par-GFP, and pSK9111, encoding GAL4 AD-Par-GFP (Table 2.2).

S. cerevisiae AH109 cells were transformed simultaneously with plasmid pairs pSK9107/pSK9111 (GAL4 BD-Par/GAL4 AD-Par-GFP) or pSK9108/pSK9110 (GAL4 BD-Par-GFP/GAL4 AD-Par) (Table 2.2) using the small-scale LiAc yeast transformation procedure (Section 2.10.2). Y2H assays were performed as described in Section 2.10.3 to determine whether Par and Par-GFP bait and prey fusion proteins interact. As shown in Figure 5.10A, yeast cells grew on high-stringency selection medium when both full-length Par (ParFL) and Par-GFP were present, regardless of whether the proteins were fused to GAL4 BD or GAL AD. Neither the Par-GFP bait nor prey proteins showed self-activation of the reporter genes or interaction with the empty plasmids (Figure 5.10A), which indicates that growth of yeast cells containing Par and Par-GFP was the result of specific interactions and activation of the reporter genes. (It has already been shown that Par bait and prey fusion proteins do not interact with empty Y2H plasmids; see Figures 3.10A and 3.11A). The interaction between Par and Par-GFP was supported by α -galactosidase assays (Section 2.10.5), which revealed similar levels of α -galactosidase activity regardless of whether Par or Par-GFP was fused to GAL4 BD or GAL4 AD (Figure 5.10B). The α -galactosidase activities resulting from the interaction between Par and Par-GFP were comparable to the level of activity resulting from Par self-interaction (Figure 5.10B). The indications provided by the Y2H and α -galactosidase assays, therefore, suggest that Par and Par-GFP have the capacity to interact with each other,


Figure 5.10 Interaction between Par and Par-GFP

A. Y2H assays of interactions between Par and Par-GFP. Pairwise Y2H assays were performed between GAL4 BD (bait) and GAL4 AD (prey) protein fusions to full-length Par (ParFL) and Par-GFP, according to the methods described in Section 5.4.4.3. *S. cerevisiae* AH109 cells containing bait and prey plasmids were patched on high-stringency selection medium (SD/-Leu/-Trp/-His/-Ade/X- α -Gal) (Table 2.3). Growth indicates activation of the *HIS3* and *ADE2* reporter genes. Blue pigmentation indicates α -galactosidase activity from yeast cells. *S. cerevisiae* AH109 cells expressing the prey protein fusion, simian virus T antigen (GAL4 AD-T), and the bait protein fusions, murine p53 (GAL4 BD-53) or human lamin protein (GAL4 BD-Lam), were included as positive and negative controls, respectively.

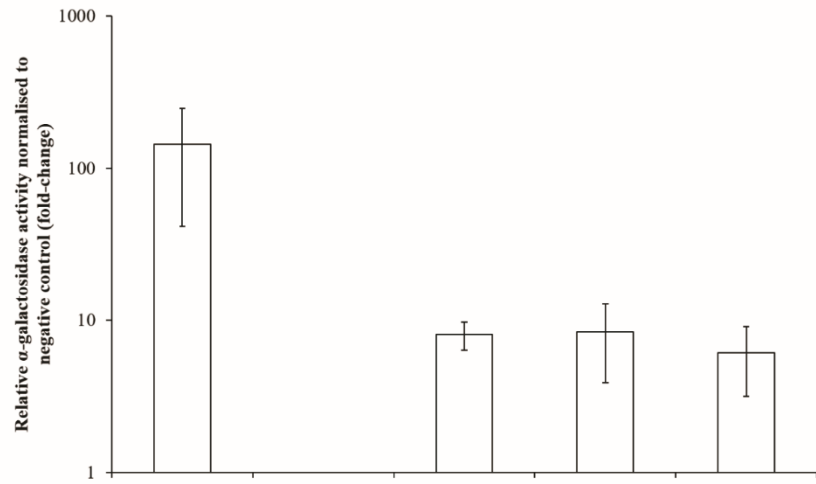
B. Relative interaction strengths between Par and Par-GFP. α -galactosidase assays were performed on *S. cerevisiae* AH109 cells containing Par and Par-GFP bait and prey fusion proteins, according to the protocol described in Section 2.10.5. For comparison of relative interaction strengths, α -galactosidase activity was calculated as described in Section 2.10.5 and expressed as fold-change relative to the negative control strain containing GAL4 BD-Lam and GAL4 AD-T. The interaction between the GAL4 BD-53 and GAL4 AD-T was included as a positive control. Each data point represents the mean of at least three independent assays, each performed in triplicate. Error bars represent standard error of the mean.

A.

Bait (GAL4 BD fusion)	53	Lam	ParFL	ParFL	Par-GFP	Par-GFP	pGBKT7
Prey (GAL4 AD fusion)	T	T	ParFL	Par-GFP	ParFL	pGADT7	Par-GFP



B.



Bait (GAL4 BD fusion)	53	Lam	ParFL	Par	Par-GFP
Prey (GAL4 AD fusion)	T	T	ParFL	Par-GFP	Par

which, combined with the stability assay data that showed a stabilising effect of Par on pSK9088 ($P_{par}::par-gfp$) (Section 5.4.4.2), provides support for the interpretation of Par-GFP localisation as being reflective of Par localisation.

5.4.4.4 Epifluorescence microscopy of Par-GFP in *S. aureus*, supplied *in trans* with Par

The results from plasmid stability assays (Section 5.4.4.2) and Y2H assays (Section 5.4.4.3) suggested that the production of Par *in trans* to the *par-gfp* partitioning system on pSK9088 (Table 2.2) led to an increase in plasmid stability, probably as a result of interaction between Par and the partially functional Par-GFP. Epifluorescence microscopy was, therefore, performed on *S. aureus* cells harbouring pSK9088 ($P_{par}::par-gfp$) in the presence and absence of Par *in trans*, on the premise that Par-GFP localisation would be representative of Par localisation.

S. aureus SK8250 cells were co-electroporated (Section 2.3.4) with pSK9088 and pSK9104 ($P_{spac}::par$) (Table 2.2), and single colonies were cultured to mid-exponential phase in the presence of antibiotic selection for each plasmid (Section 2.11.2). In order for the localisation of Par-GFP to be assessed in the presence and absence of Par *in trans*, cells carrying both pSK9088 and pSK9104 were treated with or without 1 mM IPTG, which was the level of *par* induction shown to complement the segregational stability of pSK9088 *in trans* (Figure 5.8C). Exponentially-growing cells were prepared for live cell epifluorescence microscopy as described in Section 2.11.2, and nucleoid DNA was stained with DAPI.

Due to the role of Par in plasmid segregation, the localisation of Par-GFP relative to the cell poles and/or division septum might provide useful information on the

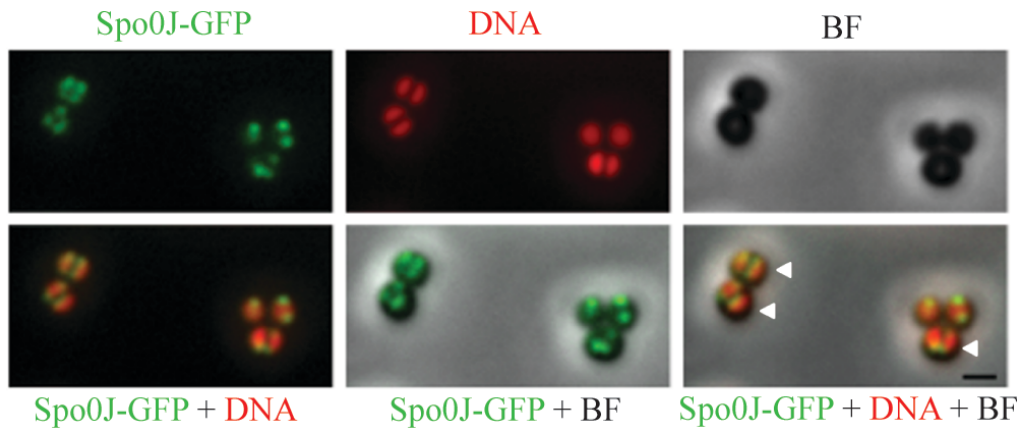
mechanism of *par*-mediated plasmid segregation. However, it was difficult to determine the localisation of the cell poles, which was due in part to the spherical shape of *S. aureus* cells, in addition to the staphylococcal mode of cell division in three orthogonal planes (Tzagoloff and Novick 1977). Fluorescent protein fusions to the Spo0J protein, which binds to the chromosomal origin of replication, *oriC*, in *B. subtilis* (Lin and Grossman 1998, Breier and Grossman 2007), were shown to localise near the cell poles in *S. aureus* (Pinho and Errington 2004, Veiga *et al.* 2011). Hence, to compare Par-GFP localisation relative to the staphylococcal cell poles, epifluorescence microscopy was performed on a Spo0J-GFP fusion protein. *S. aureus* RN4220 cells were electroporated (Section 2.3.4) with pSK9086 (Table 2.2), which expresses *spo0J-gfp* from the IPTG-inducible P_{spac} promoter. Cells were grown to early-exponential phase, before Spo0J-GFP production was induced with 1 mM IPTG for 1 h. Cells were then prepared for microscopy as described above. As shown in Figures 5.11i–ii, and consistent with published results (Pinho and Errington 2004, Veiga *et al.* 2011), the staphylococcal cell poles were clearly marked by Spo0J-GFP foci, and were particularly evident in cells that were orientated to show the bilobed nucleoid. In these cells, highlighted by white arrowheads in Figures 5.11i–ii, Spo0J-GFP foci, usually two or four visible in this orientation, were evenly distributed on either side of the division septum located between the two nucleoid lobes.

A comparison of representative micrographs obtained of Par-GFP in *S. aureus*, shown in Figures 5.12A–B, revealed no obvious differences in fluorescence localisation patterns, whether Par-GFP was produced in the presence (Figures 5.12Bi–ii) or absence (Figures 5.12Ai–iii) of Par *in trans*. Par-GFP was detected as

Figure 5.11 Fluorescence localisation of the cell division marker, Spo0J-GFP, in *S. aureus* cells

i–ii. *S. aureus* SK8250 cells harbouring pSK9086 ($P_{spac}::spo0J-gfp$) were grown to early-exponential phase, before *spo0J-GFP* expression was induced with 1 mM IPTG from pSK9086 (Section 5.4.4.4). Nucleoid DNA was stained with DAPI, and cells were prepared for epifluorescence microscopy as described in Section 2.11.2. Cells shown are biological replicates. From top left to bottom right: Spo0J-GFP; DNA; bright-field (BF); overlay of Spo0J-GFP and DNA; overlay of bright-field (BF) and Spo0J-GFP; overlay of bright-field (BF), Spo0J-GFP and DNA. Arrowheads indicate cells containing Spo0J-GFP foci located in opposite cell hemispheres. Scale bar = 1 μm .

i. *S. aureus* (*spo0J-gfp*)



ii.

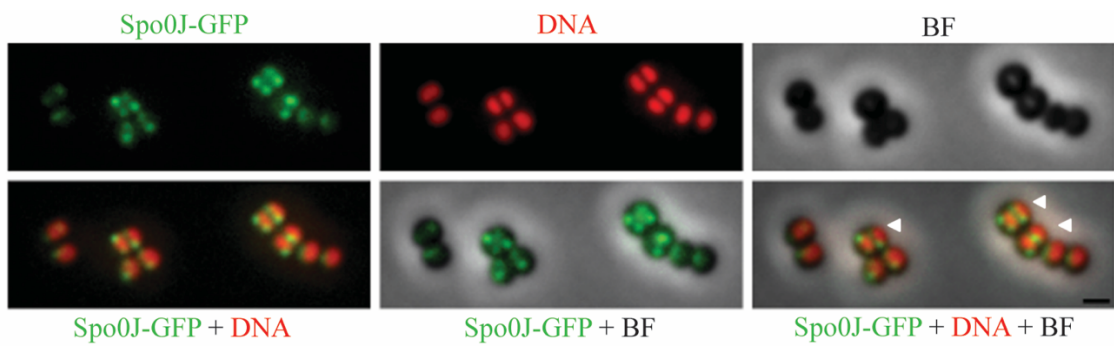
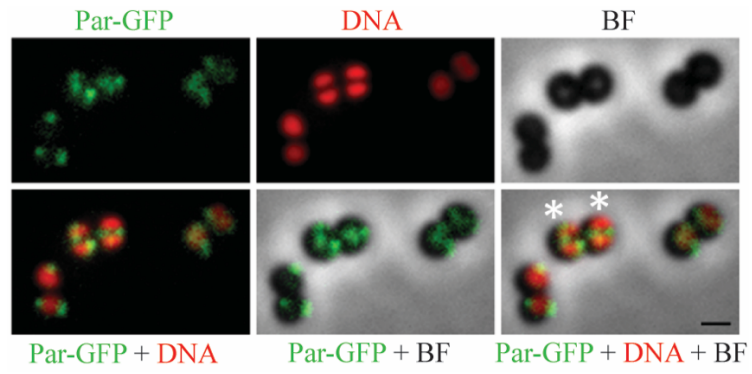


Figure 5.12 Fluorescence localisation of Par-GFP in *S. aureus* cells, in the presence and absence of Par supplied *in trans*

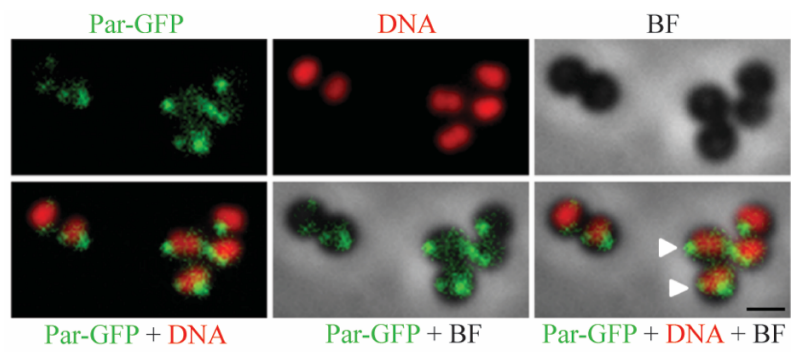
The localisation of Par-GFP was visualised by epifluorescence microscopy on *S. aureus* SK8250 cells harbouring pSK9088 and pSK9104 ($P_{spac}::par$) in the absence (Ai–iii) and presence (Bi–ii) of 1 mM IPTG induction of *par* expression from pSK9104. Cells were grown to mid-exponential phase (in the presence of IPTG where applicable), and prepared for epifluorescence microscopy as described in Section 2.11.2. Nucleoid DNA was stained with DAPI. Cells in each of (A) and (B) are biological replicates. From top left to bottom right: Par-GFP; DNA; bright-field (BF); overlay of Par-GFP and DNA; overlay of bright-field (BF) and Par-GFP; overlay of bright-field (BF), Par-GFP and DNA. Arrowheads indicate cells containing Par-GFP foci located in opposite cell hemispheres. Asterisks indicate cells containing Par-GFP foci positioned between nucleoid lobes. Scale bar = 1 μ m.

A. *S. aureus* (*par-gfp*) + Par + 0 mM IPTG

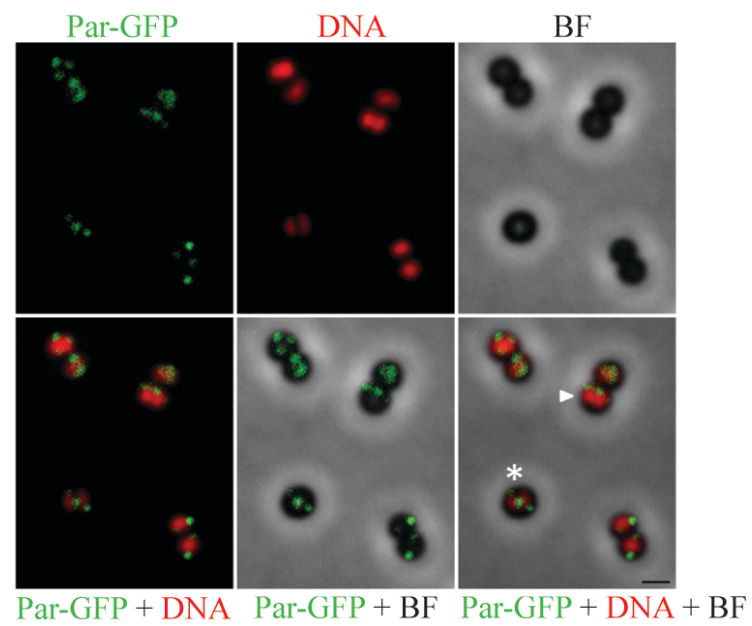
i.



ii.

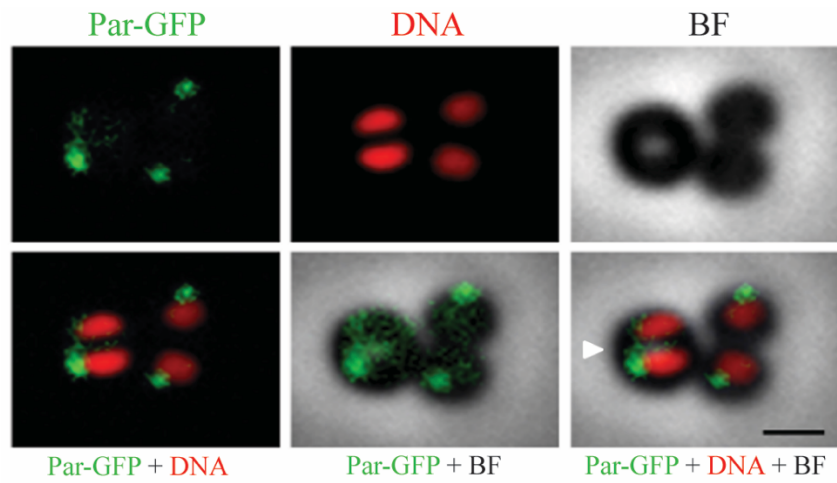


iii.

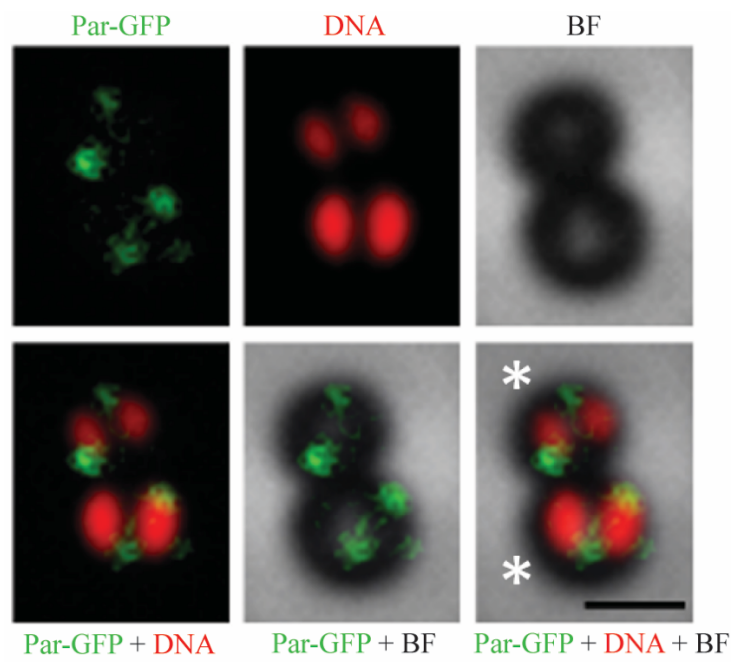


B. *S. aureus* (*par-gfp*) + Par + 1 mM IPTG

i.



ii.



foci, primarily located towards the cell periphery, with typically 1–4 foci observed per cell, regardless of whether Par was present (Figures 5.12A–B). The localisation pattern of Par-GFP foci in some, but not all, cells (depending on cell orientation) resembled the localisation of Spo0J-GFP (compare Figures 5.11 and 5.12), indicating that Par-GFP may have been localised to the cell poles at the time of image capture.

Cells in late divisional stage appeared larger than pre-divisional stage cells, and when viewed at an appropriate orientation, nucleoids appeared bilobed with large separation between the lobes, in preparation for cell division (Figures 5.12A–B, arrowheads and asterisks). These cells typically contained two or more Par-GFP foci, each in separate hemispheres of the cell, presumably on either side of the division septum, and each appearing to be associated with a separate lobe of the nucleoid (Figures 5.12A–B, white arrowheads). In this configuration, it is envisaged that subsequent cell division would result in each daughter cell receiving at least one Par-GFP focus. Examples were also observed whereby Par-GFP foci appeared between the lobes of the nucleoid, presumably at, or near, the division septum (Figures 5.12A–B, asterisks). Note that the Par-GFP localisation patterns described here were found irrespective of whether Par-GFP was supplied *in trans* with Par.

5.4.4.4.1 Association between Par-GFP and nucleoid DNA in *S. aureus*

Non-specific interactions with nucleoid DNA have been demonstrated for ParA and SopA proteins from Type Ia plasmid partitioning systems (Bouet *et al.* 2007, Ringgaard *et al.* 2009, Vecchiarelli *et al.* 2010, Hwang *et al.* 2013, Vecchiarelli *et al.* 2013b), and has been proposed for the pilot-fish mechanism of R388 plasmid

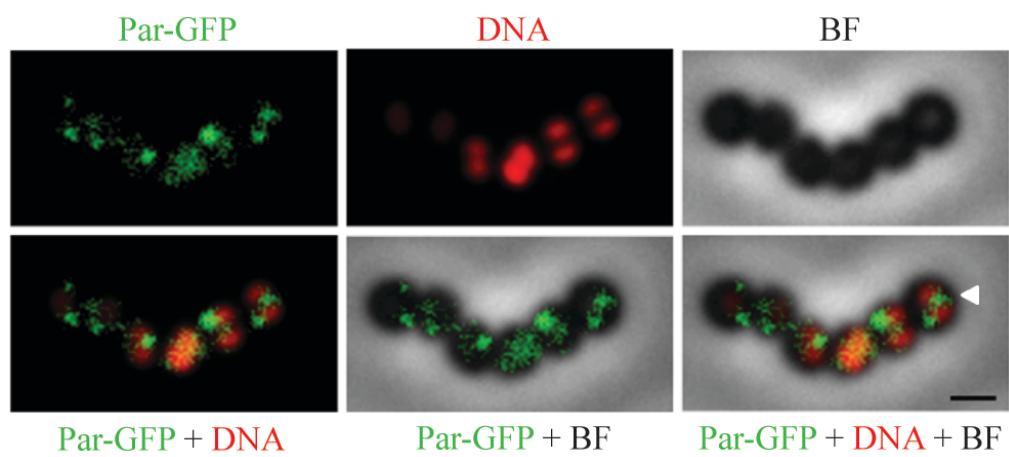
partitioning (Guynet *et al.* 2011). From the fluorescence micrographs in Figures 5.12A–B, there appeared to be a close association between some Par-GFP foci and nucleoid DNA, particularly at the outer edges of the nucleoid. As a result of these observations, and due to the resemblance of Par-GFP with Spo0J localisation (Section 5.4.4.4), the potential association between Par-GFP and nucleoid DNA was investigated by treating *S. aureus* cells with chloramphenicol in order to condense nucleoids (Section 2.11.2). It has been hypothesised that chloramphenicol acts to condense nucleoid DNA by inhibiting protein synthesis and disrupting the nucleoid-expanding force generated by this process, and that this in turn results in the compaction of nucleoids (Woldringh *et al.* 1995). Due to the large volume occupied by the nucleoid in *S. aureus* cells, condensation of nucleoid DNA has been particularly useful in staphylococcal microscopy studies (for example, see Veiga *et al.* 2011). As shown in Figures 5.13A–B, treatment of cells with chloramphenicol led to the compaction of nucleoid DNA, which resulted in a larger space between the nucleoid and the cell periphery. This allowed for clearer observation of Par-GFP localisation relative to the nucleoid and cell periphery. Whether or not Par-GFP foci were associated with nucleoid DNA was sometimes difficult to determine, and depended on the extent of nucleoid condensation and the orientation of the cells. Indeed, examples were seen in cells with and without Par production *in trans*, whereby Par-GFP foci were localised away from the cell periphery and appeared associated with the compacted nucleoid DNA (Figures 5.13A–B, arrowheads). However, there were also some examples, highlighted by asterisks in Figures 5.13A–B, whereby Par-GFP foci were detected at the cell periphery, with an obvious separation from the condensed nucleoid. This was more commonly observed in cells

Figure 5.13 Effect of nucleoid condensation on the fluorescence localisation of Par-GFP in *S. aureus* cells, in the presence and absence of Par supplied *in trans*

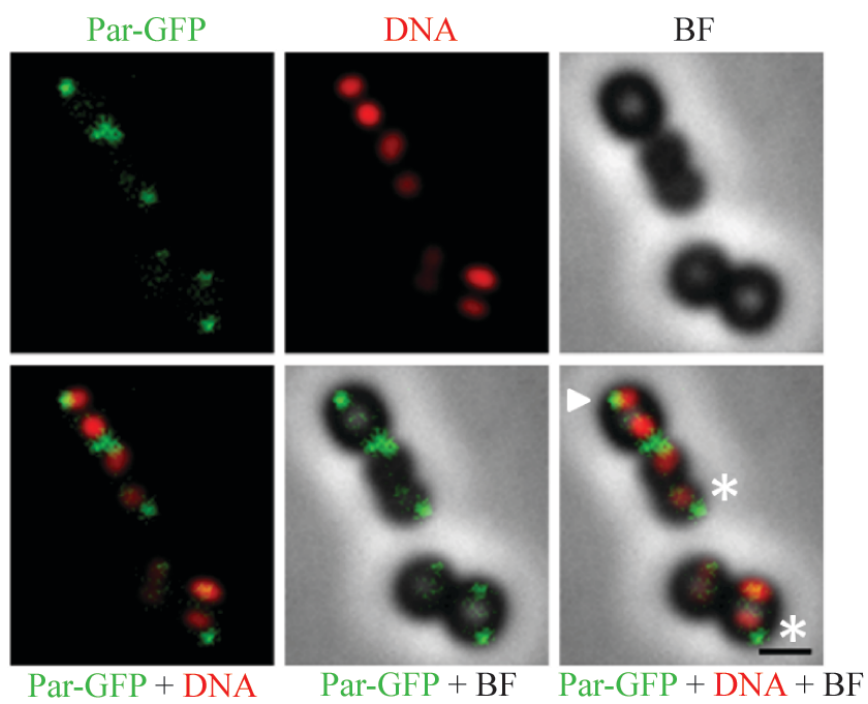
The localisation of Par-GFP was visualised by epifluorescence microscopy on *S. aureus* SK8250 cells harbouring pSK9088 and pSK9104 ($P_{spac}::par$) in the absence (Ai-ii) and presence (Bi-iii) of 1 mM IPTG induction of *par* expression from pSK9104. Cells were grown to mid-exponential phase (in the presence of IPTG where applicable), and then treated with 25 μ g/ml chloramphenicol for 1 h to condense nucleoids (Section 2.11.2). Nucleoid DNA was stained with DAPI and epifluorescence microscopy was performed as described in Section 2.11.2. Cells in each of (A) and (B) are biological replicates. From top left to bottom right: Par-GFP; DNA; bright-field (BF); overlay of Par-GFP and DNA; overlay of bright-field (BF) and Par-GFP; overlay of bright-field (BF), Par-GFP and DNA. Arrowheads indicate cells containing Par-GFP foci that appeared to associate with condensed nucleoids. Asterisks indicate cells containing Par-GFP foci that did not appear to associate with condensed nucleoids. Scale bar = 1 μ m.

A. *S. aureus* (*par-gfp*) + Par + 0 mM IPTG + Cm25

i.

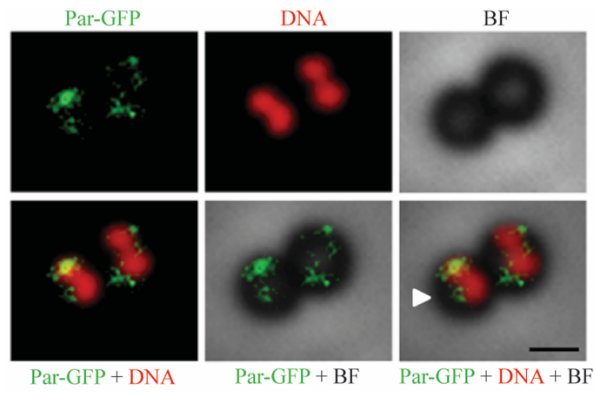


ii.

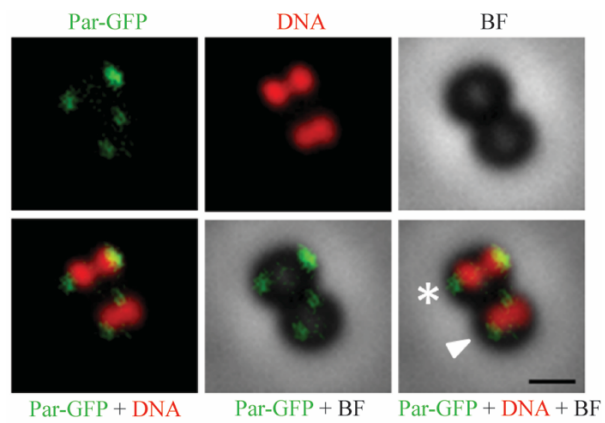


B. *S. aureus* (*par-gfp*) + Par + 1 mM IPTG + Cm25

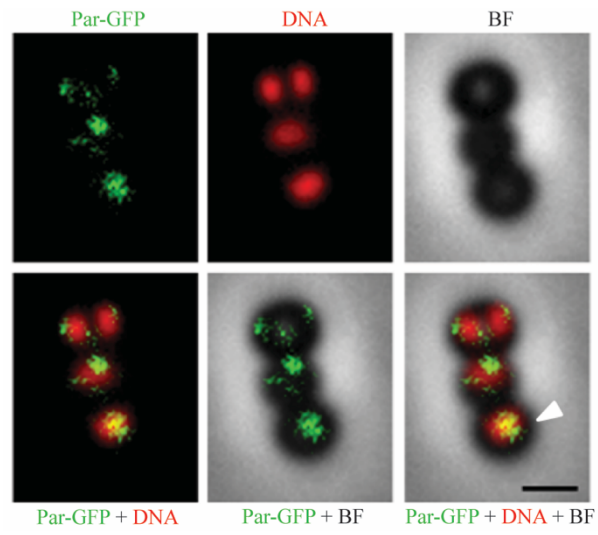
i.



ii.



iii.



that did not produce Par *in trans*, which suggests that the partial functionality of Par-GFP in the absence of Par may have contributed to the observed loss in potential associations between Par-GFP and nucleoid DNA.

5.4.5 Development of a pSK1 *par* system with inducible, *in trans* expression of *par-gfp*

The segregational stability assays performed in Section 5.4.2 showed that the N- and C-terminal GFP fusions to Par were both impaired in functionality when produced *in cis* at wild-type levels from P_{par}. Although segregational stability of pSK9088 (P_{par}::*par-gfp*) (Table 2.2) could be improved with the supply of Par *in trans* (Section 5.4.4.2), the localisation of Par-GFP in the presence and absence of Par could not be easily differentiated (Section 5.4.4.4). Hence, an alternative strategy was employed for the determination of Par localisation, and involved the titration of Par-GFP *in trans* to the wild-type *par* system on the pSK1 minireplicon, pSK4829 (Table 2.2). In this way, Par would be produced at wild-type levels from pSK4829, and controlled expression of *par-gfp* from a co-resident plasmid would allow Par-GFP to incorporate into the *par* system and decorate structures and components of the system, whilst minimising disruption to Par function.

5.4.5.1 Construction of an IPTG-inducible *par-gfp* expression plasmid

In order to titrate Par-GFP *in trans* to the wild-type *par* system on the pSK1 minireplicon, pSK4829 (Table 2.2), an inducible *par-gfp* expression plasmid was generated using pJEG015 (Table 2.2). As described in Section 5.4.4.1, pJEG015 contains features that are compatible with the pSK1 minireplicons used in this study. The *par-gfp* expression plasmid was constructed in the same way as described for

the construction of the *par* expression plasmid, pSK9104 (Table 2.2) (Section 5.4.4.1), except that primers SJ69 and SJ70 were used for the amplification of the *par* RBS and coding sequence, such that the stop codon was excluded. Subsequent ligation of the amplicon to the restricted *SalI* and *BamHI* sites of pJEG015 resulted in an N-terminal fusion of *par* in-frame with the GFP coding sequence present on the vector. Recombinant plasmids were identified by agarose gel electrophoresis (Section 2.4.3) of isolated plasmid DNA (Section 2.4.1) that had been restriction digested (Section 2.4.6) with *SalI* and *BamHI*. Recombinant plasmids were sequenced (Section 2.4.14) using primers HC18, SJ69 and SJ70 (Table 2.6), and the plasmid of correct sequence encoding Par-GFP downstream of P_{spac} and the *par* RBS was named pSK9097 (Table 2.2).

GFP fusions to the Par DNA-binding mutant, ParK15A, and the Par multimerisation mutant, Par Δ CC (Figgett 2007, Lai 2008), were also generated in pJEG015, exactly as described for the generation of pSK9097, except using pSK7721 and pSK7764 template DNA (Table 2.2) for the PCR-amplification of ParK15A and Par Δ CC coding regions, respectively. The pJEG015-derived expression plasmids with IPTG-inducible expression of *parK15A-gfp* and *par Δ CC-gfp* from the P_{spac} promoter were named pSK9102 and pSK9103, respectively (Table 2.2).

5.4.5.2 Effect of Par-GFP on plasmid segregational stability *in trans*

In order to determine the functionality of Par-GFP *in trans*, plasmid segregational stability assays were performed on *S. aureus* cells producing Par-GFP *in trans* to the *par* centromere-like site on a pSK1 minireplicon. *S. aureus* SK8250 cells were simultaneously electroporated (Section 2.3.4) with the pSK1 minireplicon, pSK4833

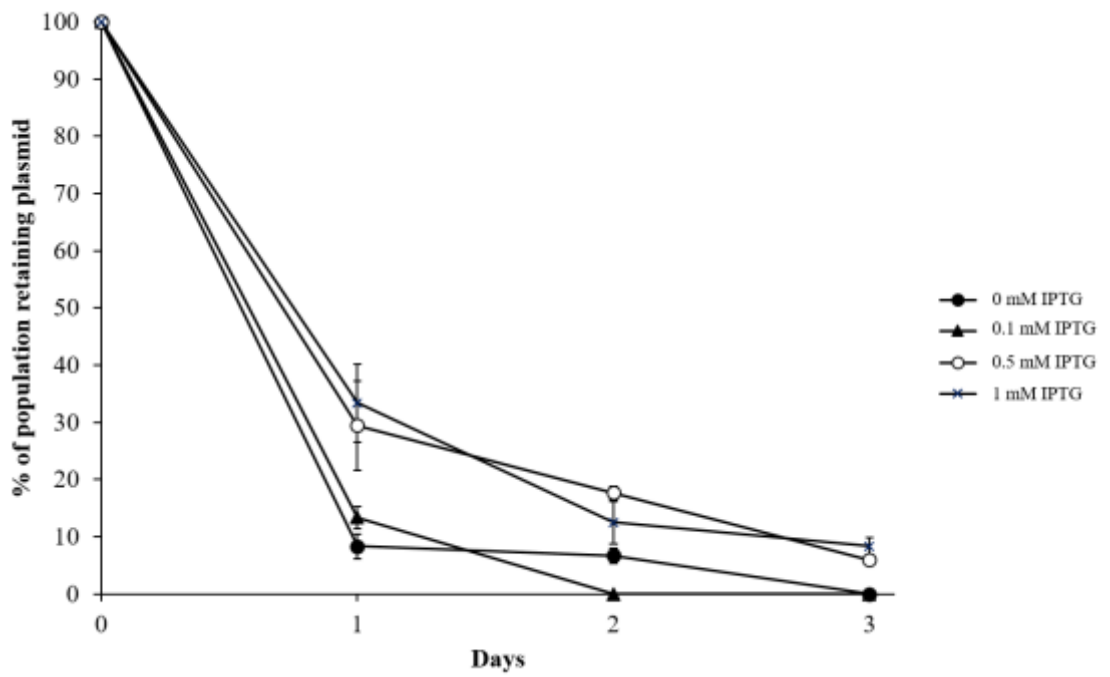
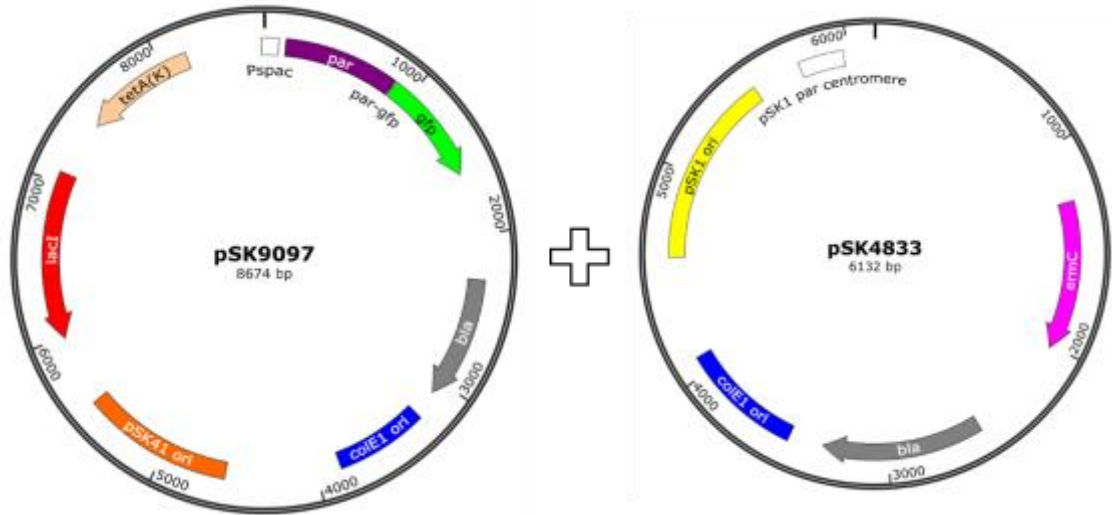
(Δpar), and the IPTG-inducible *par-gfp* expression plasmid, pSK9097 ($P_{spac}::par-gfp$) (Table 2.2), and selected for erythromycin and tetracycline resistance (Table 2.4). Stability assays were performed as described in Section 2.7, except with continuous tetracycline selection for pSK9097 ($P_{spac}::par-gfp$) and continuous IPTG induction of *par-gfp* expression with 0, 0.1, 0.5 or 1 mM IPTG. The proportion of the population retaining pSK4833 was determined using erythromycin selection, and was measured over three days, which was equivalent to approximately 50 generations. As shown in Figure 5.14A, pSK4833 was rapidly lost from the population when *par-gfp* expression was uninduced from pSK9097, with only $8\pm 2\%$ of the population carrying the plasmid after one day of the assay, and complete loss of the plasmid by the end of three days. A similar trend was observed when *par-gfp* expression was induced with 0.1 mM IPTG (Figure 5.14A). At 0.5 mM and 1 mM IPTG induction, a slightly higher proportion of the population retained pSK4833 on Day 1 ($29\pm 8\%$ and $33\pm 7\%$, respectively) and approximately 6–8% retained the plasmid at the end of the assay. These results show that Par-GFP, even when induced with maximum IPTG levels, was unable to stabilise a pSK1 minireplicon *in trans* as effectively as wild-type Par (Figure 5.8A), which suggests that Par-GFP has reduced functionality *in trans*.

To determine the effect of the supply of Par-GFP *in trans* to a pSK1 minireplicon carrying the wild-type *par* system, plasmid segregational stability assays were performed, as described above, on *S. aureus* cells harbouring pSK4829 (*par*) and pSK9097 ($P_{spac}::par-gfp$) (Table 2.2). As shown in Figure 5.14B, titration of pSK4829 with Par-GFP resulted in little effect on the segregational stability of pSK4829, at all IPTG levels tested. Because the stability assays performed on *S.*

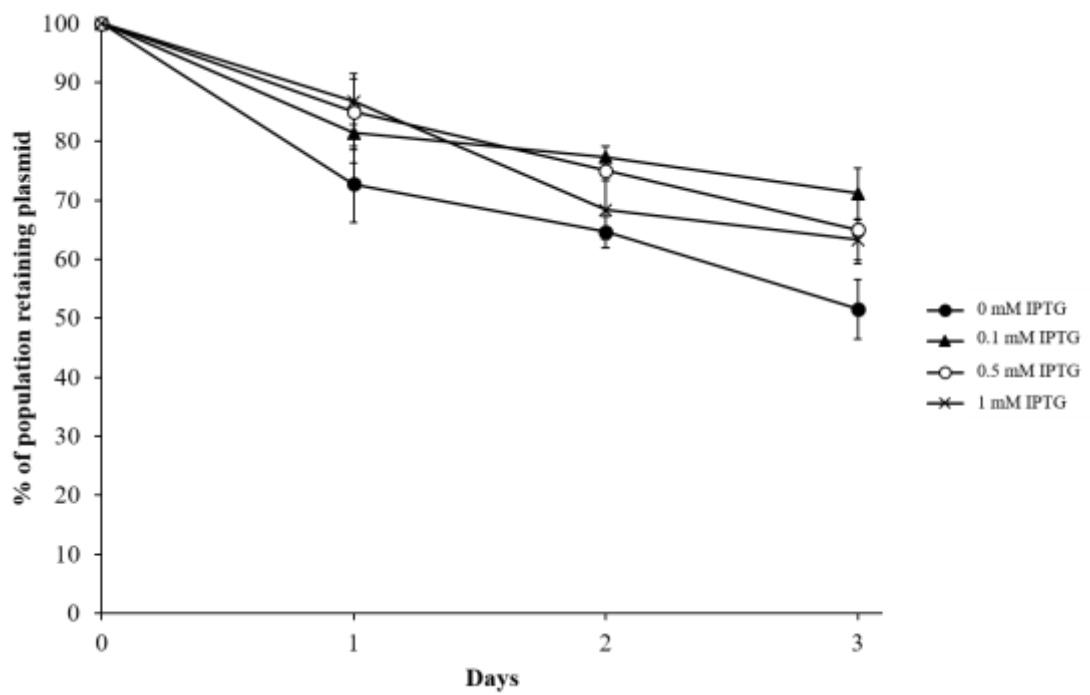
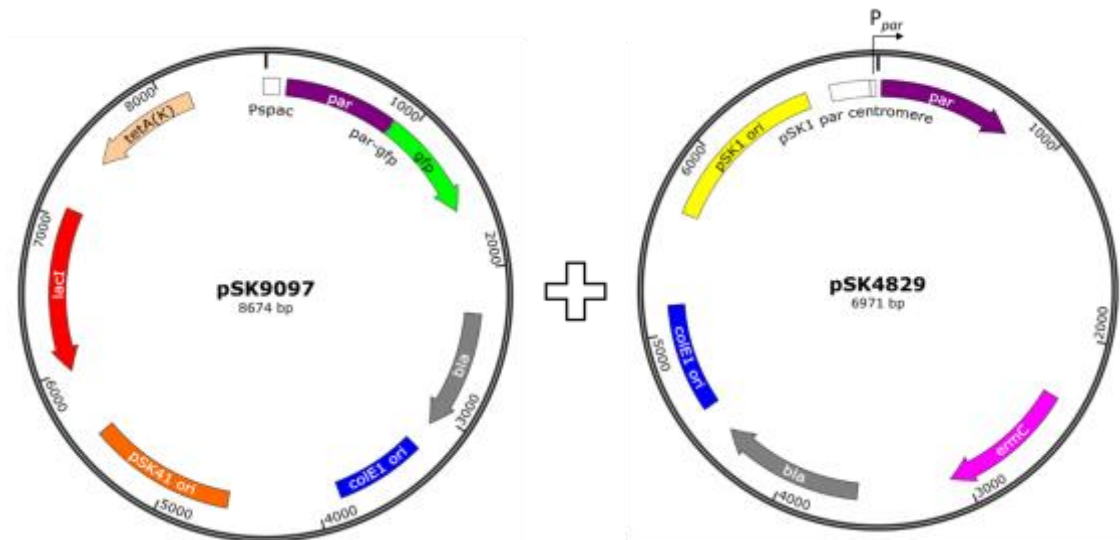
Figure 5.14 Effect of Par-GFP on plasmid segregational stability, *in trans*

Plasmid segregational stability assays of pSK1 minireplicons in the presence of Par-GFP, supplied *in trans*. The retention of pSK4833 (Δpar) (**A**) and pSK4829 (*par*) (**B**) in *S. aureus* SK8250 cells was determined as described in Section 2.7. Par-GFP was supplied *in trans* from a co-resident plasmid, pSK9097 ($P_{spac}::par-gfp$), by induction of *par-gfp* expression with 0 (●), 0.1 (▲), 0.5 (○) or 1 mM (×) IPTG. Assays were performed with continuous tetracycline selection for pSK9097. Three days of serial subculture represents approximately 50 generations. Data are normalised to 100% plasmid retention on Day 0. The averages of three independent assays are shown. Error bars represent standard error of the mean. Illustrative maps of the plasmids contained in the assayed *S. aureus* strains are shown above the graphs.

A.



B.



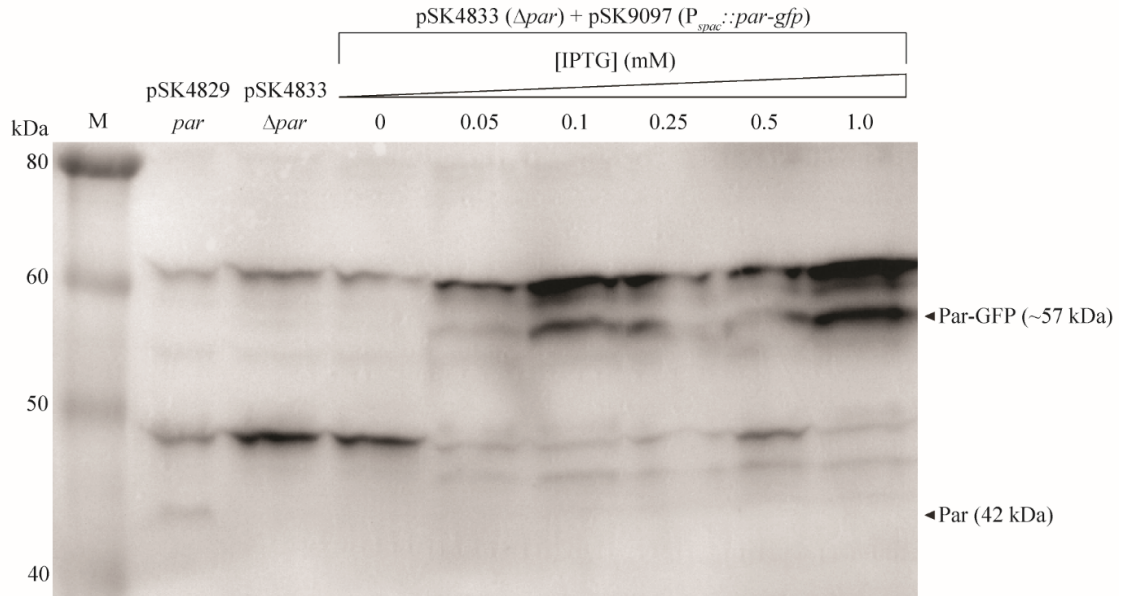
aureus cells carrying pSK4833 (Δpar) and pSK9097 indicated that Par-GFP had little functionality *in trans* (Figure 5.14A), it was expected that titration of pSK4829 with Par-GFP might negatively affect the stability of pSK4829. However, this was not the case, since stability assays did not provide any indication of an adverse interaction between Par-GFP and the *par* system on pSK4829. Therefore, because the stability of pSK4829 was unaffected by Par-GFP, potential interactions between pSK1 *par* and Par-GFP could not be assumed with any certainty.

To show that Par-GFP was indeed induced from pSK9097 ($P_{spac}::par-gfp$) during the stability assays, Western blot analyses were performed on the *S. aureus* strains assayed above. *S. aureus* SK8250 cells carrying pSK9097 and either pSK4833 (Δpar) or pSK4829 (*par*) were grown to mid-exponential phase in the presence of erythromycin and tetracycline selection, as well as 0, 0.1, 0.5 or 1 mM IPTG, which was added at the time of subculture (Section 2.1). Whole cell lysates, prepared as described in Section 2.5.8, were fractionated by SDS-PAGE (Section 2.5.6) and transferred to a PVDF membrane for Western blotting (Section 2.5.9) using anti-Par peptide antibodies (Section 2.6.3). The Western blots in Figure 5.15 show an approximately 57 kDa band corresponding to Par-GFP that is present only in lanes containing lysates from *S. aureus* cells carrying pSK9097 and treated with IPTG. An approximately 42 kDa band corresponding to Par was detected in the lysates of cells carrying pSK4829 and not pSK4833 (compare Figures 5.15A and B). For cells carrying pSK4829 as well as pSK9097, both Par and Par-GFP proteins were detected in the lysates of cells treated with IPTG (Figure 5.15B). These results confirm that IPTG induction resulted in the production of Par-GFP from pSK9097, which was supplied *in trans* to the pSK1 minireplicons, pSK4833 (Δpar) and pSK4829 (*par*).

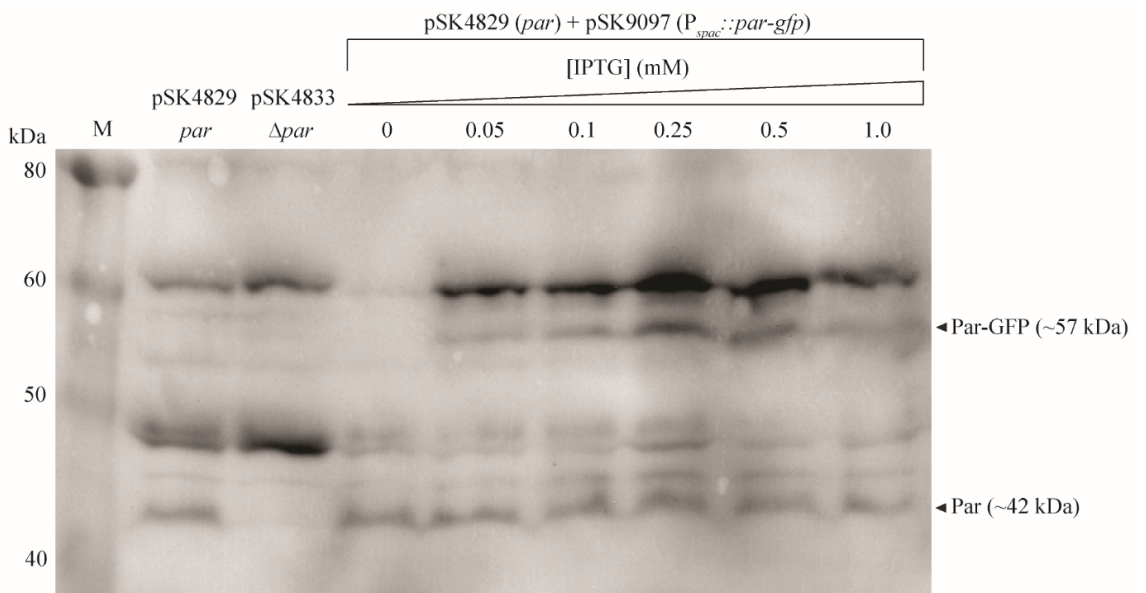
Figure 5.15 Immunodetection of Par, supplied *in trans* to pSK1 minireplicons

S. aureus SK8250 cells carrying pSK9097 ($P_{spac}::par-gfp$) and either pSK4833 (Δpar) (A) or pSK4829 (*par*) (B) were grown to mid-exponential phase with 0, 0.05, 0.1, 0.25, 0.5 or 1 mM IPTG induction of *par-gfp* expression from pSK9097 ($P_{spac}::par-gfp$) (Section 5.4.5.2). Cleared cell lysates were fractionated by SDS-PAGE (Section 2.5.6) and subjected to Western blotting (Section 2.5.9) using anti-Par peptide antibodies (Section 2.6.3). Samples were co-electrophoresed with cleared lysates from mid-exponential phase *S. aureus* SK8250 cells carrying pSK4829 (*par*) or pSK4833 (Δpar), for positive and negative controls, respectively. Lane M contains prestained protein markers, with marker sizes indicated in kDa on the left of each blot. Positions of relevant proteins and their approximate measured sizes are indicated by black arrowheads.

A.



B.



Whether Par-GFP interacted with components of the pSK1 *par* system on pSK4833 or pSK4829 remains to be shown.

5.4.5.3 Epifluorescence microscopy of Par-GFP in *S. aureus*, supplied *in trans* to Par

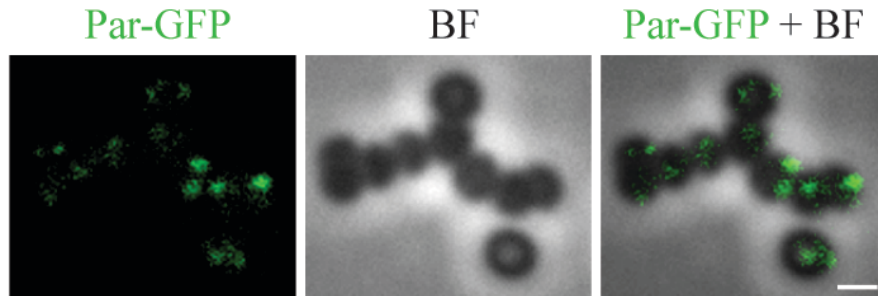
Although *in vivo* evidence of interaction between Par-GFP and components of *par* on pSK4829 is inconclusive, epifluorescence microscopy was nonetheless performed to compare the localisation pattern of Par-GFP to that of C-terminal GFP fusions to the Par DNA-binding mutant, ParK15A, and to the multimerisation mutant, Par Δ CC, in the presence of pSK1 *par* centromere DNA. In this way, the localisation patterns of ParK15A-GFP and Par Δ CC-GFP might reveal a correlation between Par activity and the formation of Par-GFP foci.

S. aureus RN4220 cells carrying the plasmid pairs pSK4829 (*par*) and pSK9097 ($P_{spac}::par-gfp$); pSK4833 (Δpar) and pSK9097 ($P_{spac}::par-gfp$); pSK7764 (*parK15A*) and pSK9102 ($P_{spac}::parK15A-gfp$); or pSK7721 (*par Δ CC*) and pSK9103 ($P_{spac}::par\Delta CC-gfp$), were grown to mid-exponential phase in the presence of antibiotic selection and 0.1 mM IPTG, and cells were prepared for live-cell epifluorescence microscopy as described in Section 2.11.2. The micrographs showed that, despite being non-functional *in trans*, Par-GFP formed foci, both in the presence (Figure 5.16A) and absence (Figures 5.16Bi–ii) of Par, that resembled those observed for Par-GFP from pSK9088 ($P_{par}::par-gfp$) (Section 5.4.4.4, Figures 5.12A–B). Similarly, foci were observed for the DNA-binding mutant, ParK15A-GFP (Figure 5.16C), which suggests that the formation of Par-GFP foci was independent of DNA-binding activity. Conversely, the multimerisation mutant,

Figure 5.16 Fluorescence localisation of Par-GFP in *S. aureus* cells, supplied *in trans* to pSK1 minireplicons

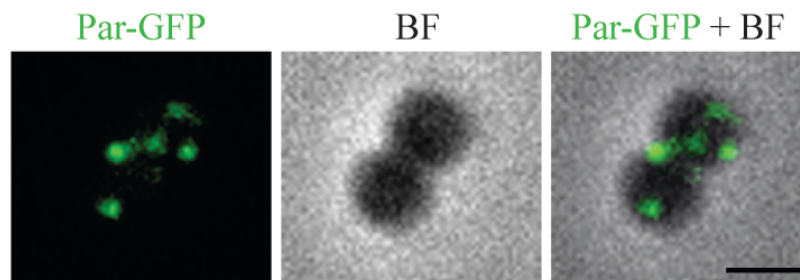
S. aureus RN4220 cells carrying pSK1 minireplicons, with and without *par* (or *par* mutants), were grown to mid-exponential phase with 0.1 mM IPTG induction of *par-gfp* (or mutant derivatives) expression from a co-resident expression plasmid (Section 5.4.5.2). **A.** Cells harbouring pSK4829 (*par*) and pSK9097 ($P_{spac}::par-gfp$). **Bi–ii.** Cells harbouring pSK4833 (Δpar) and pSK9097 ($P_{spac}::par-gfp$). Cells shown are biological replicates. **C.** Cells harbouring pSK7764 (*parK15A*) and pSK9102 ($P_{spac}::parK15A-gfp$). **D.** Cells harbouring pSK7721 (*par* ΔCC) and pSK9103 ($P_{spac}::par\Delta CC-gfp$). From left to right: Par-GFP (or mutant derivatives); bright-field (BF); overlay of bright-field (BF) and Par-GFP (or mutant derivatives). Scale bar = 1 μm .

A. *S. aureus* (*par*)

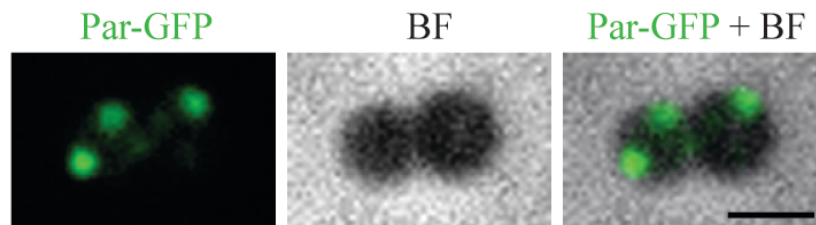


B. *S. aureus* (Δpar)

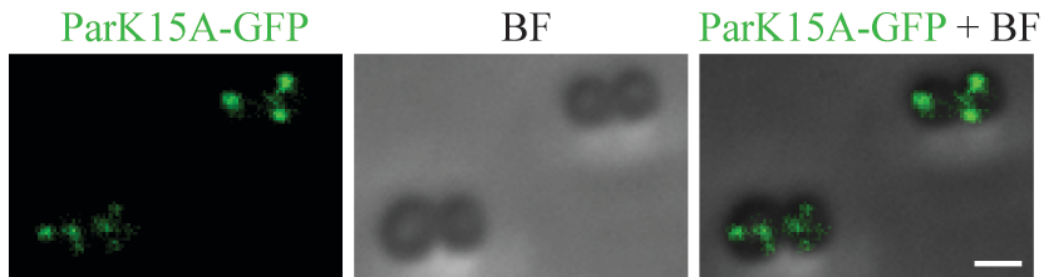
i.



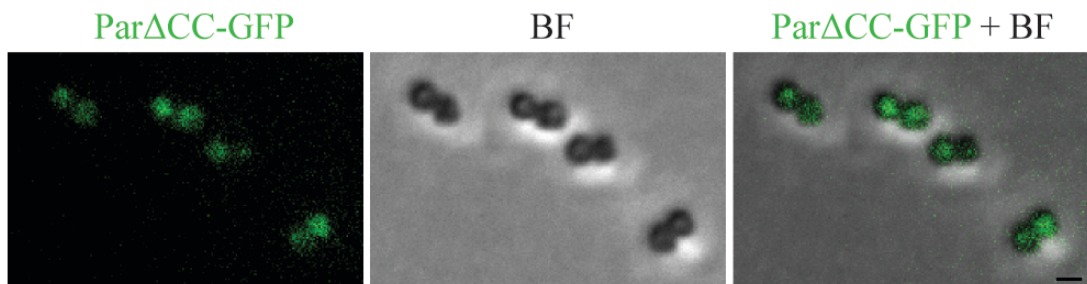
ii.



C. S. aureus (*parK15A*)



D. S. aureus (*parΔCC*)



Par Δ CC-GFP, did not form foci, but rather, exhibited diffuse fluorescence (Figure 5.16D). Taken together, the fluorescence localisation patterns exhibited by the Par-GFP mutants revealed that Par multimerisation, rather than DNA-binding activity, contributed to the formation of Par-GFP foci in *S. aureus*. The diffuse localisation of Par Δ CC-GFP also excludes the possibility that the observed foci were artefacts of GFP aggregation, which has been observed in fluorescence microscopy studies of some GFP-tagged proteins (Landgraf *et al.* 2012).

5.4.6 Epifluorescence microscopy of Par GFP fusions in *S. aureus*, in the absence of centromere DNA

Unpublished data from electron microscopy of purified RGSH₆-Par protein revealed filaments that formed in the absence of DNA and any nucleotide cofactor (Barton, D. A., Jensen, S. O. and Firth, N., unpublished data). As such, it was anticipated that filamentous Par-GFP structures might also be observed *in vivo*. However, the epifluorescence microscopy experiments performed in Sections 5.4.4.4 and 5.4.5.3 showed that Par-GFP, expressed *in cis* or *in trans* to the *par* centromere-like site, was detected only as foci, with no other structures observed. Although the appearance of Par-GFP foci was found to be independent of DNA-binding (Section 5.4.5.3), it is not inconceivable that some of the Par-GFP foci may have corresponded to the positions of pSK1 minireplicons that were bound by Par-GFP. Therefore, in order to eliminate any potential influence of the centromere-like site on Par-GFP structure formation, *par-gfp* expression was induced from the P_{spac} promoter on pSK9097 (Table 2.2), in the absence of centromere DNA, to determine whether Par-GFP might form structures other than foci.

S. aureus SK8250 cells were electroporated (Section 2.3.4) with pSK9097 ($P_{spac}::par-gfp$) and selected for tetracycline resistance (Table 2.4). Individual colonies were cultured for epifluorescence microscopy as described in Section 2.11.2, with the addition of low (0.1 mM) or high (1 mM) concentrations of IPTG to the growth media at the time of subculture. Figures 5.17Ai–ii show that induction of *par-gfp* expression with 0.1 mM IPTG resulted in the formation of Par-GFP foci, which generally localised towards the cell periphery, similar to previous observations in the presence of centromere DNA (see Figures 5.12A–B and 5.16A). No other Par-GFP localisation patterns were observed. Furthermore, when nucleoids were condensed with chloramphenicol treatment (Section 2.11.2), some Par-GFP foci appeared to be associated with the condensed nucleoids (Figure 5.17B, arrowheads), whereas others did not (Figure 5.17B, asterisks).

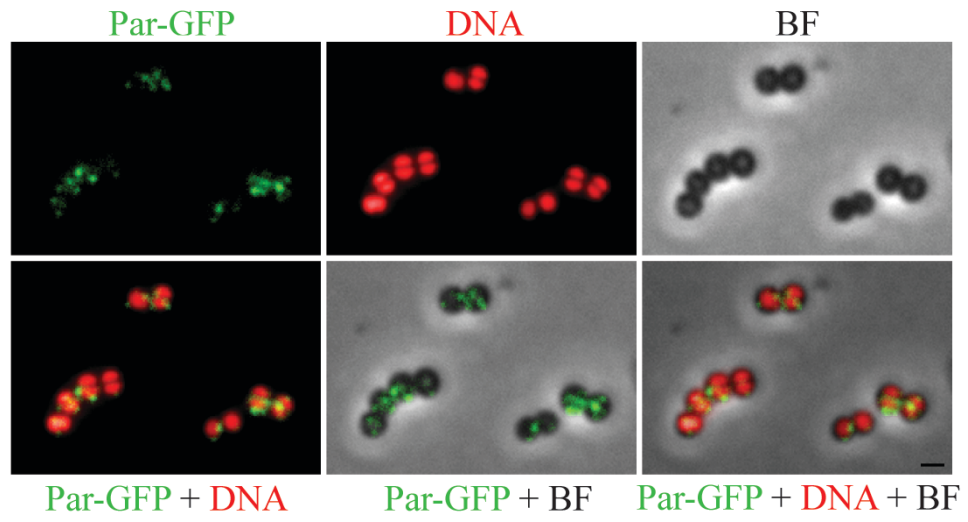
With maximum induction using 1 mM IPTG, Par-GFP formed brighter foci, and cells typically contained at least two foci (Figures 5.17Ci–iii). In addition, potential bands or arcs were visualised around the cell periphery or in the nucleoid-free space, some of which may or may not have appeared to be associated with condensed nucleoids (Figures 5.17Cii–iii, arrowheads and asterisks, respectively). It is unclear whether these patterns represent true filaments or whether they are artefacts of Par-GFP overproduction and/or bright foci that could not be resolved by the resolution limits of conventional light microscopy. Nevertheless, this localisation pattern was only observed when *par-gfp* expression was maximally induced in the absence of centromere DNA, and hence is not representative of the natural situation. However, if the observed patterns are indeed those of filamentous structures, this would hint at the potential of Par to form filaments *in vivo*, which would support the filament

Figure 5.17 Fluorescence localisation of Par-GFP in *S. aureus* cells, in the absence of pSK1 *par* centromere-like site

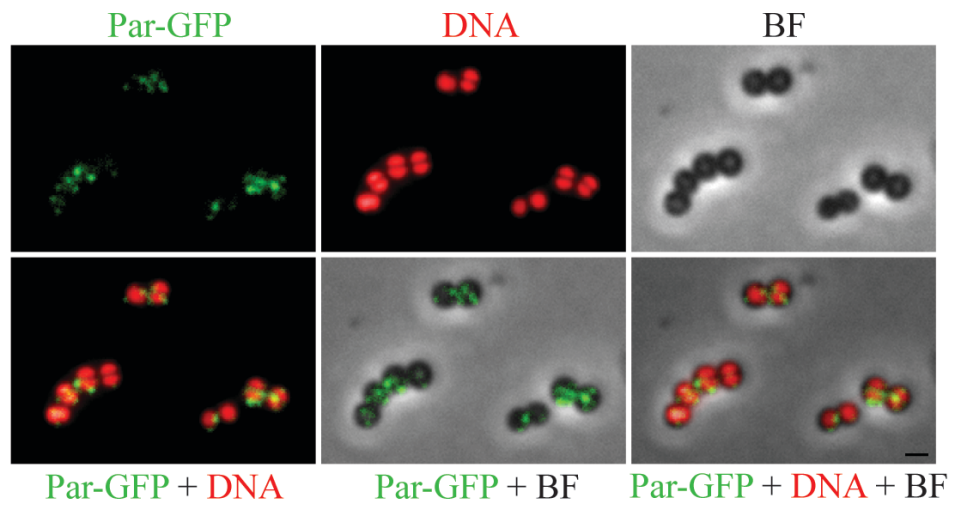
S. aureus SK8250 cells harbouring pSK9097 ($P_{spac}::par-gfp$) were grown to mid-exponential phase with IPTG induction of *par-gfp* expression (Section 5.4.6). Where applicable, nucleoids were condensed with 25 $\mu\text{g/ml}$ chloramphenicol for 1 h. Nucleoid DNA was stained with DAPI, and cells were prepared for epifluorescence microscopy as described in Section 2.11.2. **Ai–ii.** Cells producing Par-GFP induced with 0.1 mM IPTG. **B.** Cells producing Par-GFP induced with 0.1 mM IPTG, and treated with chloramphenicol. **Ci–iii.** Cells producing Par-GFP induced with 1 mM IPTG, and treated with chloramphenicol. Cells shown from each of (A) and (C) are biological replicates. From top left to bottom right: Par-GFP; DNA; bright-field (BF); overlay of Par-GFP and DNA; overlay of bright-field (BF) and Par-GFP; overlay of bright-field (BF), Par-GFP and DNA. Arrowheads indicate cells containing Par-GFP foci that appeared to associate with condensed nucleoids. Asterisks indicate cells containing Par-GFP foci that did not appear to associate with condensed nucleoids. Scale bar = 1 μm .

A. *S. aureus* (*par-gfp*) + 0.1 mM IPTG

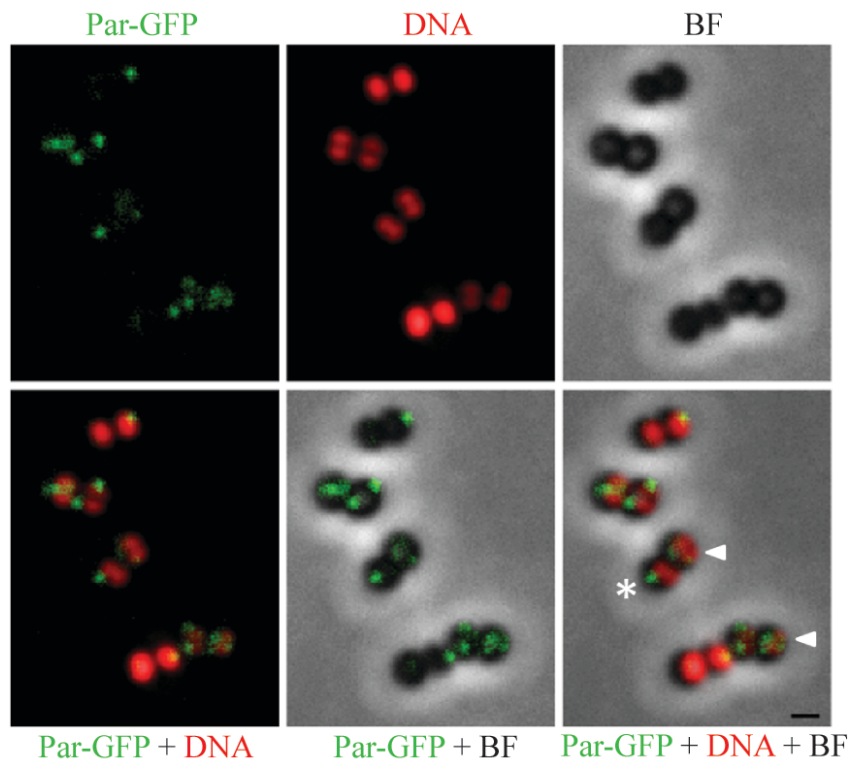
i.



ii.

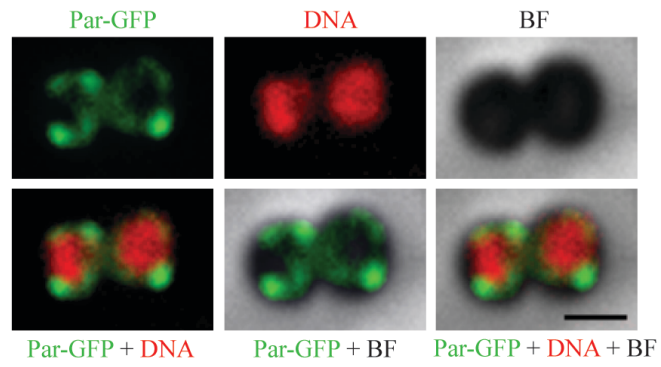


B. *S. aureus* (*par-gfp*) + 0.1 mM IPTG + Cm25

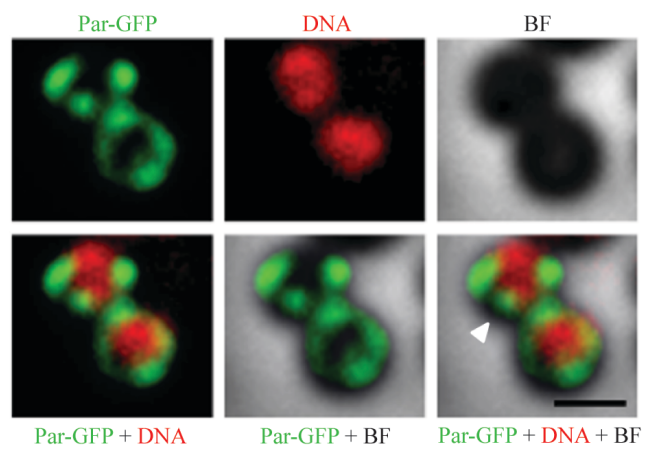


C. S. aureus (*par-gfp*) + 1 mM IPTG + Cm25

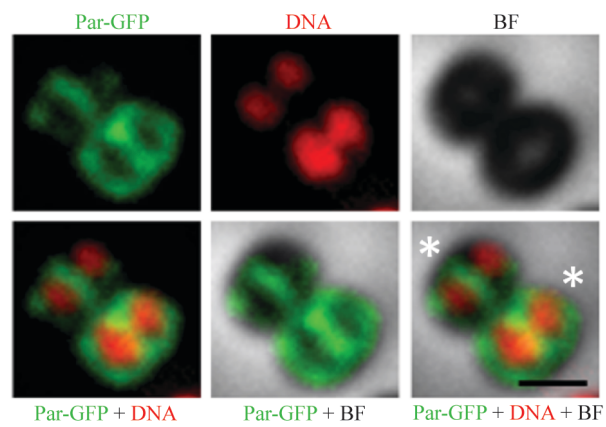
i.



ii.



iii.



formation observed *in vitro* by electron microscopy (Barton, D. A., Jensen, S. O. and Firth, N., unpublished data). At the least, these observations confirm the conclusions drawn from Section 5.4.5.3, that the formation of foci by Par-GFP is independent of centromere DNA and DNA-binding activity, and is most likely the result of Par multimerisation.

5.4.7 Distribution of Par-GFP focus numbers in *S. aureus*

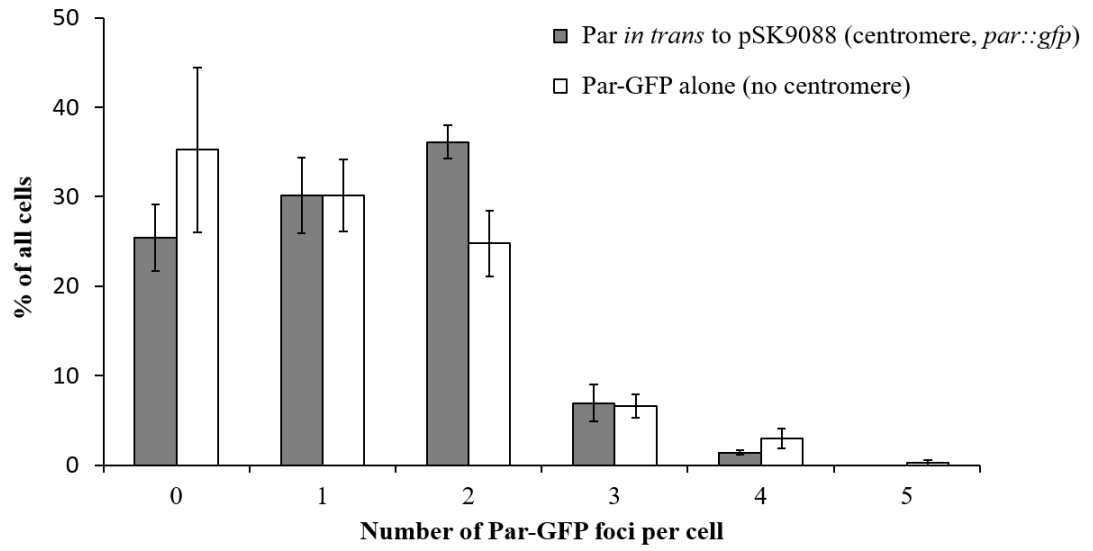
Because Par-GFP was found to produce foci irrespective of the functionality of the system or the presence of Par or centromere DNA (Sections 5.4.4.4, 5.4.5.3 and 5.4.6), the number of Par-GFP foci per cell was counted to determine whether there were differences in the distribution of focus numbers between cells containing Par-GFP in a functional plasmid stability system (pSK9088+pSK9104, Section 5.4.4) and cells producing Par-GFP in isolation (pSK9097, Section 5.4.6).

Fluorescence micrographs were obtained of *S. aureus* SK8250 cells carrying pSK9088 ($P_{par}::par-gfp$) and pSK9104 ($P_{spac}::par$) and producing Par *in trans* to *par-gfp* on pSK9088 (Section 5.4.4.4), and of *S. aureus* SK8250 cells carrying pSK9097 ($P_{spac}::par-gfp$) and producing Par-GFP in the absence of centromere DNA (Section 5.4.6). The number of Par-GFP foci present in each cell was counted using ImageJ software as described in Section 2.11.2, and the distribution of focus numbers per cell is presented in Figures 5.18A–B. Approximately $25\pm 4\%$ of cells carrying pSK9088 with 1 mM IPTG induction of Par from pSK9104 contained no Par-GFP focus (Figure 5.18A), possibly due to loss of the pSK9088 plasmid, even though antibiotic selection was applied. Another $30\pm 4\%$ of the population contained one focus, while $36\pm 2\%$ of cells contained two Par-GFP foci (Figure 5.18A). When

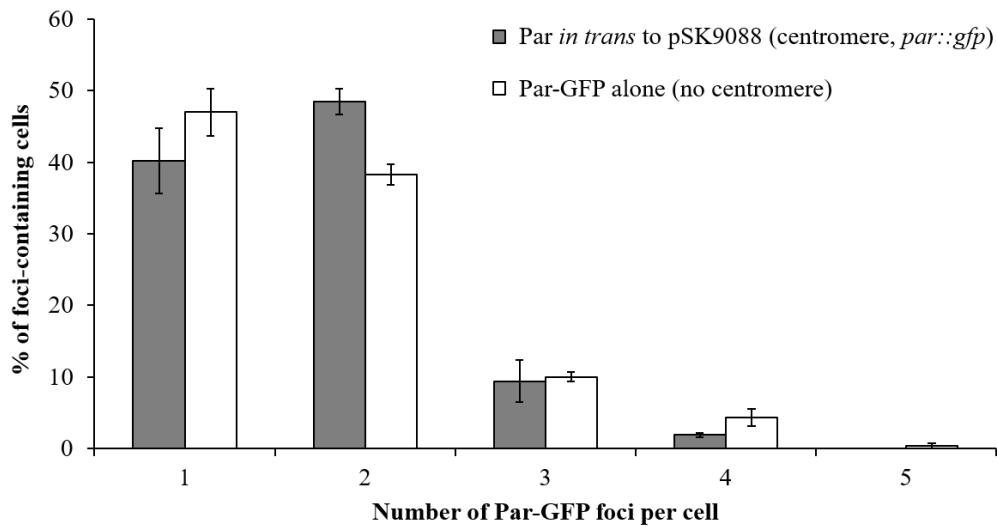
Figure 5.18 Distribution of the number of fluorescent Par-GFP foci per cell

The number of fluorescent Par-GFP foci per cell, detected by epifluorescence microscopy, was determined for *S. aureus* SK8250 cells producing Par-GFP. Grey bars represent *S. aureus* cells harbouring pSK9088 ($P_{par}::par-gfp$) and pSK9104 ($P_{spac}::par$), with 1 mM IPTG induction of *par* expression from pSK9104 (Section 5.4.4.4). Par was supplied *in trans* to *par-gfp* on pSK9088 (total number of cells = 462). White bars represent *S. aureus* cells harbouring pSK9097 ($P_{spac}::par-gfp$) with 0.1 mM IPTG induction of *par-gfp* expression from pSK9097 (total number of cells = 473) (Section 5.4.6). **A.** Histogram plotting the percentage of all cells against the number of Par-GFP foci per cell. **B.** Histogram plotting the percentage of foci-containing cells against the number of fluorescent Par-GFP foci per cell. The averages of three independent microscopy experiments are shown. Error bars represent standard error of the mean.

A.



B.



only foci-containing cells were considered, the proportion of cells that contained one Par-GFP focus was approximately $40\pm 5\%$, and approximately $48\pm 2\%$ for foci-containing cells with two foci (Figure 5.18B).

For cells that produced Par-GFP alone (from pSK9097), it appeared that the only notable difference from cells that produced Par *in trans* to *par-gfp* on pSK9088, was the proportion of cells that contained two Par-GFP foci. In the absence of centromere DNA on pSK9097, only $25\pm 4\%$ of cells had two Par-GFP foci (Figure 5.18A), which represented approximately $38\pm 1\%$ of foci-containing cells (Figure 5.18B). This suggests that, compared to cells producing Par-GFP alone, the presence of Par and the centromere-like site in a functional *par-gfp* partitioning system increased the proportion of cells containing two Par-GFP foci. It is anticipated that in cells containing pSK9088 and pSK9104, at least some of the Par-GFP foci might have corresponded to Par-GFP bound to plasmid DNA. The correlation between the number of Par-GFP foci and the number of plasmid foci per cell is examined in Section 5.8.5 below.

5.5. Immunofluorescence microscopy of Par in *E. coli*

Due to background signals and non-specific immunodetection of Par in *S. aureus* by IFM (Section 5.3.1), a heterologous host was considered for the visualisation of structures formed *in vivo* by non-tagged Par molecules. *E. coli* was chosen as an alternative host for the production of Par and Par-GFP, since the available pSK1 minireplicons encoding Par or Par-GFP (Table 2.2) contain the high copy-number pUC18 ColE1 origin of replication that facilitates plasmid replication in *E. coli* (Yanisch-Perron *et al.* 1985). Even though Par is non-functional in *E. coli* (Davies,

D. and Firth, N., unpublished data), the high copy-number of these pSK1 minireplicons in *E. coli* suggests that Par should be readily detected by IFM when expressed from these plasmids.

IFM was performed on mid-exponential phase *E. coli* DH5 α cells carrying pSK4829 (*par*) or pSK4833 (Δ *par*) (Table 2.2), as described in Section 2.11.1, using a 1:10,000 dilution of anti-Par peptide antibodies and a 1:5,000 dilution of Alexa Fluor 488-conjugated goat anti-rabbit IgG antibodies. Unlike IFM performed in *S. aureus* cells (Section 5.3.1), Par was readily detected in *E. coli*, as shown by the micrographs in Figures 5.19Ai-ii. Par was detected as foci that were localised towards the cell periphery, with some bands observed between foci, either along the perimeter of the cell or transversing the width of the cell (Figures 5.19Ai-ii). No fluorescence localisation patterns were observed in *E. coli* cells carrying pSK4833 (Δ *par*) (Figure 5.19B), which suggests that the fluorescence patterns observed from IFM of Par in *E. coli* cells carrying pSK4829 were specific to Par localisation.

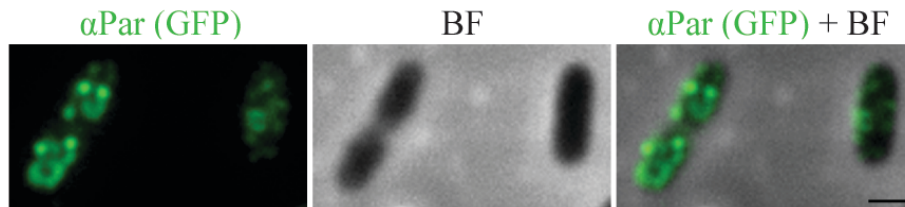
The relatively strong level of fluorescence exhibited by IFM of Par in *E. coli* enabled optical sections to be obtained along the z-axis of cells. In this way, a more complete image of 3-dimensional fluorescence structures could be obtained following deconvolution of image stacks. Fluorescence micrographs of *E. coli* cells producing Par from pSK4829, prepared as described above, were taken at eight 240 nm intervals along the z-axis of the cells, and images were deconvolved as maximum intensity projections using Zen software (Section 2.11.1). Deconvolved image stacks revealed transverse bands between Par foci that resembled possible helices or spirals

Figure 5.19 Immunofluorescence microscopy of Par in *E. coli* cells

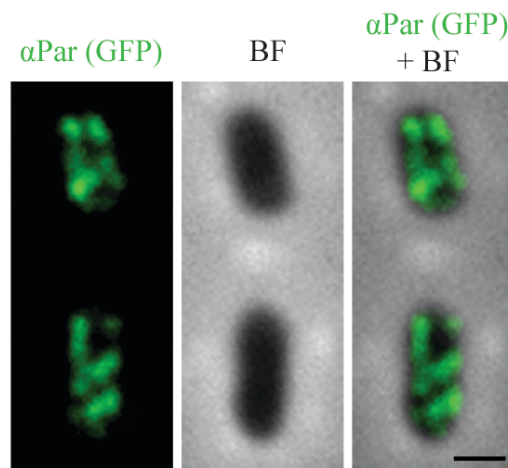
Mid-exponential phase *E. coli* DH5 α cells harbouring pSK4829 (*par*) (**Ai–ii**) or pSK4833 (Δ *par*) (**B**) were prepared for immunofluorescence microscopy (IFM) using anti-Par peptide antibodies and goat anti-rabbit IgG Alexa Fluor 488-conjugated antibodies, as described in Section 5.5. Cells shown in (A) are biological replicates. From left to right: Par; bright-field (BF); overlay of bright-field (BF) and Par. Scale bar = 1 μ m

A. *E. coli* (*par*)

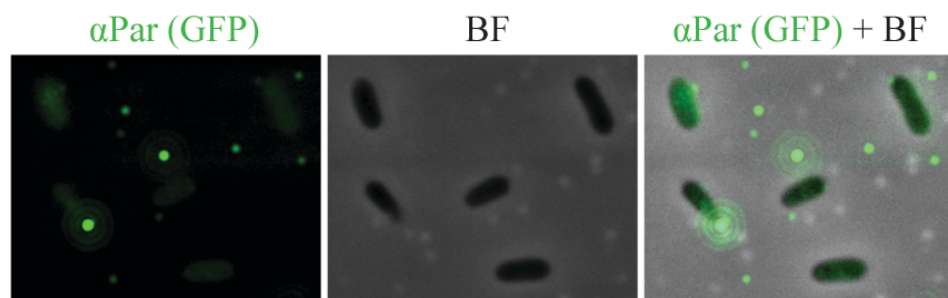
i.



ii.



B. *E. coli* (Δ *par*)



(Figures 5.20A–C), which suggests that, in *E. coli*, Par may be able to multimerise into filamentous structures.

5.6. Live cell epifluorescence microscopy of fluorescently-tagged Par in *E. coli*

In order to determine the localisation pattern of Par in live *E. coli* cells, epifluorescence microscopy was performed on cells producing Par protein fusions to GFP. *E. coli* DH5 α cells were transformed with pSK9087 or pSK9088 (Table 2.2) (Section 2.3.2), which, as described in Section 5.4.1, are pSK1 minireplicons that contain the pSK1 *par* system encoding GFP-Par and Par-GFP, respectively, instead of Par. Cells were cultured to mid-exponential phase and prepared for epifluorescence microscopy according to the methods in Section 2.11.2.

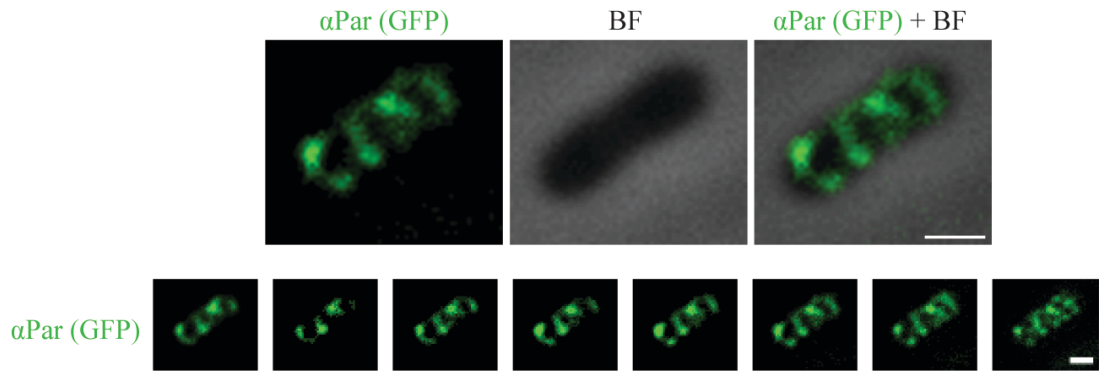
As shown in Figures 5.21Ai–ii, GFP-Par, when produced in *E. coli* cells carrying pSK9087, were visualised as fluorescent foci dispersed around the cell periphery, with potential arcs observed at some cell poles. Par-GFP, however, when expressed from pSK9088, showed a different localisation pattern, with foci generally located at mid-cell or polar positions (Figures 5.21Bi–ii). In filamentous *E. coli* cells, Par-GFP appeared at regular intervals along the cell filament, possibly at points marking the cell septa (Figure 5.21C).

Remarkably, when cells were treated with 300 μ g/ml chloramphenicol in order to condense nucleoid DNA (Section 2.11.2), a clear correlation was observed between the localisation of both N- and C- terminal Par GFP fusions and the condensed nucleoids (Figures 5.22A–B). For GFP-Par, each condensed nucleoid was typically

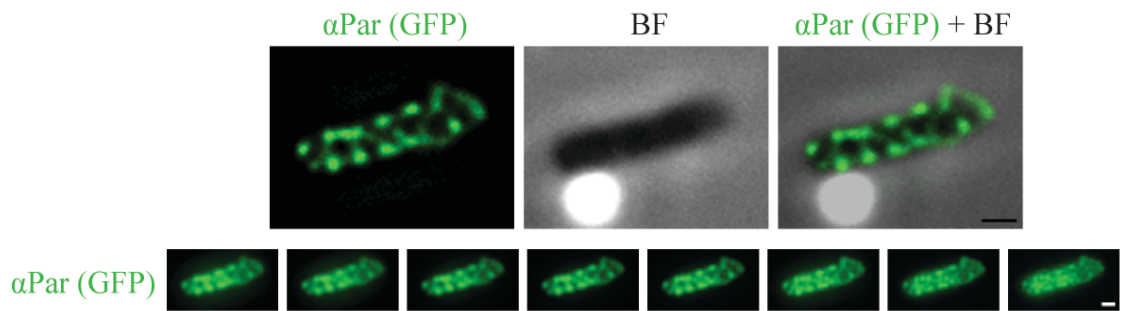
Figure 5.20 Deconvolved immunofluorescence microscopy images of Par in *E. coli* cells

A–C. Mid-exponential phase *E. coli* DH5 α cells harbouring pSK4829 (*par*) were prepared for immunofluorescence microscopy (IFM) using anti-Par peptide antibodies and goat anti-rabbit IgG Alexa Fluor 488-conjugated antibodies, as described in Section 5.5. Fluorescence images were taken in 240 nm intervals along the z-axis of cells, and image stacks were deconvolved as maximum intensity projections (Section 2.11.1). Top left to top right: deconvolved IFM image of Par; bright-field (BF); overlay of bright-field (BF) and deconvolved image of Par. Bottom: unprocessed fluorescence microscopy sections taken from low to high positions in the z-axis of cells. Scale bar = 1 μ m.

A. *E. coli* (*par*)



B.



C.

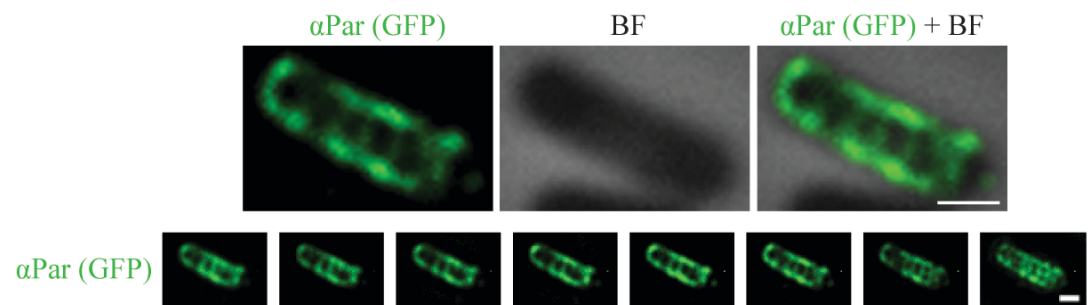
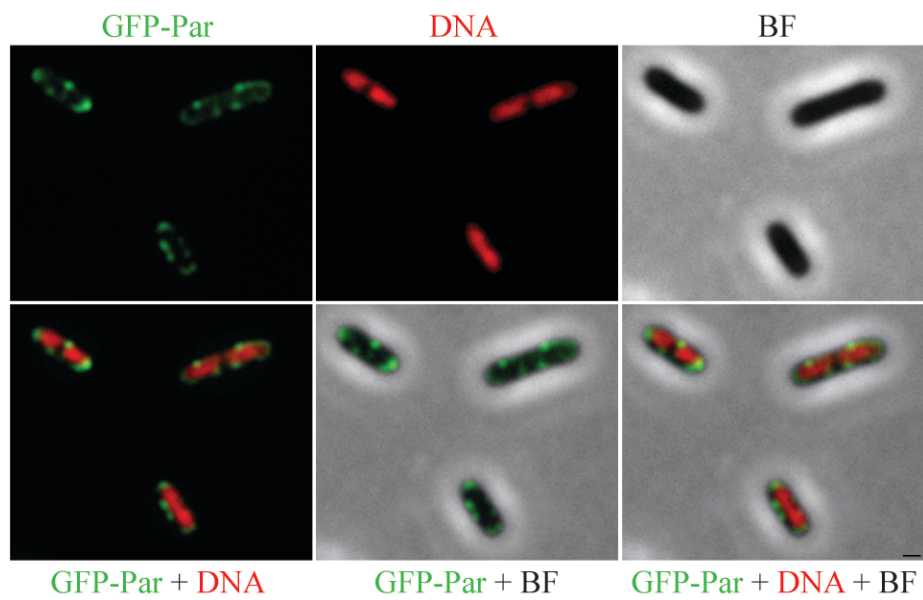


Figure 5.21 Fluorescence localisation of Par GFP fusion proteins in *E. coli* cells

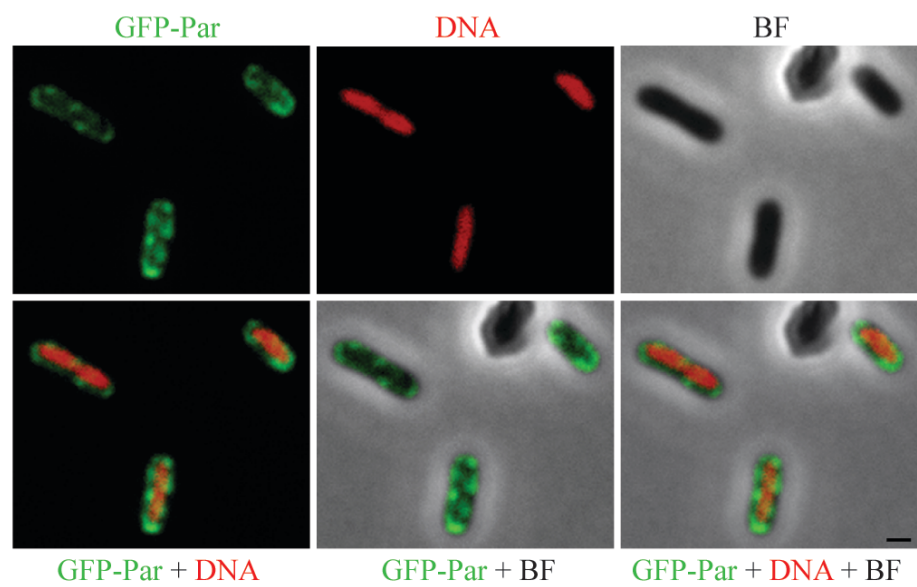
The localisation of GFP-Par (**Ai-ii**) and Par-GFP (**Bi-ii**) was visualised by epifluorescence microscopy of mid-exponential phase *E. coli* cells harbouring pSK9087 ($P_{par}::gfp-par$) or pSK9088 ($P_{par}::par-gfp$), respectively (Section 2.11.2). **C.** Filamentous *E. coli* cell producing Par-GFP, encoded by pSK9088. Nucleoid DNA was stained with DAPI, and cells were prepared for epifluorescence microscopy as described in Section 2.11.2. Cells in each of (A) and (B) are biological replicates. From top left to bottom right: Par GFP fusion proteins; DNA; bright-field (BF); overlay of Par GFP fusion proteins and DNA; overlay of bright-field (BF) and Par GFP fusion proteins; overlay of bright-field (BF), Par GFP fusion proteins and DNA. Scale bar = 1 μm .

A. *E. coli* (*gfp-par*)

i.

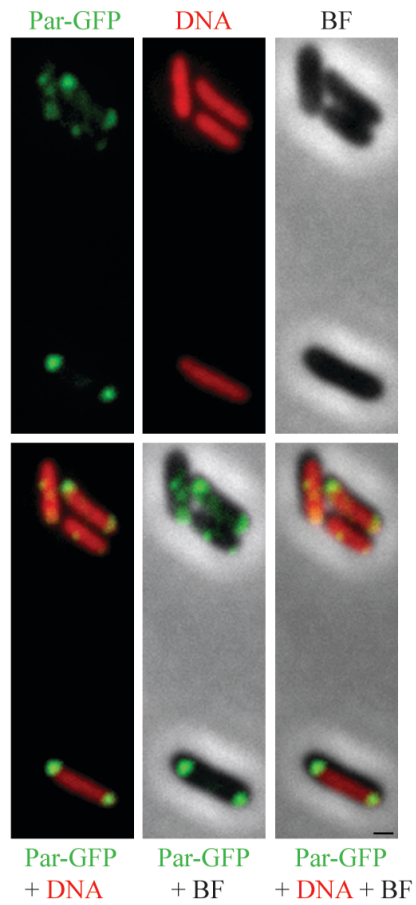


ii.

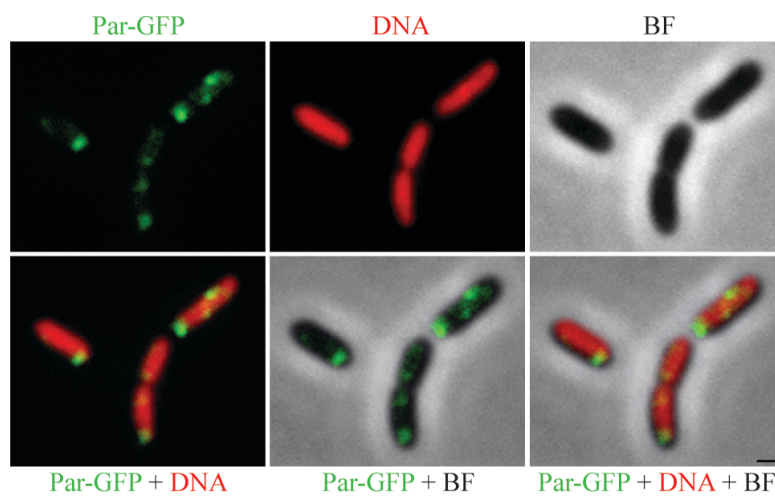


B. *E. coli* (*par-gfp*)

i.



ii.



C. Filamentous *E. coli* (*par-gfp*)

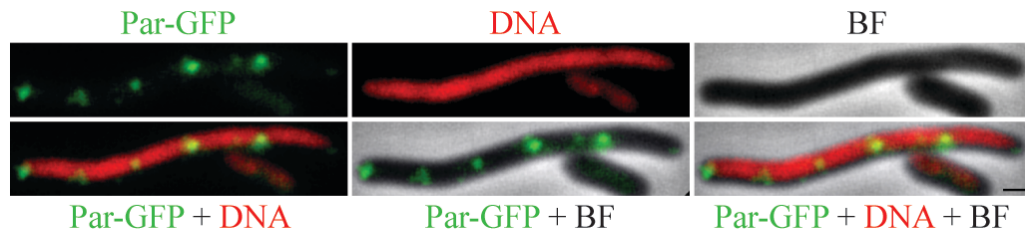
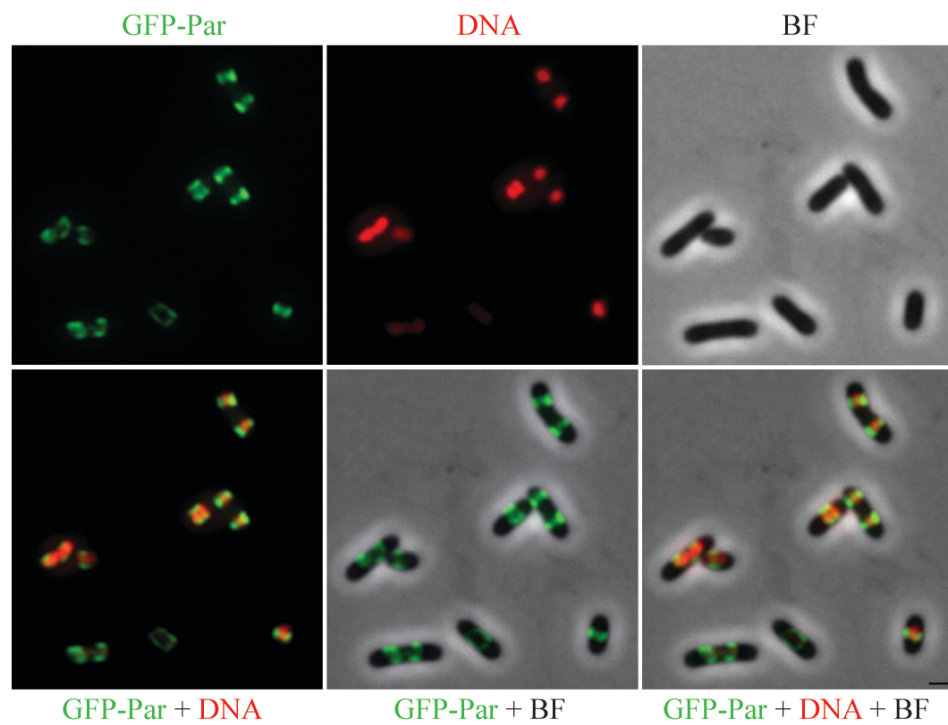


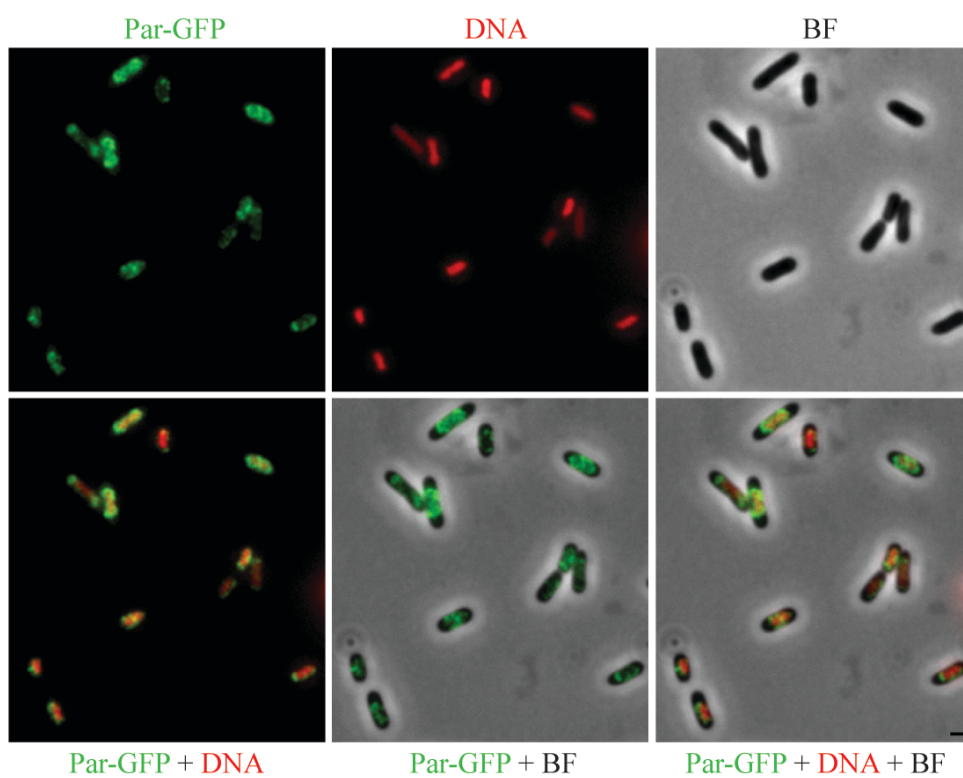
Figure 5.22 Effect of nucleoid condensation on the fluorescence localisation of Par GFP fusion proteins in *E. coli* cells

The localisation of GFP-Par (**A**) and Par-GFP (**B**) was visualised by epifluorescence microscopy of *E. coli* cells harbouring pSK9087 ($P_{par}::gfp-par$) or pSK9088 ($P_{par}::par-gfp$), respectively (Section 2.11.2). Cells were grown to mid-exponential phase and then treated with 300 $\mu\text{g/ml}$ chloramphenicol for 1.5 h to condense nucleoids (Section 2.11.2). Nucleoid DNA was stained with DAPI, and cells were prepared for epifluorescence microscopy as described in Section 2.11.2. From top left to bottom right: Par GFP fusion proteins; DNA; bright-field (BF); overlay of Par GFP fusion proteins and DNA; overlay of bright-field (BF) and Par GFP fusion proteins; overlay of bright-field (BF), Par GFP fusion proteins and DNA. Scale bar = 1 μm .

A. *E. coli* (*gfp-par*) + Cm300



B. *E. coli* (*par-gfp*) + Cm300



associated with two fluorescent GFP-Par foci, with foci located opposite each other across the width of the cell (Figure 5.22A). However, the localisation pattern of Par-GFP upon nucleoid condensation appeared to be less well-defined (Figure 5.22B). Nonetheless, there remained a clear association of Par-GFP with nucleoid DNA, since Par-GFP generally occupied the same space as the condensed nucleoids (Figure 5.22B). The observations from the nucleoid condensation treatments, therefore, suggest that GFP-Par and Par-GFP interact, either directly or indirectly, with *E. coli* chromosomal DNA.

5.6.1 Fluorescence localisation of GFP-Par mutants in *E. coli*

Because the localisation pattern displayed by GFP-Par in live *E. coli* cells more closely resembled the patterns observed from IFM of Par in *E. coli* (compare Figures 5.21A and 5.19–5.20), the fluorescence localisation of GFP-Par was interpreted as being more representative of the structures that might be formed by Par *in vivo*. For this reason, the N-terminal GFP Par fusion protein was used for subsequent live cell microscopy studies. The apparent association between GFP-Par and nucleoid DNA was intriguing (Section 5.6), and was further explored in order to determine the contribution of DNA-binding activity to this observed behaviour. To this end, an N-terminal GFP fusion to the Par DNA-binding mutant, ParK15A, was constructed as described in Section 5.4.1, except using pSK7764 template DNA (Table 2.2) for the PCR-amplification (Section 2.4.4) of the ParK15A coding region. The pSK1 minireplicon expressing *gfp-parK15A* from the P_{par} promoter was named pSK9166 (Table 2.2).

E. coli DH5 α cells were transformed (Section 2.3.2) with pSK9166 (*gfp-parK15A*) (Table 2.2) and the fluorescence localisation of GFP-ParK15A in *E. coli* was determined by epifluorescence microscopy as described in Section 2.11.2. Fluorescence micrographs of GFP-ParK15A, shown in Figure 5.23A, revealed similar localisation patterns to GFP-Par in *E. coli* (see Figures 5.21Ai–ii), with foci and patches of GFP-ParK15A observed around the periphery of the cells. This suggests that the formation of foci is independent of DNA-binding activity, a conclusion also drawn for Par-GFP foci in *S. aureus* (Section 5.4.5.3 and Section 5.4.6). However, in contrast to GFP-Par, condensation of nucleoids with chloramphenicol (Section 2.11.2) revealed that the DNA-binding mutant derivative, GFP-ParK15A, did not associate with condensed nucleoids, and instead remained as foci at the cell periphery (Figure 5.23B). Taken together, these results suggest that the DNA-binding of Par, either to *E. coli* chromosomal DNA or to centromere (plasmid) DNA, is required for its potential association with the nucleoid.

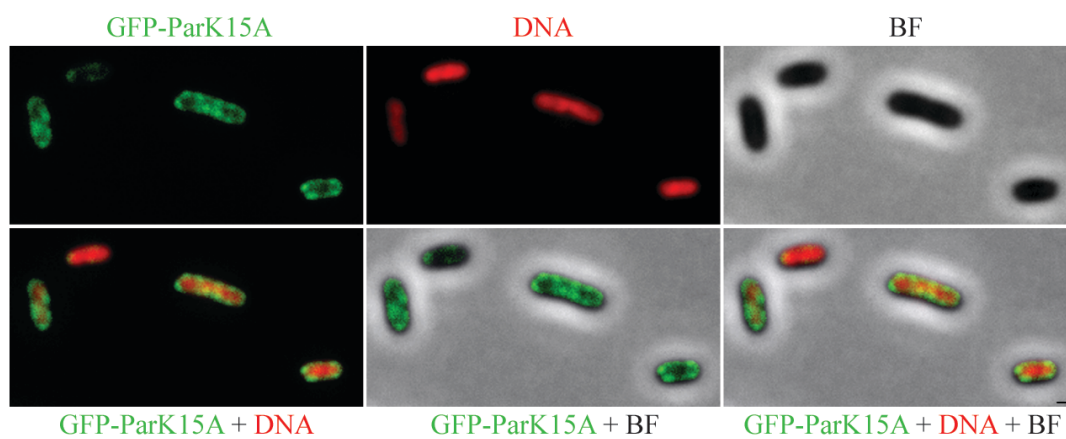
5.6.2. Construction of an IPTG-inducible *gfp-par* expression plasmid

In order to determine whether the apparent association of GFP-Par with the *E. coli* nucleoid is dependent on binding to the pSK1 *par* centromere-like site or to *E. coli* chromosomal DNA, GFP-Par was produced in the absence of centromere DNA. Regulated expression of *gfp-par* was facilitated by the IPTG-inducible P_{tac} promoter and *lac* operator element on the high copy-number *E. coli* expression plasmid, pTTQ18RGSH₆ (Table 2.2). pTTQ18RGSH₆ also encodes the Lac repressor, which controls the $P_{tac}/lacO$ promoter-operator element to regulate gene expression. A 1.5 kb DNA fragment encoding GFP-Par was PCR-amplified (Section 2.4.4) from

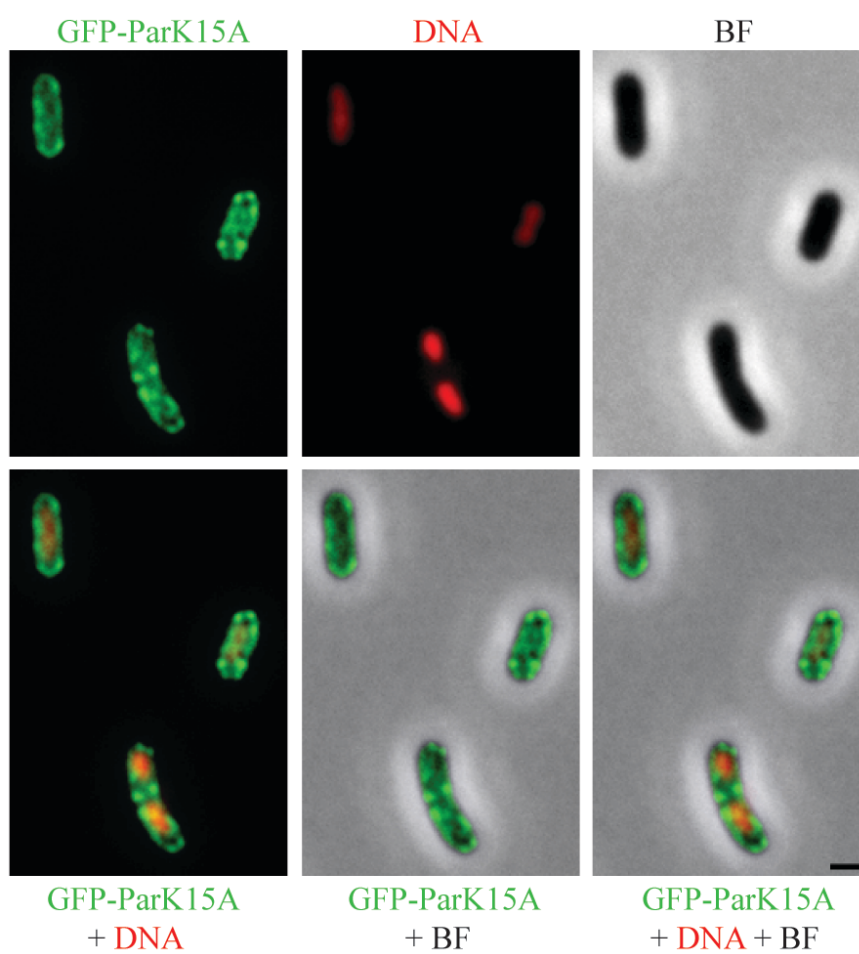
Figure 5.23 Fluorescence localisation of GFP-ParK15A in *E. coli* cells

A–B. Epifluorescence microscopy was performed on mid-exponential phase *E. coli* cells harbouring pSK9166 (*gfp-parK15A*) and producing GFP-ParK15A (Section 2.11.2). In (B), mid-exponential phase cultures were treated with 300 µg/ml chloramphenicol for 1.5 h to condense nucleoids (Section 2.11.2). Nucleoid DNA was stained with DAPI, and cells were prepared for epifluorescence microscopy as described in Section 2.11.2. From top left to bottom right: GFP-ParK15A; DNA; bright-field (BF); overlay of GFP-ParK15A and DNA; overlay of bright-field (BF) and GFP-ParK15A; overlay of bright-field (BF), GFP-ParK15A and DNA. Scale bar = 1 µm.

A. *E. coli* (*gfp-parK15A*)



B. *E. coli* (*gfp-parK15A*) + Cm300



pSK9087 template DNA (Table 2.2) using primers HC17 and HC21 (Table 2.6). HC21 contains a stop codon to prevent fusion of the vector-encoded RGS_{H6} tag to the C-terminal end of GFP-Par. The PCR product was subsequently electrophoresed on an agarose gel (Section 2.4.3) and gel-purified (Section 2.4.7), prior to restriction endonuclease digestion of the 3' end with *Hind*III (Section 2.4.6). The pTTQ18RGS_{H6} vector was concurrently digested with *Hind*III and the blunt-end cutter, *Sma*I (Section 2.4.6), and then dephosphorylated with Antarctic phosphatase (Section 2.4.10). In order to facilitate the blunt-end ligation of the 5' end of *gfp-par* with pTTQ18RGS_{H6}, the *Hind*III-restricted amplicon was treated with T4 PNK (Section 2.4.9) to phosphorylate the undigested end of *gfp*, which contained the sequence of the HC17 oligonucleotide. Ligation of *gfp-par* to the restricted and dephosphorylated *Sma*I and *Hind*III sites of pTTQ18RGS_{H6} proceeded as described in Section 2.4.11, after which the reactions were used to transform chemically-competent *E. coli* DH5 α cells to ampicillin resistance (Section 2.3.2). Plasmid DNA was isolated (Section 2.4.1) from selected transformants and recombinants were screened by restriction digestion with *Eco*RI and *Hind*III (Section 2.4.6). Restricted plasmid DNA was fractionated by agarose gel electrophoresis (Section 2.4.3), and plasmids displaying the expected restriction profile of recombinants were sequenced using primers HC2, HC11, HC17 and HC20 (Table 2.6). The pTTQ18RGS_{H6} plasmid containing the correct sequence of *gfp-par* was named pSK9178 (Table 2.2).

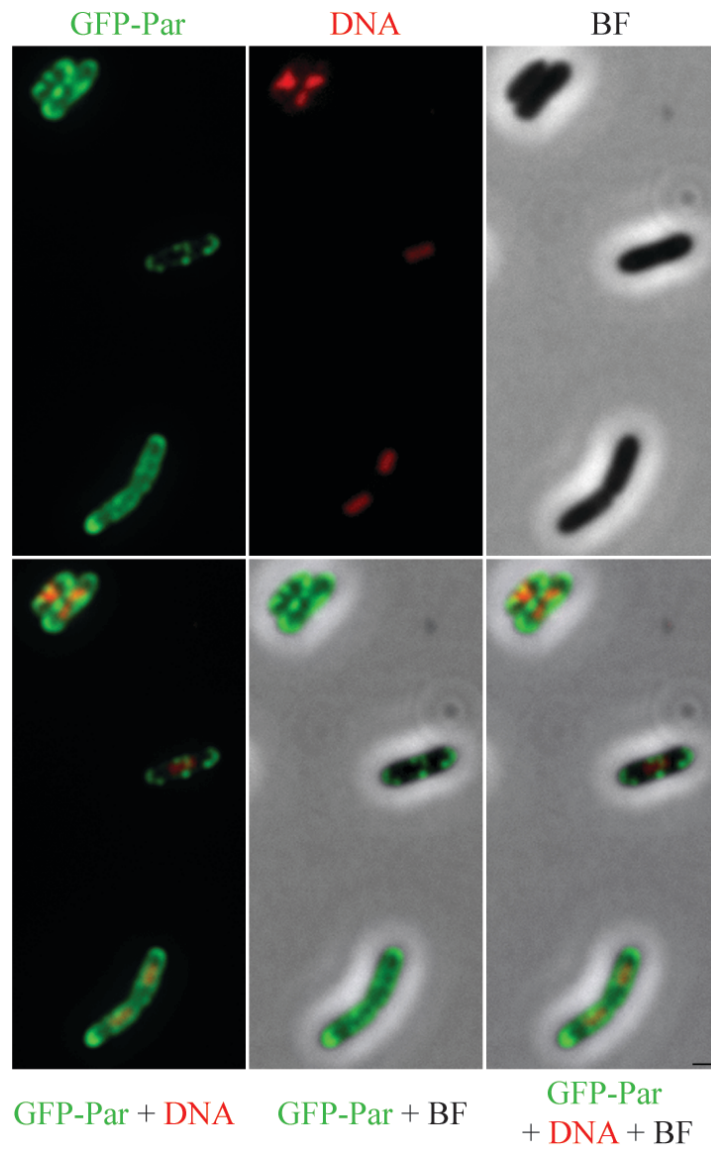
5.6.3. Fluorescence localisation of GFP-Par in *E. coli*, in the absence of centromere DNA

The contribution of the pSK1 *par* centromere-like site to the apparent association between GFP-Par and *E. coli* nucleoid DNA was assessed by performing epifluorescence microscopy of live *E. coli* cells producing GFP-Par in the absence of centromere DNA. Cells carrying pSK9178 ($P_{tac}::gfp-par$) (Table 2.2) were grown to mid-exponential phase in the presence of 0.1 mM IPTG, and then treated with chloramphenicol as described in Section 2.11.2 to condense nucleoids. Subsequent epifluorescence microscopy showed that GFP-Par, when produced in isolation in *E. coli*, formed fluorescent foci that were located around the periphery of the cell, as well as potential arcs at some cell poles (Figure 5.24). This was similar to the fluorescence localisation pattern of GFP-Par produced from pSK9087 (Table 2.2) in the presence of the pSK1 *par* centromere-like site (see Figures 5.21Ai–ii). Notably, in the absence of centromere DNA, GFP-Par did not associate with condensed nucleoids (Figure 5.24). This observation is consistent with those from epifluorescence microscopy of GFP-ParK15A, which also showed an apparent loss of association between the DNA-binding mutant and nucleoid DNA (see Figure 5.23B). These results, therefore, imply that the observed association of GFP-Par with the *E. coli* nucleoid was dependent on the binding of GFP-Par to the pSK1 *par* centromere-like site.

Figure 5.24 Fluorescence localisation of GFP-Par in *E. coli* cells, in the absence of pSK1 *par* centromere-like site

E. coli cells harbouring pSK9178 ($P_{tac}::gfp-par$) were grown to mid-exponential phase with 0.1 mM IPTG induction of *gfp-par* expression. Cells were then treated with 300 μ g/ml chloramphenicol for 1.5 h to condense nucleoids (Section 2.11.2). Nucleoid DNA was stained with DAPI, and cells were prepared for epifluorescence microscopy as described in Section 2.11.2. From top left to bottom right: GFP-Par; DNA; bright-field (BF); overlay of GFP-Par and DNA; overlay of bright-field (BF) and GFP-Par; overlay of bright-field (BF), GFP-Par and DNA. Scale bar = 1 μ m.

E. coli (*gfp-par*), no centromere-like site



5.7. Fluorescence *in situ* hybridisation of pSK1 minireplicons in *S. aureus*

In order to compare the observations of Par-GFP localisation in *S. aureus* (Section 5.4.4.4) with plasmid localisation, fluorescence *in situ* hybridisation (FISH) was performed on fixed *S. aureus* cells to localise pSK1 minireplicons with and without *par*. Cy3-labelled DNA probes were prepared by restriction digestion of pSK4833 DNA (Table 2.2) with the frequent-cutting enzymes *Hae*III, *Fok*I, *Dpn*I and *Rsa*I (Section 2.4.6). Reactions were electrophoresed on a 3% (w/v) agarose gel (Section 2.4.3), and DNA fragments smaller than 500 bp were gel-excised and purified (Section 2.4.7). The 3'-termini of DNA fragments were subsequently end-labelled with 5-Propargylamino-dCTP-Cy3 (Cy3-dCTP) using terminal deoxynucleotidyl transferase, as described in Section 2.11.3.1.

S. aureus SK8250 cells carrying either pSK4829 (*par*), pSK4833 (Δ *par*) (Table 2.2) or no plasmid DNA, were grown to mid-exponential phase and FISH was performed largely as described in Section 2.11.3.2. Only very faint fluorescence was detected, with no visible difference between the fluorescence from cells carrying pSK4829, pSK4833 or cells without any plasmid (data not shown). Despite altering various parameters such as the fixative used (methanol, paraformaldehyde), lysostaphin concentration (10–300 μ g/ml), cell lysis time (1–30 min), cell lysis temperature (RT, 37°C, 42°C), wash time (1–10 min), wash temperature (RT, 37°C), incubation time (1 h–overnight) and temperature (RT, 37°C, 42°C) with labelled probe, and the concentration of labelled probe added to the cells (5–50 ng/ μ l), non-specific fluorescence was detected regardless of whether the cells contained plasmid DNA.

Due to the problems encountered with the detection of plasmid DNA in fixed *S. aureus* cells using FISH, this method for plasmid localisation was not pursued further, and an alternative strategy was used for plasmid localisation in live *S. aureus* cells (see Section 5.8 below).

5.8. Fluorescence localisation of pSK1 minireplicons in live *S. aureus* cells

As described in Section 5.7, FISH could not specifically localise pSK1 minireplicons in fixed *S. aureus* cells. Therefore, an alternative method, based on a fluorescent repressor-operator system (FROS) (Robinett *et al.* 1996), was used for plasmid localisation in live *S. aureus* cells. FROS utilises a fluorescently-tagged repressor protein that binds to an array of operator elements present on the plasmid to be localised. In this way, epifluorescence microscopy can be performed to detect the fluorescence emitted from the fluorescent repressor protein such that localisation of the repressor is representative of the localisation of the plasmid to which it is bound. This system, therefore, enables plasmid localisation in live cells and allows plasmid movement to be tracked over time. Tagging of plasmids using FROS has been useful for studying the localisation of plasmids such as F plasmid (Gordon *et al.* 1997, Gordon *et al.* 2004, Hatano *et al.* 2007), P1 (Gordon *et al.* 1997, Gordon *et al.* 2004), pB171 (Ringgaard *et al.* 2009), R1 (Jensen and Gerdes 1999, Møller-Jensen *et al.* 2003) and RK2 (Pogliano *et al.* 2001, Ho *et al.* 2002), as well as high copy-number ColE1-type *E. coli* plasmids (Pogliano *et al.* 2001, Reyes-Lamothe *et al.* 2014). To facilitate the localisation of plasmid DNA in *S. aureus*, the FROS used in this study

consisted of *tetO* operator arrays located on pSK1 minireplicons, which provided binding sites for TetR-GFP repressor proteins.

5.8.1 Construction of pSK1 minireplicons carrying *tetO* arrays

In order to localise pSK1 minireplicons in *S. aureus* using FROS, *tetO* operator arrays were inserted into pSK4829 (*par*) and pSK4833 (Δ *par*) (Table 2.2). The *tetO* operator array used in this study was generated by Lau *et al.* (2003) on the plasmid pLAU44 (Table 2.2), which was provided by Dr. Ian Grainge (University of Newcastle, Australia). pLAU44 contains two arrays of 120 Tn10 *tetO* operators, located either side of a gentamycin resistance gene (Lau *et al.* 2003). Each array is comprised of three tandemly repeating *tetO* operators, repeated to form an array of 120 *tetO* operators. Each operator is separated by 10 bp of random sequence, as described in (Lau *et al.* 2003).

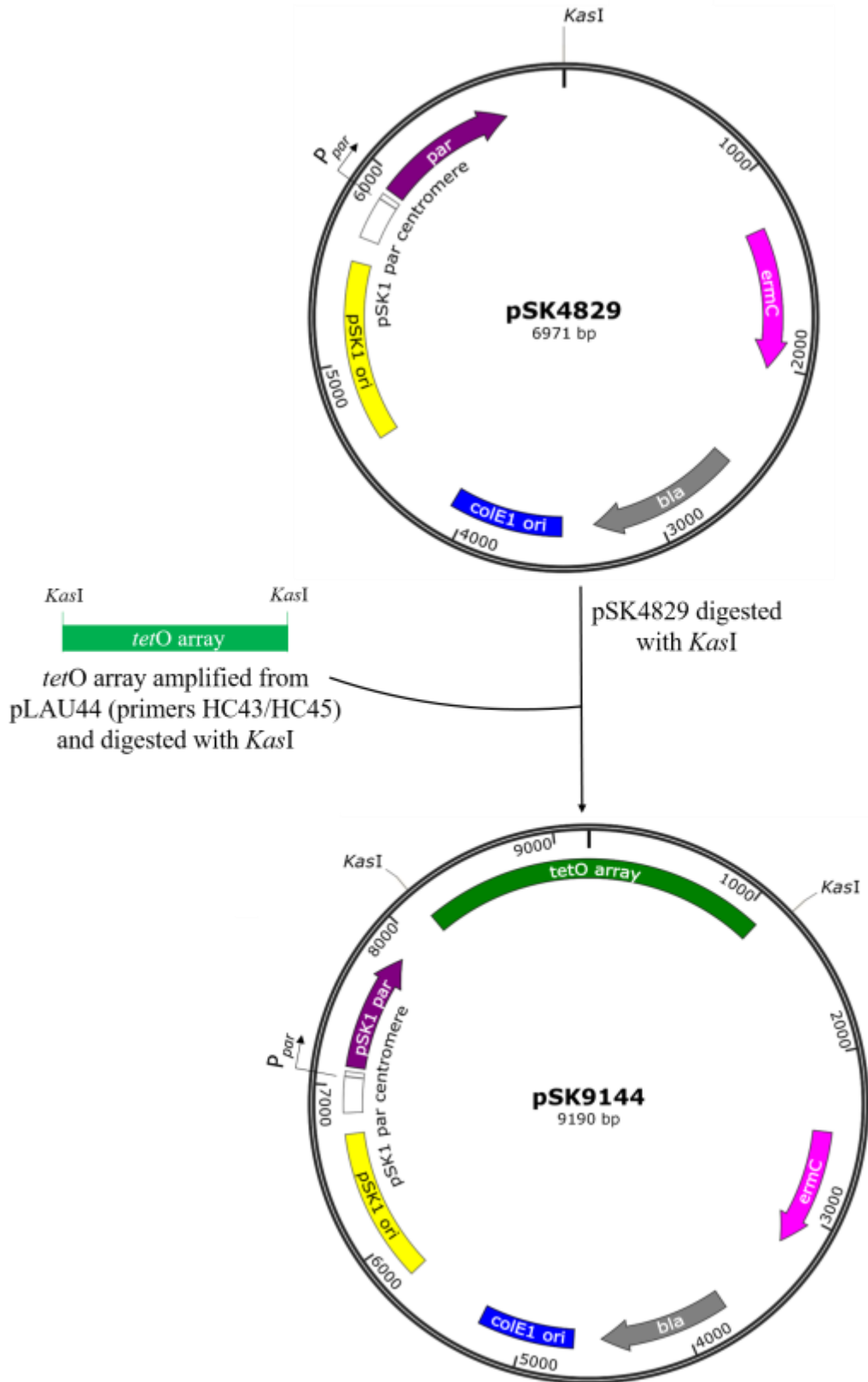
An overview of the molecular cloning processes used for the construction of pSK1 minireplicons containing the *tetO* array is shown in Figure 5.25. In order to minimise the size of the DNA fragment introduced into the pSK1 minireplicons, primers HC43 and HC45 (Table 2.6) were used to PCR-amplify (Section 2.4.4) a 4.5 kb region from pLAU44 template DNA (Table 2.2) containing an array of 120 *tetO* operators located downstream of the gentamycin resistance gene. The amplicon was electrophoresed on an agarose gel (Section 2.4.3), gel-purified (Section 2.4.7) and then restriction digested with *KasI* (Section 2.4.6) to further reduce the *tetO* array to a size of 2.2 kb. Following agarose gel electrophoresis of the digest (Section 2.4.3), the 2.2 kb fragment was gel-purified (Section 2.4.7) and then separately ligated to the *KasI*-restricted (Section 2.4.6) and dephosphorylated (Section 2.4.10) ends of

Figure 5.25 Construction of pSK1 minireplicons carrying *tetO* arrays

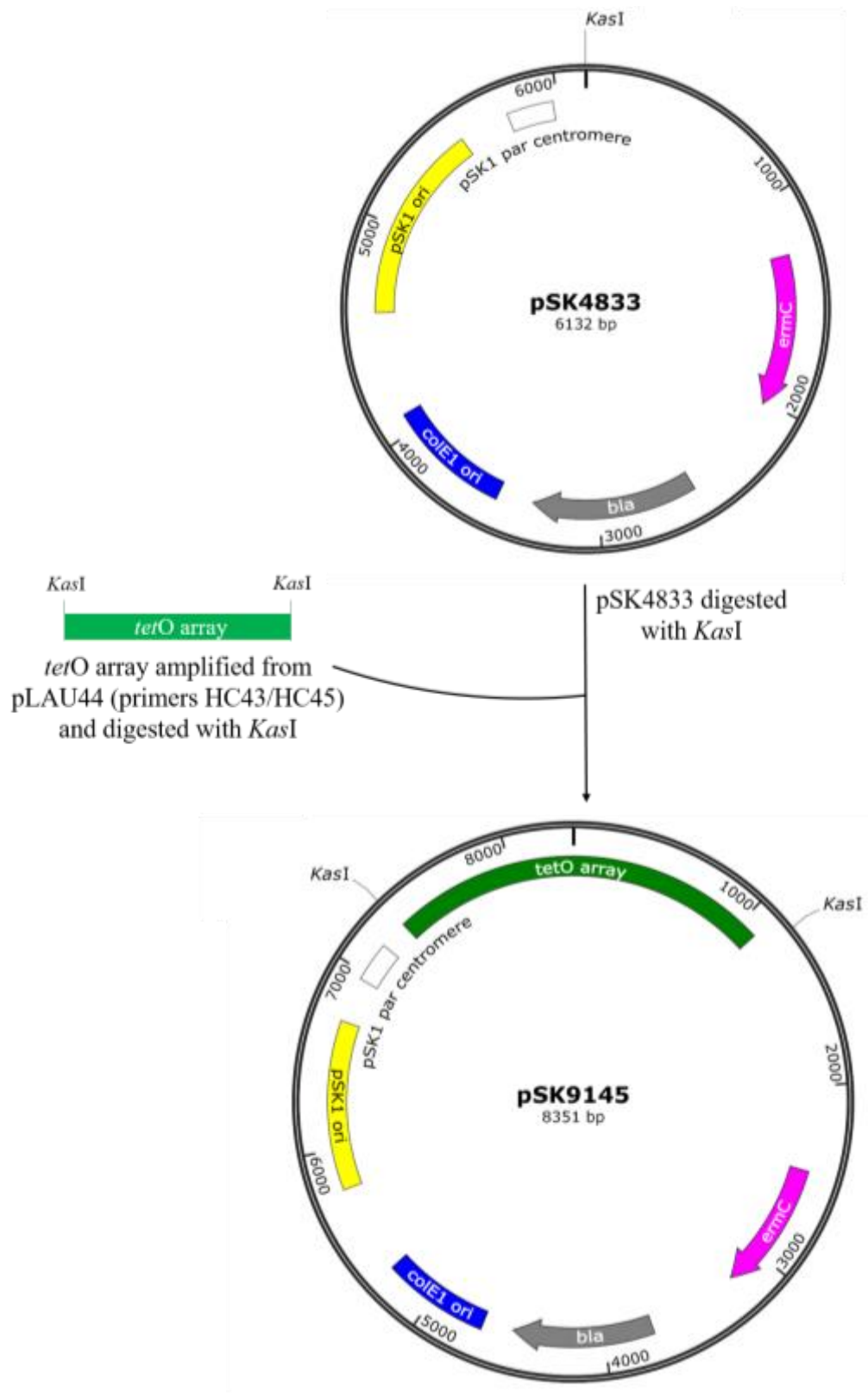
The insertion of *tetO* arrays in the pSK1 minireplicons, pSK4829 (*par*) (A) and pSK4833 (Δ *par*) (B) is described in detail in Section 5.8.1. Briefly, a *tetO* array was amplified from pLAU44 (Lau *et al.* 2003) using primers HC43 and HC45 (Table 2.6). The amplicon was then restriction digested with *KasI* (Section 2.4.6), resulting in a 2.2 kb fragment consisting of approximately 60 copies of *tetO*. The restricted *tetO* array was ligated to *KasI*-digested pSK4829 (*par*) or pSK4833 (Δ *par*) (Section 2.4.11), generating pSK9144 and pSK9145, respectively (Table 2.2).

Genes: *bla*, gene conferring ampicillin resistance in *E. coli*; *ermC*, gene conferring erythromycin resistance in *S. aureus*; ColE1 *ori*, high-copy-number *E. coli* origin of replication; pSK1 *ori*, origin of replication from *S. aureus* multiresistance plasmid pSK1; *tetO* array, array of approximately 60 copies of Tn10 Tet operators, amplified from pLAU44 (Lau *et al.* 2003); pSK1 *par*, gene encoding the plasmid maintenance protein, Par, from *S. aureus* multiresistance plasmid pSK1.

A.



B.



pSK4829 (*par*) and pSK4833 (Δ *par*) (Table 2.2). Ligation reactions were subsequently used to transform *E. coli* DH5 α cells to ampicillin resistance (Section 2.3.2). To identify recombinant plasmids containing the *tetO* array, plasmid DNA was isolated (Section 2.4.1) from selected transformants, digested with *KasI* (Section 2.4.6), and then electrophoresed on an agarose gel (Section 2.4.3). However, it was found that the isolated plasmids contained either no insert or carried an insert that was smaller than the expected size. This might have been due to instability of the *tetO* array in *E. coli* DH5 α , a RecA⁻ rather than RecA⁺ strain (Lau *et al.* 2003), which might have caused deletions of parts of the array. Therefore, to reduce potential instability, *E. coli* cells were transformed with the ligation mixtures and were incubated at a reduced temperature of 30°C instead of 37°C. Plasmid DNA was isolated from transformants grown at 30°C, and recombinant plasmids were identified by restriction digestion with *KasI* and agarose gel electrophoresis, as described above. Recombinant pSK4829 (*par*) and pSK4833 (Δ *par*) plasmids, carrying a 2.2 kb *tetO* array containing approximately 60 copies of the *tetO* operator, were named pSK9144 and pSK9145, respectively (Table 2.2).

5.8.2 Construction of an IPTG-inducible *tetR-gfp* expression plasmid

To provide the fluorescent repressor to bind the *tetO* arrays located on the pSK1 minireplicons constructed in Section 5.8.1, an IPTG-inducible *tetR-gfp* expression plasmid was generated. An *S. aureus* expression plasmid, pSK9067 (Table 2.2), that allows titratable expression of GFP protein fusions from the P_{*spac*} promoter, was constructed by Brzoska and Firth (2013). pSK9067 is an *E. coli*-*S. aureus* shuttle plasmid that utilises a pSK41 origin of replication in *S. aureus*, which makes it

compatible with the pSK1 minireplicons to be used in FROS. A MCS is located upstream of the GFP coding sequence, which enables the generation of C-terminal GFP fusions to protein coding regions cloned in-frame of *gfp*. Expression of GFP protein fusions is regulated by the IPTG-inducible P_{spac} promoter and vector-encoded Lac repressor.

However, selection for pSK9067 in *S. aureus* is provided by the *ermC* gene (Horinouchi and Weisblum 1982), which encodes erythromycin resistance and is also used to select for the FROS pSK1 minireplicons, pSK9144 and pSK9145 (Table 2.2). Therefore, to ensure plasmid compatibility and the independent selection of both plasmids in FROS, pSK9067 was modified by replacing the *ermC* gene with the *aadD* gene (McKenzie *et al.* 1986), which confers neomycin resistance in *S. aureus*. Modification of pSK9067, depicted graphically in Figure 5.26A, was performed by restriction digestion of the plasmid with *KpnI* and *ClaI* (Section 2.4.6) to release a 1.2 kb fragment containing *ermC*. Agarose gel electrophoresis (Section 2.4.3) of the restriction digestion reaction allowed for recovery of the remaining 6.7 kb of vector DNA via gel-purification (Section 2.4.7). A DNA fragment containing the *aadD* gene was excised from pSK9065 (Table 2.2) by restriction digestion of the plasmid DNA with *NcoI* and *SphI* (Section 2.4.6). The 1 kb DNA band containing *aadD* was subsequently gel-purified (Section 2.4.7) after agarose gel electrophoresis of the digests (Section 2.4.3). Overhangs on the digested 6.7 kb pSK9067 vector DNA and the 1 kb *aadD* fragment were filled-in using the Klenow fragment of DNA polymerase I (Section 2.4.8), and the blunted fragments were ligated using T4 DNA ligase (Section 2.4.11). *E. coli* DH5 α cells were transformed with the ligation reaction and selected for ampicillin resistance (Section 2.3.2), after which plasmid

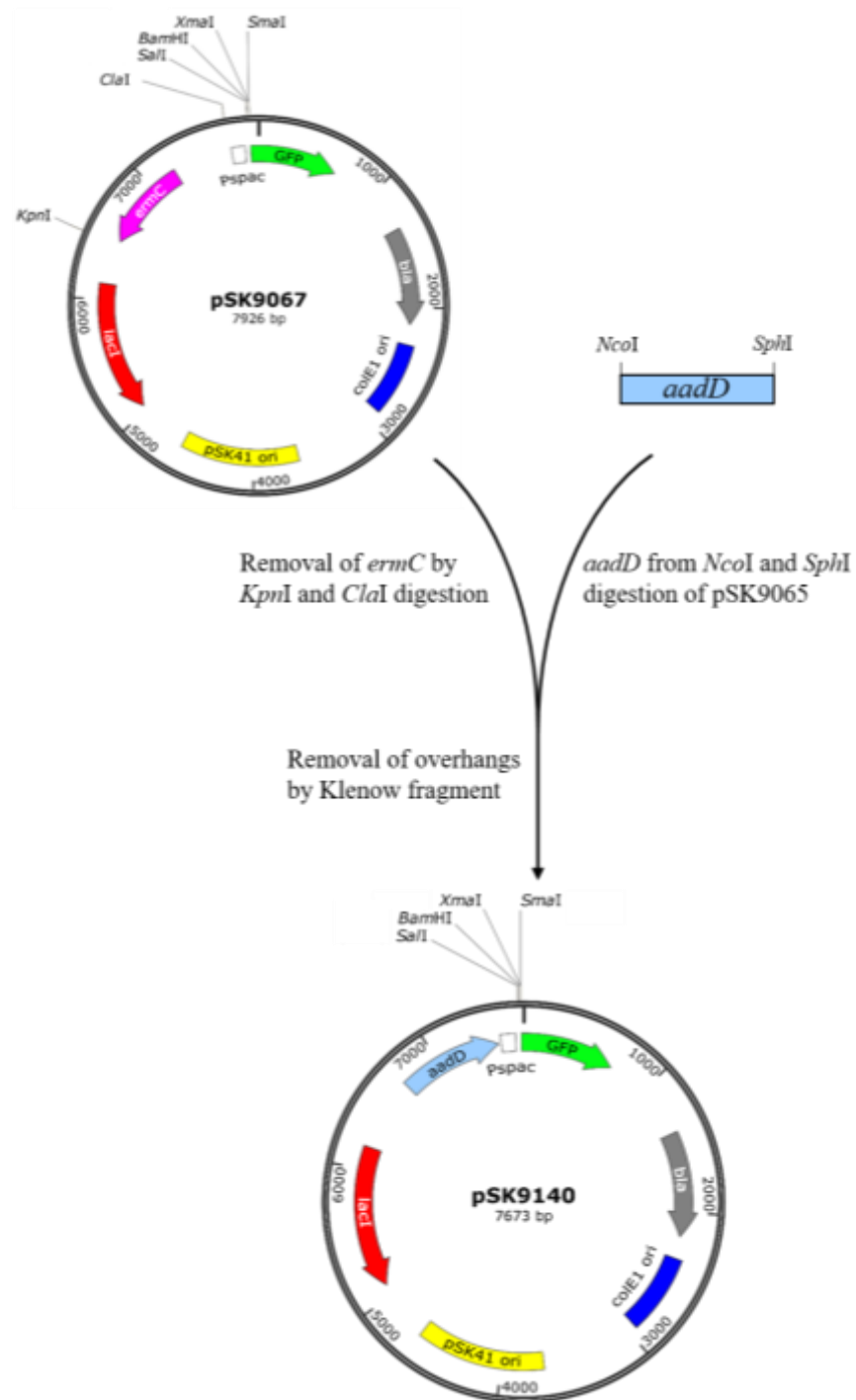
Figure 5.26 Construction of an inducible *tetR-gfp* expression plasmid

A. Modification of an *S. aureus* expression plasmid for *gfp* fusions to confer neomycin resistance in *S. aureus*. The *ermC* erythromycin resistance gene on the *S. aureus* expression plasmid pSK9067 (Brzoska and Firth 2013) was replaced with the *aadD* neomycin resistance gene, as detailed in Section 5.8.2. Briefly, a 1.2 kb DNA fragment containing *ermC* was removed from pSK9067 by restriction digestion with *KpnI* and *ClaI* (Section 2.4.6), and the remaining 6.7 kb DNA fragment was gel-purified (Section 2.4.7). The *aadD* gene was obtained from pSK9065 by restriction digestion with *NcoI* and *SphI* (Section 2.4.6) and subsequent gel-purification of the 1 kb DNA fragment containing *aadD* (Section 2.4.7). Overhangs on purified DNA fragments were removed using the Klenow fragment of DNA polymerase I (Section 2.4.8), and fragments were ligated using T4 DNA polymerase (Section 2.4.11), resulting in pSK9140 (Table 2.2). **B.** Overview of the molecular cloning of Tn10 *tetR* to generate an inducible TetR-GFP fusion protein in *S. aureus*. Details of the construction of pSK9142 (Table 2.2) are described in Section 5.8.2. Briefly, Tn10 *tetR* was amplified from pSK9065 (Table 2.2) using primers HC38 and HC39 (Table 2.6) (Section 2.4.4), which contain the strong *S. aureus* superoxide dismutase (SOD) ribosome binding site (RBS) and a five-codon linker. The *tetR* amplicon was then restricted with *SalI* and *BamHI* (Section 2.4.6) and ligated to the similarly restricted and dephosphorylated *SalI* and *BamHI* sites of pSK9140 (Table 2.2) (Section 2.4.11) to generate pSK9142 (Table 2.2).

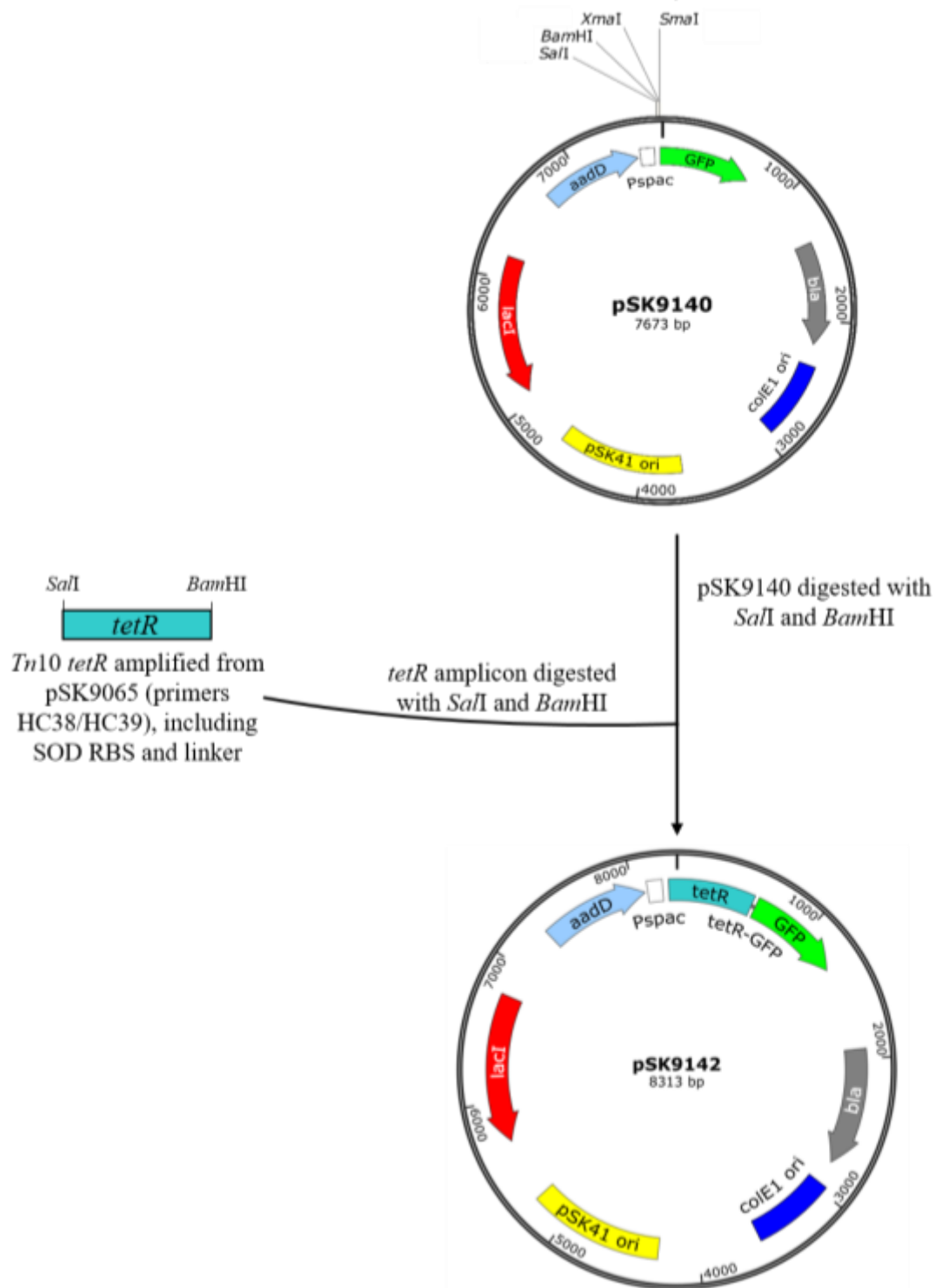
Genes: *bla*, gene conferring ampicillin resistance in *E. coli*; *aadD*, gene conferring neomycin resistance in *S. aureus*; *ermC*, gene conferring erythromycin resistance in *S. aureus*; ColE1 *ori*, high-copy-number *E. coli* origin of replication; pSK41 *ori*, origin of replication from *S. aureus* multiresistance plasmid pSK41; *lacI*, gene encoding the

repressor of the P_{spac} promoter; *gfp*, *gfpmut-1* gene encoding the green fluorescent protein; *tetR*, gene encoding the repressor that binds to Tn10 Tet operators.

A.



B.



DNA was isolated (Section 2.4.1) from selected transformants. Isolated plasmid DNA was screened for recombination by restriction digestion with *Pst*I and *Eco*RV (Section 2.4.6), followed by agarose gel electrophoresis of the digests (Section 2.4.3). Recombinant plasmids were identified by the presence of a 5.4 kb and 2.1 kb band. Neomycin resistance conferred by the modified pSK9067 plasmid was confirmed by electroporation of *S. aureus* RN4220 cells (Section 2.3.4) with recombinant plasmids and growth of transformants on NYE-agar (Table 2.3) containing 15 µg/ml neomycin. The pSK9067 plasmid derivative that conferred neomycin resistance in *S. aureus* was named pSK9140 (Table 2.2).

To construct a *tetR-gfp* expression plasmid, the *Tn10 tetR* gene was PCR-amplified (Section 2.4.4) from pSK9065 plasmid DNA (Table 2.2) using primers HC38 and HC39 (Table 2.6). The sense primer, HC38, contains a *Sal*I restriction site as well as the strong RBS from the *S. aureus* superoxide dismutase (SOD) gene (Clements *et al.* 1999) to promote efficient translation of the *tetR-gfp* transcript. In addition to a *Bam*HI restriction site, the antisense primer, HC39, also encodes a linker, SCGAS (Veiga *et al.* 2011), to be incorporated between the TetR and GFP proteins to minimise interference of TetR structure and function by GFP (Chen *et al.* 2013). The 0.7 kb PCR product was purified (Section 2.4.7) and digested with *Sal*I and *Bam*HI (Section 2.4.6), as was pSK9140 vector DNA (Table 2.2). The digested pSK9140 DNA was dephosphorylated (Section 2.4.10) and used in a ligation reaction (Section 2.4.11) with the digested *tetR* amplicon to insert the *tetR* coding region upstream and in-frame of *gfp* (Figure 5.26B). The ligation mixture was used to transform *E. coli* DH5α cells to ampicillin resistance (Section 2.3.2), after which plasmid DNA was isolated (Section 2.4.1) from selected transformants to screen for recombinants by

restriction digestion with *SalI* and *BamHI* (Section 2.4.6), followed by agarose gel electrophoresis (Section 2.4.3). Plasmids showing the expected restriction profile of recombinants were sequenced (Section 2.4.14) using primers HC38 and HC39 (Table 2.6). The plasmid containing the correct sequence of the SOD RBS and *tetR* in-frame of *gfp* was named pSK9142 (Table 2.2) (Figure 5.26B).

5.8.3 Effect of TetR-GFP on plasmid segregational stability

To determine whether *par* enhances the segregational stability of pSK1 minireplicons carrying the *tetO* array, and whether the production and binding of TetR-GFP to the *tetO* array affects Par function, plasmid segregational stability assays were performed on *S. aureus* cells carrying the two FROS plasmids. Because transformation efficiencies were low when *S. aureus* cells were simultaneously electroporated with pSK9142 ($P_{spac}::tetR-gfp$) and either pSK9144 (*par*, 60×*tetO*) or pSK9145 (Δpar , 60×*tetO*) (Table 2.2) (data not shown), *S. aureus* SK8250 cells were first electroporated (Section 2.3.4) with pSK9142 only, and transformants were selected on NYE-agar (Table 2.3) containing neomycin (Table 2.4). Electrocompetent *S. aureus* SK8250 cells carrying pSK9142 were prepared as described in Section 2.3.3, and then electroporated with either pSK9144 or pSK9145. Transformants were grown at 30°C with selection on NYE-agar (Table 2.3) containing both neomycin (to select for retention of pSK9142) and erythromycin (to select for transformants carrying pSK9144 or pSK9145) (Table 2.4).

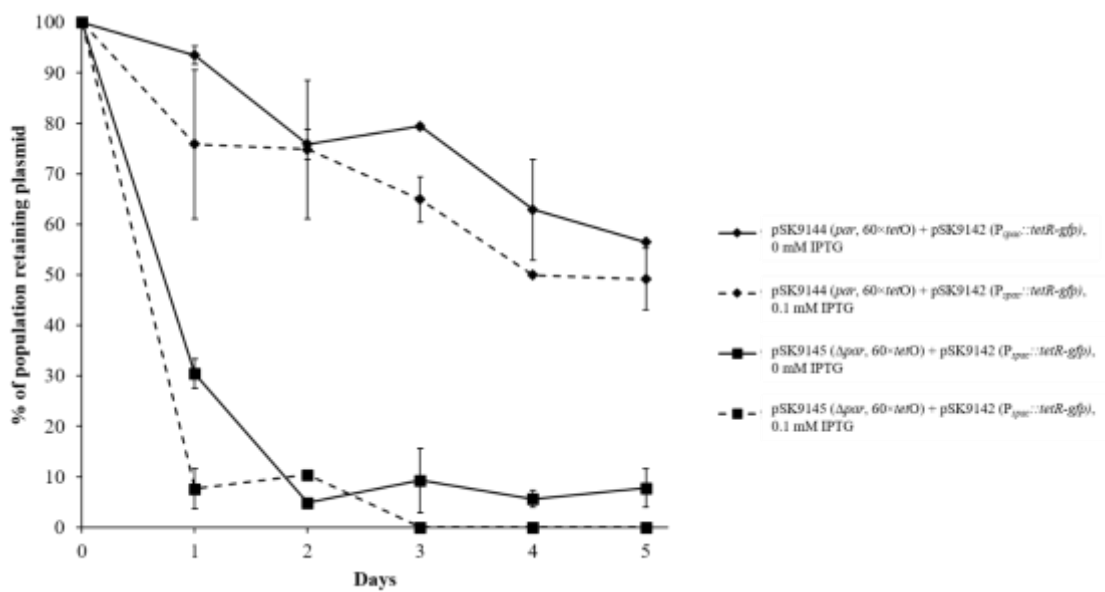
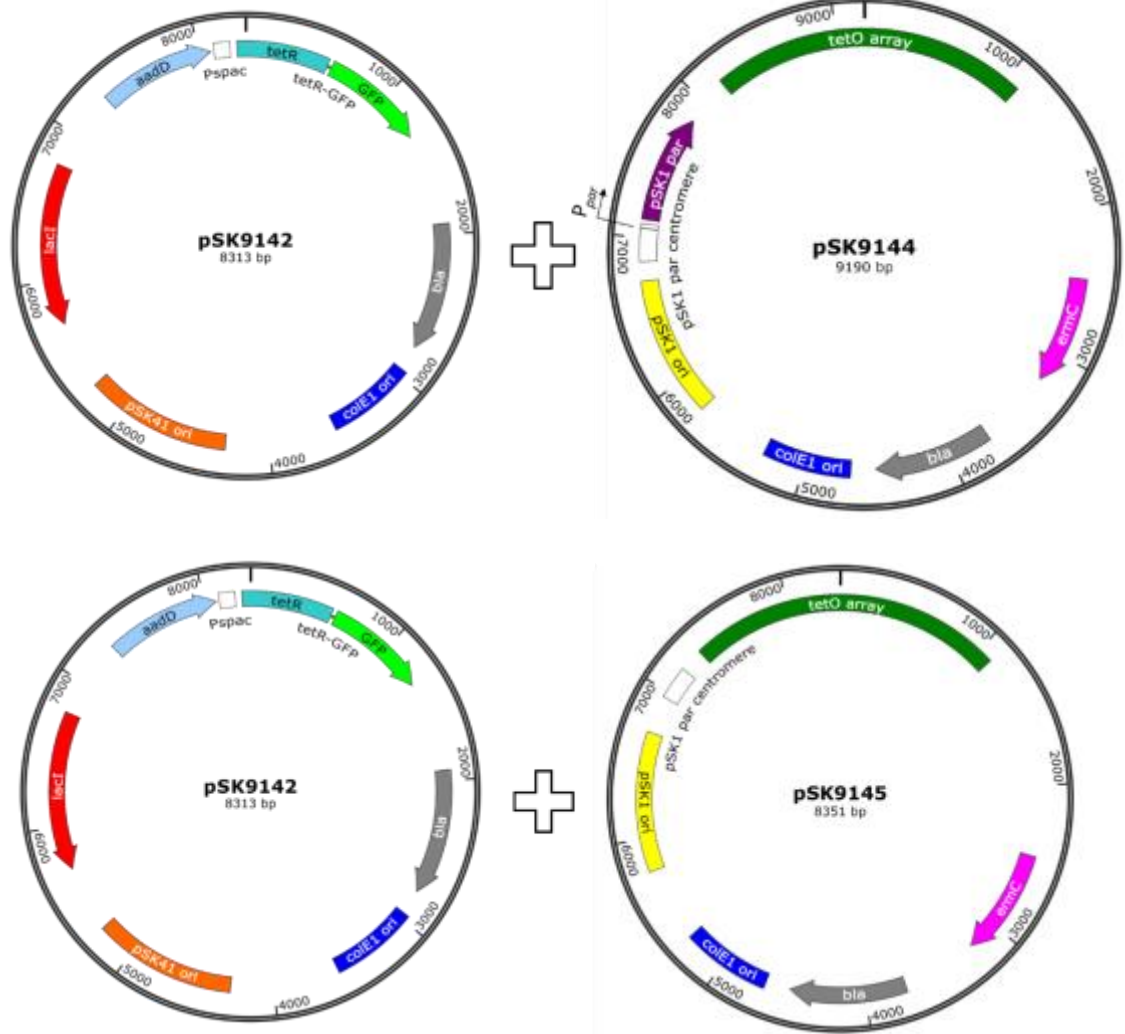
Plasmid segregational stability assays were performed on *S. aureus* cells carrying pSK9142 ($P_{spac}::tetR-gfp$) and either pSK9144 (*par*, 60×*tetO*) or pSK9145 (Δpar , 60×*tetO*) as described in Section 2.7. In order to minimise potential instability of the

tetO array, as experienced with *E. coli* cells when grown at 37°C (Section 5.8.1), serial subcultures for the stability assays were performed at 30°C. Throughout the assays, continuous selection for pSK9142 was applied using neomycin in the culture media. Serial subcultures and viable counts were performed in the absence of erythromycin, and retention of pSK1 minireplicons carrying the *tetO* array was assayed by growth of cells on media containing both erythromycin and neomycin. Expression of *tetR-gfp* was either uninduced or induced from pSK9142 using 0.1 mM IPTG, which was added to the LB-broth used for subculture.

Following five days of continuous subculture, approximately 56% of the cell population retained pSK9144 (*par*, 60×*tetO*) when expression of *tetR-gfp* was uninduced (Figure 5.27). This was compared to 8±4% of the population that retained pSK9145 (Δ *par*, 60×*tetO*) after five days of the assay in the absence of TetR-GFP induction (Figure 5.27). These results, therefore, suggest that *par* enhances the segregational stability of a pSK1 minireplicon carrying the *tetO* array. When *tetR-gfp* expression was induced with 0.1 mM IPTG, no dramatic effects were observed on the segregational stability of pSK9144 or pSK9145; at the conclusion of the assay, pSK9144 was retained by a larger proportion of the population (49±6%) compared to pSK9145, which was completely lost from the population after three days of the assay (Figure 5.27). Therefore, induction of *tetR-gfp* expression from pSK9142 using 0.1 mM IPTG did not appear to interfere with Par function or disrupt plasmid segregational stability. The enhanced segregational stability of pSK9144 compared to pSK9145, even in the presence of TetR-GFP, demonstrates the functionality of *par* and validates the suitability of these plasmid pairs for the study of plasmid localisation in *S. aureus* using FROS.

Figure 5.27 Effect of TetR-GFP on the segregational stability of pSK1 minireplicons containing *tetO* arrays

Plasmid segregational stability assays of pSK1 minireplicons carrying *tetO* arrays. The retention of pSK1 minireplicons pSK9144 (*par*, 60×*tetO*) (◆) and pSK9145 (Δ *par*, 60×*tetO*) (■) in *S. aureus* SK8250 cells was determined as described in Section 2.7. Expression of *tetR-gfp* was induced from a co-resident plasmid, pSK9142 ($P_{spac}::tetR-gfp$), with 0 mM IPTG (solid lines) or 0.1 mM IPTG (dashed lines). Assays were performed with continuous neomycin selection for pSK9142. Five days of serial subculture represents approximately 75 generations. Data are normalised to 100% plasmid retention on Day 0. The averages of three independent assays are shown. Error bars represent standard error of the mean. Illustrative maps of the plasmids contained in the assayed *S. aureus* strains are shown above the graphs.



5.8.4 Fluorescence localisation of pSK1 minireplicons using a fluorescent repressor-operator system in live *S. aureus* cells

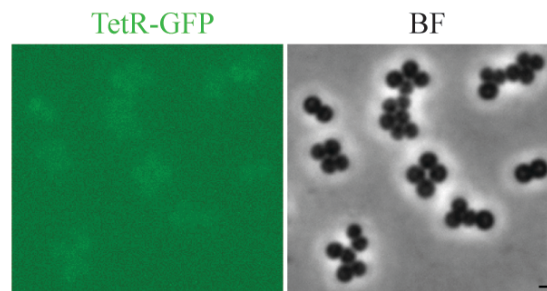
The localisation of pSK1 minireplicons in *S. aureus* cells was determined by epifluorescence microscopy using FROS, which consisted of pSK9142 ($P_{spac}::tetR-gfp$) and either pSK9144 (*par*, $60\times tetO$) or pSK9145 (Δpar , $60\times tetO$) (Table 2.2). Stationary phase cultures of *S. aureus* SK8250 cells grown at 30°C and carrying the two pairs of FROS plasmids (with and without *par*), were used to inoculate fresh LB-broth (Table 2.3) containing antibiotic selection for both plasmids (Table 2.4) (Section 2.11.2). Cultures were grown at 30°C to mid-exponential phase, after which 0.1 mM IPTG was added to induce *tetR-gfp* expression. Expression was induced at 30°C for 2 h, and, when necessary, nucleoids were condensed with 25 µg/ml chloramphenicol for a further 1 h at 30°C (Section 2.11.2). *S. aureus* cells were prepared for epifluorescence microscopy and nucleoid DNA was stained with DAPI as described in Section 2.11.2.

The fluorescence micrograph in Figure 5.28A shows that when *tetR-gfp* expression was uninduced in *S. aureus* cells carrying the FROS plasmids pSK9142 ($P_{spac}::tetR-gfp$) and pSK9144 (*par*, $60\times tetO$), no fluorescence was detected. However, when *tetR-gfp* expression was induced with 0.1 mM IPTG, fluorescent foci were observed (Figures 5.28Bi–iv), which suggests that expression of *tetR-gfp* could be tightly regulated, and that the fluorescence detected was emitted specifically from TetR-GFP. Furthermore, when *S. aureus* cells harboured pSK9142 and pSK4829 (Table 2.2), which lacks the *tetO* array present on pSK9144, TetR-GFP produced only diffuse fluorescence when induced with 0.1 mM IPTG (Figure 5.28C). Therefore,

Figure 5.28 Fluorescence localisation of pSK1 minireplicons in *S. aureus* cells by tagging with TetR-GFP

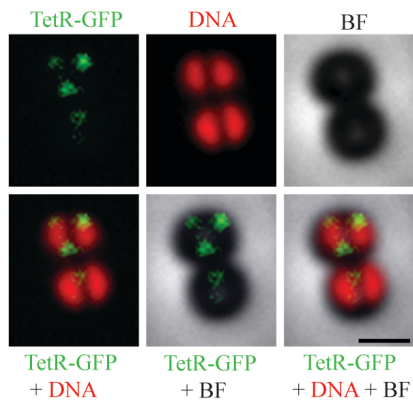
The localisation of pSK1 minireplicons pSK9144 (*par*, 60×*tetO*) (**A** and **Bi–iv**), pSK4829 (**C**) and pSK9145 (Δ *par*, 60×*tetO*) (**Di–v**) in mid-exponential phase *S. aureus* SK8250 cells was visualised by tagging with TetR-GFP using a fluorescent repressor-operator system. Expression of *tetR-gfp* from pSK9142 ($P_{spac}::tetR-gfp$) was uninduced (**A**) or induced with 0.1 mM IPTG (Section 5.8.4) (**B–D**). Nucleoid DNA was stained with DAPI (**B** and **D**), and cells were prepared for epifluorescence microscopy as described in Section 2.11.2. Cells in each of (**B**) and (**D**) are biological replicates. In (**A**), from left to right: TetR-GFP, bright-field (BF). In (**B**) and (**D**), from top left to bottom right: TetR-GFP; DNA; bright-field (BF); overlay of TetR-GFP and DNA; overlay of bright-field (BF) and TetR-GFP; overlay of bright-field (BF), TetR-GFP and DNA. In (**C**), from left to right: TetR-GFP; bright-field (BF); overlay of bright-field (BF) and TetR-GFP. Scale bar = 1 μ m.

A. *S. aureus* (*par*, 60×*tetO*) + TetR-GFP + 0 mM IPTG

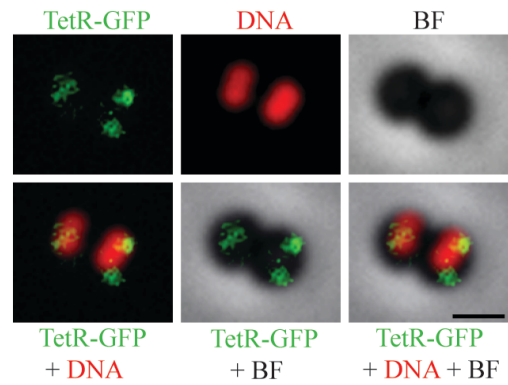


B. *S. aureus* (*par*, 60×*tetO*) + TetR-GFP + 0.1 mM IPTG

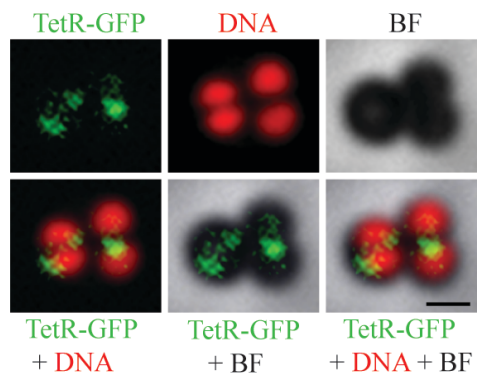
i.



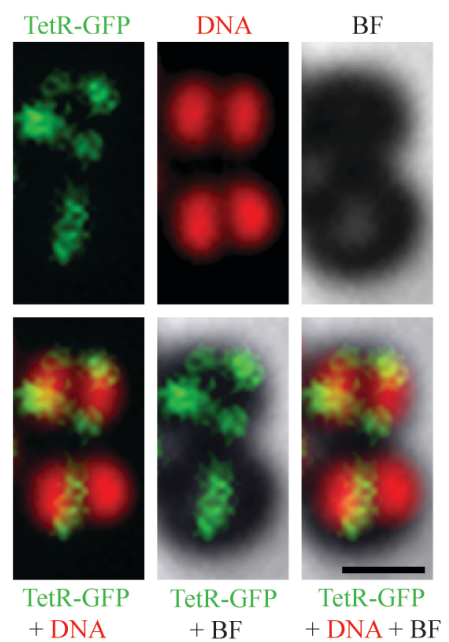
ii.



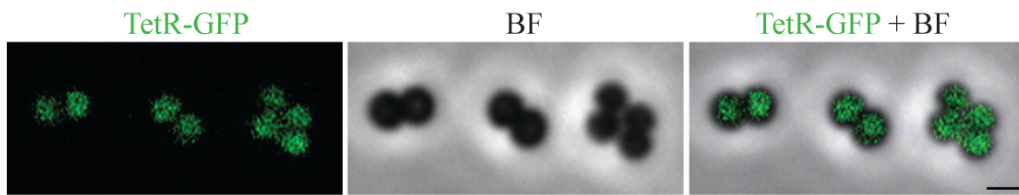
iii.



iv.

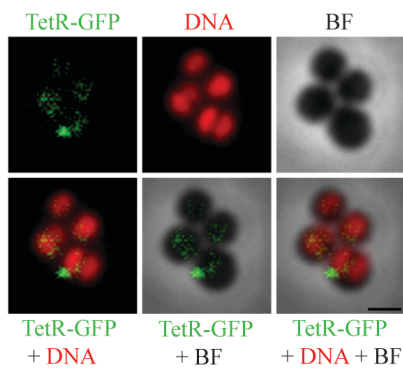


C. *S. aureus* (*par*) + TetR-GFP + 0.1 mM IPTG

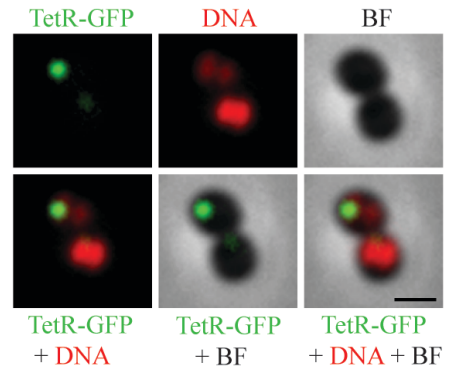


D. *S. aureus* (Δpar , $60\times tetO$) + TetR-GFP + 0.1 mM IPTG

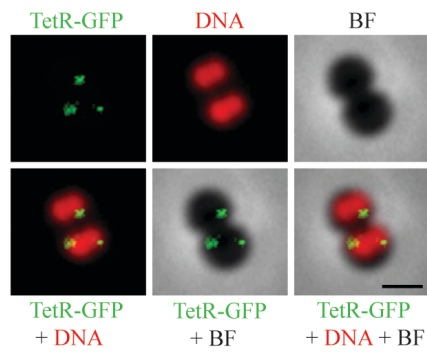
i.



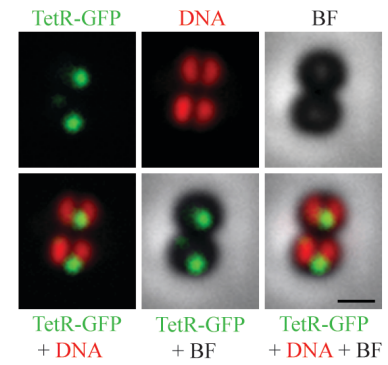
ii.



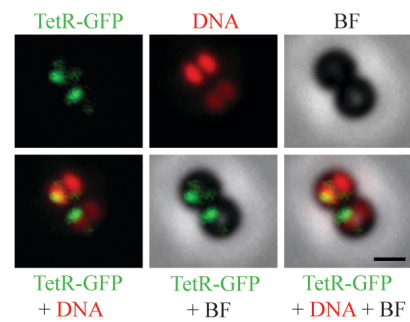
iii.



iv.



v.



fluorescent foci were only observed in *S. aureus* cells when both the *tetO* array and TetR-GFP were present in FROS. This strongly suggests that the observed foci resulted from TetR-GFP binding to the *tetO* array on the pSK1 minireplicons, and therefore, TetR-GFP localisation was interpreted as a strong indicator of plasmid localisation.

Typically, one to four fluorescent foci were observed in each *S. aureus* cell carrying pSK9142 ($P_{spac}::tetR-gfp$) and pSK9144 (*par*, $60\times tetO$) (Figures 5.28Bi–iv). In cells displaying one plasmid focus ($24\pm 2\%$ of all cells), the focus tended to localise at the division septum, between the two hemispheres of nucleoid DNA (Figure 5.28Bi, bottom cell). Where two foci were present ($37\pm 2\%$), each focus was generally associated with a separate hemisphere of nucleoid DNA, with the two foci either on the same or opposite sides of the cell (Figure 5.28Bii, right cell and Figure 5.28Biii, left cell). However, examples were also observed whereby the two foci were localised in the space between two nucleoids (Figure 5.28Biv, bottom cell). A third focus would sometimes be observed at the division septum ($11\pm 2\%$) (Figure 5.28Bi, top cell). In examples where four fluorescent foci were visualised ($3\pm 1\%$), foci typically assumed the positions of the cell poles (Figure 5.28Biv, top cell), similar to the polar localisation pattern observed for Spo0J-GFP shown in Figures 5.11i–ii. Furthermore, TetR-GFP foci appeared to be of similar intensities between cell hemispheres (Figures 5.28Bi–iv).

When *par* was absent, in cells carrying pSK9142 ($P_{spac}::tetR-gfp$) and pSK9145 (Δpar , $60\times tetO$), the majority of cells ($55\pm 1\%$) had no fluorescent foci and only showed diffuse fluorescence (Figure 5.28Di, top three cells), which was probably

due to the unstable segregational stability of pSK9145, as demonstrated by stability assays performed in Section 5.8.3. Of the cells that did contain foci, a large proportion contained only one focus ($23\pm 1\%$ of all cells; $50\pm 2\%$ of foci-containing cells), which was often of high fluorescence intensity and at times located between the two hemispheres of nucleoid DNA, potentially at the division septum (Figure 5.28Dii; Figure 5.28Diii, top cell and Figure 5.28Div, top cell). When more than one focus was present, examples were observed whereby plasmid foci were located on the same side of the division septum, in the same hemisphere of the cell (Figure 5.28Dv, bottom cell). In some cells lacking *par*, TetR-GFP foci displayed uneven fluorescence intensities between hemispheres, with extremely bright foci observed (Figure 5.28Div, bottom cell and Figure 5.28Dv). This could possibly be due to an uneven distribution of TetR-GFP, and hence pSK9145, between cell hemispheres. Overall, although *par*-deficient plasmid foci were localised towards the periphery of the cell, foci did not appear to assume the polar-like localisation pattern observed for plasmids containing *par*.

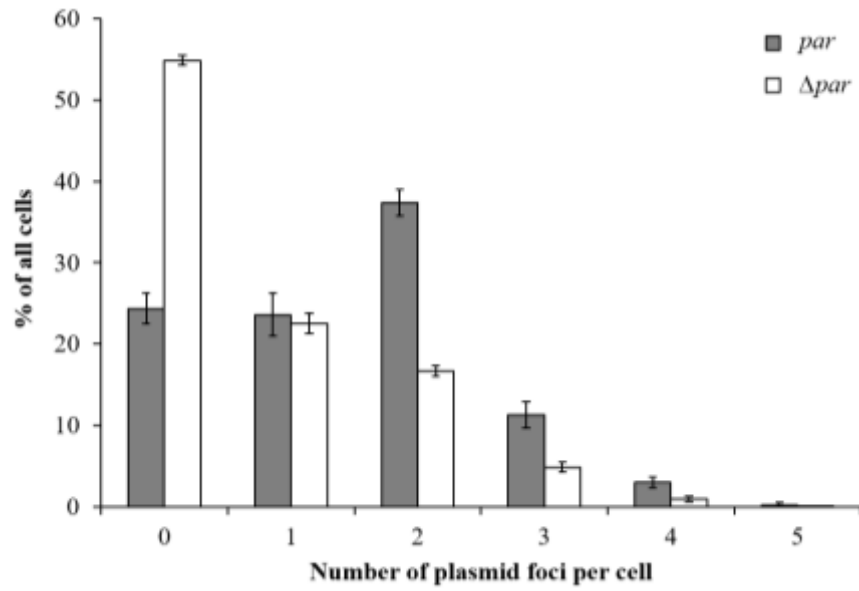
5.8.5 Distribution of TetR-GFP focus numbers in *S. aureus*

The distribution of the number of fluorescent TetR-GFP foci present in each cell, in the presence and absence of *par*, is presented in Figures 5.29A–B. Since it was established that TetR-GFP foci were formed as a result of TetR-GFP binding to *tetO* arrays (Section 5.8.4), the number of foci should, therefore, be reflective of the number of plasmids, or plasmid clusters, present in each *S. aureus* cell. The histograms in Figure 5.29A show that the mode for cells carrying pSK9144 (*par*, $60\times tetO$) is 2 plasmid foci per cell ($37\pm 2\%$), and that the distribution of plasmid

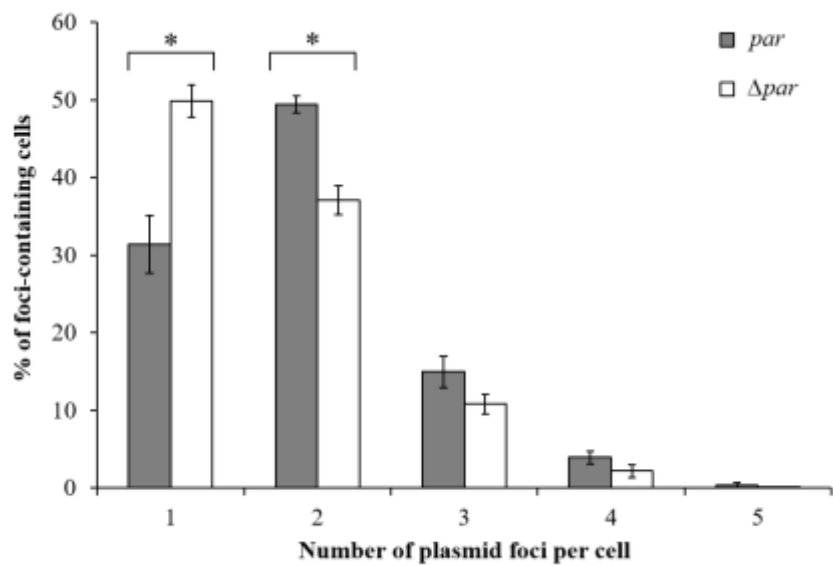
Figure 5.29 Distribution of the number of plasmid foci per cell

The number of fluorescent plasmid foci per cell, detected by epifluorescence microscopy, was determined for *S. aureus* SK8250 cells harbouring pSK1 minireplicons pSK9144 (*par*, 60×*tetO*) (grey bars; total number of cells = 1,362) or pSK9145 (Δ *par*, 60×*tetO*) (white bars; total number of cells = 1,616). Plasmids were visualised by tagging with TetR-GFP using a fluorescent repressor-operator system. Expression of *tetR-gfp* from pSK9142 ($P_{spac}::tetR-gfp$) was induced with 0.1 mM IPTG (Section 5.8.4). **A.** Histogram plotting the percentage of all cells against the number of plasmid foci per cell. **B.** Histogram plotting the percentage of foci-containing cells against the number of plasmid foci per cell. The averages of four independent microscopy experiments are shown. Error bars represent standard error of the mean.

A.



B.



* $p < 0.05$

focus numbers is centred around the mode. In the absence of *par*, the mode is 0 foci per cell ($55\pm 1\%$), with decreasing proportions of the population containing higher plasmid focus numbers. A Chi-squared test for homogeneity indicated that the distribution of plasmid focus numbers in cells with and without *par* was significantly different ($p < 2.2 \times 10^{-16}$). Importantly, the proportion of the population without any plasmid focus was substantially higher in cell populations lacking *par* compared to cells containing *par* ($24\pm 2\%$) (Figure 5.29A). Therefore, the presence of *par* on pSK1 minireplicons affected the distribution of the number of plasmid foci per cell, and increased the likelihood of cells containing at least one plasmid focus.

A more accurate reflection of the effect of pSK1 *par* on plasmid localisation might be obtained by analysing plasmid focus numbers in foci-containing cells only. Again, a Chi-squared test for homogeneity indicated that the distribution of plasmid focus numbers in foci-containing cells with and without *par* was significantly different ($p < 2.6 \times 10^{-9}$). Specifically, when only foci-containing cells were considered, there appeared to be a difference in the proportion of cells containing 1 or 2 foci (Figure 5.29B). In the absence of *par*, approximately half the foci-containing cells contained 1 plasmid focus ($50\pm 2\%$), which is significantly higher than the proportion of cells that contained 1 focus when *par* was present ($31\pm 4\%$) ($p < 0.05$; Figure 5.29B). Furthermore, compared to cells lacking *par*, a significantly higher proportion of cells carrying pSK9144 (*par*, $60\times tetO$) contained 2 plasmid foci ($49\pm 1\%$ compared to $37\pm 2\%$ without *par*; $p < 0.05$), which is also the mode for cells carrying pSK9144 (Figure 5.29B).

Overall, it appears that the absence of *par* significantly increased the likelihood of plasmid loss (no TetR-GFP foci) and the likelihood of cells containing 1 plasmid focus, and that the presence of *par* significantly increased the proportion of cells containing 2 plasmid foci. To ensure that the distributions of plasmid focus numbers per cell were not influenced by potential biases in the counting method, the number of plasmid foci per cell was calculated for a subset of both populations by an independent individual in a blind experiment, and were consistent with the results obtained. Interestingly, the number of TetR-GFP foci per cell, in both the presence and absence of *par*, was less than the expected copy-number for pSK1 minireplicons in *S. aureus* (estimated to be 3–10 copies per cell) (Grkovic *et al.* 2003, LeBard 2005), which is perhaps suggestive of plasmid clustering. This is discussed further in Section 5.9.2.

5.8.6 Association between TetR-GFP and nucleoid DNA in *S. aureus*

Similar to observations with Par-GFP foci in *S. aureus* (Section 5.4.4.4), TetR-GFP foci appeared to be associated with nucleoid DNA, in both the presence and absence of *par* (see Figures 5.28Bi–iv and Di–v). Therefore, to determine whether TetR-GFP, and hence plasmid DNA, was associated with *S. aureus* nucleoid DNA, *S. aureus* SK8250 cells carrying pSK9142 ($P_{spac}::tetR-gfp$) and either pSK9144 (*par*, $60\times tetO$) or pSK9145 (Δpar , $60\times tetO$) (Table 2.2) were prepared for epifluorescence microscopy as described in Section 5.8.4, and treated with chloramphenicol to induce nucleoid condensation (Section 2.11.2).

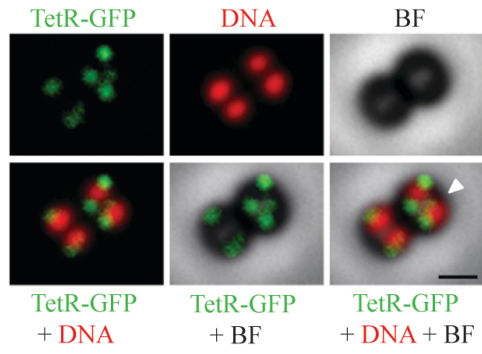
As shown in Figures 5.30Ai–v, most examples of cells carrying the FROS plasmids containing *par* clearly showed an apparent association between TetR-GFP and

Figure 5.30 Effect of nucleoid condensation on the fluorescence localisation of pSK1 minireplicons in *S. aureus* cells

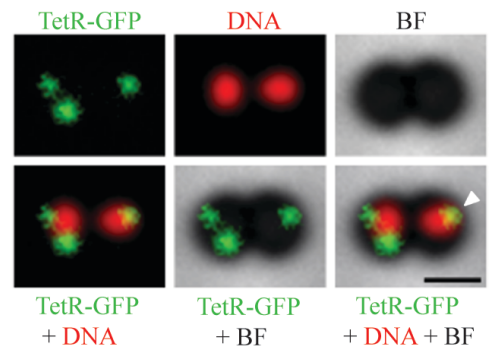
The localisation of pSK1 minireplicons pSK9144 (*par*, 60×*tetO*) (**Ai–v**) and pSK9145 (Δ *par*, 60×*tetO*) (**Bi–iii**) in *S. aureus* SK8250 cells was visualised by tagging with TetR-GFP using a fluorescent repressor-operator system. Expression of *tetR-gfp* from pSK9142 ($P_{spac}::tetR-gfp$) was induced with 0.1 mM IPTG (Section 5.8.4). Cells were grown to mid-exponential phase and then treated with 25 μ g/ml chloramphenicol for 1 h to condense nucleoids (Section 2.11.2). Nucleoid DNA was stained with DAPI, and cells were prepared for epifluorescence microscopy as described in Section 2.11.2. Cells in each of (A) and (B) are biological replicates. From top left to bottom right: TetR-GFP; DNA; bright-field (BF); overlay of TetR-GFP and DNA; overlay of bright-field (BF) and TetR-GFP; overlay of bright-field (BF), TetR-GFP and DNA. Arrowheads indicate cells containing plasmid foci that appeared to associate with condensed nucleoids. Asterisks indicate cells containing plasmid foci that did not appear to associate with condensed nucleoids. Scale bar = 1 μ m.

A. *S. aureus* (*par*, $60\times tetO$) + TetR-GFP + 0.1 mM IPTG + Cm25

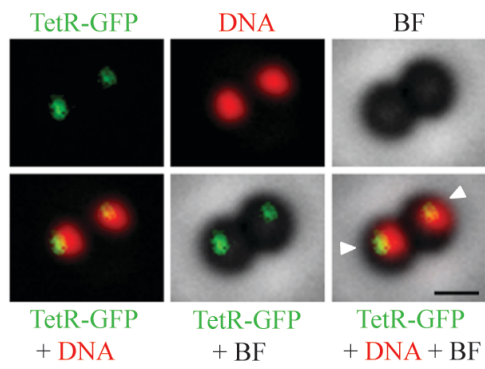
i.



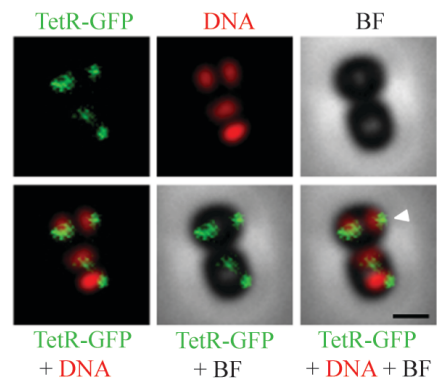
ii.



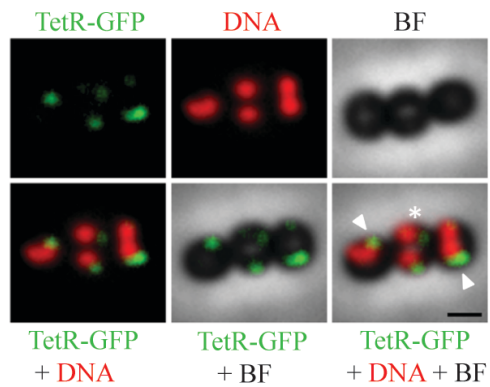
iii.



iv.

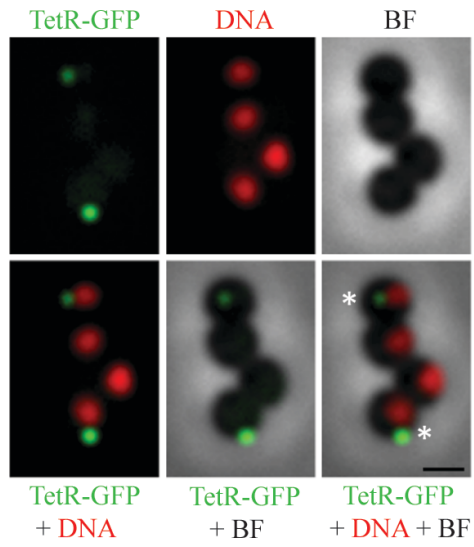


v.

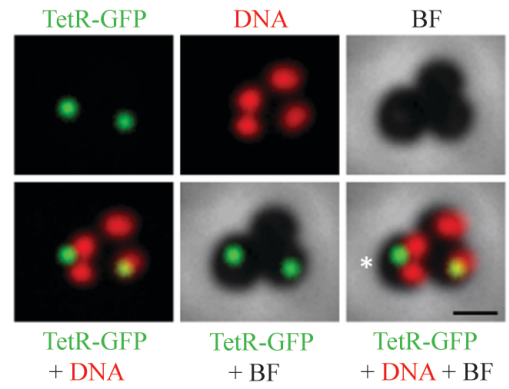


B. *S. aureus* (Δpar , $60\times tetO$) + TetR-GFP + 0.1 mM IPTG + Cm25

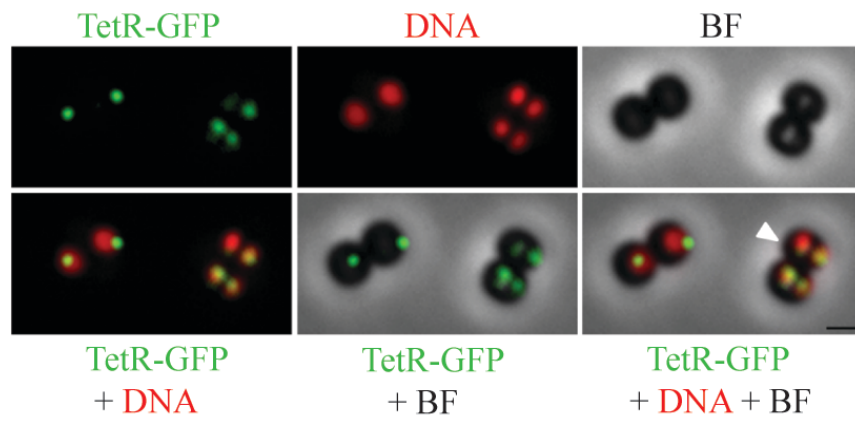
i.



ii.



iii.



condensed nucleoids. This apparent association was highlighted by the displacement of TetR-GFP foci away from the cell periphery and towards the centre of the cell, where the nucleoids had condensed (Figures 5.30Ai–v, arrowheads). However, examples were also observed whereby an association of TetR-GFP with nucleoid DNA was less pronounced (Figure 5.30Av, asterisk). In the absence of *par*, a number of examples showed an obvious space between TetR-GFP foci and condensed nucleoid DNA (Figure 5.30Bi–ii, asterisks), however, an apparent association was also observed in some cells (Figure 5.30Biii, arrowhead). The results from the chloramphenicol treatment of *S. aureus* nucleoids are, therefore, inconclusive and do not provide strong evidence of an association between plasmid DNA and chromosomal DNA, in the presence or absence of *par*.

5.8.7 Time-lapse epifluorescence microscopy of plasmid localisation in *S. aureus*

One of the advantages of implementing FROS for the localisation of plasmid DNA in live *S. aureus* cells is the ability to track plasmid localisation over time. Time-lapse epifluorescence microscopy was performed on *S. aureus* cells carrying the pairs of FROS plasmids, with and without *par*, to determine the localisation of pSK1 minireplicons during the cell cycle. FROS experiments were performed as described above in Section 5.8.4, and fluorescence micrographs were captured at 1 min intervals for up to 6 min.

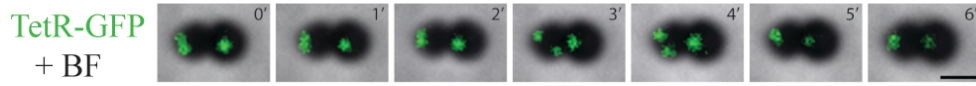
The series of micrographs presented in Figures 5.31Ai–iv, and shown as movies in Supplementary Movies 1–4, depicts the localisation of pSK9144 (*par*, 60×*tetO*) (Table 2.2) in *S. aureus* SK8250 cells over time. In the presence of *par*, TetR-GFP

Figure 5.31 Time-lapse microscopy of the fluorescence localisation of pSK1 minireplicons in *S. aureus* cells by tagging with TetR-GFP

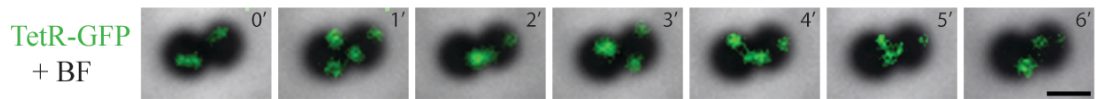
The localisation of pSK1 minireplicons pSK9144 (*par*, 60×*tetO*) (**Ai-iv**) and pSK9145 (Δ *par*, 60×*tetO*) (**Bi-iii**) in mid-exponential phase *S. aureus* SK8250 cells was visualised by tagging with TetR-GFP using a fluorescent repressor-operator system. Expression of *tetR-gfp* from pSK9142 ($P_{spac}::tetR-gfp$) was induced with 0.1 mM IPTG (Section 5.8.4). Cells were prepared for epifluorescence microscopy as described in Section 2.11.2, and images were taken at 1 min intervals for up to six minutes (0'–6'). Cells in each of (A) and (B) are biological replicates. Images shown are overlays of bright-field (BF) and TetR-GFP micrographs. Scale bar = 1 μ m. Movies of time-lapse micrographs are shown in Supplementary Movies 1–7.

A. *S. aureus* (*par*, 60×*tetO*) + TetR-GFP + 0.1 mM IPTG

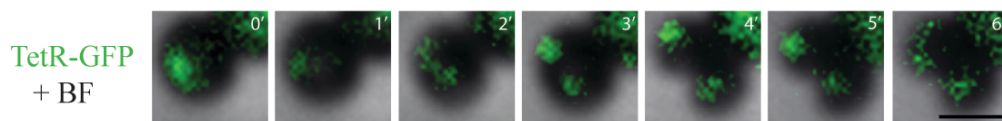
i.



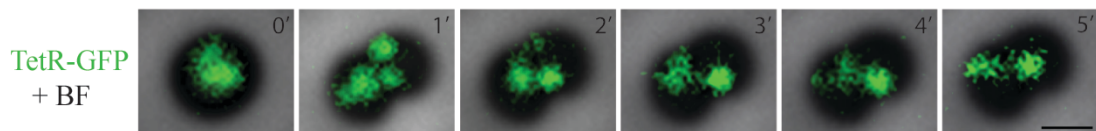
ii.



iii.

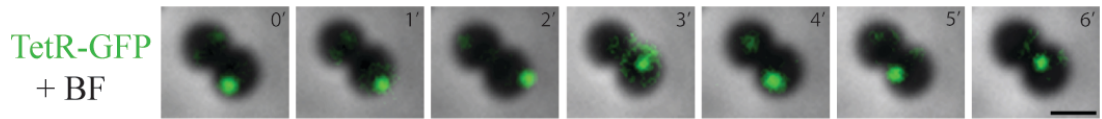


iv.

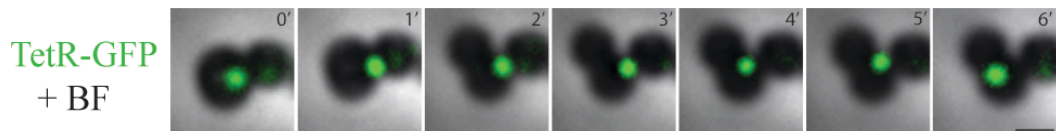


B. *S. aureus* (Δpar , $60\times tetO$) + TetR-GFP + 0.1 mM IPTG

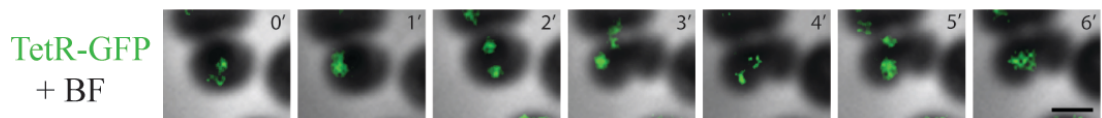
i.



ii.



iii.



foci, and hence plasmid DNA, were either static or confined to a small area, and appeared to have a restricted trajectory predominantly along the cell periphery (Figures 5.31Ai–ii; Supplementary Movies 1–2). Plasmid foci were observed to converge and separate during the time-lapse experiments, and thus the number of plasmid foci varied during the cell cycle (Figures 5.31Ai–ii and Biii; Supplementary Movies 1–2 and 7). In predivisional cells, which appeared larger than non-dividing cells, plasmid foci were located near the division site (and presumably near the division septum) and appeared as one larger, more intense focus, possibly representing a pair or cluster of replicated plasmids (Figures 5.31Aiii–iv, panel 0'; Supplementary Movies 3–4). The large focus then appeared to separate into two or more foci, which were segregated into individual daughter cells prior to cell division (Figures 5.31Aiii, panels 2'–4' and 5.31Aiv, panels 1'–3'; Supplementary Movies 3–4).

In contrast to the restricted movement of pSK1 minireplicons in the presence of *par*, the mobility of pSK9145 (Δpar , 60 $\times tetO$) (Table 2.2) seemed more unrestricted, and foci often appeared to traverse the cell diameter (Figure 5.31Bi; Supplementary Movie 5). The cumulative distance travelled by TetR-GFP foci during the observation period also seemed greater in the absence of *par* compared to when *par* was present, possibly suggesting that plasmid DNA moved more quickly and/or more freely in the absence of *par*. However, foci movement was not quantitated because the path of movement between time points was unknown, and hence, distance and velocity could not be determined with confidence.

Because many cells carrying pSK9142 ($P_{spac}::tetR-gfp$) and pSK9145 (Δpar , $60\times tetO$) contained no or only one TetR-GFP focus (Figures 5.29A–B), it was expected that plasmid segregation would be inefficient. Indeed, when predivisional cells contained a single focus, the pSK9145 plasmid focus did not separate into more foci, unlike what was observed for pSK9144 (above). Upon cell division, the single focus remained within the mother cell and was not inherited by the daughter cell (Figure 5.31Bii; Supplementary Movie 6). Even when two plasmid foci were observed, one daughter cell did not appear to inherit any plasmid focus (Figure 5.31Biii; Supplementary Movie 7), which demonstrates the reduced plasmid segregational stability of *par*-deficient pSK1 minireplicons. Photobleaching of TetR-GFP fluorescence signals prevented fluorescence localisation of plasmid DNA over more than one cell cycle.

5.9. Discussion

A summary of the results described in this chapter is presented in Table 5.1.

5.9.1 Fluorescence localisation of Par

Anti-Par peptide antibodies that were generated against two predicted antigenic Par peptides were shown to be reactive against the full-length Par protein (Figure 5.2A). Although the antibodies were affinity-purified against the peptides by the supplier (Mimotopes Pty Ltd), a number of non-specific protein bands were detected in Western blots of Par in *S. aureus* cell lysates (Figure 5.2A). The extraneous protein bands may have been caused by non-specific binding of *S. aureus* proteins to the anti-Par peptide antibodies. The *S. aureus* strain used for Western blot analyses, *S.*

Table 5.1 Summary of properties of Par derivatives (Chapter 5)

Protein	Plasmid stabilisation^a	Localisation^b	Association with nucleoid DNA^c	Protein interactions^d
RGSH ₆ -Par	No	N. D.	N. D.	N. D.
Par	N. D.	<i>E. coli</i> : Foci around cell periphery, possible filaments/helices/spirals	N. D.	N. D.
GFP-Par (P _{par})	No	<i>S. aureus</i> : Foci around cell periphery <i>E. coli</i> : Foci and patches around cell periphery; potential arcs at cell poles	<i>E. coli</i> : Yes, centromere-dependent	N. D.
Par-GFP (P _{par})	Partial	<i>S. aureus</i> : Foci around cell periphery <i>E. coli</i> : Foci at mid-cell or cell poles	<i>E. coli</i> : Yes, centromere-dependent	N. D.
GFP-ParK15A (P _{par})	N. D.	<i>E. coli</i> : Foci and patches around cell periphery	<i>E. coli</i> : No	N. D.
Δpar + Par (P _{spac}) <i>in trans</i>	Titrateable	N. D.	N. D.	N. D.
GFP-Par (P _{par}) + Par (P _{spac}) <i>in trans</i>	Titrateable	N. D.	N. D.	N. D.
Par-GFP (P _{par}) + Par (P _{spac}) <i>in trans</i>	Titrateable to wild-type levels with 0.5–1.0 mM IPTG	<i>S. aureus</i> : Foci around cell periphery in the presence and absence of Par	<i>S. aureus</i> : Possible	N. D.
Δpar + Par-GFP (P _{spac}) <i>in trans</i>	Titrateable	<i>S. aureus</i> : Foci around cell periphery	N. D.	N. D.

Table 5.1 Summary of properties of Par derivatives (Chapter 5) (continued)

Protein	Plasmid stabilisation^a	Localisation^b	Association with nucleoid DNA^c	Protein interactions^d
Par (P _{par}) + Par-GFP (P _{spac}) <i>in trans</i>	Yes	<i>S. aureus</i> : Foci around cell periphery	N. D.	N. D.
ParK15A (P _{par}) + ParK15A-GFP (P _{spac}) <i>in trans</i>	N. D.	<i>S. aureus</i> : Foci around cell periphery	N. D.	N. D.
ParΔCC (P _{par}) + ParΔCC-GFP (P _{spac}) <i>in trans</i>	N. D.	<i>S. aureus</i> : Disperse, cytoplasmic	N. D.	N. D.
Par-GFP (P _{spac}) (no centromere)	N. D.	<i>S. aureus</i> : Foci around cell periphery (0.1 mM IPTG); bright foci, possible bands/arcs (1.0 mM IPTG)	<i>S. aureus</i> : Possible	N. D.
GFP-Par (P _{tac}) (no centromere)	N. D.	<i>E. coli</i> : Foci around cell periphery, possible arcs at cell poles	<i>E. coli</i> : No	N. D.
GAL4 BD-ParFL	N. D.	N. D.	N. D.	GAL4 AD -ParFL, -ParGFP
GAL4 BD-ParGFP	N. D.	N. D.	N. D.	GAL4 AD -ParFL

^aPlasmid stabilisation ability assessed by plasmid segregational stability assays (Sections 5.3.4, 5.4.2, 5.4.4.2 and 5.4.5.2).

^bLocalisation assessed using epifluorescence microscopy (Sections 5.3–5.6).

^cAssociation with nucleoid DNA assessed by nucleoid condensation using chloramphenicol (25 µg/ml *S. aureus*; 300 µg/ml *E. coli*) (Sections 5.4 and 5.6).

^dProtein interactions assessed by yeast two-hybrid (Y2H) assays (Section 5.4.4.3).

N. D. Not determined in experiments described in Chapter 5.

aureus SK8250 (Table 2.1), is deficient in the expression of the immunoglobulin-binding protein, Protein A (Liu 2012), and indeed, bands of approximately 50 kDa and higher, corresponding to the sizes of Protein A and Protein A complexes, were not observed on the blots (Figures 5.2A–C). There remains, however, at least one other known immunoglobulin-binding protein in *S. aureus* – the 50 kDa protein, Sbi, which has been shown to interact with the Fc part of immunoglobulins (Zhang *et al.* 1998). Hence, the presence of at least one of the non-specific protein bands on Par Western blots might be explained by the binding of Sbi to anti-Par antibodies. Indeed, incubation of the blots with normal goat serum prior to incubation with the primary antibodies reduced background bands (Figures 5.2B–C), presumably due to the blocking of immunoglobulin-binding proteins with antibodies present in the goat serum. However, non-specific protein bands, at approximately 48 kDa and 58 kDa, were detected even in the presence of normal goat serum (Figures 5.2B–C). The detection of these bands may have been the product of cross-reactivity of anti-Par antibodies with *S. aureus* proteins.

The titration of anti-Par peptide antibodies shown in Figure 5.2C revealed that the detection of Par required relatively low antibody dilutions (1:100–1:1,000), which might have contributed to the potential cross-reactivity with *S. aureus* proteins. Whereas higher antibody dilutions might have minimized cross-reactivity, higher dilutions of the antibody resulted in reduced signal intensities for both Par and non-specific protein bands (Figure 5.2C), and hence the specificity of Par immunodetection using anti-Par peptide antibodies could not be improved without a loss in sensitivity. This could be due to a number of factors, such as low Par

expression levels, poor antigenicity of the Par peptides used for antibody production, or weak interaction between anti-Par peptide antibodies and Par epitopes.

When the anti-Par antibodies were applied in IFM of Par in fixed *S. aureus* cells, the antibodies were unable to specifically detect Par (Section 5.3.1). This was despite successful localisation of FtsZ by IFM (Figure 5.3D), which indicates that the IFM protocol was suitable for detection of proteins in *S. aureus*. Note that a considerably higher dilution of anti-FtsZ antibodies was used (1:20,000 compared to 1:100–1:10,000 tested for IFM of Par), probably due to higher levels of FtsZ in *S. aureus* and/or higher specificity of the antibodies for FtsZ, which would have minimised cross-reactivity with *S. aureus* proteins. Therefore, the inability to specifically detect Par in *S. aureus* using IFM was most likely due to a combination of low levels of Par protein in cells (as described in Section 3.2.2), low sensitivity of the anti-Par peptide antibodies, and cross-reactivity of the antibodies with non-specific *S. aureus* proteins (as shown on the Western blots in Figure 5.2C).

An epitope-tagged derivative of Par, RGS_{H6}-Par, was generated for its potential use in IFM using monoclonal anti-His antibodies against the epitope (Section 5.3.3). It was anticipated that monoclonal antibodies would provide greater sensitivity and potentially reduce the cross-reactivity experienced with polyclonal anti-Par peptide antibodies. Plasmid segregational stability assays revealed a lack of functionality of RGS_{H6}-tagged Par (Figure 5.4), which made it unsuitable for use in IFM as a substitute for Par. Given additional time, monoclonal antibodies could be generated against Par or predicted antigenic Par peptides, on the premise that monoclonal antibodies might be more specific to the target antigen, and that the absence of serum

components might reduce cross-reactivity with non-specific *S. aureus* proteins. However, it is anticipated that low Par expression levels in *S. aureus* would remain a major challenge in future IFM attempts.

It was unexpected that the relatively small-sized RGSH₆ tag would interfere with Par functionality, especially since DNA-binding and multimerisation activities had been demonstrated *in vitro* for purified RGSH₆-Par proteins (Sections 3.4 and 3.5.1). In light of this, it should be stressed that the results described in Chapter 3 are still valid for characterising the functional activities of Par. The observed loss of functionality of RGSH₆-Par might have resulted from an alteration of DNA-binding, autoregulation or multimerisation activity. Nonetheless, these remain undeniably functional properties of Par.

The difficulties encountered with IFM of Par in *S. aureus* were not experienced when IFM of Par was performed in *E. coli*. This may have been due to the higher copy-number of pSK4829 (*par*) (Table 2.2) in *E. coli* compared to *S. aureus*, which allowed Par to be detected using relatively high dilutions (1:10,000) of the anti-Par peptide antibodies in IFM (Figures 5.19A and 5.20). The high antibody dilution may have reduced non-specific binding of the antibodies to *E. coli* proteins, which, in addition to the larger cell size, allowed for clear visualisation of Par foci as well as potential arcs, helices or spirals that were present only in cells producing Par (Figures 5.19Ai–ii). Although Par has not demonstrated functionality in *E. coli* (Davies, D. and Firth, N., unpublished data), the localisation of Par in this heterologous host may provide insights into the structural properties of Par *in vivo*, particularly with respect to filament formation, as suggested by data obtained from

electron microscopy of purified RGSH₆-Par (Barton, D. A., Jensen, S. O. and Firth, N., unpublished data).

Deconvolution of IFM images of Par in *E. coli* revealed potential 3-dimensional structures, such as helices or spirals (Figures 5.20A–C), that were reminiscent of those observed for ParA and SopA of the Type Ia plasmid partitioning system (Ebersbach and Gerdes 2004, Adachi *et al.* 2006, Ringgaard *et al.* 2009). No helical or spiral patterns were detected for Par-GFP in *S. aureus*, except perhaps when Par-GFP was maximally induced from pSK9097 in the absence of centromere DNA (Figures 5.17Ci–iii). The inability to readily detect Par-GFP filaments in *S. aureus* may have been due to the significantly fainter levels of fluorescence detected, which may have resulted in the detection of foci and not fainter structures. Furthermore, fluorescence detection of structures in spherical *S. aureus* cells could have been improved by obtaining images along the z-axis of the cells, followed by deconvolution of the image stacks to visualise fluorescence from multiple planes, as performed for IFM of Par in *E. coli*. However, the faint fluorescence of Par-GFP resulted in rapid photobleaching, which prevented the acquisition of z-stacks. Of course, it is also possible that the helical or spiral structures observed in *E. coli* do not exist in *S. aureus*, and were instead the product of Par overproduction in a heterologous host.

It should also be noted that, although filamentous structures appear to have been observed in *E. coli* (Figures 5.19Ai–ii and 5.20A–C), and also potentially in *S. aureus* when Par-GFP was overproduced from pSK9097 in the absence of centromere DNA (Figure 5.17Ci–iii), it is unclear whether these patterns represent

true Par filaments or unresolved Par foci that were proximally located. Indeed, there is uncertainty about whether ParA forms filaments, or only short polymers or multimers, *in vivo* (Vecchiarelli *et al.* 2012). Interpretation of Par localisation patterns is limited by the spatial resolution of conventional wide-field epifluorescence microscopy, which has an optical resolution of 180–700 nm (Schermelleh *et al.* 2010). Since the width of *E. coli* cells and the diameter of *S. aureus* cells is only approximately 1 μm , resolution of the spatial localisation of subcellular proteins is undoubtedly limited. Super-resolution microscopy methods, such as 3-dimensional structured illumination microscopy (3D-SIM) or cryo-electron tomography (cryo-ET), provide optical resolutions of approximately 100–300 nm and 5 nm, respectively (Murphy and Jensen 2007, Gustafsson *et al.* 2008). 3D-SIM has been useful for the visualisation of the ring structure formed by FtsZ-GFP in *S. aureus* (Strauss *et al.* 2012, Turnbull *et al.* 2014), while cryo-ET has been used to visualise R1 ParM bundles in *E. coli* (Bharat *et al.* 2015). Both methods have provided more detailed images than can be achieved by conventional fluorescence microscopy. Super-resolution microscopy techniques could, therefore, provide increased resolution and sharper images to confirm the presence or absence of filamentous Par structures in *E. coli* and, more importantly, in *S. aureus*.

The fusion of GFP to Par enabled a representative visualisation of Par localisation in live *S. aureus* cells. Ideally, the localisation of Par GFP fusions would correlate to the localisation of Par as determined by IFM. However, because the cellular localisation of Par in fixed *S. aureus* cells could not be specifically detected using IFM (Section 5.3.1), it cannot be assumed with absolute confidence that the localisation patterns of Par GFP fusions in live *S. aureus* cells are accurate

representations of Par localisation. It should also be emphasised that Par-GFP was shown to exhibit reduced functionality (Figure 5.6B), and that even though the impaired functionality of the *par-gfp* partitioning system on pSK9088 (Table 2.2) could be complemented with the supply of Par *in trans* from pSK9104 (Table 2.2) (Figure 5.8C), the components of this system were produced in a non-natural arrangement that differs from the wild-type genetic organisation pSK1 *par*. Therefore, without IFM data to verify the localisation of Par-GFP in *S. aureus*, it is imperative that the above considerations are noted and that subsequent analyses of Par-GFP localisation patterns are interpreted cautiously.

Plasmid segregational stability assays showed that GFP-Par was non-functional, whereas Par-GFP was partially functional (Figure 5.6B). The expression of both proteins was confirmed by Western blotting of *S. aureus* cell lysates (Figure 5.6A), which indicates that the lack of plasmid segregational stability was a result of impaired protein function and not the complete absence of protein. The reduced functionality of Par GFP fusions was not unexpected, as the addition of GFP (27 kDa) to Par (29 kDa) probably caused disruptions to Par protein folding or protein interactions, which may have resulted in the observed reduction in partitioning function. It is interesting to note that N-terminal fusions to Par, for example with RGSH₆ or GFP, both resulted in a loss of Par function (see Figures 5.4 and 5.6B), which is perhaps suggestive of a disruption to the N-terminal HTH domain and DNA-binding activity. Alternative fusions of tags to Par could be generated, using different linker compositions, lengths and insert positions, to try to minimise disruption to Par function, such that a functional Par GFP fusion protein can be used for localisation studies.

The pSK1 minireplicons pSK9088 ($P_{par}::par-gfp$) (Table 2.2) and pSK9087 ($P_{par}::gfp-par$) (Table 2.2) displayed dose-dependent increases in segregational stability with IPTG induction of Par expression from a co-resident plasmid, pSK9104 ($P_{pac}::par$) (Table 2.2) (Figures 5.8B–C). The segregational stability of pSK9088 ($P_{par}::par-gfp$), but not pSK9087 ($P_{par}::gfp-par$), could be improved to the stability level of pSK4829 (par) (Table 2.2) with maximum induction of Par expression (0.5 mM and 1 mM IPTG) (Figures 5.8B–C). Western blot analyses verified the inducible production of Par from pSK9104 (Figures 5.9B–C), indicating that the increase in plasmid stability was the result of an increase in Par protein levels. Although increasing IPTG concentrations should have corresponded to increasing amounts of Par, uneven sample loading might not have clearly demonstrated Par titration in the Western blots (Figures 5.9B–C). The blots nonetheless show that Par was induced in the presence of IPTG, and the effect of increasing levels of Par induction was reflected in the stability assays in Figures 5.8B–C.

Because a loading control was not used for quantifying relative protein amounts from the Western blots in Figures 5.9B–C, it is unclear whether increasing IPTG concentrations also resulted in an increase in GFP-Par levels. The apparent overexpression of GFP-Par compared to WT Par, at all Par induction levels, may have contributed to the lower stability of pSK9087 ($P_{par}::gfp-par$) compared to pSK9088 ($P_{par}::par-gfp$), since overexpression of partitioning proteins have been shown to result in plasmid instability (Funnell 1988a).

With regard to the improved segregational stability of pSK9088, the nature of the contribution of Par to the observed increase is unclear. However, it may be the result of direct interaction between Par and the centromere-like site on pSK9088, and/or interaction of Par with partially functional Par-GFP to improve DNA-binding, autoregulation or multimerisation activities. Previous studies have shown that Par, when expressed from the chromosome, is functional *in trans* as an autorepressor of P_{par} (LeBard 2005). Therefore, it is conceivable that the potential *in trans* autoregulation of *par-gfp* on pSK9088 by Par from pSK9104 ($P_{spac}::par$), may have contributed to the increased plasmid stability. Although interestingly, no obvious *in trans* repression of GFP-Par (Figure 5.9B) or Par-GFP (Figure 5.9C) expression was observed by Western blotting of lysates from *S. aureus* cells producing Par *in trans* to pSK9087 or pSK9088, respectively. At the least, since Par alone was unable to fully complement the unstable, *par*-deficient plasmid, pSK4833 (Figure 5.8A), *in trans*, it appears that a *cis*-acting protein, in this case Par-GFP of pSK9088, or alternatively, higher overall protein levels, is required for complete complementation of the partial functionality of a *trans*-acting Par protein.

Since the fluorescence localisation of Par-GFP should be representative of Par localisation in this artificial, yet seemingly functional, plasmid stability system, it was important to demonstrate interaction of Par from pSK9104 ($P_{spac}::par$) with components of the *par-gfp* partitioning system on pSK9088. To this end, the Y2H and α -galactosidase assays performed in Section 5.4.4.3 showed interaction between Par and Par-GFP bait and prey fusion proteins (Figures 5.10A–B), which suggests that the increased segregational stability of pSK9088 might have involved interaction of Par with Par-GFP. Except for the apparent stabilising effect of Par on pSK9088

(Figure 5.8C), no direct evidence has been obtained for the interaction of Par with Par-GFP *in vivo* under the conditions used for fluorescence localisation studies. *in vivo* cross-linking experiments using DSP on *S. aureus* cells expressing Par and Par-GFP were attempted (data not shown), however, as demonstrated by Figure 3.8B, *in vivo* cross-linking in *S. aureus*, and the subsequent detection of cross-linked Par complexes, was difficult to interpret due to non-specific background bands. Problems were compounded by the potential sizes of Par:Par-GFP complexes, which would depend on the ratio of Par and Par-GFP in cross-linked complexes. As an alternative, to elucidate whether Par and Par-GFP interact in *S. aureus*, immunoprecipitation experiments (Bonifacino *et al.* 2001) could be performed on *S. aureus* cells harbouring pSK9088 ($P_{par}::par-gfp$) and pSK9104 ($P_{spac}::par$) using either anti-Par or anti-GFP antibodies to isolate and precipitate potential Par:Par-GFP complexes that may have formed *in vivo*.

When Par-GFP, produced from pSK9088, was supplied *in trans* with Par to increase plasmid stability, fluorescent foci were observed around the periphery of *S. aureus* cells (Figures 5.12Bi–ii). The localisation pattern of some Par-GFP foci appeared reminiscent of Spo0J-GFP localisation, which marked the cell poles at the tips of elongated nucleoid lobes (Figures 5.11i–ii). Although this localisation pattern was not observed for all Par-GFP foci, it is possible that Par-GFP may have localised to the cell poles at specific stages of plasmid partitioning. Nonetheless, it was difficult to discern the spatial organisation of these foci with respect to subcellular structures. This was largely due to the small, coccoid shape and orthogonal mode of staphylococcal cell division (Tzagoloff and Novick 1977), which presented challenges for the identification of cell orientation without co-visualisation of other

subcellular components. Although staining of the nucleoid with DAPI aided in the identification of cell orientation, it would be useful to perform simultaneous fluorescence localisation of Par-GFP and fluorescently-tagged cell division proteins, such as FtsZ or EzrA, which have previously been localised in *S. aureus* (Pereira *et al.* 2010, Veiga *et al.* 2011). Cell structures such as the cell membrane or cell wall, could also be stained using fluorescent dyes such as Nile Red and the fluorescent vancomycin derivative, Van-FL, respectively. The dual visualisation of Par-GFP and other fluorescently-tagged proteins in *S. aureus* might present challenges due to the presence of two existing plasmids (pSK9088 and pSK9104) in the *S. aureus* strain used for Par-GFP localisation. Coordination of dual visualisation would require consideration of the compatibilities of origins of replication, antibiotic selection, promoters, inducers and inducer levels. A balance of protein induction levels would need to be achieved for optimal visualisation of both proteins, whilst minimising potential interference with the *par-gfp* plasmid segregational stability system.

It was expected that the increased segregational stability of pSK9088 ($P_{par}::par-gfp$) in the presence of Par might result in different Par-GFP localisation patterns compared to patterns observed in the absence of Par. However, no obvious differences were detected (Figures 5.7A–B and 5.12A–B). It may be that the localisation of Par-GFP was not affected by differences in the stability of pSK9088 in the presence and absence of Par, and that other factors, such as DNA-binding, autoregulation or multimerisation, might have been affected by the partially-functional *par-gfp* system. It is also important to note that the fluorescence localisation of Par-GFP was only captured at a single point in time, and hence further insight into the potential effects of Par on the localisation of Par-GFP might be

achieved by performing time-lapse fluorescence microscopy to track Par-GFP localisation over the course of the cell cycle. Unfortunately, due to faint fluorescence signals from Par-GFP, time-lapse experiments caused significant photobleaching of GFP fluorescence, which made interpretation of localisation difficult.

Furthermore, the localisation of Par-GFP from pSK9088 ($P_{par}::par-gfp$), in the presence or absence of Par (Figures 5.7A–B and 5.12A–B), did not appear to differ dramatically from that of Par-GFP when produced in the absence of the pSK1 *par* centromere-like site (pSK9097) (Figures 5.17Ai–ii), or when Par-GFP was produced *in trans* to the centromere-like site on pSK4829 (*par*) or pSK4833 (Δpar) (Figures 5.16A–B). The localisation of the DNA-binding mutant derivative, ParK15A-GFP, was also similar to that of Par-GFP (Figure 5.16C). In all cases, Par-GFP and ParK15A-GFP appeared as foci, which were most likely formed as the result of Par multimerisation via the CC domain, since Par Δ CC-GFP did not form foci and showed only diffuse fluorescence (Figure 5.16D). This confirmed that Par-GFP foci were not artefacts of GFP aggregation, a problem that has resulted in misinterpretation of the localisation of some proteins (Landgraf *et al.* 2012). The absence of Par Δ CC-GFP foci is consistent with *in vitro* cross-linking data, which suggests that the CC domain is crucial for Par multimerisation (Lai 2008). The epifluorescence microscopy observations presented here, therefore, provide *in vivo* evidence of the role of the CC domain in Par multimerisation. Furthermore, the observation of fluorescent foci for ParK15A-GFP (Figure 5.16C), and for Par-GFP when produced in the absence of the centromere-like site (Figures 5.17Ai–ii), implies that focus formation is independent of the presence of centromere DNA and DNA-binding activity. The implications of these observations for the mechanism of

par-mediated plasmid partitioning are discussed further in Chapter 6. Note that it remains to be shown that Par-GFP binds directly to centromere DNA on pSK1 minireplicons. To investigate this, EMSAs should be performed to assess the DNA-binding of Par-GFP to radiolabelled probes containing the pSK1 *par* centromere-like site, as described for the EMSAs performed on purified RGSH₆-Par proteins in Section 3.4. Ultimately, dual localisation of plasmid DNA and Par would be required to verify whether Par-GFP binds to plasmid DNA. However, dual localisation would require re-consideration of the experimental designs used to individually localise Par and plasmid DNA in this study.

The potential association of Par-GFP and TetR-GFP plasmid foci with *S. aureus* nucleoid DNA was explored by observing the localisation of these fluorescent foci following condensation of nucleoids using chloramphenicol. The results from the nucleoid condensation experiments were inconclusive (Figures 5.13A–B, 5.17B–C and 5.30A–B), although it is important to note that the observed localisation of Par-GFP or TetR-GFP foci relative to nucleoid DNA was likely influenced by the stage of cell division and plasmid partitioning at the time of image capture, as well as the orientation at which the cells were viewed. While there appeared to be some clear examples of a close association between condensed nucleoids and Par-GFP or TetR-GFP, this was not the case for all condensed nucleoids, regardless of whether Par was present (Figures 5.13A–B, 5.17B–C and 5.30A–B). If indeed an association did exist, it would not be unreasonable to suggest that the foci would not remain associated with the nucleoid at all times during the cell cycle.

Sometimes, it was unclear whether fluorescent Par-GFP or TetR-GFP foci were associated with condensed *S. aureus* nucleoids. This was in contrast to the nucleoid condensations performed in *E. coli*, which clearly showed an association of GFP-Par and Par-GFP with nucleoid DNA, and that the association was dependent on the presence of the centromere-like site and DNA-binding activity (Figures 5.23B and 5.24). As described above, the small size of *S. aureus* cells is a major limitation to the spatial resolution of subcellular objects using conventional light microscopy techniques. Therefore, super-resolution microscopy might be better suited for the visualisation of Par-GFP and TetR-GFP localisation with respect to the edges of *S. aureus* nucleoids. In this regard, 3D-SIM might be able to resolve fluorescent foci and edges of the nucleoid to determine whether the foci colocalise with parts of the nucleoid.

Another method that could be used for the detection of associations between fluorescent foci and nucleoid DNA is fluorescence resonance energy transfer (FRET) (Förster 1948). FRET has been used to detect protein-DNA (Cremazy *et al.* 2005) and protein-RNA (Lorenz 2009) interactions by fluorescence microscopy. Cremazy *et al.* (2005) used the SytoxOrange nucleic acid stain as the FRET energy acceptor, which was excited by the emission energy transferred from nearby DNA-binding proteins fused to GFP and YFP energy donors. It is, therefore, conceivable that FRET could be used to determine whether Par-GFP or TetR-GFP is located within close proximity of the nucleoid. Potential associations of Par-GFP (and Par) with nucleoid DNA could also be investigated using *in vitro* methods, such as chromatin immunoprecipitation, for the identification of potential chromosome binding sites (Collas 2010).

5.9.2 Fluorescence localisation of plasmid DNA

In cells carrying the functional *par-gfp* system, with Par provided *in trans*, the number of Par-GFP foci per cell (Figures 5.18A–B) could be expected to correlate with the number of TetR-GFP plasmid foci observed for pSK9144 (*par*, 60×*tetO*) (Table 2.2) in FROS experiments (Figures 5.29A–B). This assumes that all Par-GFP foci represented plasmids bound by Par-GFP. However, it cannot be verified that all Par-GFP proteins were bound to the centromere DNA, and since it was shown that the centromere DNA and DNA-binding activity were not required for the formation of Par-GFP foci (Figures 5.16C and 5.17Ai–ii), the observed foci might, therefore, represent a mix of Par-GFP proteins that were bound to plasmids, and Par-GFP multimers that were not engaged in DNA-binding. In contrast, TetR-GFP foci were only observed in the presence of *tetO* arrays (Section 5.8.4), and hence it is almost certain that all TetR-GFP foci represented TetR-GFP proteins bound to plasmid DNA. Furthermore, the functionality of *par* in enhancing the segregational stability of pSK1 minireplicons containing the *tetO* array was demonstrated by plasmid segregational stability assays of pSK9144 (*par*, 60×*tetO*) and pSK9145 (Δ *par*, 60×*tetO*) (Table 2.2) in *S. aureus*, which also showed that the production of TetR-GFP from pSK9142 (Table 2.2) did not affect plasmid stability (Figure 5.27). Overall, the distribution of the number of Par-GFP and TetR-GFP foci per cell appears consistent between the populations, and both data sets showed a significantly higher proportion of cells containing two foci when Par was present (Figures 5.18A–B and 5.29A–B). However, for the reasons mentioned above, plasmid localisation would most accurately be represented by the localisation of TetR-GFP rather than

Par-GFP, and therefore subsequent analyses of plasmid localisation were carried out using data obtained from the FROS experiments performed in Section 5.8.4.

The issues raised previously regarding the challenges of determining the spatial organisation of Par-GFP foci with respect to subcellular components also apply to the localisation of TetR-GFP foci. Namely, that the localisation of TetR-GFP foci and analysis of focus numbers may be influenced by the small size of *S. aureus* cells, which imposes limitations on the resolution of TetR-GFP foci using conventional microscopy techniques. With respect to the analysis of TetR-GFP focus numbers, it should be taken into consideration that due to the spherical shape and random orientation of *S. aureus* cells, the single focal plane imaged may have excluded foci located at other points along the z-axis of the cells. To ensure that foci in all planes can be visualised, images could be taken at various points on the z-axis to obtain a z-stack, which can then be deconvolved, as performed for IFM of Par in *E. coli* (Section 5.5). However, the fluorescence intensity of foci in *S. aureus* cells was relatively low compared to the fluorescence detected from *E. coli* cells, and thus problems with photobleaching would need to be overcome. Furthermore, counts of TetR-GFP foci were performed on images captured at a single point in time, and time-lapse microscopy showed that the number of plasmid foci varied during the cell cycle (Figures 5.31Ai–ii and Biii). However, it was anticipated that the scoring of TetR-GFP focus numbers from a large sample of cells ($n > 1,300$) would account for variations in cell orientation and stages of the cell cycle.

Since TetR-GFP binds to the *tetO* arrays located on pSK1 minireplicons, it was expected that the number of TetR-GFP foci per cell would correspond to the

approximate copy-number of pSK1 minireplicons, which is estimated to be 3–10 copies per cell (Grkovic *et al.* 2003, LeBard 2005). However, the majority of cells contained fewer than 3 plasmid foci per cell (Figures 5.29A–B), which suggests that each plasmid focus represented multiple plasmids. The discrepancy between observed focus numbers and expected plasmid copy-numbers has also been noted for other plasmids, for example P1 (Li and Austin 2002, Gordon *et al.* 2004), F (Gordon *et al.* 2004), RK2 (Pogliano *et al.* 2001) and pUC19 (Pogliano *et al.* 2001). It is possible that the plasmid foci represented plasmid clustering, either by physical linking of plasmid molecules, or the colocalisation of multiple plasmids at a specific site in the cell. Intriguingly, it would appear that the supposed plasmid clusters form independently of *par*, since bright plasmid foci were also observed for pSK1 minireplicons lacking *par* (Figures 5.28Di–v).

In *S. aureus* cells harbouring pSK1 minireplicons containing the full *par* system (pSK9144) (Table 2.2), most cells ($37\pm 2\%$) showed two plasmid foci that were evenly distributed between cell hemispheres (Figure 5.28Bii, right cell and Figure 5.28Biii, left cell). When only one focus was present ($24\pm 3\%$ of cells), the focus was usually of bright intensity and located in the septal region (Figure 5.28Bi, bottom cell). The plasmid localisation described here is supported by data obtained from time-lapse microscopy, which showed that *par*⁺ plasmids were clustered as one plasmid focus located near the site of cell division (Figures 5.31Aiii–iv, panel 0'). The single focus then separated into two or more new foci, which were segregated into daughter cells prior to cell division, resulting in the inheritance of at least one plasmid focus by each daughter cell (Figure 5.31Aiii, panels 2'–4' and Figure 5.31Aiv, panels 1'–3'). A similar sequence of events has been described for the Type

Ia *parABS* system of P1 and for the *par2* system of pB171 in *E. coli* cells, whereby a single plasmid focus is positioned at midcell, before the focus is fragmented into two new foci, which are segregated into the daughter cells immediately before cell division (Li and Austin 2002, Ebersbach and Gerdes 2004).

Due to the spherical shape and random orientation of *S. aureus* cells, the localisation of *par*⁺ plasmid foci at mid-cell was not easily recognisable. For example, the plasmid foci in cells shown in Figure 5.31Aiv, appear to have been located at mid-cell prior to plasmid segregation, whereas plasmid foci in Figure 5.31Aiii may or may not have been positioned at mid-cell. Covisualisation of plasmid DNA with markers of cell orientation, such as FtsZ or EzrA (Pereira *et al.* 2010, Veiga *et al.* 2011), may aid in the localisation of plasmid foci relative to division septa. Nevertheless, based on the direction of cell division, it is conceivable that *par*⁺ plasmid foci were located in the vicinity of the division septum, which is consistent with observations described for Type Ia partitioning systems (Li and Austin 2002, Ebersbach and Gerdes 2004).

The majority of cells carrying pSK1 minireplicons that lacked *par* (pSK9145) (Table 2.2), did not contain any plasmid foci (Figure 5.29A). However, of the cells that did contain plasmid foci, a larger proportion of cells contained one focus compared to any other number of foci (Figure 5.29B). The proportion of cells containing one plasmid focus was also significantly higher for cells carrying pSK9145 (Δpar , 60 $\times tetO$) compared to pSK9144 (*par*, 60 $\times tetO$) (Figure 5.29B). The prevalence of cells containing only one plasmid focus for partition-deficient plasmids could be the result of plasmid loss due to segregational instability (Figure 5.27), and/or reduced

copy-number of *par*⁻ compared to *par*⁺ plasmids. The copy-number of the *tetO*-containing pSK1 minireplicons, pSK9144 and pSK9145, have yet to be determined, and could be calculated using gel electrophoresis and densitometric analysis of plasmid DNA bands (Projan *et al.* 1983, Pushnova *et al.* 2000), or using quantitative PCR methods (Lee *et al.* 2006) to establish whether pSK9144 and pSK9145 copy-numbers differ. Although, as described above, the number of fluorescent plasmid foci did not appear to reflect plasmid copy-number, and hence the high proportion of cells carrying one pSK9145 plasmid focus could be independent of plasmid copy-number.

Time-lapse microscopy showed that, unlike *par*⁺ plasmids, partition-deficient plasmid foci (pSK9145) failed to separate into new foci prior to cell division, and consequently, one daughter cell was left without any plasmid focus (Figures 5.31Bii–iii). This was similar to observations of plasmid mis-segregation in the absence of functional P1 *parABS* or pB171 *par2* partitioning systems in *E. coli* (Li and Austin 2002, Ebersbach and Gerdes 2004). In these studies, *E. coli* cells carrying partition-deficient plasmids contained a single plasmid focus, which was inherited by only one daughter cell following cell division (Li and Austin 2002, Ebersbach and Gerdes 2004). The time-lapse microscopy of cells carrying pSK9145 (Δpar , $60\times tetO$), therefore, demonstrated the inability of a single plasmid focus to separate into new foci in the absence of *par*. This might explain the absence of plasmid foci in most cells and the prevalence of cells carrying one pSK9145 focus (Figures 5.29A–B). Similarly, the effect of *par* on plasmid segregation is likely reflected in the significantly higher proportion of cells containing two pSK9144 (*par*, $60\times tetO$) plasmid foci (Figure 5.29A–B), which were conceivably derived from the separation

of a single plasmid focus into two new foci, in preparation for segregation into daughter cells.

It is also interesting to note that pSK9145 (Δpar , $60\times tetO$) plasmid foci appeared to move more quickly and in a more unrestricted fashion compared to pSK9144 (par , $60\times tetO$) plasmid foci, which appeared to have restricted movement (compare Figures 5.31Bi and 5.31Ai-ii). This phenomenon was also observed in studies of the partitioning systems of F, P1 and RK2 plasmids, which showed that partition-deficient plasmids were more mobile than par^+ plasmids (Gordon *et al.* 2004, Derman *et al.* 2008). Analysis of the localisation of pSK1 minireplicons using particle-tracking software may be able to provide quantitative information about plasmid displacement, such as the total distance travelled by plasmid foci, and the rate of plasmid movement. However, tracking plasmid foci in *S. aureus* may be challenging using conventional fluorescence microscopy, for reasons mentioned previously, and hence the use of super-resolution microscopy might be more suitable for this purpose. As discussed further in Chapter 6, a restriction in the movement of par^+ plasmid foci might suggest anchoring of plasmid DNA to subcellular structures.

In light of the data obtained from FROS experiments, the correlation between Par-GFP localisation and Par functionality remains ambiguous. This is partly due to the indistinguishable localisation patterns of Par-GFP foci in *S. aureus* cells, regardless of whether the $par-gfp$ partitioning system on pSK9088 (Table 2.2) was complemented *in trans* with Par (Section 5.4.4.4). Furthermore, as explained earlier, it is possible that not all Par-GFP foci were bound to plasmid DNA. It would, therefore, be interesting to simultaneously localise Par and plasmid DNA to illustrate

the role of DNA-binding in plasmid partitioning, *in vivo*. However, given that the setup used for the localisation of Par-GFP and plasmid DNA in *S. aureus* each involves two plasmids, it would be unfeasible to introduce both pairs of plasmids into *S. aureus* cells for dual localisation studies. Similarly, localisation of Par-GFP from pSK9088 required titration with WT Par from pSK9104 (see Section 5.4.4). Hence, dual localization of Par-GFP with fluorescently-labelled staphylococcal cell division markers, such as DivIVA or Spo0J, although desirable, would be difficult using the present plasmid configurations. One alternative could involve the expression of one or more components of the Par or plasmid localisation systems from the chromosome. In any instance, careful consideration would be required for the generation of an *S. aureus* strain that enables visualisation of stable pSK1 minireplicons carrying *par*, in the presence of functional, fluorescently-tagged Par protein.

Unfortunately, the fluorescence localisation of pSK1 minireplicons using FROS could not be independently verified using FISH. Despite varying many parameters, FISH was unsuccessful in the detection of pSK1 minireplicons in fixed *S. aureus* cells (Section 5.7). The use of FISH for the localisation of low copy-number plasmids in *S. aureus* is not widely reported in the literature, and most FISH protocols for *S. aureus* describe the detection of high-copy 16S rRNA for the identification or localisation of whole *S. aureus* cells (Kempf *et al.* 2000, Poppert *et al.* 2010, Lawson *et al.* 2011a, Lawson *et al.* 2011b). The low copy-number of the pSK1 minireplicons used in this study (approximately 3 copies per cell for pSK4829) (LeBard 2005) might have been a significant factor in the inability to detect the plasmids using FISH. Furthermore, the labelling and/or specificity of the

probes might not have been sufficient for the hybridisation and subsequent detection of low copy-number plasmid DNA. Instead of generating probes from restriction digestion of pSK4833 DNA (Section 5.7), probes could be generated against multiple specific target sequences on the plasmid DNA, and alternative probe labelling methods could be trialled, such as the incorporation of fluorochrome-labelled dNTPs by PCR, nick translation or random primed labelling (Wiegant and Raap 2001). It might also be useful to verify the FISH protocol in *S. aureus* by using the Sau 16S69 probe specific for *S. aureus* 16S rRNA (Kempf *et al.* 2000).

Although the localisation of plasmids using FROS could not be verified by FISH, the observation of fluorescent foci only in the presence of *tetO*-containing plasmids (Figures 5.28B–D) indicates that the fluorescent foci were not non-specific aggregates of TetR-GFP, but rather, were formed as a result of TetR-GFP binding to the *tetO* array. Importantly, segregational stability assays confirmed the stabilising effect of *par* on *tetO*-containing plasmids, even in the presence of TetR-GFP binding (Figure 5.27). As such, the observed effect of *par* on the segregation of TetR-GFP foci into daughter cells strongly suggests that TetR-GFP foci were representative of plasmid clusters that could be influenced by *par*. It should be noted that although the time-lapse microscopy images presented in this study are representative and were reproducible in replicate experiments, the possibility cannot be excluded that plasmid segregation in other cells of the population may have exhibited a different sequence of events to those described here. Nonetheless, time-lapse microscopy has demonstrated the functionality of pSK1 *par* in the segregation of plasmid copies into daughter cells, and the mis-segregation of plasmids in the absence of *par*. However, the mechanism driving plasmid segregation remains unclear, and hence the

microscopy data will require supplementation with *in vitro* data on Par activity, such as those presented in Chapters 3 and 4, in order for the mechanism of *par*-mediated plasmid segregational stability to be understood. This will be discussed in detail in Chapter 6.

CHAPTER 6

General discussion

Low copy-number plasmids usually encode plasmid segregational stability determinants to ensure their accurate inheritance by daughter cells during bacterial cell division. A number of active plasmid partitioning systems have been described to date, and are generally classified under three different types, types I–III, according to the type of NTPase that they encode. In these systems, the partitioning locus consists of three components: a centromere-like site, and a bicistronic operon that encodes a centromere-binding protein (CBP) and a force-generating NTPase motor protein (Ebersbach and Gerdes 2005, Hayes and Barilla 2006, Schumacher 2008, Salje 2010, Baxter and Funnell 2014). A fourth potential type of plasmid partitioning system, *stbABC*, has also been described for the *E. coli* low copy-number plasmid, R388, which comprises a putative centromere-like site and the plasmid stability determinant, StbA (Guynet *et al.* 2011, Guynet and de la Cruz 2011).

In contrast to the separate CBPs and force-generating NTPases encoded by the types I–III partitioning systems, the *par* plasmid segregational stability determinant on the low copy-number staphylococcal multiresistance plasmid, pSK1, encodes only a single protein, Par (Simpson *et al.* 2003). Interestingly, previous work shows that the predicted HTH and CC domains of Par are critical to DNA-binding and Par multimerisation activity, respectively (Lai 2008). Both activities, which are central to the types I–III active plasmid partitioning systems (Ebersbach and Gerdes 2005, Hayes and Barilla 2006, Schumacher 2008, Salje 2010, Baxter and Funnell 2014),

are also essential for Par function in plasmid maintenance. However, the extraordinary feature distinguishing pSK1 *par* from typical plasmid partitioning systems is the demonstration of both DNA-binding and multimerisation activity by a single protein, instead of separate CBP and NTPase proteins. Therefore, the mechanism of plasmid segregation by pSK1 *par* clearly does not conform to the mechanisms used by conventional tripartite active plasmid partitioning systems.

In this chapter, the results presented in this thesis will be discussed in the context of deciphering the potential mechanisms employed by pSK1 *par* to mediate plasmid segregational stability. Understanding the mechanistic details of pSK1 *par* is paramount for the identification of suitable targets for the development of strategies to interfere with Par function and plasmid inheritance.

6.1. Functional significance of Par C-terminal domain in the partition complex

With regard to the role of Par domains in plasmid maintenance, the work conducted as part of this study focussed on determining the functional significance of the third putative domain of Par – the acidic and predicted disordered C-terminal domain (CTD). The predicted disordered nature of the Par CTD was implied by Simpson *et al.* (2003), and indeed, analysis of the Par amino acid sequence (GenBank Accession Number AAF63251) using the protein disorder prediction server, PrDOS (Ishida and Kinoshita 2007), indicates a high probability of disorder in the CTD (residues 156–245) (Supplementary Figure S5). Although the predicted disorder of the Par CTD has yet to be confirmed, the failure to obtain well-diffracting crystals of the full-length Par protein for X-ray crystallography (Schumacher, M. A. and Firth, N.,

unpublished data), supports the probability of Par at least containing a flexible CTD, since flexible segments are often not amenable to crystallisation (Oldfield *et al.* 2005, Slabinski *et al.* 2007).

Disordered domains are defined as protein domains that lack secondary structure, or at least, are highly flexible or structurally unstable (Wright and Dyson 1999, Dunker *et al.* 2002). It is estimated that around 6–33% of bacterial proteins contain extended regions of disorder (>40 residues), with approximately 4.5% of *S. aureus* proteins predicted to contain contiguous regions of disorder greater than 30 residues in length (Ward *et al.* 2004). The plasticity afforded by intrinsically disordered protein regions often imparts roles in molecular interactions, such as protein-protein or protein-DNA interactions, to execute functions in protein signalling, regulation and DNA-binding (Dunker *et al.* 2002, Tompa 2002, Dyson and Wright 2005, Tompa 2012). Intrinsically disordered proteins also commonly function as modulators of these binding interactions (Dunker *et al.* 2002, Dyson and Wright 2005). As such, it was anticipated that the Par CTD might interact with other predicted domains of Par, either intra- or inter- molecularly, or with host-encoded proteins.

Since potential interactions of the CTD with the N-terminal HTH or central CC domains might influence the DNA-binding and multimerisation activities of Par, respectively, the contribution of the CTD to these activities was investigated in Chapter 3 of this study. Results confirmed that the CTD is essential for Par function, as shown by plasmid segregational stability assays in Figure 3.2A. Furthermore, the combined results from several *in vitro* experiments suggested that the CTD influences Par DNA-binding, self-interaction and multimerisation activities (Sections

3.7.3–3.7.5). Specifically, *in vitro* cross-linking of purified RGSH₆-Par Δ CTD revealed a predominance of RGSH₆-Par Δ CTD dimers compared to multimers of higher molecular weight (Figure 3.7B), which suggests an impairment of Par to form larger multimers in the absence of the CTD. This most likely resulted in the reduced cooperativity of Par Δ CTD DNA-binding activity, as reflected by the formation of intermediate RGSH₆-Par Δ CTD-DNA species in EMSAs, which caused a more gradual shift in DNA probe mobility compared to DNA bound by RGSH₆-Par (compare Figures 3.6C and G to Figures 3.6A and F).

Taken together, the results presented in Chapter 3 suggest a role of the Par CTD in partition complex formation. In most characterised active plasmid partitioning systems, formation of the partition complex requires the recruitment and assembly of multiple CBPs at the centromere-like site (Bouet *et al.* 2000, Møller-Jensen *et al.* 2003, Schumacher and Funnell 2005, Schumacher *et al.* 2007a, Aylett and Löwe 2012). Intermolecular interactions between DNA-bound CBPs stabilise the nucleoprotein complex, which often causes a conformational change in the DNA. X-ray crystallography studies revealed that the type II pB171 ParR/*parC* partition complex forms a super-helical structure, with centromere DNA wrapped around 12 ParR dimers per helical turn (Møller-Jensen *et al.* 2007). The disordered C-terminal ends of ParR molecules are oriented towards the centre of the helix and are thought to play a role in interdimer contacts to stabilise the partition complex (Møller-Jensen *et al.* 2007). Wrapping of DNA around the partition complex has also been described for P1 ParB/*parS* (Funnell and Gagnier 1993), pSK41 ParR/*parC* (Schumacher *et al.* 2007a), and pBtoxis TubR/*tubC* binding (Aylett and Löwe 2012). Consistent with this, DNaseI footprinting suggests that the binding of pSK1 Par to centromere DNA

probably causes a topological change in the DNA, since a number of nucleotides in the centromeric region appeared to be hypersensitive to DNaseI digestion upon Par binding (LeBard 2005). It can, therefore, be envisaged that assembly of the Par partition complex is a cooperative process that might involve intermolecular interactions between the CTDs of neighbouring Par proteins in the segrosome. Consequently, truncation of, or mutations to, the CTD would result in inefficient partition complex formation and/or destabilisation of the partition complex, causing reduced cooperativity of centromere-binding, as observed in Figures 3.6C and G–I.

Furthermore, yeast two-hybrid (Y2H) and α -galactosidase assays showed that removal of, or deleterious mutations to, the Par CTD resulted in self-interactions that induced expression of the α -galactosidase reporter gene to a greater extent compared to activation by self-interacting wild-type Par fusion proteins (Figures 3.10A–B). This suggests that interaction between Par CTD mutants, presumably via their CC domains, is stronger than interactions between wild-type Par. It seems, therefore, that in addition to its role in stabilising the partition complex, the predicted disordered Par CTD may also have a role in negatively modulating Par self-interactions, possibly by sterically hindering strong interactions between Par CC domains. Consistent with the function of disordered regions as flexible linkers (Dunker *et al.* 2002, Tompa 2002), the disordered CTD might achieve modulation of Par self-interaction by acting as a molecular spacer to regulate distances between Par protein domains.

Therefore, in light of the role of disordered protein domains in molecular interactions (Dunker *et al.* 2002, Tompa 2002, Dyson and Wright 2005, Tompa 2012), the results

generated in this study give rise to the proposal that the predicted disordered CTD of Par might function as a modulator of Par interactions by promoting, or stabilising, the formation of higher-order Par multimers, whilst also modulating self-interaction of Par proteins, particularly the formation of Par dimers. A similar such modulation domain has been described for the N-terminal disordered domain of the type Ia partitioning protein KorB, which modulates DNA-binding activity and cellular localisation (Rajasekar *et al.* 2010). KorB also contains a region of disorder located between the central DNA-binding domain and the C-terminal multimerisation domain (Rajasekar *et al.* 2010). This disordered region is predicted to be involved in transcriptional repression and protein-protein interactions (Rajasekar *et al.* 2010).

Besides KorB, it seems that disordered, or at least flexible, regions are relatively common among other centromere-binding partitioning proteins. As described above, the C-terminal end of ParR from the type II partitioning system on pB171 is believed to be disordered (Møller-Jensen *et al.* 2007), whereas the type Ib TP228 ParG protein exhibits a highly disordered N-terminal tail (Golovanov *et al.* 2003), and the P1 ParB protein has a flexible linker between its DNA-binding and dimerisation domains (Schumacher and Funnell 2005). The prevalence of flexible and disordered regions amongst CBPs, therefore, highlights their importance in plasmid partitioning, particularly in the modulation of protein-protein and protein-DNA interactions.

The exact nature by which the CTD might contribute to the modulation of Par activity remains unclear, since Y2H assays only indicated direct interactions between two C-terminal domains, and did not indicate direct interactions of the CTD with the

NTD or CC domains (Figure 3.11A). However, as described in Section 4.6.1, it should be noted that centromere-DNA, and thus DNA-binding activity, was absent in the Y2H system, and hence CTD interactions that might be triggered subsequent to specific DNA-binding would not have been accounted for. Nonetheless, it could be speculated that the CTD modulates interactions, perhaps sterically, between Par domains to regulate Par self-interaction, multimerisation and complex formation.

6.2. Potential mechanisms of pSK1 *par*-mediated plasmid segregational stability

The mechanism of Par function in plasmid segregational stability is of immense interest due to the notable genetic difference between the pSK1 *par* system and characterised active plasmid partitioning systems. Namely, that only a single protein, Par, is encoded by pSK1 *par*, and that Par lacks any NTPase activity that might provide a mechanism for plasmid segregation, as observed in other partitioning systems. Although the plasmid partitioning systems studied thus far differ in their modes of plasmid segregation, especially with regard to the NTPase involved, the sequence of events is similar. Broadly, CBPs recognise and bind to repetitive DNA sequences at the centromere-like site, usually as a dimer or dimer-of-dimers (Bouet *et al.* 2000, Schumacher and Funnell 2005, Schumacher *et al.* 2007a, Aylett and Löwe 2012). The cooperative binding of multiple CBP multimers to the centromere-like site results in the formation of the segrosome, or partition complex, to which cognate NTPase proteins are recruited in an NTP-dependent conformation (Bouet and Funnell 1999, Møller-Jensen *et al.* 2003, Ni *et al.* 2010). Interaction between the partition complex and NTPase is integral to plasmid segregation (Davis *et al.* 1992,

Davey and Funnell 1997, Jensen and Gerdes 1997, Møller-Jensen *et al.* 2003, Ah-Seng *et al.* 2009).

Considering the knowledge gained from the molecular characterisation of pSK1 *par* from this and previous studies, potential mechanisms of Par action can be put forward, and are discussed in detail below.

6.2.1. Centromere-binding

The first stage, as is the case for all plasmid partitioning systems, is the sequence-specific binding of Par to the pSK1 *par* centromere-like site. DNaseI footprinting shows that Par binds specifically to seven 12-bp repeats found in the *par* centromere-like site (LeBard 2005), and that binding occurs via the N-terminal HTH domain, to which the K15 residue is critical (Lai 2008).

Consistent with the behaviour of other CBPs, preliminary X-ray crystallography data of pSK1 Par DNA-binding revealed Par dimers bound to DNA consisting of a palindromic sequence of the consensus binding site, TTAGGTAGTAAA (Schumacher, M. A. and Firth, N., unpublished data). However, with regard to the mechanistic order of events, it is unclear whether these dimeric interactions form subsequent to DNA-binding, or whether Par binds centromere DNA as dimers. The collective results from several experiments in this study provide support for the latter proposition, that Par forms dimers, or multimers, prior to DNA-binding. In particular, Par multimerisation studies, such as Y2H assays and *in vitro* cross-linking of purified RGS_{H6}-Par (Sections 3.6.2 and 3.5.1, respectively), showed that Par self-interacts and forms multimers (dimers, trimers, hexamers and higher-order multimers) *in vitro* and in the absence of DNA, which suggests that Par

multimerisation is not dependent on DNA-binding. Furthermore, *in vivo* cross-linking data showed that ParK15A, which lacks DNA-binding activity, forms cross-linked dimers in *S. aureus* cell lysates (Figure 3.8B), while epifluorescence microscopy showed the formation of fluorescent Par-GFP foci in the absence of the centromere-like site (Figure 5.17Ai–ii) and DNA-binding activity (ParK15A-GFP, Figure 5.16C). These results provide further support for the ability of Par to multimerise in the absence of DNA-binding.

Perhaps the strongest indicator of Par binding centromere DNA as a multimer is derived from the lack of DNA-binding activity exhibited by Par Δ CC mutants in EMSAs (Supplementary Figure S3B) (Lai 2008). Par Δ CC, which contains a deletion of the central CC domain from residues 83–155, is incapable of dimerisation (Supplementary Figures S2A–B) (Lai 2008, Jensen, S. O. and Firth, N., unpublished data). Since Par Δ CC retains the wild-type HTH DNA-binding domain, the severe impairment of Par Δ CC DNA-binding activity strongly indicates that the formation of Par multimers, or at least dimers, is required for centromere-binding, and that Par most likely binds centromere DNA as a multimer.

Specifically, the possibility of Par binding centromere DNA as a dimer is suggested by cross-linking experiments that showed a higher proportion of RGSH₆-Par Δ CTD dimers compared to higher-order multimers (Figures 3.7B–C). Since RGSH₆-Par Δ CTD readily bound centromere DNA in EMSAs (Figures 3.6C and G), it is conceivable that Par binds DNA as a dimer, after which a larger partition complex is assembled following the cooperative recruitment of additional Par dimers, analogous to partition complex assembly described for other plasmid partitioning systems

(Bouet *et al.* 2000, Møller-Jensen *et al.* 2003, Schumacher and Funnell 2005, Schumacher *et al.* 2007a, Aylett and Löwe 2012). Finally, as detailed in Section 6.1, interactions between the CTDs of Par proteins could contribute to stabilisation of the higher-order pSK1 *par* partition complex.

6.2.2. Plasmid pairing

For many plasmid partitioning systems, replicated plasmids are paired, or clustered, prior to active segregation. The pairing of plasmids is essential to efficient plasmid inheritance, and both the type I ParB and type II ParR proteins have been implicated in plasmid pairing via their cognate centromere-like sites (Jensen *et al.* 1998, Edgar *et al.* 2001, Schumacher and Funnell 2005, Ringgaard *et al.* 2007, Schumacher *et al.* 2007b). Preliminary structural data of Par DNA-binding reveals potential interactions between the NTDs of dimer pairs that are bound to separate DNA duplexes (Schumacher, M. A. and Firth, N., unpublished data). Furthermore, the number of fluorescent plasmid foci observed in *S. aureus* cells was generally less than the expected copy-number of pSK1 minireplicons (Figures 5.29A–B) (Grkovic *et al.* 2003, LeBard 2005). Interpretation of the combined data suggests DNA bridging and the potential of Par interactions to mediate plasmid pairing, or clustering. However, alanine substitution of the residues predicted to be involved in these interdimer NTD interactions, E10 and Y43, had little effect on Par function (Figure 3.13C). Since only residues 2–53 were visible in the crystal structure, it cannot be excluded that potential DNA pairing might be mediated by interactions involving other regions of Par, such as the CC or C-terminal domains.

6.2.3. Plasmid segregation

From a mechanistic perspective, the sequence of events that occurs subsequent to Par centromere-binding, in particular, how plasmids are physically segregated to daughter cells, remains to be revealed. However, perhaps one of the most notable findings from this study revealed a significant difference in the distribution of plasmid focus numbers between cell populations carrying plasmids with and without *par*. Specifically, cells carrying *par*⁺ plasmids were significantly more likely to contain two plasmid foci, whereas a significantly higher proportion of cells carrying *par*⁻ plasmids had only one focus (Figure 5.29 B). From time-lapse fluorescence imaging of plasmid localisation, described in Section 5.8.7, it appears that replicated *par*⁺ pSK1 minireplicons converge, or cluster, to form a single fluorescent focus near the division septum. The focus then separates into two or more foci, at least one of which is inherited by each daughter cell (Figures 5.31Aiii–iv). Plasmids lacking *par* failed to separate and segregate into daughter cells (Figure 5.31Bii–iii). This sequence of events reflects those described for type I plasmid partitioning systems observed in *E. coli* (Li and Austin 2002, Ebersbach and Gerdes 2004).

In most systems, the energy for plasmid segregation is derived from NTP hydrolysis by the motor proteins, which is stimulated by interaction of the NTPases with CBPs in the partition complex (Davis *et al.* 1992, Davey and Funnell 1997, Jensen and Gerdes 1997, Møller-Jensen *et al.* 2003, Ah-Seng *et al.* 2009). Plasmids are then actively driven apart using mechanisms such as the proposed diffusion-ratchet model for type Ia partitioning systems (Vecchiarelli *et al.* 2010, Vecchiarelli *et al.* 2013b), pushing by dynamically unstable actin-like filaments in type II systems (Møller-

Jensen *et al.* 2003, Garner *et al.* 2007), and treadmilling of tubulin-like filaments in type III systems (Ni *et al.* 2010). Importantly, motor proteins with reduced NTPase activity have detrimental effects on plasmid segregational stability, and are associated with an inability to separate plasmid clusters (Davis *et al.* 1996, Jensen and Gerdes 1997, Fung *et al.* 2001, Larsen *et al.* 2007, Ah-Seng *et al.* 2013). NTPase activity is, therefore, central to most plasmid partitioning systems described to date, and plays a key role in plasmid segregation dynamics.

However, with no NTPase activity apparent for Par, the force-generating component of plasmid segregation is unclear. Furthermore, the lack of evidence for Par filament formation *in vivo* (Sections 5.4.3, 5.4.4.4, 5.4.5.3 and 5.4.6) suggests that filament formation and NTPase activity might not be involved in Par mechanism. Although, as discussed in Section 5.9.1, this needs further validation using methods such as super-resolution microscopy or cryo-electron tomography. Therefore, based on data obtained in this study, a number of mechanisms are plausible, and are discussed below.

6.2.3.1. Molecular switches

In the absence of NTP hydrolysis, it could be hypothesised that certain biological events, for example post-translational modification or binding to DNA or proteins, could stimulate changes in protein conformation, particularly in the predicted disordered CTD (Dunker *et al.* 2002, Dyson and Wright 2005, Tompa 2012). For example, in the Phd/Doc toxin-antitoxin system of bacteriophage P1, interaction of the toxin, Doc, with binding sites in the disordered C-terminal domain of the antitoxin, Phd, results in a shift to the folded state of Phd, which in turn changes the

disordered N-terminal DNA-binding domain from to a low- to a high- DNA affinity state (Garcia-Pino *et al.* 2008, Garcia-Pino *et al.* 2010). Phd/Doc complexes bound to the operator of the *phd/doc* operon are disrupted by the binding of high amounts of Doc toxin, which results in de-repression of *phd* expression, and increased Phd production to counter the effects of Doc. This allosteric coupling, which is commonly observed for regulatory proteins containing disordered regions (Hilser and Thompson 2007), enables Phd to switch between its role as both a repressor and an antitoxin.

Similarly, particular stimuli, such as post-translational modification or Par DNA-binding, might trigger a disorder-to-order transition in the Par CTD. Such a shift could then cause Par to switch between its DNA-binding and multimerisation states, or promote subsequent protein-protein or force-generating interactions that might facilitate plasmid segregation. Mass spectrometry (Silva *et al.* 2013) could be used to determine whether such post-translational modifications are made to Par.

6.2.3.2. Pilot-fish or hitch-hiking

Although NTP hydrolysis plays a major role in many plasmid partitioning systems, there is, however, a possible exception to the need for NTPase activity. The recently-described StbA plasmid stabilisation protein encoded by the *stbABC* locus on the *E. coli* plasmid R388, is thought to attach to the host chromosome in a pilot-fish mechanism of plasmid segregation, such that plasmids are segregated in concert with chromosome segregation (Guynet *et al.* 2011, Guynet and de la Cruz 2011). In this way, the partitioning function of the *stbABC* operon does not require a motor protein to be encoded.

The pilot-fish mechanism of plasmid partitioning for R388 in *E. coli* is analogous to the hitch-hiking mechanism proposed for the segregation of plasmids from other kingdoms of life, such as the yeast 2 μ m plasmid (Velmurugan *et al.* 2000, Mehta *et al.* 2002, Jayaram *et al.* 2004, Sau *et al.* 2015) and viral plasmid DNA (Lehman and Botchan 1998, Ilves *et al.* 1999). These types of models describe the physical attachment of plasmid DNA to host chromosomal DNA, such that plasmids are efficiently partitioned by coupling plasmid segregation with chromosome segregation. It is, therefore, conceivable that a similar mechanism could be utilised by pSK1 Par, especially considering that no other protein is encoded by the *par* locus, and that no nucleotide-binding or NTPase activities have been detected.

6.2.3.3. Host factors

The reliance of pSK1 *par*-mediated plasmid segregation on host factors, such as chromosomal DNA or host-encoded proteins, is highly possible. Plasmid partitioning systems are typically self-contained functional units and usually do not require a host-factor. However, for the type Ia plasmid partitioning system, the host-encoded protein, integration host factor (IHF), although dispensable for plasmid segregational stability, significantly increases the cooperativity of ParB binding to *parS* (Funnell 1988b, Funnell 1991).

Although results from this study do not provide any direct evidence of interaction with host factors, time-lapse fluorescence localisation studies of plasmid DNA in *S. aureus* cells revealed restricted plasmid movement in the presence of *par*, compared to quicker, stochastic movement without *par* (Figures 5.31A–B, Supplementary Movies 1–7). A restriction in the movement of *par*⁺ plasmid foci might suggest

tethering or anchoring of plasmid DNA to host structures or receptors, a conclusion that was also drawn from similar observations of P1, F and RK2 plasmid segregation dynamics (Pogliano *et al.* 2001, Gordon *et al.* 2004, Derman *et al.* 2008).

6.2.3.3.1. Host factors: nucleoid DNA

Binding of pSK1 Par to the bacterial nucleoid, either directly or indirectly, may have a role in plasmid segregation. Indeed, EMSAs showed that Par binds to non-specific DNA in the absence of other proteins (Figure 4.10A). However, nucleoid condensation experiments were inconclusive for identifying associations between Par-GFP and *S. aureus* nucleoid DNA (Figures 5.13A–B). Nevertheless, it is unlikely that Par binds non-specifically to the nucleoid, since Par-GFP did not co-localise with the bacterial nucleoid in a manner that was observed for the localisation of nucleoid-binding partitioning proteins such as ParA and SopA (Hatano *et al.* 2007, Castaing *et al.* 2008, Hatano and Niki 2010). Rather, Par-GFP formed foci in *S. aureus* cells, regardless of whether DNA-binding activity or the pSK1 *par* centromere were present (Figures 5.16C and 5.17Ai–ii). Therefore, if Par does bind directly to chromosomal DNA, it would likely be via sequence-specific interactions.

As discussed in Sections 4.6.2 and 5.9.1, a search for Par binding sites using chromatin immunoprecipitation (ChIP) (Collas 2010) might identify binding sites on the chromosome, which may or may not be similar to sequences found at the pSK1 *par* centromere-like site. Indeed, the centromere-like repeats of pSK1 *par* and the homologous stability determinant identified on the *S. epidermidis* pSERP plasmid are quite dissimilar (compare Figures 1.5 and 4.1C), which suggests that the functionality of Par homologues in *S. aureus* might rely on binding to nucleoid DNA

either non-specifically, or to sequences conserved in the staphylococcal genome. ChIP experiments for both pSK1 Par and Par-pSERP, performed in *S. aureus* and the pSERP native host, *S. epidermidis*, and performed in the presence of their respective centromere-like sites, would provide validation on whether potential interactions between Par and the nucleoid are specific or non-specific. It would not be unreasonable to anticipate similar or identical binding sites for both Par and Par-pSERP if the interaction involves specific binding to conserved chromosomal sequences. The identification of chromosomal binding sites, whether specific or non-specific, would favour a pilot-fish or hitch-hiking mechanism, whereby Par exploits chromosome segregation to mediate stable plasmid inheritance (Section 6.2.3.2) (Figure 6.1A). Chromatin conformation capture techniques, such as 3C (Marbouty *et al.* 2014) and Hi-C (Beitel *et al.* 2014) could be used to determine whether plasmids and nucleoids are linked.

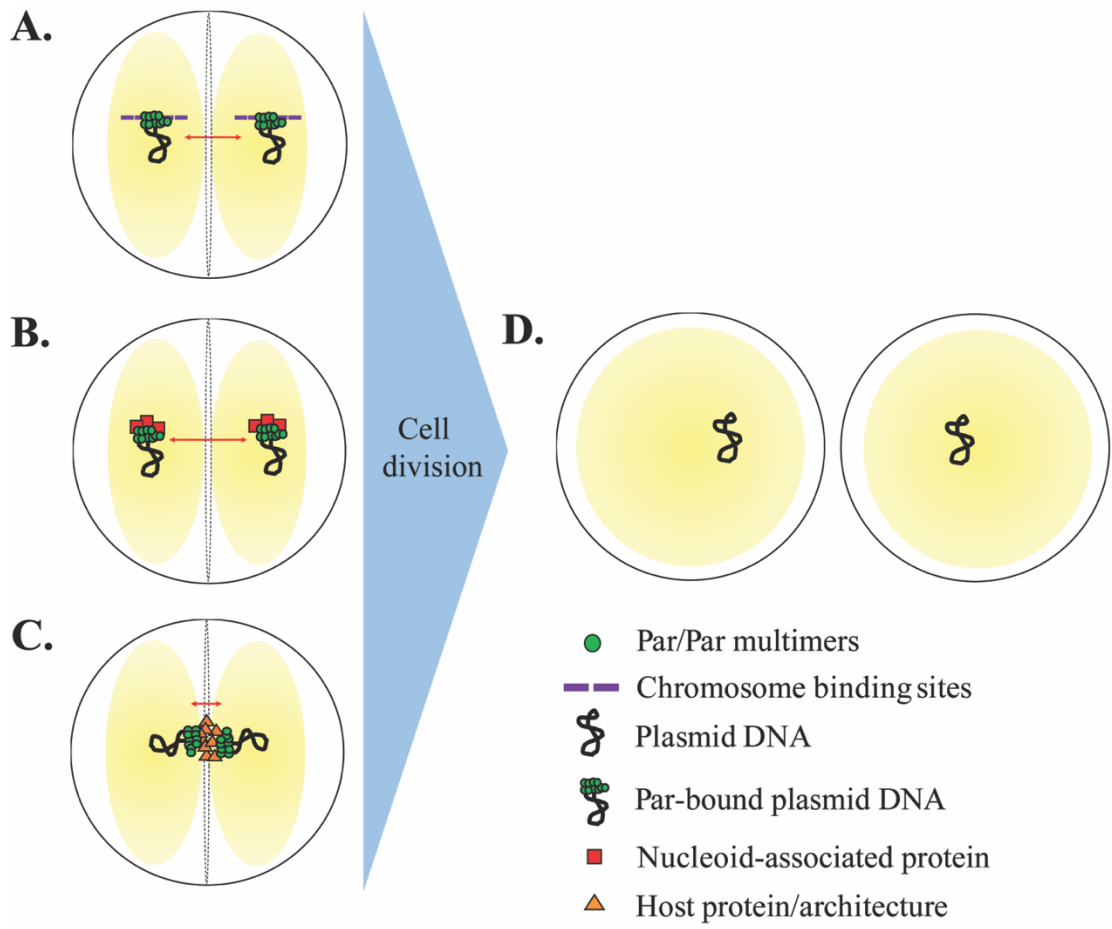
Although ambiguous in *S. aureus*, nucleoid condensation experiments in *E. coli* showed strong, presumably non-specific, association of GFP-Par with nucleoid DNA, but only in the presence of the pSK1 *par* centromere-like site and DNA-binding activity (compare Figures 5.22A to Figures 5.23B and 5.24). This suggests that the association between GFP-Par and nucleoid DNA depends on the binding of GFP-Par to the centromere-like site on plasmid DNA. From these observations, although made from a heterologous host, it can be hypothesised that either Par interacts with chromosomal DNA subsequent to centromere-binding (Figure 6.1A), or that a host protein (which may have a homologue in *E. coli*) interacts with the partition complex to tether plasmids to the nucleoid (Figure 6.1B). In either case, it

Figure 6.1 Proposed models for pSK1 *par* plasmid segregation

A–B. Par exploits chromosome segregation by hitch-hiking on the bacterial nucleoid DNA (yellow). **A.** Par binds to the plasmid centromere-like site and directly to specific sequences on chromosomal DNA. **B.** Par acts as an adapter between plasmid DNA and nucleoid-associated proteins. Par-bound plasmid DNA is therefore tethered to the nucleoid, such that plasmids are segregated (red arrows) together with chromosomes.

C. Par-bound plasmid DNA is anchored to specifically-localised host-encoded proteins or components of the host cell architecture, such as the division septum or cell poles. Correct subcellular localisation of plasmid DNA at predetermined positions ensures accurate plasmid segregation upon cell division (**D**).

S. aureus cells are represented by black circles, and the division site is represented by dotted lines. For clarity, only one pair of plasmids is shown for each dividing cell.



can be argued that a pilot-fish or hitch-hiking model (Section 6.2.3.2) could be used to mediate plasmid segregation.

6.2.3.3.2. Host factors: host-encoded proteins

In most active plasmid partitioning systems, CBPs act as adapter proteins between plasmid DNA and the NTPases that drive plasmid segregation (Bouet and Funnell 1999, Møller-Jensen *et al.* 2003, Ni *et al.* 2010). Since pSK1 Par is a CBP, it is possible that it too acts as an adapter to bridge plasmid DNA with host-encoded proteins that might provide the energy or spatio-temporal cues for plasmid segregation (Figure 6.1C). Since epifluorescence microscopy showed that Par-GFP and plasmid DNA are localised towards the cell periphery (Figures 5.12A–B and 5.28Bi–iv), Par might bridge plasmid DNA to membrane-bound or peripherally-located proteins, possibly via its C-terminal domain.

The potential interaction of Par with a candidate membrane-bound protein, DivIVA, was explored using Y2H assays (Section 4.4.3), since it was thought that the similar HTH and CC structures between Par and *B. subtilis* RacA (Figure 4.8) might reflect an interaction dynamic analogous to the RacA-DivIVA interaction during *Bacillus* chromosome segregation (Ben-Yehuda *et al.* 2003, Schumacher *et al.* 2016). Importantly, and as described in Section 4.4.3, *S. aureus* appears to lack a RacA homologue. However, in *Bacillus*, RacA binds specifically and non-specifically to DNA sequences on the bacterial chromosome, and interacts with the polarly-localised and membrane-bound protein, DivIVA, to anchor sister chromosomes to the cell poles (Ben-Yehuda *et al.* 2003, Wu and Errington 2003, Ben-Yehuda *et al.* 2005). In doing so, the RacA-DivIVA interaction ensures accurate segregation of

chromosomal DNA during cell division. Although no interaction was detected between Par and *S. aureus* DivIVA using Y2H assays (Figure 4.9), and although Y2H screening did not identify relevant protein interaction partners (Sections 4.4.1–4.4.2), there remains the possibility of the involvement of other host proteins in pSK1 *par* mechanism. As described in Section 4.6.1, co-immunoprecipitation experiments (Free *et al.* 2001) in the presence of the pSK1 *par* centromere-like site and DNA-binding activity, might provide an alternative means of identifying potential Par interaction partners. In this method, lysates from *S. aureus* SK8250 cells (*spa*⁻) (Table 2.1) containing Par and pSK1 minireplicons carrying the *par* centromere-like site, could be incubated with anti-Par peptide antibodies that are coupled to a resin, such as Protein A agarose beads. Subsequent precipitation and purification of Par-protein complexes using the anti-Par-coupled resin would enable the identification of potential Par interaction partners via mass spectroscopy.

6.2.4. Autoregulation

Finally, another unresolved mechanistic feature of pSK1 *par* action is the separation, or otherwise, of the autoregulation and partitioning functions of Par. Our studies have shown that binding of Par to the centromere-like site, which overlaps the *par* promoter (Figure 1.4), contributes to repression of *par* expression, as indicated by transcriptional reporter gene assays conducted in *S. aureus* (LeBard 2005). For P1 ParA, the ADP- and ATP- bound states exhibit different protein conformations, which determine the specificity of ParA binding to the *par* operator and to the ParB/*parC* partition complex, respectively (Davey and Funnell 1997, Bouet and Funnell 1999). Likewise, as mentioned in Section 6.2.3.1, interaction of Doc with

Phd dictates the role of Phd as a repressor or as an antitoxin (Garcia-Pino *et al.* 2010). However, unlike type Ia partitioning systems, whereby the centromere-like site and operator regions are spatially separated (Figure 1.2), the pSK1 *par* promoter is located within the centromere-like site (Figure 1.6). This is similar to the genetic organisation of types Ib, II and III systems (Figure 1.2), however, in these systems, autoregulation and plasmid segregation activities are carried out by two separate proteins (Section 1.5). pSK1 *par* only encodes a single protein that exhibits both autoregulation and plasmid maintenance functions, and little is known about how these roles are regulated. It would, therefore, be interesting to further investigate the structural and mechanistic properties of pSK1 Par to understand the interplay between its autoregulation and partitioning activities. For example, the autoregulation activity of Par could be further examined by performing reporter gene assays, such as chloramphenicol acetyl transferase (CAT) assays (Kwong *et al.* 2004, LeBard 2005), on Par mutants, particularly the Par CTD mutants (described in Section 3.2.1), to determine whether inefficiencies in DNA-binding, self-interaction or multimerisation, have an effect on autoregulation activity. This might provide some insight into potential differences in the conformation or multimerisation states of Par during centromere-binding and operator-binding, which may contribute to regulation of the partitioning and autoregulation roles of Par, respectively.

6.3. Concluding remarks

The efficiency with which low copy-number plasmids are maintained and accurately inherited in bacterial populations, even in the absence of antibiotic selection, is significantly enhanced by plasmid-encoded partitioning systems. The plasmid

segregational stability determinant, *par*, on the staphylococcal multiresistance plasmid, pSK1, is believed to enhance plasmid maintenance using a plasmid partitioning mechanism (Simpson *et al.* 2003). Homologues of Par are widely distributed amongst large staphylococcal multiresistance and pathogenicity plasmids, with approximately 80% encoding a Par-like protein (Shearer *et al.* 2011). However, distinct from typical bicistronic *par* operons, which encode a DNA-binding protein as well as a separate NTPase, only a single Par is protein encoded by this partitioning locus. pSK1 *par*, therefore, represents a potentially novel mechanism of plasmid partitioning.

Results from this and previous studies (LeBard 2005, Figgett 2007, Lai 2008) have provided molecular and functional characterisations of pSK1 Par activity, including autoregulation, centromere-binding, self-interaction and multimerisation. In conjunction with results from interaction and localisation studies presented in this thesis, these studies offer insight into the mechanistic details of pSK1 *par*-mediated plasmid segregation. Still, there remain unanswered questions about the pSK1 *par* mechanism of plasmid partitioning, and further research needs to be undertaken in order to increase our understanding of this process. Of particular interest are questions surrounding the force that drives the physical separation of plasmid DNA into daughter cells – is segregation an active process, and does it involve a host-encoded factor? Also, does Par exhibit different conformational states to execute autoregulatory, centromere-binding and multimerisation functions?

Deciphering the mechanism of pSK1 *par* will aid in the identification of novel targets for therapies, or eco-evo drugs, aimed to interfere with Par function. In this

way, disrupting the inheritance of multiresistance plasmids could help address the serious threat of antimicrobial resistance in *S. aureus* and in other bacteria that might utilise a similar mode of plasmid segregation.

APPENDIX A

Abbreviations

%	percent
<	less than
>	greater than
Δ	deletion
°C	degrees Celsius
μF	microfarads
μg	microgram(s)
μl	microlitre(s)
μm	micrometre(s)
μM	micromolar
aa	amino acid(s)
AD	activation domain
Ade	adenine
ADP	adenosine diphosphate
Ap	ampicillin
APS	ammonium persulfate
ATP	adenosine triphosphate
BD	DNA-binding domain
BHI	brain heart infusion
ble	bleomycin
bp	base pair(s)
BSA	bovine serum albumin
CA-MRSA	community-acquired MRSA

CAT	chloramphenicol acetyl transferase
CBP	centromere-binding protein
CC	coiled-coil
ChIP	chromatin immunoprecipitation
cm	centimetre(s)
Cm	chloramphenicol
cpm	counts per minute
CTD	C-terminal domain
C-terminal	carboxy-terminal
Cy3	5-propargylamino-dCTP-Cy3
Da	Dalton(s)
DAPI	4',6-diamidino-2-phenylindole
dATP	2'-deoxyadenosine 5'-triphosphate
dCTP	2'-deoxycytidine 5'-triphosphate
dGTP	2'-deoxyguanosine 5'-triphosphate
DMSO	dimethyl sulfoxide
DNA	deoxyribonucleic acid
DNase	deoxyribonuclease
dNTP	2'-deoxynucleotide 5'-triphosphate
DSP	dithiobis(succinimidyl propionate)
DTT	dithiothrietol
dTTP	2'-deoxythymidine 5'-triphosphate
ECL	enhanced chemiluminescence
EDTA	ethylenediaminetetra-acetic acid
Em	erythromycin
EMSA	electrophoretic mobility shift assay
FISH	fluorescence <i>in situ</i> hybridisation

FL	full-length
FnBP	fibronectin-binding protein
FROS	fluorescent reporter-operator system
GFP	green fluorescent protein
Gm	gentamicin
GTE	glucose-tris-EDTA
h	hour(s)
HA	haemagglutinin
His	histidine
HRP	horseradish peroxidase
HTH	helix-turn-helix
IFM	immunofluorescence microscopy
IgG	immunoglobulin G
IHF	integration host factor
IPTG	isopropyl- β -D-thiogalactopyranoside
IR	inverted repeat
IS	insertion sequence
kb	kilobase(s)
kDa	kilodalton(s)
Km	kanamycin
kV	kilovolt(s)
LB	Luria broth
Leu	leucine
LEU ⁺	leucine autotrophy
M	molar
MCS	multiple cloning site
mg	milligram(s)

min	minute(s)
ml	millilitre(s)
mM	millimolar
mRNA	messenger RNA
MRSA	methicillin-resistant <i>Staphylococcus aureus</i>
ng	nanogram(s)
Ni ²⁺ -NTA	nickel-nitrilotriacetic acid
nm	nanometre(s)
nM	nanomolar
Nm	neomycin
nt	nucleotide(s)
N-terminal	amino-terminal
NYE	nutrient yeast
OD	optical density
ORF	open reading frame
<i>oriC</i>	chromosomal origin of replication
<i>oriT</i>	origin of transfer
PAGE	polyacrylamide gel electrophoresis
<i>par</i> ⁻	in the absence of <i>par</i>
<i>par</i> ⁺	in the presence of <i>par</i>
PBP	penicillin binding protein
PBS	phosphate-buffered saline
PCR	polymerase chain reaction
PEG	polyethylene glycol
PFU	plaque-forming units
Pn	penicillin
PNK	polynucleotide kinase

poly(dI-dC)	poly(deoxyinosinic-deoxycytidylic)
<i>psk</i>	post-segregational killing
PVDF	polyvinylidene difluoride
R	resistance/resistant
RBS	ribosome binding site
RC	rolling circle
RFP	red fluorescent protein
RHH	ribbon-helix-helix
Rif	rifampicin
RNA	ribonucleic acid
rpm	revolutions per minute
RT	room temperature
s	second(s)
SAPI	<i>Staphylococcus aureus</i> pathogenicity island
SCC	staphylococcal cassette chromosome
SD	synthetic dropout
SDS	sodium dodecyl sulfate
spc	spectinomycin
SSC	saline sodium citrate
SSCT	saline sodium citrate Tween-20
TA	toxin-antitoxin
TAE	tris-acetate EDTA
TBE	tris-borate EDTA
TBS	tris-buffered saline
Tc	tetracycline
TE	tris-EDTA
TEMED	N, N, N', N'-tetramethyl-ethylene-diamine

Tn	transposon
Tp	trimethoprim
<i>tra</i>	conjugative transfer
Trp	tryptophan
TRP ⁺	tryptophan autotrophy
TSP	transcription start point
UV	ultraviolet
V	volt(s)
v/v	volume per volume
VISA	vancomycin-intermediate <i>Staphylococcus aureus</i>
w/v	weight per volume
WL	wash and lysis
X- α -Gal	5-bromo-4-chloro-3-indolyl- β -D-galactopyranoside
Y2H	yeast two-hybrid
YPD	yeast peptone dextrose
Ω	ohms

APPENDIX B

Supplementary

Supplementary Methods S1. Bioinformatics techniques

Identification of conserved residues in the C-terminal domain (CTD) of pSK1 Par was achieved using BLASTP (Altschul *et al.* 1990) to search the non-redundant protein sequences database. The amino acid sequence of the Par CTD (residues 156–245 of pSK1 Par; GenBank Accession Number AAF63251) was used as the query sequence. Selected sequences showing sequence identity were chosen and a multiple sequence alignment was generated using the ClustalW2 (Fast) program (Thompson *et al.* 1994, Larkin *et al.* 2007). Conservation of residues within the sequence alignment was visualised by levels of shading, created using the Gene Doc multiple sequence alignment editor and shading utility (Nicholas and Nicholas 1997)

Supplementary Figure S1 Identification of conserved residues in the Par CTD

Multiple sequence alignment of selected pSK1 Par CTD homologues. Selected amino acid sequences, identified as sharing homology with the pSK1 Par CTD sequence (residues 156–245; GenBank Accession Number AAF63251), were aligned using ClustalW2 (Supplementary Methods S1). For clarity, only residues 141–269 of the multiple sequence alignment are shown. Sources of the sequences (strain or plasmid) are listed on the left. Sources are shaded according to the bacterial species from which they were derived: *S. aureus* (blue); *S. epidermidis* (pink), *S. saprophyticus* (green); *S. hominis* (red); *S. warneri* (purple); *S. capitis* (black); *S. haemolyticus* (brown); *Enterococcus faecalis* (grey). Two sequences from *Lactococcus lactis*, which were not detected by searching using the CTD sequence but were identified as homologous to the full-length Par sequence by Figgett (2007), are included in the alignment to highlight sequence conservation across bacterial genera. These two sources are unshaded. Amino acid positions for individual sequences are shown on the right; positions for the alignment are shown at the top. Amino acid residues showing 100% conservation amongst the aligned sequences are shaded in orange, and those with greater than 90% conservation are shaded in yellow. Insertions and deletions are indicated by dashes. Residues 128–155 of Par, encompassing the coiled-coil (CC) domain, is indicated above the alignment.

GenBank Accession Numbers for the aligned sequences are given as follows: pSK1 (AAF63251); SAP062C (ACZ69356); pWBG755 (ACZ66059); pWBG746 (ACZ58711); pMS97 (BAD86531); SAP102A (ADA80779); pMW2 (AP004832); VSRAp (AP003367); SAP105B (ADA80166); M23864_W1 (ZP_04818772); pSSP2 (YP_302584); C80 (ZP_07844536); L37603 (ZP_04678483); SK14 (ZP_03614476); pNVH97A (CAB94810); HH22 (ZP_03986057); pCI305 (AAF86680); pAH33 (AAF17613).

Par CC domain

```

      *           160           *           180           *           200           *
pSK1      : KLEENQCIILALESNKRIQKLEHQLEEEERQLSYSFKSTNDRNFVDVGEASYTSDSVNTDQYCKEEKK--P : 197
SAP062C   : KLEENQCIILALESNKRIQKLEHQLEEEERQLSYSFKSTNDRNFVDVGEASYTSDSVNTDQYCKEEKK--P : 192
pWBG755   : KLEENQCIILALESNKRIQKLEHQLEEEERQLNYSFDTATNDRQSINPGEATFTEEYQNSNQCKKIPIEA : 209
pMS97     : KLEENQCIILALESNKRIQKLEHQLEEEERQLNYSFDTATNDRQSINPGEATFTEEYQNSNQCKKIPIEA : 130
SAP102A   : KLEENQCIILALESNKRIQKLEHQLEEEERQLNYSFDTATNDRQSINPGEATFTEEYKNSNQCKKIPIEA : 205
pMW2      : KLEENQCVLALESNKRIQKLEHQLEEEERQLNYSFDTATNDRQNVDAQEKTYTTSFVNINRDCEE--TKET : 190
VRSAp     : KLEENQCIILSLENNKRIQKLESQLEEEERQLKYSFDTTMNDRQNINPGEATFTEESQINQCKKCEQP--T : 200
SAP105B   : KLEENQCIILALESNKRIQKLESQLEEEERQLNYSFDTATNDRQNINPGEATFTEESQINQCKTKRQP--T : 200
M23864 W1 : KLEENQCIILALESNKRIQKLESQLEEEERQLNYSFDTATNDRQNINPGEATFTEESQINQCKTKRQP--T : 203
pSSP2     : RLLENQCIILALESNKRIQKLEHQLEEEERQLNYSFDTSVNDRQNVNSGEATFTEEPKIDIDQECENEHP--T : 174
C80       : KLEENQCIILALESNKRIQKLESQLEEEERQLNYSFDTATNDRQNINPGEATFTEESQINQCKTKRQP--T : 200
L37603    : KLEENQCVLALESNKRIQKLEHQLEEEERQLNYSFDTSSNDRQNVNAQGEATFTEESKDNQCKEENQTTDK : 192
SK14      : KLEENQCIILALESNKRIQKLESQLEEEERQLNYSFDTATNDRQNINPGEATFTEESQINQCKTKRQP--T : 200
pNVH97A   : KLEENQCVLALESNKRIQKLESQLEEEERQLNYSFDTATNDRQNIDPGEATFTEESQINQCKTK--CQPT : 190
HH22      : KLEENQCIILALESNKRIQKLEHQLEEEERQLNYSFDTSTNDRKKNFDVGEASYTSDSVNTNQYCKEEIN--P : 200
pCI305    : EQIKNK--DNQISVWDEQIKSLVEAQQIQNLLIQ----QQLLALQDKKLLLEYKAENDRLKVLKMPSC : 160
pAH33     : EQIKNK--DNQISVWDEQIKSLVEAQQIQNLLIQ----QQLLALQDKKLLLEYKAENDRLKVLKMPSC : 160

```

```

      220           *           240           *           260
pSK1      : EVQPRDISESQQDEKSQQQDDSFN-----QNDKDIAIEETQT---KKGFW SRLFGG : 245
SAP062C   : EVQPRDISESQQDEKSQQQDDSFN-----QNDKDIAIEETQT---KKGFW SRLFGG : 240
pWBG755   : ELNHKGITKARKKDDSNEDVLRDDKLSSEIEESGPEP-REVETP---KKGFW SRLFGS : 263
pMS97     : ELNHKGITKARKKDDSNEDVLRDDKLSSEIEESGPEP-REVETP---KKGFW SRLFGS : 184
SAP102A   : ELNHKGITKARKKDDSNEDVLRDDKLSSEIEESGPEP-REVETP---KKGFW SRLFGS : 259
pMW2      : EIQYKDISGSQSDSTQGEAQRED--VSANPNNDSDIEEKSEETA KKGFW SRLFGN : 247
VRSAp     : EVNHRNITEENKHDSFD--ELTKEDKFVEETKNDSSDNREVEPPP---KKGFW SRLFGN : 253
SAP105B   : EVNNKDIAEEKKNDSDEGELTKEDKFVEETKSDPDDNREVEPPP---KKGFW SRFFGN : 255
M23864 W1 : EVNYKDIAEEKKNDSDEGELTKEDKFVEETKSDPDDNREVEPPP---KKGFW SRLFGN : 258
pSSP2     : EVQHRDVAEEKGDSEIKEDFKDDKLSSEIEESGPEP-REVETP---KKGFW SRLFGN : 228
C80       : EVNYKDIAEEKKNDSDEGELTKEDKFVEETKNDPDDNREVEPPP---KKGFW SRFFGN : 255
L37603    : DIDPRVIFEEENRNEDINQSTNAKEN--ERVEKQDPNTNDEVERP---SKKGFW SRLFGN : 246
SK14      : EVNYKDIAEEKKNDSDEGELTKEDKFVEETKSDPDDNREVEPPP---KKGFW SRFFGN : 255
pNVH97A   : EVNYKDIAEEKKNDSDEGELTKEDKFVEETKSDPDDNREVEPPP---KKGFW SRLFGN : 245
HH22      : VVQSRGISENQDGEKQK-----ENDRGIAIEETQT---KKGFW SRLFGG : 242
pCI305    : ETEFRHLDNQYKDEVNALKKLEN---LQEQIKDKRIEIQEKP----RKWVG-LWRK : 210
pAH33     : ETEFRHLDNQYKDEVNALKKLEN---LQEQIKDKRIEIQEKP----RKWVG-LWRK : 210

```

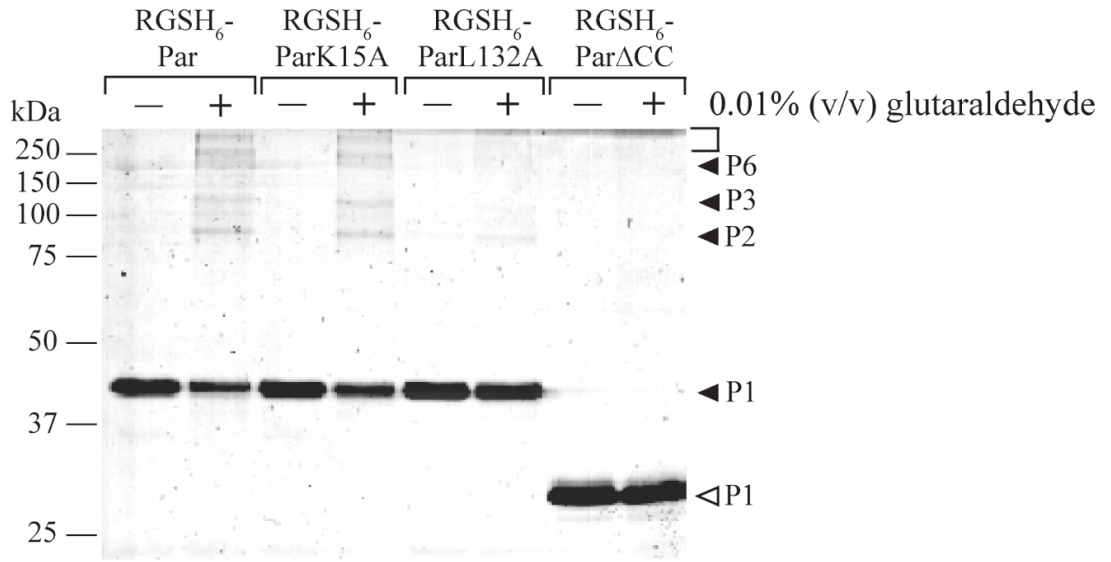
Supplementary Figure S2 Cross-linking of Par proteins

A. 10% (w/v) SDS polyacrylamide gel of RGS_{H6}-Par proteins cross-linked with glutaraldehyde. Purified RGS_{H6}-Par proteins were incubated with (+) or without (-) 0.01% (v/v) glutaraldehyde, as described in Section 2.9.1. Cross-linking reactions were analysed by SDS-PAGE and Coomassie Brilliant Blue staining (Section 2.5.6). Data obtained from Jensen, S. O. and Firth, N., unpublished data.

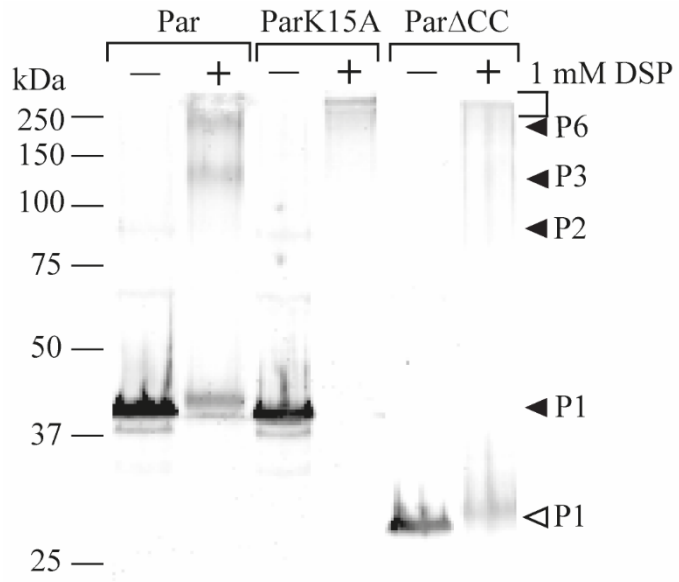
B. Western blot of cross-linked Par proteins in *E. coli*. *E. coli* DH5 α cells containing pSK4829 (Par), pSK7764 (ParK15A) or pSK7721 (Par Δ CC) were incubated with (+) or without (-) 1 mM DSP, according to Section 2.9.2. Cell lysates were electrophoresed on 10% (w/v) SDS polyacrylamide gels under non-reducing conditions, and Par proteins were detected by Western blotting using rabbit anti-Par antiserum (Section 2.5.9). Data obtained from Jensen, S. O. and Firth, N., unpublished data.

Sizes of prestained protein markers are indicated in kDa on the left of each gel or blot. Where appropriate, the positions of monomers (P1) and potential dimers (P2), trimers (P3) and hexamers (P6) are indicated by solid arrowheads for full-length RGS_{H6}-Par proteins, and by an open arrowhead for RGS_{H6}-Par Δ CC. The positions of higher-order multimers are bracketed.

A.



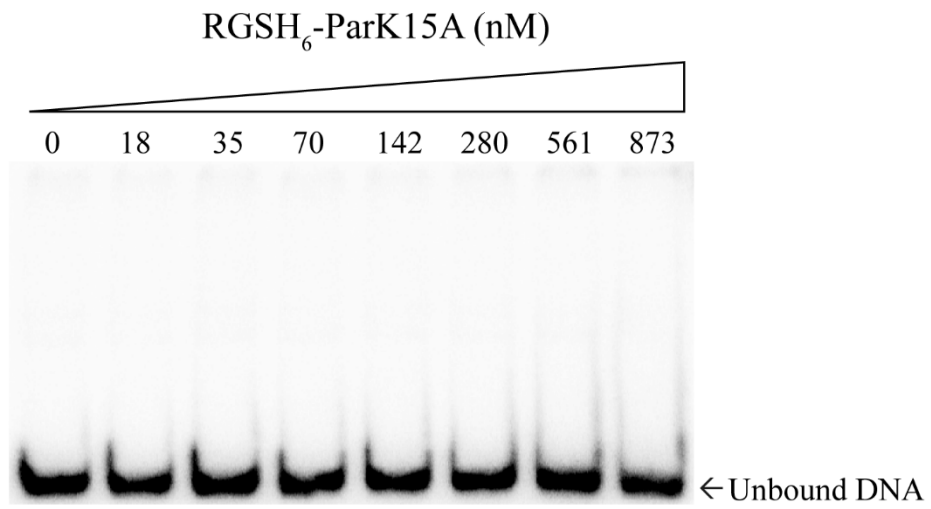
B.



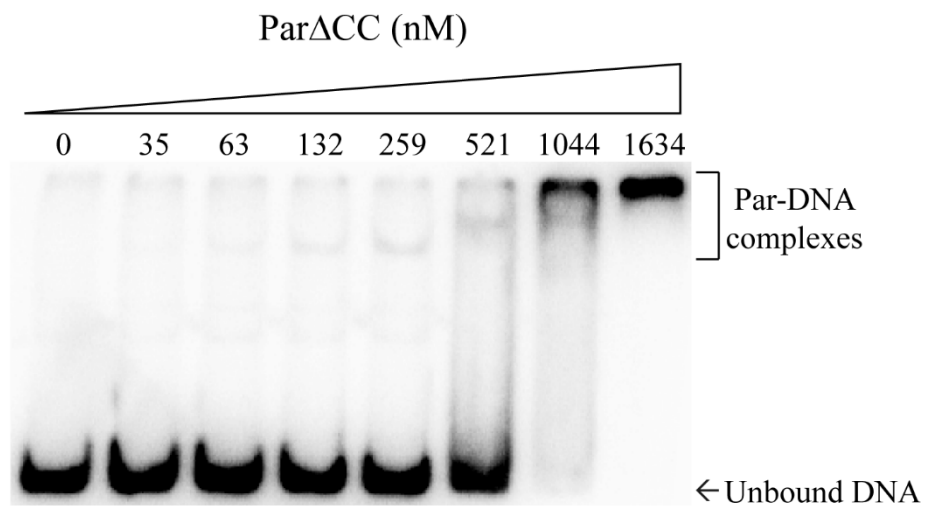
Supplementary Figure S3 DNA-binding activity of Par mutants

Electrophoretic mobility shift assays (EMSAs) of RGSH₆-ParK15A (**A**) and RGSH₆-ParΔCC (**B**) binding to the pSK1 *par-rep* intergenic region. Approximately 500 cpm of a radiolabelled *par-rep* intergenic DNA probe (nt 1689–1900, GenBank Accession Number GU565967; Figure 1.5) was incubated with increasing concentrations of purified RGSH₆-ParK15A or RGSH₆-ParΔCC, as described in Section 2.8. EMSAs were electrophoresed on 5% (w/v) polyacrylamide gels, and radiolabelled DNA probes were detected by phosphor imaging. Protein concentrations (nM) are shown above each lane. The positions of unbound DNA are indicated by black arrowheads.

A.



B.



Supplementary Figure S4 Sequence alignment of pSK1 Par with an enterococcal Par homologue

Pairwise sequence alignment of pSK1 Par and a Par homologue identified in *Enterococcus faecalis*. Amino acid sequences of pSK1 Par (GenBank Accession Number AAF63251) and an *E. faecalis* Par homologue (GenBank Accession Number EOI28424), which was identified from a BLASTP search (Altschul *et al.* 1990) using the Par amino acid sequence, were aligned using Clustal Omega (Sievers *et al.* 2011). Amino acid positions for individual sequences are shown on the right; positions for the alignment are shown above the alignment. Amino acid residues common to both aligned sequences are shaded in orange and denoted in uppercase below the alignment. Insertions and deletions are indicated by dashes.

```

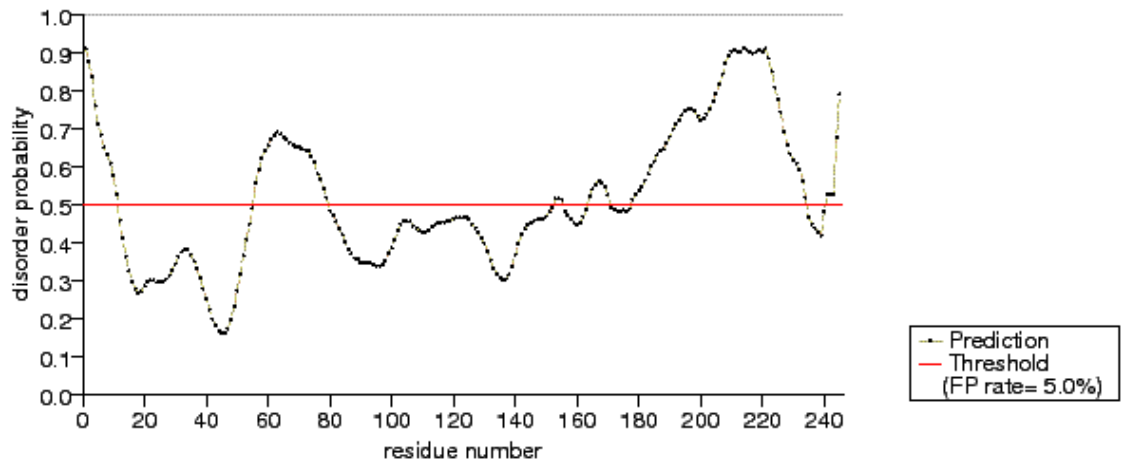
      *          20      *          40      *          60      *          80      *          100      *          120
S. aureus : MKTIKVADELNVTKQTVVNNAKMINISFEKENGVNYIDNDYLIKIVEKITKKERTTQNKENKSEIT---YENTENRYNNSDGFETLTKVNELEKQVEIFETRAKNDKEYIENLTKQLDQQ : 121
E. faecalis : ~~~~~~VLLGMFLSIKTLRYKRT---VWPFYFYTIIRTL-----SNKESVKKELFDENTAKVEKYIYNNSNSSETLTKVNELEKQIEIFETRAKNDKEYIENLTKQLDQQ : 98
              L      K      I      I      NKE  K  E      EK  YNNS  ETLTKVNELEKQ EIFETRAKNDKEYIENLTKQLDQQ

      *          140      *          160      *          180      *          200      *          220      *          240
S. aureus : NSNVNTLNKLLNQILALESNKKIQKLEHQLEEEERQLSYSFDKSTNDRNFDVQEASYSVNTDQYQKEEKKPEVQPKDISEQQDEKSKQDDSFNQNDKIDIAIEETQTKKGFWSRLFGG : 245
E. faecalis : NSNVNTLNKLLNQILALESNKKIQKLEHQLEEEERQLNYSFDKSTNDRKNFDVQEASYSVNTNQYQKEEINPVVQSKGISENQDGEKQ-----KENDRGIAIEETQTKKGFWSRLFGG : 216
      NSNVNTLNKLLNQILALESNKKIQKLE QLEEEERQL YSFDKSTNDR NFDVQEASYSVNT QYQKEE P VQ K ISE QQD Q      NDK IAIEETQTKKGFWSRLFGG

```

Supplementary Figure S5 Prediction of disordered Par protein regions

Residues of disorder were predicted for the pSK1 Par amino acid sequence (GenBank Accession Number AAF63251) using the protein disorder prediction server, PrDOS (Ishida and Kinoshita 2007), with a prediction false positive (FP) rate of 5%. The disorder probability is shown for each Par residue, with the disorder probability threshold set to 0.5 (red line). Residues with disorder probabilities above the red line are predicted to be disordered.



Supplementary Movies S1–S7 Time-lapse microscopy of the fluorescence localisation of pSK1 minireplicons in *S. aureus* cells by tagging with TetR-GFP

The localisation of pSK1 minireplicons pSK9144 (*par*, 60×*tetO*) (S1–S4) and pSK9145 (Δ *par*, 60×*tetO*) (S5–S7) in mid-exponential phase *S. aureus* SK8250 cells was visualised by tagging with TetR-GFP using a fluorescent repressor-operator system. Expression of *tetR-gfp* from pSK9142 ($P_{spac}::tetR-gfp$) was induced with 0.1 mM IPTG (Section 5.8.4). Cells were prepared for epifluorescence microscopy as described in Section 2.11.2, and images were taken at 1 min intervals for up to six minutes (0'–6'). Cells in each of S1–S4 and S5–S7 are biological replicates. Images shown are overlays of bright-field and TetR-GFP micrographs.

Supplementary Table S1. pSK1 *par* centromere-like sites on *S. aureus* chromosomal DNA

Strand	Match	Position on pSK1		Mismatches
		Start (nt)	Stop (nt)	
+	TTAATTAGTAAA	34853	34864	2
+	TTAGATAGTAAT	46686	46697	2
+	TCAGGAAGTAAA	75119	75130	2
+	ATAGGTAGTAAG	80964	80975	2
+	TTAGGTAGAAAA	91977	91988	1
+	TTAGCTGGTAAA	93163	93174	2
+	TTTGGTTGTAAA	102607	102618	2
+	TTAGATAGTAAT	109841	109852	2
+	TTAGGTACGAAA	122804	122815	2
+	TTAGGTAGCAAG	127539	127550	2
+	TTAGGTAATATA	130601	130612	2
+	TTAGTTGGTAAA	141035	141046	2
+	TTAGGTAGTATA	167582	167593	1
+	TTTGATAGTAAA	176086	176097	2
+	TTTAGTAGTAAA	178285	178296	2
+	TTAGATATTTAAA	178883	178894	2
+	TTACGTAGTGAA	183400	183411	2
+	TCAGTTAGTAAA	189918	189929	2
+	TTCGGTATTTAAA	204404	204415	2
+	TTAGGTCGTACA	206721	206732	2
+	TTAGGCAGAAAA	235943	235954	2
+	TTATGTAGTCAA	237758	237769	2
+	TTAAGTAGTGAA	240476	240487	2
+	TTTGATAGTAAA	240849	240860	2
+	TTTGGTATTTAAA	248044	248055	2
+	TGAGGTAGTAGA	251040	251051	2
+	CTAGGTAATAAA	255056	255067	2
+	TAAGGTAGTAAA	274308	274319	1
+	TTAGATGGTAAA	280862	280873	2
+	TTTTGTAGTAAA	302302	302313	2
+	TTCGGTATTTAAA	302550	302561	2
+	TTAATTAGTAAA	304212	304223	2
+	TTAGGTGTTAAA	304563	304574	2
+	TTTGCTAGTAAA	312842	312853	2
+	TTTGGTAGTAAC	315388	315399	2
+	TTACGTAATAAA	332571	332582	2
+	TTAGGAAGTCAA	333861	333872	2
+	TTATCTAGTAAA	339181	339192	2
+	TTAGGTAGTAAT	339847	339858	1
+	TTGGCTAGTAAA	340289	340300	2
+	TTACGTGGTAAA	350475	350486	2
+	TTACGTAGTAAA	358540	358551	1
+	TTAGGTAATAAA	359267	359278	1
+	TTAGCTAGTAAC	363637	363648	2
+	TTTGAAGTAAA	369925	369936	2
+	TTAGGTGGTAAA	381989	382000	1
+	TCAGGTAATAAAA	382706	382717	2
+	TTACGTAATAAAA	389214	389225	2
+	TTAGTTGGTAAA	392170	392181	2
+	TTAGGTGATAAAA	395843	395854	2
+	TTACGTAATAAAA	396229	396240	2

Strand	Match	Position on pSK1		Mismatches
		Start (nt)	Stop (nt)	
+	TTAGCTAGTATA	408951	408962	2
+	TTTGGTGGTAAA	420190	420201	2
+	TCAGGTAGTACA	435648	435659	2
+	TTAGCTAGTAAA	439289	439300	1
+	TTAAGAAGTAAA	445200	445211	2
+	TTAAGCAGTAAA	451387	451398	2
+	TTAAGTAGAAAA	465087	465098	2
+	CTAGGCAGTAAA	467155	467166	2
+	TTAGTAAGTAAA	468831	468842	2
+	TTAGTGAGTAAA	472978	472989	2
+	TTACTTAGTAAA	475915	475926	2
+	TTAGGTAGAACA	477094	477105	2
+	TTAGGTGGGAAA	479095	479106	2
+	TTATGAAGTAAA	485662	485673	2
+	TTAGGTAGTAAT	489086	489097	1
+	TTAAGCAGTAAA	495666	495677	2
+	TTACGTAATAAAA	500576	500587	2
+	TTAGATATTTAAA	501371	501382	2
+	TTAGGTAGAAAC	524419	524430	2
+	TTAGTTGGTAAA	524680	524691	2
+	TTAGGTCTTAAA	529334	529345	2
+	TTAGATGGTAAA	530532	530543	2
+	TTAGGTAATAAAA	531599	531610	2
+	TTATGTTGTAAA	552289	552300	2
+	TTAGAAAGTAAA	555297	555308	2
+	TTAGGTAGTGGA	564599	564610	2
+	TTAGGATGTAAA	565751	565762	2
+	TTAGGTAGTAAA	570512	570523	0
+	TTACATAGTAAA	573766	573777	2
+	TTAGCGAGTAAA	578068	578079	2
+	TTACGTATTTAAA	579065	579076	2
+	TTTAGTAGTAAA	579150	579161	2
+	TTAGGAAGTAAT	586575	586586	2
+	TTAAGTAATAAAA	587497	587508	2
+	ATAAGTAGTAAA	589634	589645	2
+	TTAGGTAGTATC	589656	589667	2
+	ATAGGTAATAAAA	591861	591872	2
+	TTAGGTAATACA	629836	629847	2
+	TTTGGTAGTAAT	635001	635012	2
+	TTAAATAGTAAA	639982	639993	2
+	TTAGGTATTAAC	643320	643331	2
+	TTAGGAATTTAAA	655101	655112	2
+	TTAGGTATTACA	656238	656249	2
+	TTATGTAATAAAA	656911	656922	2
+	TTAGTTTGTAAA	657219	657230	2
+	TTATATAGTAAA	660384	660395	2
+	TTAGCTAATAAAA	669663	669674	2
+	TTAGGTAGAGAA	671962	671973	2
+	TTAGGTAGTCAT	685472	685483	2
+	TGAGTTAGTAAA	692006	692017	2
+	ATTGGTAGTAAA	692994	693005	2
+	TTAGCTAATAAAA	695369	695380	2
+	TTTGATAGTAAA	700808	700819	2

Strand	Match	Position on pSK1		Mismatches
		Start (nt)	Stop (nt)	
+	TTTGGTATTAAA	702438	702449	2
+	TTAGGTGTTAAA	710255	710266	2
+	TTAGGTGGTACA	714415	714426	2
+	TTAGGTATTAAA	720485	720496	1
+	TCAGCTAGTAAA	727430	727441	2
+	TTAGATACTAAA	727928	727939	2
+	TCAGGTAGCAAA	740774	740785	2
+	TTAGGAAGTATA	749746	749757	2
+	AAAGGTAGTAAA	754655	754666	2
+	TTTGGTAATAAA	767242	767253	2
+	TTAGGTATTACA	767701	767712	2
+	TTATGTAGTAGA	769497	769508	2
+	TTTGGTAGTGAA	771854	771865	2
+	TTAGTTATTAAA	774629	774640	2
+	TTAGGTAGACAA	776497	776508	2
+	TTACCTAGTAAA	791836	791847	2
+	TTTGTTAGTAAA	792832	792843	2
+	ATAGGTAGTACA	794051	794062	2
+	TTAAGTAATAAA	800962	800973	2
+	TTAGTTGGTAAA	816544	816555	2
+	TTCGGTATTAAA	836533	836544	2
+	TTACGAAGTAAA	841019	841030	2
+	TTATGTAGCAAA	842349	842360	2
+	ATTGGTAGTAAA	843286	843297	2
+	TTAGTTGGTAAA	843904	843915	2
+	ATAGGTATTAAA	860211	860222	2
+	TTAGTTACTAAA	862182	862193	2
+	TTAGCTGGTAAA	865901	865912	2
+	TTAAGTCGTAAA	883212	883223	2
+	TTAGGAAATAAA	890205	890216	2
+	TTAGGTATCAAA	898515	898526	2
+	TTAGGTTATAAA	901093	901104	2
+	TTAGATAATAAA	907117	907128	2
+	TTAGGTTACTAAA	909676	909687	1
+	TTAAGTAATAAA	919460	919471	2
+	TTAGGTGCTAAA	920121	920132	2
+	TTAGTTAATAAA	947784	947795	2
+	GTAGGTGGTAAA	949008	949019	2
+	TTAGATAATAAA	982975	982986	2
+	TCAGGTAATAAA	984978	984989	2
+	TTAGATAGTATA	1007368	1007379	2
+	TTAGGTGTTAAA	1012742	1012753	2
+	TTAGGTGGAAAA	1013864	1013875	2
+	ATAGGTAATAAA	1013886	1013897	2
+	TCAGTTAGTAAA	1014456	1014467	2
+	TTAGGTATTACA	1014981	1014992	2
+	TTAGTTAGAAAA	1028770	1028781	2
+	TTAGCTATTAAA	1034341	1034352	2
+	TTAAGTAATAAA	1039927	1039938	2
+	TTAGGTAAAAAA	1051985	1051996	2
+	TTATGTAGTCAA	1054761	1054772	2
+	TTTGGTGGTAAA	1068744	1068755	2
+	TTAGTTAATAAA	1070446	1070457	2

Strand	Match	Position on pSK1		Mismatches
		Start (nt)	Stop (nt)	
+	TTAGGTGGTAAT	1082668	1082679	2
+	TTATTTAGTAAA	1085669	1085680	2
+	TTAGTTATTTAAA	1086108	1086119	2
+	TTAGGTGGTATA	1097102	1097113	2
+	TTAGGTGTTAAA	1099380	1099391	2
+	TTAGGTGGTAAA	1106209	1106220	1
+	TTAGGTATCAAAA	1113707	1113718	2
+	TTAGATAGTGAA	1117718	1117729	2
+	TTAGGTGGTCAA	1119217	1119228	2
+	TCAGGTATTTAAA	1123003	1123014	2
+	TTTGTTAGTAAA	1138083	1138094	2
+	TTGGTAATAAAA	1139316	1139327	2
+	TTAGGTCTTAAA	1139595	1139606	2
+	TTAGATATTTAAA	1141290	1141301	2
+	CTAGGTACTAAA	1148079	1148090	2
+	TTAGGTAATGAA	1161172	1161183	2
+	TTACGTGGTAAA	1161853	1161864	2
+	TTATGTTGTTAAA	1167011	1167022	2
+	TTAGGTAAAAAAA	1167951	1167962	2
+	TCAGGTGGTAAA	1168830	1168841	2
+	TTAGGTAAGAAA	1172884	1172895	2
+	TTACGTAGTAAA	1201659	1201670	1
+	TTATGTAGTAGA	1208436	1208447	2
+	TTAGCTAGAAAA	1214288	1214299	2
+	TTACATAGTAAA	1220732	1220743	2
+	TGAGGTAGTAAG	1226986	1226997	2
+	ATAGATAGTAAA	1248813	1248824	2
+	ATAGATAGTAAA	1250487	1250498	2
+	TTAGGGAGTATA	1257169	1257180	2
+	TTAAGTAGTAAA	1258776	1258787	1
+	TGATGTAGTAAA	1261519	1261530	2
+	ATATGTAGTAAA	1273242	1273253	2
+	TTAGCTAGAAAA	1278888	1278899	2
+	TTAGGTAGTAAG	1282345	1282356	1
+	TTAGGTGATAAAA	1285166	1285177	2
+	TTAGGTGTTAAA	1289549	1289560	2
+	TTATGTAATAAAA	1307276	1307287	2
+	TTAGGTAGAAAA	1313030	1313041	1
+	TTAGGTATTTAAA	1318486	1318497	1
+	TTAGGTGTTAAA	1323442	1323453	2
+	TTAGTTAATAAAA	1340650	1340661	2
+	TTTGGTATTTAAA	1344525	1344536	2
+	TGAGGTGGTAAA	1346746	1346757	2
+	TTAAGTAGTAAT	1351434	1351445	2
+	TTAAGTAGTCAA	1355765	1355776	2
+	TTCTGTAGTAAA	1358810	1358821	2
+	TTAGGAAGTATA	1375459	1375470	2
+	CTAGCTAGTAAA	1376632	1376643	2
+	TTAGCTAGTTAA	1434794	1434805	2
+	TTAGGTAATACA	1464572	1464583	2
+	TTAGAAAAGTAAA	1503709	1503720	2
+	TTGGGTAGTAGA	1517062	1517073	2
+	TTAGGTACCAAAA	1521596	1521607	2

Strand	Match	Position on pSK1		Mismatches
		Start (nt)	Stop (nt)	
+	TTAGTTAATAAAA	1542595	1542606	2
+	TTGGATAGTAAA	1564160	1564171	2
+	TTAGGTAATAAG	1567231	1567242	2
+	GTAGGTATTTAAA	1571800	1571811	2
+	GAAGGTAGTAAA	1580531	1580542	2
+	TTATATAGTAAA	1588202	1588213	2
+	CTAGGTAGTCAA	1593815	1593826	2
+	TTAGTTATTTAAA	1597888	1597899	2
+	TTTAGTAGTAAA	1601713	1601724	2
+	TTAGCTACTAAA	1616244	1616255	2
+	TTAGGTAGTGGA	1619965	1619976	2
+	ATAGGTATTTAAA	1663875	1663886	2
+	TTTGGTACTAAA	1668724	1668735	2
+	TTATGTATTTAAA	1687901	1687912	2
+	TTAGGTAGCATA	1700932	1700943	2
+	TTAGGTGGCAAAA	1705468	1705479	2
+	TTAGTTGGTAAA	1743794	1743805	2
+	TTATGTATTTAAA	1747108	1747119	2
+	TTATGAAGTAAA	1761567	1761578	2
+	TTATATAGTAAA	1764030	1764041	2
+	TTAGTAAGTAAA	1775282	1775293	2
+	TCAGGTATTTAAA	1777867	1777878	2
+	CTAGGTTCGTAAA	1780302	1780313	2
+	TTAGCTACTAAA	1798888	1798899	2
+	TTATGTAGTAAA	1826653	1826664	1
+	TTAGTTACTAAA	1836468	1836479	2
+	TTTGGTAGTAAG	1840439	1840450	2
+	TTAGGTAGTATA	1850193	1850204	1
+	TTAAATAGTAAA	1850652	1850663	2
+	CGAGGTAGTAAA	1861701	1861712	2
+	TTCGGTATTTAAA	1883547	1883558	2
+	ATACGTAGTAAA	1892365	1892376	2
+	ATAGGTACTAAA	1896403	1896414	2
+	TCAGTTAGTAAA	1898379	1898390	2
+	ATAGGTATTTAAA	1904749	1904760	2
+	TTAGGTAGTAAA	1946310	1946321	0
+	TTAGGTTGTAAT	1954407	1954418	2
+	TTAGCTAGTATA	1965092	1965103	2
+	ATATGTAGTAAA	1975244	1975255	2
+	TTAGGTAGTAGA	2003296	2003307	1
+	TTAGGTTGGAAA	2008083	2008094	2
+	TTAGGTTATAAAA	2013405	2013416	2
+	TTAGGTGTTAAA	2019372	2019383	2
+	TTTGGTAGTAAT	2026550	2026561	2
+	TTAGGTGTTAAA	2043766	2043777	2
+	TTAGGTCATAAAA	2074467	2074478	2
+	TTAGCTACTAAA	2091573	2091584	2
+	TTAGGCAGTGAA	2096126	2096137	2
+	GTAGGTACTAAA	2132431	2132442	2
+	CTAGGTATTTAAA	2138002	2138013	2
+	TTAAGTAGTCAA	2144866	2144877	2
+	TTCGTTAGTAAA	2160970	2160981	2
+	TTAGTTAGTAAG	2184317	2184328	2

Strand	Match	Position on pSK1		Mismatches
		Start (nt)	Stop (nt)	
+	TTAGGCACTAAA	2185099	2185110	2
+	TTACGTAATAAAA	2220861	2220872	2
+	TTAGTACTAAA	2230764	2230775	2
+	TCAGTTAGTAAA	2238334	2238345	2
+	TTATGTAATAAAA	2249838	2249849	2
+	ATGGGTAGTAAA	2275070	2275081	2
+	TTAGATTGTAAA	2282790	2282801	2
+	TTTGGTAGTAAC	2313930	2313941	2
+	TTTGGTAGTAAT	2330196	2330207	2
+	TTAGGGAGTAAG	2335982	2335993	2
+	TTATATAGTAAA	2356617	2356628	2
+	GTAGGTGGTAAA	2362532	2362543	2
+	TTATATAGTAAA	2376348	2376359	2
+	TTAGGTAGAAAC	2379331	2379342	2
+	TCAGGTGGTAAA	2385607	2385618	2
+	TTAGGTGGCAA	2410711	2410722	2
+	TTACATAGTAAA	2411071	2411082	2
+	TTAGATAGTAAA	2435882	2435893	1
+	TTAGCTAGTAAC	2447256	2447267	2
+	TTAGGTAAGAAA	2455955	2455966	2
+	TTAGGTTATAAAA	2479614	2479625	2
+	ATAGCTAGTAAA	2492649	2492660	2
+	TTAGGTCCTAAA	2510222	2510233	2
+	TTAGCTAGTAAA	2544217	2544228	1
+	TTAGGTAGTACA	2550493	2550504	1
+	ATACGTAGTAAA	2558617	2558628	2
+	TTAGGTGTTAAA	2584000	2584011	2
+	ATAGTTAGTAAA	2589304	2589315	2
+	TAAGGCAGTAAA	2592773	2592784	2
+	ATGGGTAGTAAA	2602857	2602868	2
+	TTAGGTATTCAA	2631853	2631864	2
+	TCAGGTAGCAA	2634467	2634478	2
+	TTAAGAAGTAAA	2635085	2635096	2
+	TTTGGTAATAAAA	2635256	2635267	2
+	TCAGGTAGTAAT	2649982	2649993	2
+	TAAGGTAGAAAA	2653757	2653768	2
+	TTAAGTAGAAAA	2659534	2659545	2
+	TTAGGAACTAAA	2662957	2662968	2
+	TTAGGTAGTGAA	2663443	2663454	1
+	TTAGGTCTTAAA	2672429	2672440	2
+	TCAGGTTGTAAA	2694020	2694031	2
+	TTTGGTAATAAAA	2707706	2707717	2
+	CTAGTTAGTAAA	2708378	2708389	2
+	TTAGCTAGTAAA	2712403	2712414	1
+	TCAGGTAATAAAA	2731414	2731425	2
+	CTCGGTAGTAAA	2732811	2732822	2
+	TTTGATAGTAAA	2734722	2734733	2
+	ATAGGTAGTAAC	2781842	2781853	2
+	TTTAGTAGTAAA	2809974	2809985	2
+	TTAGGTCGTAAG	2811059	2811070	2
+	TTACGTAATAAAA	2812933	2812944	2
-	TTAGGTGGTAAT	2816506	2816495	2
-	TTAAGTAATAAAA	2814628	2814617	2

Strand	Match	Position on pSK1		Mismatches
		Start (nt)	Stop (nt)	
-	TTAGGTAGCAAG	2812068	2812057	2
-	TTGGTAGGAAA	2810941	2810930	2
-	TAAGGTTGTAAG	2808848	2808837	2
-	TTAGGAAGTTAA	2799362	2799351	2
-	TTAGGTGGTATA	2793264	2793253	2
-	TTGGTAATAAAA	2779619	2779608	2
-	TTAGGTTGTAAG	2775149	2775138	2
-	TTAGGTAACAAA	2765792	2765781	2
-	TCAGCTAGTAAA	2764220	2764209	2
-	TCAGGTAGTACA	2763626	2763615	2
-	ATAGGTATTAAA	2718436	2718425	2
-	TTAGATGGTAAA	2704294	2704283	2
-	ATAGATAGTAAA	2691367	2691356	2
-	TTAGGTGATAAA	2669344	2669333	2
-	TTATGTAGTAAA	2659607	2659596	1
-	GCAGGTAGTAAA	2657664	2657653	2
-	TTATCTAGTAAA	2654757	2654746	2
-	CTAGGTATTAAA	2648961	2648950	2
-	TTAGCTTGTAAG	2646063	2646052	2
-	TTAATTAGTAAA	2616872	2616861	2
-	TTAGCTAATAAAA	2610549	2610538	2
-	GTAGGTAGTATA	2609301	2609290	2
-	TCAGGTAGTAAT	2601065	2601054	2
-	ATAGGTAGTACA	2595410	2595399	2
-	TTATATAGTAAA	2592153	2592142	2
-	TTATGTAATAAAA	2579429	2579418	2
-	TTATTTAGTAAA	2574159	2574148	2
-	TCACGTAGTAAA	2561258	2561247	2
-	TCACGTAGTAAA	2560373	2560362	2
-	TGAGGTATTAAA	2533112	2533101	2
-	TTAGGTGGTATA	2529741	2529730	2
-	CTAGGTAGTAAG	2522282	2522271	2
-	TTAGGTAATAAT	2511247	2511236	2
-	GTAGGTATTAAA	2507315	2507304	2
-	TTAAGTACTAAA	2491912	2491901	2
-	TTAGAAAGTAAA	2474244	2474233	2
-	TTATGGAGTAAA	2471603	2471592	2
-	TTATGTAGTAAG	2468101	2468090	2
-	TTGGGTACTAAA	2463706	2463695	2
-	TCAGGTAATAAAA	2460942	2460931	2
-	TTAGGTGATAAA	2455853	2455842	2
-	ATAGATAGTAAA	2454042	2454031	2
-	TTGGTAGTAAT	2436917	2436906	2
-	TTTTGTAGTAAA	2436074	2436063	2
-	TTAGGTAGCATA	2435519	2435508	2
-	TTAAGTACTAAA	2422907	2422896	2
-	TTAGGTATTAAA	2403243	2403232	1
-	TTAGATAGTGAA	2401101	2401090	2
-	TTATGTAGTAAA	2389434	2389423	1
-	TTATGTAGCAAA	2384319	2384308	2
-	TTATGTAATAAAA	2380124	2380113	2
-	ATAGGTATTAAA	2363271	2363260	2
-	TAAGTTAGTAAA	2356401	2356390	2

Strand	Match	Position on pSK1		Mismatches
		Start (nt)	Stop (nt)	
-	TTAGGTGGTAAT	2351359	2351348	2
-	TTAGGACGTAAA	2346990	2346979	2
-	TAAGATAGTAAA	2346569	2346558	2
-	TCAGATAGTAAA	2343783	2343772	2
-	TTAAGAAGTAAA	2334862	2334851	2
-	TTAGGTGTAAA	2333539	2333528	2
-	ATAAGTAGTAAA	2330124	2330113	2
-	TTAGGTAAGAAA	2325644	2325633	2
-	TTAGATAATAAAA	2322385	2322374	2
-	TTAGGTTTTAAA	2321389	2321378	2
-	TTAGGAAGAAAA	2317787	2317776	2
-	TTAGGTGTAAA	2311855	2311844	2
-	TTTGGTAATAAAA	2311072	2311061	2
-	TTAGGTCTAAA	2309501	2309490	2
-	TTAGGTCGTAAA	2304682	2304671	1
-	TTAGGTAAAAAA	2304444	2304433	2
-	TTAGGTAGAAAT	2296339	2296328	2
-	TTAGGTATTTAA	2295537	2295526	2
-	ATAGGTAATAAAA	2295290	2295279	2
-	TTAGTTATTTAAA	2287799	2287788	2
-	TTAGGTATTTAAA	2274685	2274674	1
-	TTAGTAAGTAAA	2269498	2269487	2
-	GTAGGTATTTAAA	2253357	2253346	2
-	TTTGGTATTTAAA	2248688	2248677	2
-	TTAAGCAGTAAA	2241691	2241680	2
-	TTAGTTATTTAAA	2231655	2231644	2
-	TTAGATACTAAA	2230719	2230708	2
-	TTAGATACTAAA	2229708	2229697	2
-	TTAGGTAGTCCA	2221758	2221747	2
-	TTAGGTCATAAAA	2217776	2217765	2
-	TTAGCAAGTAAA	2210686	2210675	2
-	TTAGGTAGAGAA	2191176	2191165	2
-	TTAGGTATTCAA	2191065	2191054	2
-	TTAGATGGTAAA	2190807	2190796	2
-	TTAGGTGGTACA	2190387	2190376	2
-	TTAGGTCGTGAA	2184610	2184599	2
-	TTAGATCGTAAA	2183230	2183219	2
-	TTAGCTGGTAAA	2176087	2176076	2
-	TTTGGTACTAAA	2175670	2175659	2
-	TTAGGTAGTCAT	2174882	2174871	2
-	TTAGATGGTAAA	2167963	2167952	2
-	ATTGGTAGTAAA	2161049	2161038	2
-	TGATGTAGTAAA	2154634	2154623	2
-	TAAGGTAGCAAAA	2152686	2152675	2
-	TTAGGCATTTAAA	2140495	2140484	2
-	TTAGGTATTTAAA	2136286	2136275	1
-	TTAGGTAGTGAT	2129760	2129749	2
-	TTAAGCAGTAAA	2125204	2125193	2
-	TTAGGTAAAAAA	2104306	2104295	2
-	CTAGGTATTTAAA	2098034	2098023	2
-	TTATGTAGTAAT	2096810	2096799	2
-	TCAGGTGGTAAA	2077266	2077255	2
-	TTTGCTAGTAAA	2074434	2074423	2

Strand	Match	Position on pSK1		Mismatches
		Start (nt)	Stop (nt)	
-	CTAGGTAATAAAA	2073473	2073462	2
-	TTAGTTAGTGAA	2073350	2073339	2
-	GTAGGTAATAAAA	2072353	2072342	2
-	TTAGGTTTTAAA	2068526	2068515	2
-	TTAGGTATTAAG	2066250	2066239	2
-	TTGGCAGTAAA	2064106	2064095	2
-	TTAGGTATTAAC	2058268	2058257	2
-	TTAGATAATAAAA	2054510	2054499	2
-	TTAGGTGGGAAA	2047344	2047333	2
-	TTAGGTGGTAAG	2043364	2043353	2
-	GTAGGTAATAAAA	2042977	2042966	2
-	TTAGGTGGTATA	2041234	2041223	2
-	TTAGGTCATAAAA	2025550	2025539	2
-	TTAGGTGGTAAT	2025238	2025227	2
-	TTAGGTCTAAA	2021870	2021859	2
-	TTAGGCACTAAA	1995379	1995368	2
-	TTAGGTGTAAA	1995181	1995170	2
-	TTAGGTATTGAA	1994773	1994762	2
-	TTTGGTACTAAA	1989119	1989108	2
-	TTAGATACTAAA	1988654	1988643	2
-	CTAGGTAATAAAA	1965815	1965804	2
-	TTAGCTAGGAAA	1960886	1960875	2
-	TTAGGAATTA AAA	1958387	1958376	2
-	TTAGATAGCAAAA	1957090	1957079	2
-	GTAAGTAGTAAA	1952394	1952383	2
-	ATAGGTAATAAAA	1925308	1925297	2
-	TTAGCTAGTAAA	1921326	1921315	1
-	TTAAGTAGTAAA	1914799	1914788	1
-	TTAGATATTA AAA	1914370	1914359	2
-	TTAGGTGGTAGA	1911282	1911271	2
-	TCCGGTAGTAAA	1910916	1910905	2
-	TTAAGCAGTAAA	1903808	1903797	2
-	TTAGGTAATGAA	1894271	1894260	2
-	TTAGGTAGAAAA	1867622	1867611	1
-	TTAGGTGGTAGA	1859335	1859324	2
-	TTGGTAGTAAA	1852260	1852249	1
-	TTAGGTATGAAA	1851122	1851111	2
-	TTTTGTAGTAAA	1848760	1848749	2
-	TTAAATAGTAAA	1842576	1842565	2
-	TTCGATAGTAAA	1838094	1838083	2
-	TTGGGTAGAAAA	1833549	1833538	2
-	TTAGTTAGTATA	1821151	1821140	2
-	TTAGGTAGTAAG	1817360	1817349	1
-	TTAGATGGTAAA	1801508	1801497	2
-	TTAGGAAGTATA	1788110	1788099	2
-	TTAGGTCGTATA	1787214	1787203	2
-	TTAGGTACAAAA	1784598	1784587	2
-	TGATGTAGTAAA	1784335	1784324	2
-	TTAGTTACTAAA	1760096	1760085	2
-	TTAGCTAGTAAA	1757172	1757161	1
-	TTAGGTAATAAT	1756129	1756118	2
-	TTCGGTATTA AAA	1730316	1730305	2
-	TTAGGTATTAAT	1716299	1716288	2

Strand	Match	Position on pSK1		Mismatches
		Start (nt)	Stop (nt)	
-	TTAGGTATTATA	1711166	1711155	2
-	TTAGCTATTA AAA	1711097	1711086	2
-	TTCGGTATTA AAA	1709185	1709174	2
-	TTATGTAGAAAA	1708160	1708149	2
-	ATAGGTATTA AAA	1698944	1698933	2
-	TTTGGTGGTAAA	1671215	1671204	2
-	TTAGGTGCTAAA	1658770	1658759	2
-	TTAGTTATTA AAA	1652892	1652881	2
-	TTAGAAAAGTAAA	1649476	1649465	2
-	TGAGGTAATA AAA	1636981	1636970	2
-	TTAGGTGGTCAA	1622193	1622182	2
-	TGAGGTATTA AAA	1611450	1611439	2
-	TTAGTTAGTGAA	1608666	1608655	2
-	TCAGGTGGTAAA	1608546	1608535	2
-	TTTGAAGTAAA	1604238	1604227	2
-	TTAGCTAGTAGA	1598907	1598896	2
-	TTAGGTATTGAA	1593340	1593329	2
-	GTTGGTAGTAAA	1590291	1590280	2
-	TTAGGTTGTAAA	1589610	1589599	1
-	TTAGGTAATAAT	1584665	1584654	2
-	TTTGGTTGTAAA	1577449	1577438	2
-	TTAGGTGGTATA	1569129	1569118	2
-	TTAAGTAATA AAA	1547308	1547297	2
-	TTAGGTAAAAAAA	1542259	1542248	2
-	TTAGGTAAAAAAA	1539257	1539246	2
-	TTAGGTAGAAAA	1537832	1537821	1
-	TTATGTATTA AAA	1533705	1533694	2
-	TTAGGTGGGAAA	1531457	1531446	2
-	TTAATTAGTAAA	1509414	1509403	2
-	TTAGGAAGAAAA	1508988	1508977	2
-	CTAGGTAATA AAA	1507210	1507199	2
-	TTAGTTAGTGAA	1507087	1507076	2
-	TTATTTAGTAAA	1506384	1506373	2
-	GTAGGTAATA AAA	1506088	1506077	2
-	TTAGGTAATGAA	1503667	1503656	2
-	TTAGGTTTTAAA	1497878	1497867	2
-	TCAGGTAATA AAA	1496306	1496295	2
-	GTAAGTAGTAAA	1494687	1494676	2
-	TTAGGGAGTAAA	1490790	1490779	1
-	TTAGGTAATA AAA	1472008	1471997	1
-	TTAGGAAGTCAA	1467282	1467271	2
-	TTAGGAAATA AAA	1460437	1460426	2
-	TTATGAAGTAAA	1452599	1452588	2
-	TTAGGTAGTCCA	1441374	1441363	2
-	TTAGGTATTGAA	1438988	1438977	2
-	TTAGGAATTA AAA	1433887	1433876	2
-	TTAAGTAATA AAA	1433734	1433723	2
-	TTAGGTATTAAT	1424861	1424850	2
-	TTTGGTAGTAAA	1420910	1420899	1
-	TTAGGCAGTAAT	1404037	1404026	2
-	TTAGGTAATA AAA	1400746	1400735	2
-	TTAGTTATTA AAA	1397962	1397951	2
-	TTAAGAAGTAAA	1369165	1369154	2

Strand	Match	Position on pSK1		Mismatches
		Start (nt)	Stop (nt)	
-	TCAGGTAGAAAA	1368586	1368575	2
-	TTAGGTTATAAA	1365900	1365889	2
-	TTAGGAAGTAAA	1364191	1364180	1
-	TTAAATAGTAAA	1363081	1363070	2
-	AAAGGTAGTAAA	1322841	1322830	2
-	TTAGTTAATAAA	1308124	1308113	2
-	TTAAGAAGTAAA	1301364	1301353	2
-	TTATGTAGTAGA	1284588	1284577	2
-	TTAGGTATTAAT	1272702	1272691	2
-	TTAGCTACTAAA	1260588	1260577	2
-	CTAGGTAATAAA	1240109	1240098	2
-	TTAGATACTAAA	1236108	1236097	2
-	TTAGGTGTTAAA	1216673	1216662	2
-	TAAGATAGTAAA	1214628	1214617	2
-	TTAGGGAATAAA	1202403	1202392	2
-	GTAGGTAGTCAA	1181892	1181881	2
-	TTACGTAATAAA	1171937	1171926	2
-	TTAAGGAGTAAA	1171680	1171669	2
-	TTAAGTAGTTAA	1131873	1131862	2
-	TTAAGTAGTCAA	1109235	1109224	2
-	TTACGTAGTAAT	1100177	1100166	2
-	GTAGGTATTAATAAA	1096466	1096455	2
-	TTACCTAGTAAA	1088751	1088740	2
-	TTAGGTTGCAAAA	1087270	1087259	2
-	TTTGGTAGTGAA	1040840	1040829	2
-	TTAGATAATAAA	1028768	1028757	2
-	TTTTGTAGTAAA	1015670	1015659	2
-	TTTGGTGGTAAA	1014651	1014640	2
-	TTAGATGGTAAA	979105	979094	2
-	TTAGGTGGTCAA	976055	976044	2
-	TTAGATAGTAAT	967736	967725	2
-	TTAGGTAATCAA	966404	966393	2
-	CTAGGTGGTAAA	961714	961703	2
-	TTAGGAATTAATAAA	956623	956612	2
-	TTTGATAGTAAA	954728	954717	2
-	TAAGGTATTAATAAA	915849	915838	2
-	ATATGTAGTAAA	909472	909461	2
-	TTAGATAGTAAG	898734	898723	2
-	TTAGCTAGTGAA	886115	886104	2
-	TTAAGTGGTAAA	880723	880712	2
-	TTAGGTTCTAAA	871509	871498	2
-	TTAGCTAGTAAC	866339	866328	2
-	TTAAGTAGTAAT	860770	860759	2
-	TTAGGAGGTAAA	849314	849303	2
-	TTAAGTACTAAA	847244	847233	2
-	TTAGTTAGTACA	840619	840608	2
-	TTATGTAGTAAT	827495	827484	2
-	TTAGGTTTTAAA	825786	825775	2
-	TTAAATAGTAAA	819660	819649	2
-	TTAAGTAGTAAG	801617	801606	2
-	TTAGGTTCTAAA	770274	770263	2
-	TTAGGTAGTTAA	757165	757154	1
-	TTAGCTTGTAATAAA	744915	744904	2

Strand	Match	Position on pSK1		Mismatches
		Start (nt)	Stop (nt)	
-	TTAACTAGTAAA	734507	734496	2
-	TTAGTTAGTAAT	723478	723467	2
-	TTAGATAATAAAA	710133	710122	2
-	TTATGTAGTTAA	710085	710074	2
-	TTAGCTAGTAAT	679163	679152	2
-	TTAGATAGTACA	666268	666257	2
-	TTAGATAGTAAA	664062	664051	1
-	TTAGTTTGTAATA	649738	649727	2
-	TTAAGTAATAAAA	649591	649580	2
-	TTAAGTATTAATA	646929	646918	2
-	TTAGCTAGTAAC	638707	638696	2
-	TTAGGTAATAAG	627049	627038	2
-	TTAATTAGTAAA	625706	625695	2
-	TCAGGTAATAAAA	621986	621975	2
-	TTAGGTATGAAA	621179	621168	2
-	TTCAGTAGTAAA	601632	601621	2
-	GTAGGTATTAATA	595082	595071	2
-	ATAGGTAATAAAA	591062	591051	2
-	TTAGGTAGTAAG	583830	583819	1
-	TTAACTAGTAAA	583344	583333	2
-	TTAGCTGGTAAA	576565	576554	2
-	TTAACTAGTAAA	573112	573101	2
-	TGAGGTAATAAAA	556596	556585	2
-	TTAGTTTGTAATA	539838	539827	2
-	TTAGTTAATAAAA	538327	538316	2
-	TTAGCTTGTAATA	531503	531492	2
-	TTAGTAAGTAAA	529887	529876	2
-	TTAGGAAGAAAA	483787	483776	2
-	TTAGGTTGTAAT	400765	400754	2
-	TTAGAAAAGTAAA	370345	370334	2
-	TTAGGTAGAAAA	352113	352102	1
-	CAAGGTAGTAAA	336383	336372	2
-	TTGGTAGTAAA	326861	326850	1
-	GAAGGTAGTAAA	311056	311045	2
-	TTAGGAAGGAAA	298731	298720	2
-	TTGGTGGTAAA	262074	262063	2
-	TTGGTAATAAAA	259993	259982	2
-	TTACGTAATAAAA	246511	246500	2
-	TTACGTAGCAAAA	241188	241177	2
-	ATAGGTAATAAAA	236800	236789	2
-	TTAGATACTAAA	228629	228618	2
-	TTAAATAGTAAA	209406	209395	2
-	TTATGTACTAAA	200188	200177	2
-	TTAGGTAATATA	195790	195779	2
-	TTAGCTAATAAAA	176431	176420	2
-	TTGGGTAGGAAA	166260	166249	2
-	TTGGTGGTAAA	164927	164916	2
-	TTATGTACTAAA	158324	158313	2
-	TTAGGCAGTATA	156927	156916	2
-	TTAGATACTAAA	139557	139546	2
-	TTGGTATTAATA	128914	128903	2
-	TTGGTATTAATA	109076	109065	2
-	TTAGGTGTTAAA	79311	79300	2

Strand	Match	Position on pSK1		Mismatches
		Start (nt)	Stop (nt)	
-	TTTTGTAGTAAA	78754	78743	2
-	TTAGGCATTAAA	73214	73203	2
-	GTAGGAAGTAAA	71217	71206	2
-	ATAGGTAATAAAA	48964	48953	2
-	TTAGGTAATAAAA	41976	41965	1
-	ATATGTAGTAAA	32655	32644	2
-	TTAAGTAATAAAA	31023	31012	2
-	TTTGTTAGTAAA	8695	8684	2
-	TGAGGTAATAAAA	2540	2529	2

BIBLIOGRAPHY

Abajy, M. Y., Kopec, J., Schiwon, K., Burzynski, M., Doring, M., Bohn, C. and Grohmann, E. (2007). A type IV-secretion-like system is required for conjugative DNA transport of broad-host-range plasmid pIP501 in gram-positive bacteria. *J Bacteriol* **189**: 2487-2496.

Abeles, A. L., Friedman, S. A. and Austin, S. J. (1985). Partition of unit-copy miniplasmids to daughter cells: III. The DNA sequence and functional organization of the P1 partition region. *J Mol Biol* **185**: 261-272.

Adachi, S., Hori, K. and Hiraga, S. (2006). Subcellular positioning of F plasmid mediated by dynamic localization of SopA and SopB. *J Mol Biol* **356**: 850-863.

Addinall, S. G., Bi, E. and Lutkenhaus, J. (1996). FtsZ ring formation in *fts* mutants. *J Bacteriol* **178**: 3877-3884.

Ah-Seng, Y., Lopez, F., Pasta, F., Lane, D. and Bouet, J. Y. (2009). Dual role of DNA in regulating ATP hydrolysis by the SopA partition protein. *J Biol Chem* **284**: 30067-30075.

Ah-Seng, Y., Rech, J., Lane, D. and Bouet, J. Y. (2013). Defining the role of ATP hydrolysis in mitotic segregation of bacterial plasmids. *PLoS Genet* **9**: e1003956.

Akhtar, P., Anand, S. P., Watkins, S. C. and Khan, S. A. (2009). The tubulin-like RepX protein encoded by the pXO1 plasmid forms polymers *in vivo* in *Bacillus anthracis*. *J Bacteriol* **191**: 2493-2500.

Alonso, A., Sánchez, P. and Martínez, J. L. (2001). Environmental selection of antibiotic resistance genes. *Environ Microbiol* **3**: 1-9.

Altschul, S. F., Gish, W., Miller, W., Myers, E. W. and Lipman, D. J. (1990). Basic local alignment search tool. *J Mol Biol* **215**: 403-410.

Altschul, S. F., Madden, T. L., Schäffer, A. A., Zhang, J., Zhang, Z., Miller, W. and Lipman, D. J. (1997). Gapped BLAST and PSI-BLAST: a new generation of protein database search programs. *Nucleic Acids Res* **25**: 3389-3402.

Amábile-Cuevas, C. F. and Heinemann, J. A. (2004). Shooting the messenger of antibiotic resistance: plasmid elimination as a potential counter-evolutionary tactic. *Drug Discov Today* **9**: 465-467.

Andersen, K. R., Leksa, N. C. and Schwartz, T. U. (2013). Optimized *E. coli* expression strain LOBSTR eliminates common contaminants from His-tag purification. *Proteins* **81**: 1857-1861.

Apisiridej, S., Leelaporn, A., Scaramuzzi, C. D., Skurray, R. A. and Firth, N. (1997). Molecular analysis of a mobilizable theta-mode trimethoprim resistance plasmid from coagulase-negative staphylococci. *Plasmid* **38**: 13-24.

Archer, G. L. and Johnston, J. L. (1983). Self-transmissible plasmids in staphylococci that encode resistance to aminoglycosides. *Antimicrob Agents Ch* **24**: 70-77.

Austin, S. and Abeles, A. (1983). Partition of unit-copy miniplasmids to daughter cells: II. The partition region of miniplasmid P1 encodes an essential protein and a centromere-like site at which it acts. *J Mol Biol* **169**: 373-387.

Aylett, C. H. S., Izoré, T., Amos, L. A. and Löwe, J. (2013). Structure of the tubulin/FtsZ-like protein TubZ from *Pseudomonas* bacteriophage Φ KZ. *J Mol Biol* **425**: 2164-2173.

Aylett, C. H. S. and Löwe, J. (2012). Superstructure of the centromeric complex of TubZRC plasmid partitioning systems. *Proc Natl Acad Sci USA* **109**: 16522-16527.

Aylett, C. H. S., Wang, Q., Michie, K. A., Amos, L. A. and Löwe, J. (2010). Filament structure of bacterial tubulin homologue TubZ. *Proc Natl Acad Sci USA* **107**: 19766-19771.

Bächi, B. (1980). Physical mapping of *Bgl*I, *Bgl*II, *Pst*I and *Eco*RI restriction fragments of staphylococcal phage Φ 11 DNA. *Mol Gen Genet* **180**: 391-398.

Baquero, F., Coque, T. M. and de la Cruz, F. (2011). Ecology and evolution as targets: the need for novel eco-evo drugs and strategies to fight antibiotic resistance. *Antimicrob Agents Ch* **55**: 3649-3660.

Baquero, F., Lanza, V. F., Cantón, R. and Coque, T. M. (2015). Public health evolutionary biology of antimicrobial resistance: priorities for intervention. *Evol Appl* **8**: 223-239.

Barillà, D., Carmelo, E. and Hayes, F. (2007). The tail of the ParG DNA segregation protein remodels ParF polymers and enhances ATP hydrolysis via an arginine finger-like motif. *Proc Natl Acad Sci USA* **104**: 1811-1816.

Barillà, D. and Hayes, F. (2003). Architecture of the ParF-ParG protein complex involved in prokaryotic DNA segregation. *Mol Microbiol* **49**: 487-499.

Baron, S. (1996). Medical Microbiology. University of Texas Medical Branch at Galveston, Galveston.

Barr, V., Barr, K., Millar, M. R. and Lacey, R. W. (1986). β -lactam antibiotics increase the frequency of plasmid transfer in *Staphylococcus aureus*. *J Antimicrob Chemoth* **17**: 409-413.

Bataineh, H. A. (2006). Resistance of *Staphylococcus aureus* to vancomycin in Zarqa, Jordan. *Pak J Med Sci* **22**: 144-148.

Baxter, J. C. and Funnell, B. E. (2014). Plasmid partition mechanisms. *Microbiol Spectr* **2**.

Beitel, C. W., Froenicke, L., Lang, J. M., Korf, I. F., Michelmore, R. W., Eisen, J. A. and Darling, A. E. (2014). Strain- and plasmid-level deconvolution of a synthetic metagenome by sequencing proximity ligation products. *PeerJ* **2**: e415.

Ben-Yehuda, S., Fujita, M., Liu, X. S., Gorbatyuk, B., Skoko, D., Yan, J., Marko, J. F., Liu, J. S., Eichenberger, P., Rudner, D. Z. and Losick, R. (2005). Defining a centromere-like element in *Bacillus subtilis* by identifying the binding sites for the chromosome-anchoring protein RacA. *Mol Cell* **17**: 773-782.

Ben-Yehuda, S., Rudner, D. Z. and Losick, R. (2003). RacA, a bacterial protein that anchors chromosomes to the cell poles. *Science* **299**: 532-536.

Benachour, A., Frère, J., Flahaut, S., Novel, G. and Auffray, Y. (1997). Molecular analysis of the replication region of the theta-replicating plasmid pUCL287 from *Tetragenococcus (Pediococcus) halophilus* ATCC33315. *Mol Gen Genet* **255**: 504-513.

- Berg, T., Firth, N., Apisiridej, S., Hettiaratchi, A., Leelaporn, A. and Skurray, R. A.** (1998). Complete nucleotide sequence of pSK41: evolution of staphylococcal conjugative multiresistance plasmids. *J Bacteriol* **180**: 4350-4359.
- Bernard, P. and Couturier, M.** (1992). Cell killing by the F plasmid CcdB protein involves poisoning of DNA-topoisomerase II complexes. *J Mol Biol* **226**: 735-745.
- Betley, M. J. and Mekalanos, J. J.** (1985). Staphylococcal enterotoxin A is encoded by phage. *Science* **229**: 185-187.
- Bharat, T. A. M., Murshudov, G. N., Sachse, C. and Löwe, J.** (2015). Structures of actin-like ParM filaments show architecture of plasmid-segregating spindles. *Nature* **523**: 106-110.
- Bonhoeffer, S., Lipsitch, M. and Levin, B. R.** (1997). Evaluating treatment protocols to prevent antibiotic resistance. *Proc Natl Acad Sci USA* **94**: 12106-12111.
- Bonifacino, J. S., Dell'Angelica, E. C. and Springer, T. A.** (2001). Immunoprecipitation. *Curr Protoc Mol Biol* **48**: 10.16.11–10.16.29.
- Bonnin, R. and Bouloc, P.** (2015). RNA degradation in *Staphylococcus aureus*: diversity of ribonucleases and their impact. *International Journal of Genomics* **2015**: 12.
- Bork, P., Sander, C. and Valencia, A.** (1992). An ATPase domain common to prokaryotic cell cycle proteins, sugar kinases, actin, and hsp70 heat shock proteins. *Proc Natl Acad Sci USA* **89**: 7290-7294.
- Bottomley, A. L., Kabli, A. F., Hurd, A. F., Turner, R. D., Garcia-Lara, J. and Foster, S. J.** (2014). *Staphylococcus aureus* DivIB is a peptidoglycan-binding protein that is required for a morphological checkpoint in cell division. *Mol Microbiol* **94**: 1041-1064.
- Boucher, H. W. and Corey, G. R.** (2008). Epidemiology of methicillin-resistant *Staphylococcus aureus*. *Clin Infect Dis* **46**: S344-S349.
- Bouet, J., Ah-Seng, Y., Benmeradi, N. and Lane, D.** (2007). Polymerization of SopA partition ATPase: regulation by DNA binding and SopB. *Mol Microbiol* **63**: 468-481.

Bouet, J. Y. and Funnell, B. E. (1999). P1 ParA interacts with the P1 partition complex at *parS* and an ATP-ADP switch controls ParA activities. *EMBO J* **18**: 1415-1424.

Bouet, J. Y., Surtees, J. A. and Funnell, B. E. (2000). Stoichiometry of P1 plasmid partition complexes. *J Biol Chem* **275**: 8213-8219.

Bradford, M. M. (1976). A rapid and sensitive method for the quantitation of microgram quantities of protein utilizing the principle of protein-dye binding. *Anal Biochem* **72**: 248-254.

Breier, A. M. and Grossman, A. D. (2007). Whole-genome analysis of the chromosome partitioning and sporulation protein Spo0J (ParB) reveals spreading and origin-distal sites on the *Bacillus subtilis* chromosome. *Mol Microbiol* **64**: 703-718.

Brennan, R. G. and Matthews, B. W. (1989). The helix-turn-helix DNA binding motif. *J Biol Chem* **264**: 1903-1906.

Broedersz, C. P., Wang, X., Meir, Y., Loparo, J. J., Rudner, D. Z. and Wingreen, N. S. (2014). Condensation and localization of the partitioning protein ParB on the bacterial chromosome. *Proc Natl Acad Sci USA* **111**: 8809-8814.

Brumfitt, W. and Hamilton-Miller, J. (1989). Methicillin-resistant *Staphylococcus aureus*. *New Engl J Med* **320**: 1188-1196.

Brzoska, A. J. and Firth, N. (2013). Two-plasmid vector system for independently controlled expression of green and red fluorescent fusion proteins in *Staphylococcus aureus*. *Appl Environ Microbiol* **79**: 3133-3136.

Burkhard, P., Stetefeld, J. and Strelkov, S. V. (2001). Coiled coils: a highly versatile protein folding motif. *Trends Cell Biol* **11**: 82-88.

Byrne, M. E., Gillespie, M. T. and Skurray, R. A. (1990). Molecular analysis of a gentamicin resistance transposonlike element on plasmids isolated from North American *Staphylococcus aureus* strains. *Antimicrob Agents Ch* **34**: 2106-2113.

Byrne, M. E., Gillespie, M. T. and Skurray, R. A. (1991). 4',4" adenylyltransferase activity on conjugative plasmids isolated from *Staphylococcus aureus* is encoded on an integrated copy of pUB110. *Plasmid* **25**: 70-75.

Byrne, M. E., Rouch, D. A. and Skurray, R. A. (1989). Nucleotide sequence analysis of IS256 from the *Staphylococcus aureus* gentamicin-tobramycin-kanamycin-resistance transposon Tn4001. *Gene* **81**: 361-367.

Campbell, C. S. and Mullins, R. D. (2007). In vivo visualization of type II plasmid segregation: bacterial actin filaments pushing plasmids. *J Cell Biol* **179**: 1059-1066.

Canchaya, C., Fournous, G., Chibani-Chennoufi, S., Dillmann, M. L. and Brüßow, H. (2003). Phage as agents of lateral gene transfer. *Curr Opin Microbiol* **6**: 417-424.

Carmelo, E., Barillà, D., Golovanov, A. P., Lian, L. Y., Derome, A. and Hayes, F. (2005). The unstructured N-terminal tail of ParG modulates assembly of a quaternary nucleoprotein complex in transcription repression. *J Biol Chem* **280**: 28683-28691.

Carrel, M., Perencevich, E. N. and David, M. Z. (2015). USA300 methicillin-resistant *Staphylococcus aureus*, United States, 2000–2013. *Emerg Infect Dis* **21**: 1973.

Castaing, J., Bouet, J. and Lane, D. (2008). F plasmid partition depends on interaction of SopA with non-specific DNA. *Mol Microbiol* **70**: 1000-1011.

CDC (1999). Four pediatric deaths from community-acquired methicillin-resistant *Staphylococcus aureus*-Minnesota and North Dakota, 1997-1999. *Morb Mortal Wkly Rep* **48**: 707-710.

CDC (2002). *Staphylococcus aureus* resistant to vancomycin - United States, 2002. *Morb Mortal Wkly Rep* **51**: 565-567.

CDC (2013). Antibiotic resistance threats in the United States, 2013.

CDC (2014). Active bacterial core surveillance report, emerging infections program network, methicillin resistant *Staphylococcus aureus*, 2014.

Chalker, A. F., Ingraham, K. A., Lunsford, R. D., Bryant, A. P., Bryant, J., Wallis, N. G., Broskey, J. P., Pearson, S. C. and Holmes, D. J. (2000). The *bacA* gene, which determines bacitracin susceptibility in *Streptococcus pneumoniae* and *Staphylococcus aureus*, is also required for virulence. *Microbiology* **146**: 1547-1553.

- Chambers, H. F.** (2001). The changing epidemiology of *Staphylococcus aureus*? *Emerg Infect Dis* **7**: 178-182.
- Chan, H. Y.** (2011). Plasmid stability determinant of pSK1 from *Staphylococcus aureus*. Honours thesis. The University of Sydney.
- Chen, X., Zaro, J. and Shen, W.** (2013). Fusion protein linkers: property, design and functionality. *Adv Drug Deliver Rev* **65**: 1357-1369.
- Chen, Y. and Erickson, H. P.** (2008). *In vitro* assembly studies of FtsZ/tubulin-like proteins (TubZ) from *Bacillus* Plasmids: evidence for a capping mechanism. *J Biol Chem* **283**: 8102-8109.
- Chongtrakool, P., Ito, T., Ma, X. X., Kondo, Y., Trakulsomboon, S., Tiensasitorn, C., Jamklang, M., Chavalit, T., Song, J. H. and Hiramatsu, K.** (2006). Staphylococcal cassette chromosome *mec* (SCC*mec*) typing of methicillin-resistant *Staphylococcus aureus* strains isolated in 11 Asian countries: a proposal for a new nomenclature for SCC*mec* elements. *Antimicrob Agents Ch* **50**: 1001-1012.
- Chopra, I.** (1976). Mechanisms of resistance to fusidic acid in *Staphylococcus aureus*. *J Gen Microbiol* **96**: 229-238.
- Clements, M. O., Watson, S. P. and Foster, S. J.** (1999). Characterization of the major superoxide dismutase of *Staphylococcus aureus* and its role in starvation survival, stress resistance, and pathogenicity. *J Bacteriol* **181**: 3898-3903.
- Collas, P.** (2010). The current state of chromatin immunoprecipitation. *Mol Biotechnol* **45**: 87-100.
- Cookson, B. D. and Phillips, I.** (1988). Epidemic methicillin-resistant *Staphylococcus aureus*. *J Antimicrob Chemoth* **21**: 57-65.
- Cormack, B. P., Valdivia, R. H. and Falkow, S.** (1996). FACS-optimized mutants of the green fluorescent protein (GFP). *Gene* **173**: 33-38.
- Corn, J. E. and Berger, J. M.** (2006). Regulation of bacterial priming and daughter strand synthesis through helicase-primase interactions. *Nucleic Acids Res* **34**: 4082-4088.

Corvaglia, A. R., François, P., Hernandez, D., Perron, K., Linder, P. and Schrenzel, J. (2010). A type III-like restriction endonuclease functions as a major barrier to horizontal gene transfer in clinical *Staphylococcus aureus* strains. *Proc Natl Acad Sci USA* **107**: 11954-11958.

Cremazy, F. G. E., Manders, E. M. M., Bastiaens, P. I. H., Kramer, G., Hager, G. L., van Munster, E. B., Verschure, P. J., Gadella Jr, T. J. and van Driel, R. (2005). Imaging *in situ* protein–DNA interactions in the cell nucleus using FRET–FLIM. *Exp Cell Res* **309**: 390-396.

Dandekar, T. and Dandekar, G. (2010). Pharmacogenomic strategies against microbial resistance: from bright to bleak to innovative. *Pharmacogenomics* **11**: 1193-1196.

Daum, R. S., Ito, T., Hiramatsu, K., Hussain, F., Mongkolrattanothai, K., Jamklang, M. and Boyle-Vavra, S. (2002). A novel methicillin-resistance cassette in community-acquired methicillin-resistant *Staphylococcus aureus* isolates of diverse genetic backgrounds. *J Infect Dis* **186**: 1344-1347.

Davey, M. J. and Funnell, B. E. (1997). Modulation of the P1 plasmid partition protein ParA by ATP, ADP, and P1 ParB. *J Biol Chem* **272**: 15286-15292.

Davis, M. A., Martin, K. A. and Austin, S. J. (1992). Biochemical activities of the ParA partition protein of the P1 plasmid. *Mol Microbiol* **6**: 1141-1147.

Davis, M. A., Radnedge, L., Martin, K. A., Hayes, F., Youngren, B. and Austin, S. J. (1996). The P1 ParA protein and its ATPase activity play a direct role in the segregation of plasmid copies to daughter cells. *Mol Microbiol* **21**: 1029-1036.

Derman, A. I., Lim-Fong, G. and Pogliano, J. (2008). Intracellular mobility of plasmid DNA is limited by the ParA family of partitioning systems. *Mol Microbiol* **67**: 935-946.

Diep, B. A., Gill, S. R., Chang, R. F., Phan, T. H., Chen, J. H., Davidson, M. G., Lin, F., Lin, J., Carleton, H. A., Mongodin, E. F., Sensabaugh, G. F. and Perdreau-Remington, F. (2006). Complete genome sequence of USA300, an epidemic clone of community-acquired methicillin-resistant *Staphylococcus aureus*. *Lancet* **367**: 731-739.

Dougan, D. A., Micevski, D. and Truscott, K. N. (2012). The N-end rule pathway: from recognition by N-recognins, to destruction by AAA+proteases. *BBA-Mol Cell Res* **1823**: 83-91.

Dubin, D. T., Matthews, P. R., Chikramane, S. G. and Stewart, P. R. (1991). Physical mapping of the *mec* region of an American methicillin-resistant *Staphylococcus aureus* strain. *Antimicrob Agents Ch* **35**: 1661-1665.

Dunker, A. K., Brown, C. J., Lawson, J. D., Iakoucheva, L. M. and Obradović, Z. (2002). Intrinsic disorder and protein function. *Biochemistry* **41**: 6573-6582.

Dunny, G. M., Lee, L. N. and LeBlanc, D. J. (1991). Improved electroporation and cloning vector system for gram-positive bacteria. *Appl Environ Microbiol* **57**: 1194-1201.

Dyer, D. W., Rock, M. I., Lee, C. Y. and Iandolo, J. J. (1985). Generation of transducing particles in *Staphylococcus aureus*. *J Bacteriol* **161**: 91-95.

Dyke, K. G. and Gregory, P. (1997). Resistance mediated by β -lactamase. In Crossley, K. B. and Archer, G. L. *The staphylococci in human disease*. New York, USA, Churchill Livingstone.

Dyson, H. J. and Wright, P. E. (2005). Intrinsically unstructured proteins and their functions. *Nat Rev Mol Cell Biol* **6**: 197-208.

Ebersbach, G. and Gerdes, K. (2001). The double *par* locus of virulence factor pB171: DNA segregation is correlated with oscillation of ParA. *Proc Natl Acad Sci USA* **98**: 15078-15083.

Ebersbach, G. and Gerdes, K. (2004). Bacterial mitosis: partitioning protein ParA oscillates in spiral-shaped structures and positions plasmids at mid-cell. *Mol Microbiol* **52**: 385-398.

Ebersbach, G. and Gerdes, K. (2005). Plasmid segregation mechanisms. *Annu Rev Genet* **39**: 453-479.

Edgar, R., Chatteraj, D. K. and Yarmolinsky, M. (2001). Pairing of P1 plasmid partition sites by ParB. *Mol Microbiol* **42**: 1363-1370.

Edwards, J. S., Betts, L., Frazier, M. L., Pollet, R. M., Kwong, S. M., Walton, W. G., Ballentine, W. K., Huang, J. J., Habibi, S., Del Campo, M., Meier, J. L., Dervan, P. B., Firth, N. and Redinbo, M. R. (2013). Molecular basis of antibiotic multiresistance transfer in *Staphylococcus aureus*. *Proc Natl Acad Sci USA* **110**: 2804-2809.

Erdmann, N., Petroff, T. and Funnell, B. E. (1999). Intracellular localization of P1 ParB protein depends on ParA and *parS*. *Proc Natl Acad Sci USA* **96**: 14905-14910.

Erickson, H. P. and O'Brien, E. T. (1992). Microtubule dynamic instability and GTP hydrolysis. *Annu Rev Biophys Biomol Struct* **21**: 145-166.

Fields, S. and Song, O. (1989). A novel genetic system to detect protein-protein interactions. *Nature* **340**: 245-246.

Figgett, W. A. (2007). Partitioning system of the staphylococcal multiresistance plasmid pSK1. Honours thesis. The University of Sydney, Australia.

Filice, G., Nyman, J., Lexau, C., Lees, C. H., Bockstedt, L. A., Como-Sabetti, K., Leshner, L. J. and Lynfield, R. (2010). Excess costs and utilization associated with methicillin resistance for patients with *Staphylococcus aureus* infection. *Infect Control Hosp Epidemiol* **31**: 365-373.

Fink, G. and Löwe, J. (2015). Reconstitution of a prokaryotic minus end-tracking system using TubRC centromeric complexes and tubulin-like protein TubZ filaments. *Proc Natl Acad Sci USA* **112**: E1845-E1850.

Firth, N., Apisiridej, S., Berg, T., O'Rourke, B. A., Curnock, S., Dyke, K. G. and Skurray, R. A. (2000). Replication of staphylococcal multiresistance plasmids. *J Bacteriol* **182**: 2170-2178.

Firth, N., Ridgway, K. P., Byrne, M. E., Fink, P. D., Johnson, L., Paulsen, I. T. and Skurray, R. A. (1993). Analysis of a transfer region from the staphylococcal conjugative plasmid pSK41. *Gene* **136**: 13-25.

Firth, N. and Skurray, R. A. (1998). Mobile elements in the evolution and spread of multiple-drug resistance in staphylococci. *Drug Resist Update* **1**: 49-58.

Firth, N. and Skurray, R. A. (2000). The *Staphylococcus*-Genetics: Accessory elements and genetic exchange. In Fischetti, V. A., Novick, R. P., Ferretti, J. J.,

Portnoy, D. A. and Rood, J. I. *Gram-positive pathogens*. Washington, D. C., ASM press.

Fischbach, M. A. and Walsh, C. T. (2009). Antibiotics for emerging pathogens. *Science* **325**: 1089-1093.

Forsberg, K. J., Reyes, A., Wang, B., Selleck, E. M., Sommer, M. O. A. and Dantas, G. (2012). The shared antibiotic resistome of soil bacteria and human pathogens. *Science* **337**: 1107-1111.

Forsgren, A. and Sjöquist, J. (1966). "Protein A" from *S. aureus*: I. Pseudo-immune reaction with human γ -globulin. *J Immunol* **97**: 822-827.

Förster, T. (1948). Intermolecular energy migration and fluorescence. *Ann. Phys.* **437**: 55-75.

Fozo, E. M., Hemm, M. R. and Storz, G. (2008). Small toxic proteins and the antisense RNAs that repress them. *Microbiol Mol Biol R* **72**: 579-589.

Francia, M. V., Fujimoto, S., Tille, P., Weaver, K. E. and Clewell, D. B. (2004). Replication of *Enterococcus faecalis* pheromone-responding plasmid pAD1: location of the minimal replicon and *oriV* site and RepA involvement in initiation of replication. *J Bacteriol* **186**: 5003-5016.

Free, R. B., Hazelwood, L. A. and Sibley, D. R. (2001). Identifying Novel Protein-Protein Interactions Using Co-Immunoprecipitation and Mass Spectroscopy. *Current Protocols in Neuroscience*. John Wiley & Sons, Inc.

Friedman, S. A. and Austin, S. J. (1988). The P1 plasmid-partition system synthesizes two essential proteins from an autoregulated operon. *Plasmid* **19**: 103-112.

Fung, E., Bouet, J. Y. and Funnell, B. E. (2001). Probing the ATP-binding site of P1 ParA: partition and repression have different requirements for ATP binding and hydrolysis. *EMBO J* **20**: 4901-4911.

Funnell, B. E. (1988a). Mini-P1 plasmid partitioning: excess ParB protein destabilizes plasmids containing the centromere *parS*. *J Bacteriol* **170**: 954-960.

Funnell, B. E. (1988b). Participation of *Escherichia coli* integration host factor in the P1 plasmid partition system. *Proc Natl Acad Sci USA* **85**: 6657-6661.

Funnell, B. E. (1991). The P1 plasmid partition complex at *parS*. The influence of *Escherichia coli* integration host factor and of substrate topology. *J Biol Chem* **266**: 14328-14337.

Funnell, B. E. (2014). How to build segregation complexes in bacteria: use bridges. *Gene Dev* **28**: 1140-1142.

Funnell, B. E. and Gagnier, L. (1993). The P1 plasmid partition complex at *parS*. II. Analysis of ParB protein binding activity and specificity. *J Biol Chem* **268**: 3616-3624.

Garcia-Pino, A., Balasubramanian, S., Wyns, L., Gazit, E., De Greve, H., Magnuson, R. D., Charlier, D., van Nuland, N. A. J. and Loris, R. (2010). Allosteric and intrinsic disorder mediate transcription regulation by conditional cooperativity. *Cell* **142**: 101-111.

Garcia-Pino, A., Christensen-Dalsgaard, M., Wyns, L., Yarmolinsky, M., Magnuson, R. D., Gerdes, K. and Loris, R. (2008). Doc of prophage P1 is inhibited by its antitoxin partner Phd through fold complementation. *J Biol Chem* **283**: 30821-30827.

Garneau, J. E., Dupuis, M.-E., Villion, M., Romero, D. A., Barrangou, R., Boyaval, P., Fremaux, C., Horvath, P., Magadan, A. H. and Moineau, S. (2010). The CRISPR/Cas bacterial immune system cleaves bacteriophage and plasmid DNA. *Nature* **468**: 67-71.

Garner, E. C., Campbell, C. S. and Mullins, R. D. (2004). Dynamic instability in a DNA-segregating prokaryotic actin homolog. *Science* **306**: 1021-1025.

Garner, E. C., Campbell, C. S., Weibel, D. B. and Mullins, R. D. (2007). Reconstitution of DNA segregation driven by assembly of a prokaryotic actin homolog. *Science* **315**: 1270-1274.

Gayathri, P., Fujii, T., Møller-Jensen, J., van den Ent, F., Namba, K. and Löwe, J. (2012). A bipolar spindle of antiparallel ParM filaments drives bacterial plasmid segregation. *Science* **338**: 1334-1337.

Gayathri, P., Fujii, T., Namba, K. and Löwe, J. (2013). Structure of the ParM filament at 8.5 Å resolution. *J Struct Biol* **184**: 33-42.

Gennaro, M. L., Kornblum, J. and Novick, R. P. (1987). A site-specific recombination function in *Staphylococcus aureus* plasmids. *J Bacteriol* **169**: 2601-2610.

Gerdes, K., Christensen, S. K. and Lobner-Olesen, A. (2005). Prokaryotic toxin-antitoxin stress response loci. *Nat Rev Microbiol* **3**: 371-382.

Gerdes, K., Howard, M. and Szardenings, F. (2010). Pushing and pulling in prokaryotic DNA segregation. *Cell* **141**: 927-942.

Gerdes, K. and Wagner, E. G. H. (2007). RNA antitoxins. *Curr Opin Microbiol* **10**: 117-124.

Gillespie, M. T., Lyon, B. R., Messerotti, L. J. and Skurray, R. A. (1987). Chromosome- and plasmid-mediated gentamicin resistance in *Staphylococcus aureus* encoded by Tn4001. *J Med Microbiol* **24**: 139-144.

Gillespie, M. T., Lyon, B. R. and Skurray, R. A. (1988). Structural and evolutionary relationships of β -lactamase transposons from *Staphylococcus aureus*. *J Gen Microbiol* **134**: 2857-2866.

Gillet, Y., Issartel, B., Vanhems, P., Fournet, J.-C., Lina, G., Bes, M., Vandenesch, F., Piémont, Y., Brousse, N., Floret, D. and Etienne, J. (2002). Association between *Staphylococcus aureus* strains carrying gene for Panton-Valentine leukocidin and highly lethal necrotising pneumonia in young immunocompetent patients. *Lancet* **359**: 753-759.

Golovanov, A. P., Barillà, D., Golovanova, M., Hayes, F. and Lian, L. Y. (2003). ParG, a protein required for active partition of bacterial plasmids, has a dimeric ribbon-helix-helix structure. *Mol Microbiol* **50**: 1141-1153.

Gonzalez, B. E., Martinez-Aguilar, G., Hulten, K. G., Hammerman, W. A., Coss-Bu, J., Avalos-Mishaan, A., Mason, E. O. and Kaplan, S. L. (2005). Severe staphylococcal sepsis in adolescents in the era of community-acquired methicillin-resistant *Staphylococcus aureus*. *Pediatrics* **115**: 642-648.

Gorak, E. J., Yamada, S. M. and Brown, J. D. (1999). Community-acquired methicillin-resistant *Staphylococcus aureus* in hospitalized adults and children without known risk factors. *Clin Infect Dis* **29**: 797-800.

Gordon, G. S., Sitnikov, D., Webb, C. D., Teleman, A., Straight, A., Losick, R., Murray, A. W. and Wright, A. (1997). Chromosome and low copy plasmid segregation in *E. coli*: visual evidence for distinct mechanisms. *Cell* **90**: 1113-1121.

Gordon, S., Rech, J., Lane, D. and Wright, A. (2004). Kinetics of plasmid segregation in *Escherichia coli*. *Mol Microbiol* **51**: 461-469.

Gould, I. M., Reilly, J., Bunyan, D. and Walker, A. (2010). Costs of healthcare-associated methicillin-resistant *Staphylococcus aureus* and its control. *Clin Microbiol Infect* **16**: 1721-1728.

Graham, T. G. W., Wang, X., Song, D., Etsen, C. M., van Oijen, A. M., Rudner, D. Z. and Loparo, J. J. (2014). ParB spreading requires DNA bridging. *Gene Dev* **28**: 1228-1238.

Greene, C., McDevitt, D., Francois, P., Vaudaux, P. E., Lew, D. P. and Poster, T. J. (1995). Adhesion properties of mutants of *Staphylococcus aureus* defective in fibronectin-binding proteins and studies on the expression of *fnb* genes. *Mol Microbiol* **17**: 1143-1152.

Greenfield, T. J., Ehli, E., Kirshenmann, T., Franch, T., Gerdes, K. and Weaver, K. E. (2000). The antisense RNA of the *par* locus of pAD1 regulates the expression of a 33-amino-acid toxic peptide by an unusual mechanism. *Mol Microbiol* **37**: 652-660.

Greenfield, T. J., Franch, T., Gerdes, K. and Weaver, K. E. (2001). Antisense RNA regulation of the *par* post-segregational killing system: structural analysis and mechanism of binding of the antisense RNA, RNAII and its target, RNAI. *Mol Microbiol* **42**: 527-537.

Greenfield, T. J. and Weaver, K. E. (2000). Antisense RNA regulation of the pAD1 *par* post-segregational killing system requires interaction at the 5' and 3' ends of the RNAs. *Mol Microbiol* **37**: 661-670.

Grice, E. A. and Segre, J. A. (2011). The skin microbiome. *Nat Rev Microbiol* **9**: 244-253.

Grkovic, S., Brown, M. H., Hardie, K. M., Firth, N. and Skurray, R. A. (2003). Stable low-copy-number *Staphylococcus aureus* shuttle vectors. *Microbiology* **149**: 785-794.

Gu, B., Kelesidis, T., Tsiodras, S., Hindler, J. and Humphries, R. M. (2013). The emerging problem of linezolid-resistant *Staphylococcus*. *J Antimicrob Chemoth* **68**: 4-11.

Gustafsson, M. G. L., Shao, L., Carlton, P. M., Wang, C. J. R., Golubovskaya, I. N., Cande, W. Z., Agard, D. A. and Sedat, J. W. (2008). Three-dimensional resolution doubling in wide-field fluorescence microscopy by structured illumination. *Biophys J* **94**: 4957-4970.

Guynet, C., Cuevas, A., Moncalián, G. and de la Cruz, F. (2011). The *stb* operon balances the requirements for vegetative stability and conjugative transfer of plasmid R388. *PLoS Genet* **7**: 1-12.

Guynet, C. and de la Cruz, F. (2011). Plasmid segregation without partition. *Mob Genet Elements* **1**: 236-241.

Hanssen, A. M. and Ericson Sollid, J. U. (2006). *SCCmec* in staphylococci: genes on the move. *FEMS Immunol Med Microbiol* **46**: 8-20.

Hao, J. J. and Yarmolinsky, M. (2002). Effects of the P1 plasmid centromere on expression of P1 partition genes. *J Bacteriol* **184**: 4857-4867.

Hartman, B. J. and Tomasz, A. (1984). Low-affinity penicillin-binding protein associated with beta-lactam resistance in *Staphylococcus aureus*. *J Bacteriol* **158**: 513-516.

Hatano, T. and Niki, H. (2010). Partitioning of P1 plasmids by gradual distribution of the ATPase ParA. *Mol Microbiol* **78**: 1182-1198.

Hatano, T., Yamaichi, Y. and Niki, H. (2007). Oscillating focus of SopA associated with filamentous structure guides partitioning of F plasmid. *Mol Microbiol* **64**: 1198-1213.

Havey, J. C., Vecchiarelli, A. G. and Funnell, B. E. (2012). ATP-regulated interactions between P1 ParA, ParB and non-specific DNA that are stabilized by the plasmid partition site, *parS*. *Nucleic Acids Res* **40**: 801-812.

Hayden, M. K., Rezai, K., Hayes, R. A., Lolans, K., Quinn, J. P. and Weinstein, R. A. (2005). Development of daptomycin resistance *in vivo* in methicillin-resistant *Staphylococcus aureus*. *J Clin Microbiol* **43**: 5285-5287.

Hayes, F. (2000). The partition system of multidrug resistance plasmid TP228 includes a novel protein that epitomizes an evolutionarily distinct subgroup of the ParA superfamily. *Mol Microbiol* **37**: 528-541.

Hayes, F. and Barilla, D. (2006). The bacterial segrosome: a dynamic nucleoprotein machine for DNA trafficking and segregation. *Nature Rev Microbiol* **4**: 133-143.

Henriques-Normark, B. and Normark, S. (2014). Bacterial vaccines and antibiotic resistance. *Upsala J Med Sci* **119**: 205-208.

Herold, B. C., Immergluck, L. C., Maranan, M. C., Lauderdale, D. S., Gaskin, R. E., Boyle-Vavra, S., Leitch, C. D. and Daum, R. S. (1998). Community-acquired methicillin-resistant *Staphylococcus aureus* in children with no identified predisposing risk. *JAMA* **279**: 593-598.

Hester, C. M. and Lutkenhaus, J. (2007). Soj (ParA) DNA binding is mediated by conserved arginines and is essential for plasmid segregation. *Proc Natl Acad Sci USA* **104**: 20326-20331.

Hilser, V. J. and Thompson, E. B. (2007). Intrinsic disorder as a mechanism to optimize allosteric coupling in proteins. *Proc Natl Acad Sci USA* **104**: 8311-8315.

Hiramatsu, K., Cui, L., Kuroda, M. and Ito, T. (2001). The emergence and evolution of methicillin-resistant *Staphylococcus aureus*. *Trends Microbiol* **9**: 486-493.

Hiramatsu, K., Hanaki, H., Ino, T., Yabuta, K., Oguri, T. and Tenover, F. C. (1997). Methicillin-resistant *Staphylococcus aureus* clinical strain with reduced vancomycin susceptibility. *J Antimicrob Chemoth* **40**: 135-136.

Ho, T. Q., Zhong, Z., Aung, S. and Pogliano, J. (2002). Compatible bacterial plasmids are targeted to independent cellular locations in *Escherichia coli*. *EMBO J* **21**: 1864-1872.

Hong, H., Park, S., Flores Jiménez, R. H., Rinehart, D. and Tamm, L. K. (2007). Role of aromatic side chains in the folding and thermodynamic stability of integral membrane proteins. *J Am Chem Soc* **129**: 8320-8327.

Horinouchi, S. and Weisblum, B. (1982). Nucleotide sequence and functional map of pE194, a plasmid that specifies inducible resistance to macrolide, lincosamide, and streptogramin type B antibiotics. *J Bacteriol* **150**: 804-814.

Hoshino, S. and Hayashi, I. (2012). Filament formation of the FtsZ/tubulin-like protein TubZ from the *Bacillus cereus* pXO1 plasmid. *J Biol Chem* **287**: 32103-32112.

Howden, B. P., Davies, J. K., Johnson, P. D. R., Stinear, T. P. and Grayson, M. L. (2010). Reduced vancomycin susceptibility in *Staphylococcus aureus*, including vancomycin-intermediate and heterogeneous vancomycin-intermediate strains: resistance mechanisms, laboratory detection, and clinical implications. *Clin Microbiol Rev* **23**: 99-139.

Hwang, L. C., Vecchiarelli, A. G., Han, Y. W., Mizuuchi, M., Harada, Y., Funnell, B. E. and Mizuuchi, K. (2013). ParA-mediated plasmid partition driven by protein pattern self-organization. *EMBO J* **32**: 1238-1249.

Iandolo, J. J., Worrell, V., Groicher, K. H., Qian, Y., Tian, R., Kenton, S., Dorman, A., Ji, H., Lin, S., Loh, P., Qi, S., Zhu, H. and Roe, B. A. (2002). Comparative analysis of the genomes of the temperate bacteriophages ϕ 11, ϕ 12 and ϕ 13 of *Staphylococcus aureus* 8325. *Gene* **289**: 109-118.

Ileri, A. and Savino, C. (2008). Protein structure determination by X-ray crystallography. *Methods Mol Biol* **452**: 63-87.

Ilves, I., Kivi, S. and Ustav, M. (1999). Long-term episomal maintenance of bovine papillomavirus Type 1 plasmids is determined by attachment to host chromosomes, which is mediated by the viral E2 protein and its binding sites. *J Virol* **73**: 4404-4412.

Ishida, T. and Kinoshita, K. (2007). PrDOS: prediction of disordered protein regions from amino acid sequence. *Nucleic Acids Res* **35**: W460-W464.

Ito, T., Katayama, Y., Asada, K., Mori, N., Tsutsumimoto, K., Tiensasitorn, C. and Hiramatsu, K. (2001). Structural comparison of three types of staphylococcal cassette chromosome *mec* integrated in the chromosome in methicillin-resistant *Staphylococcus aureus*. *Antimicrob Agents Ch* **45**: 1323-1336.

Ito, T., Katayama, Y. and Hiramatsu, K. (1999). Cloning and nucleotide sequence determination of the entire *mec* DNA of pre-methicillin-resistant *Staphylococcus aureus* N315. *Antimicrob Agents Ch* **43**: 1449-1458.

Ito, T., Ma, X. X., Takeuchi, F., Okuma, K., Yuzawa, H. and Hiramatsu, K. (2004). Novel type V staphylococcal cassette chromosome *mec* driven by a novel cassette chromosome recombinase, *ccrC*. *Antimicrob Agents Ch* **48**: 2637-2651.

Ito, T., Okuma, K., Ma, X. X., Yuzawa, H. and Hiramatsu, K. (2003). Insights on antibiotic resistance of *Staphylococcus aureus* from its whole genome: genomic island SCC. *Drug Resist Update* **6**: 41-52.

IWG-SCC (2009). Classification of staphylococcal cassette chromosome *mec* (SCC*mec*): guidelines for reporting novel SCC*mec* elements, *Antimicrob Agents Ch*. **53**: 4961-4967.

Jayaram, M., Mehta, S., Uzri, D. and Velmurugan, S. (2004). Segregation of the yeast plasmid: similarities and contrasts with bacterial plasmid partitioning. *Plasmid* **51**: 162-178.

Jensen, R. B., Dam, M. and Gerdes, K. (1994). Partitioning of plasmid R1. The *parA* operon is autoregulated by *parR* and its transcription is highly stimulated by a downstream activating element. *J Mol Biol* **236**: 1299-1309.

Jensen, R. B. and Gerdes, K. (1997). Partitioning of plasmid R1. The ParM protein exhibits ATPase activity and interacts with the centromere-like ParR-*parC* complex. *J Mol Biol* **269**: 505-513.

Jensen, R. B. and Gerdes, K. (1999). Mechanism of DNA segregation in prokaryotes: ParM partitioning protein of plasmid R1 co-localizes with its replicon during the cell cycle. *EMBO J* **18**: 4076-4084.

Jensen, R. B., Lurz, R. and Gerdes, K. (1998). Mechanism of DNA segregation in prokaryotes: Replicon pairing by *parC* of plasmid R1. *Proc Natl Acad Sci USA* **95**: 8550-8555.

Jensen, R. B. and Shapiro, L. (1999). The *Caulobacter crescentus smc* gene is required for cell cycle progression and chromosome segregation. *Proc Natl Acad Sci USA* **96**: 10661-10666.

Jensen, S. O., Apisiridej, S., Kwong, S. M., Yang, Y. H., Skurray, R. A. and Firth, N. (2010). Analysis of the prototypical *Staphylococcus aureus* multiresistance plasmid pSK1. *Plasmid* **64**: 135-142.

Jensen, S. O. and Lyon, B. R. (2009). Genetics of antimicrobial resistance in *Staphylococcus aureus*. *Future Microbiol* **4**: 565-582.

Jevons, M. P. (1961). "Celbenin" - resistant staphylococci. *Brit Med J* **1**: 124-125.

John, S. H., Lelitha, S. D. K. and Surendran, R. (2017). Clinico-microbiological study of community acquired and health care associated methicillin-resistant *Staphylococcus aureus* from skin and soft tissue infections. *Int J Res Med Sci* **4**: 7.

Kahn, M., Kolter, R., Thomas, C., Figurski, D., Meyer, R., Remaut, E. and Helinski, D. R. (1979). Plasmid cloning vehicles derived from plasmids ColE1, F, R6K, and RK2. *Methods in Enzymology*. Academic Press, USA **68**: 268-280.

Kaneko, J., Kimura, T., Narita, S., Tomita, T. and Yoshiyuki, K. (1998). Complete nucleotide sequence and molecular characterization of the temperate staphylococcal bacteriophage ϕ PVL carrying Panton–Valentine leukocidin genes. *Gene* **215**: 57-67.

Karimova, G., Pidoux, J., Ullmann, A. and Ladant, D. (1998). A bacterial two-hybrid system based on a reconstituted signal transduction pathway. *Proc Natl Acad Sci USA* **95**: 5752-5756.

Katayama, Y., Ito, T. and Hiramatsu, K. (2000). A new class of genetic element, staphylococcus cassette chromosome *mec*, encodes methicillin resistance in *Staphylococcus aureus*. *Antimicrob Agents Ch* **44**: 1549-1555.

Katayama, Y., Takeuchi, F., Ito, T., Ma, X. X., Ui-Mizutani, Y., Kobayashi, I. and Hiramatsu, K. (2003). Identification in methicillin-susceptible *Staphylococcus hominis* of an active primordial mobile genetic element for the staphylococcal cassette chromosome *mec* of methicillin-resistant *Staphylococcus aureus*. *J Bacteriol* **185**: 2711-2722.

- Kempf, V. A. J., Trebesius, K. and Autenrieth, I. B.** (2000). Fluorescent *in situ* hybridization allows rapid identification of microorganisms in blood cultures. *J Clin Microbiol* **38**: 830-838.
- Khan, S.** (1997). Rolling-circle replication of bacterial plasmids. *Microbiol Mol Biol R* **61**: 442-455.
- Khan, S. A.** (2005). Plasmid rolling-circle replication: highlights of two decades of research. *Plasmid* **53**: 126-136.
- Khan, S. A. and Novick, R. P.** (1983). Complete nucleotide-sequence of pT181, a tetracycline-resistance plasmid from *Staphylococcus aureus*. *Infect Control Hosp Epidemiol* **22**: 99-104.
- Khare, D., Ziegelin, G., Lanka, E. and Heinemann, U.** (2004). Sequence-specific DNA binding determined by contacts outside the helix-turn-helix motif of the ParB homolog KorB. *Nat Struct Mol Biol* **11**: 656-663.
- King, M. D., Humphrey, B. J., Wang, Y. F., Kourbatova, E. V., Ray, S. M. and Blumberg, H. M.** (2006). Emergence of community-acquired methicillin-resistant *Staphylococcus aureus* USA 300 clone as the predominant cause of skin and soft-tissue infections. *Ann Intern Med* **144**: 309-317.
- Klein, E., Smith, D. L. and Laxminarayan, R.** (2007). Hospitalizations and deaths caused by methicillin-resistant *Staphylococcus aureus*, United States, 1999–2005. *Emerg Infect Dis* **13**: 1840-1846.
- Kluytmans, J., van Belkum, A. and Verbrugh, H.** (1997). Nasal carriage of *Staphylococcus aureus*: epidemiology, underlying mechanisms, and associated risks. *Clin Microbiol Rev* **10**: 505-520.
- Koepsel, R. R., Murray, R. W., Rosenblum, W. D. and Khan, S. A.** (1985). The replication initiator protein of plasmid pT181 has sequence-specific endonuclease and topoisomerase-like activities. *Proc Natl Acad Sci USA* **82**: 6845-6849.
- Koepsell, S. A., Larson, M. A., Griep, M. A. and Hinrichs, S. H.** (2006). *Staphylococcus aureus* helicase but not *Escherichia coli* helicase stimulates *S. aureus* primase activity and maintains initiation specificity. *J Bacteriol* **188**: 4673-4680.

Kraemer, James A., Erb, Marcella L., Waddling, Christopher A., Montabana, Elizabeth A., Zehr, Elena A., Wang, H., Nguyen, K., Pham, Duy Stephen L., Agard, David A. and Pogliano, J. (2012). A phage tubulin assembles dynamic filaments by an atypical mechanism to center viral DNA within the host cell. *Cell* **149**: 1488-1499.

Kushnirov, V. V. (2000). Rapid and reliable protein extraction from yeast. *Yeast* **16**: 857-860.

Kwan, T., Liu, J., DuBow, M., Gros, P. and Pelletier, J. (2005). The complete genomes and proteomes of 27 *Staphylococcus aureus* bacteriophages. *Proc Natl Acad Sci USA* **102**: 5174-5179.

Kwong, S. M. and Firth, N. (2015). Structural and sequence requirements for the antisense RNA regulating replication of staphylococcal multiresistance plasmid pSK41. *Plasmid* **78**: 17-25.

Kwong, S. M., Jensen, S. O. and Firth, N. (2010). Prevalence of Fst-like toxin-antitoxin systems. *Microbiology* **156**: 975-977.

Kwong, S. M., Lim, R., LeBard, R. J., Skurray, R. A. and Firth, N. (2008). Analysis of the pSK1 replicon, a prototype from the staphylococcal multiresistance plasmid family. *Microbiology* **154**: 3084-3094.

Kwong, S. M., Skurray, R. A. and Firth, N. (2004). *Staphylococcus aureus* multiresistance plasmid pSK41: analysis of the replication region, initiator protein binding and antisense RNA regulation. *Mol Microbiol* **51**: 497-509.

Kwong, S. M., Skurray, R. A. and Firth, N. (2006). Replication control of staphylococcal multiresistance plasmid pSK41: an antisense RNA mediates dual-level regulation of Rep expression. *J Bacteriol* **188**: 4404-4412.

Lacey, R. W. (1980). Evidence for two mechanisms of plasmid transfer in mixed cultures of *Staphylococcus aureus*. *J Gen Microbiol* **119**: 423-435.

Laemmli, U. K. (1970). Cleavage of structural proteins during the assembly of the head of bacteriophage T4. *Nature* **227**: 680-685.

Lai, E. (2008). Analysis of a plasmid segregational stability determinant from *Staphylococcus aureus*. Honours thesis. The University of Sydney, Australia.

Landgraf, D., Okumus, B., Chien, P., Baker, T. A. and Paulsson, J. (2012). Segregation of molecules at cell division reveals native protein localization. *Nat Meth* **9**: 480-482.

Larkin, M. A., Blackshields, G., Brown, N. P., Chenna, R., McGettigan, P. A., McWilliam, H., Valentin, F., Wallace, I. M., Wilm, A., Lopez, R., Thompson, J. D., Gibson, T. J. and Higgins, D. G. (2007). Clustal W and Clustal X version 2.0. *Bioinformatics* **23**: 2947-2948.

Larsen, R. A., Cusumano, C., Fujioka, A., Lim-Fong, G., Patterson, P. and Pogliano, J. (2007). Treadmilling of a prokaryotic tubulin-like protein, TubZ, required for plasmid stability in *Bacillus thuringiensis*. *Gene Dev* **21**: 1340-1352.

Lau, I. F., Filipe, S. R., Søballe, B., Økstad, O. A., Barre, F. X. and Sherratt, D. J. (2003). Spatial and temporal organization of replicating *Escherichia coli* chromosomes. *Mol Microbiol* **49**: 731-743.

Lawson, T. S., Connally, R. E., Vemulpad, S. and Piper, J. A. (2011a). Express fluorescence *in situ* hybridization methods for the detection of *Staphylococcus aureus*. *Clin Lab* **59**: 789-794.

Lawson, T. S., Connally, R. E., Vemulpad, S. and Piper, J. A. (2011b). Optimization of a two-step permeabilization fluorescence *in situ* hybridization (FISH) assay for the detection of *Staphylococcus aureus*. *J Clin Lab Anal* **25**: 359-365.

Laxminarayan, R., Duse, A., Wattal, C., Zaidi, A. K. M., Wertheim, H. F. L., Sumpradit, N., Vlieghe, E., Hara, G. L., Gould, I. M., Goossens, H., Greko, C., So, A. D., Bigdeli, M., Tomson, G., Woodhouse, W., Ombaka, E., Peralta, A. Q., Qamar, F. N., Mir, F., Kariuki, S., Bhutta, Z. A., Coates, A., Bergstrom, R., Wright, G. D., Brown, E. D. and Cars, O. (2013). Antibiotic resistance—the need for global solutions. *Lancet Infect Dis* **13**: 1057-1098.

LeBard, R. J. (2005). Molecular characterisation of plasmid stability mechanisms in *Staphylococcus aureus*. PhD thesis. The University of Sydney, Australia.

LeBard, R. J., Jensen, S. O., Arnaiz, I. A., Skurray, R. A. and Firth, N. (2008). A multimer resolution system contributes to segregational stability of the

prototypical staphylococcal conjugative multiresistance plasmid pSK41. *FEMS Microbiol Lett* **284**: 58-67.

Lederberg, J. (1952). Cell genetics and hereditary symbiosis. *Physiol Rev* **32**: 403-430.

Lee, C. L., Ow, D. S. W. and Oh, S. K. W. (2006). Quantitative real-time polymerase chain reaction for determination of plasmid copy number in bacteria. *J Microbiol Meth* **65**: 258-267.

Leelaporn, A., Firth, N., Byrne, M. E., Roper, E. and Skurray, R. A. (1994). Possible role of insertion sequence IS257 in dissemination and expression of high- and low-level trimethoprim resistance in staphylococci. *Antimicrob Agents Ch* **38**: 2238-2244.

Leelaporn, A., Firth, N., Paulsen, I. and Skurray, R. (1996). IS257-mediated cointegration in the evolution of a family of staphylococcal trimethoprim resistance plasmids. *J Bacteriol* **178**: 6070-6073.

Lehman, C. W. and Botchan, M. R. (1998). Segregation of viral plasmids depends on tethering to chromosomes and is regulated by phosphorylation. *Proc Natl Acad Sci USA* **95**: 4338-4343.

Li, Y. and Austin, S. (2002). The P1 plasmid is segregated to daughter cells by a 'capture and ejection' mechanism coordinated with *Escherichia coli* cell division. *Mol Microbiol* **46**: 63-74.

Liang, Y. (2008). Applications of isothermal titration calorimetry in protein science. *Acta Bioch Bioph Sin* **40**: 565-576.

Liew, A. T. F., Theis, T., Jensen, S. O., Garcia-Lara, J., Foster, S. J., Firth, N., Lewis, P. J. and Harry, E. J. (2011). A simple plasmid-based system that allows rapid generation of tightly controlled gene expression in *Staphylococcus aureus*. *Microbiology* **157**: 666-676.

Lim, G. E., Derman, A. I. and Pogliano, J. (2005). Bacterial DNA segregation by dynamic SopA polymers. *Proc Natl Acad Sci USA* **102**: 17658-17663.

Lin, D. C. and Grossman, A. D. (1998). Identification and characterization of a bacterial chromosome partitioning site. *Cell* **92**: 675-685.

Lindsay, J. A. (2010). Genomic variation and evolution of *Staphylococcus aureus*. *Int J Med Microbiol* **300**: 98-103.

Lindsay, J. A. (2013). Hospital-associated MRSA and antibiotic resistance—what have we learned from genomics? *Int J Med Microbiol* **303**: 318-323.

Lindsay, J. A. (2014). *Staphylococcus aureus* genomics and the impact of horizontal gene transfer. *Int J Med Microbiol* **304**: 103-109.

Lindsay, J. A., Moore, C. E., Day, N. P., Peacock, S. J., Witney, A. A., Stabler, R. A., Husain, S. E., Butcher, P. D. and Hinds, J. (2006). Microarrays reveal that each of the ten dominant lineages of *Staphylococcus aureus* has a unique combination of surface-associated and regulatory genes. *J Bacteriol* **188**: 669-676.

Lindsay, J. A., Ruzin, A., Ross, H. F., Kurepina, N. and Novick, R. P. (1998). The gene for toxic shock toxin is carried by a family of mobile pathogenicity islands in *Staphylococcus aureus*. *Mol Microbiol* **29**: 527-543.

Littlejohn, T. G., DiBerardino, D., Messerotti, L. J., Spiers, S. J. and Skurray, R. A. (1991). Structure and evolution of a family of genes encoding antiseptic and disinfectant resistance in *Staphylococcus aureus*. *Gene* **101**: 59-66.

Liu, M. A. (2012). Replication initiation in the staphylococcal multiresistance plasmid pSK41. PhD thesis. The University of Sydney, Australia.

Liu, M. A., Kwong, S. M., Jensen, S. O., Brzoska, A. J. and Firth, N. (2013). Biology of the staphylococcal conjugative multiresistance plasmid pSK41. *Plasmid* **70**: 42-51.

Łobocka, M. and Yarmolinsky, M. (1996). P1 plasmid partition: a mutational analysis of ParB. *J Mol Biol* **259**: 366-382.

Löfblom, J., Kronqvist, N., Uhlén, M., Ståhl, S. and Wernérus, H. (2007). Optimization of electroporation-mediated transformation: *Staphylococcus carnosus* as model organism. *J Appl Microbiol* **102**: 736-747.

Löfdahl, S., Zabielski, J. and Philipson, L. (1981). Structure and restriction enzyme maps of the circularly permuted DNA of staphylococcal bacteriophage Φ 11. *J Virol* **37**: 784-794.

Looman, A. C., Bodlaender, J., Comstock, L. J., Eaton, D., Jhurani, P., de Boer, H. A. and van Knippenberg, P. H. (1987). Influence of the codon following the AUG initiation codon on the expression of a modified *lacZ* gene in *Escherichia coli*. *EMBO J* **6**: 2489-2492.

Lorenz, M. (2009). Visualizing protein–RNA interactions inside cells by fluorescence resonance energy transfer. *RNA* **15**: 97-103.

Lundblad, J. R., Laurance, M. and Goodman, R. H. (1996). Fluorescence polarization analysis of protein-DNA and protein-protein interactions. *Mol Endocrinol* **10**: 607-612.

Luong, T. T., Ouyang, S., Bush, K. and Lee, C. Y. (2002). Type 1 capsule genes of *Staphylococcus aureus* are carried in a staphylococcal cassette chromosome genetic element. *J Bacteriol* **184**: 3623-3629.

Lyon, B. R., Iuorio, J. L., May, J. W. and Skurray, R. A. (1984a). Molecular epidemiology of multiresistant *Staphylococcus aureus* in Australian hospitals. *J Med Microbiol* **17**: 79-89.

Lyon, B. R., May, J. W. and Skurray, R. A. (1983). Analysis of plasmids in nosocomial strains of multiple-antibiotic-resistant *Staphylococcus aureus*. *Appl Environ Microbiol* **23**: 817-826.

Lyon, B. R., May, J. W. and Skurray, R. A. (1984b). Tn4001: A gentamicin and kanamycin resistance transposon in *Staphylococcus aureus*. *Mol Gen Genet* **193**: 554-556.

Lyon, B. R. and Skurray, R. (1987). Antimicrobial resistance of *Staphylococcus aureus*: genetic basis. *Microbiol Rev* **51**: 88-134.

Maiques, E., Úbeda, C., Tormo, M. Á., Ferrer, M. D., Lasa, Í., Novick, R. P. and Penadés, J. R. (2007). Role of staphylococcal phage and SaPI integrase in intra- and interspecies SaPI transfer. *J Bacteriol* **189**: 5608-5616.

Malachowa, N. and DeLeo, F. R. (2010). Mobile genetic elements of *Staphylococcus aureus*. *Cell Mol Life Sci* **67**: 3057-3071.

Mangili, A., Bica, I., Snyderman, D. R. and Hamer, D. H. (2005). Daptomycin-resistant, methicillin-resistant *Staphylococcus aureus* bacteremia. *Clin Infect Dis* **40**: 1058-1060.

Marass, F. and Upton, C. (2009). Sequence Searcher: A Java tool to perform regular expression and fuzzy searches of multiple DNA and protein sequences. *BMC Res Notes* **2**: 1-3.

Marbouty, M., Cournac, A., Flot, J. F., Marie-Nelly, H., Mozziconacci, J. and Koszul, R. (2014). Metagenomic chromosome conformation capture (meta3C) unveils the diversity of chromosome organization in microorganisms. *eLife* **3**: e03318.

Marincola, G., Schäfer, T., Behler, J., Bernhardt, J., Ohlsen, K., Goerke, C. and Wolz, C. (2012). RNase Y of *Staphylococcus aureus* and its role in the activation of virulence genes. *Mol Microbiol* **85**: 817-832.

Martínez, J. L. (2008). Antibiotics and antibiotic resistance genes in natural environments. *Science* **321**: 365-367.

McCarthy, A. J. and Lindsay, J. A. (2012). The distribution of plasmids that carry virulence and resistance genes in *Staphylococcus aureus* is lineage associated. *BMC Microbiol* **12**: 104-104.

McDonnell, R. W., Sweeney, H. M. and Cohen, S. (1983). Conjugational transfer of gentamicin resistance plasmids intra- and interspecifically in *Staphylococcus aureus* and *Staphylococcus epidermidis*. *Antimicrob Agents Ch* **23**: 151-160.

McKenzie, T., Hoshino, T., Tanaka, T. and Sueoka, N. (1986). The nucleotide sequence of pUB110: some salient features in relation to replication and its regulation. *Plasmid* **15**: 93-103.

Mehta, S., Yang, X. M., Chan, C. S., Dobson, M. J., Jayaram, M. and Velmurugan, S. (2002). The 2 micron plasmid purloins the yeast cohesin complex: a mechanism for coupling plasmid partitioning and chromosome segregation? *J Cell Biol* **158**: 625-637.

Mendes, R. E., Deshpande, L. M., Bonilla, H. F., Schwarz, S., Huband, M. D., Jones, R. N. and Quinn, J. P. (2013). Dissemination of a pSCFS3-like *cfr*-carrying plasmid in *Staphylococcus aureus* and *Staphylococcus epidermidis* clinical isolates recovered from hospitals in Ohio. *Antimicrob Agents Ch* **57**: 2923-2928.

Mitsuhashi, S., Oshima, H., Kawaharada, U. and Hashimoto, H. (1965). Drug resistance of staphylococci I. Transduction of tetracycline resistance with phage lysates obtained from multiply resistant staphylococci. *J Bacteriol* **89**: 967-976.

Møller-Jensen, J., Borch, J., Dam, M., Jensen, R. B., Roepstorff, P. and Gerdes, K. (2003). Bacterial mitosis: ParM of plasmid R1 moves plasmid DNA by an actin-like insertional polymerization mechanism. *Mol Cell* **12**: 1477-1487.

Møller-Jensen, J., Jensen, R. B., Löwe, J. and Gerdes, K. (2002). Prokaryotic DNA segregation by an actin-like filament. *EMBO J* **21**: 3119-3127.

Møller-Jensen, J., Ringgaard, S., Mercogliano, C. P., Gerdes, K. and Löwe, J. (2007). Structural analysis of the ParR/*parC* plasmid partition complex. *EMBO J* **26**: 4413-4422.

Mongkolrattanothai, K., Boyle, S., Murphy, T. V. and Daum, R. S. (2004). Novel non-*mecA*-containing staphylococcal chromosomal cassette composite island containing *pbp4* and *tagF* genes in a commensal staphylococcal species: a possible reservoir for antibiotic resistance islands in *Staphylococcus aureus*. *Antimicrob Agents Ch* **48**: 1823-1836.

Monk, I. R., Shah, I. M., Xu, M., Tan, M. and Foster, T. J. (2012). Transforming the untransformable: application of direct transformation to manipulate genetically *Staphylococcus aureus* and *Staphylococcus epidermidis*. *mBio* **3**: 1-11.

Montabana, E. A. and Agard, D. A. (2014). Bacterial tubulin TubZ-Bt transitions between a two-stranded intermediate and a four-stranded filament upon GTP hydrolysis. *Proc Natl Acad Sci USA* **111**: 3407-3412.

Montelione, G. T., Zheng, D., Huang, Y. J., Gunsalus, K. C. and Szyperski, T. (2000). Protein NMR spectroscopy in structural genomics. *Nat Struct Mol Biol* **7**: 982-985.

Morales, G., Picazo, J. J., Baos, E., Candel, F. J., Arribi, A., Peláez, B., Andrade, R., de la Torre, M.-Á., Fereres, J. and Sánchez-García, M. (2010). Resistance to linezolid is mediated by the *cfr* gene in the first report of an outbreak of linezolid-resistant *Staphylococcus aureus*. *Clin Infect Dis* **50**: 821-825.

- Morikawa, K., Takemura, A. J., Inose, Y., Tsai, M., Nguyen Thi, L. T., Ohta, T. and Msadek, T.** (2012). Expression of a cryptic secondary sigma factor gene unveils natural competence for DNA transformation in *Staphylococcus aureus*. *PLoS Pathog* **8**: e1003003.
- Morton, T. M., Johnston, J. L., Patterson, J. and Archer, G. L.** (1995). Characterization of a conjugative staphylococcal mupirocin resistance plasmid. *Antimicrob Agents Ch* **39**: 1272-1280.
- Motallebi-Veshareh, M., Rouch, D. A. and Thomas, C. M.** (1990). A family of ATPases involved in active partitioning of diverse bacterial plasmids. *Mol Microbiol* **4**: 1455-1463.
- Murphy, G. E. and Jensen, G. J.** (2007). Electron cryotomography. *Biotechniques* **43**: 413–415.
- Naimi, T. S., LeDell, K. H., Como-Sabetti, K., Borchardt, S. M., Boxrud, D. J., Etienne, J., Johnson, S. K., Vandenesch, F., Fridkin, S., O'Boyle, C., Danila, R. N. and Lynfield, R.** (2003). Comparison of community- and health care-associated methicillin-resistant *Staphylococcus aureus* infection. *JAMA* **290**: 2976-2984.
- Narita, S., Kaneko, J., Chiba, J., Piémont, Y., Jarraud, S., Etienne, J. and Kamio, Y.** (2001). Phage conversion of Panton-Valentine leukocidin in *Staphylococcus aureus*: molecular analysis of a PVL-converting phage, ϕ SLT. *Gene* **268**: 195-206.
- Nguyen, B., Tanious, F. A. and Wilson, W. D.** (2007). Biosensor-surface plasmon resonance: Quantitative analysis of small molecule–nucleic acid interactions. *Methods* **42**: 150-161.
- Ni, L., Xu, W., Kumaraswami, M. and Schumacher, M. A.** (2010). Plasmid protein TubR uses a distinct mode of HTH-DNA binding and recruits the prokaryotic tubulin homolog TubZ to effect DNA partition. *Proc Natl Acad Sci USA* **107**: 11763-11768.
- Nicholas, K. B. and Nicholas, H. B.** (1997). "GeneDoc: a tool for editing and annotating multiple sequence alignments." from <http://www.psc.edu/biomed/genedoc>.

Nordström, K. and Austin, S. J. (1989). Mechanisms that contribute to the stable segregation of plasmids. *Annu Rev Genet* **23**: 37-69.

Novick, R. P. (1989). Staphylococcal plasmids and their replication. *Annu Rev Microbiol* **43**: 537-563.

Novick, R. P. (1990). The *Staphylococcus* as a molecular genetic system. *Molecular Biology of the Staphylococci*. Novick, R. P. VCH Press, New York, USA **1**: 1-37.

Novick, R. P., Christie, G. E. and Penadés, J. R. (2010). The phage-related chromosomal islands of Gram-positive bacteria. *Nat Rev Microbiol* **8**: 541-551.

Novick, R. P., Edelman, I. and Lofdahl, S. (1986). Small *Staphylococcus aureus* plasmids are transduced as linear multimers that are formed and resolved by replicative processes. *J Mol Biol* **192**: 209-220.

Novick, R. P., Schlievert, P. and Ruzin, A. (2001). Pathogenicity and resistance islands of staphylococci. *Microbes Infect* **3**: 585-594.

Novick, R. P. and Subedi, A. (2007). The SaPIs: mobile pathogenicity islands of *Staphylococcus*. *Chem Immunol Allergy* **93**: 42-57.

Nübel, U., Roumagnac, P., Feldkamp, M., Song, J. H., Ko, K. S., Huang, Y. C., Coombs, G., Ip, M., Westh, H., Skov, R., Struelens, M. J., Goering, R. V., Strommenger, B., Weller, A., Witte, W. and Achtman, M. (2008). Frequent emergence and limited geographic dispersal of methicillin-resistant *Staphylococcus aureus*. *Proc Natl Acad Sci USA* **105**: 14130-14135.

O'Brien, F. G., Yui Eto, K., Murphy, R. J. T., Fairhurst, H. M., Coombs, G. W., Grubb, W. B. and Ramsay, J. P. (2015). Origin-of-transfer sequences facilitate mobilisation of non-conjugative antimicrobial-resistance plasmids in *Staphylococcus aureus*. *Nucleic Acids Res* **43**: 7971-7983.

Ogura, Y., Ogasawara, N., Harry, E. J. and S, M. (2003). Increasing the ratio of Soj to Spo0J promotes replication initiation in *Bacillus subtilis*. *J Bacteriol* **185**: 6316-6324.

Ojala, V., Laitalainen, J. and Jalasvuori, M. (2013). Fight evolution with evolution: plasmid-dependent phages with a wide host range prevent the spread of antibiotic resistance. *Evol Appl* **6**: 925-932.

Oldfield, C. J., Ulrich, E. L., Cheng, Y., Dunker, A. K. and Markley, J. L. (2005). Addressing the intrinsic disorder bottleneck in structural proteomics. *Proteins* **59**: 444-453.

Oliva, M. A., Martin-Galiano, A. J., Sakaguchi, Y. and Andreu, J. M. (2012). Tubulin homolog TubZ in a phage-encoded partition system. *Proc Natl Acad Sci USA* **109**: 7711-7716.

Orlova, A., Garner, E. C., Galkin, V. E., Heuser, J., Mullins, R. D. and Egelman, E. H. (2007). The structure of bacterial ParM filaments. *Nat Struct Mol Biol* **14**: 921-926.

Page, R. and Peti, W. (2016). Toxin-antitoxin systems in bacterial growth arrest and persistence. *Nat Chem Biol* **12**: 208-214.

Pallen, M. J. and Wren, B. W. (2007). Bacterial pathogenomics. *Nature* **449**: 835-842.

Paulsen, I. T., Gillespie, M. T., Littlejohn, T. G., Hanvivatvong, O., Rowland, S. J., Dyke, K. G. H. and Skurray, R. A. (1994). Characterisation of *sin*, a potential recombinase-encoding gene from *Staphylococcus aureus*. *Gene* **141**: 109-114.

Pellequer, J. L. and Westhof, E. (1993). PREDITOP: A program for antigenicity prediction. *J Mol Graphics* **11**: 204-210.

Pelton, J. T. and McLean, L. R. (2000). Spectroscopic methods for analysis of protein secondary structure. *Anal Biochem* **277**: 167-176.

Pereira, P. M., Veiga, H., Jorge, A. M. and Pinho, M. G. (2010). Fluorescent reporters for studies of cellular localization of proteins in *Staphylococcus aureus*. *Appl Environ Microbiol* **76**: 4346-4353.

Pérez-Roth, E., Kwong, S. M., Alcoba-Florez, J., Firth, N. and Méndez-Álvarez, S. (2010). Complete nucleotide sequence and comparative analysis of pPR9, a 41.7-kilobase conjugative staphylococcal multiresistance plasmid conferring high-level mupirocin resistance. *Antimicrob Agents Ch* **54**: 2252-2257.

Pérez-Roth, E., López-Aguilar, C., Alcoba-Florez, J. and Méndez-Álvarez, S. (2006). High-level mupirocin resistance within methicillin-resistant *Staphylococcus aureus* pandemic lineages. *Antimicrob Agents Ch* **50**: 3207-3211.

Pinho, M. G. and Errington, J. (2003). Dispersed mode of *Staphylococcus aureus* cell wall synthesis in the absence of the division machinery. *Mol Microbiol* **50**: 871-881.

Pinho, M. G. and Errington, J. (2004). A *divIVA* null mutant of *Staphylococcus aureus* undergoes normal cell division. *FEMS Microbiol Lett* **240**: 145-149.

Pinho, M. G. and Errington, J. (2005). Recruitment of penicillin-binding protein PBP2 to the division site of *Staphylococcus aureus* is dependent on its transpeptidation substrates. *Mol Microbiol* **55**: 799-807.

Pinho, M. G., Kjos, M. and Veening, J. (2013). How to get (a)round: mechanisms controlling growth and division of coccoid bacteria. *Nat Rev Micro* **11**: 601-614.

Plorde, J. J. and Sherris, J. C. (1974). Staphylococcal resistance to antibiotics: origin, measurement, and epidemiology. *Ann NY Acad Sci* **236**: 413-434.

Pogliano, J., Ho, T. Q., Zhong, Z. and Helinski, D. R. (2001). Multicopy plasmids are clustered and localized in *Escherichia coli*. *Proc Natl Acad Sci USA* **98**: 4486-4491.

Pollet, R. M., Ingle, J. D., Hymes, J. P., Eakes, T. C., Eto, K. Y., Kwong, S. M., Ramsay, J. P., Firth, N. and Redinbo, M. R. (2016). Processing of nonconjugative resistance plasmids by conjugation nicking enzyme of Staphylococci. *J Bacteriol* **198**: 888-897.

Ponomarenko, J., Bui, H., Li, W., Fussedder, N., Bourne, P. E., Sette, A. and Peters, B. (2008). ElliPro: a new structure-based tool for the prediction of antibody epitopes. *BMC Bioinformatics* **9**: 1-9.

Popp, D., Xu, W., Narita, A., Brzoska, A. J., Skurray, R. A., Firth, N., Goshdastider, U., Maéda, Y., Robinson, R. C. and Schumacher, M. A. (2010). Structure and filament dynamics of the pSK41 actin-like ParM protein: implications for plasmid DNA segregation. *J Biol Chem* **285**: 10130-10140.

Poppert, S., Riecker, M., Wellinghausen, N., Frickmann, H. and Essig, A. (2010). Accelerated identification of *Staphylococcus aureus* from blood cultures by a modified fluorescence *in situ* hybridization procedure. *J Med Microbiol* **59**: 65-68.

Prescott, L. M., Harley, J. P. and Klein, D. A. (2005). Microbiology. McGraw Hill, New York.

Projan, S. J. and Archer, G. L. (1989). Mobilization of the relaxable *Staphylococcus aureus* plasmid pC221 by the conjugative plasmid pGO1 involves three pC221 loci. *J Bacteriol* **171**: 1841-1845.

Projan, S. J., Carleton, S. and Novick, R. P. (1983). Determination of plasmid copy number by fluorescence densitometry. *Plasmid* **9**: 182-190.

Pushnova, E. A., Geier, M. and Zhu, Y. S. (2000). An easy and accurate agarose gel assay for quantitation of bacterial plasmid copy numbers. *Anal Biochem* **284**: 70-76.

Rajasekar, K., Muntaha, S. T., Tame, J. R. H., Kommareddy, S., Morris, G., Wharton, C. W., Thomas, C. M., White, S. A., Hyde, E. I. and Scott, D. J. (2010). Order and disorder in the domain organization of the plasmid partition protein KorB. *J Biol Chem* **285**: 15440-15449.

Rammelkamp, C. H. and Maxon, T. (1942). Resistance of *Staphylococcus aureus* to the action of penicillin. *P Soc Exp Biol Med* **51**: 386-389.

Ramsay, J. P., Kwong, S. M., Murphy, R. J. T., Yui Eto, K., Price, K. J., Nguyen, Q. T., O'Brien, F. G., Grubb, W. B., Coombs, G. W. and Firth, N. (2016). An updated view of plasmid conjugation and mobilization in *Staphylococcus*. *Mob Genet Elements* **6**: e1208317.

Reyes-Lamothe, R., Tran, T., Meas, D., Lee, L., Li, A. M., Sherratt, D. J. and Tolmasky, M. E. (2014). High-copy bacterial plasmids diffuse in the nucleoid-free space, replicate stochastically and are randomly partitioned at cell division. *Nucleic Acids Res* **42**: 1042-1051.

Ridder, A., Skupjen, P., Unterreitmeier, S. and Langosch, D. (2005). Tryptophan supports interaction of transmembrane helices. *J Mol Biol* **354**: 894-902.

Ringgaard, S., Löwe, J. and Gerdes, K. (2007). Centromere pairing by a plasmid-encoded type I ParB protein. *J Biol Chem* **282**: 28216-28225.

Ringgaard, S., van Zon, J., Howard, M. and Gerdes, K. (2009). Movement and equipositioning of plasmids by ParA filament disassembly. *Proc Natl Acad Sci USA* **106**: 19369-19374.

Robinett, C. C., Straight, A., Li, G., Wilhelm, C., Sudlow, G., Murray, A. and Belmont, A. S. (1996). *In vivo* localization of DNA sequences and visualization of large-scale chromatin organization using *lac* operator/repressor recognition. *J Cell Biol* **135**: 1685-1700.

Rocker, A. and Meinhart, A. (2016). Type II toxin: antitoxin systems. More than small selfish entities? *Curr Genet* **62**: 287-290.

Rodionov, O., Lobočka, M. and Yarmolinsky, M. (1999). Silencing of genes flanking the P1 plasmid centromere. *Science* **283**: 546-549.

Rodionov, O. and Yarmolinsky, M. (2004). Plasmid partitioning and the spreading of P1 partition protein ParB. *Molecular Microbiology* **52**: 1215-1223.

Rossi, F., Diaz, L., Wollam, A., Panesso, D., Zhou, Y., Rincon, S., Narechania, A., Xing, G., Di Gioia, T. S. R., Doi, A., Tran, T. T., Reyes, J., Munita, J. M., Carvajal, L. P., Hernandez-Roldan, A., Brandão, D., van der Heijden, I. M., Murray, B. E., Planet, P. J., Weinstock, G. M. and Arias, C. A. (2014). Transferable vancomycin resistance in a community-associated MRSA lineage. *New Engl J Med* **370**: 1524-1531.

Rouch, D. A., Byrne, M. E., Kong, Y. C. and Skurray, R. A. (1987). The *aacA-aphD* gentamicin and kanamycin resistance determinant of Tn4001 from *Staphylococcus aureus*: expression and nucleotide sequence analysis. *J Gen Microbiol* **133**: 3039-3052.

Rouch, D. A., Messerotti, L. J., Loo, L. S. L., Jackson, C. A. and Skurray, R. A. (1989). Trimethoprim resistance transposon Tn4003 from *Staphylococcus aureus* encodes genes for a dihydrofolate reductase and thymidylate synthetase flanked by three copies of IS257. *Mol Microbiol* **3**: 161-175.

Rountree, P. M. (1951). The role of certain electrolytes in the adsorption of staphylococcal bacteriophages. *J Gen Microbiol* **5**: 673-680.

Rowland, S. J. and Dyke, K. G. (1989). Characterization of the staphylococcal beta-lactamase transposon Tn552. *EMBO J* **8**: 2761-2773.

Rowland, S. J. and Dyke, K. G. H. (1990). Tn552, a novel transposable element from *Staphylococcus aureus*. *Mol Microbiol* **4**: 961-975.

Rudin, L., Sjöström, J., Lindberg, M. and Philipson, L. (1974). Factors affecting competence for transformation in *Staphylococcus aureus*. *J Bacteriol* **118**: 155-164.

Ruiz-Echevarría, M. J., Giménez-Gallego, G., Sabariego-Jareño, R. and Díaz-Orejas, R. (1995). Kid, a small protein of the *parD* stability system of plasmid R1, is an inhibitor of DNA replication acting at the initiation of DNA synthesis. *J Mol Biol* **247**: 568-577.

Rush, M. G., Gordon, C. N., Novick, R. P. and Warner, R. C. (1969). Penicillinase plasmid DNA from *Staphylococcus aureus*. *Proc Natl Acad Sci USA* **63**: 1304-1310.

Ruzin, A., Lindsay, J. and Novick, R. P. (2001). Molecular genetics of SaPII – a mobile pathogenicity island in *Staphylococcus aureus*. *Mol Microbiol* **41**: 365-377.

Salgado, C. D., Farr, B. M. and Calfee, D. P. (2003). Community-acquired methicillin-resistant *Staphylococcus aureus*: a meta-analysis of prevalence and risk factors. *Clin Infect Dis* **36**: 131-139.

Salje, J. (2010). Plasmid segregation: how to survive as an extra piece of DNA. *Crit Rev Biochem Mol* **45**: 296-317.

Salje, J. and Löwe, J. (2008). Bacterial actin: architecture of the ParMRC plasmid DNA partitioning complex. *EMBO J* **27**: 2230-2238.

Salje, J., Zuber, B. and Löwe, J. (2009). Electron cryomicroscopy of *E. coli* reveals filament bundles involved in plasmid DNA segregation. *Science* **323**: 509-512.

Sambrook, J. and Russell, D. W. (2001). Molecular cloning: a laboratory manual. Cold Spring Harbour Laboratory, Cold Spring Harbour, New York.

Sanchez, A., Cattoni, Diego I., Walter, J.-C., Rech, J., Parmeggiani, A., Nollmann, M. and Bouet, J. Y. (2015). Stochastic self-assembly of ParB proteins builds the bacterial DNA segregation apparatus. *Cell Syst* **1**: 163-173.

Sanchez, A., Rech, J., Gasc, C. and Bouet, J. (2013). Insight into centromere-binding properties of ParB proteins: a secondary binding motif is essential for bacterial genome maintenance. *Nucleic Acids Res* **41**: 3094-3103.

Sau, S., Liu, Y. T., Ma, C. H. and Jayaram, M. (2015). Stable persistence of the yeast plasmid by hitchhiking on chromosomes during vegetative and germ-line divisions of host cells. *Mob Genet Elements* **5**: 21-28.

Schenk, S. and Laddaga, R. A. (1992). Improved method for electroporation of *Staphylococcus aureus*. *FEMS Microbiol Lett* **94**: 133-138.

Schermelleh, L., Heintzmann, R. and Leonhardt, H. (2010). A guide to super-resolution fluorescence microscopy. *J Cell Biol* **190**: 165-175.

Schneewind, O., Model, P. and Fischetti, V. A. (1992). Sorting of protein A to the staphylococcal cell wall. *Cell* **70**: 267-281.

Schreiter, E. R. and Drennan, C. L. (2007). Ribbon-helix-helix transcription factors: variations on a theme. *Nat Rev Microbiol* **5**: 710-720.

Schumacher, Maria A. (2008). Structural biology of plasmid partition: uncovering the molecular mechanisms of DNA segregation. *Biochem J* **412**: 1-18.

Schumacher, M. A. (2012). Bacterial plasmid partition machinery: a minimalist approach to survival. *Curr Opin Struct Biol* **22**: 72-79.

Schumacher, M. A. and Funnell, B. E. (2005). Structures of ParB bound to DNA reveal mechanism of partition complex formation. *Nature* **438**: 516-519.

Schumacher, M. A., Glover, T. C., Brzoska, A. J., Jensen, S. O., Dunham, T. D., Skurray, R. A. and Firth, N. (2007a). Segrosome structure revealed by a complex of ParR with centromere DNA. *Nature* **450**: 1268-1271.

Schumacher, M. A., Lee, J. and Zeng, W. (2016). Molecular insights into DNA binding and anchoring by the *Bacillus subtilis* sporulation kinetochore-like RacA protein. *Nucleic Acids Res* **44**: 5438-5449.

Schumacher, M. A., Mansoor, A. and Funnell, B. E. (2007b). Structure of a four-way bridged ParB-DNA complex provides insight into P1 segrosome assembly. *J Biol Chem* **282**: 10456-10464.

Schumacher, M. A., Piro, K. M. and Xu, W. (2010). Insight into F plasmid DNA segregation revealed by structures of SopB and SopB-DNA complexes. *Nucleic Acids Res* **38**: 4514-4526.

Schumacher, M. A., Tonthat, N. K., Kwong, S. M., Chinnam, N. b., Liu, M. A., Skurray, R. A. and Firth, N. (2014). Mechanism of staphylococcal multiresistance plasmid replication origin assembly by the RepA protein. *Proc Natl Acad Sci USA* **111**: 9121-9126.

Selinger, L. B., McGregor, N. F., Khachatourians, G. G. and Hynes, M. F. (1990). Mobilization of closely related plasmids pUB110 and pBC16 by *Bacillus* plasmid pXO503 requires *trans*-acting open reading frame beta. *J Bacteriol* **172**: 3290-3297.

Semon, D., Movva, N. R., Smith, T. F., El Alama, M. and Davies, J. (1987). Plasmid-determined bleomycin resistance in *Staphylococcus aureus*. *Plasmid* **17**: 46-53.

Sengupta, M., Nielsen, H. J., Youngren, B. and Austin, S. (2010). P1 plasmid segregation: accurate redistribution by dynamic plasmid pairing and separation. *J Bacteriol* **192**: 1175-1183.

Shalita, Z., Murphy, E. and Novick, R. P. (1980). Penicillinase plasmids of *Staphylococcus aureus*: structural and evolutionary relationships *Plasmid* **3**: 291-311.

Shearer, J. E. S., Wireman, J., Hostetler, J., Forberger, H., Borman, J., Gill, J., Sanchez, S., Mankin, A., LaMarre, J., Lindsay, J. A., Bayles, K., Nicholson, A., O'Brien, F., Jensen, S. O., Firth, N., Skurray, R. A. and Summers, A. O. (2011). Major families of multiresistant plasmids from geographically and epidemiologically diverse staphylococci. *G3 (Bethesda)* **1**: 581-591.

Shirai, A., Matsuyama, A., Yashiroda, Y., Hashimoto, A., Kawamura, Y., Arai, R., Komatsu, Y., Horinouchi, S. and Yoshida, M. (2008). Global analysis of gel mobility of proteins and its use in target identification. *J Biol Chem* **283**: 10745-10752.

Shokeen, S., Greenfield, T. J., Ehli, E. A., Rasmussen, J., Perrault, B. E. and Weaver, K. E. (2009). An intramolecular upstream helix ensures the stability of a toxin-encoding RNA in *Enterococcus faecalis*. *J Bacteriol* **191**: 1528-1536.

Shokeen, S., Patel, S., Greenfield, T. J., Brinkman, C. and Weaver, K. E. (2008). Translational regulation by an intramolecular stem-loop is required for intermolecular RNA regulation of the *par* addiction module. *J Bacteriol* **190**: 6076-6083.

Shore, A. C., Lazaris, A., Kinnevey, P. M., Brennan, O. M., Brennan, G. I., O'Connell, B., Feßler, A. T., Schwarz, S. and Coleman, D. C. (2016). First report of *cfr*-carrying plasmids in the pandemic sequence type 22 methicillin-resistant *Staphylococcus aureus* staphylococcal cassette chromosome *mec* type IV clone. *Antimicrob Agents Ch* **60**: 3007-3015.

Sievers, F., Wilm, A., Dineen, D., Gibson, T. J., Karplus, K., Li, W., Lopez, R., McWilliam, H., Remmert, M., Söding, J., Thompson, J. D. and Higgins, D. G. (2011). Fast, scalable generation of high-quality protein multiple sequence alignments using Clustal Omega. *Molecular systems biology* **7**: 539.

Signäs, C., Raucci, G., Jönsson, K., Lindgren, P. E., Anantharamaiah, G. M., Höök, M. and Lindberg, M. (1989). Nucleotide sequence of the gene for a fibronectin-binding protein from *Staphylococcus aureus*: use of this peptide sequence in the synthesis of biologically active peptides. *Proc Natl Acad Sci USA* **86**: 699-703.

Silva, A. M. N., Vitorino, R., Domingues, M. R. M., Spickett, C. M. and Domingues, P. (2013). Post-translational modifications and mass spectrometry detection. *Free Radical Bio Med* **65**: 925-941.

Simpson, A. E. (2002). Mobile elements and the molecular evolution of antimicrobial resistance in *Staphylococcus aureus*. PhD thesis. The University of Sydney, Australia.

Simpson, A. E., Skurray, R. A. and Firth, N. (2000). An IS257-derived hybrid promoter directs transcription of a *tetA(K)* tetracycline resistance gene in the *Staphylococcus aureus* chromosomal *mec* region. *J Bacteriol* **182**: 3345-3352.

Simpson, A. E., Skurray, R. A. and Firth, N. (2003). A single gene on the staphylococcal multiresistance plasmid pSK1 encodes a novel partitioning system. *J Bacteriol* **185**: 2143-2152.

Sjöström, J., Löfdahl, S. and Philipson, L. (1979). Transformation of *Staphylococcus aureus* by heterologous plasmids. *Plasmid* **2**: 529-535.

Skibbens, R. V. (2008). Mechanisms of sister chromatid pairing. *Int Rev Cell Mol Biol* **269**: 283-339.

Slabinski, L., Jaroszewski, L., Rodrigues, A. P. C., Rychlewski, L., Wilson, I. A., Lesley, S. A. and Godzik, A. (2007). The challenge of protein structure determination—lessons from structural genomics. *Protein Sci* **16**: 2472-2482.

Sowash, M. G. and Uhlemann, A. C. (2014). Community-associated methicillin-resistant *Staphylococcus aureus* case studies. *Method Mol Biol* **1085**: 25-69.

Stefani, S., Chung, D. R., Lindsay, J. A., Friedrich, A. W., Kearns, A. M., Westh, H. and MacKenzie, F. M. (2012). Methicillin-resistant *Staphylococcus aureus* (MRSA): global epidemiology and harmonisation of typing methods. *Int J Antimicrob Ag* **39**: 273-282.

Stenström, C. M., Jin, H., Major, L. L., Tate, W. P. and Isaksson, L. A. (2001). Codon bias at the 3'-side of the initiation codon is correlated with translation initiation efficiency in *Escherichia coli*. *Gene* **263**: 273-284.

Stewart, P. R., Waldron, H. G., Lee, J. S. and Matthews, P. R. (1985). Molecular relationships among serogroup B bacteriophages of *Staphylococcus aureus*. *J Virol* **55**: 111-116.

Strauss, M. P., Liew, A. T. F., Turnbull, L., Whitchurch, C. B., Monahan, L. G. and Harry, E. J. (2012). 3D-SIM super resolution microscopy reveals a bead-like arrangement for FtsZ and the division machinery: implications for triggering cytokinesis. *PLoS Biol* **10**: e1001389.

Stryjewski, M. E. and Chambers, H. F. (2008). Skin and soft-tissue infections caused by community-acquired methicillin-resistant *Staphylococcus aureus*. *Clin Infect Dis* **46**: S368-S377.

Stryjewski, M. E. and Corey, G. R. (2014). Methicillin-resistant *Staphylococcus aureus*: an evolving pathogen. *Clin Infect Dis* **58**: S10-S19.

Subedi, A., Ubeda, C., Adhikari, R. P., Penadés, J. R. and Novick, R. P. (2007). Sequence analysis reveals genetic exchanges and intraspecific spread of SaPI2, a pathogenicity island involved in menstrual toxic shock. *Microbiology* **153**: 3235-3245.

Summers, D. K., Beton, C. W. H. and Withers, H. L. (1993). Multicopy plasmid instability: the dimer catastrophe hypothesis. *Mol Microbiol* **8**: 1031-1038.

Summers, D. K. and Sherratt, D. J. (1984). Multimerization of high copy number plasmids causes instability: ColE1 encodes a determinant essential for plasmid monomerization and stability. *Cell* **36**: 1097-1103.

Surtees, J. A. and Funnell, B. E. (2001). The DNA binding domains of P1 ParB and the architecture of the P1 plasmid partition complex. *J Biol Chem* **276**: 12385-12394.

Szabo, A., Stolz, L. and Granzow, R. (1995). Surface plasmon resonance and its use in biomolecular interaction analysis (BIA). *Curr Opin Struct Biol* **5**: 699-705.

Tang, M., Bideshi, D. K., Park, H. W. and Federici, B. A. (2006). Minireplicon from pBtoxis of *Bacillus thuringiensis* subsp. *israelensis*. *Appl Environ Microbiol* **72**: 6948-6954.

Tang, M., Bideshi, D. K., Park, H. W. and Federici, B. A. (2007). Iteron-binding ORF157 and FtsZ-like ORF156 proteins encoded by pBtoxis play a role in its replication in *Bacillus thuringiensis* subsp. *israelensis*. *J Bacteriol* **189**: 8053-8058.

Tang, S. L., Chang, B. C. H. and Halgamuge, S. K. (2010). Gene functionality's influence on the second codon: A large-scale survey of second codon composition in three domains. *Genomics* **96**: 92-101.

Taylor, J. A., Pastrana, C. L., Butterer, A., Pernstich, C., Gwynn, E. J., Sobott, F., Moreno-Herrero, F. and Dillingham, M. S. (2015). Specific and non-specific interactions of ParB with DNA: implications for chromosome segregation. *Nucleic Acids Res* **43**: 719-731.

Tennent, J. M., Lyon, B. R., Midgley, M., Jones, G., Purewal, A. S. and Skurray, R. A. (1989). Physical and biochemical characterization of the *qacA* gene encoding antiseptic and disinfectant resistance in *Staphylococcus aureus*. *J Gen Microbiol* **135**: 1-10.

- Tenover, F. C. and Goering, R. V.** (2009). Methicillin-resistant *Staphylococcus aureus* strain USA300: origin and epidemiology. *J Antimicrob Chemoth* **64**: 441-446.
- Tenover, F. C., McDougal, L. K., Goering, R. V., Killgore, G., Projan, S. J., Patel, J. B. and Dunman, P. M.** (2006). Characterization of a strain of community-associated methicillin-resistant *Staphylococcus aureus* widely disseminated in the United States. *J Clin Microbiol* **44**: 108-118.
- Thompson, J. D., Higgins, D. G. and Gibson, T. J.** (1994). CLUSTAL W: improving the sensitivity of progressive multiple sequence alignment through sequence weighting, position-specific gap penalties and weight matrix choice. *Nucleic Acids Res* **22**: 4673-4680.
- Thompson, J. K. and Collins, M. A.** (2003). Completed sequence of plasmid pIP501 and origin of spontaneous deletion derivatives. *Plasmid* **50**: 28-35.
- Tinsley, E. and Khan, S. A.** (2006). A novel FtsZ-like protein is involved in replication of the anthrax toxin-encoding pXO1 plasmid in *Bacillus anthracis*. *J Bacteriol* **188**: 2829-2835.
- Tiwari, H. K. and Sen, M. R.** (2006). Emergence of vancomycin resistant *Staphylococcus aureus* (VRSA) from a tertiary care hospital from northern part of India. *BMC Infect Dis* **6**: 156-156.
- Tompa, P.** (2002). Intrinsically unstructured proteins. *Trends Biochem Sci* **27**: 527-533.
- Tompa, P.** (2012). Intrinsically disordered proteins: a 10-year recap. *Trends Biochem Sci* **37**: 509-516.
- Ton-That, H., Faull, K. F. and Schneewind, O.** (1997). Anchor structure of staphylococcal surface proteins: a branched peptide that links the carboxyl terminus of proteins to the cell wall. *J Biol Chem* **272**: 22285-22292.
- Towbin, H., Staehelin, T. and Gordon, J.** (1979). Electrophoretic transfer of proteins from polyacrylamide gels to nitrocellulose sheets: procedure and some applications. *Proc Natl Acad Sci USA* **76**: 4350-4354.

Townsend, D. E., Ashdown, N., Annear, D. I. and Grubb, W. B. (1985). A conjugative plasmid encoding production of a diffusible pigment and resistance to aminoglycosides and macrolides in *Staphylococcus aureus*. *Aust J Exp Biol Med Sci* **63**: 573-586.

Townsend, D. E., Ashdown, N., Bolton, S., Bradley, J., Duckworth, G., Moorhouse, E. C. and Grubb, W. B. (1987). The international spread of methicillin-resistant *Staphylococcus aureus*. *J Hosp Infect* **9**: 60-71.

Tsiodras, S., Gold, H. S., Sakoulas, G., Eliopoulos, G. M., Wennersten, C., Venkataraman, L., Moellering Jr, R. C. and Ferraro, M. J. (2001). Linezolid resistance in a clinical isolate of *Staphylococcus aureus*. *Lancet* **358**: 207-208.

Turlej, A., Hryniewicz, W. and Empel, J. (2011). Staphylococcal cassette chromosome *mec* (SCC*mec*) classification and typing methods: an overview. *Pol J Microbiol* **60**: 95-103.

Turnbull, L., Strauss, M. P., Liew, A. T. F., Monahan, L. G., Whitchurch, C. B. and Harry, E. J. (2014). Super-resolution imaging of the cytokinetic Z ring in live bacteria using fast 3D-structured illumination microscopy (f3D-SIM). *J Viz Exp* e51469 DOI: 10.3791/51469

Tzagoloff, H. and Novick, R. (1977). Geometry of cell division in *Staphylococcus aureus*. *J Bacteriol* **129**: 343-350.

Úbeda, C., Maiques, E., Barry, P., Matthews, A., Tormo, M. Á., Lasa, Í., Novick, R. P. and Penadés, J. R. (2008). SaPI mutations affecting replication and transfer and enabling autonomous replication in the absence of helper phage. *Mol Microbiol* **67**: 493-503.

Udo, E. E., Wei, M. Q. and Grubb, W. B. (1992). Conjugative trimethoprim resistance in *Staphylococcus aureus*. *FEMS Microbiol Lett* **97**: 243-248.

Unterholzner, S. J., Poppenberger, B. and Rozhon, W. (2013). Toxin–antitoxin systems: biology, identification, and application. *Mob Genet Elements* **3**: e26219.

van den Ent, F., Møller-Jensen, J., Amos, L. A., Gerdes, K. and Löwe, J. (2002). F-actin-like filaments formed by plasmid segregation protein ParM. *EMBO J* **21**: 6935-6943.

Van Melderen, L. and Saavedra De Bast, M. (2009). Bacterial Toxin–Antitoxin Systems: More Than Selfish Entities? *PLOS Genetics* **5**: e1000437.

Vaughan, S., Wickstead, B., Gull, K. and Addinall, S. G. (2004). Molecular evolution of FtsZ protein sequences encoded within the genomes of archaea, bacteria, and eukaryota. *J Mol Evol* **58**: 19-29.

Vecchiarelli, A. G., Han, Y. W., Tan, X., Mizuuchi, M., Ghirlando, R., Biertümpfel, C., Funnell, B. E. and Mizuuchi, K. (2010). ATP control of dynamic P1 ParA–DNA interactions: a key role for the nucleoid in plasmid partition. *Mol Microbiol* **78**: 78-91.

Vecchiarelli, A. G., Havey, J. C., Ing, L. L., Wong, E. O. Y., Waples, W. G. and Funnell, B. E. (2013a). Dissection of the ATPase active site of P1 ParA reveals multiple active forms essential for plasmid partition. *J Biol Chem* **288**: 17823-17831.

Vecchiarelli, A. G., Hwang, L. C. and Mizuuchi, K. (2013b). Cell-free study of F plasmid partition provides evidence for cargo transport by a diffusion-ratchet mechanism. *Proc Natl Acad Sci USA* **110**: E1390-E1397.

Vecchiarelli, A. G., Mizuuchi, K. and Funnell, B. E. (2012). Surfing biological surfaces: exploiting the nucleoid for partition and transport in bacteria. *Mol Microbiol* **86**: 513-523.

Veiga, H., Jorge, A. M. and Pinho, M. G. (2011). Absence of nucleoid occlusion effector Noc impairs formation of orthogonal FtsZ rings during *Staphylococcus aureus* cell division. *Mol Microbiol* **80**: 1366-1380.

Velmurugan, S., Yang, X. M., Chan, C. S. M., Dobson, M. and Jayaram, M. (2000). Partitioning of the 2- μ m circle plasmid of *Saccharomyces cerevisiae*: functional coordination with chromosome segregation and plasmid-encoded Rep protein distribution. *J Cell Biol* **149**: 553-566.

Waldron, D. E. and Lindsay, J. A. (2006). Sau1: a novel lineage-specific type I restriction-modification system that blocks horizontal gene transfer into *Staphylococcus aureus* and between *S. aureus* isolates of different lineages. *J Bacteriol* **188**: 5578-5585.

Walker, J. E., Saraste, M., Runswick, M. J. and Gay, N. J. (1982). Distantly related sequences in the alpha- and beta-subunits of ATP synthase, myosin, kinases

and other ATP-requiring enzymes and a common nucleotide binding fold. *EMBO J* **1**: 945-951.

Wang, X. and Wood, T. K. (2011). Toxin-antitoxin systems influence biofilm and persister cell formation and the general stress response. *Appl Environ Microbiol* **77**: 5577-5583.

Ward, J. J., Sodhi, J. S., McGuffin, L. J., Buxton, B. F. and Jones, D. T. (2004). Prediction and functional analysis of native disorder in proteins from the three kingdoms of life. *J Mol Biol* **337**: 635-645.

Weaver, K. E., Jensen, K. D., Colwell, A. and Sriram, S. (1996). Functional analysis of the *Enterococcus faecalis* plasmid pAD1-encoded stability determinant *par*. *Mol Microbiol* **20**: 53-63.

Weaver, K. E., Kwong, S. M., Firth, N. and Francia, M. V. (2009a). The RepA_N replicons of Gram-positive bacteria: a family of broadly distributed but narrow host range plasmids. *Plasmid* **61**: 94-109.

Weaver, K. E., Reddy, S. G., Brinkman, C. L., Patel, S., Bayles, K. W. and Endres, J. L. (2009b). Identification and characterization of a family of toxin-antitoxin systems related to the *Enterococcus faecalis* plasmid pAD1 *par* addiction module. *Microbiology* **155**: 2930-2940.

Weigel, L. M., Clewell, D. B., Gill, S. R., Clark, N. C., McDougal, L. K., Flannagan, S. E., Kolonay, J. F., Shetty, J., Killgore, G. E. and Tenover, F. C. (2003). Genetic analysis of a high-level vancomycin-resistant isolate of *Staphylococcus aureus*. *Science* **302**: 1569-1571.

Weitao, T., Dasgupta, S. and Nordström, K. (2000). Plasmid R1 is present as clusters in the cells of *Escherichia coli*. *Plasmid* **43**: 200-204.

Wen, J., Arakawa, T. and Philo, J. S. (1996). Size-exclusion chromatography with on-line light-scattering, absorbance, and refractive index detectors for studying proteins and their interactions. *Anal Biochem* **240**: 155-166.

Wen, Y., Behiels, E. and Devreese, B. (2014). Toxin-antitoxin systems: their role in persistence, biofilm formation, and pathogenicity. *Pathog Dis* **70**: 240-249.

Wertheim, H. F. L., Melles, D. C., Vos, M. C., van Leeuwen, W., van Belkum, A., Verbrugh, H. A. and Nouwen, J. L. (2005). The role of nasal carriage in *Staphylococcus aureus* infections. *Lancet Infect Dis* **5**: 751-762.

Wheeler, D. L., Church, D. M., Federhen, S., Lash, A. E., Madden, T. L., Pontius, J. U., Schuler, G. D., Schriml, L. M., Sequeira, E., Tatusova, T. A. and Wagner, L. (2003). Database resources of the National Center for Biotechnology. *Nucleic Acids Res* **31**: 28-33.

WHO (2015). Global action plan on antimicrobial resistance. Available at http://www.who.int/drugresistance/global_action_plan/en/.

Wiegant, J. and Raap, A. K. (2001). Probe labeling and fluorescence *in situ* hybridization. *Curr Protoc Cytom* **00**: 8.3.1–8.3.21.

Winstel, V., Liang, C., Sanchez-Carballo, P., Steglich, M., Munar, M., Bröker, B. M., Penadés, J. R., Nübel, U., Holst, O., Dandekar, T., Peschel, A. and Xia, G. (2013). Wall teichoic acid structure governs horizontal gene transfer between major bacterial pathogens. *Nat Commun* **4**: 2345.

Woldringh, C. L., Jensen, P. R. and Westerhoff, H. V. (1995). Structure and partitioning of bacterial DNA: determined by a balance of compaction and expansion forces? *FEMS Microbiol Lett* **131**: 235-242.

Wright, P. E. and Dyson, H. J. (1999). Intrinsically unstructured proteins: re-assessing the protein structure-function paradigm. *J Mol Biol* **293**: 321-331.

Wu, L. J. and Errington, J. (2003). RacA and the Soj-Spo0J system combine to effect polar chromosome segregation in sporulating *Bacillus subtilis*. *Mol Microbiol* **49**: 1463-1475.

Wu, Z., Li, F., Liu, D., Xue, H. and Zhao, X. (2015). Novel type XII staphylococcal cassette chromosome *mec* harboring a new cassette chromosome recombinase, CcrC2. *Antimicrob Agents Ch* **59**: 7597-7601.

Xia, G., Corrigan, R. M., Winstel, V., Goerke, C., Gründling, A. and Peschel, A. (2011). Wall teichoic acid-dependent adsorption of staphylococcal siphovirus and myovirus. *J Bacteriol* **193**: 4006-4009.

Yamaguchi, T., Hayashi, T., Takami, H., Nakasone, K., Ohnishi, M., Nakayama, K., Yamada, S., Komatsuzawa, H. and Sugai, M. (2000). Phage conversion of exfoliative toxin A production in *Staphylococcus aureus*. *Mol Microbiol* **38**: 694-705.

Yanisch-Perron, C., Vieira, J. and Messing, J. (1985). Improved M13 phage cloning vectors and host strains: nucleotide sequences of the M13mp18 and pUC19 vectors. *Gene* **33**: 103-119.

Yau, W. M., Wimley, W. C., Gawrisch, K. and White, S. H. (1998). The preference of tryptophan for membrane interfaces. *Biochemistry* **37**: 14713-14718.

Zhang, L., Jacobsson, K., Vasi, J., Lindberg, M. and Frykberg, L. (1998). A second IgG-binding protein in *Staphylococcus aureus*. *Microbiology* **144**: 985-991.